The release of lipids from dairy food matrices under *in vitro* gastrointestinal digestive conditions

A thesis presented in partial fulfilment of the requirements for the degree of

Doctor of Philosophy

in

Food Technology

at Massey University, Manawatū, Palmerston North, New Zealand

Patrick Tai

2022

Abstract

The milk fat globule membrane (MFGM) is a trilayer phospholipid and protein interface that separates the triacylglycerides from the serum phase. Consumption of MFGM phospholipids decreases serum cholesterol in adults with high risk for hypercholesterolemia and modulates serum cholesterol in healthy adults. The biochemical mechanism behind this putative effect is currently unknown.

The large majority (~80%) of the cholesterol in the milk fat globule is localized in the MFGM in complexation with sphingomyelin to form liquid-ordered (L_o) domains. The nutritional and digestive implications of consuming L_o domains have been scarcely considered.

Considering sphingomyelin strongly complexes with cholesterol, the MFGM is rich in sphingomyelin, and the consumption of MFGM material has shown to modulate serum cholesterol, there is a likely link between the presence of L_o domains and the nutritional benefit of consuming MFGM material.

Model bilayer systems, phospholipid liposomes/vesicles, were created from phospholipids derived from natural sources: soy phosphatidylcholine (SPC), porcine brain phosphatidylcholine (BPC), egg sphingomyelin (ESM), milk sphingomyelin (MSM), milk fat globule membrane (MFGM) phospholipids extracted from bovine beta-serum, and ovine cholesterol. The structural and thermotropic properties of the vesicles were investigated under *in vitro* gastrointestinal conditions.

First, a screening test was performed on MSM/cholesterol multilamellar vesicles (MLVs). Instruments were capable of detecting shifts in the vesicles from solid-ordered (S_o) and liquid-disordered (L_d) to liquid-ordered at 2 × the MSM concentration found in raw milk.

Incubation with physiologically relevant concentrations of bovine bile demonstrated 3:2 mol/mol MSM/cholesterol MLVs were capable of resisting detergent-induced solubilization by bile salts. The SPC/cholesterol, BPC/cholesterol, and MFGM/cholesterol phospholipid vesicles were disrupted. At the endpoint of *in vitro* gastrointestinal digestion, 3:2 mol/mol MSM/cholesterol MLVs also experienced micellization – however there was no statistically significant difference in the total bilayer order of the vesicles, implying a degree of structure possibly remained.

Further investigation on the detergent solubilization of MFGM phospholipid vesicles by bile salts revealed that although the vesicle was disrupted, the mixed micellar size growth was minimal. That is, there was a lack of phospholipid exchange between vesicle and micelle.

These findings set the stage for further research into the bioactive potential of milk phospholipids.

Acknowledgements

Just one more experiment left –

Five timeless words that I told everyone who asked me how my Ph.D. was progressing at the beginning of this year. It wasn't a lie and it never turned into lie. Just one more experiment left, then just one more experiment left, and now I'm writing this acknowledgements page in July 2022. I didn't want to stop. Looking back, my almost four years spent constructing this thesis were the most fruitful and possibly happiest times in my life. Now, time to say thank you.

First, my supervisors: Dr. David Everett for introducing me to the Riddet Institute and taking me on as his student. At the beginning of my Ph.D. I asked one of his former students, Dr. Ali Rashidinejad, for his opinion on Dr. Everett. Without a beat, he said, "one of the greatest men I've ever had the pleasure of meeting." I raised an eyebrow back then; I don't anymore. Dr. Harjinder Singh, the director of the Riddet. I was worried he wouldn't have time for me, considering how busy he was. He did have the time and even welcomed all his Ph.D students to his home. Finally, Dr. Matt Golding. Whenever I had a problem understanding a result, I would finish banging my head against the wall, cross the parking lot to the Riddet Complex, go up the stairs, pass the Food Chemistry lab, and knock-on Dr. Golding's door. He would always have at least three suggestions, all good, and I would go back to my desk a little more confident in what I was interpreting, at least, until the next problem arose. I couldn't have done better for an advisory panel.

Next are those who supported my work: Maggie Zou, the tireless lab manager for the Riddet who none of the Riddet students would get anything done without, and Steve Glasglow for his help with access and operating the Food Chemistry equipment. From AgResearch, Dr. Caroline, Carol, Thum, who lent me her digestion reagents during the global supply chain crisis, and Dr. Mariza Gomes-Reis, who showed me how to quantify my phospholipids on her HPLC. Linda and Jacinda from the Te Ohu Rangahau Kai Operations for setting up the new building and helping everyone adjust to working at PC2. From the Department of Fundamental Sciences at Massey University, Dr. Mark Waterland for all his help and advice on Raman spectroscopy, Sam Brooke, Dr. Waterland's Ph.D. student who always ensured the Raman set-up would obtain the highest resolution spectra possible, and Trevor Loo for his expertise on the nano-DSC. The Manawatū Microscopy and Imaging Centre who make the Formvar grids and run the electron microscopes. Without them, I wouldn't have known what I was looking at. Dr. Ben Boyd from Monash University for giving me the opportunity use the Australian Synchrotron and introducing me to Dr. Andrew, Andy, Clulow who has been the greatest resource for x-ray scattering a graduate student with no background in x-ray scattering could hope for.

The Food Chemistry and Structures Team at AgResearch for adopting me as one of their own, especially our Team Leader, Dr. Linda Samuelson. I can now admit I am very afraid of disappointing

you by not showing up to meetings. I don't know how the other teams operate, but you've been such an exemplary team leader, I don't think I care to know.

A huge thank you to the Riddet administration, John, Terri, and Meg for all the work they do, which allows us to focus on research. You're the only reason why my samples even go to Australia for the (actual) last experiment. The other Dr. Golding, Sarah, who was like a mother to us graduate students, tirelessly championing effective science communication and professional development. And, of course, Ansley. The Riddet isn't the same without you.

To the original Bunker Group + Anika. It's been a wild ride. We'll go our separate ways, but I'm sure a part of us will remain in that slightly cramped room that has been repurposed into a sensory lab. To the remaining graduate students left in Ecology, I wish you all the best. You'll make it.

Of the students past and present, Debashree, who showed me around my first day; Zheng, who shared a sample freezer box and gym time with me; Siqi for conducting almost all my initial equipment training; Isuri, the only other postgrad who knew what it was like walking to Fundamental Sciences every day; Taciana, who lent me her buttermilk powder and showed me how to get more. Finally, not graduate students, but Rory, I consider you my lab bench mate, and Stephen Giteru, I consider you my fume hood mate even if you only used the water baths opposite the fume hood.

Lastly, my parents and brother in California for supporting me during my four years in New Zealand. My partner, Sarah, who made sure I was alive to do another day of research and in the writing on the thesis would give me a mug of water before promptly saying, "get back to work, slave."

Table of contents

Abstract ..... **II**
Acknowledgements ..... **III**
Table of contents ..... **V**
List of figures ..... **X**
List of tables ..... **XV**
List of abbreviations ..... **XVI**
List of publications, proposals, and awards ..... **XVIII**
Chapter 1 – Introduction **1**
1.1 General introduction 1
1.2 Objectives of the thesis 2
1.3 Format of the thesis 3
Chapter 2 – Literature review **7**
2.1 Background 7
2.2 The secretion of milk fat globule 8
2.3 The physical characteristics of the milk fat globule and its membrane 9
2.4 Milk fat globule membrane proteins 12
2.5 Milk fat globule membrane polar lipid and putative health benefits 12
2.5.1 Milk polar lipid composition 12
2.5.2 The anticholesteremic effect of milk polar lipids 15
2.6 Milk fat globule membrane architecture 18
2.6.1 Lipid rafts and (L_o) liquid-ordered domains 19
2.6.2 Sphingomyelin and cholesterol complexation to form (L_o) liquid-ordered domains 20
2.6.3 Properties of liquid-ordered domains in the milk fat globule membrane 23
2.7 Physiological response to milk fat globule membrane components 26
2.7.1 Gastric digestion 27
2.7.2 Intestinal digestion 29
2.7.3 Alkaline sphingomyelinase 31
2.8 Techniques for modelling and investigating the milk fat globule membrane 34
2.8.1 Model membrane systems 34
2.8.2 INFOGEST in vitro digestion 37
2.8.3 Dynamic light scattering 39
2.8.4 Zeta potential 40
2.8.5 Confocal laser scanning microscopy 41
2.8.6 Transmission electron microscopy 42
2.8.7 Differential scanning calorimetry 43
2.8.8 Raman spectroscopy 44

2.8.9 X-ray diffraction 47
2.8.10 Atomic force microscopy 49
2.8.11 Nuclear magnetic resonance spectroscopy 50
2.8.12 Electron spin resonance spectroscopy 52
2.9 Conclusions 54
Chapter 3 – Milk sphingomyelin/cholesterol multilamellar vesicles and properties 74
3.1 Introduction 74
3.2 Methods and Materials 75
3.2.1 Phospholipid vesicle systems 75
3.2.2 Physical characteristics of milk sphingomyelin multilamellar vesicles 75
3.2.3 Transmission electron microscopy (TEM) 76
3.2.4 Differential scanning calorimetry (DSC) 76
3.2.5 Raman spectroscopy 76
3.2.6 Synchrotron x-ray scattering 77
3.2.7 Statistical analysis 77
3.3 Results and Discussion 77
3.3.1 Physical properties of milk sphingomyelin and cholesterol multilamellar vesicles 77
3.3.2 Thermotropic behaviour of milk sphingomyelin and cholesterol multilamellar vesicles 81
3.3.3 Intra- and inter-molecular behaviour of milk sphingomyelin bilayers 91
3.4 Conclusions 95
Chapter 4 – Cholesterol-phospholipid interactions resist the detergent effect of bovine bile 100
4.1 Introduction 100
4.2. Materials and methods 102
4.2.1. Sample preparation 102
4.2.1.1 Vesicle preparation 102
4.2.1.2 Particle size 102
4.2.1.3. Bile addition 102
4.2.2 Interactions between vesicles and bovine bile 103
4.2.2.1 Negative stain transmission electron microscopy 103
4.2.2.2 Optical density 103
4.2.2.3 Raman spectroscopy 103
4.2.3. Statistical analysis 104
4.3. Results and discussion 104
4.3.1. Physical characterization of phospholipid vesicles 104
4.3.2. The solubilization and micellization of natural phospholipid and phospholipid/cholesterol vesicles by bovine bile 107
4.3.2.1 Optical density of binary phospholipid/cholesterol vesicles 107

4.3.2.2 Optical density of ternary phospholipid vesicles 111
4.3.2.2 Raman spectroscopy 114
4.3.2.2.1 The effect of cholesterol on phospholipid acyl chain interchain interactions and gauche/trans conformational isomerism 115
4.3.2.2.2 Effect of bile and cholesterol additions on phospholipid acyl chain interchain interactions and gauche/trans conformational isomerism 121
4.3.2.2.3. Bovine bile interactions with the PC ester and MSM amide regions 123
4.4. Conclusions 125
Chapter 5 – Structural analysis of vesicles comprised of milk fat globule membrane phospholipid extracted from bovine beta-serum 132
5.1. Introduction 132
5.2. Materials and methods 133
5.2.1. MFGM phospholipid extraction 133
5.2.2 MFGM phospholipid characterization 134
5.2.3 Vesicle preparation and characterization 134
5.2.4. Bovine bile addition to MFGM phospholipid vesicles 135
5.2.4.1 Transmission electron microscopy 136
5.2.4.2 Optical density 136
5.2.4.3 Raman spectroscopy 136
5.2.4.4 X-ray diffraction 136
5.2.5. Statistical analysis 137
5.3. Results and discussion 137
5.3.1. Polar lipid composition of beta-serum extract 137
5.3.2. Physical and thermotropic properties of MFGM phospholipid vesicles 139
5.3.3. Detergent-induced micellization of MFGM phospholipid vesicles 142
5.3.4. The effect of detergent-induced micellization on the inter- and intra hydrocarbon chain order of MFGM phospholipid 146
5.3.5. Small angle X-ray scattering 153
5.4. Conclusions 155
Chapter 6 – The structural fate of liquid-ordered domains during i*n vitro* digestion of phospholipid/cholesterol vesicles 162
6.1. Introduction 162
6.2. Materials and methods 165
6.2.1 Milk fat globule membrane phospholipid extraction 165
6.2.2 Phospholipid vesicle preparation 166
6.2.3 Gastrointestinal static *in vitro* digestion 166
6.2.4 Negative stain transmission electron microscopy 168
6.2.5 Raman spectroscopy 168
6.2.6 Differential scanning calorimetry 168

6.2.7 Statistical analysis 168
6.3.1 Results and discussion 171
6.3.1. Microstructure of phospholipid/cholesterol vesicles under *in vitro* digestion conditions 171
6.3.2. Bilayer order of phospholipid MLVs after being subjected to *in vitro* digestion 173
6.3.2.1. Bilayer order of milk sphingomyelin and cholesterol vesicles under *in vitro* digestive conditions 176
6.3.2.2. Bilayer order of phosphatidylcholine and cholesterol vesicles under *in vitro* digestive conditions 183
6.3.2.3. Bilayer order of milk fat globule membrane phospholipid extract and cholesterol vesicles under *in vitro* digestive conditions 188
6.3.3. Phase transitions and thermotropic behaviour of milk phospholipids 191
6.3.3.1. Thermotropic behaviour of milk sphingomyelin vesicles before and after in vitro digestion 192
6.3.3.2. Thermotropic behaviour of milk fat globule membrane phospholipid vesicles before and after *in vitro* digestion 197
6.4 Conclusions 200
Chapter 7 – Structural alterations of biliary micelles in the presence of phospholipid/cholesterol vesicles during detergent-induced solubilization by bile salts 208
7.1 Introduction 208
7.2 Materials and methods 210
7.2.1 Milk fat globule membrane phospholipid extraction 210
7.2.2 Phospholipid vesicle preparation for temperature-controlled SR-XRD and detergent-induced vesicle → micelle transition by bovine bile 211
7.2.3 Temperature-controlled SR-SAXS experiments 211
7.2.4 Detergent-induced vesicle → micelle transition by bile salt SR-SAXS experiments 212
7.2.5 SR-SAXS data analysis 213
7.3 Results and discussion 214
7.3.1 Diffuse scattering of milk fat globule membrane and soy phosphatidylcholine vesicles 214
7.3.2. Sphingomyelin and cholesterol multilamellarvesicles retain lamellar structure when heated 214
7.3.3. Sphingomyelin and cholesterol multilamellar vesicles retain lamellarity during detergent-induced micellization by bile salts 219
7.3.4. Increasing cholesterol concentration reduces micellar swelling during detergent-induced solubilization by bile salt 223
7.4. Conclusions 229
Chapter 8 – Key findings and future research directions 237
8.1. Key findings 237
8.1.1. Cholesterol induces structural changes in sphingomyelin multilamellar vesicles at near-physiological concentrations 237

8.1.2. Sphingomyelin and cholesterol multilamellar vesicles resist detergent-induced solubilization by bovine bile 238
8.1.3. Milk fat globule membrane phospholipid vesicles are susceptible to detergent-induced solubilization by bovine bile 242
8.1.4. Bile and pancreatin solubilize the detergent-resistant L_o phase 244
8.1.5. Milk sphingomyelin and cholesterol multilamellar vesicles retain lamellar structure in the presence of bovine bile 246
8.1.6 Novelty of the research conducted 249
8.2. Further research 250
8.2.1 The function of liquid ordered domains on the milk fat globule membrane 250
8.2.2 Additional considerations for investigating the *in vitro* digestion of milk fat globule membrane phospholipids 253
8.3 Closing remarks 254
Appendix 261
Appendix: Chapter 3 261
Appendix: Chapter 4 262
Appendix: Chapter 5 277
Appendix: Chapter 6 286
Appendix: Chapter 7 304

List of figures

Chapter 2 – Literature Review

Figure 2.1. Summary of MFG secretion 8

Figure 2.2. Structures of common polar lipids within the milk fat globule membrane 13

Figure 2.3. Updated model of the milk fat globule membrane as a heterogenous patchwork of polar lipids..... 18

Figure 2.4. Confocal laser scanning micrograph of milk fat globules from raw cream stained with rhodamine dioleoyl-*sn*-glycero-3-phosphoethanolamine (Rd-DOPE) 24

Figure 2.5. Current model of *in vitro* gastrointestinal milk fat globule membrane (MFGM) digestion 27

Figure 2.6. Confocal laser scanning microscopy (CLSM) of whole milk after *in vitro* gastric digestion.. 29

Figure 2.7. Digestion of dietary sphingomyelin (SM) 34

Figure 2.8. Two-dimensional schematic representation of how Rd-DOPE (denoted in the original figure as Rh-PE) partitions into the L_d phase of a phospholipid trilayer. 42

Figure 2.9. Raman spectra of various phospholipids in powered form..... 46

Figure 2.10. Bragg's Law (reproduced from the Science Education Resource Center at Carleton College); d, spacing between crystal layer; λ = wavelength, θ = angle between the incident and plane. 48

Figure 2.11. Self-assembled lyotropic liquid crystalline structures from lipase-catalysed digestion of bovine milk with and without bile salts 49

Figure 2.12. ^{2}H NMR spectra of PSM-31d and DPPC-31d MLVs, respectively 52

Figure 2.13 Schematic of possible MFGM interaction with bile salts and pancreatic lipase observed using ESR. 53

Chapter 3 - Milk sphingomyelin/cholesterol multilamellar vesicles and properties

Figure 3.1. Particle size distribution of milk sphingomyelin multilamellar vesicles 78

Figure 3.2. Milk sphingomyelin multilamellar vesicles (a-d), native milk fat globules (e)..... 79

Figure 3.3. Zeta potential of milk sphingomyelin multilamellar vesicles comprised of varying amounts of cholesterol..... 80

Figure 3.4. Differential scanning calorimetry thermotropic profile of milk sphingomyelin vesicles of varying concentrations. 81

Figure 3.5. Differential scanning calorimetry plot of milk sphingomyelin (MSM) vesicles with varying concentrations of cholesterol 83

Figure 3.6. SAXS of milk sphingomyelin concentration gradient 84

Figure 3.7. Schematic of $L_{\beta 1}$ to $L_{\beta 2}$ phase transition in milk sphingomyelin. 86

Figure 3.8. SAXS of milk sphingomyelin vesicles without cholesterol as a function of temperature. 88

Figure 3.9. SAXS of milk sphingomyelin (MSM) multilamellar vesicles (MLVs) with varying concentrations of cholesterol 89

Figure 3.10. WAXS d-spacing of milk sphingomyelin (MSM) multilamellar vesicles (MLVs) with varying concentrations of cholesterol during heating 90

Figure 3.11. Raman spectra of milk sphingomyelin vesicles without cholesterol labelled with the regions of interest and their assignments 91

Figure 3.12. Raman spectra of milk sphingomyelin (MSM) multilamellar vesicles (MLVs) with varying concentrations of cholesterol 94

Chapter 4 - Cholesterol-phospholipid interactions resist the detergent effect of bovine bile

Figure 4.1. Negative stain transmission electron micrographs of milk sphingomyelin (MSM) vesicles 105

Figure 4.2. Negative stain transmission electron micrographs, brain phosphatidylcholine (BPC).... 106

Figure 4.3. Optical density 630 nm of milk sphingomyelin (MSM) multilamellar vesicles incubated with taurocholic acid (5 mM) for 2 h at 37 °C with control (PIPES buffer with bovine bile) subtracted.. 107

Figure 4.4. Optical density at 630 nm of phospholipid vesicles incubated with bovine bile (10 mM) for 2 h at 37 °C with control (PIPES buffer with bovine bile) subtracted 109

Figure. 4.5. Optical density measurements at 405 nm of the detergent-induced micellization of phospholipid vesicles for 2 h and at 37 °C..... 113

Figure 4.6. Optical density measurements of the detergent induced micellization of milk sphingomyelin (MSM, % mol variable), soy phosphatidylcholine (SPC, % mol variable), and cholesterol vesicles for 2 h and at 37 °C where cholesterol is constant (27% mol). 114

Figure 4.7. Raman spectra of milk sphingomyelin (MSM) vesicles with no cholesterol (MSM100) and 3:2 mol:mol MSM:cholesterol (MSM60). 117

Figure 4.8. Lateral interchain packing (I_{2850}/I_{2880}) of phospholipid/cholesterol vesicles. 118

Figure 4.9. Lateral interchain plus the degree of intrachain packing (I_{2930}/I_{2880}) of phospholipid/cholesterol vesicles.. 119

Figure 4.10. Intrachain rotational conformation (I_{1085}/I_{1130}) of phospholipid/cholesterol vesicles.... 120

Figure 4.11. Raman spectra of the MSM vesicle amide region (1600 – 1700 cm^{-1})..... 124

Chapter 5 - Structural analysis of phosopholipid vesicles comprised of milk fat globule membrane phospholipid extracted from bovine beta-serum

Figure 5.1. Chromatograms of MFGM phospholipid extracts.. 139

Figure 5.2. Size and thermotropic behaviour properties of phospholipid vesicles created from milk fat globule membrane phospholipids derived from beta-serum (MFGM) 141

Figure 5.3. Transmission electron micrographs of phospholipid vesicles made from milk fat globule membrane (MFGM) phospholipids extracted from beta-serum powder. 142

Figure 5.4. Transmission electron microscopy of milk fat globule membrane (MFGM) phospholipid vesicles after incubation with bovine bile 144

Figure 5.5. The kinetics of detergent-induced micellization of milk fat globule membrane (MFGM) phospholipid vesicles by optical density 145

Figure 5.6. Raman spectra of MFGM100 and MFGM60 vesicles 149

Figure 5.7. Raman spectrum of MFGM100 and MFGM60 vesicles after bile addition 150

Figure 5.8. Raman peak intensity ratios for hydrocarbon inter and intrachain order of milk fat globule phospholipid vesicles with varying concentrations of cholesterol before (MFGM) and after (MFGMB) bovine bile addition 152

Figure 5.9. Small angle x-ray scattering profiles of milk fat globule membrane (MFGM) vesicles. 154

Chapter 6 - The structural fate of liquid-ordered domains during *in vitro* digestion of phospholipid/cholesterol vesicles

Figure 6.1. Experimental design for static *in vitro* digestion of phospholipid vesicles 170

Figure 6.2. The addition of rabbit gastric extract to phospholipid/cholesterol vesicles 172

Figure 6.3. Phospholipid vesicles post-gastric and intestinal *in vitro* digestion 174

Figure 6.4 The morphology of micellar intermediates from perforated vesicles and open bilayers.. 175

Figure. 6.5. Marginal means of the overall peak intensity ratios of milk sphingomyelin vesicles (i.e., no alk-SMase and with alk-SMase results have been pooled together) 179

Figure 6.6. Milk sphingomyelin and cholesterol multilamellar vesicles have been divided into two independent experiments. Pre-digestion, gastric, and intestinal digestion with alk-SMase and without.

pd = pre-digestion, gs = gastric phase, ma = intestinal phase, n = no alk-SMase, y= alk-SMase. Each point represents one replicate..... 182

Figure 6.7. Marginal means of the overall peak intensity ratios of brain phosphatidylcholine vesicles. 184

Figure 6.8. Marginal means of the overall peak intensity ratios of soy phosphatidylcholine vesicles. 185

Figure 6.9. Difference in I_{2850}/I_{2880} (No SMase - SMase) for intestinal soy phosphatidylcholine vesicles. 187

Figure 6.10. Marginal means of the overall peak intensity ratios of milk fat globule membrane phospholipid vesicles. 189

Figure 6.12. Thermotropic behaviour of milk sphingomyelin (MSM) multilamellar vesicles during *in vitro* digestion. 193

Figure 6.13. Structural model of D-*erythro*-sphingomyelin molecule..... 194

Figure. 6.14. Thermotropic behaviour of milk sphingomyelin (MSM) multilamellar vesicles (MLVs) during *in vitro* intestinal digestion 196

Figure. 6.15. Thermotropic behaviour of milk fat globule membrane (MFGM) phospholipid vesicles during *in vitro* digestion..... 198

Figure. 6.16. Thermotropic behaviour of milk fat globule membrane (MFGM) phospholipid vesicles post-intestinal *in vitro* digestion..... 199

Chapter 7 - Structural alterations of biliary micelles in the presence of phospholipid/cholesterol vesicles during detergent-induced solubilization by bile salts

Figure 7.1. Diffuse scattering of a) soy phosphatidylcholine vesicles and b) milk fat globule membrane phospholipid vesicle..... 215

Figure 7.2. Small angle x-ray scattering of milk sphingomyelin and cholesterol multilamellar vesicles. 216

Figure 7.3. Small angle x-ray scattering of egg sphingomyelin and cholesterol multilamellar vesicles. 218

Figure. 7.4. Small angle x-ray scattering of PIPES buffer after bile addition on a log-log scale 219

Figure. 7.5. Small angle x-ray scattering of milk sphingomyelin phospholipid vesicles on a log-log scale 221

Figure 7.6. Small angle x-ray scattering of 4:1 egg sphingomyelin/cholesterol.. 223

Figure 7.7. The radius of gyration (R_g) of phospholipid vesicles during incubation with bovine bile. 226

Chapter 8 - Key findings and future research directions

Figure 8.1. Schematic of the proposed solubilization behaviour of MSM multilamellar vesicles (MLV) at 37 °C 240

Figure 8.2. Schematic of the proposed solubilization behaviour of BPC and SPC vesicles at 37 °C. 242

Figure 8.3. Schematic of hypothesized gastric lipase interactions with bilayers and the resulting effect on bilayer order 245

Figure 8.4. Schematic for the solubilization of milk fat globule membrane (MFGM) phospholipid vesicles by bile salts 249

List of tables

Table 2.1. General milk fat globule membrane composition. 10

Table 2.2. Relative proportion of each class of polar lipids in the bovine milk fat globule membrane based on fat globule size.. 11

Table 2.3. Polar lipid composition in bovine milk fat globule membrane. 13

Table 2.4. Reported health benefits from polar lipids in the milk fat globule membrane.. 14

Table 2.5. Raman active bands and their assignments for PC, PE, SM. 47

Table 3.1 Raman active modes for milk sphingomyelin.. 92

Table 4.1. Reference Raman band assignments for phospholipid vesicles. 115

Table 5.1. Polar lipid concentration of MLVs created from recombined MFGM phospholipid extract. 135

Table 5.2. Relative proportion of polar lipids found in beta-serum powder. 138

Table 5.3 Raman assignments, reference modes and Raman active bands for MFGM phospholipid vesicles before and after bovine bile addition. 147

Table 6.1. Phospholipid and cholesterol concentrations used for MFGM phospholipid vesicles..... 166

Table 7.1. Phospholipid and cholesterol concentrations used for MFGM phospholipid vesicles..... 211

List of abbreviations

Materials and reagents

alk-SMase = Alkaline sphingomyelinase

BPC = Porcine brain phosphatidylcholine

BSP2 = Beta serum powder from TATUA Co-operative Dairy Company

ESM = Egg sphingomyelin

MFG = Milk fat globule

MFGM = Milk fat globule membrane

MSM = Milk sphingomyelin

PC = Phosphatidylcholine

PE = Phosphatidylethanolamine

PI = Phosphatidylinositol

PIPES = Piperazine-N,N'-bis(2-ethanesulfonic acid)

PS = Phosphatidylserine

Rd-DOPE = Dioleoyl-sn-glycero-3-phosphoethanolamine head-labelled fluorescent rhodamine

RGE = Rabbit gastric extract

RGL = Rabbit gastric lipase

SGF = Simulated gastric fluid

SIF = Simulated intestinal fluid

SSF = Simulated salivary fluid

SM = Sphingomyelin

SPC = Soy phosphatidylcholine

Instruments

CLSM = Confocal laser scanning microscopy

DLS = Dynamic light scattering

DSC = Differential scanning calorimetry

ESR = Electron spin resonance (also known as electron paramagnetic resonance)

OD = Optical density

SR–SAXS = Synchrotron radiation small-angle x-ray scattering

SR–WAXS = Synchrotron radiation wide-angle x-ray scattering

TEM = Transmission electron microscopy

Types of liposomes/vesicles

MLV = Multilamellar vesicle

SUV = Small unilamellar vesicle

LUV = Large unilamellar vesicle

GUV = Giant unilamellar vesicle

Sample label key

Bile salt experiments:

BPC70 = Porcine brain phosphatidylcholine vesicles with 7/3 mol/mol BPC/cholesterol

BPC70B = Porcine brain phosphatidylcholine vesicles with 7/3 mol/mol BPC/cholesterol incubated with bovine bile at 37 °C for 2 h (endpoint of incubation)

BPC70B0.3 = Porcine brain phosphatidylcholine vesicles with 7/3 mol/mol BPC/cholesterol incubated with bovine bile at 37 °C for 20 s

In vitro digestion experiments:

BPC70 = Porcine brain phosphatidylcholine vesicles with 7/3 mol/mol BPC/cholesterol before being submitted to digestion

GBPC70 = Porcine brain phosphatidylcholine vesicles with 7/3 mol/mol BPC/cholesterol after being submitted to the gastric stage and the gastric enzymes have been inactivated

IaBPC70 = Porcine brain phosphatidylcholine vesicles with 7/3 mol/mol BPC/cholesterol after being submitted to the intestinal stage with alkaline sphingomyelinase and the intestinal enzymes have been inactivated

InBPC70 = Porcine brain phosphatidylcholine vesicles with 7/3 mol/mol BPC/cholesterol after being submitted to the intestinal stage without alkaline sphingomyelinase and the intestinal enzymes have been inactivated

Other

d-spacing = The distance between planes of atoms that give rise to diffraction peaks

HDL = High density lipoprotein

L_d = Liquid-disordered phase ($> T_m$)

LDL = Low density lipoprotein

L_o = Liquid-ordered phase

S_o = Solid-ordered phase ($< T_m$), does not distinguish between the various polymorphs that arise from interdigitation

TAG = Triacylglyceride

T_m = Melting temperature

List of publications, proposals, and awards

Publications

- Tai, P., Golding, M., Singh, H., Waterland, M., & Everett, D. W. (2021). Cholesterol-phospholipid interactions resist the detergent effect of bovine bile. *Colloids and Surfaces B: Biointerfaces, 205*, 111842. https://doi.org/10.1016/j.colsurfb.2021.111842
- Tai, P., Golding, M., Singh, H., & Everett, D. (2022). The bovine milk fat globule membrane – Liquid ordered domain formation and anticholesteremic effects during digestion. *Food Reviews International*, 1–27 (Ahead of publication). https://doi.org/10.1080/87559129.2021.2015773

Awards

Third Place, 3-Minute Thesis Competition, American Dairy Science Association Conference, 2022

Second Place, 3-Minute Pitch Competition, New Zealand Institute of Food Technologists Conference, 2021

Third Place, Student Presentation, Riddet Institute Student Colloquium, 2021

Third Place, 3-Minute Pitch Competition, New Zealand Institute of Food Technologists Conference, 2019

Proposals

Tai P., Clulow A., Boyd B., Everett D. (PI), Liquid-ordered phases in milk fat globule membrane and its role in digestion, Australian Synchrotron, 2021

Conference Proceedings

Tai P., Clulow, A., Everett, D., Golding M., Singh H., The *in vitro* digestion of milk sphingomyelin and cholesterol model membranes, American Dairy Science Association; Kansas City, USA. (Oral)

Tai P., Digesting rafts: Milk fat globule membrane microstructure's influence on lipid digestion, AgResearch/Riddet Dairy Industry Workshop; Palmerston North, NZ. 2021 (Oral)

Tai P., Everett, D., Golding M., Singh H., Milk fat globule membrane: The structural complexity of sphingomyelin, World Congress on Oils and Fats; Sydney, AUS. 2020. (Oral)

Tai P., Singh H., Everett, D., Milk sphingomyelin interactions with cholesterol in binary mixtures. NZIFST Conference; Christchurch, NZ. 2019. (Poster)

Chapter 1 – Introduction

1.1 General introduction

Milk is a biologically secreted oil-in-water emulsion that has been consumed throughout human history. Capitalizing on to the rich protein and lipid content, the food industry has processed milk to create high value dairy products such as cheese, yogurt, and butter which can have a considerable a cholesterol content. The cholesterol in dairy products have been historically demonized in the mainstream media as a cause of metabolic disease (Taubes Gary, 2001). The 2015 – 2020 US Dietary Guidelines removed the limit restricting dietary cholesterol that was previously set at 300 mg/day (Carson et al., 2020). This recommendation was the culmination of decades of clinical research indicating elevated serum cholesterol could not be solely linked to the intake of dietary cholesterol. Hidden within the guideline revocation are profundities that question the nature of how we study food.

Food rich in cholesterol that are also rich in phospholipids such as eggs and buttermilk have been known to modulate or even reduce serum cholesterol, a leading risk factor for heart disease. There are currently two treatments for reducing serum cholesterol, reducing endogenous cholesterol synthesis, and reducing dietary cholesterol absorption which in turn reduces biliary cholesterol reabsorption (Howles, 2016). The mechanism of action for foods rich in phospholipids is presumed to be the latter – the phospholipids are somehow capable of reducing intestinal cholesterol absorption.

In milk, the phospholipids are part of a complex microstructure known as the milk fat globule membrane (MFGM), which in turn is a component of a macrostructure, the fat globule. Food structure is an increasing consideration in the nutritional field, particularly dairy nutrition. A prime example is the ability of liquid milk to form a curd in the stomach due to the low pH conditions, delaying gastric emptying. As per this example, the health benefits that the macrostructure (clot) provide requires a specific microstructure (partially hydrolysed kappa-casein aggregated protein network entrapping coalesced fat globules). Conversely the opposite may also be true in milk, a secretion bioengineered for neonatal consumption. The architecture of a specific macrostructure (fat globule) may be the result of nutritional requirements that a microstructure (milk fat globule membrane) provides. Investigating the possible relationship between putative health benefits, microstructure, and the resulting macrostructure in dairy products is a novel area ripe for rigorous studies.

The MFGM, an interface that encases energy-dense triacylglycerides, separating them from the bulk serum phase, is one such intersection of nutrition, macrostructure, and complex microstructure. A multitude of clinical studies have shown that although the MFGM is rich in cholesterol, a cholesterol modulating effect can be observed when participants consume products rich in MFGM, such as buttermilk. The phospholipids and proteins that comprise the trilayer membrane (one outer bilayer and one inner monolayer) have been noted for other putative nutritional benefit as well. The question arises as to whether the structural components of the MFGM serve only a structural function and the nutrition benefits are the result of mere composition, or whether there are synergies between the function and structure of this phospholipid-protein interface. One manifestation of hypothetical synergy could be structural heterogeneities predominately laterally clustered on the outer leaflet known as liquid ordered (L_o) domains, assemblies of sphingomyelin (SM) and cholesterol. The main research question of the thesis is whether L_o domains are purely a structural feature of the MFGM or whether it has some effect on digestion. The unique characteristics and formation of L_o domains will be explained in more detail within the literature review.

Using the milk fat globule membrane as a focus of study, the role of microstructure on physical macrostructure will be assessed to better understand the structural interactions and biochemical interplay of lipids during gastrointestinal digestion.

1.2 Objectives of the thesis

The composition and lateral structure of the native MFGM has been regularly updated in the scientific literature, and while not exhaustively understood, some foundational knowledge exists. There is a dearth of information regarding how the structure of the membrane changes when gastro-intestinal components such as gastric lipase, bile, and alkaline sphingomyelinase are sequentially applied during digestion.

The assumption that underpins this research is that structural changes which may occur within the MFGM during digestion are observable and measurable. If this is the case, these structural changes that influence the digestion of membrane components can be quantified. It is well understood that cholesterol and sphingomyelin are absorbed through the intestine and therefore sphingomyelin–cholesterol complexation does not prevent digestion. The current literature suggests that the complexation of these two lipids is capable of reducing cholesterol absorption, yet does not present a comprehensive mechanism of action.

In short, this thesis will aim to understand the digestion of milk fat globule membrane with a focus on the formation, properties, and gastro-intestinal digestion of L_o regions created from phospholipid and cholesterol derived from biological sources. This structural peculiarity that will be described in detail in the next chapter may link MFGM morphology with its putative nutritional effects.

The objectives for each research chapter are as follows:

1) Confirm the presence of L_o domains when cholesterol is incorporated into milk sphingomyelin (MSM) bilayers. Assess the structural changes that occurs from such an interaction.
2) Compare cholesterol interactions with MSM and other naturally occurring phospholipids (derived from porcine brain and soy) to determine whether the structural changes that potentially occur in MFGM systems are exceptional.
3) Determine whether the MSM model membrane system is applicable to a more complex phospholipid system featuring recombined MFGM phospholipids.
4) Investigate how the structures of these model membrane systems changed under digestive conditions, refining the current model of MFGM digestion to include L_o domains.

The final objectives of the thesis are as follows:

1) Update the current model of milk fat globule digestion to include the ultimate fate of L_o domains.
2) Determine whether Lo structures persist during gastro-intestinal digestion and conversely whether gastro-intestinal components are capable of altering the domains structure.
3) Generate a greater understanding of the role of L_o domains in the digestion of the MFGM and milk fat globules.
4) Identify a direction for further study on the digestive impact of L_o domains.

1.3 Format of the thesis

Chapter 2 is a critical assessment of the literature. The secretion of MFGM is described, followed by a discussion of the physical characteristics, elaboration of the chemical components of the membrane and the structural interactions, cataloguing pre-clinical, animal, and clinical studies that investigate the nutritional benefits of consuming MFGM, assessing the current model of MFGM digestion, and finally an exploration of the techniques and

instruments commonly used to investigate phospholipid membranes. The literature review concludes with identifying areas where further consideration are necessary and what learnings are to be applied to the thesis.

Chapter 3 (*research question 1*) consists of the preliminary experiments that explored the various techniques and instruments that can be employed to investigate phospholipid membranes. This chapter also seeks to confirm the interaction between sphingomyelin and cholesterol to determine which experiments would be feasible.

Chapter 4 (*research question 2*), the first part of the main work, compares the phospholipid/cholesterol interactions of different species of phospholipids derived from natural sources and then tests the resistance to rehydrated bile as a proxy for L_o domain forming capacity.

Chapter 5 (*research question 3*) takes the findings from Chapter 4 and asks whether they hold up with a complex blend of phospholipids formed from a recombined MFGM phospholipid extract. This extract was initially characterized and the structural changes that occur when bile is added to model membranes was investigated.

Chapter 6 (*research question 4*) is the culmination of the work, all model membrane systems underwent the INFOGEST static *in-vitro* digestion protocol, and structural changes to the membranes were measured.

Chapter 7 (*research questions 2 and 3*) includes a deeper investigation of detergent phospholipid interactions using synchrotron radiation small angle x-ray scattering. The experiment sought to confirm some of the hypothesis made in Chapter 4 and 5 and to promote the application of x-ray scattering as an invaluable tool for digestion work.

Chapter 8 synthesizes all previous chapters to arrive at tentative conclusions regarding MFGM digestion. A direction for future work is described and promising techniques that are in development are discussed.

The thesis and the core concepts of each chapter are below:

Chapter 1 – Introduction

Chapter 2 – Literature review

Chapter 3 - Milk sphingomyelin/cholesterol multilamellar vesicles and properties: a preliminary study

- Characterization of phospholipid model membrane system (particle size, zeta potential, morphology)
- The thermotropic behaviour of the model membrane system

Chapter 4 - Cholesterol-phospholipid interactions resist the detergent effect of bovine bile

- Interactions between physiological bile and phospholipids derived from natural sources
- Solubilization and micellization of phospholipid model membranes at different phase states

Chapter 5 - Structural analysis of vesicles comprised of milk fat globule membrane phospholipid extracted from bovine beta-serum

- Extraction and characterization of milk fat globule membrane phospholipids from beta-serum
- Interactions between physiological bile and milk fat globule membrane phospholipids

Chapter 6 - The structural fate of liquid-ordered domains during *in vitro* digestion of phospholipid/cholesterol vesicles

- Gastric digestion of phospholipid model membranes
- Intestinal digestion of phospholipid model membranes
- Analysis of the changes in bilayer order during *in vitro* gastrointestinal digestion

Chapter 7 - Determination of detergent-induced phase transitions and structural alterations of phospholipid/cholesterol vesicles

- Structural examination of naturally derived phospholipids and the thermotropic behaviour
- Micellar intermediates that form during the detergent-induced solubilization and micellization of phospholipid model membranes by bovine bile

Chapter 8 – Key findings and future research directions

References

Carson, J. A. S., Lichtenstein, A. H., Anderson, C. A. M., Appel, L. J., Kris-Etherton, P. M., Meyer, K. A., Petersen, K., Polonsky, T., Van Horn, L., & On behalf of the American Heart Association Nutrition Committee of the Council on Lifestyle and Cardiometabolic Health; Council on Arteriosclerosis, Thrombosis and Vascular Biology; Council on Cardiovascular and Stroke Nursing; Council on Clinical Cardiology; Council on Peripheral Vascular Disease; and Stroke Council. (2020). Dietary Cholesterol and Cardiovascular Risk: A science advisory from the American heart association. *Circulation*, *141*(3).

Howles, P.N. (2016). Cholesterol Absorption and Metabolism. In: Proetzel, G., Wiles, M. (eds) *Mouse Models for Drug Discovery. Methods in Molecular Biology*, vol 1438. Humana Press, New York, NY.

Taubes Gary. (2001). The Soft Science of Dietary Fat. *Science*, *291*(5513), 2536–2545.

Chapter 2 – Literature review

The bovine milk fat globule membrane – liquid ordered domain formation, anticholesteremic effects during digestion, current techniques and their applications

2.1 Background

The bovine milk fat globule membrane (MFGM) is a complex assembly of polar lipids, cholesterol, and proteins that envelope a triacylglyceride (TAG) core. With a unique composition and structure, this interface is intricately involved in milk lipid digestion and metabolism. The MFGM is best known for aiding neonates in brain and gut development (Gallier et al., 2015). Isolated MFGM components (in particular, phospholipids) are now widely part of the fortification effort for infant formula. In adults, the regular consumption of MFGM has been clinically shown to modulate serum cholesterol (Conway, Gauthier, & Pouliot., 2013) and is therefore a possible alternative to ingredients such as plant sterols in cholesterol-lowering foods. Despite clinical evidence, research to elucidate the mechanisms behind the anticholesteremic effect of the MFGM remain unexplored. Research in this direction may clarify and strengthen both awareness and confidence in the functionality of MFGM components for human health in both the scientific community and with consumers.

Recently, there has been a concerted effort in the field of food science and nutrition to look beyond a simple reductionist approach when assigning nutritional functions to food components, and to instead examine the synergies that food structures and their component interactions may engender, as well as the resultant digestive behaviour (Somaratne et al., 2020). The MFGM, with a complex array of proteins and polar lipids, heterogenous structure, and multitude of ascribed physiological effects, is a relevant and important candidate for such an evaluation.

Identifying research gaps between the interplay of MFGM composition, structure, digestive behaviour, and observed health outcomes is foundational to understanding the nuances behind MFGM functionality. Consequently, the objective of this review is to critically examine the recent work on the MFGM structure within the context of digestion to identify potential mechanisms for its anticholesteremic effect. This review begins with an overview of milk secretion as it relates to the unique composition of MFGM polar lipids before focusing on a discussion of:

- The proteins and polar lipids that comprise the MFGM with a focus on preclinical, animal, and human clinical studies that evaluate the anticholesteremic potential.

This chapter is an update of a review article published in Food Reviews International (2022)

- The current model of the MFGM, in particular, the structural implications of liquid ordered (L_o) domains.
- The roles of alkaline sphingomyelinase (alk-SMase) also known as ectonucleotide pyrophosphatase/phosphodiesterase family member 7 (E-NPP7), and cholesterol in MFGM gastrointestinal lipid digestion.
- The methodologies and techniques commonly used to investigate model membrane systems, including a critical examination of the state-of-the-art structural data that can be potentially obtained from model membrane or dairy systems.

This review concludes with a summary of the gaps in the literature and determines the direction and foci of the thesis.

2.2 The secretion of milk fat globule

Heid and Keenan (2005) provide a detailed review of milk fat globule (MFG) secretion and the formation of the MFGM (Fig. 2.1) which underpins our understanding of this phenomenon. Literature that updates this model have been recently quite exhaustively reviewed (Thum et al., 2021).

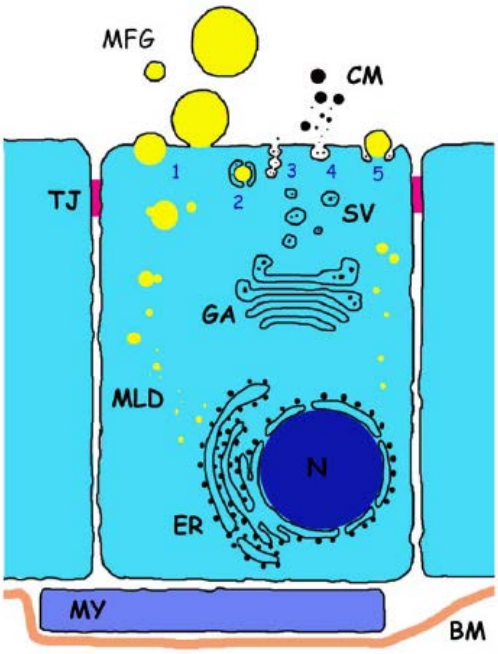

Figure 2.1. Summary of MFG secretion. 1) Secretion by envelopment and "pinching off" the apical membrane. 2) Fusion of secretory vesicles and fat droplets. 3) Secretion of serum (non-fat) components by compound exocytosis. 4) Secretion of serum (non-fat) components. 5) Unknown mechanism for the direct secretion of MLDs. TJ = tight junction; CM = casein micelle; GA = Golgi apparatus; SV = secretory vesicle; MLD = microlipid droplet; N = nucleus; ER = endoplasmic reticulum; MY = myoepithelial cell; BM = basement membrane (Heid & Keenan, 2005).

The precursor of MFGs, microlipid droplets (MLD), are produced in the endoplasmic reticulum (ER) of lactocytes within the mammary gland. When finally released into the

cytosol, the MLD takes the outer membrane of the ER (Mather, 2011). There is strong proteomic evidence this becomes the innermost layer of the MFGM (Wu et al., 2000). Possible site specificity for the nucleation and growth of the MLD in the ER, as well as how this process is regulated, is currently being explored (Ben M'barek et al., 2017).

After an MLD is formed, it follows super diffusive behaviour (moving via predetermined pathways) through the cytoplasm, fusing with other droplets until it reaches the apical membrane (Masedunskas et al., 2017). When the droplet makes contact with the apical plasma membrane bilayer, butyrophilin (BTN), a major MFGM protein, forms a transient, pH-dependent oligomeric complex with xanthine oxidase (XO) that is essential for secretion (Jeong et al., 2013; Monks et al., 2016). As the lipid droplet grows, it pushes against the apical membrane, incorporating apical components such as the glycoprotein mucin 1 (MUC1), and sphingolipids such as sphingomyelin (SM). Finally, the droplet is liberated from the apical membrane through an oxytocin mediated G-protein coupled reaction which releases Ca^{2+}, causing a contraction in the epithelial cell, sealing or "pinching off" the milk fat droplet (Gimpl & Fahrenholz, 2001; Masedunskas et al.,2017).

The concurrent secretion of casein replenishes the depleting apical membrane allowing for the continuous secretion of MFGs. These secretory vesicles originate from the Golgi apparatus. As such, proteins associated with the Golgi, like BTN, have been found in the MFGM (Wooding & Sargeant, 2015; Honvo-Houéto et al., 2016). An alternative mechanism proposes that MLDs become progressively entrapped within secretory vesicles at the apical cytoplasm, leading to the formation of intracytoplasmic vacuoles that contain both caseins as well as MLDs. These vacuoles would then be released from the apical membrane via exocytosis (Wooding, 1971). Although this hypothesis may account for the protein composition of the MFGM, it fails to express why cellular apical components such as SM are present in MFGM.

Wooding & Mather (2017) recently claimed those domains were holes in the membrane due to post-secretory reorganization based on immunological evidence and claimed domains visible with CLSM were due to a lack in unit membrane. The latter has been shown to be inaccurate, but the paper mentioned demonstrates the structure of the membrane is still under consideration.

2.3 The physical characteristics of the milk fat globule and its membrane

The resulting MFG is comprised of a TAG core encapsulated within three membrane layers, an innermost monolayer, and an outer bilayer. This trilayer envelope is known as the MFGM, a 10 – 50 nm thick membrane (Lopez, Cauthy & Guyomarc'h, 2018) containing phospholipids, sphingolipids, and proteins. Phospholipids and proteins account for over 95% of the dry weight

of the membrane (Table 2.1) (Walstra, Wouters, Geurts, 2006). However, it should be noted that the isolation method can greatly alter the amount and ratios of phospholipids and proteins (Gallier et al., 2010 a).

Table 2.1. General milk fat globule membrane composition. Adapted with permission from Walstra, Wouters, Geurts, (2006)

Component	mg per 100 g fat globules	Percentage of membrane material (db)
Protein	1800	70
Phospholipids	650	25
Cerebrosides	80	3
Cholesterol	40	2
Monoglycerides	traces	n.d.
Water	traces	n.d.
Carotenoids + Vit. A	0.04	n.d.
Fe	0.3	n.d.
Cu	0.01	n.d.

db = dry basis; n.d. = not determined.

Bovine milk fat globules with a diameter smaller than 1 µm are estimated to represent 80% of the MFGs, yet only make up 5% of the volume of milk lipid. Globules that are 1-8 µm make up 94% of lipid in the milk whereas the remaining lipid content is made up of MFGs greater than 8 µm (Huppertz & Kelly, 2006). When comparing MFG size amongst bovine milk, seasonality, feed nutrition, and breed can induce differences (Wiking et al., 2004; Carroll et al., 2006; Couvreur et al., 2007; Barłowska et al., 2009).

Fat globule size in bovine milk is negatively correlated with total content of polar lipids (Table 2.2) with membrane material emphasized to be the limiting factor (Wiking et al., 2004). How fat globule size affects the ratios of specific polar lipids is still unknown as the results of the few studies available are conflicting. Lopez et al. (2011 a) used microfiltration to separate bulk milk into a two separate fractions. The small MFG fraction (~1.6 µm) had a higher proportion of phosphatidylethanolamine (PE) and phosphatidylserine (PS), but a lower proportion of phosphatidylinositol (PI) and phosphatidylcholine (PC) when compared to the large MFG fraction (~6.5 µm). The relative proportions of SM and PS were outside the range of the small and large values. The authors suggest the differences in polar lipid composition is due to small MFGs having higher curvatures and therefore a higher amount of polar lipid desorption during secretion. Another theory is the formation of small, microsome-like particles that subsequently dislodge from the fat globule in a process known as vesiculation (Evers, 2004). PC, concentrated in the outmost layer of the MFGM, would be a likely target of this process in small MFGs.

Table 2.2. Relative proportion of each class of polar lipids in the bovine milk fat globule membrane based on fat globule size. Adapted with permission from Lopez et al., (2011 a).

Polar lipids	Relative proportion of polar lipids (%)	
	Small MFGM fraction (~1.6 μm)	Large MFG fraction (~6.5 μm)
PC	22.4 ± 1.4 a	26.7 ± 0.8 b
PE	25.5 ± 3.8 b	20.1 ± 0.7 a
PI	9.8 ± 0.7 a	12.7 ± 0.5 b
PS	19.7 ± 1.8 b	17.9 ± 0.5 a
SM	22.6 ± 1.2 b	22.6 ± 0.9 b

PC = phosphatidylcholine; PE = phosphatidylethanolamine; PI = phosphatidylinositol; PS = phosphatidylserine; SM = sphingomyelin; MFG = milk fat globule. Different letters across rows designate significant differences ($p < 0.05$).

In a study by Lu et al. (2016), two fractions of milk fat globules were isolated by centrifugation. The small MFG fraction ($d_{4,3}$ = 3.32 ± 1.21 μm, $d_{3,2}$ =2.93 ± 1.06 μm) had a higher weight percentage of PE, but a lower percentage of PI compared to the large MFG fraction ($d_{4,3}$ = 7.61 ± 0.90 μm, $d_{3,2}$ = 4.31 ± 0.17 μm). When determining natural variation in a herd of Holstein-Friesian cows, Logan et al. (2014) reported proportionally higher percentages of PC (29.8 ± 1.3% vs. 26.5 ± 0.9%) in the fat globules of cows that consistently produced smaller fat globules (mean 3.6 ± 0.2 μm) compared to those that produced larger fat globules (mean 4.6 ± 0.3 μm). Such inconsistent results can be in part explained by different isolation and quantification methodologies used, though lactation stage has shown to significantly alter phospholipid composition even when fat globule size has been taken into account (Mesilati-Stahy & Argov-Argaman, 2014).

Ensuring that a biological emulsion remains stable may not be the only factor driving MFGM phospholipid composition. The composition may be critical in meeting a nutritional requirement. Lactation stage influences MFG polar lipid:triacylglyceride, a proxy for changes in MFG size (Bitman & Wood, 1990). Larger MFGs are known to contain higher concentrations of host defence proteins (antimicrobial peptides/proteins) in the form of cathelicidins. Their affinity for larger MFG and selective accumulation in the MFGM requires further investigation (Lu et al., 2016). An addition of phenolic compounds from *Pistacia lentiscus* to reduce the oxidative stress of bovine mammary epithelial cells leads to the production of larger milk fat globules (20% increase in size) compared to the control; however, phospholipid composition remains constant (Hadaya et al., 2020). Therefore, mammary cells with reduced oxidative stress tend to secrete larger milk fat globules which may have greater nutritional benefits. Although research into the nutritional differences of differently sized MFGs is only presently coming to the fore, the possible interaction between structure and function is an important question with no simple answer. Differently sized MFG have differing phospholipid and proteins contents (Lopez

et al., 2011 a; Lu et al., 2016). If large and small MFGs fulfil different nutritional requirements, are these supposed variable nutrient profiles wrought from changing phospholipid content, protein content, or both?

2.4 Milk fat globule membrane proteins

The protein content of the MFGM accounts for 25 – 60% of the mass of the membrane material and 1 – 2% of total bovine milk proteins (Mather, 2011). Although over 100 MFGM proteins are present, the most extensively studied proteins in the MFGM, which also happen to present at the highest concentrations, are XO, BTN, MUC1, adipophilin (ADPH), PAS 6/7, and fatty-acid-binding protein (FABP) (Reinhardt & Lippolis, 2006). Some evidence exists that these MFGM proteins have potential as nutraceuticals in preventing the development of breast cancer, colon cancer, and gastric diseases (Spitsberg, 2005).

Proteins within the MFGM are commonly transmembrane (e.g., BTN), peripheral (e.g., XO), or loosely attached (e.g., PAS 6/7) (Mather, 2000). The functions of these proteins vary from membrane/protein trafficking, immunoprotection, and fat transport/metabolism. Of the immune-protective proteins, glycoproteins form the MFGM glycocalyx which covers the entire surface of the fat globule. The carbohydrate moieties (also known as glycoconjugates) are attached to the proteins protruding into the aqueous phase and are known to serve as bacterial and viral ligands, acting as competitors or decoys for pathogenic receptors that target cells (O'Riordan et al., 2014; Douëllou et al., 2017).

Processing can modify lipid-protein or protein-protein interactions which transform the structure of the MFGM. For instance, XO and BTN form a complex due to intermolecular disulphide bonds at pasteurization temperatures (> 60 °C) (Ye et al., 2002), potentially altering digestion behaviour.

2.5 Milk fat globule membrane polar lipid and putative health benefits

2.5.1 Milk polar lipid composition

Polar lipids only account for about 0.5 – 1% of all milk lipids yet serve as the structural foundation of the MFGM (Jiménez-Flores & Brisson, 2008). The concentration of polar lipids in the MFGM varies, depending upon the size of the fat globule. Smaller fat globules have a higher summative surface-area to volume ratio than a larger population of globules, and therefore, will proportionally have higher amounts of membrane polar lipids, assuming constant fat content (Lopez et al., 2011 a).

Phospholipids such as PE, PC, PS, and PI as well as sphingolipids such as SM, make up the large majority of the polar lipids in the bovine MFGM (average polar lipid content, 299 mg L^{-1}) (Fig 2.2; Table 2.3) (Zheng, Jiménez-Flores, & Everett, 2014 a; Yao et al., 2016 a; Lopez,

2020). The hydrocarbon composition of milk sphingomyelin (MSM) is of particular interest. The amide-linked acyl chain of MSM is mostly (> 60 mol%) composed of C22:0, 23:0, and 24:0 (Noh & Koo, 2004). This abundance of long chain saturated hydrocarbon chains, uncommon in dietary SM, allows for strong hydrophobic interactions with cholesterol (Et-Thakafy et al., 2018). For instance, in eggs, another food source high in SM, the sphingomyelin (egg-SM) is mostly composed of C16:0 (86 mol%).

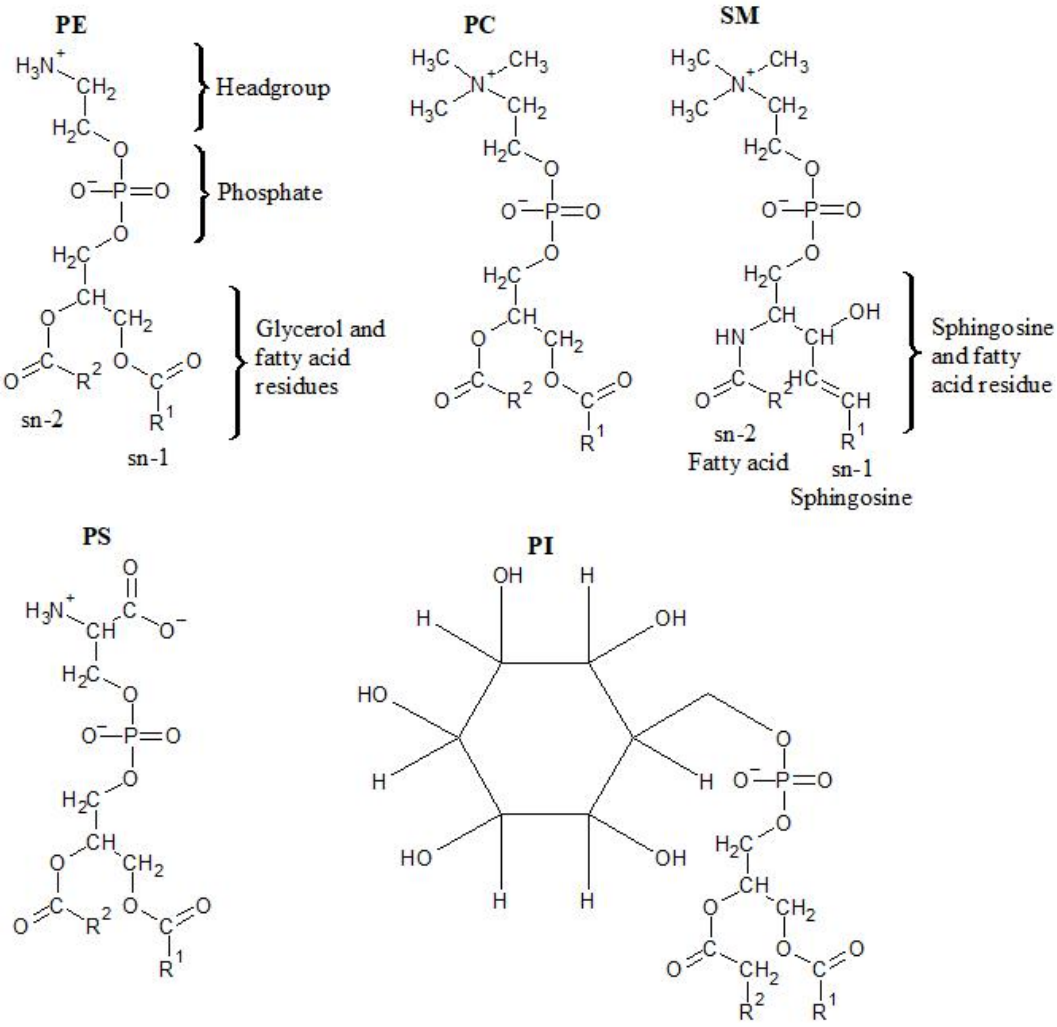

Figure 2.2. Structures of common polar lipids within the milk fat globule membrane. PE = phosphatidylethanolamine; PC = phosphatidylcholine; SM = sphingomyelin; PS = phosphatidylserine; PI = phosphatidylinositol.

Table 2.3. Polar lipid composition in bovine milk fat globule membrane. Adapted with permission from Yao et al., (2016 a).

Polar lipids	**Percentage present in bovine milk (%w/w of total phospholipids)**
Phosphatidylcholine	33.12 ± 0.21
Phosphatidylethanolamine	23.42 ± 0.13
Phosphatidylinositol	8.97 ± 0.06
Phosphatidylserine	9.07 ± 0.07
Sphingomyelin	25.40 ± 0.19

The bioactive potential of MFGM polar lipids is well-documented (Table 2.4). Some of the nutritional aspects are not health benefits attributed with the consumption of MFGM materials but rather MFGM components have been linked to nutritional effect. Furthermore, although these nutritional aspects have been identified to be related to these individual components, whether the component was consumed as is or part of the greater MFGM matrix has not been distinguished. Finally, further research is required in this field as there is only weak evidence of some of the beneficial effects of MFGM to humans (Dewettinck et al., 2008).

Table 2.4. Reported health benefits from polar lipids in the milk fat globule membrane. Adapted with permission from Gallier, Laubscher, & Rafael Jiménez-Flores, (2014 a); Dewettinck et al., (2008).

Component	PL%	Nutritional Aspects
Sphingolipids and metabolites	18 - 34.1	Reduction of the number of aberrant crypt foci and adenocarcinomas. Shift in tumour type (malignant to benign). Anticholesteremic. Protection of the liver from fat- and cholesterol-induced steatosis. Suppression of gastrointestinal pathogens. Neonatal gut maturation. Myelination of the developing central nervous system. Endogenous modulators of vascular function. Associated with age-related diseases and the development of Alzheimer's disease.
Sphingosine 1-phosphate		Mitogenic.
Phosphatidylcholine (PC)	19.2 - 37.3	Supports liver recovery from toxic chemical attack or viral damage. Protects the human GI mucosa against toxic attack. Reduction of necrotizing enterocolitis. Alleviates orotic acid-induced fatty liver.
Lysophosphatidylcholine (lysoPC)	2	Bacteriostatic and bactericidal capacity. Strong gastroprotective role in duodenal mucosa.
Phosphatidylethanolamine (PE)	19 - 42	Maintains hemostasis.
Phosphatidylinositol (PI)	5 - 11	Substrate in cell signalling. Promotes plasma cholesterol transport and metabolism.
Phosphatidylserine (PS)	1.9 - 10.5	Helps memory in a variety of tasks. Positive effect on Alzheimer's disease patients. Improves exercise capacity of exercising humans.

2.5.2 The anticholesteremic effect of milk polar lipids

Phospholipids derived from milk potentially help regulate intestinal cholesterol and lipid absorption (Dewettinck et al., 2008; Cohn et al., 2010). Clinical and animal studies demonstrate that a reduction in blood cholesterol from the consumption of MFGM arises from synergies between components and the structural organization within the MFGM (Noh & Koo, 2004; Conway et al., 2013; Rosqvist et al., 2015; Lovegrove & Givens, 2016). The first known study detailing this effect was Howards and Mark (1979). Participants who consumed 35 g of spray-dried buttermilk (high in milk phospholipids) every day for two weeks had significantly lower serum cholesterol (-6.4%) compared to participants who consumed 80 g of butterfat at the same frequency and duration (+9.8% serum cholesterol). Participants who consumed 160 g of cream (80 g fat/day) showed no significant increase in serum cholesterol. The authors made special note that butterfat was hypercholesterolemic, yet neither the cream nor the buttermilk increased plasma cholesterol. This led to the hypothesis that MFGM, depleted in butterfat, may contain an anticholesteremic factor.

There are currently three hypotheses that may provide some insight into the anticholesteremic effect of the MFGM: structural, enzymatic, and topogenic (Cohn et al., 2010). The structural hypothesis is as follows: the incorporation of cholesterol and SM into mixed micelles shifts cholesterol molecules from the micellar to the vesicular phase thus reducing intraluminal micellar cholesterol solubilisation and monomeric cholesterol uptake (Ros, 2000; Eckhardt et al., 2002). Foundational to this hypothesis is work that shows saturated SM and PC preferentially distribute into vesicles due to more efficient packing, whereas unsaturated PC distributes into micelles (Cohen & Carey, 1991). Micelles are the ideal physical form for maximal cellular uptake of cholesterol whereas the vesicular (lamellar) form is poorly absorbed by the brush border cholesterol binding protein that mediates cholesterol absorption via a collision-induced transfer mechanism (Thurnhofer & Hauser, 1990). If SM were to saturate a vesicle that contains cholesterol, a higher concentration of bile salt would be required to solubilize the vesicle into micelles, thus hindering cholesterol transport though the intestinal mucosa and epithelium.

The second hypothesis is that an excess of dietary polar lipids in the small intestine interferes with micellar polar lipid hydrolysis which is necessary for cholesterol uptake. In a Caco-2 cell model, the addition of PC micelles reduced cholesterol uptake whereas the addition of pancreatic phospholipase A2 (pPLA2) increased absorption (Homan & Hamelehle, 1998). SM has been shown to inhibit secretory Type II phospholipase A2 (sPLA2 – II), a structurally similar enzyme to pPLA2. Therefore, it is possible that high SM concentrations inhibit pPLA2

as well. As pPLA2 activity is necessary for efficient cholesterol uptake, inhibition would lead to reduced PC hydrolysis which would in turn reduce cholesterol absorption (Chung et al., 2013).

The third hypothesis is that polar lipids change the composition of intestinal enterocytes. The orientation of the transmembrane domains of membrane proteins is dependent upon membrane phospholipid composition during the initial assembly of the membrane, as well as post assembly. Furthermore, the lateral organization of membrane proteins is dynamic and dependent upon the surrounding environment (Dowhan & Bogdanov, 2009). Large quantities of dietary SM may modify the folding of transmembrane proteins through electrostatic or hydrophobic interactions, reducing the ability to absorb cholesterol monomers through the intestinal epithelium.

Animal studies, most commonly rat models, have shown that consumption of SM significantly decreases serum cholesterol when compared to a control diet (Imaizumi et al., 1992; Kobayashi et al., 1997; Norris et al., 2016). Moreover, rats with cannulated mesenteric lymph ducts, and an indwelling catheter infused with a lipid emulsion containing MSM and cholesterol introduced into the upper duodenum, showed lower levels of circulating cholesterol in the lymphatic system than those infused with egg-SM and cholesterol (Noh & Koo, 2003; Noh & Koo, 2004). This suggests that the highly saturated MSM is more capable at reducing cholesterol absorption due to a hydrophobic interaction.

On the other hand, clinical studies demonstrate that consuming pure SM has little effect on serum cholesterol levels in humans. Participants who consumed 1 g of MSM dissolved in corn oil as a daily supplement showed no difference in total serum cholesterol compared to a control diet (Ramprasath et al., 2013). There are two possible explanations for these discrepancies. Humans are one of the few animals that have alk-SMase present in both bile and in the intestinal tract (Duan et al., 1996). This enzyme, which hydrolyses SM into ceramide, is endogenous only in the small intestine for most other mammals, including rats (Duan, Nyberg, & Nilsson, 1995; Duan, 2006; Duan, 2007). Consequently, equivalent concentrations of SM that are sufficiently functional in rodents may not offer the same health benefits in humans due to the presence of alk-SMase in the bile. Additionally, although humans consume on average 300 – 400 mg of SM per day (Ramprasath et al., 2013), dietary SM is not commonly consumed as pure SM. It is always a component of a food product within a complex molecular structure, such as in egg yolk, or within the MFGM which envelopes MFGs.

Clinical studies have demonstrated that when a natively structured food rich in SM is consumed, a cholesterol modulating effect becomes evident. Participants who consumed a buttermilk beverage containing 700 mg of MSM daily did not have altered serum cholesterol levels,

whereas consumption of an unstructured control beverage (119 mg MSM) made from skim milk powder in which two-thirds of the milk phospholipids were replaced by egg polar lipid isolate significantly elevated (+2.2%) total cholesterol (Ohlsson et al., 2009). This experiment demonstrates the ability of the milk lipid structure to counteract increased serum lipid concentration.

The same trend is evident in participants who consumed a control beverage versus a ready-to-drink structured buttermilk beverage (11.81 mg of MSM). Those who consumed the buttermilk beverage had lower serum cholesterol (-3.1%), low-density lipoprotein (LDL) cholesterol (-3.1%) and triglycerides (-10.7%) than the control group (Conway et al., 2013). Overweight participants who consumed whipping cream (19.8 mg milk phospholipid/day) showed a significant reduction in total cholesterol (~ -1%). Those who consumed the control diet which incorporated butterfat (1.3 mg milk phospholipid/day) showed a significantly elevated total cholesterol (5.3%) (Rosqvist et al., 2015), showing structure- and concentration-dependent effects.

Recently, overweight, post-menopausal women who consumed MFGM-supplemented cream cheese (5 g milk polar lipids) for breakfast each day for four weeks had significantly larger decreases in serum total cholesterol and LDL cholesterol (-7% and -9%, respectively) when compared to their counterparts who consumed the control cream cheese (-0.7% total cholesterol and -1% LDL cholesterol). Those who consumed the 5 g milk polar lipid supplemented cream cheese were within the normal levels for serum and LDL cholesterol at the end of study (Vors et al., 2019).

It should be noted that the clinical trials reviewed showed an anticholesteremic effect when the participants persistently consumed MFGM. Daily consumption of high levels of milk phospholipid may not be convenient for all those who want access to this nutritional benefit – therefore, it is worthwhile considering whether the sporadic intake of MFGM or the complementation of MFGM with other dietary sources of phospholipids demonstrate similar putative health outcomes.

In one such study, Baumgartner et al. (2013) reported that the molecular matrix of food plays a role in cholesterol absorption. When participants were given either one egg, two eggs, or a buttermilk beverage mixed with one egg yolk to consume per day, serum cholesterol and LDL cholesterol were significantly higher in women who consumed two eggs (+7% and +45% higher) than the control (one egg), although egg-SM is known to reduce serum cholesterol when consumed (Noh & Koo, 2003). Yet, the serum and LDL cholesterol of women who consumed the buttermilk beverage plus egg yolk group were not significantly different compared to the

one egg group. The authors hypothesized that SM present in the buttermilk beverage interfered with intestinal cholesterol absorption.

The currently available literature indicates that humans consuming pure SM alone do not exhibit an anticholesteremic effect. This may be due to the unique composition of human bile in which contains an appreciable concentration of alk-SMase. Yet, despite our increased capacity to digest SM, foods with complex structures, such as the MFGM, do exhibit anticholesteremic properties when consumed, implying that the microstructure that the phospholipids are a part of play a significant role in determining the anticholesteremic effect of the MFGM.

2.6 Milk fat globule membrane architecture

The exact, native structure of the MFGM has not yet been discerned; however, various models have been proposed and updated (Fig. 2.3) (Danthine et al., 2000; Dewettinck et al., 2008; Lopez, 2011; Lopez et al., 2015).The distribution of phospholipids and proteins within the bilayer is asymmetric with the inner monolayer being rich in PI, PS, and PE whereas SM, PC, and cholesterol are concentrated within the outer bilayer (Deeth 1997; Mather & Keenan 1998 Jeong et al., 2013; Zheng, Jiménez-Flores, & Everett, 2014 a). The SM and cholesterol in the outer bilayer are tightly packed together forming complexes known as liquid-ordered (L_o) domains. These domains are analogous in phospholipid composition and structure to biological lipid or membrane rafts (Gallier et al., 2010 b).

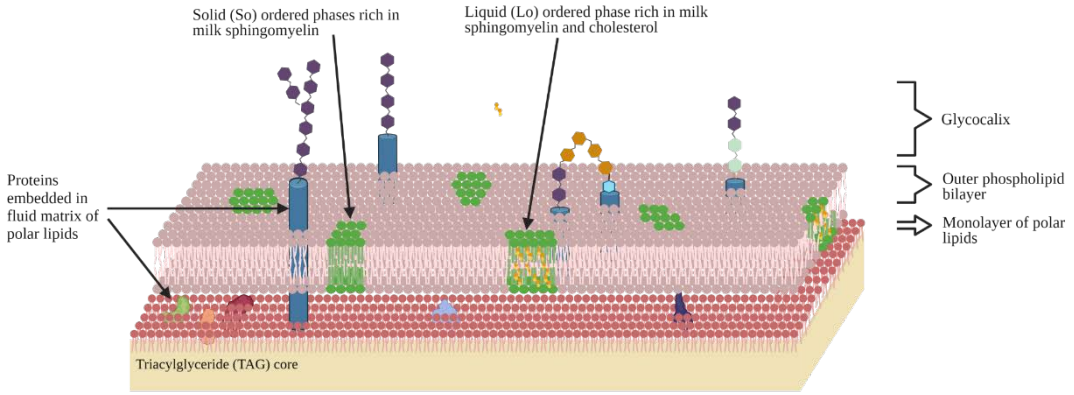

Figure 2.3. Updated model of the milk fat globule membrane as a heterogenous patchwork of polar lipids. The proteins are embedded within the liquid disordered portion of the membrane. Not to scale (the protein fraction makes up a much larger proportion of the membrane than what is shown) Adapted with permission from Lopez, Cauty, & Guyomarc'h (2018 a). Created with BioRender.com

The location of PE within the MFGM has been a point of contention. Deeth (1997) reported that MFGM phospholipid asymmetry is similar to the membrane of red blood cells, therefore PE may exist within the inner MFGM monolayer. Inhibition of the phosphatidylserine

decarboxylase pathway with sodium azide and sodium fluoride to reduce PE synthesis in mammary epithelial cells has been shown to sharply limit the formation of large intercellular lipid droplets (> 2μm) (Cohen et al., 2017). The authors concluded that the PE content of lipid droplets played a valuable role in determining droplet fusion and therefore MFG size. Conversely, Zheng, Jiménez-Flores, & Everett (2014 a) asserts that as the critical packing parameter of PE (which determines the preferred association structure of molecular shape dependent upon the effective volume of FA, length of FA, and head group area) is greater than 1, the phospholipid should have an inverted truncated cone critical packing shape, and therefore suited to an inverted packing structure (Iraelachvili, 2010) in the inner leaflet of the bilayer rather than the inner monolayer.

2.6.1 Lipid rafts and (L_o) liquid-ordered domains

Due to the co-presence of SM and cholesterol in the outer bilayer, the existence of structures analogous to lipid rafts have been hypothesized to be present in the MFGM. Lipid rafts were first proposed to describe heterogeneous regions in the plasma membrane of cells serving as transient microdomains that act as centres for a variety of membrane activity (i.e., dynamic catalytic platforms) (Simons & Ikonen, 1997). The original operating definition of a lipid raft was for it to be insoluble in 1% cold Triton X-100 and float in the upper half of a 5-30% sucrose density gradient (Pike, 2004). It has since been observed that not all detergent-resistant membranes (DRMs) happen to be lipid rafts (Hope & Pike, 1996). A new definition of lipid rafts as being 10–200 nm in size, heterogeneous, highly dynamic, sterol- and sphingolipid-enriched domains that compartmentalize cellular processes was later affirmed, specifically applying to cellular microdomains (Pike, 2006). As lipid rafts are formed from membrane regions known as L_o domains, the L_o domains in the MFGM which do not compartmentalize cellular processes cannot be considered “true” lipid rafts under the cellular definition of the term.

Liquid-ordered (L_o) domains are enriched with SM and cholesterol compared to the bulk of the fluid membrane that is in the liquid-disordered (L_d) phase (Quinn & Wolf, 2009). The cholesterol tightly packs (condensation effect) the SM while increasing the fluidity of the packed domains (fluidizing effect) allowing for the assembly of the mobile platforms heterogeneous on the surface of the membrane (McIntosh et al., 1992). Electron spin resonance (ESR) has been used to great effect in determining the structure of the L_o phase. Spin-label probes embedded within the L_o phase show motion typical of probes embedded within L_d phases; however, the reorientational motion around the axis of rotation of the probe is closer to that of probes embedded within a solid ordered (S_o) phase (also known as a gel phase) of phospholipids. The properties of the L_o phase can therefore be summarized as an intermediate

between a fluid bilayer and a gel phase (Collado et al., 2005). ESR probes further show that the two-site exchange rate of the spin labelled probe between L_o domains and other less ordered domains occur on the order of nanoseconds, suggesting the L_o phase is formed through the accumulation of transient associations between randomly distributed SM and cholesterol complexes (Chachaty et al., 2005).

As for the conditions that allow for the existence of L_o domains, calorimetric studies show that the addition of cholesterol prevents SM from phase partitioning into the S_o phase at temperatures below the SM melting temperature (for MSM that is T_m < 34 °C); wide-angle x-ray scattering (WAXS) confirms the disappearance of the S_o phase as cholesterol is added, forming an L_o phase (Lopez, Cheng, & Perez, 2018 b). The disappearance of the S_o hexagonal lattice as cholesterol is incorporated into the MSM bilayers, and d-spacing (periodicity, membrane width) intermediate between S_o and L_d domains (Lopez, Cheng, & Perez, 2018 b), are in agreement with the aforementioned ESR results.

2.6.2 Sphingomyelin and cholesterol complexation to form (L_o) liquid-ordered domains

Multiple hypotheses have been proposed to explain the mechanism behind SM and cholesterol complexation. The classic "umbrella model" suggests that the non-polar cholesterol finds shelter amongst a forest of acyl chains underneath a canopy of the polar head group (Huang & Zhao, 1995; Smith, Quinn & Lorenz, 2020). When embedded in a bilayer, cholesterol is known to reorient so that the polar hydroxyl group is pointed towards the hydrophilic choline headgroup (Smondyrev & Berkowitz, 1999). This orientation not only minimizes hydrophobic size mismatch between sterol molecules and long acyl chains but has been speculated to promote hydrogen bonding networks throughout the bilayer (Pandit, Bostick & Berkowitz, 2004; Jaikishan & Slotte 2011). Thus, phospholipids and sphingolipids with longer acyl chains are more attracted to the non-polar cholesterol carbon rings (Simons & Vaz, 2004).

The condensed complex model postulates that phospholipid and cholesterol mixing is non-ideal. Even binary mixtures of phospholipids (high T_m values) and cholesterol exhibit three phases, phospholipids, cholesterol, and a mixed phase of cholesterol and phospholipids (McConnell & Raddhkrishnan, 2003). The mixed phase is an intermediate complex which can be defined as cholesterol and phospholipid molecules reversibly reacting (Radhakrishnan & McConnell, 1999).

$$nq\mathrm{C} + np\mathrm{P} \rightleftharpoons C_{nq}P_{np} \qquad (2.1)$$

where C and P are cholesterol and a phospholipid; q and p are stoichiometric integers; and n is the cooperative factor, the inherent tendency of a specific phospholipid and cholesterol to form

a complex, usually 3 – 5 (Radhakrishnan et al. 2001). McConnell & Radhakrishnan (2003), use the analogy of a titration. Cholesterol is added to the phospholipid membrane until there is neither excess cholesterol nor excess phospholipid, an equivalence point. In phospholipid/cholesterol monolayers, this equivalence point can range from 25 – 43% mol cholesterol depending upon the phospholipid composition of the monolayer (Radhakrishnan & McConnell, 1999).

The mixed phase of cholesterol and phospholipid contains molecules with a lower-than-expected average area per molecule. These regions of "condensed" complexes are therefore accountable for the condensation effect of cholesterol and can repel other phospholipids, leading to immiscibility in ternary mixtures (Radhakrishnan & McConnell, 2005). Although the condensed complex model offers an explanation for why SM and cholesterol form complexes, the model provides no mechanism of action that addresses the intermolecular interactions that make the formation of condensed complexes possible.

Finally, a superlattice model features membrane lipids existing in regular distributions within the membrane, in contrast to the classic fluid-mosaic model (Somerharju, Virtanen & Cheng, 1999). Singer and Nicolson's fluid mosaic model proposes that the plasma membrane is a fluid bilayer of phospholipids with intercalated membrane proteins. Due to the fluidity of the membrane, protein and phospholipid are given a high degree of lateral freedom (Nicolson, 2014). Conversely, the superlattice model implies that there are a limited number of lipid conformations which are considered the most energetically favourable. Superlattices are not rigid monolithic structures; multiple superlattices can exist within a membrane. Furthermore, superlattices may exist in both phospholipid headgroups as well as acyl chains (Somerharju et al., 2009). The superlattice model attempts to explain SM/cholesterol complexation and the formation of liquid ordered domains through headgroup steric interference. The bulky SM (and PC) headgroup leads to "packing frustration," where spaces remain in the acyl chain region of the bilayer. Spaces that unsaturated PE and cholesterol are capable of filling resulting in thermodynamically favourable and tightly packed domains (Fenske et al., 1990; Virtanen et al., 1995). The superlattice model predicts that SM (and PC) interactions with cholesterol form hexagonal superlattices at both 20% and 25% mol cholesterol and this was experimentally shown to be the case (Chong et al., 1996).

Although useful for conceptualizing the lateral organization of model phospholipid bilayers due to the numerous factors that influence phospholipid/cholesterol interactions (e.g., hydrocarbon chain length, saturation, headgroup charge, presence of transmembrane proteins), none of these models can wholly explain why SM and cholesterol form L_o domains (Björkbom et al., 2010).

Outside of lateral lipid-lipid interactions, another plausible theory involves the hydroxyl group in cholesterol forming a hydrogen bond with the sphingosine amide group present in SM, or the ester oxygen in glycerophospholipids (Boggs, 1987). To test this theory, Arsov and Quaroni (2008) created egg-SM/cholesterol liposomes at varying relative molar ratios. Using attenuated total reflectance–Fourier transform infrared (ATR–FTIR) spectroscopy, these authors investigated changes to the amide I band (1643 cm^{-1}). This band is solely linked to the interactions between SM and cholesterol, confirming the existence of a hydrogen bond network within the liposomes. In spite of such a promising result, they were unable to conclusively verify the existence of direct SM/cholesterol hydrogen bonds, as SM may form intramolecular hydrogen bonds and the complexity of this network prevented the isolation of one specific interaction. This result challenges a previous study that claims the 1643 cm^{-1} band is a deformation mode of water molecules involved in a hydrogen-bond network (Lamba et al., 1991). To clarify the identity of the 1643 cm^{-1} band, the Raman spectrum of egg-SM hydrated in water was compared to egg-SM hydrated in D_2O. The addition of D_2O did not shift the band in question neither did changing the hydrocarbon chain length of SM affect the presence of the 1643 cm^{-1}. However, when ^{13}C replaced the carbon adjacent to the amide group, the subsequent Raman shift was shown to be consistent with expected values, offering strong evidence that the identification of the amide I band was valid (Shirota et al., 2016). The amide I band was also confirmed as a marker to detect SM clusters in bilayers using an all-atom molecular dynamics simulation (Yagi et al. 2015).

Deuterium NMR, comparing the cholesterol affinity of 14:0/14:$0_{(d27)}$-PC against 14:$0_{(d27)}$-SM bilayers, demonstrates that cholestatrienol (fluorescent cholesterol analogue) has a two-fold greater partition coefficient for SM bilayers. Furthermore, when the SM was heated so it had the same hydrocarbon chain order (determined with diphenylhexatriene anisotropy and the deuterium order parameter from ^2H-NMR) as the PC, although the difference between the PC and SM partition coefficient decreased, SM still had a significantly higher partition coefficient, suggesting that hydrophobic interactions must not be the only type of interaction that significantly contributes to cholesterol and SM complexation (Lönnfors et al., 2011). These authors ascribe this result to either a direct hydrogen bond between SM and cholesterol, or an inter-lipid hydrogen bonding network amongst SM. Although the presence of hydrogen bonding in SM bilayers, and the ability of cholesterol to modify those bonds is well known, there is still no evidence of a direct stabilizing hydrogen bond between cholesterol apical hydroxyl group and the amide group of SM (Lala, 1981; Guo et al., 2002; Slotte, 2016). A wealth of additional studies have indirectly indicated the existence and importance of cholesterol-promoted inter-lipid hydrogen bonding amongst SM molecules (Veiga, 2001; Zidar et al., 2009; Yasuda et al.,

2014; Sodt, Pastor & Lyman, 2015; Rowlands et al., 2020). The network of SM hydrogen bonds is believed to push cholesterol molecules further into the bilayer, minimizing entropic penalties.

Although the presence of inter-lipid hydrogen bonding has been confirmed, hydrogen bonding alone cannot support SM and cholesterol complexation at dilute concentrations. *In silico* simulations of ternary palmitoylsphingomyelin (PSM)/1-palmitoyl-2-oleoyl-*sn*-glycero-3-phosphocholine (POPC)/cholesterol bilayers show that cholesterol preferentially forms hydrogen bonds with POPC rather than PSM (Aittoniemi et al., 2007). However, PSM charge-pairing of choline nitrogen with cholesterol hydroxyl groups, hydrophobic interactions, and van der Waal interactions reduces the tilt angle of cholesterol so that the choline headgroup more readily serves as a shield against water. Yet, the role of the amide group in this complexation cannot be underestimated. Substituting the amide with an ester bond increases enzymatic oxidation of SM/cholesterol small unilamellar vesicles (SUV) 2.5-fold, suggesting that cholesterol becomes more accessible (Bittman et al, 1994).

In summary, the role of hydrogen bonding in SM/cholesterol complexation remains controversial, and although the above work has provided strong evidence for an exceptional interaction between SM and cholesterol, there are still gaps in understanding the intermolecular nuances to SM and cholesterol complexation.

2.6.3 Properties of liquid-ordered domains in the milk fat globule membrane

Liquid-ordered domains are well-studied in biological systems and model membranes, but scarcely examined in dairy matrices. This is partly because the presence of L_o domains in the MFGM have been proposed much later than in biological systems (Lopez et al., 2008 a). Confocal laser scanning microscopy of MFGs stained with lecithin fluorescent probes has revealed heterogeneities in the MFGM (Evers et al., 2008). These heterogeneities were further analysed using exogenous phospholipid dioleoyl-*sn*-glycero-3-phosphoethanolamine head-labelled fluorescent rhodamine (Rd-DOPE) to show that the heterogeneities were not localized proteins but regions of tightly packed polar lipids (Fig. 2.4) (Gallier et al., 2010 b; Lopez, Madec & Jimenez-Flores, 2010). Based on these results, the most accepted of the current MFGM models are based on the following assumptions: 1) MSM and cholesterol are major lipid components in the outer bilayer of the MFGM, 2) SM and cholesterol are known to preferentially form a complex (Engberg et al., 2020; Codini, Garcia-Gil & Albi, 2021), and 3) analogous lipid rafts occur in biological membranes when the above two criteria are met (Pike, 2006; Lopez, Cauty & Guyomarc'h, 2018 a).

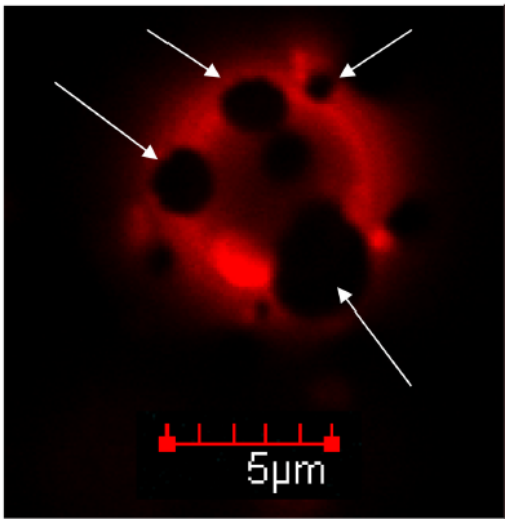

Figure 2.4. Confocal laser scanning micrograph of milk fat globules from raw cream stained with rhodamine dioleoyl-*sn*-glycero-3-phosphoethanolamine (Rd-DOPE). Arrows pointing at suspected liquid-ordered domains. Reprinted with permission from Gallier et al. (2010). Copyright 2010 American Chemical Society.

Using the same Rd-DOPE staining technique, Et-Thakafy, Guymoarc'h, & Lopez (2017 a) measured the dynamics of L_o domains in multiple species of MFGM as a function of temperature. At temperatures lower than T_m, the S_o and L_o phases co-exist and visible domains appear irregular in shape, highlighting the limitations of confocal microscopy with fluorescent phospholipid probes to differentiate L_o domains from the S_o phase (Zheng et al., 2014 b). Although this is less of an issue at temperatures much greater than 36 °C (T_m of MFGM) where the S_o phase is non-existent (Et-Thakafy, Guymoarc'h, & Lopez, 2017 a), care must be taken when drawing conclusions about L_o domains at temperatures < 36 °C by the use of confocal laser scanning microscopy alone, as one cannot be sure that what is being visualized is an S_o or L_o domain. At temperatures higher than T_m, depending upon the saturated polar lipid and cholesterol content of the membrane, the size and number of domains may decrease (melting of the S_o phase), the domains may coalesce (a behaviour common in L_o domains but not S_o domains) (Chen & Santore, 2014), or the domains visible below T_m may completely melt leaving a fat globule with no visible domains. Those fat globules with domains remaining above T_m exhibit irregular and angular domains when cooled. These angular fragments are likely to be the emerging S_o phase, implying that the L_o phase has become akin to a point of nucleation for S_o phase, likely due to the hydrophobic mismatching that occurs at the boundaries of L_o domains.

Conversely, if at temperatures greater than T_m the globule has no domains, small circular domains or a network of elongated domains form when cooled below T_m. The small circular domains are hypothesized to be where the supersaturated fluid phase is a point of nucleation to form small S_o domains. Those S_o domains do not coalesce but instead rapidly connect.

Extended storage at a temperature lower than the T_m of the MFGM leads to coalescence, and both angular domains and elongated domains reform the original circular domains which are thermodynamically more favourable.

Segregation that results from the presence of L_o domains introduce lateral heterogeneity to the membrane. Monolayer model systems show L_o domains are approximately 0.8 nm higher than the surrounding L_d area at room temperature, whereas the S_o phase is 1 nm higher than the L_d phase (Gallier et al., 2010 c; Guyomarc'h et al., 2014; Guyomarc'h et al., 2017). This increase in height is due to either the formation of an S_o phase or to cholesterol-induced ordering, respectively, increasing the proportion of *trans* isomers (Simons & Vas, 2004). The height differences are indicative of not only lateral phase separation but also mechanical heterogeneities in the outer bilayer. The rupture force of the MSM S_o phase is 30 nN, compared to 15 nN for the L_d phase and 12 nN for the L_o phase at 20 °C (Murthy, Guyomarc'h & Lopez., 2016). That is, molecules in the L_o phase possess higher lateral mobility than those in the S_o. One consequence of this mobility is the tendency to part when, for example, an atomic force microscope (AFM) probe comes into contact with the bilayer (Guyomarc'h et al., 2014). Due to multiple types of phospholipids that comprise the MFGM, the melting exotherm of MFGM is rather broad, exhibiting melting behaviour from as low as 15 °C to as high as 40 °C although the maximum of the endotherm is centred on 36 °C (Murthy, Guyomarc'h, & Lopez, 2016). Within the human intestine (at 37 °C), the majority of the MFGM exists as L_o domains littering a sea of L_d. Therefore, the susceptibility of L_o domain to rupture may affect lipolytic enzymatic reactions leading to altered digestion behaviour.

In a binary MSM/cholesterol system with the cholesterol concentration at 40 mol %, the S_o to L_d phase transition is undetectable at any temperature with DSC and the lateral packing structure of the phospholipids is no longer hexagonal, thus the entire system is in the L_o phase (Lopez, Cheng, & Perez, 2018 b). This phenomenon was reproduced in a recombined MFGM phospholipid extract monolayer with a MFGM extract/cholesterol molar ratio of 2.6:1 (MSM:cholesterol molar ratio 1:1) (Lopez, Cauty & Guyomarc'h, 2018 a). Animal studies have shown that cholesterol absorption is at its lowest when rats are fed a dispersion comprising a 1:1 molar ratio of MSM and cholesterol, hinting that one of the native functions of MSM is to regulate cholesterol uptake (Nyberg, Duan, & Nilsson, 2000). Such a result may seem counterintuitive. The condensed complex model indicates that the integral stoichiometry of egg-SM and cholesterol is 2:1 (Radhadkrishnan & McConnell, 1999), and longer length *sn-2* acyl chains of SM have no effect on the SM/cholesterol mixed phase equivalence point (Radhakrishnan et al., 2001). Thus, one might assume the equivalence point of MSM and cholesterol to also be 2:1. However, phospholipids with a higher T_m are known to require less

cholesterol to reach an equivalence point (Keller, Radhakrishnan, & McConnell, 2000) so it is quite likely MSM, which is richer in 22:0, 23:0, and 24:0 hydrocarbon chains, requires less cholesterol to reach this point. The phospholipid composition of the recombined MFGM phospholipid monolayer adds another layer of complexity. The presence of L_o domains cannot wholly be ascribed to SM/cholesterol interaction. Six percent of PC in buttermilk powder is saturated (Gallier et al., 2010 a), and capable of forming L_o domains. Stoichiometric considerations are necessary to understand the digestive implications of L_o domains, although current techniques are not yet capable of establishing unambiguous values for binary and ternary mixtures (Radhakrishnan et al., 2001), leaving aside native phospholipid mixtures, such as the MFGM.

Nascent inquiries into MFGM lipid-lipid interactions have structure have consistently revealed greater heterogeneity and complexity than expected. At the forefront are L_o domains and the inherent enigmatic digestive and structural roles. Notwithstanding, lipid-lipid interactions in the MFGM are the metaphorical tip of the iceberg, so to speak, with lipid-transmembrane milk protein interactions and the effect of processing on MFGM structure being essential factors to consider, but outside the scope of this thesis.

2.7 Physiological response to milk fat globule membrane components

In vitro digestion models are split into four steps, the oral phase, the gastric phase, the intestinal phase, and finally the colonic phase (Alegria, Garcia-Llata & Cilla, 2015). The digestive role of the oral phase depends upon the food matrix examined. As far as the MFGM in the native form is concerned, fluid milk does not require mastication, does not form a bolus, nor does it contain digestible starch. The primary function of the oral phase for fluid milk digestion is dilution with saliva. On the other hand, for solid dairy products, such as cheese, that contain MFGM fragments, particle size must first be reduced by chewing before dilution with saliva (Minekus et al., 2014). The authors are unaware of any detailed studies on oral processing of the MFGM; however, the charged mucin in saliva associating with the fat globule is known to cause flocculation in raw milk and homogenized milk globules to flocculate (Smoczyński and Staniewski, 2014). The flocculation may influence the resulting gastrointestinal digestion, the particulars of which require further investigation. The physical and chemical changes of the MFGM during the gastric and intestinal phase will be further discussed in the following sub-sections.

Probing the MFGM during digestion has been difficult due to the structural complexity of the membrane. The available literature predominantly employs confocal microscopy to visualize how proteins interact with fat globules, model membranes to track phase transitions, and construction of Langmuir monolayers to examine the effect of bile salts. For a simple overview,

Figure 2.5 summarizes the current gastrointestinal model of the digestion of fat globules coated with MFGM.

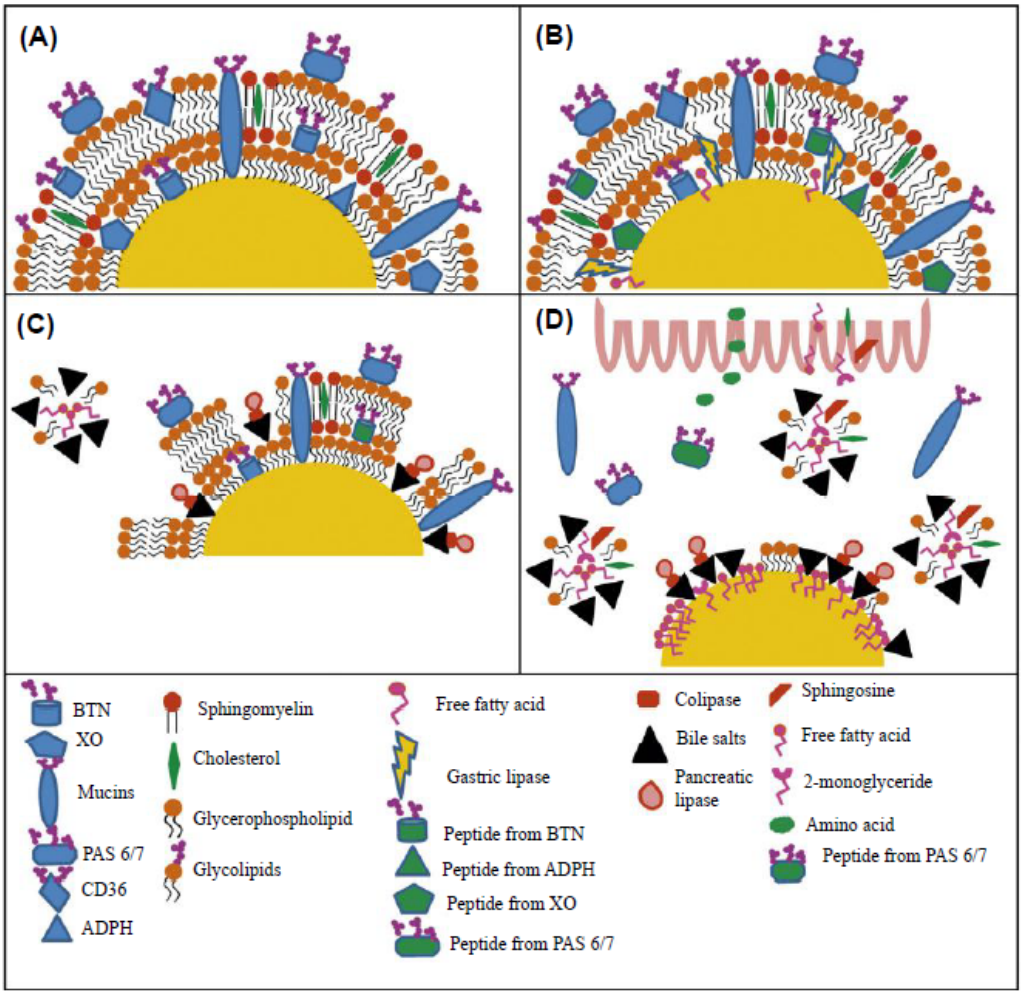

Figure 2.5. Current model of *in vitro* gastrointestinal milk fat globule membrane (MFGM) digestion. A) Native MFGM. B) Gastric digestion of milk fat globules (MFG). Gastric lipase hydrolyses triacylglyceride core to form protrusions of free fatty acids (FFA) that trap lipase and limit gastric lipolysis. Pepsin hydrolyses MFGM proteins; however, some glycoproteins are resistant. C) Intestinal digestion begins. Bile salts adsorb onto the surface of the MFGM displacing portions, allowing co-lipase to accumulate on the interface and recruit pancreatic lipase to form a pancreatic lipase and co-lipase complex. D) The remaining MFGM proteins are hydrolysed by trypsin and chymotrypsin. As the pancreatic lipase hydrolyses the triacylglyceride core, the resulting fatty acids and cholesterol are incorporated into phospholipid-bile salt mixed micelles to be further hydrolysed into monomers before being transported through the intestinal wall. Reproduced with permission from Gallier, Ye, & Singh (2012).

2.7.1 Gastric digestion

The gastric digestion phase has been shown to impact the MFGM in three ways: (1) gastric lipase generates free fatty acids that may aid in pancreatic lipase binding, (2) proteolytic enzymes (e.g., pepsin) digest MFGM proteins, and (3) the low pH causes caseins in the milk to aggregate, thus forming a closely knit network which entraps fat globules. As the protein network density increases, fat globules aggregate and coalesce (Singh and Gallier, 2017).

As commercial gastric lipase was unavailable until recently and due to a lack of attention, gastric lipolysis has often not been considered in previous *in vitro* models (Gallier, Ye, & Singh, 2012; Minekus et al, 2014). Be that as it may, *in vivo* models have shown that gastric lipases are able to reach the triacylglyceride (TAG) core of the MFG, hydrolysing long hydrocarbons (> C16), thus increasing the amount of free fatty acids that make up the gastric chyme (Gallier et al., 2013 a). The free fatty acids produced are known to promote the activation of the pancreatic co-lipase complex (Michalski, 2009). A peculiar observation is that lamellar structures observed as spherical protrusions on the interface of the MFG almost act as plugs limiting further gastric lipase activity (Gallier & Singh, 2012, Gallier et al., 2013 a). These spherical protrusions consist of free protonated fatty acids (74%), phospholipids (16%), monoglycerides (5%), diacylglycerols (4%), free cholesterol (1%), triacylglycerols (<1%) and human gastric lipase, not only signifying disruption of the MFGM structure may be occurring in the stomach, but also implying possible trapping of human gastric lipase (Pafumi et al., 2003). Considering gastric digestion is known to result in the hydrolysis of approximately 10 - 30% of lipids in adults, it is unlikely these spherical protrusions, only 200 nm in size and irregularly covering the surface of a lipid droplet, are the sole limiting factor of human gastric lipase activity.

Pepsin mediates protein hydrolysis during the gastric phase. Major proteins vary in hydrolysis rates, with BTN being much more resistant than XO or PAS 6 or 7 (Ye, Cui, & Singh, 2011). Yet, the high degree of glycosylation of MFGM glycoproteins from the glycocalyx, such as MUC1, impedes adherence and therefore hydrolysis by proteolytic enzymes (Hamosh et al., 1999).

Proteases and the low pH environment during gastric digestion cause the casein in milk to aggregate (Ye et al., 2016). The effect of this network on the fat globules depends upon the conditions of digestion. When bovine raw milk is digested *in vitro* under static, simulated fasting conditions, fat globules retained a globular structure (Gallier, Ye & Singh., 2012). Globular structure is also conserved under *in vivo* conditions when rats are fed raw or pasteurized cream, which is low in casein (Gallier et al., 2013 a). Yet, when bovine milk (raw, pasteurized) undergoes *in vitro* digestion under dynamic conditions using a human gastric simulator, fat globules show coalescence after 20 minutes (Ye et al., 2016; Roy et al., 2021). As these experiments did not use gastric lipase, this coalescence is solely due to the shear force from the nascent protein clot acting on the milk fat globules. The observed coalescence and subsequential potential for interfacial changes (Fig. 2.6.) call into question the previous assumption that the lateral organization of polar lipids and L_o domains of the MFGM in raw milk is conserved during gastric digestion.

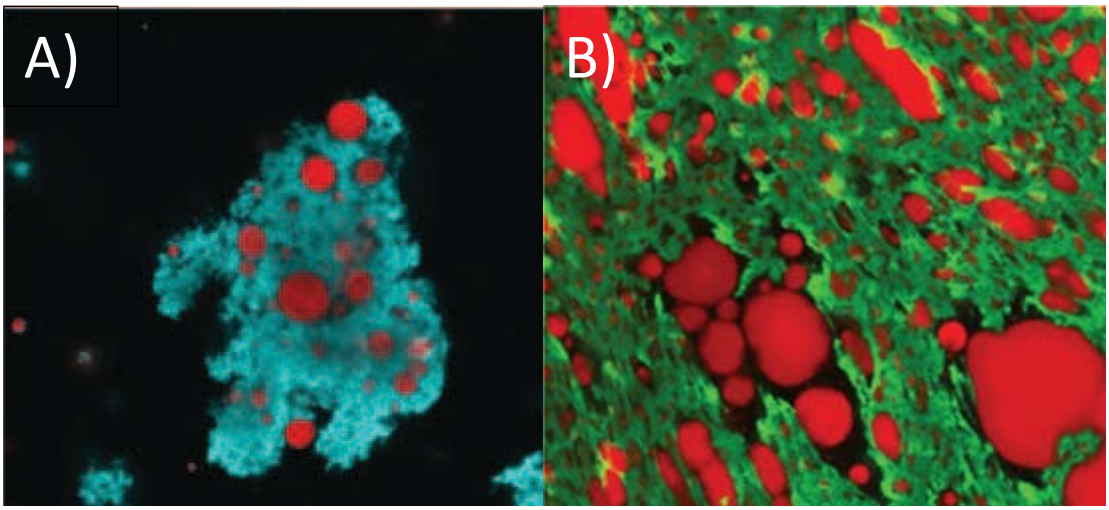

Figure 2.6. Confocal laser scanning microscopy (CLSM) of whole milk after *in vitro* gastric digestion. Red shows the fat; blue/green shows the protein. A) Static *in vitro* gastric digestion under fasting conditions for 120 min Gallier, Ye, & Singh, (2012). B) Dynamic *in vitro* gastric digestion for 90 min Roy et al., (2021).

2.7.2 Intestinal digestion

Lipolysis is an interfacial process, and consequently, the interfacial properties of milk fat globules play a large role in determining the rate of lipolysis during small intestinal digestion. During the intestinal phase, bile salts adsorb onto the MFGM surface, allowing pancreatic lipase (after forming a complex with the co-lipase) to access the TAG core. The resulting monoglycerides, fatty acids, phospholipids, and cholesterol self-assemble (with the addition of intestinal bile salts) to form mixed micelles which transport the lipolytic products into the enterocyte (Michalski, 2009).

The importance of the MFGM in limiting hydrolysis of the core triacylglycerides is evident when comparing the digestion of raw and recombined milk, the latter releasing fatty acids more easily during digestion. Where the native MFGM envelopes raw milk fat globules, the surface of recombined milk (in this case, mixing 4% (w/w) anhydrous milk fat in skim milk) consists largely of casein micelles and serum proteins (Ye, Cu & Singh, 2010). The lipoprotein lipase in milk is known to preferentially (70%) bind to casein micelles with the remainder existing as a casein-enzyme complex in the serum (Anderson, 1982). In the process of digestion, pancreatic lipase may have the same affinity for casein as its amino acid sequence and relevant binding sites bear some degree of homology with milk lipoprotein lipase (Ben-Avram et al., 1986). In which case, the high affinity for casein would bring the enzyme into close proximity to the interface of the casein and whey coated recombined fat globule. An alternative explanation is that when the adsorbed casein is hydrolysed under digestive conditions, the pancreatic lipase quickly adsorbs onto the uncovered surface allowing access to the lipid interior. Pancreatic lipase is known be highly surface active with an initial adsorption rate similar to bile salts (Corsten et al., 2017).

The difference between the rate of lipid hydrolysis of recombined milk and raw milk is erased with the addition of bile salts to the system (Ye, Cu &, Singh, 2010) highlighting the role of bile in lipid digestion. Model membrane systems are often relied upon to unravel nuances in the interaction between bile salts and L_o domains (Eckhardt et al., 1999; Zhou et al., 2013; Coreta-Gomes et al., 2015; Eckstein, Holzhütter, & Berndt, 2018). Bile salts displace polar lipids located in the outer layer of the MFGM (Patton et al., 1986), and rapidly decrease MFGM fluidity to form mixed micelles with interfacial MFGM components, as examined by electron spin resonance (Alshehab et al., 2019). Furthermore, in the presence of pancreatic lipase, although reduced, bile salt detergent effects still dominate, displacing interfacial components so the pancreatic lipase can hydrolyse the triacylglyceride core.

Bile salts preferentially adhere to the L_o domains of MFGM phospholipid extract monolayers leading to the creation of "snowflake" shaped domains due to an increase in the negative surface charge. Bile salts are hypothesized to disrupt either the domain boundaries, or position within the L_o domain, reducing the density of lipid packing (Gallier et al., 2014 b). When a critical concentration of bile salts or detergent is reached, the preferential affinity of SM for cholesterol is nullified (van Erpecum & Carey, 1997). Furthermore, a reduction in packing density promotes lipase/co-lipase complex adherence onto these snowflake domains (Chu et al., 2010).

The structural properties of a micelle is dependent upon the phospholipid lipid:bile salt ratio with mixed micelles being bile salt rich whereas phospholipid rich particles better resemble vesicles (Suys et al., 2017). Inserting an abundance of SM into mixed micelles containing cholesterol so that the concentration of phospholipid exceeds the solubilizing capacity of the bile salts reverts cholesterol molecules from the easily absorbed micellar phase (through the intestinal epithelial layer) into the poorly absorbed lamellar (vesicular) phase (Eckhardt et al, 2002). The addition of 40 % mol cholesterol was reported to make egg-PC/egg-SM 60:40 mol/mol small unilamellar vesicles highly resistant to taurocholate-induced micellization, and lead to the formation of large vesicular aggregates (Moschetta et al., 2002). Moreover, saturated soy-PC and cholesterol liposomes in the L_o phase resist up to 56 mM bile salts (Hermida et al., 2014), more than five times the physiological concentration of bile. Therefore, it is likely that at least a portion of SM and cholesterol in the MFGM is not micellized in the small intestine and retains a vesicular form. How this conservation of structure may affect subsequent lipolysis is unknown.

Cholesterol uptake occurs throughout the entire length of the small intestine but predominately in the duodenum and proximal jejunum (Lammert & Wang, 2005), therefore, the colonic phase should offer no new insights into how SM and cholesterol complexation in the form of L_o domains induce an anticholesteremic effect. Faecal samples can help confirm the ability of SM

to interact with cholesterol in the small intestine to inhibit cholesterol absorption. Rats given a high fat diet with an egg-SM supplement (6 mg/g) were reported to deposit 48% and 37% higher amounts of total lipid and cholesterol, respectively, into faeces than rats that only consumed a high fat diet, showing the unabsorbed cholesterol being excreted (Chung et al., 2013).

Supplementation of MSM in the diet may have some effect on colonic flora. Ileostomy patients who consumed pure MSM incorporated into skim milk had significantly higher amounts of PSM, N-docosanoylsphingosine-1-phosphocholine (C22-SM), and N-(tricosanoyl)-sphing-4-enine-1-phosphocholine (C23-SM) in the contents of their ileostomy bags. These long chain saturated hydrocarbons are characteristic of MSM and demonstrate that the consumption of MSM results in the retention of MSM components in the ileum which could be a source of nutrients further down the gastrointestinal tract (Ohlsson et al., 2010). In contrast, Vors et al. (2019) were unable to find any differences in gut microbiota in overweight post-menopausal women after a four-week intervention of cream cheese supplemented with 5 g of milk polar lipids from buttermilk concentrate. In 4-month-old neonates, the supplementation of MFGM and lactoferrin results in slightly altered microflora in the stool (Chichlowski et al., 2021). Although much attention has been placed on the role of the microbiome in human nutrition, investigating the effect of MSM on the microbiome to the level of depth it deserves is beyond the scope of this review.

2.7.3 Alkaline sphingomyelinase

One possible key player in the digestion of L_o domains is E-NPP7 a sphingomyelinase native to the small intestine. Two other sphingomyelinase types exist in the human body, acid-SMase and neutral-SMase, but these are only similar to alk-SMase (E-NPP7) in enzymatic function. Based on its amino acid sequence, alk-SMase shares 30% similarity with NPP enzymes. These are ecto-enzymes which attach to the outer leaflet of the plasma membrane via the N- or C-terminus transmembrane domain (Duan, 2006). In alk-SMase, the C-terminus transmembrane domain anchors the enzyme onto the intestinal brush border. Other alk-SMase motifs include a “cap” subdomain and a catalytic domain which enclose two zinc ions. In addition to the zinc-phosphate interaction, the crystal structure of the enzyme has one phosphate oxygen hydrogen-bonded to an Asn-96 side chain, and the choline quaternary ammonium group forming a cation-π box with two surrounding aromatic side chains. When the substrate is in position, the two zinc ions bind the SM phosphate group allowing a Thr_{75} hydroxyl side chain to engage in a nucleophilic attack of the phosphorus atom activated by one of the zinc ions, resulting in a ceramide leaving group and a phosphocholyl-threonine intermediate (Gorelik et al., 2017). To

reform the Thr_{75} side chain and release the bound phosphocholine the intermediate undergoes a nucleophilic attack by a water molecule activated by a remaining zinc ion (Gorelik et al., 2017).

For most mammals, alk-SMase is anchored to the intestinal mucosa surrounding the microvilli membrane. In humans there is a separate source of alk-SMase present in the bile (Duan et al., 1996). Biliary alk-SMase is likely produced in the liver, localized in the canalicular membrane, dissociated by bile acid, and then concentrated in the gallbladder before being released into the intestine with bile (Duan, 2006). There is high alk-SMase activity in gallbladder bile (1000 ± 180 nmol/h/mg protein) yet the concentration in the gallbladder mucosa (90 ± 24 nmol/h/mg protein) is too low to be considered as the location where alk-SMase originates. Conversely, the moderate amount found in hepatic bile (400 ± 60 nmol/h/mg protein) clearly suggests alk-SMase is produced in the liver and then concentrated in the gallbladder bile (Nyberg et al, 1996). Furthermore, northern blot analysis shows high levels of alk-SMase mRNA levels in the human liver (Duan et al., 2003 a).

Intuitively, one might expect this bile to be the source of the alk-SMase attached to the intestinal mucosa that is common in mammals. Bile taken from most non-human mammals (rat, guinea pig, pig, cow, sheep) has no alk-SMase activity, and hamster bile only has 20% of the activity present in human bile (both at pH 7.5) (Duan et al., 1996). Northern blots have further shown alk-SMase is only present in the jejunum for rats (Wu et al., 2005). The evidence above constructs a clear picture: in humans, alk-SMase mRNA is present in both the liver and small intestine, and both hepatic bile and intestinal mucosa have alk-SMase activity. In rats, alk-SMase is only present in the small intestine and not the bile. It can be concluded humans have two individual sources of alk-SMase: biliary alk-SMase originating from the liver and secreted into the bile and intestinal alk-SMase anchored to the brush border of mucosal cells. A larger question is the role of alk-SMase in the bile and why humans have evolved such a capacity.

Within the small intestine, alk-SMase is located at the surface of microvillar membrane in the enterocyte within the jejunum. In that section of the intestine, the pH is approximately 7; however, as suggested by the name, alk-SMase is more active at pH 9 (Nyberg et al., 1997). Alk-SMase has another dependency - bile salts. The stimulatory effect of bile salts is due to the electrostatic attraction between the positively charged alk-SMase that holds the active site, and the anionic bile salt micelles are anionic. The two most effective bile salts being taurocholate and taurochenodeoxycholate, two major bile salts present in human bile (Hofmann, 1999). Substitution of a Arg-271 + Arg-343 loop near the micelle absorption area with anionic glutamates reduced SMase activity (Gorelick et al., 2017). Furthermore, substitution of hydrophobic residues Ile-344 + Val-346 + Phe-348 with less hydrophobic residues also greatly reduces SMase activity, suggesting active site interactions with hydrocarbon chains are also

necessary for optimal enzyme activity (Gorelick et al., 2017). Maximal activation of the enzyme occurs at the biliary critical micelle concentration. Each bile salt will therefore have a different stimulatory effort on alk-SMase. Conversely, an excess of bile salts which exceeds the critical micelle concentration will inhibit enzymatic activity; however, the mechanism has not been experimentally determined. Taking into account the enzyme's electrostatic preferences, substrate non-competitive inhibition due to the high concentration of anionic micelles may occur. The CMC may result in the ideal lipid:bile salt ratio for mixed micelles containing the zwitterionic SM in disk-like bilayers (Maldonado-Valderrama et al., 2011) to adhere onto the active site. Physiologically, the upper small intestine is where most bile salt-induced lipid digestion occurs, but the concentration of bile salts is usually too high for alk-SMase to be effective (Duan & Nilsson, 1997).

Alkaline sphingomyelinase secretion and digestion in humans is depicted in Figure 2.7. After a meal is consumed, intestinal endocrine cells release cholecystokinin which has two separate but related roles: stimulating the gall bladder to release alk-SMase along with bile salts into bile and triggering the pancreas to secrete trypsin which hydrolyses the C-terminus of the intestinal alk-SMase, releasing the enzyme from the intestinal mucosa (Olsson et al., 2004; Duan, 2006).

After SM is hydrolysed into ceramide, the ceramide is subsequently hydrolysed into sphingosine by an intestinal neutral ceramidase. Intestinal neutral ceramidase carries many similarities to alk-SMase; it is a brush border enzyme, resistant to trypsin-mediated inhibition, and activated by bile salts (Olsson et al., 2004). The sphingosine is absorbed through the enterocyte, converted into fatty acids, and incorporated into chylomicrons. The presence of SM and cholesterol mixed micelles has been shown to almost completely (94%) inhibit sphingosine absorption in Caco-2 and HT-29-D4 cell lines (Garmy et al., 2005). The authors suggest that SM and cholesterol complexes stabilize sphingosine in an extended low-energy confirmation interfering which interferes with binding to Niemann-Pick C1-Like 1 (NPC1L1), an apical protein on intestinal epithelial cells that significantly mediates cholesterol absorption. The presence of egg-SM micelles decreases mRNA (-22%) and protein expression (- 9%) of NPC1LI as well as reducing apical to basolateral uptake of cholesterol by 72% (Yang et al., 2018).

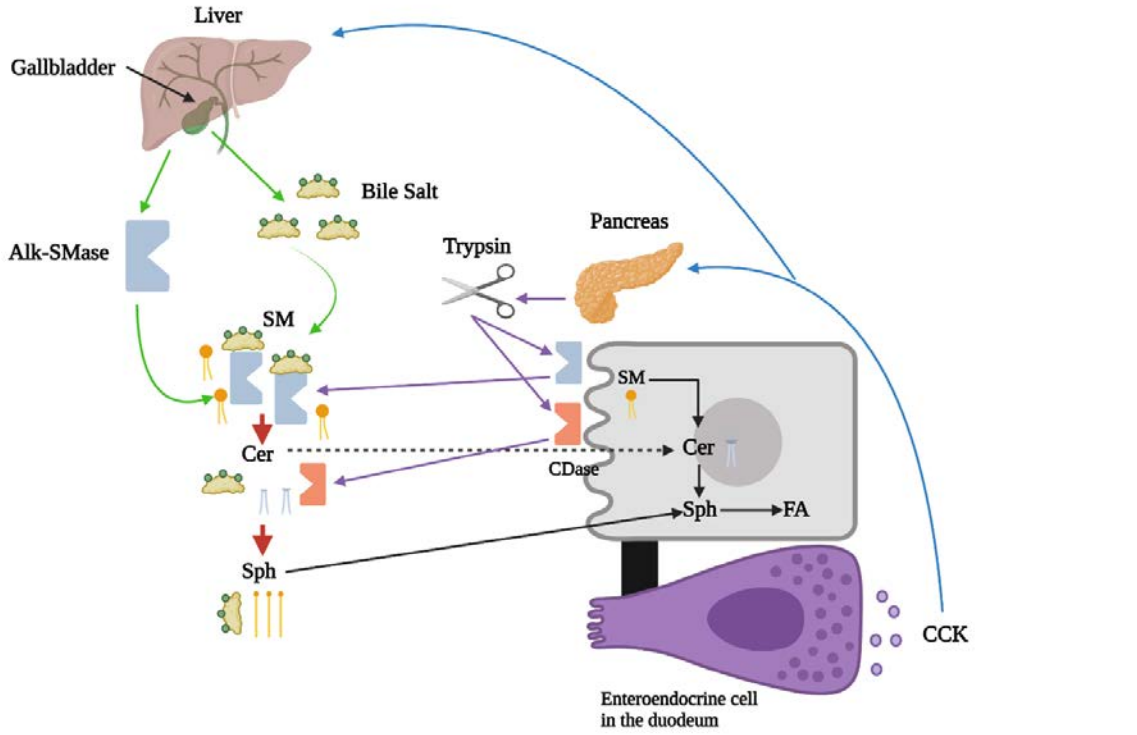

Figure 2.7. Digestion of dietary sphingomyelin (SM). Humans have alkaline SM (alk-SMase; blue bars) in both the bile and bound to the intestinal mucosa. After a meal is consumed, cholecystokinin (CCK) induces the secretion of alk-SMase into the bile, and trypsin to the intestinal lumen. The trypsin hydrolyses alk-SMase and neutral ceramidase (C-Dase) from the mucosa. The sphingosine (Sph) is transported and converted to fatty acids (FA) or ceramide (Cer). The SM in the enterocyte indicates endogenous synthesized SM by mucosal cells and is located on the brush borders. Reproduced with modification from Duan (2006). Created with BioRender.com

The digestion of the MFGM can be summarized as such: (1) the oral phase dilutes and causes MFGs to flocculate; (2) gastric lipase partially hydrolyses MFG core triacylglycerides promoting eventual activity by pancreatic lipase and its co-lipase in the small intestine; and (3) the secreted bile salts convert the MFG into mixed micelles which are then hydrolysed and taken up into the intestinal epithelium. A unique feature of the MFGM is the sphingomyelin and cholesterol interaction which forms L_o domains. Although, cell models indicate these assemblies resist epithelial absorption, how the aforementioned digestive processes affect (or fail to affect) L_o domains are still unknown.

2.8 Techniques for modelling and investigating the milk fat globule membrane

2.8.1 Model membrane systems

Four liposome/vesicle systems are commonly considered for model phospholipid bilayers: multilamellar vesicles (MLV), giant unilamellar vesicles (GUV), large unilamellar vesicles (LUV), and small unilamellar vesicles (SUV). This section will describe how each is created

and their general physical characteristics. Monolayer and supported bilayers will be touched upon later.

The first liposome system employed was MLVs by the Bangham thin film hydration method (Bangham, Standish, & Watkins, 1965). Pure phospholipids are dissolved in solvent which is then evaporated to form a thin lipid film. Hydrating this lipid film above its T_m and vortexing the suspension until turbid produces polydisperse vesicles comprising of multiple lamellae, otherwise known as MLVs. These multilamellar vesicles are irregularly shaped, polydisperse and will sediment when given enough time. Multilamellar vesicles have poor size homogeneity but are usually greater than 1 μm. These make MLVs, in terms of size, the model most similar to the majority of MFG membranes.

Different MLV preparations often incorporate additional processes to increase homogeneity or reduce the number of layers, for example, sonication after swelling to increase homogeneity or freeze-thaw cycling of the hydrated lipid film below freezing and above the T_m (Filippov, Orädd, & Lindblom, 2006; Quinn, 2013; Keyvanloo et al., 2018). The principle behind freeze-thaw cycling works as follows: MLVs have two water components, the bulk water in which the vesicle is suspended, and interlamellar water embedded in or between the layers. This interlamellar water, embedded in membrane layers of the vesicle, is less likely to contain nucleating agents (minerals, impurities) than the bulk water, and therefore is susceptible to supercooling. As the bulk water around the vesicle freezes, osmotic stress causes the vesicle to eject interlamellar water, dehydrating the vesicle and reducing the lamellarity (Kaasgaard et al., 2003).

The advantage of GUV is their size (30 – 150 μm), making them a powerful tool for studying the morphology of biological membranes using CLSM (Bagatolli & Gratton, 2000; Sot et al., 2008). Vesicles of this size were traditionally prepared through a gentle hydration of a dried lipid film with water saturated nitrogen for two or more hours, before dilution with an aqueous buffer (Reeves & Dowben, 1969). An assortment of improved protocols has since been developed: osmotic shock, gel assisted swelling, peptide-induced fusion of smaller precursor vesicles, detergent-mediated reconstitution, droplet-transfer, and inkjet-based formation (Witkowska, Jablonski, & Jahn, 2018). The most popular is known as electroformation which involves running an electric current through a rehydrated lipid film supported on a glass slide coated with a conductive material, commonly tin oxide (Angelova, Hristova, & Tsoneva, 1999). The principle behind electroformation lies in manipulating the second step of the traditional thin layer hydration to swell the lipid in the buffer in four ways: a minor direct electrostatic interaction between the electric field and lipid charges; redistribution of lipid counter-ions which govern bilayer thickness; decreasing membrane surface and line tension, which is the key

driver for vesicle formation, but can also lead to holes in the bilayer; and electroosmosis (Dimitrov & Angelova, 1987). Electroosmotic forces primarily occur when an electric alternating current is applied during electroformation. The periodic motion of the buffer aids in dislodging and separating the newly formed membrane from the bulk lipid.

Using GUVs as a platform, Zheng et al. (2014 b) investigated the nature of L_o domains using DPPC, DOPE, MSM, and cholesterol. Binary GUVs of DPPC and DOPE showed clear phase separation between the saturated DPPC and the unsaturated DOPE. GUVs entirely made of MSM displayed elongated domains, attributed to hydrocarbon chain mismatch which alters the lateral phospholipid molecular packing. Finally, Rd-DOPE, commonly used to distinguish L_o domains from the L_d phase in milk fat globules, was unable to distinguish between S_o and L_o domains. These authors suggested that more robust methods were necessary to elucidate L_o structures within the MFGM.

Large unilamellar vesicles (LUV) are produced after extruding a hydrated lipid film through a filter while keeping the temperature of the preparation above the lipid's T_m. The most common filter for LUVs is two stacked polycarbonate Nucleopore filters with a pore size of 100 nm producing vesicles which have an average diameter of 90 – 105 nm (Basáñez et al., 1997; Ferraretto et al., 1997; Arnulphi et al., 2007; Skočaj et al., 2014). In contrast, small unilamellar vesicles (SUV) require brief sonication of the hydrated lipid film to supply vesicles that are ~ 60 nm (Moschetta, et al., 2002; Murthy, Guyomarc'h, & Lopez, 2018). These two techniques allow a higher level of control over the resulting vesicle size and ensure relatively consistent monodispersity, making them the most used model membrane system for structural and functional experiments.

Monolayers, in particular, Langmuir-Blodgett (LB) films are commonly used in to investigate the phase coexistence and physical behaviour of phospholipids. Although a monolayer is only half a bilayer membrane, the pressure, temperature, and subphase of LB troughs are easily independently controlled. The greatest advantage of a monolayer is the ability to separately measure lateral packing density and lipid composition, allowing hydrocarbon chain order to be investigated as a function of surface pressure and temperature.

An LB trough consists of an interface between two phases, most commonly air-water. Molecules are deposited on the interface forming a thin monolayer. In the case of phospholipids, the hydrophilic headgroups face the water with the tails facing the air. To make an LB film, a solid hydrophobic substrate is dipped into the trough, collecting a layer of phospholipids (McCullough & Regen, 2004). Subsequent dips and retrievals lead to the assembly of multiple layers on the support. Studies of phospholipid monolayers in LB troughs

form the basis of the condensed complex model discussed in *Section 2.6.1*. Mixed phases of MSM and cholesterol have higher intermolecular forces acting upon them than pure phases of MSM or cholesterol alone. The interfacial area of the MSM and cholesterol monolayer is at its most condensed (i.e. when attractive forcers are at the highest) at 7:3 mol/mol cholesterol:sphingomyelin (Cheng, Ropers, & Lopez, 2017).

Although the LB technique lacks the specificity to pinpoint the exact contributions of a particular species, monolayer techniques lend themselves well to investigating the phase transitions of the complex composition of MFGM. Dark domains that correspond to L_o domains grow in size with the addition of sphingomyelin and cholesterol in dairy-based phospholipid monolayers (Gallier et al., 2010 b). Phospholipid composition, surface pressure, and temperature further modifies the morphology of these domains whereas the addition of cholesterol increases the number of domains.

Compared to the self-assembled bilayers described at the beginning of the section, it is relatively simple to deposit proteins onto a monolayer, rendering the system closer in semblance to the native MFGM (Gallier et al., 2014 b). Recently, ultrafiltration and solvent washing have been used to create a non-surface-active milk permeate subphase for Langmuir trough experiments for the purpose of validating the aforenoted studies (Real Hernandez & Jimenez-Flores, 2019).

Langmuir-Blodgett films can serve as an intermediate stage in the production of supported lipid bilayer (SLB), another model membrane system commonly used to investigate MFGM topography. An SLB is a bilayer that rests on top a solid substrate; the inner leaflet of the phospholipid is not directly standing on the support – there exists a thin layer of water to maintain fluidity. Therefore, substrates should be hydrophilic and smooth, ideally fused silica, borosilicate glass, mica, or oxidized silicon.

To manufacture an SLB from an LB film, the monolayer is pulled from the trough and the upper leaflet is transferred by the Langmuir-Schaefer procedure, horizontally dipping the monolayer into the trough once more to fuse the upper leaflet with the bottom leaflet (Tamm & McConnell, 1985). An alternate method is to take the LB film monolayer and fuse SUVs onto the monolayer, meaning the SUV vesicles deform and rupture after encountering the hydrocarbon chains (Kalb, Frey, & Tamm, 1992). A third method involves the direct adsorption of a vesicle from an aqueous suspension onto the supported substrate.

2.8.2 INFOGEST in vitro *digestion*

In recent years, there has been an effort to harmonize digestion protocols, leading to the creation of a standardized method known as INFOGEST (Minekus et al., 2014). Two variations of the

INFOGEST method currently exist: a static digestion model consisting of three separate phases (oral, gastric, and small intestinal) (Brodkorb et al., 2019) that is restricted to the measurement of endpoints, and a semi-dynamic model (Mulet-Cabero et al., 2020) that allows for intermittent time point sampling during the gastric phase which carries through to the small intestinal phase. The volume of milk fat globule membrane phospholipid preparations is too low to consider a semi-dynamic model; therefore, this section will only describe the static model.

After solid foods are mechanically broken down in the oral phase, salivary amylase begins to degrade starches. There may be a role for salivary mucin to flocculate colloidal components of the food such as fat globules. In the previous version of the INFOGEST protocol, the oral phase could be skipped if the food in question has a short residence time and is resistant to amylase, i.e., liquids that do not contain starch (Minekus et al., 2014). A recent amendment to this protocol recommends that all food be diluted with simulated oral fluid at a 1:1 wt/wt ratio (Brodkorb et al., 2019).

The gastric phase follows on from the oral phase of digestion. A static model is unable to model a dynamic digestive system with varying pH levels in different sections but does offer convenience in terms of volume digested and equipment necessary. For static models, the suggested pH is 3 and the recommended duration for gastric digestion is 2 h at 37 °C. Both pepsin and gastric lipase are present in the stomach. The static model suggests the use of porcine pepsin (84% homologous to human pepsin) and rabbit gastric lipase (Brodkorb et al., 2019). Increasing the pH to intestinal conditions (7) after the gastric phase is complete, or the addition of chemical inhibitors such as Pepstatin A and Orlistat, can be used to inactive the pepsin and gastric lipase, respectively.

The final phase occurs in the small intestine. Two options exist at this point, the use of porcine pancreatin, or the individual enzymes: porcine trypsin, bovine chymotrypsin, porcine pancreatic lipase and colipase, and porcine pancreatic α-amylase. Furthermore, the addition of 10 mM bile salts as rehydrated bovine bile is necessary (Brodkorb et al., 2019). As the digestion of L_o regions is the topic of this research, recombinant alk-SMase will be incorporated at this stage. Choosing a representative concentration of alk-SMase to include in the procedure is difficult as alk-SMase has never been used in previous *in-vitro* digestion studies. After purification, the activity of human intestinal alk-SMase is 183 nmol/min/ug enzyme (Duan et al., 2003 b). As is, the activity of alk-SMase in bile is 2.4 nmol/min/mL bile (Duan & Nilsson, 1997). Also worth considering, the alk-SMase activity of the small intestinal contents of newborns is 0.22 nmol/min/mL intestinal contents. Using these figures, a crude estimate of alk-SMase activity in the intestine can be obtained.

Heat-shock treatment or freezing are commonly used to inactivate intestinal enzymes. Lowering the pH to near gastric levels will also inactivate intestinal enzymes if the gastric enzymes have already been inactivated. Porcine pancreatic lipase is an alkaline, mesophilic enzyme with an optimal pH of 7.3 – 9.0 and temperature of 35 – 45 °C (Mendes, Oliveira, & de Castro, 2012). About 30% of enzyme activity remains when assayed at pH 5 and 37 °C, and less than 20% enzyme activity remains when incubated for 20 min at 60 °C and pH 8 (Evran & Telefoncu, 2005). The inactivation conditions for alk-SMase are similar to pancreatic lipase. About 20% enzyme activity remains when incubated for 1 h at 60 °C (Cheng et al., 2002) and 10% remains at pH 5 (Duan & Nilsson, 1997). Heating may alter the food structure and thawing the samples for subsequent analysis invites residual enzymatic activity. Chemical inhibitors include Pefabloc SC for trypsin and chymotrypsin, and 4-bromopheylboronic acid or methanol/chloroform for lipase. Chloroform is known to change phospholipid structure (Turkyilmaz et al., 2009; Reigada, 2011).

2.8.3 Dynamic light scattering

Dynamic light scattering (DLS), also known as photon correlation spectroscopy and quasi-elastic light scattering is a non-invasive, non-destructive, analytical technique that is often used to measure the particle size distributions of nanomaterials. This technique takes advantage of the differences in the velocity of particles in solution due to Brownian motion. There are many excellent reviews on DLS and its applications (Dalgleish & Hallett, 1995; Bhattacharjee, 2016). The basic principle of this technique is as follows: the Einstein-Stokes equation (Eq. 2.2) below shows the speed of diffusion of a particle is inversely proportional to the hydrodynamic diameter:

$$d = \frac{kT}{3\pi\eta D} \tag{2.2}$$

where d = the hydrodynamic diameter, the theoretical diameter of a hard sphere that diffuses at the same speed as the particle in question, k = the Boltzmann constant, T = absolute temperature, η = dispersant viscosity, and D = diffusion coefficient of the particle. Evident from the equation is the inherent assumption that the particles are spherical. Properties of the dispersant, as well as that of the particle such as ionic strength, surface structure, and the aforementioned shape of the particle, affect the accuracy of dH as an estimate of particle size.

The constant, random movements of the particles within the dispersant cause the scattered light (mostly Mie scattering) from a light source (i.e., laser) to constructively and destructively interfere, creating a speckled pattern of light and dark that fluctuates over time. A photodetector analyses this pattern, delivering an initial intensity signal. More signals are taken at different time points (also known as delay times) and compared to the initial signal. As Brownian motion

is random, one expects a loss of correlation between the initial signal and the signal sampled as time increases (Hassan, Rana, & Verma, 2015). Using this information, a correlation function can be constructed:

$$G(\tau) = A \cdot e^{-Dq^2\tau} + B \quad (2.3)$$

where, G (τ) = is the correlation at delay time τ, A = amplitude of the correlation function, D = diffusion of the particle, B = the baseline, and q = scattering vector which is expressed as:

$$|q| = \frac{4\pi n_0}{\lambda_0 sin\frac{\theta}{2}} \quad (2.4)$$

Here, n_0 = the refractive index (RI) of the dispersant, λ_0 = is the wavelength of the laser, and θ = is the angle of detection. Eqs. (2.3) and (2.4) are used to calculate D, which is then used to determine d in Eq. 2.2. The clear advantage of this method is that few variables are necessary (RI, viscosity of dispersant, and temperature, detection angle) to obtain particle size data.

2.8.4 Zeta potential

Zeta potential (ζ) is commonly used in the colloid sciences as an indicator of nanoparticle stability. The rule of thumb is that system with a zeta potential ≥ |30| mV, indicates the particles will not self-aggregate (Honary & Zahir, 2013). Hunter (1981) provides a comprehensive in-depth volume on the applications of zeta potential and uses in colloid sciences. Bhattacharjee (2016) supplies an excellent review on the theory, instrumentation, and factors to consider when measuring ζ-potential.

Fundamentally, ζ-potential measures the potential difference between the hydrodynamic particle surface of shear (the slipping plane) as it moves under the application of an electric field, and a point at infinite distance from the particle. This surface of shear is located within the electric diffuse double layer, an ionic atmosphere surrounding the charged colloidal particle. As the ζ-potential of a particle cannot be directly measured, it is calculated from the electrophoretic mobility (μ_e) of a charged particle in an electric field (Eq. 2.5).

$$\mu_e = \frac{V}{E} \quad (2.5)$$

where V = particle velocity (μm/s), E = electric field strength (Volt/cm). Using the value of μe, the ζ-potential can be obtained from Henry's equation (Eq. 2.6).

$$\mu_e = \frac{2\varepsilon_r\varepsilon_0\zeta f(\kappa a)}{3\eta} \quad (2.6)$$

where ε_r = relative permittivity/dielectric constant, ε_0 = permittivity of a vacuum, f(κa) = Henry's function, η = viscosity of sample at measurement temperature, and ζ = zeta potential. A variation of Henry's equation, called the Helmholtz-Smoluchowski approximation where f(κa) = 1.5 is necessary when the thickness of the electric double layer is much smaller than the particle radius. This applies to large particles (up to, and greater than 1 μm) within aqueous solutions at salt concentrations of 10 mM and higher, which is very common for MLVs and MFGs dispersions.

Due to the positive choline headgroup and negative phosphate group, SM is a zwitterion. The zeta potential of SUVs composed entirely of MSM is 4.2 ± 0.5 mV whereas SUVs comprised of MFGM polar lipid extracts are -4.6 ± 0.5 mV due to the presence of anionic polar lipids, such as PS and PI, which bear negative head groups (Obeid et al., 2019). With such low absolute zeta potential values, these model membrane systems are expected to show aggregation. This is not a surprise as MFG themselves only have a zeta potential of -16 to -10 mV depending upon the calcium concentration (Dalgleish, 1984; Lopez et al., 2008 b; Ménard et al., 2010).

2.8.5 Confocal laser scanning microscopy

The premier method for investigating the MFGM, as well as the surface morphology of model membranes, is undoubtedly confocal laser scanning microscopy (CLSM). By taking a stack of images of a thick sample it is possible to develop a three-dimensional construct of a milk fat globule. To accomplish this, four elements are necessary for a CLSM system: a fluorophore (dye), an excitation source, wavelength filters to isolate emission photons from excitation photons, and a detector to transform the emission photons into an image.

Fluorophores are unreactive fluorescence dyes and can be a component of a probe, which have highly specific biochemical targets. For dairy products, Nile Red (9-diethylamino-5H-benzo[a]phenoxazine-5-one) is used to fluoresce neutral lipids whereas Fast Green FCF (acid blue 3) which is derived from triphenylmethane and triphenylcarbinol stains the protein. When used in concert to double stain the sample, the distribution of the lipids within the protein matrix becomes visible. For phospholipids, Rd-DOPE (1,2-dioleoyl-sn-glycero-3-phosphoethanolamine-N-(lissamine rhodamine B sulfonyl, also abbreviated as Rh-PE) is a PE molecule with a rhodamine dye attached to the ethanolamine headgroup. Due to the low melting temperature of DOPE (-7.3 °C) (Koynova & Tenchov, 2013), the probe partitions into the L_d phase (Fig 2.8). The S_o and L_o regions do not fluoresce, giving the mistaken appearance of holes at first glance.

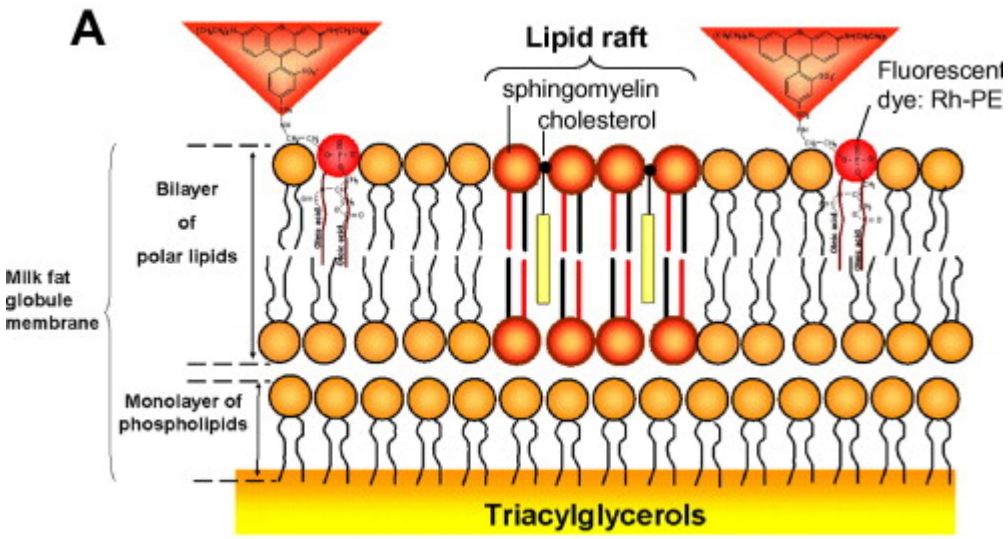

Figure 2.8. Two-dimensional schematic representation of how Rd-DOPE (denoted in the original figure as Rh-PE) partitions into the L_d phase of a phospholipid trilayer. Reproduced from Lopez et al., (2010).

The sources used to excite the fluorophores most commonly used to stain the MFGM are Ar^+ lasers and laser diodes for the lipids and a He-Ne laser for protein. The exact emission and collection wavelength will depend upon the experiment in question and the operational parameters of the instrument.

2.8.6 Transmission electron microscopy

The principle behind transmission electron microscopy (TEM) is to bombard a dry sample in a vacuum with an electron beam to visualize an image. Firing electrons at a sample leads to elastic and inelastic scattering (Williams & Carter, 1996). Elastic scattering occurs when the combined kinetic energy and momentum of the electron and the atom with which the electron is interacting remains constant, delivering high resolution information. Conversely, inelastic scattering occurs when an electron transfers energy to the sample, causing radiation damage. As electrons which are elastically scattered will interact differently with the lens compared to those which are inelastically scattered, differences in focal length occur. To correct these focal length aberrations, an electromagnetic lens in the barrel of the TEM is used.

Collecting the elastically scattered electrons is like shining a light through a grating. Most of the electrons pass through unhindered; however, some constructively or destructively interfere, forming a diffraction pattern. The objective lens is placed at the back focal point to recombine the electrons and form an image (Franken et al., 2020). Electron dense regions in the sample appear dark whereas an area that allows the transmission of electrons will appear light. The clear advantage of this technique over visible light microscopy and CLSM is the ability to produce high quality images of structures with nanometre resolution.

The most common style of TEM when studying model membrane systems is time resolved cryo-TEM (TRC-TEM) where the sample is flash frozen with liquid ethane and transferred under liquid nitrogen into the microscope (Thompson et al., 2016). The freezing occurs so quickly that ice crystals do not form, allowing one to directly visualize soft materials like phospholipid vesicles in high structural detail. Furthermore, without a drying step the sample can be visualized under a variety of conditions (pH, in the middle of a reaction, etc.) (Basáñez et al., 1997).

Although lower in structural fidelity, negative stain TEM has shown to be sufficient for visualizing not only the structure of SM liposomes but also the hydrocarbon chain order (Tokudome et al., 2010). Negative staining involves applying a sample onto a mesh grid with a thin carbon resin cover. A heavy metal salt can be used to the stain the sample to alter the number of scattering events. Scattering is proportional to atomic number (Z), the size of the nucleus with elastic scattering increasing with $Z^{4/3}$ and inelastic scattering by $Z^{1/3}$ (Franken et al., 2020). Limitations include the stain interacting with the vesicle thus changing the structure, and vesicles interacting with the carbon films to give rise to anomalous structures like torn or folded liposomes (Baxa, 2018; Robson et al., 2018). Nevertheless, negative stain TEM remains the simplest method to obtain highly resolved images of vesicles.

2.8.7 Differential scanning calorimetry

Differential scanning calorimetry (DSC) measures the change in physical material properties over time and temperature which is represented as the difference between exothermic or endothermic energy between an analyte and a reference. The material of interest and the reference (usually buffer or dispersant) are placed in separate cells (pans, capillaries) and heated. Constant energy is supplied to both cells to maintain an identical temperature. As the cells are heated, the analyte may undergo a thermally induced transition. In this case, excess energy is required to ensure both cells maintain identical temperatures. The energy necessary to keep both samples at identical temperatures at each previously specified time point is subtracted from the other, producing a thermograph (Prenner & Chiu, 2011).

In the lipid sciences, DSC is primarily used to study oxidation and phase transitions (T_m and T_c). The latter show up as endothermic or exothermic events, peaks, in the thermograph. The temperature at which the maximum height of the peak occurs is the temperature of phase transition. However, the peaks of many phospholipid thermograms are asymmetrical. In those cases, the width of the transition at half the peak height (FWHM, $T_{1/2}$) can be used to gauge the physical transition. Another thermotropic parameter that can be calculated from a DSC thermograph is enthalpy:

$$\Delta S = H_{Cal}/T_m \quad (2.7)$$

The free energy (G) is zero at the phase transition; hence, H_{Cal} corresponds to the area under a peak.

Phospholipid phase transitions occur at well-defined temperatures based on the type, hydrocarbon chain length, and saturation (Heerklotz, 2004). Differences in vesicle morphology can alter the thermograms. Multilamellar vesicles are the most commonly used system for DSC experiments as they prove reproducible and provide high resolution phase transition peaks (Heerklotz, 2004). DSC thermograms of SUVs contain fewer pre-transition enthalpic transitions. Furthermore, when SUVs are heated, they form LUVs which may bias the cooling thermogram.

There are generally three different types of phase transitions that occur for a pure phospholipid bilayer. The two of interest are the S_o to L_d transition and S_o to a ripple phase. The ripple phase is an intermediate phase between S_o and L_d that is named after its periodicity. There is no conclusive explanation for the formation of a ripple phase. Possible hypotheses include relieving the packing frustration of phospholipids that are no longer tilted (Scott & McCullough, 1993), thermodynamic stability (McCullough, Perk, & Scott, 1990), or increasing headgroup exposure to the hydrophilic bulk phase (Cevc, 1991).

The later chapters of this thesis shall discuss the splitting and broadening of the S_o peaks when cholesterol is incorporated into vesicles. For now, it should be understood that whereas the $S_o \rightarrow L_o$ is an observable and measurable change, unlike an S_o to L_d transition, what is being measured is the absence of a transition – the larger the proportion of the vesicle existing in the L_o phase, the less of a transition is present. This makes discriminating between an L_o phase and the absence of a signal difficult. Thus, although DSC is a powerful tool for investigating phase transitions in lipids, it has limited applications for mixtures of cholesterol and phospholipids.

2.8.8 Raman spectroscopy

Vibrational spectroscopy measures the vibrations of molecular bonds. There are six different types of molecular vibrations, also known as the normal modes of vibration: asymmetric stretching, symmetric stretching, wagging, scissoring, twisting, and rocking. As long as these modes change the molecules dipole moment, they will absorb infrared (IR) light at specific frequencies. A detector measures the amount of IR light transmitted through the sample at a certain wavelength producing a spectrum (Stuart, 2015).

Raman spectroscopy utilizes an intense, monochromatic light source (most commonly a laser) to raise a molecule from a ground vibrational state to an excited state. The electromagnetic radiation from the laser induces a dipole within the molecule, changing its polarizability. The

selection rule for Raman spectroscopy requires asymmetric polarizability for vibrational modes to be detected. After the molecule returns to the ground state, most of the light is elastically scattered (Rayleigh scattering) – the wavelength of the scattered light having the same wavelength as the incident light. About one in a million photons undergo inelastic scattering, where the wavelength of the scattered light is higher or lower than the wavelength of the incident light. If the wavelength is longer, the scattered light is known as Stokes-Raman scattering. When the wavelength is shorter, it is known as anti-Stokes Raman scattering. Most Raman spectroscopy measures Stokes-Raman scattering (Vandenabeele, 2013). The spectrum of Stokes-Raman scattered light is then dispersed using a grating before being collected in a detector to product a spectrum. The wavenumber, intensity, and shape of a Raman spectra gives detailed information on the chemical and physical nature of the sample, allowing the structural changes of a sample when concentration, composition, and other parameters are altered to be elucidated.

The Raman spectrum of phospholipids can be divided into active bands that describe the headgroups and those that describe the apolar tails. The bands for the headgroups occur at 700 – 900 cm^{-1}. For instance, the ethanolamine group for PE occurs at 760 cm^{-1}. Curiously, even though PC and SM are both composed of a choline headgroup, the symmetric and asymmetric stretching vibrations in PC are 719 and 876 cm^{-1} whereas SM is 723 and 882 cm^{-1}. The reason for shift is not yet known. The saturation, length, and orientation of the apolar tails make up the remaining spectrum from 1000 cm^{-1} onwards.

The Raman spectrum of SM is very typical of phospholipids (Fig. 2.9). Table 2.5 details the assignments Czamara et al. (2015) has drawn from the literature, although caution must as exercised as the exact Raman assignments in the CH region (2800 – 3000 cm^{-1}) are often conflicting (Batenjany et al., 1994; Lee & Bain, 2005; Argov et al., 2008; Yao et al., 2016 b).

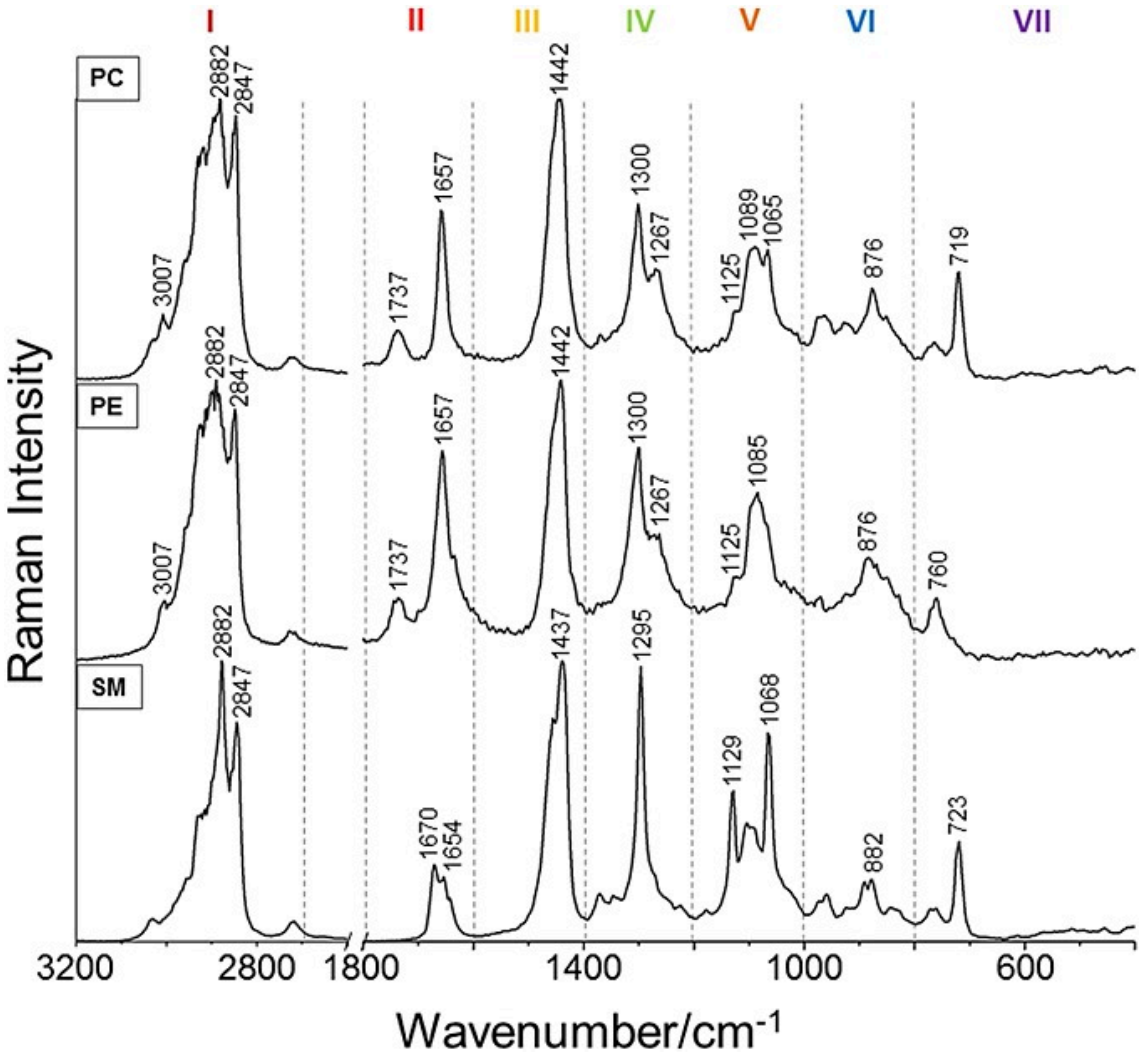

Figure 2.9. Raman spectra of various phospholipids in powered form. Reproduced from Czamara et al., (2015).

The major similarities between the Raman spectra of phospholipids are strong signals in the CH and C-C regions. The most remarkable difference between SM and PC which shares a choline headgroup is that SM is missing a band at 1737 cm^{-1} (carboxyl ester stretching vibration). Instead, SM has a band composed of two counterparts at 1670 and 1645 cm^{-1} which denote the carboxyl stretching coupled with amide bending vibrations (Krafft et al., 2005). As previously mentioned in Section *2.6.2*, this amide group is hypothesized to be a keystone in the sphingomyelin inter-lipid hydrogen bonding network. The 1130, 1085, and 1068 cm^{-1} bands are the C-C vibrations related to the length of the hydrocarbon chain and tail length and are directly related to the proportion of *trans*/*gauche* rotamers (Okotrub et al., 2020). At room temperature, the intensity ratios for 1130/1085 cm^{-1} and 1068/1085 cm^{-1} for SM is generally higher than that of PC, indicating SM bilayers have a higher proportion of *trans* hydrocarbon chain, i.e., a higher amount of bilayer is in the S_o phase. Sphingomyelin bilayers commonly lack a signal at 3007 cm^{-1} (=CH stretching) which is present in more unsaturated phospholipid species (Borchman, Tang, & Yappert, 1999). Finally, the 2880 cm^{-1} (asymmetric CH_2, sp3 stretch) peak is higher in

intensity than in PC and SM. This band is more sensitive to both inter- and intra-chain interactions.

Table 2.5. Raman Active Bands and their assignments for PC, PE, SM. Adapted from Czamara et al., (2015).

Modes[1]	**PC**	**PE**	**SM**
ν(=CH)	3007	3007	
$\nu_{as}(=CH_3)$	2959	2959	2959
$\nu_{s}(=CH_3)$	2925	2920	
$\nu_{as}(=CH_2)$	2882	2882	2880
$\nu_{s}(=CH_2)$	2847	2847	2847
ν(C=O)	1737	1737	
ν(C=C)	1657	1657	1670, 1654
$\alpha(CH_2/CH_3)$	1442	1442	1437
$\tau(CH_2)$	1300	1300	1295
δ(=CH)	1267	1267	
ν(C - C)	1125	1125	1129
ν(P - O)	1096	1096	1096
$\nu_{as}N^{+}(CH_3)_3$	876		882
Ethanolamine		760	
$\nu_{as}N^{+}(CH_3)_3$	719		723

[1] α, scissoring; δ, deformation; τ, twisting; ν, stretching (s, symmetric; as, symmetric).

2.8.9 X-ray diffraction

X-ray diffraction (XRD) can generate high resolution structural data from crystalline substances. Although an unreasonably high concentrations of vesicles material is often necessary for laboratory scale XRD instruments, beamlines in synchrotron facilities are capable of investigating MLVs at micromolar concentrations. The basis of XRD is Bragg's equation:

$$n\lambda = 2d \sin\theta \tag{2.8}$$

where n is an integer, λ is the wavelength of the X-ray, d is the spacing of the crystal layer, and θ is the angle between the incident ray and the plane (Fig 2.10). At the heart of this equation is when a beam of X-rays is passed through a highly ordered material, the diffracted beam is in-phase, resulting in constructive interference. In this case, in-phase means the sum of the distance travelled by the incident ray and the scattered ray when divided by the wavelength of the X-ray is an integer. From this imaginary right-angle triangle positioned in an array of atoms, the distance between the planes can be calculated.

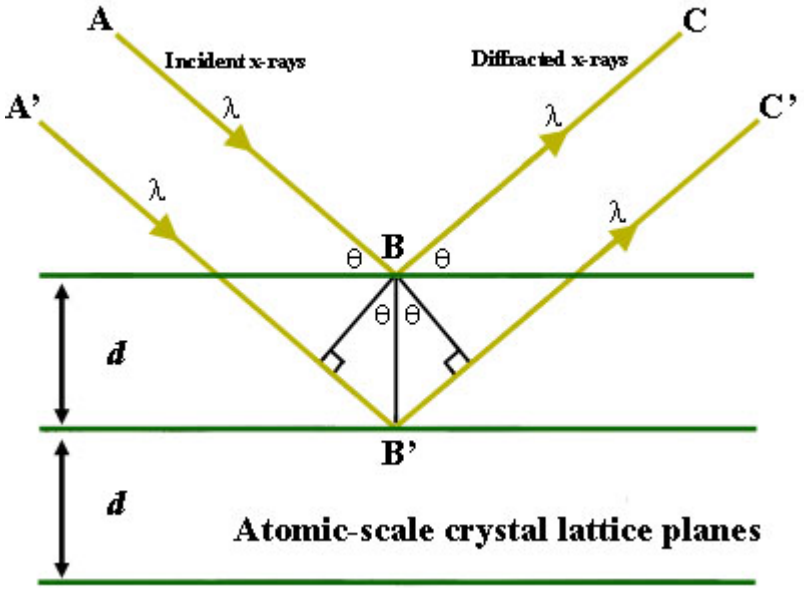

Figure 2.10. Bragg's Law (reproduced from the Science Education Resource Center at Carleton College); d, spacing between crystal layer; λ = wavelength, θ = angle between the incident and plane.

Interest in applying synchrotron XRD to phospholipid bilayers is mainly a biological pursuit to understand cellular membranes. The digestion of dietary phospholipids is a recent scholarly pursuit. Great strides have been made on the *in vitro* digestion of milk triglycerides and the investigation of various crystal structures formed during this process. During the lipolysis of milk triglycerides, a large quantity of highly amphiphilic polar lipids species (mono- and diglycerides) are released (Salentinig et al., 2011) and self-assemble to form a variety of lyotropic liquid crystalline structures which are somewhat dependent upon the species origin of the milk (Clulow et al., 2018) (Fig. 2.11). In the absence of bile, lipase digestion of commercial bovine milk produce inverse, oil-continuous micelles within the O/W emulsion droplets, as well as persistent lamellar structures within 1 min of lipase addition (Salentinig et al., 2013). At 2 min, these structures pack into an *Fd3m* lattice (micelles arranged in a cubic lattice). Half a minute later a transient inverse hexagonal phase that vanishes after 15 minutes of digestion is present. After 10 min of digestion, the water content increases, owing to the formation of a *Pn3m* (Salentinig et al., 2013) or *Im3m* structure (both are bicontinuous cubic phases) (Clulow et al., 2018). Furthermore, large uni- and multilamellar vesicles, tubular structures, and multilamellar fragments can be observed in the midst of transitioning into cubosomes with Cryo-TEM.

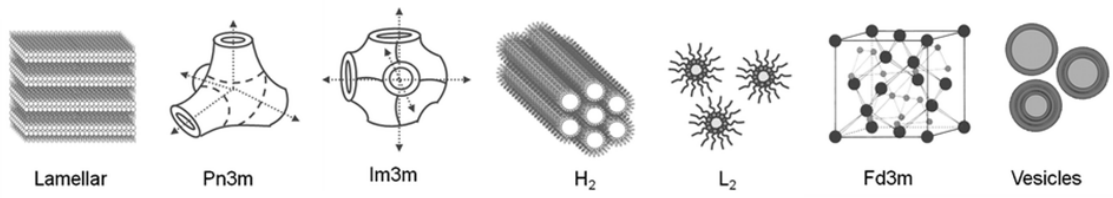

Figure 2.11. Self-assembled lyotropic liquid crystalline structures from lipase-catalysed digestion of bovine milk with and without bile salts. Reproduced from Kulkarni et al., (2011). *Pn3m* = diamond inverse bicontinuous cubic, *Lm3m* = primitive inverse bicontinuous cubic, H_2 = inverse hexagonal, L_2 = disordered inverse micellar, *Fd3m* = inverse micellar cubic.

In the presence of bile salts, milk triacylglycerides were digested more quickly. The inverse hexagonal structure takes 6 min of digestion to form and only lasts 3 min before devolving into a broad peak. Towards the end of the digestion period, vesicular structures begin to develop on the surface of the cubosomes rather than into them. As such, after 30 min of digestion, vesicles of varying structures dominate. In the context of this thesis, the abundance of vesicles as the digestion reaches completion is promising as one of the hypotheses for the putative bioactivity of SM as an anticholesteremic agent is due to the ability of the sphingolipid to maintain a poorly absorbed lamellar form in the presence of cholesterol. It is highly possible there are synergistic effects between the digestion of milk triacylglycerides and phospholipids.

2.8.10 Atomic force microscopy

Atomic force microscopy (AFM) is powerful scanning technique for probing supported phospholipid bilayers. AFM consists of a sharp cantilever tip which identifies the sample surface topography. As the cantilever tip is brought close in proximity to the surface, various forces repel the tip, deflecting a laser beam. Photon detectors measure the reflected light and produce a measurement. Three different modes exist: non-contact, keeping the tip slightly away from the surface and measuring the shift from its natural position; contact, monitoring the force required to keep the tip on the sample surface; and tapping, uses both non-contact and contact modes.

Atomic force microscopy has also been used to determine the mechanical properties of phospholipid systems. Calculating the Young modulus, the ratio between the force applied to an area (tensile stress) and the amount of extension per unit length (tensile strain) of DOPC SUVs (T_m = -20 °C) and DDPC SUVs (T_m = 41 °C) at 20 °C showed a ten-fold difference (Et-Thakafy et al., 2017 b), thus DDPC liposomes that were wholly in the S_o were invariably stiffer than the DOPC liposomes which were wholly in the L_d phase. Applying this methodology to MSM, Et-Thakafy et al., (2018) further uncovered that the Young's modulus of MSM at 20 °C was lower than that of the S_o DPPC. Considering MSM is rich in C24:0 hydrocarbon chains, one would except the S_o phase to be stiffer than DDPC which is made up of C16:0; however, the lower T_m SM species act as "defects" in the bilayer lateral organization.

The mechanical properties of liposomes or monolayers notwithstanding, AFM can be directly applied to physically characterized L_o domains in dairy systems. AFM was originally a complementary method to CLSM, and used to confirm domains as visually (Gallier et al., 2010 b), L_o domains look like holes where the Rd-DOPE dye could not intercalate. The technique was further applied to compliment the epifluorescence microscopy of β-casein–phospholipid monolayers to investigate protein-lipid interactions that would occur on the milk fat globule interface (Gallier et al., 2012). Phase images show the height differences between L_o and S_o domains as well as flower shaped β-casein–phospholipid domains that are suggested to arise from electrostatic and hydrophobic interactions between the protein and phospholipid. The driving force behind protein-phospholipid attraction was analogized to be close to protein dissolution in a solvent system – proteins partition preferentially in either L_o or L_d depending upon chemical character (electrostatic, hydrophobicity).

2.8.11 Nuclear magnetic resonance spectroscopy

Nuclear magnetic resonance (NMR) spectroscopy is a high-resolution tool capable of determining chemical structure, physical structure, and molecular dynamics through the oscillatory response of certain nuclei with non-zero nuclear spins when placed in a magnetic field. The difference in oscillatory response leads to an energy difference:

$$\Delta E = \gamma\hbar(1 - \sigma)B_0 \tag{2.9}$$

where γ is the gyromagnetic ratio, a constant associated with each nuclei; B_o is the strength of the magnetic field; σ is the chemical shielding around a nucleus; $\hbar$ is the reduced Planck's constant divided by 2π. The reduced Planck's constant is the fundamental quantum unit of angular momentum, i.e. the amount of spin of a nucleus (Reif et al., 2021). As Eq. (2.9). indicates, the electrons that shield the nucleus from the magnetic field causes the axis of rotation to precess around the magnetic field. Differing numbers of electrons will result in different amounts of shielding (σ), which in turn, alter the Larmor frequency, the frequency of the rotation of the nucleus around the magnetic field. These differing frequencies are visible as chemical shifts, the deviation between the frequency of the nucleus being analysed and a standard.

Four nuclei are commonly targeted when studying phospholipids with solid state NMR: ^{1}H, ^{13}C, ^{31}P, and ^{2}H for deuterated samples. Of the four, the first two are universally applied to lipid analysis, and magic angle spinning variants have been used to study the phospholipid orientation, lateral diffusion, and membrane dynamics (Schiller et al., 2007). The magic angle in question is 54.74° with respect to the magnetic field. This angle has been coined as "magic," due to the anisotropic nature of nuclear magnetic interactions. The orientation of the magnetic moment of the sample to the static magnet field will affect the energy levels and corresponding

resonance frequencies of the nuclei under analysis. Magic angle spinning is often used in solid-state NMR where the less mobile molecules do not average out anisotropic interactions, leaving broad bands with reduced sensitivity. When the sample is spun at the magic angle (54.74 °) many of these anisotropic interactions are averaged out at the cost of some structural and dynamic detail (Polenova et al., 2015). Often, a combination of nuclei must be analysed to investigate the inter- and intra-molecular interactions of phospholipids.

Although NMR techniques have been prolifically applied to investigate model membranes and sphingomyelin/cholesterol interactions, as mentioned in Section *2.6.2*. Little has been reported on structural analysis of milk derived phospholipids with NMR. In the dairy sciences, the technique, especially ^{31}P, is used to profile and characterize phospholipid species (MacKenzie, Vyssotski, & Nekrasov, 2009). The varying headgroups among dairy phospholipids result in different chemical shifts, and with the use of standards, phospholipids can be identified and quantified although this method was shown to be slightly less sensitive than the 2D thin layer chromatography (TLC) employed to separate dairy phospholipids extracted from fresh cream. (MacKenzie, Vyssotski, & Nekrasov, 2009). Phosphatidic acid and three other unidentifiable compounds were detected using the 2D-TLC system. These components represented 2.8% mol of the total phospholipid composition. Thus, in practice, ^{31}P NMR was capable of identifying and quantifying all major phospholipid types. Metabolomics is another area of focus for NMR in the dairy sciences, with ^{1}H, ^{13}C, and ^{31}P used to identify novel bioactive compounds (Sundekilde, Larsen, & Bertram, 2013).

One advantage NMR has over DSC, X-ray diffraction, and CLSM is that the L_o domains are visible rather than assumed to exist due to the broadening of a phase transition, disappearance of the hexagonal hydrocarbon packing peak, or the absence of fluorescence (Fig. 2.12). ^{2}H NMR and perdeuterated DDPC-d31and PSM-d31 (C16:0) are capable of distinguishing the structural features the S_o, L_o, and L_d phases. The L_d phase (A1, A2) consists of superimposed doublets, corresponding to a labelled carbon. The sharp repeating pattern represents the bond order – in the case of L_d, a high proportion of hydrocarbons are in the *gauche* conformation with lipids undergoing rapid isomerization and symmetric reorientation (Keyvanloo et al., 2018). The S_o phase (C1, C2) PSM and DPPC bell pattern show the opposite of the L_d phase, highly restricted movement due to the tilted *trans* conformation of the hydrocarbon chains. The L_o phase is an intermediate. Although it is an accurate representation of the three phases and their physical characters, it may be difficult to tell apart an L_o phase and a vesicle with L_d to S_o phases co-existing.

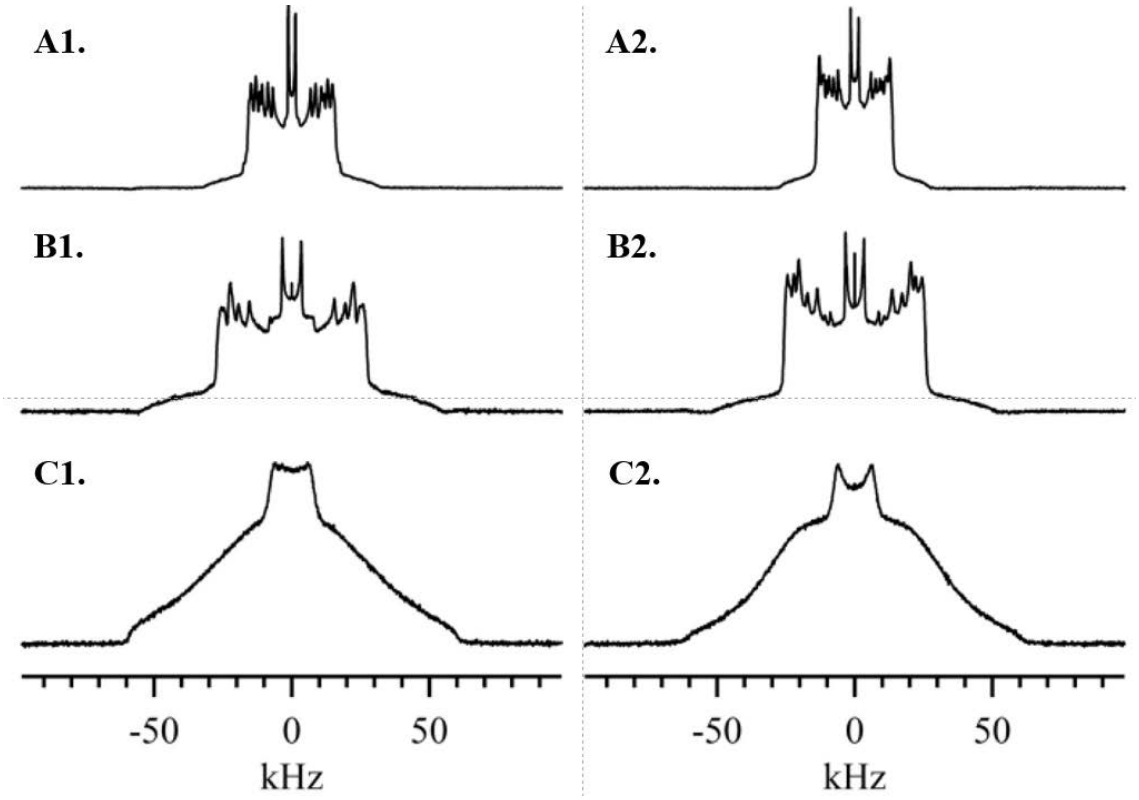

Figure 2.12. ^{2}H NMR spectra of PSM-31d and DPPC-31d MLVs, respectively. A1 and A2 L_d phase above 41 °C. B1 and B2 L_o phases with 40 mol % cholesterol at 48 °C. C1 and C2 S_o phase below 39 °C. Reproduced from Keyvanloo et al., (2018).

2.8.12 Electron spin resonance spectroscopy

Electron spin resonance (ESR) or otherwise known as electron paramagnetic spin resonance is similar to NMR; the analyte is placed within a static magnetic field and microwave radiation is applied. Unlike NMR which analyses the nucleus of individual atoms, ESR focuses on the interactions between the external magnetic field and unpaired electrons. In the membrane sciences, ESR is a complementary technique to NMR and vibrational spectroscopic methods. ESR is better suited for analysing the conformation of fluid hydrocarbon chains whereas Raman and infrared methods specialize in determining the order of hydrocarbon chains (Marsh, 1974).

As is, membrane bilayers lack paramagnetism, stable free radicals, also known as spin labels, must be incorporated into membrane to obtain a signal (Marsh, 1974). There are multiple methods for incorporating lipid spin labels into the bilayer – the most common is to dissolve the spin label in solvent (ethanol, methanol) which is added to the aqueous suspension of liposomes or vesicles. After centrifugation, the phospholipid pellet can be re-suspended in fresh buffer and the spin label reapplied until a high enough concentration of the spin label is present in the bilayer (Alshehab et al., 2019). Phospholipids labelled with a ESR sensitive doxyl radical on the sn-2 chain are also commercially available (Chachaty et al., 2005).

Recently, ESR has been used to measure the fluidity as well as changes in the local viscosity and polarity of the MFGM during simulated digestion (Alshehab et al., 2019). Rigidification of the MFGM due to the presence of bile salts is indicative of micellization. The authors also noted that after 5 min of incubation, phase separation was apparent. Adsorption of pancreatic lipase onto the MFGM increases surface pressure at the interface, loosening phospholipid hydrocarbon chains (Bagatolli & Mouritsen, 2013). When examined together, the bile salts adsorb more quickly to the MFGM phospholipid interface compared to the pancreatic lipase, thus the increased order in lateral packing from micellization dominates. From interpreting the data obtained from ESR experiments, a model describing the bile salt and pancreatic lipase interactions with MFGs was developed (Fig. 2.13).

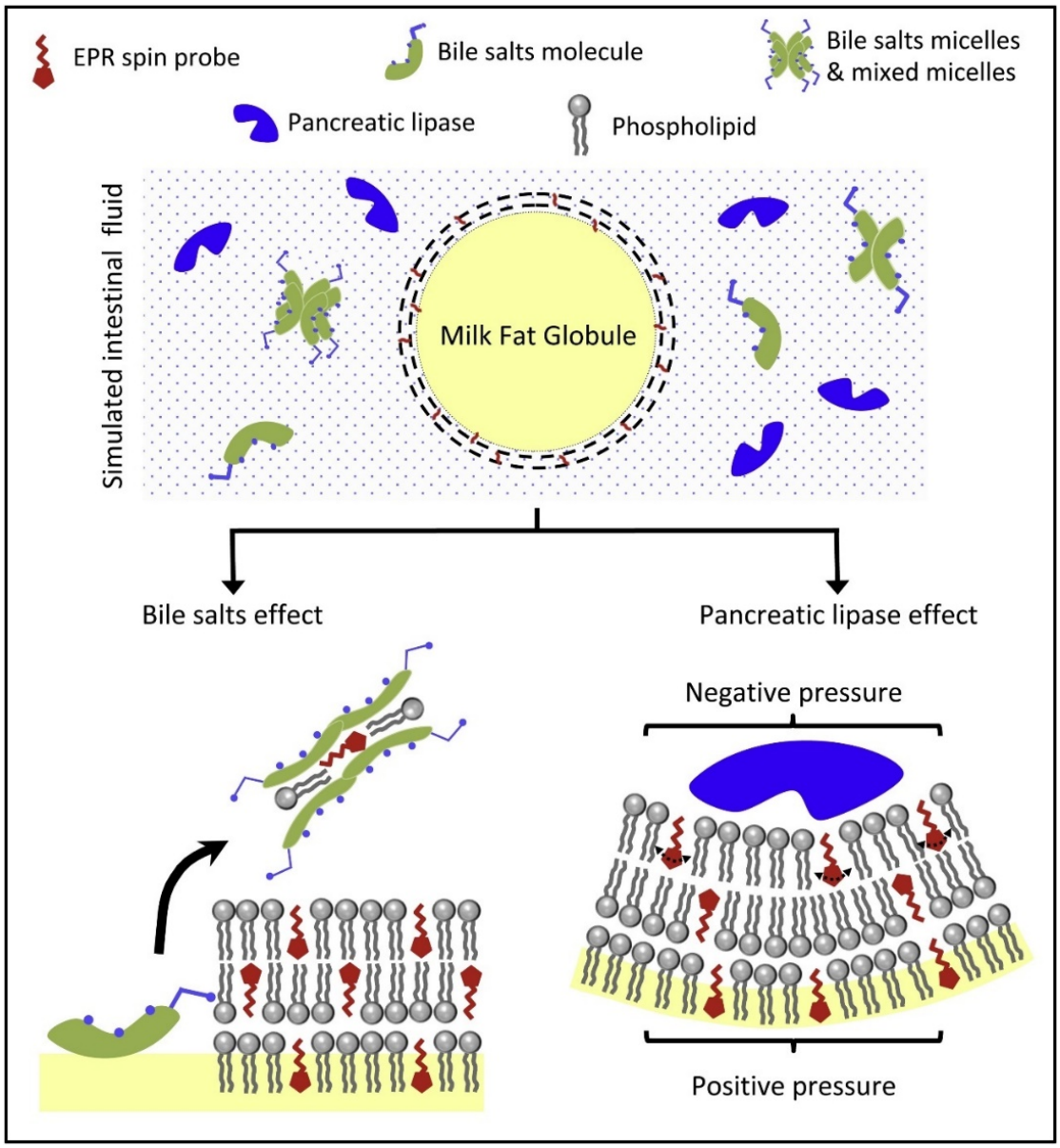

Figure 2.13 Schematic of possible MFGM interaction with bile salts and pancreatic lipase observed using ESR. Not to scale. Reproduced from Alshehab et al., (2019).

2.9 Conclusions

To shed light on the mechanism behind the many putative bioactive effects attributed to milk phospholipids, the structural complexity of the MFGM must be investigated. It is well understood in the current literature that phospholipid bedrock of the MFGM is structurally heterogenous. The boundaries are demarked by clusters of high T_m phospholipid species, of which sphingomyelin is noteworthy. The complexation of cholesterol to these regions that are rich in sphingomyelin, spawns L_o domains which are tightly packed together and are more structurally ordered than the bulk L_d domain of the membrane. The interaction between cholesterol and sphingomyelin has been hypothesized as the mechanism for the observed anticholesteremic effect of milk phospholipid consumption. The consumed sphingomyelin and cholesterol interact with the mixed micelles forming structures resistant to cholesterol uptake. Conversely, the idea of a complex that partially consists of cholesterol from an external source being responsible for modulating cholesterol uptake seems nonsensical, almost a Catch-22. Thus, the question becomes, for what purpose does cholesterol and therefore the L_o domains exist within the MFGM?

To answer such a question, the following gaps in the literature reviewed have been determined:

- The structural differences between L_o domains in model membranes and the native MFGM?
- The interactions between L_o domains and digestive biochemical factors?
- The resistance of L_o domain structures to gastrointestinal digestion?
- The impact of alk-SMase on L_o domain digestion as the phospholipase is not commonly included in *in vitro* digestion protocols.
- The role of the SM amide region and hydrogen bonding in the formation of L_o domains.
- The composition of the MFGM results in both nutritionally beneficial bioactive function and structural elements. It is unknown if the synergy between structural elements and composition is responsible for such bioactive effects.

This thesis will attempt to answers these questions, at least in part, using model membrane systems. As reviewed above, model membranes systems only offer a simplified version of reality. However, because these systems are simplified, an entire vesicle can be made into the L_o phase which is easier to study that L_o domains on a heterogenous membrane. These model systems offer valuable insights into the fundamental physical chemistry of the components that make up the MFGM. This is of great value not only due to the lucrative health benefits the MFGM is rightly renowned for, but also because lipid digestion is an interfacial process. The digestion of dairy products is unable to be truly understood without understanding how the interface of fat globules, the MFGM, is digested. This understanding is the first step to reverse

engineer these biological interfacial layers in artificial emulsion systems to better deliver nutrients and bioactive compounds among other biotechnological advances.

References

Aittoniemi, J., Niemelä, P. S., Hyvönen, M. T., Karttunen, M., & Vattulainen, I. (2007). Insight into the putative specific interactions between cholesterol, sphingomyelin, and palmitoyl-oleoyl phosphatidylcholine. *Biophysical Journal*, *92*(4), 1125–1137.

Alegria, A.; Garcia-Llatas, G.; Cilla, A. (2015). Static digestion models: General introduction. In D. Swiatecka, A. Mackie (Eds.), *The impact of food bioactives on health:* In vitro *and* ex vivo *models* (pp. 3-13). London, UK: Springer.

Alshehab, M., Budamagunta, M. S., Voss, J. C., & Nitin, N. (2019). Real-time measurements of milk fat globule membrane modulation during simulated intestinal digestion using electron paramagnetic resonance spectroscopy. *Colloids and Surfaces B: Biointerfaces*, *184*, 110511.

Anderson, M. (1982). Factors affecting the distribution of lipoprotein lipase activity between serum and casein micelles in bovine milk. *Journal of Dairy Research*, *49*(01), 51.

Angelova, M. I., Hristova, N., & Tsoneva, I. (1999). DNA-induced endocytosis upon local microinjection to giant unilamellar cationic vesicles. *European Biophysics Journal*, *28*(2), 142–150.

Argov, N., Lemay, D. G., & German, J. B. (2008). Milk fat globule structure and function: Nanoscience comes to milk production. *Trends in Food Science & Technology*, *19*(12), 617–623.

Arnulphi, C., Sot, J., García-Pacios, M., Arrondo, J.-L. R., Alonso, A., & Goñi, F. M. (2007). Triton X-100 partitioning into sphingomyelin bilayers at subsolubilizing detergent concentrations: Effect of lipid phase and a comparison with dipalmitoylphosphatidylcholine. *Biophysical Journal*, *93*(10), 3504–3514.

Arsov, Z., & Quaroni, L. (2008). Detection of lipid phase coexistence and lipid interactions in sphingomyelin/cholesterol membranes by ATR-FTIR spectroscopy. *Biochimica et Biophysica Acta (BBA) - Biomembranes*, *1778*(4), 880–889.

Bagatolli, L. A., & Gratton, E. (2000). Two photon fluorescence microscopy of coexisting lipid domains in giant unilamellar vesicles of binary phospholipid mixtures. *Biophysical Journal*, *78*(1), 290–305.

Bagatolli, L. A., & Mouritsen, O. G. (2013). Is the fluid mosaic (and the accompanying raft hypothesis) a suitable model to describe fundamental features of biological membranes? What may be missing? *Frontiers in Plant Science*, *4* (457). 1 – 6.

Bangham, A. D., Standish, M. M., & Watkins, J. C. (1965). Diffusion of univalent ions across the lamellae of swollen phospholipids. *Journal of Molecular Biology, 13(1)*, 238-282.

Barłowska, J., Litwińczuk, Z., Wolanciuk, A., & Brodziak, A. (2009). Relationship of somatic cell count to daily yield and technological usefulness of milk from. *Polish Journal of Veterinary Sciences*, *12*(1), 75–79.

Basáñez, G., Ruiz-Argüello, M. B., Alonso, A., Goñi, F. M., Karlsson, G., & Edwards, K. (1997). Morphological changes induced by phospholipase C and by sphingomyelinase on large unilamellar vesicles: A cryo-transmission electron microscopy study of liposome fusion. *Biophysical Journal*, *72*(6), 2630–2637.

Baumgartner, S., Kelly, E. R., van der Made, S., Berendschot, T. TJM., Husche, C., Lütjohann, D., & Plat, J. (2013). The influence of consuming an egg or an egg-yolk buttermilk drink for 12 wk on serum lipids, inflammation, and liver function markers in human volunteers. *Nutrition*, *29*(10), 1237–1244.

Batenjany, M. M., Wang, Z., Huang, C., & Levin, I. W. (1994). Bilayer packing characteristics of mixed chain phospholipid derivatives: Raman spectroscopic and differential scanning calorimetric studies of 1-stearoyl-2-capryl-sn-glycero-3-phosphocholine (C(18): C(10)PC) and 1-stearoyl-2-capryl-sn-glycero-3-phospho-N-trimethylpropanolamine (C(18): C(10)TMPC). *Biochimica et Biophysica Acta (BBA) - Biomembranes*, *1192*(2), 205–214.

Baxa, U. (2018). Imaging of liposomes by transmission electron microscopy. In S. E. McNeil (Ed.), *Characterization of Nanoparticles Intended for Drug Delivery* (Vol. 1682, pp. 73–88). New York, USA: Springer.

Ben-Avram, C. M., Ben-Zeev, O., Lee, T. D., Haaga, K., Shively, J. E., Goers, J., Pedersen, M. E., Reeve, J. R., & Schotz, M. C. (1986). Homology of lipoprotein lipase to pancreatic lipase. *Proceedings of the National Academy of Sciences*, *83*(12), 4185–4189.

Ben M'barek, K., Ajjaji, D., Chorlay, A., Vanni, S., Forêt, L., & Thiam, A. R. (2017). ER membrane phospholipids and surface tension control cellular lipid droplet formation. *Developmental Cell*, *41*(6), 591-604.

Bhattacharjee, S. (2016). DLS and zeta potential – What they are and what they are not? *Journal of Controlled Release*, *235*, 337–351.

Bitman, J., & Wood, D. L. (1990). Changes in milk fat phospholipids during lactation. *Journal of Dairy Science*, *73*(5), 1208–1216.

Bittman, R., Kasireddy, C. R., Mattjus, P., & Slotte, J. P. (1994). Interaction of cholesterol with sphingomyelin in monolayers and vesicles. *Biochemistry*, *33*(39), 11776–11781.

Björkbom, A., Róg, T., Kaszuba, K., Kurita, M., Yamaguchi, S., Lönnfors, M., Nyholm, T. K. M., Vattulainen, I., Katsumura, S., & Slotte, J. P. (2010). Effect of sphingomyelin headgroup size on molecular properties and interactions with cholesterol. *Biophysical Journal*, *99*(10), 3300–3308.

Boggs, J. M. (1987). Lipid intermolecular hydrogen bonding: Influence on structural organization and membrane function. *Biochimica et Biophysica Acta (BBA) - Reviews on Biomembranes*, *906*(3), 353–404.

Borchman, D., Tang, D., & Yappert, M. C. (1999). Lipid composition, membrane structure relationships in lens and muscle sarcoplasmic reticulum membranes. *Biospectroscopy*, *5*(3), 151–167.

Brodkorb, A., Egger, L., Alminger, M., Alvito, P., Assunção, R., Ballance, S., Bohn, T., Bourlieu-Lacanal, C., Boutrou, R., Carrière, F., Clemente, A., Corredig, M., Dupont, D., Dufour, C., Edwards, C., Golding, M., Karakaya, S., Kirkhus, B., Le Feunteun, S., … Recio, I. (2019). INFOGEST static in vitro simulation of gastrointestinal food digestion. *Nature Protocols*, *14*(4), 991–1014.

Carroll, S. M., DePeters, E. J., Taylor, S. J., Rosenberg, M., Perez-Monti, H., & Capps, V. A. (2006). Milk composition of Holstein, Jersey, and Brown Swiss cows in response to increasing levels of dietary fat. *Animal Feed Science and Technology*, *131*(3–4), 451–473.

Cevc, G. (1991). How membrane chain-melting phase-transition temperature is affected by the lipid chain asymmetry and degree of unsaturation: An effective chain-length model. *Biochemistry*, *30*(29), 7186–7193.

Chachaty, C., Rainteau, D., Tessier, C., Quinn, P. J., & Wolf, C. (2005). Building up of the liquid-ordered phase formed by sphingomyelin and cholesterol. *Biophysical Journal*, *88*(6), 4032–4044.

Chen, D., & Santore, M. M. (2014). 1,2-Dipalmitoyl- *sn* -glycero-3-phosphocholine (DPPC)-rich domain formation in binary phospholipid vesicle membranes: Two-dimensional nucleation and growth. *Langmuir*, *30*(31), 9484–9493.

Cheng, Y., Nilsson, Å., Tömquist, E., & Duan, R.-D. (2002). Purification, characterization, and expression of rat intestinal alkaline sphingomyelinase. *Journal of Lipid Research*, *43*(2), 316–324.

Cheng, K., Ropers, M.-H., & Lopez, C. (2017). The miscibility of milk sphingomyelin and cholesterol is affected by temperature and surface pressure in mixed Langmuir monolayers. *Food Chemistry*, *224*, 114–123.

Chichlowski, M., Bokulich, N., Harris, C. L., Wampler, J. L., Li, F., Berseth, C. L., Rudolph, C., & Wu, S. S. (2021). Effect of bovine milk fat globule membrane and lactoferrin in infant formula on gut microbiome and metabolome at 4 months of age. *Current Developments in Nutrition*, *5*(5), 1-9.

Chong, P. L.-G., Liu, F., Wang, M. M., Truong, K., Sugar, I. P., & Brown, R. E. (1996). Fluorescence evidence for cholesterol regular distribution in phosphatidylcholine and in sphingomyelin lipid bilayers. *Journal of Fluorescence*, *6*(4), 221–230.

Chu, B.-S., Gunning, A. P., Rich, G. T., Ridout, M. J., Faulks, R. M., Wickham, M. S. J., Morris, V. J., & Wilde, P. J. (2010). Adsorption of bile salts and pancreatic colipase and lipase onto digalactosyldiacylglycerol and dipalmitoylphosphatidylcholine monolayers. *Langmuir*, *26*(12), 9782–9793.

Chung, R. W. S., Kamili, A., Tandy, S., Weir, J. M., Gaire, R., Wong, G., Meikle, P. J., Cohn, J. S., & Rye, K.-A. (2013). Dietary sphingomyelin lowers hepatic lipid levels and inhibits intestinal cholesterol absorption in high-fat-fed mice. *PLoS ONE*, *8*(2), e55949.

Clulow, A. J., Salim, M., Hawley, A., & Boyd, B. J. (2018). A closer look at the behaviour of milk lipids during digestion. *Chemistry and Physics of Lipids*, *211*, 107–116.

Cohen, D. E., & Carey, M. C. (1991). Acyl chain unsaturation modulates distribution of lecithin molecular species between mixed micelles and vesicles in model bile. Implications for particle structure and metastable cholesterol solubilities. *Journal of Lipid Research. 32*, 1291-1302.

Cohen, B.-C., Raz, C., Shamay, A., & Argov-Argaman, N. (2017). Lipid Droplet Fusion in Mammary Epithelial Cells is Regulated by Phosphatidylethanolamine Metabolism. *Journal of Mammary Gland Biology and Neoplasia*, *22*(4), 235–249.

Cohn, J., Kamili, A., Wat, E., Chung, R. W., & Tandy, S. (2010). Dietary phospholipids and intestinal cholesterol absorption. *Nutrients*, *2*(2), 116–127.

Collado, M. I., Goñi, F. M., Alonso, A., & Marsh, D. (2005). Domain formation in sphingomyelin/cholesterol mixed membranes studied by spin-label electron spin resonance spectroscopy. *Biochemistry*, *44*(12), 4911–4918.

Conway, V., Couture, P., Richard, C., Gauthier, S. F., Pouliot, Y., & Lamarche, B. (2013). Impact of buttermilk consumption on plasma lipids and surrogate markers of cholesterol homeostasis in men and women. *Nutrition, Metabolism and Cardiovascular Diseases*, *23*(12), 1255–1262.

Conway, V., Gauthier, S. F., & Pouliot, Y. (2014). Buttermilk: Much more than a source of milk phospholipids. *Animal Frontiers*, *4*(2), 44–51.

Coreta-Gomes, F. M., Martins, P. A. T., Velazquez-Campoy, A., Vaz, W. L. C., Geraldes, C. F. G., & Moreno, M. J. (2015). Interaction of bile salts with model membranes mimicking the gastrointestinal epithelium: A study by isothermal titration calorimetry. *Langmuir*, *31*(33), 9097–9104.

Corstens, M. N., Osorio Caltenco, L. A., de Vries, R., Schroën, K., & Berton-Carabin, C. C. (2017). Interfacial behaviour of biopolymer multilayers: Influence of in vitro digestive conditions. *Colloids and Surfaces B: Biointerfaces*, *153*, 199–207.

Couvreur, S., Hurtaud, C., Marnet, P. G., Faverdin, P., & Peyraud, J. L. (2007). Composition of milk fat from cows selected for milk fat globule size and offered either fresh pasture or a corn silage-based diet. *Journal of Dairy Science*, *90*(1), 392–403.

Czamara, K., Majzner, K., Pacia, M. Z., Kochan, K., Kaczor, A., & Baranska, M. (2015). Raman spectroscopy of lipids: A review: Raman spectroscopy of lipids. *Journal of Raman Spectroscopy*, *46*(1), 4–20.

Dalgleish, D. G. (1984). Measurement of electrophoretic mobilities and zeta-potentials of particles from milk using laser Doppler electrophoresis. *Journal of Dairy Research*, *51*(3), 425–438.

Dalgleish, D. G., & Hallett, F. R. (1995). Dynamic light scattering: Applications to food systems. *Food Research International*, *28*(3), 181–193.

Danthine, S., Blecker, C., Paquot, M., Innocente, N., & Deroanne, C. (2000). Évolution des connaissances sur la membrane du globule gras du lait: Synthèse bibliographique. *Le Lait*, *80*(2), 209–222.

Deeth, H. (1997). The role of phospholipids in the stability of milk fat globules. *The Australian Journal of Dairy Technology. 52*, 44-46.

Dewettinck, K., Rombaut, R., Thienpont, N., Le, T. T., Messens, K., & Van Camp, J. (2008). Nutritional and technological aspects of milk fat globule membrane material. *International Dairy Journal*, *18*(5), 436–457.

Dimitrov, D. S., & Angelova, M. I. (1987). Lipid swelling and liposome formation on solid surfaces in external electric fields. In H. Hoffmann (Ed.), *New Trends in Colloid Science* (Vol. 73, pp. 48–56). Steinkopff.

Douëllou, T., Montel, M. C., & Thevenot Sergentet, D. (2017). Invited review: Anti-adhesive properties of bovine oligosaccharides and bovine milk fat globule membrane-associated glycoconjugates against bacterial food enteropathogens. *Journal of Dairy Science*, *100*(5), 3348–3359.

Dowhan, W., & Bogdanov, M. (2009). Lipid-Dependent Membrane Protein Topogenesis. *Annual Review of Biochemistry*, *78*(1), 515–540.

Duan, R.-D., Nyberg, L., & Nilsson, Å. (1995). Alkaline sphingomyelinase activity in rat gastrointestinal tract: Distribution and characteristics. *Biochimica et Biophysica Acta (BBA) - Lipids and Lipid Metabolism*, *1259*(1), 49–55.

Duan, R.-D., Hertervig, E., Nyberg, L., Hauge, T., Sternby, B., Lillienau, J., Farooqi, A., & Nilsson, Å. (1996). Distribution of alkaline sphingomyelinase activity in human beings and animals: Tissue and species differences. *Digestive Diseases and Sciences*, *41*(9), 1801–1806.

Duan, R., & Nilsson, A. (1997). Purification of a newly identified alkaline sphingomyelinase in human bile and effects of bile salts and phosphatidylcholine on enzyme activity. *Hepatology*, *26*(4), 823–830.

Duan, R.-D., Bergman, T., Xu, N., Wu, J., Cheng, Y., Duan, J., Nelander, S., Palmberg, C., & Nilsson, Å. (2003). Identification of human intestinal alkaline sphingomyelinase as a novel ecto-enzyme related to the nucleotide phosphodiesterase family. *Journal of Biological Chemistry*, *278*(40), 38528–38536.

Duan, R.-D., Cheng, Y., Hansen, G., Hertervig, E., Liu, J.-J., Syk, I., Sjöström, H., & Nilsson, Å. (2003). Purification, localization, and expression of human intestinal alkaline sphingomyelinase. *Journal of Lipid Research*, *44*(6), 1241–1250.

Duan, R., & Nilsson, A. (1997). Purification of a newly identified alkaline sphingomyelinase in human bile and effects of bile salts and phosphatidylcholine on enzyme activity. *Hepatology*, *26*(4), 823–830.

Duan, R. (2006). Alkaline sphingomyelinase: An old enzyme with novel implications. *Biochimica et Biophysica Acta (BBA) - Molecular and Cell Biology of Lipids*, *1761*(3), 281–291.

Duan, R.-D. (2007). Sphingomyelinase and ceramidase in the intestinal tract. *European Journal of Lipid Science and Technology*, *109*(10), 987–993.

Eckhardt, E. R. M., Moschetta, A., Renooij, W., Goerdayal, S. S., van Berge-Henegouwen, G. P., & van Erpecum, K. J. (1999). Asymmetric distribution of phosphatidylcholine and sphingomyelin between micellar and vesicular phases: Potential implications for canalicular bile formation. *Journal of Lipid Research, 40*, 2022-2033.

Eckhardt, E. R. M., Wang, D. Q. –H., Donovan, J. M., & Carey, M. C. (2002). Dietary sphingomyelin suppresses intestinal cholesterol absorption by decreasing thermodynamic activity of cholesterol monomers. *Gastroenterology*, *122*(4), 948–956.

Eckstein, J., Holzhütter, H.-G., & Berndt, N. (2018). The importance of membrane microdomains for bile salt-dependent biliary lipid secretion. *Journal of Cell Science*, *131*(5), jcs211524.

Et-Thakafy, O., Guyomarc'h, F., & Lopez, C. (2017). Lipid domains in the milk fat globule membrane: Dynamics investigated in situ in milk in relation to temperature and time. *Food Chemistry*, *220*, 352–361.

Et-Thakafy, O., Delorme, N., Gaillard, C., Mériadec, C., Artzner, F., Lopez, C., & Guyomarc'h, F. (2017 b). Mechanical properties of membranes composed of gel-phase or fluid-phase phospholipids probed on liposomes by atomic Force Spectroscopy. *Langmuir*, *33*(21), 5117–5126.

Et-Thakafy, O., Delorme, N., Guyomarc'h, F., & Lopez, C. (2018). Mechanical properties of milk sphingomyelin bilayer membranes in the gel phase: Effects of naturally complex heterogeneity, saturation and acyl chain length investigated on liposomes using AFM. *Chemistry and Physics of Lipids*, *210*, 47–59.

Evers, J. M. (2004). The milkfat globule membrane—Compositional and structural changes post secretion by the mammary secretory cell. *International Dairy Journal*, *14*(8), 661–674.

Evers, J. M., Haverkamp, R. G., Holroyd, S. E., Jameson, G. B., Mackenzie, D. D. S., & McCarthy, O. J. (2008). Heterogeneity of milk fat globule membrane structure and composition as observed using fluorescence microscopy techniques. *International Dairy Journal*, *18*(12), 1081–1089.

Evran, S., & Telefoncu, A. (2005). Modification of porcine pancreatic lipase with Z-Proline. *Preparative Biochemistry and Biotechnology*, *35*(3), 191–201.

Fenske, D. B., Jarrell, H. C., Guo, Y., & Hui, S. W. (1990). Effect of unsaturated phosphatidylethanolamine on the chain order profile of bilayers at the onset of the hexagonal phase transition. A deuterium NMR study. *Biochemistry*, *29*(51), 11222–11229.

Ferraretto, A., Pitto, M., Palestini, P., & Masserini, M. (1997). Lipid domains in the membrane: Thermotropic properties of sphingomyelin vesicles containing GM1 ganglioside and cholesterol, *Biochemistry, 36,* 9232-9236.

Franken, L. E., Grünewald, K., Boekema, E. J., & Stuart, M. C. (2020). A technical introduction to transmission electron microscopy for soft-matter: Imaging, possibilities, choices, and technical developments. *Small*, *16*(14), 1-15.

Filippov, A., Orädd, G., & Lindblom, G. (2006). Sphingomyelin structure influences the lateral diffusion and raft formation in lipid bilayers. *Biophysical Journal, 90(6)*, 2086–2092.

Gallier, S., Gragson, D., Cabral, C., Jiménez-Flores, R., & Everett, D. W. (2010 a). Composition and fatty acid distribution of bovine milk phospholipids from processed milk Products. *Journal of Agricultural and Food Chemistry*, *58*(19), 10503–10511.

Gallier, S., Gragson, D., Jiménez-Flores, R., & Everett, D. (2010 b). Using confocal laser scanning microscopy to probe the milk fat globule membrane and associated proteins. *Journal of Agricultural and Food Chemistry*, *58*(7), 4250–4257.

Gallier, S., Gragson, D., Jiménez-Flores, R., & Everett, D. W. (2010 c). Surface characterization of bovine milk phospholipid monolayers by Langmuir isotherms and microscopic techniques. *Journal of Agricultural and Food Chemistry*, *58*(23), 12275–12285.

Gallier, S., Gordon, K. C., Jiménez-Flores, R., & Everett, D. W. (2011). Composition of bovine milk fat globules by confocal Raman microscopy. *International Dairy Journal*, *21*(6), 402–412.

Gallier, S., Ye, A., & Singh, H. (2012). Structural changes of bovine milk fat globules during *in vitro* digestion. *Journal of Dairy Science*, *95*(7), 3579–3592.

Gallier, S., Cui, J., Olson, T. D., Rutherfurd, S. M., Ye, A., Moughan, P. J., & Singh, H. (2013 a). *In vivo* digestion of bovine milk fat globules: Effect of processing and interfacial structural changes. I. Gastric digestion. *Food Chemistry*, *141*(3), 3273–3281.

Gallier, S., Laubscher, A., & Jiménez-Flores, R. (2014 a). The milk fat globule membrane: Structure, methodology for its study, and functionality. M. Boland, M. Golding, H. Singh (Eds.) *Food structures, digestion and health* (1st edn, pp. 108-134). London, UK: Elsevier.

Gallier, S., Shaw, E., Laubscher, A., Gragson, D., Singh, H., & Jiménez-Flores, R. (2014 b). Adsorption of Bile Salts to Milk Phospholipid and Phospholipid–Protein Monolayers. *Journal of Agricultural and Food Chemistry*, *62*(6), 1363–1372.

Gallier, S., Vocking, K., Post, J. A., Van De Heijning, B., Acton, D., Van Der Beek, E. M., & Van Baalen, T. (2015). A novel infant milk formula concept: Mimicking the human milk fat globule structure. *Colloids and Surfaces B: Biointerfaces*, 136, 329–339.

Garmy, N., Taïeb, N., Yahi, N., & Fantini, J. (2005). Apical uptake and transepithelial transport of sphingosine monomers through intact human intestinal epithelial cells: Physicochemical and molecular modeling studies. *Archives of Biochemistry and Biophysics*, *440*(1), 91–100.

Gimpl, G., & Fahrenholz, F. (2001). The oxytocin receptor system: Structure, function, and regulation. *Physiological Reviews*, *81*(2), 629–683.

Gorelik, A., Liu, F., Illes, K., & Nagar, B. (2017). Crystal structure of the human alkaline sphingomyelinase provides insights into substrate recognition. *Journal of Biological Chemistry*, *292*(17), 7087–7094.

Guo, W., Kurze, V., Huber, T., Afdhal, N. H., Beyer, K., & Hamilton, J. A. (2002). A solid-state NMR study of phospholipid-cholesterol interactions: Sphingomyelin-cholesterol binary systems. *Biophysical Journal*, *83*(3), 1465–1478.

Guyomarc'h, F., Zou, S., Chen, M., Milhiet, P.-E., Godefroy, C., Vié, V., & Lopez, C. (2014). Milk sphingomyelin domains in biomimetic membranes and the role of cholesterol: Morphology and nanomechanical properties investigated using AFM and force spectroscopy. *Langmuir*, *30*(22), 6516–6524.

Guyomarc'h, F., Chen, M., Et-Thakafy, O., Zou, S., & Lopez, C. (2017). Gel-gel phase separation within milk sphingomyelin domains revealed at the nanoscale using atomic force microscopy. *Biochimica et Biophysica Acta (BBA) - Biomembranes*, *1859*(5), 949–958.

Hadaya, O., Bransi-Nicola, R., Shalev, Y., Azaizeh, H., Roth, Z., Muklada, H., Deutch, T., Landau, S. Y., & Argov-Argaman, N. (2020). Pistacia lentiscus extract enhances mammary epithelial cells' productivity by modulating their oxidative status. *Scientific Reports*, *10*(1), 20985.

Hamosh, M., Peterson, J. A., Henderson, T. R., Scallan, C. D., Kiwan, R., Ceriani, R. L., Armand, M., Mehta, N. R., & Hamosh, P. (1999). Protective function of human milk: The milk fat globule. *Seminars in Perinatology*, *23*(3), 242–249.

Hassan, P. A., Rana, S., & Verma, G. (2015). Making sense of Brownian motion: Colloid characterization by dynamic light scattering. *Langmuir*, *31*(1), 3–12.

Henry, D., Eby, N., Goodge, J., Mogk, D. (2018) X-ray reflection in accordance with Bragg's Law. Retrieved May 31, 2022, from https://serc.carleton.edu/msu_nanotech/methods/BraggsLaw.html

Heerklotz, H. (2004). The microcalorimetry of lipid membranes. *Journal of Physics: Condensed Matter*, *16*(15), R441–R467.

Heid, H. W., & Keenan, T. W. (2005). Intracellular origin and secretion of milk fat globules. *European Journal of Cell Biology*, 84(2–3), 245–258.

Hermida, L. G., Sabés-Xamaní, M., & Barnadas-Rodríguez, R. (2014). Characteristics and behaviour of liposomes when incubated with natural bile salt extract: Implications for their use as oral drug delivery systems. *Soft Matter*, *10*(35), 6677–6685.

Hofmann, A. F. (1999). The continuing importance of bile acids in liver and intestinal disease. *Archives of Internal Medicine*, *159*(22), 2647–2658.

Homan, R., & Hamelehle, K. L. (1998). Phospholipase A2 relieves phosphatidylcholine inhibition of micellar cholesterol absorption and transport by human intestinal cell line Caco-2. *Journal of Lipid Research. 39*, 1197-1209

Honary, S., & Zahir, F. (2013). Effect of Zeta Potential on the properties of nano-drug delivery systems—A review (Part 2). *Tropical Journal of Pharmaceutical Research*, *12*(2), 265–273.

Honvo-Houéto, E., Henry, C., Chat, S., Layani, S., & Truchet, S. (2016). The endoplasmic reticulum and casein-containing vesicles contribute to milk fat globule membrane. *Molecular Biology of the Cell*, *27*(19), 2946–2964.

Hope, H. R., & Pike, L. J. (1996). Phosphoinositides and phosphoinositide-utilizing enzymes in detergent-insoluble lipid domains. *Molecular Biology of the Cell*, *7*(6), 843–851.

Howards, A., & Marks, J. (1979). Effect of milk products on serum-cholesterol. *The Lancet 314* (8149), 957.

Huang, J.-B., & Zhao, G.-X. (1995). Formation and coexistence of the micelles and vesicles in mixed solution of cationic and anionic surfactant. *Colloid & Polymer Science*, *273*(2), 156–164.

Hunter, R. J. (2013). Zeta potential in colloid science: Principles and applications (Vol. 2). Academic press.

Huppertz, T.. & Kelly, A. L. (2006). Physical chemistry of milk fat globules. In P.F. Fox, P.L.H. McSweeney (Eds.), *Advanced dairy chemistry volume 2 Lipids* (3rd edn, pp. 173-222). Massachusetts, USA: Springer.

Imaizumi, K., Tominaga, A., Sato, M., & Sugano, M. (1992). Effects of dietary sphingolipids on levels of serum and liver lipids in rats. *Nutrition Research*, *12*(4–5), 543–548.

Israelachvili, J. N. (2010). Soft and biological structures. In *Intermolecular and surface forces* (3rd edn. pp. 535–576). Massachusetts, USA: Elsevier Science

Jaikishan, S., & Slotte, J. P. (2011). Effect of hydrophobic mismatch and interdigitation on sterol/sphingomyelin interaction in ternary bilayer membranes. *Biochimica et Biophysica Acta (BBA) - Biomembranes*, *1808*(7), 1940–1945.

Jeong, J., Lisinski, I., Kadegowda, A. K. G., Shin, H., Wooding, F. B. P., Daniels, B. R., Schaack, J., & Mather, I. H. (2013). A test of current models for the mechanism of milk-lipid droplet secretion: Mechanism of milk-lipid secretion. *Traffic*, *14*(9), 974–986.

Jiménez-Flores, R., & Brisson, G. (2008). The milk fat globule membrane as an ingredient: Why, how, when? *Dairy Science and Technology*, *88*(1), 5–18.

Kaasgaard, T., Mouritsen, O. G., & Jørgensen, K. (2003). Freeze/thaw effects on lipid-bilayer vesicles investigated by differential scanning calorimetry. *Biochimica et Biophysica Acta (BBA) - Biomembranes*, *1615*(1–2), 77–83.

Kalb, E., Frey, S., & Tamm, L. K. (1992). Formation of supported planar bilayers by fusion of vesicles to supported phospholipid monolayers. *Biochimica et Biophysica Acta (BBA) - Biomembranes*, *1103*(2), 307–316.

Keller, S. L., Radhakrishnan, A., & McConnell, H. M. (2000). Saturated phospholipids with high melting temperatures form complexes with cholesterol in monolayers. *The Journal of Physical Chemistry B*, *104*(31), 7522–7527.

Keyvanloo, A., Shaghaghi, M., Zuckermann, M. J., & Thewalt, J. L. (2018). The phase behaviour and organization of sphingomyelin/cholesterol membranes: A deuterium NMR Study. *Biophysical Journal*, *114*(6), 1344–1356.

Kobayashi, T., Shimizugawa, T., Osakabe, T., Watanabe, S., & Okuyama, H. (1997). A long-term feeding of sphingolipids affected the levels of plasma cholesterol and hepatic triacylglycerol but not tissue phospholipids and sphingolipids. *Nutrition Research*, *17*(1), 111–114.

Koynova, R., Tenchov, B. (2013) Phase transitions and phase behaviour of lipids. In G. C. K. Roberts (Ed), *Encyclopedia of Biophysics: P* (pp. 49). Berlin, Germany: Springer

Krafft, C., Neudert, L., Simat, T., & Salzer, R. (2005). Near infrared Raman spectra of human brain lipids. *Spectrochimica Acta Part A: Molecular and Biomolecular Spectroscopy*, *61*(7), 1529–1535.

Kulkarni, C. V., Wachter, W., Iglesias-Salto, G., Engelskirchen, S., & Ahualli, S. (2011). Monoolein: A magic lipid? *Phys. Chem. Chem. Phys.*, *13*(8), 3004–3021.

Lala, A. K. (1981). Cholesterol and phospholipids in membranes: The hydrogen bonding problem. *International Journal of Quantum Chemistry*, *20*(1), 93–97.

Lammert, F., & Wang, D. Q.-H. (2005). New insights into the genetic regulation of intestinal cholesterol absorption. *Gastroenterology*, *129*(2), 718–734.

Lee, C., & Bain, C. D. (2005). Raman spectra of planar supported lipid bilayers. *Biochimica et Biophysica Acta (BBA) - Biomembranes*, *1711*(1), 59–71.

Logan, A., Auldist, M., Greenwood, J., & Day, L. (2014). Natural variation of bovine milk fat globule size within a herd. *Journal of Dairy Science*, *97*(7), 4072–4082.

Lönnfors, M., Doux, J. P. F., Killian, J. A., Nyholm, T. K. M., & Slotte, J. P. (2011). Sterols have higher affinity for sphingomyelin than for phosphatidylcholine bilayers even at equal acyl-chain order. *Biophysical Journal*, *100*(11), 2633–2641.

Lopez, C., Briard-Bion, V., Beaucher, E., & Ollivon, M. (2008 a). Multiscale characterization of the organization of triglycerides and phospholipids in emmental cheese: From the microscopic to the molecular level. *Journal of Agricultural and Food Chemistry*, *56*(7), 2406–2414.

Lopez, C., Briard-Bion, V., Menard, O., Rousseau, F., Pradel, P., & Besle, J.-M. (2008 b). Phospholipid, sphingolipid, and fatty acid compositions of the milk fat globule membrane are modified by diet. *Journal of Agricultural and Food Chemistry*, *56*(13), 5226–5236.

Lopez, C., Madec, M.-N., & Jimenez-Flores, R. (2010). Lipid rafts in the bovine milk fat globule membrane revealed by the lateral segregation of phospholipids and heterogeneous distribution of glycoproteins. *Food Chemistry*, *120*(1), 22–33.

Lopez, C. (2011). Milk fat globules enveloped by their biological membrane: Unique colloidal assemblies with a specific composition and structure. *Current Opinion in Colloid & Interface Science*, *16*(5), 391–404.

Lopez, C., Briard-Bion, V., Ménard, O., Beaucher, E., Rousseau, F., Fauquant, J., Leconte, N., & Robert, B. (2011 a). Fat globules selected from whole milk according to their size: Different compositions and structure of the biomembrane, revealing sphingomyelin-rich domains. Food Chemistry, 125(2), 355–368.

Lopez, C., Cauty, C., & Guyomarc'h, F. (2018 a). Unravelling the complexity of milk fat globules to tailor bioinspired emulsions providing health benefits: The key role played by the biological membrane. *European Journal of Lipid Science and Technology, 121*, 1800201.

Lopez, C., Cheng, K., & Perez, J. (2018 b). Thermotropic phase behaviour of milk sphingomyelin and role of cholesterol in the formation of the liquid ordered phase examined using SR-XRD and DSC. *Chemistry and Physics of Lipids, 215*, 46–55.

Lopez, C., Cauty, C., & Guyomarc'h, F. (2015). Organization of lipids in milks, infant milk formulas and various dairy products: Role of technological processes and potential impacts. *Dairy Science & Technology*, *95*(6), 863–893.

Lopez, C. (2020). Intracellular origin of milk fat globules, composition and structure of the milk fat globule membrane highlighting the specific role of sphingomyelin. In P. L. H. McSweeney, P. F. Fox, & J. A. O'Mahony (Eds.), *Advanced Dairy Chemistry, Volume 2* (pp. 107–131). Switzerland: Springer International Publishing.

Lovegrove, J. A., & Givens, D. I. (2016). Dairy food products: Good or bad for cardiometabolic disease? *Nutrition Research Reviews, 29*(02), 249–267.

Lu, J., Argov-Argaman, N., Anggrek, J., Boeren, S., van Hooijdonk, T., Vervoort, J., & Hettinga, K. A. (2016). The protein and lipid composition of the membrane of milk fat globules depends on their size. *Journal of Dairy Science*, *99*(6), 4726–4738.

MacKenzie, A., Vyssotski, M., & Nekrasov, E. (2009). Quantitative analysis of dairy phospholipids by 31P NMR. *Journal of the American Oil Chemists' Society*, *86*(8), 757–763.

Maldonado-Valderrama, J., Wilde, P., Macierzanka, A., & Mackie, A. (2011). The role of bile salts in digestion. *Advances in Colloid and Interface Science*, *165*(1), 36–46.

Masedunskas, A., Chen, Y., Stussman, R., Weigert, R., & Mather, I. H. (2017). Kinetics of milk lipid droplet transport, growth, and secretion revealed by intravital imaging: Lipid droplet release is intermittently stimulated by oxytocin. *Molecular Biology of the Cell*, *28*(7), 935–946.

Marsh, D. (1974). Statistical mechanics of the fluidity of phospholipid bilayers and membranes. *The Journal of Membrane Biology*, *18*(1), 145–162.

Mather, I. H., & Keenan, T. W. (1998). Origin and Secretion of Milk Lipids. *Journal of Mammary Gland Biology and Neoplasia. 3*, 259-273.

Mather, I. H. (2000). A review and proposed nomenclature for major proteins of the milk-fat globule membrane,. *Journal of Dairy Science*, *83*(2), 203–247.

Mather, I. H. (2011) Milk lipids: Milk fat globule membrane. In J.W. Fuquay, P.F. Fox and P.L.H. McSweeney (Eds.), *Encyclopedia of dairy sciences* (2nd edn., pp. 680-690). San Diego, USA: Academic Press.

McConnell, H. M., & Radhakrishnan, A. (2003). Condensed complexes of cholesterol and phospholipids. *Biochimica et Biophysica Acta (BBA) - Biomembranes*, *1610*(2), 159–173.

McCullough, W. S., Perk, J. H. H., & Scott, H. L. (1990). Analysis of a model for the ripple phase of lipid bilayers. *The Journal of Chemical Physics*, *93*(8), 6070–6080.

McCullough, III, D. H., & Regen, S. L. (2004). Don't forget Langmuir–Blodgett films. *Chem. Commun.*, *24*, 2787–2791.

Ménard, O., Ahmad, S., Rousseau, F., Briard-Bion, V., Gaucheron, F., & Lopez, C. (2010). Buffalo vs. cow milk fat globules: Size distribution, zeta-potential, compositions in total fatty acids and in polar lipids from the milk fat globule membrane. *Food Chemistry*, *120*(2), 544–551.

McIntosh, T. J., Simon, S. A., Needham, D., & Huang, C. H. (1992). Structure and cohesive properties of sphingomyelin/cholesterol bilayers. *Biochemistry*, *31*(7), 2012–2020.

Mendes, A. A., Oliveira, P. C., & de Castro, H. F. (2012). Properties and biotechnological applications of porcine pancreatic lipase. *Journal of Molecular Catalysis B: Enzymatic*, *78*, 119–134.

Mesilati-Stahy, R., & Argov-Argaman, N. (2014). The relationship between size and lipid composition of the bovine milk fat globule is modulated by lactation stage. *Food Chemistry*, *145*, 562–570.

Michalski, M.-C. (2009). Specific molecular and colloidal structures of milk fat affecting lipolysis, absorption and postprandial lipemia. *European Journal of Lipid Science and Technology*, *111*(5), 413–431.

Minekus, M., Alminger, M., Alvito, P., Ballance, S., Bohn, T., Bourlieu, C., Carrière, F., Boutrou, R., Corredig, M., Dupont, D., Dufour, C., Egger, L., Golding, M., Karakaya, S., Kirkhus, B., Le Feunteun, S., Lesmes, U., Macierzanka, A., Mackie, A., … Brodkorb, A. (2014). A standardised static *in vitro* digestion method suitable for food – an international consensus. *Food Function.*, *5*(6), 1113–1124.

Moschetta, A., Frederik, P. M., Portincasa, P., vanBerge-Henegouwen, G. P., & van Erpecum, K. J. (2002). Incorporation of cholesterol in sphingomyelin-phosphatidylcholine vesicles has profound effects on detergent-induced phase transitions. *Journal of Lipid Research*, *43*(7), 1046–1053.

Monks, J., Dzieciatkowska, M., Bales, E. S., Orlicky, D. J., Wright, R. M., & McManaman, J. L. (2016). Xanthine oxidoreductase mediates membrane docking of milk-fat droplets but is not essential for apocrine lipid secretion: Xanthine oxidoreductase and milk fat secretion. *The Journal of Physiology*, *594*(20), 5899–5921.

Mulet-Cabero, A.-I., Egger, L., Portmann, R., Ménard, O., Marze, S., Minekus, M., Le Feunteun, S., Sarkar, A., Grundy, M. M.-L., Carrière, F., Golding, M., Dupont, D., Recio, I., Brodkorb, A., & Mackie, A. (2020). A standardised semi-dynamic *in vitro* digestion method suitable for food – an international consensus. *Food & Function*, *11*(2), 1702–1720.

Murthy, A. V. R., Guyomarc'h, F., & Lopez, C. (2016). Cholesterol decreases the size and the mechanical resistance to rupture of sphingomyelin rich domains, in lipid bilayers studied as a model of the milk fat globule membrane. *Langmuir*, *32*(26), 6757–6765.

Murthy, A. V. R., Guyomarc'h, F., & Lopez, C. (2018). Palmitoyl ceramide promotes milk sphingomyelin gel phase domains formation and affects the mechanical properties of the fluid phase in milk-SM/DOPC supported membranes. *Biochimica et Biophysica Acta (BBA) - Biomembranes*, *1860*(3), 635–644.

Nicolson, G. L. (2014). The fluid—mosaic model of membrane structure: Still relevant to understanding the structure, function and dynamics of biological membranes after more than 40 years. *Biochimica et Biophysica Acta (BBA) - Biomembranes*, *1838*(6), 1451–1466.

Noh, S. K., & Koo, S. I. (2003). Egg sphingomyelin lowers the lymphatic absorption of cholesterol and α-tocopherol in rats. *The Journal of Nutrition*, *133*(11), 3571–3576.

Noh, S. K., & Koo, S. I. (2004). Milk sphingomyelin is more effective than egg sphingomyelin in inhibiting intestinal absorption of cholesterol and fat in rats. *The Journal of Nutrition*, *134*(10), 2611–2616.

Norris, G. H., Jiang, C., Ryan, J., Porter, C. M., & Blesso, C. N. (2016). Milk sphingomyelin improves lipid metabolism and alters gut microbiota in high fat diet-fed mice. *The Journal of Nutritional Biochemistry*, *30*, 93–101.

Nyberg, L., Duan, R.-D., Axelson, J., & Nilsson, Å. (1996). Identification of an alkaline sphingomyelinase activity in human bile. *Biochimica et Biophysica Acta (BBA) - Lipids and Lipid Metabolism*, *1300*(1), 42–48.

Nyberg, L., Nilsson, Å., Lundgren, P., & Duan, R.-D. (1997). Localization and capacity of sphingomyelin digestion in the rat intestinal tract. *The Journal of Nutritional Biochemistry*, *8*(3), 112–118.

Nyberg, L., Duan, R.-D., & Nilsson, Å. (2000). A mutual inhibitory effect on absorption of sphingomyelin and cholesterol. *The Journal of Nutritional Biochemistry*, *11*(5), 244–249.

Obeid, S., Guyomarc'h, F., David-Briand, E., Gaucheron, F., Riaublanc, A., & Lopez, C. (2019). The phase and charge of milk polar lipid membrane bilayers govern their selective interactions with proteins as demonstrated with casein micelles. *Journal of Colloid and Interface Science*, *534*, 279–290.

Ohlsson, L., Hertervig, E., Jönsson, B. A., Duan, R.-D., Nyberg, L., Svernlöv, R., & Nilsson, Å. (2010). Sphingolipids in human ileostomy content after meals containing milk sphingomyelin. *The American Journal of Clinical Nutrition*, *91*(3), 672–678.

Okotrub, K. A., Zykova, V. A., Adichtchev, S. V., & Surovtsev, N. V. (2020). Deciphering the orientation of lipid molecules by principal component analysis of Raman mapping data. *The Analyst*, *145*(4), 1466–1472.

Olsson, M., Duan, R.-D., Ohlsson, L., & Nilsson, Å. (2004). Rat intestinal ceramidase: Purification, properties, and physiological relevance. *American Journal of Physiology-Gastrointestinal and Liver Physiology*, *287*(4), G929–G937.

O'Riordan, N., Kane, M., Joshi, L., & Hickey, R. M. (2014). Structural and functional characteristics of bovine milk protein glycosylation. *Glycobiology*, *24*(3), 220–236.

Pafumi, Y., Lairon, D., de la Porte, P. L., Juhel, C., Storch, J., Hamosh, M., & Armand, M. (2002). Mechanisms of inhibition of triacylglycerol hydrolysis by human gastric lipase. *Journal of Biological Chemistry*, 277(31), 28070–28079.

Pandit, S. A., Bostick, D., & Berkowitz, M. L. (2004). Complexation of phosphatidylcholine lipids with cholesterol. *Biophysical Journal*, *86*(3), 1345–1356.

Patton, S., Borgström, B., Stemberger, B. H., & Welsch, U. (1986). Release of Membrane from Milk Fat Globules by Conjugated Bile Salts. *Journal of Pediatric Gastroenterology and Nutrition*, *5*(2), 262-267.

Pike, L. J. (2004). Lipid rafts: Heterogeneity on the high seas. *Biochemical Journal*, *378*(2), 281–292.

Pike, L. J. (2006). Rafts defined: A report on the Keystone symposium on lipid rafts and cell function. *Journal of Lipid Research*, *47*(7), 1597–1598.

Polenova, T., Gupta, R., & Goldbourt, A. (2015). Magic angle spinning NMR spectroscopy: A versatile technique for structural and dynamic analysis of solid-phase systems. *Analytical Chemistry*, *87*(11), 5458–5469.

Prenner, E., & Chiu, M. (2011). Differential scanning calorimetry: An invaluable tool for a detailed thermodynamic characterization of macromolecules and their interactions. *Journal of Pharmacy and Bioallied Sciences*, *3*(1), 39.

Quinn, P. J., & Wolf, C. (2009). The liquid-ordered phase in membranes. *Biochimica et Biophysica Acta (BBA) - Biomembranes*, *1788*(1), 33–46.

Quinn, P. J. (2013). Structure of sphingomyelin bilayers and complexes with cholesterol forming membrane rafts. *Langmuir*, *29*(30), 9447–9456.

Radhakrishnan, A., & McConnell, H. M. (1999). Condensed complexes of cholesterol and phospholipids. *Biophysical Journal*, *77*, 1507 – 1517.

Radhakrishnan, A., Li, X.-M., Brown, R. E., & McConnell, H. M. (2001). Stoichiometry of cholesterol–sphingomyelin condensed complexes in monolayers. *Biochimica et Biophysica Acta (BBA) - Biomembranes*, *1511*(1), 1–6.

Ramprasath, V. R., Jones, P. J., Buckley, D. D., Woollett, L. A., & Heubi, J. E. (2013). Effect of dietary sphingomyelin on absorption and fractional synthetic rate of cholesterol and serum lipid profile in humans. *Lipids in Health and Disease*, *12*(1), 125.

Real Hernandez, L., & Jimenez-Flores, R. (2019). Preparation of non-surface-active Langmuir trough subphases from milk. *ACS Omega*, *4*(12), 14920–14927.

Reeves, J. P., & Dowben, R. M. (1969). Formation and properties of thin-walled phospholipid vesicles. *Journal of Cellular Physiology*, *73*(1), 49–60.

Reif, B., Ashbrook, S. E., Emsley, L., & Hong, M. (2021). Solid-state NMR spectroscopy. *Nature Reviews Methods Primers*, *1*(2), 1 – 23.

Reigada, R. (2011). Influence of chloroform in liquid-ordered and liquid-disordered phases in lipid membranes. *The Journal of Physical Chemistry B*, *115*(11), 2527–2535.

Reinhardt, T. A., & Lippolis, J. D. (2006). Bovine milk fat globule membrane proteome. *Journal of Dairy Research*, *73*(04), 406-416.

Robson, A.-L., Dastoor, P. C., Flynn, J., Palmer, W., Martin, A., Smith, D. W., Woldu, A., & Hua, S. (2018). Advantages and limitations of current imaging techniques for characterizing liposome morphology. *Frontiers in Pharmacology*, *9* (80), 1 – 8.

Ros, E. (2000). Intestinal absorption of triglyceride and cholesterol. Dietary and pharmacological inhibition to reduce cardiovascular risk. *Atherosclerosis*, *151*(2), 357–379.

Rosqvist, F., Smedman, A., Lindmark-Månsson, H., Paulsson, M., Petrus, P., Straniero, S., Rudling, M., Dahlman, I., & Risérus, U. (2015). Potential role of milk fat globule membrane in modulating plasma lipoproteins, gene expression, and cholesterol metabolism in humans: A randomized study. *The American Journal of Clinical Nutrition*, *102*(1), 20–30.

Rowlands, L. J., Marks, A., Sanderson, J. M., & Law, R. V. (2020). ^{17}O NMR spectroscopy as a tool to study hydrogen bonding of cholesterol in lipid bilayers. *Chemical Communications*, *56*(92), 14499–14502.

Roy, D., Ye, A., Moughan, P. J., & Singh, H. (2021). Impact of gastric coagulation on the kinetics of release of fat globules from milk of different species. *Food & Function*, *12*(4), 1783–1802.

Salentinig, S., Sagalowicz, L., Leser, M. E., Tedeschi, C., & Glatter, O. (2011). Transitions in the internal structure of lipid droplets during fat digestion. *Soft Matter*, *7*(2), 650–661.

Salentinig, S., Phan, S., Khan, J., Hawley, A., & Boyd, B. J. (2013). Formation of highly organized nanostructures during the digestion of milk. *ACS Nano*, *7*(12), 10904–10911.

Scott, H. L., & McCullough, W. S. (1993). Lipid-cholesterol interactions in the P beta' phase. Application of a statistical mechanical model. *Biophysical Journal*, *64*(5), 1398–1404.

Schiller, J., Muller, M., Fuchs, B., Arnold, K., & Huster, D. (2007). 31P NMR spectroscopy of phospholipids: From micelles to membranes. *Current Analytical Chemistry*, *3*(4), 283–301.

Simons, K., & Ikonen, E. (1997). Functional rafts in cell membranes. *Nature*. *387*, 569-572.

Smith, P., Quinn, P. J., & Lorenz, C. D. (2020). Two coexisting membrane structures are defined by lateral and transbilayer interactions between sphingomyelin and cholesterol. *Langmuir*, *36*(33), 9786–9799.

Simons, K., & Vaz, W. L. C. (2004). Model systems, lipid rafts, and cell membranes. *Annual Review of Biophysics and Biomolecular Structure*, *33*(1), 269–295.

Singh, H., & Gallier, S. (2017). Nature's complex emulsion: The fat globules of milk. *Food Hydrocolloids*, *68*, 81–89.

Shirota, K., Yagi, K., Inaba, T., Li, P.-C., Murata, M., Sugita, Y., & Kobayashi, T. (2016). Detection of sphingomyelin clusters by Raman spectroscopy. *Biophysical Journal*, *111*(5), 999–1007.

Skočaj, M., Resnik, N., Grundner, M., Ota, K., Rojko, N., Hodnik, V., Anderluh, G., Sobota, A., Maček, P., Veranič, P., & Sepčić, K. (2014). Tracking cholesterol/sphingomyelin-rich membrane domains with the ostreolysin A-mCherry protein. *PLoS ONE*, *9*(3), e92783.

Slotte, J. P. (2016). The importance of hydrogen bonding in sphingomyelin's membrane interactions with co-lipids. *Biochimica et Biophysica Acta (BBA) - Biomembranes*, *1858*(2), 304–310.

Somerharju, P., Virtanen, J. A., & Cheng, K. H. (1999). Lateral organisation of membrane lipids: The superlattice view. *Biochimica et Biophysica Acta*, *17*, 32-48.

` Somerharju, P., Virtanen, J. A., Cheng, K. H., & Hermansson, M. (2009). The superlattice model of lateral organization of membranes and its implications on membrane lipid homeostasis. *Biochimica et Biophysica Acta (BBA) - Biomembranes*, *1788*(1), 12–23.

Sot, J., Ibarguren, M., Busto, J. V., Montes, L.-R., Goñi, F. M., & Alonso, A. (2008). Cholesterol displacement by ceramide in sphingomyelin-containing liquid-ordered domains, and generation of gel regions in giant lipidic vesicles. *FEBS Letters*, *582*(21–22), 3230–3236.

Smoczyński, M., & Staniewski, B. (2014). Saliva-induced flocculation of milk fat globules studied by image analysis. *Journal of International Scientific Publications: Agriculture and Food*, 2, 542-548.

Smondyrev, A. M., & Berkowitz, M. L. (1999). Structure of dipalmitoylphosphatidylcholine/cholesterol bilayer at low and high cholesterol concentrations: Molecular dynamics simulation. *Biophysical Journal*, *77*(4), 2075–2089.

Sodt, A. J., Pastor, R. W., & Lyman, E. (2015). Hexagonal substructure and hydrogen bonding in liquid-ordered phases containing palmitoyl sphingomyelin. *Biophysical Journal*, *109*(5), 948–955.

Somaratne, G., Ferrua, M. J., Ye, A., Nau, F., Floury, J., Dupont, D., & Singh, J. (2020). Food material properties as determining factors in nutrient release during human gastric digestion: A review. *Critical Reviews in Food Science and Nutrition*, *60*(22), 3753–3769.

Spitsberg, V. L. (2005). Invited review: Bovine milk fat globule membrane as a potential nutraceutical. *Journal of Dairy Science*, *88*(7), 2289–2294.

Stuart, B. (2015). Infrared spectroscopy. In John Wiley & Sons Inc (Ed.), *Kirk-Othmer Encyclopedia of Chemical Technology* (pp. 1–18). John Wiley & Sons, Inc.

Suys, E. J. A., Warren, D. B., Porter, C. J. H., Benameur, H., Pouton, C. W., & Chalmers, D. K. (2017). Computational models of the intestinal environment. 3. The impact of cholesterol content and pH on mixed micelle colloids. *Molecular Pharmaceutics*, *14*(11), 3684–3697.

Sundekilde, U., Larsen, L., & Bertram, H. (2013). NMR-Based milk metabolomics. *Metabolites*, *3*(2), 204–222.

Tamm, L. K., & McConnell, H. M. (1985). Supported phospholipid bilayers. *Biophysical Journal*, *47*(1), 105–113.

Thompson, R. F., Walker, M., Siebert, C. A., Muench, S. P., & Ranson, N. A. (2016). An introduction to sample preparation and imaging by cryo-electron microscopy for structural biology. *Methods*, *100*, 3–15.

Thum, C., Roy, N. C., Everett, D. W., & McNabb, W. C. (2021). Variation in milk fat globule size and composition: A source of bioactives for human health. *Critical Reviews in Food Science and Nutrition*, 1–27.

Thurnhofer, H., & Hauser, H. (1990). Uptake of cholesterol by small intestinal brush border membrane is protein-mediated. *Biochemistry*, *29*(8), 2142–2148.

Tokudome, Y., Uchida, R., Yokote, T., Todo, H., Hada, N., Kon, T., Yasuda, J., Hayashi, H., Hashimoto, F., & Sugibayashi, K. (2010). Effect of topically applied sphingomyelin-based liposomes on the ceramide level in a three-dimensional cultured human skin model. *Journal of Liposome Research*, *20*(1), 49–54.

Turkyilmaz, S., Chen, W.-H., Mitomo, H., & Regen, S. L. (2009). Loosening and reorganization of fluid phospholipid bilayers by chloroform. *Journal of the American Chemical Society*, *131*(14), 5068–5069.

van Erpecum, K. J., & Carey, M. C. (1997). Influence of bile salts on molecular interactions between sphingomyelin and cholesterol: Relevance to bile formation and stability. *Biochimica et Biophysica Acta (BBA) - Lipids and Lipid Metabolism*, *1345*(3), 269–282.

Vandenabeele, P. (2013). *Practical Raman spectroscopy: An introduction*. West Sussex; Wiley.

Veiga, M. P., Arrondo, J. L. R., Goñi, F. M., Alonso, A., & Marsh, D. (2001). Interaction of cholesterol with sphingomyelin in mixed membranes containing phosphatidylcholine, studied by spin-label ESR and IR spectroscopies. A possible stabilization of gel-phase sphingolipid domains by cholesterol. *Biochemistry*, *40*(8), 2614–2622.

Virtanen, J., Ruonala, M., Vauhkonen, M., & Somerharju, P. (1995). Lateral organization of liquid-crystalline cholesterol-dimyristoylphosphatidylcholine bilayers. Evidence for domains

with hexagonal and centered rectangular cholesterol superlattices. *Biochemistry*, *34*(36), 11568–11581.

Vors, C., Joumard-Cubizolles, L., Lecomte, M., Combe, E., Ouchchane, L., Drai, J., Raynal, K., Joffre, F., Meiller, L., Le Barz, M., Gaborit, P., Caille, A., Sothier, M., Domingues-Faria, C., Blot, A., Wauquier, A., Blond, E., Sauvinet, V., Gésan-Guiziou, G., … Michalski, M.-C. (2019). Milk polar lipids reduce lipid cardiovascular risk factors in overweight postmenopausal women: Towards a gut sphingomyelin-cholesterol interplay. *Gut*, 318155.

Walstra, P., Wouters, J., Geurts, T. (2006). *Dairy science and technology* (2nd edn., Chapt. 3).

Florida, USA: Taylor & Francis Group, LLC.

Williams, D. B., & Carter, C. B. (1996). The transmission electron microscope. In *Transmission electron microscopy* (pp. 3–17). Springer.

Wiking, L., Stagsted, J., Björck, L., & Nielsen, J. H. (2004). Milk fat globule size is affected by fat production in dairy cows. *International Dairy Journal*, *14*(10), 909–913.

Witkowska, A., Jablonski, L., & Jahn, R. (2018). A convenient protocol for generating giant unilamellar vesicles containing SNARE proteins using electroformation. *Scientific Reports*, *8*(1), 1–8.

Wooding, F. B. P. (1971). The mechanism of secretion of the milk fat globule. *Journal of Cell Science, 9,* 805-821.

Wooding, F. B. P., & Sargeant, T. J. (2015). Immunocytochemical evidence for Golgi vesicle involvement in milk fat globule secretion. *Journal of Histochemistry & Cytochemistry*, *63*(12), 943–951.

Wooding, F. B. P., & Mather, I. H. (2017). Ultrastructural and immunocytochemical evidence for the reorganisation of the milk fat globule membrane after secretion. *Cell and Tissue Research*, *367*(2), 283–295.

Wu, C. C., Howell, K. E., Neville, M. C., Yates, J. R., & McManaman, J. L. (2000). Proteomics reveal a link between the endoplasmic reticulum and lipid secretory mechanisms in mammary epithelial cells. *Electrophoresis*, *21*(16), 3470–3482.

Wu, J., Cheng, Y., Palmberg, C., Bergman, T., Nilsson, Å., & Duan, R.-D. (2005). Cloning of alkaline sphingomyelinase from rat intestinal mucosa and adjusting of the hypothetical protein XP_221184 in GenBank. *Biochimica et Biophysica Acta (BBA) - Molecular and Cell Biology of Lipids*, *1687*(1–3), 94–102.

Yagi, K., Li, P.-C., Shirota, K., Kobayashi, T., & Sugita, Y. (2015). A weight averaged approach for predicting amide vibrational bands of a sphingomyelin bilayer. *Physical Chemistry Chemical Physics*, *17*(43), 29113–29123.

Yang, F., Chen, G., Ma, M., Qiu, N., Zhu, L., & Li, J. (2018). Egg-yolk sphingomyelin and phosphatidylcholine attenuate cholesterol absorption in Caco-2 cells. *Lipids*, *53*(2), 217–233.

Yao, Y., Zhao, G., Xiang, J., Zou, X., Jin, Q., & Wang, X. (2016 a). Lipid composition and structural characteristics of bovine, caprine and human milk fat globules. *International Dairy Journal*, *56*, 64–73.

Yao, Y., Zhao, G., Yan, Y., Mu, H., Jin, Q., Zou, X., & Wang, X. (2016 b). Milk fat globules by confocal Raman microscopy: Differences in human, bovine and caprine milk. *Food Research International*, *80*, 61–69.

Yasuda, T., Kinoshita, M., Murata, M., & Matsumori, N. (2014). Detailed comparison of deuterium quadrupole profiles between sphingomyelin and phosphatidylcholine bilayers. *Biophysical Journal*, *106*(3), 631–638.

Ye, A., Singh, H., Taylor, M. W., & Anema, S. (2002). Characterization of protein components of natural and heat-treated milk fat globule membranes. *International Dairy Journal*, *12*(4), 393–402.

Ye, A., Cui, J., & Singh, H. (2010). Effect of the fat globule membrane on in vitro digestion of milk fat globules with pancreatic lipase. *International Dairy Journal*, *20*(12), 822–829.

Ye, A., Cui, J., & Singh, H. (2011). Proteolysis of milk fat globule membrane proteins during in vitro gastric digestion of milk. *Journal of Dairy Science*, *94*(6), 2762–2770.

Zheng, H., Jiménez-Flores, R., & Everett, D. W. (2014 a). Lateral lipid organization of the bovine milk fat globule membrane is revealed by washing processes. *Journal of Dairy Science*, *97*(10), 5964–5974.

Zheng, H., Jiménez-Flores, R., Gragson, D., & Everett, D. W. (2014 b). Phospholipid architecture of the bovine milk fat globule membrane using giant unilamellar vesicles as a model. *Journal of Agricultural and Food Chemistry*, *62*(14), 3236–3243.

Zhou, Y., Maxwell, K. N., Sezgin, E., Lu, M., Liang, H., Hancock, J. F., Dial, E. J., Lichtenberger, L. M., & Levental, I. (2013). Bile acids modulate signaling by functional perturbation of plasma membrane domains. *Journal of Biological Chemistry*, *288*(50), 35660–35670.

Zidar, J., Merzel, F., Hodošček, M., Rebolj, K., Sepčić, K., Maček, P., & Janežič, D. (2009). Liquid-ordered phase formation in cholesterol/sphingomyelin bilayers: All-atom molecular dynamics simulations. *The Journal of Physical Chemistry B*, *113*(48), 15795–15802.

Chapter 3 – Milk sphingomyelin/cholesterol multilamellar vesicles and properties

3.1 Introduction

Bovine milk structure plays a large role in determining nutrient bioavailability during digestion. Compared to bovine milk protein microstructure, the role of bovine milk lipid microstructure during digestion is less well-known and more difficult to study, owing to many confounding factors that obscure the exact mechanisms of action. There is growing interest in food products that mimic "natural" products, such as milk (Gallier et al., 2015) which makes understanding the changes in bovine milk lipid microstructure during digestion and its effect on human health a worthwhile pursuit.

Paramount to infant nutrition and lauded for its multitude of bioactive components, the MFGM is a complex phospholipid trilayer embedded with transmembrane glycosylated proteins. First believed to follow the homogenous fluid-mosaic model (Dewettinck et al., 2008), the lateral structure of the MFGM has later been shown to be heterogenous (Gallier et al., 2010 a). Lateral liquid ordered (L_o) domains enriched with sphingomyelin and cholesterol, which are analogous to the lipid rafts structures found in cell membranes (Lopez, 2020), exist predominately in the outer leaflet of the MFGM. The exact function of these unique domains is unknown.

Quantifying the behaviour of the native L_o domains in the MFGM has always been elusive due to their small size. Liquid ordered domains situated on the surface of the MFGM were first uncovered by confocal laser scanning microscopy using fluorescent lecithin probes and hypothesized to be glycosylated compounds that exist between the phospholipid inner leaflet and triacylglyceride core of damaged bilayers (Evers et al., 2008). This technique was later refined with exogenous phospholipid DOPE head-labelled fluorescent rhodamine dye (Rd-DOPE) (Gallier et al., 2010 a; Lopez, Madec, & Jimenez-Flores, 2010) and atomic force microscopy to show that these putative domains were not gaps in the bilayer but heterogenous regions of tightly packed sphingomyelin and cholesterol (Gallier et al., 2010 b) that possess different mechanical properties to the bulk liquid disordered (L_d) phase (Guyomarc'h et al., 2014; Murthy, Guyomarc'h, & Lopez, 2016).

Further investigation of the molecular properties of L_o domains has often required the creation of model membrane systems using binary and ternary blends of phospholipids and sphingolipids (most commonly consisting of a single species with identical alkyl chains). Phase diagrams that delineate phase transitions of various phospholipid blend have been assembled using electron spin resonance (Chiang et al., 2004), nuclear magnetic resonance (Hsueh, Zuckermann, & Thewalt, 2005), and differential scanning calorimetry (Svetlovics, Wheaten, & Almedia., 2012). Differential scanning calorimetry is a workhorse technique for membrane studies used to assess the effect of cholesterol on the thermotropic behaviour of phospholipid bilayer systems (Lopez, Cheng, & Perez, 2018). If

cholesterol is interacting with the phospholipid to form L_o domains, the size of the phase transition peak decreases as the concentration of cholesterol increases (Jobin & Alves, 2019). Similar information can be obtained by wide angle x-ray scattering (WAXS) where the dissolution of the solid ordered (S_o) phase can be measured with the disappearance of the Bragg peak that represents hexagonal packing ($q = 1.51\ Å^{-1}$) whereas small angle x-ray scattering (SAXS) resolves the lamellar repeat d-spacing, the thickness of a bilayer. Finally, vibrational spectroscopy is capable of delving into the molecular order of phospholipid hydrocarbon chains. All the aforementioned techniques have been individually used to elucidate the phase state of vesicle systems comprising of phospholipids, but rarely in concert.

The major objectives for this preliminary study were: 1) construct a model membrane system that contains measurable L_o domains; 2) determine whether it is possible to measure SM and cholesterol interactions at physiologically relevant concentrations; and 3) ensure this membrane system and the instruments used were practical for investigating the digestive behaviour of model membrane systems.

3.2 Methods and Materials

3.2.1 Phospholipid vesicle systems

A multilamellar vesicle (MLV) system was created from milk sphingomyelin and cholesterol using thin layer dispersion (Bangham, Standish, & Weissmann, 1965; Isalomboto Nkanga et al., 2019). Vesicle creation closely resembled the method of Lopez, Cheng, & Perez (2018) with a few minor changes. Final sphingomyelin concentration was 326 μM and molar ratios were 100/0, 80/20, and 60/40 mol/mol of sphingomyelin/cholesterol. Milk sphingomyelin (purity > 99% by TLC, Avanti Lipid, Alabama, USA) and cholesterol were first dissolved in 4:1 v/v chloroform/methanol (hereby known as solvent) before being dried with a gentle stream of nitrogen. The resulting dried lipid film was hydrated with Milli-Q water or PIPES buffer (piperazine-1,4-bis(2-ethanesulfonic acid)) heated to ~60 °C, above the melting point of sphingomyelin. The PIPES buffer consisted of 10 mM PIPES (purity ≥ 99%; Sigma-Aldrich NZ, Auckland, NZ) dissolved in a small volume of 1 M NaOH and mixed with 50 mM NaCl (Analytical Reagent Grade; Thermo Fisher Scientific NZ, North Shore City, NZ) and 5 mM $CaCl_2$ (Millipore, MA, USA) dissolved in Milli-Q water to match the ionic strength of milk. The pH was adjusted to 6.7 using either 2 M HCL or 4 M NaOH to match the pH of milk. After hydration, samples were maintained at 60 °C in a water bath for 30 min while being intermittently vortexed to form MLVs. The MLVs were kept quiescent for 24 h at room temperature to reduce the heterogeneity of the size distribution (Dua, Rana, & Bhandari, 2012).

3.2.2 Physical characteristics of milk sphingomyelin multilamellar vesicles

Particle size was measured using dynamic light scattering (DLS; Malvern Zetasizer Nano, Worcestershire, UK) at room temperature with data analysed using Zetasizer Software 7.10. The

dispersant refractive index was 1.330 and viscosity 1.0031 mPa. The measurement angle used was 173° backscatter. Particle size was performed in duplicate with each measurement consisting of the mean of at least 12 readings. Each replicate was measured three times. The "general purpose" analysis model native to the software was chosen for data processing. Particle size distributions were averaged using the aforementioned software.

Zeta potential for phospholipid vesicles was measured on the same instrument. The pH of the vesicles was 6.7 ± 0.1 and the charge from cholesterol was 0. The sample refractive index was 1.450 and absorption 0.001. The dispersant refractive index was 1.330, viscosity 1.003 mPa, and dielectric constant (ε) of the PIPES buffer, 80.4. As the particle size was large enough such that the Debye length was negligible in proportion to the radius of the vesicles, the Smoluchowski approximation was used (Bhattacharjee, 2016; Obeid et al., 2019).

3.2.3 Transmission electron microscopy (TEM)

Negative stain transmission electron microscopy (TEM) was conducted on an FEI Tecnai G2 Spirit BioTWIN (Czech Republic). Samples were applied onto 3.05 mm, 200 mesh copper grids (Agar Scientific, Essex, UK) pre-coated with Formvar at the Manawatu Microscopy and Imaging Centre. After allowing the sample to adhere to the carbon resin for 5 min, the residual sample was wicked off using filter paper. Uranyl acetate (2%) was used to stain the grid for 5 min before being wicked off, ensuring the grid was no longer wet before the sample was loaded onto the microscope.

3.2.4 Differential scanning calorimetry (DSC)

Differential scanning calorimetry (DSC) measurements were taken using a Nano DSC (TA instruments, New Castle, DE, USA). Samples (300 μL) were injected into capillary cells and compared to 300 μL of PIPES buffer as a reference. Samples and corresponding controls were cooled to 1 °C, pressurized to 300 kPa, and allowed to equilibrate for 10 min. Heating scans were from 1 °C to 60 °C at 1 °C/min. The start-up hook, an endothermic shift as the instrument approaches steady state, from 1 – 5 °C was removed. Data were analyzed with the NanoAnalyze software (TA Instruments, Delaware, USA).

3.2.5 Raman spectroscopy

Raman spectroscopic data was acquired, using a confocal microscope adapted from a commercially available inverted fluorescence microscope (Olympus IX70, Albany, NZ) and pumped by a 532-nm fibre-coupled diode laser. Mirrors were used to orient the beam into a 40× microscope objective (numerical aperture = 0.65). Raman scattered light was collected in a 180° back-scattering geometry through the 40× microscope objective. The scattered light was directed into a FERGIE detector (Princeton Instruments, Trenton, NJ, USA). The typical power at the sample measured 100 mW.

Frames (250 in total) each lasting 500 ms were taken for each measurement. The 250 frames were averaged and baselined via a peak averaging program written using Python.

3.2.6 Synchrotron x-ray scattering

X-ray scattering experiments were performed at the Australian Nuclear Science and Technology (ANSTO) synchrotron (Melbourne, Australia) on the SAXS/WAXS beamline operating at 14 KeV (λ= 0.88560 Å). Two 2-dimensional detectors recorded diffraction patterns in the small angle (0.02–0.3.5 $Å^{-1}$) and wide angle (1.2–1.9 $Å^{-1}$) regions to characterize lamellar structures and identify hydrocarbon chain order, respectively. Diffraction patterns were displayed as a series of concentric rings as a function of the radial scattering vector $q = 4\pi\sin\theta/\lambda$, where 2θ was the scattering angle and λ the wavelength of the incident beam. The capillary was inserted in a multi-stage set-up and XRD patterns were recorded as a function of temperature. Each reading was taken 5 °C apart. The first run was from 0 – 30 °C. After an indeterminate pause due to instrument complications, the detector was restarted and run from 30 – 80 °C.

An in-house developed software package, ScatterBrain, was used to convert the 2D SAXS pattern recorded using a Pilatus 1 M detector to a converted to plots of I (q) versus q by radial integration of the scattered X-ray intensity about the calibrated beam centre position.

3.2.7 Statistical analysis

Experiments were done with two independent replicates. To confirm results, at least two independent experiments were conducted. The only exception was for the x-ray scattering experiments. Due to the unavailability of the synchrotron, independent replicates could not be accommodated. Statistical significance was determined using one-way ANOVA and Tukey's HSD with critical $\alpha = 0.05$. The statistical software used was Minitab (State College, PA, USA).

3.3 Results and Discussion

3.3.1 Physical properties of milk sphingomyelin and cholesterol multilamellar vesicles

The majority of MLVs were larger than 1 μm and the addition of cholesterol did not have a statistical effect on particle size distribution nor polydispersity (Fig 3.1). The multilamellarity of the vesicles was confirmed with SAXS described later in the chapter. The addition of cholesterol is known to increase the lateral distance between phospholipid hydrocarbon chains and therefore, will increase the size of the liposomes (Sułkowski et al., 2005). The diameter difference between a 1-palmitoyl-2-oleoyl-sn-glycero-3-phosphocholine (POPC) LUV without cholesterol and 3:2 mol/mol POPC:cholesterol was reported to be +14% (Arriaga et al., 2009). Due the polydispersity of the constructed MLVs the statistical significance of such a difference could not be parsed using DLS. The measured particle size distribution of vesicles was nominally similar to that of milk fat globules. However, as stated in Chapter 2, bovine MFGs that are 1-8 μm make up 94% of lipid content but only

5% of the volume. In Fig 3.1, that might be the case for the 0% cholesterol, but not for the other treatments.

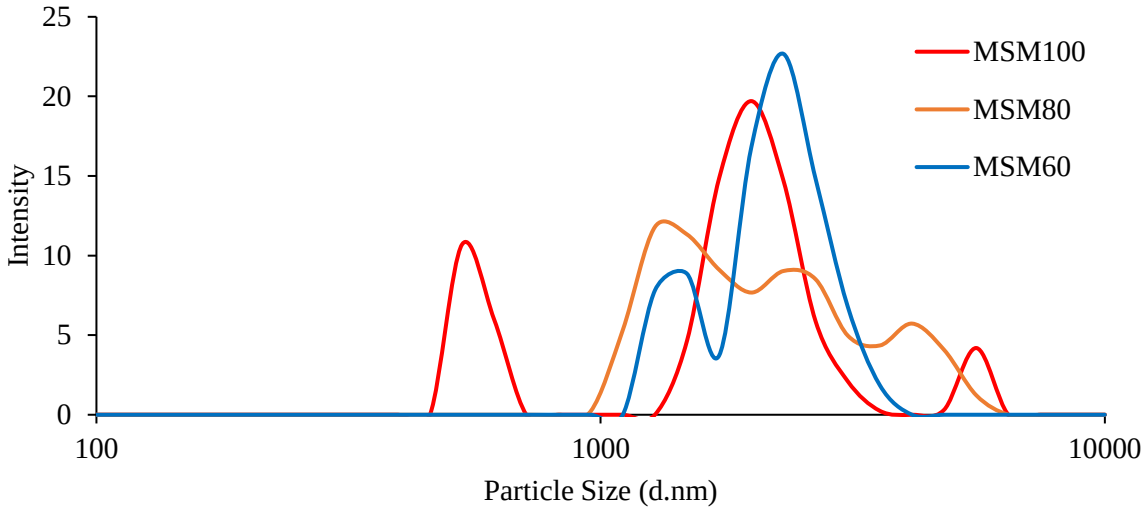

Figure 3.1. Particle size distribution of milk sphingomyelin multilamellar vesicles. MSM100 = Milk sphingomyelin with 0% cholesterol; MSM80 = Milk sphingomyelin with 20% cholesterol; MSM60 = Milk sphingomyelin with 40% cholesterol.

Transmission electron microscopy (TEM) partly confirmed DLS particle size measurements. The current protocol, negatives staining with Uranyl acetate (2%) was unable to confirm the lamellarity of the vesicles. Vesicles were distinguished from artefacts based on comparisons with the blank (PIPES buffer on Formvar grids) or with literature TEM micrographs of vesicles.

The wide range of vesicle size and the aggregation present in the micrographs were features of the MLVs predicted from particle size measurements (Fig 3.2). However, the DLS was incapable of detecting the smaller vesicles that were visible (~200 nm). Morphologically, vesicles were spherical (Fig. 3.2 b) or slightly collapsed (Fig. 3.2 d). When dried in preparation for negative staining TEM, MLVs collapsed into themselves to form irregular shapes (Baxa, 2018). These morphological anomalies are not uncommon when using negative stain TEM (Meister and Blume, 2017) and one of the advantages of the cryo-TEM technique is being able to visualize the native structure of the vesicle. There were occasions when aggregates of MLVs had collapsed on top or onto each other (Fig. 3.2 a, d). Although the polydispersity and extent of aggregation make an MLV model membrane system seem widely variable, these two features, that would be considered “defects” in a prepared emulsions or liposomal delivery system, bare striking resemblance to how native milk fat globules are naturally assembled (Fig. 3.2 e). The SEM micrograph (Fig. 3.2 e) is not for comparison but to show that both vesicles and native milk fat globules are susceptible to aggregation.

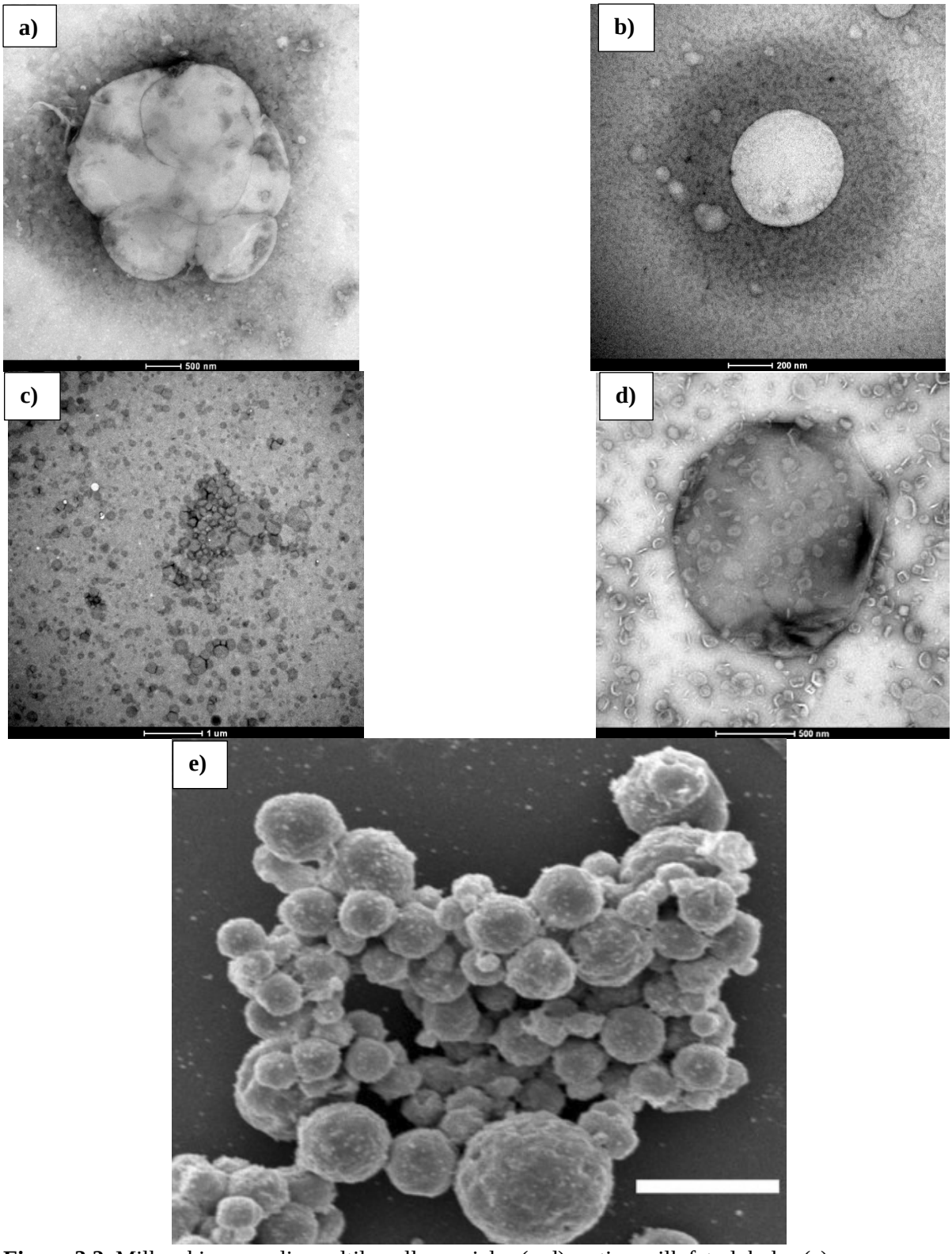

Figure 3.2. Milk sphingomyelin multilamellar vesicles (a-d), native milk fat globules (e)

a) 20,500 ×, 40% mol cholesterol, multiple small vesicles on top of a larger vesicle aggregate;
b) 60,000 ×, 40% mol cholesterol, single vesicle alongside some smaller ones;
c) 16,500 ×, 20% mol cholesterol, aggregation of many small vesicles;
d) 43,000 ×, 0% mol cholesterol, a large vesicle and multiple smaller ones. The smaller vesicles have an oval or flattened shape due to drying;
e) Scanning electron micrograph of bovine milk fat globule. Bar is approximately 5 µm. Note how aggregation is present. From Ward et al., (2004).

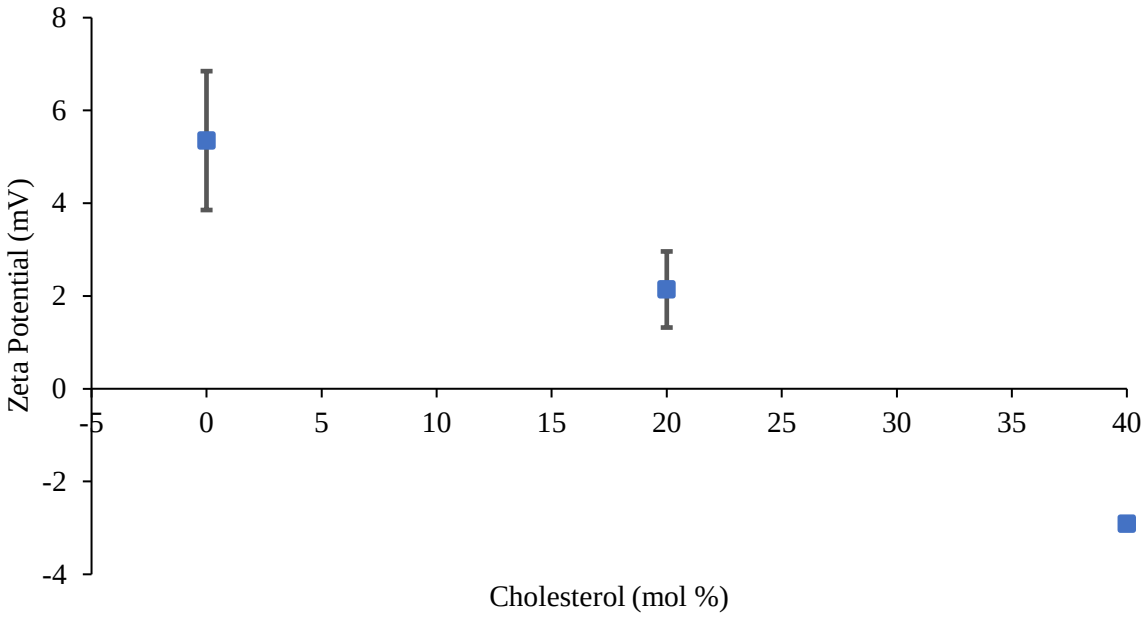

Figure 3.3. Zeta potential of milk sphingomyelin multilamellar vesicles comprised of varying amounts of cholesterol. Error bars are the standard deviation. The standard deviation for the 40% mol cholesterol MSM is present but not visible.

The zeta potential of MSM/cholesterol vesicles suspended in PIPES buffer at pH 6.7 were 5.34 ± 1.30, 2.14 ± 0.65, and -2.90 ± 0.27 mV respectively for 1:0, 4:1, and 3:2 mol/mol MSM/cholesterol MLVs (Fig. 3.3). As the absolute value of the zeta potential for any MLV never rose above/below ± 30 mV, considered to be a point above which electrostatic repulsion becomes dominant, the decrease in zeta potential as cholesterol concentration increased, albeit significant, was inconsequential when assessing the stability of the MLVs (Bhattacharjee, 2016). The low absolute zeta potential was apparent as the MLV aggregates sediment when stored overnight.

The significant decrease in zeta potential due to the addition of cholesterol hints at possible lateral bilayer interactions. Obeid et al. (2019) claims that the presence of NaCl in the PIPES buffer has a screen effect on the surface membrane charge (Sinn et al., 2006) or the Ca^{2+} binds to the carboxyl or phosphate for in PC (Melcrová et al., 2016) leading to tendency towards a positive zeta potential. The negative zeta-potential obtained for MSM60 (40% cholesterol) suggests this is not the case, at least when cholesterol is present. One explanation that addresses both the tendency for the zwitterionic MSM bilayers to display a positive zeta potential as well as the inverse impact on zeta potential by cholesterol hinges on the condensing effect of cholesterol on lateral chain order. Sodium ions are known to penetrate deeply into the bilayer and interact with the negatively charged phosphate oxygen groups of sphingomyelin. Conversely, chloride ions have been shown to only be weakly associated with choline headgroups (Böckmann et al., 2003). Therefore, the net surface charge of MSM MLVs is slightly positive. The insertion of cholesterol between the SM molecules strengthens hydrophobic interactions while partly dissembling the inter-lipid SM hydrogen bond network. This preferential

interaction between SM and cholesterol extends the hydrophobic shell, expelling Na^+ ions which were bound to the negatively charged phosphate into the bulk water (Stępniewski et al., 2010) – rendering the surface charge and therefore zeta potential negative whereas the Cl^- ions remain associated with the choline headgroups (Magarkar et al., 2015).

Particle size, zeta potential measurements, and transmission electron micrographs demonstrated that vesicles were formed, although without Cryo-TEM the lamellae was unable to be confirmed. The significant decrease in zeta potential as cholesterol was added is preliminary evidence that cholesterol is interacting with the MSM in a way that changes the properties of the vesicle, in this case, the electrostatic properties.

3.3.2 Thermotropic behaviour of milk sphingomyelin and cholesterol multilamellar vesicles

The highest concentration of SM reported to be found in milk (11.9 mg/dl) (Bitman & Wood, 1990) was used as guideline to set the lower limit of detection for nano-DSC experiments. MLVs constructed with 163 μM MSM showed a peak, a melting transition (T_m), at 33 °C, which was in agreement with other hydrated sphingomyelin vesicle calorimetry studies (Murthy et al., 2015; Cheng, Ropers, & Lopez, 2017; Lopez, Cheng, & Perez, 2018) (Fig. 3.4). The sharp cut off at 50 °C for the 163 μM SM vesicle sample was likely due to an impurity or noise as it was not present in the 186 and 326 μM. The low signal, and the sharp downturn of the 163 μM DSC curve after 50 °C were the main reasons why it was deemed unproductive to assay concentrations of MSM that were lower than 163 μM.

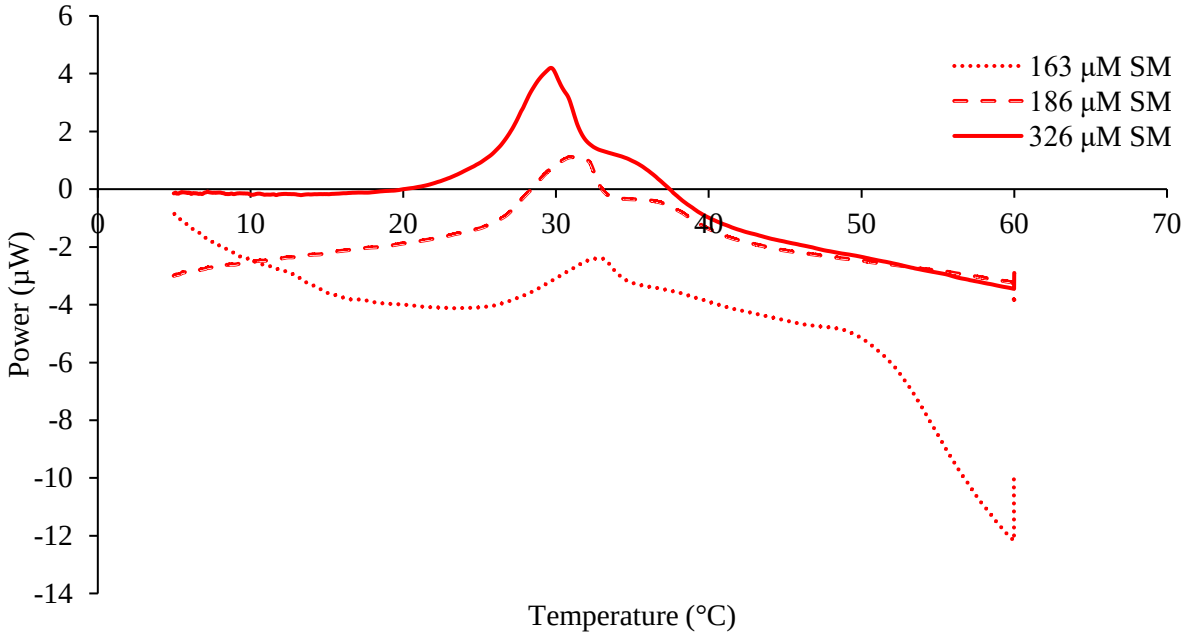

Figure 3.4. Differential scanning calorimetry thermotropic profile of milk sphingomyelin vesicles of varying concentrations. Offsets have been added for clarity.

The DSC curve of MLVs constructed with 186 and 326 μM MSM were as expected – a broad multicomponent endothermic event around 30 °C as a phase transition from the rigid, tilted solid ordered (S_o) phase to the fluid, liquid disordered (L_d) phase occurred. Milk sphingomyelin concentration had an inverse impact on transition temperature, with the MLVs containing 186 and 326 μM MSM having lower T_m values (32 °C and 29 °C, respectively). This result differs from the findings reported by Lopez, Cheng, & Perez (2018) where MSM concentration is proportional to the T_m in hydrated MSM MLVs. The directly proportional relationship between SM concentration and T_m may only exist for high concentrations of milk SM (64 – 1019 mM).

The broad shoulder from 35 – 40 °C was suggested to be from issues with sample homogeneity as the shoulder decreased as MSM concentration decreased, completely disappearing at 9:1 wt% MSM:water (127 mM) (Lopez, Cheng, & Perez, 2018). Yet as seen in Figure 3.4, this shoulder is still prominent at micromolar concentrations of MSM. The working hypothesis is that these shoulders do exist at 9:1 and 19:1 wt% MSM:water, but the instrument used in the study by Lopez, Cheng, & Perez (2018) lacked the sensitivity to detect them. In this case, the broad shoulder would not be due to homogeneity but is inherent to the MSM due to the high T_m values of the C23:0 and C24:0 acyl chains that make up 53% of MSM (Shaw et al., 2012). Interdigitation brought upon by the hydrophobic mismatch between the sphingosine backbone and acyl chain of SM species with a high T_m is known to broaden the $S_o \rightarrow L_d$ phase transition (Et-Thakafy et al., 2018). Further DSC work is necessary to confirm this.

The onset of a L_o phase at 4:1 mol/mol% MSM:cholesterol in binary MLVs is known to dissipate the sharp T_m into a broad endotherm (Lopez, Cheng, & Perez, 2018). The L_o phase is a fluid, ordered platform with structural properties intermediate of the S_o and L_d phases. Depending on the phase state of the MLV, the cholesterol fluidizes the MLV, dispersing L_o domain subunits throughout the bulk L_d phase (Murthy et al., 2015) when the MLV is in the S_o phase. The cholesterol condenses the MLV, causing the area per phospholipid molecule to decrease when the MLV is in the L_d phase (Ma et al., 2016).

At 3:2 mol% MSM:cholesterol the L_o phase completely covers the entire bilayer, rendering the endotherm no longer visible (Lopez, Cheng, & Perez, 2018). This behaviour was well conserved in MLVs containing almost a thousand-fold less lipid (Fig. 3.5). The T_m of MSM 100 was 33 °C and when 20% cholesterol was added (MSM 80) the S_o to L_d transition mostly dissipated, only showing a slight peak at 28 °C. The reduction in T_m is likely due to the hydrophobic mismatch of cholesterol with the variety of MSM hydrocarbon chain lengths (Nyholm, Nylund, & Slotte, 2003). As the S_o phase melts, the bilayer shrinks due to the introduction of *gauche* rotamers; this shrinkage invites further heterogeneities i.e. hydrocarbon chain lengths mismatching, to occur when a foreign molecule is incorporated into the bilayer. Incorporation of cholesterol decreases the T_m for PC > 18 carbon

chains and conversely increases the T_m of PC < 18 carbon chains (McMullen, Lewis, & McElhaney, 1993). This is due to the hydrophobic length of cholesterol (~ 17.5 Å) being roughly equal to the hydrocarbon chain at C17 PC and therefore, the least amount of mismatch. On the other hand, the greater the difference between the hydrophobic length of cholesterol and the hydrocarbon chain – the higher amount of mismatch resulting in a shift in T_m. In this case, the hydrocarbon chains of the MSM used are roughly 80 % > C:18 (Avanti Lipid), so the reduction in T_m is very expected.

Sphingomyelin that was not complexed with cholesterol was still capable of melting; therefore, the remnant of a possible pre-transition at 23 °C and a peak observed at 28 °C. This persistent endothermic event in 4:1 mol% MSM:cholesterol (MSM 80) indicates an $S_o \rightarrow L_d$ transition amidst a mixed-L_o phase – where the L_o domains are interspersed among the bulk L_d phase (Murthy et al., 2015) – as a phase transition would not occur in a vesicle entirely in the L_o phase. As the concentration of cholesterol is further increased to 40% (MSM60) only the faintest hint of a possible endothermic event remains. At this concentration, the interaction between cholesterol and SM has dissipated the phase transition, rendering any $S_o \rightarrow L_d$ phase transition undetectable. Whether this is the stoichiometric ratio where all SM molecules are interacting with cholesterol molecules is not something that can be determined with DSC alone.

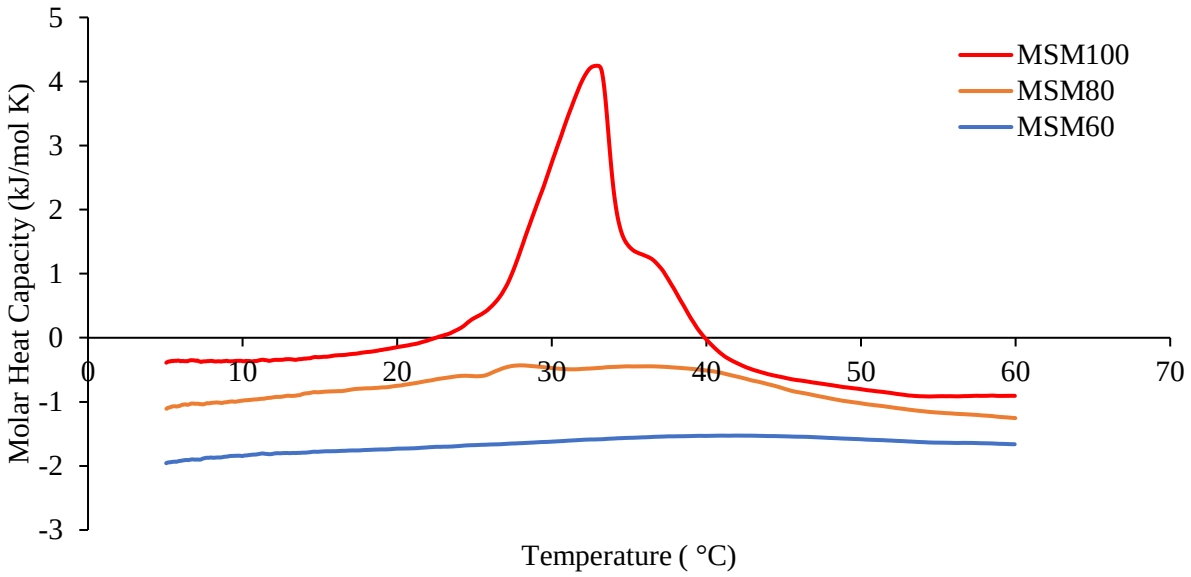

Figure 3.5. Differential scanning calorimetry plot of milk sphingomyelin (MSM) vesicles with varying concentrations of cholesterol. Offsets have been added for clarity. MSM100 = 0% mol cholesterol; MSM80 = 20% mol cholesterol; MSM60 = 40% mol cholesterol

A preliminary experiment using synchrotron radiation (SR) SAXS and WAXS examined the complex structural changes hinted by the DSC analysis. Once again, a concentration gradient of MSM was taken to determine the phospholipid concentration for subsequent experiments and to evaluate whether diffraction originating from physiologically relevant concentrations of MSM was detectable.

At the concentration of phospholipid used, Bragg peaks were not detectable with conventional laboratory XRD (Appendix 3.1).

Two Bragg peaks were visible in the small angle (Fig. 3.6 a) and a single peak was present in the wide angle (Fig. 3.6 b). In the SAXS, the second Bragg peak was almost not visible for 160 and 330 μM MSM. The extra Bragg peaks indicated for the 660 μM SM sample at q = 0.076 $Å^{-1}$ (d = 82 Å) was from an impurity as it was not present in the other MSM preparation. In the WAXS, a peak was only present at MSM concentrations greater 660 μM. Although 660 μM SM is four times the SM content in milk, this was the concentration chosen for subsequent XRD experiments.

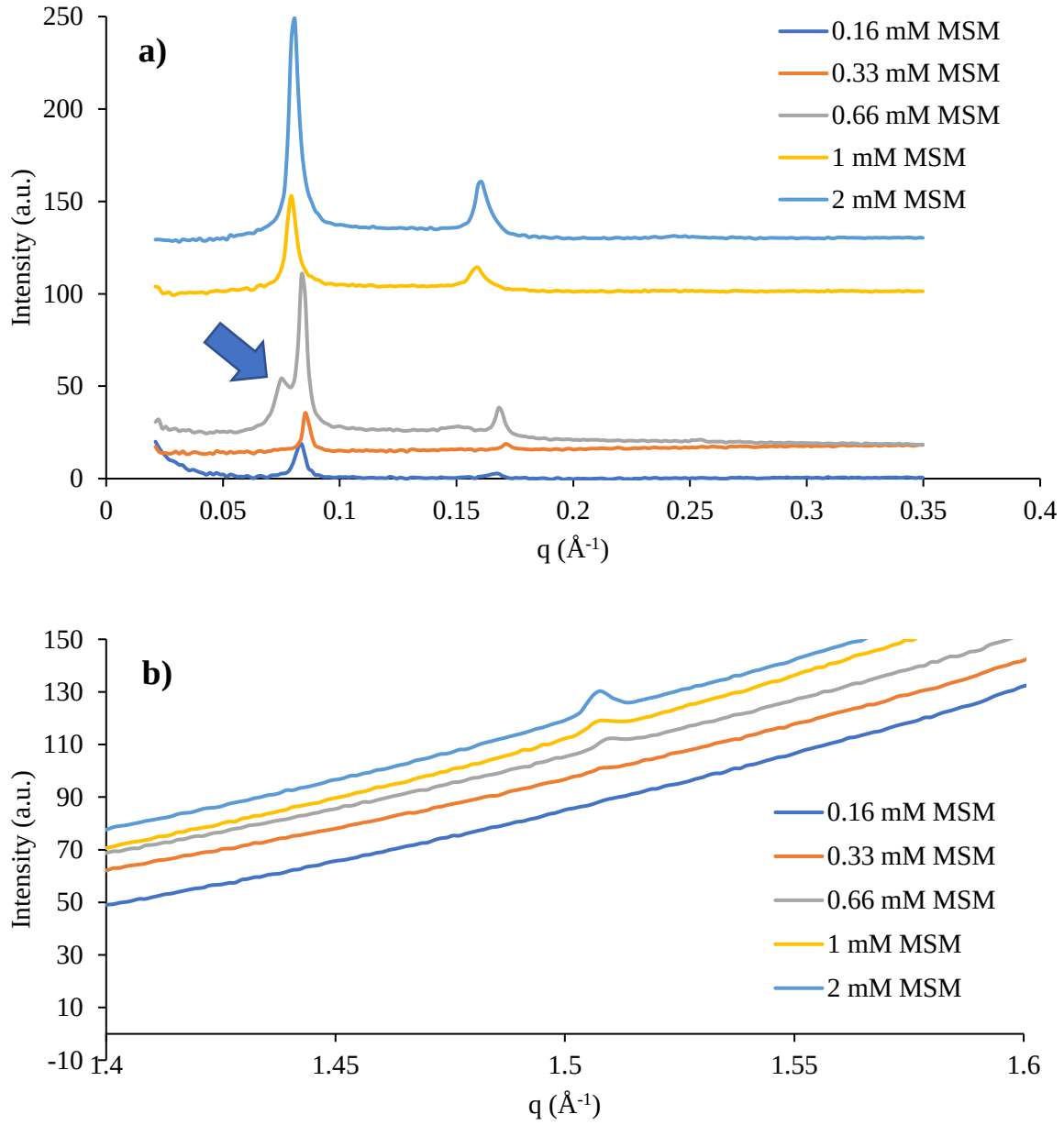

Figure 3.6. SAXS of milk sphingomyelin concentration gradient. Offsets have been added for clarity. a) small-angle scattering profile, arrow indicates the impurity in the preparation; b) wide-angle scattering profile.

At temperatures < MSM T_m (34 °C), two small-angle Bragg peaks were visible for the MSM100 (Fig 3.7 a). These are first- and second-order lamellar repeat d-spacing, the bilayer width in addition to the interlamellar spacing (Pabst et al., 2000). A minor Bragg peak at slightly higher q than the first-order Bragg peak has be reported in egg sphingomyelin (ESM) and attributed to the interdigitation of high T_m (C22:0, C24:0) MSM components (Chachaty et al., 2005). Interdigitation occurs when the lengths of the hydrocarbon chains of the sphingosine backbone and the acyl chain are mismatched. In those high T_m MSM species, this results in what is known as a mixed indigitated S_o phase ($L_{\beta 1}$ phase) where the long chain spans the entire bilayer and the two shorter chains of opposing monolayers match end to end (Levin, Keihan, & Harris, 1985; Koynova & Caffrey, 1995). However, this lamellar feature was not visible in the MSM preparations.

The first-order Bragg peak, the bilayer periodicity which represents the bilayer width and the interlamellar spacing, had a d-spacing of 72.6 Å (q = 0.856 $Å^{-1}$) at T < 30 °C. This S_o phase d-spacing evolved as a function of temperature, increasing in distance at temperatures close to T_m and then decreasing as T > T_m (Fig. 3.8 a). As the MLV was heated close to T_m, the hydrocarbon carbon chains un-tilted, resulting in a temporary increased d-spacing (Shaw et al., 2012). Other suggestions for the temporary increase in lamellar repeat d-spacing as temperature increases towards T_m include successive melting of MSM fatty acids, inefficient packing due to mismatched N-acyl chain lengths, or S_o phase polymorphism (Lopez, Cheng, & Perez, 2018). The S_o phase polymorphism occurs as a $L_{\beta 1}$ to $L_{\beta 2}$ transition (Levin, Keihan, & Harris, 1985). The $L_{\beta 1}$ phase is the state the MSM exists in for most of the S_o phase. As energy is inputted into the MSM bilayer and the low T_m MSM transition to a L_d phase, the high T_m SM unfurl to form a $L_{\beta 2}$ phase where the longer hydrocarbon chain matches the shorter hydrocarbon chain on the opposite monolayer, increasing bilayer width (Fig. 3.7) (Lopez, Cheng, & Perez. 2018).

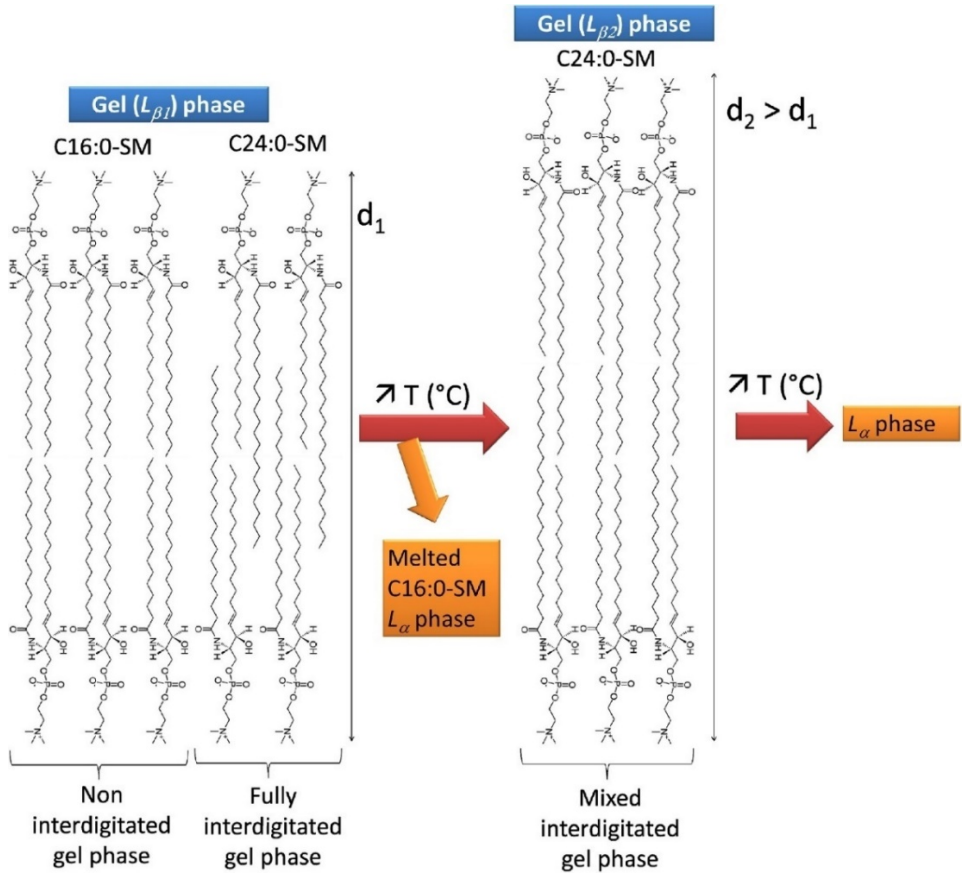

Figure 3.7. Schematic of $L_{\beta 1}$ to $L_{\beta 2}$ phase transition in milk sphingomyelin. In this figure, gel phase refers to the S_o phase and the L_α phase refers to the L_d phase. This figure uses mixed interdigitated to refer to the $L_{\beta 2}$ however other publications have used that term in reference to the $L_{\beta 1}$ phase. Reproduced from Lopez, Cheng, & Perez, (2018)

However, a complete $L_{\beta 1}$ to $L_{\beta 2}$ transition is unlikely to be reason for the shift in d-spacing at 30 °C as the transition in question is usually a 7 or 8 Å increase whereas the shift that occurred was only 2 Å which is consistent with the un-tilting of phospholipids pre $S_o \rightarrow L_d$ transition (Shaw et al., 2012). In short, if a $L_{\beta 1} \rightarrow L_{\beta 2}$ transition did occur the MSM system it only began at 30 °C and ceased before 40 °C when the L_d phase dominates (Fig 3.9 b).

At temperatures > 50 °C, when a majority of the MSM 100 vesicles were in the L_d phase, the lamellar spacing shrunk to 64.5 Å (q = 0.0968 $Å^{-1}$) (Fig 3.9 b). This trend, and the associated values, agree with previously reported lamellar repeat d-spacings of MSM (d- Lβ (S_o)=73 Å, d-L_d=66 Å) (Shaw et al., 2012). Of particular note was that the lamellar repeat d-spacing of MSM 100 remained at 67.5 Å from 40 – 45 °C (Fig 3.9 b). This pattern is consistent with the broad shoulder present in the DSC profile immediately above T_m (Fig. 3.5); however, as the shoulder in the DSC profile begins at 35 °C and ends at 40 °C further investigation is warranted.

Evidence for the disappearance of the S_o phase can be further observed in the WAXS data (Fig. 3.8 b). The peak at d = 4.13 Å (1.51 $Å^{-1}$) represents the tilted hexagonal packing of the hydrocarbon chains within the S_o phase (Chemin et al., 2008). Upon heating, hexagonal packing d-spacing steadily

increases until the T_m is reached, where it disappears – indicating the gel phase has completely melted.

The SAXS results depict the clustering effect of cholesterol on sphingomyelin bilayers quite well. Three molar ratios of MSM:cholesterol were tested, 1:0 (control), 4:1 (onset of the L_o phase), 3:2 (completion of the L_o phase) (Lopez, Cheng, & Perez, 2018). Regardless of the molar ratio of MSM:cholesterol, two Bragg peaks were present at 20 °C (Fig. 3.9 a). At 20 °C, with the addition of cholesterol, lamellar repeat d-spacing decreased from 72.6 Å (0% mol cholesterol) to 67.6 Å (40% mol cholesterol) revealing that cholesterol was capable of affecting the structure of MSM bilayers, even at temperatures < T_m (Fig. 3.9 b). Conversely, at 60 °C, the first order Bragg peak d-spacing increased from 64.5 Å (0% mol cholesterol) to 67.6 Å (40% mol cholesterol). The addition of cholesterol to MSM vesicles abates temperature-induced d-spacing shifts in either direction – expansion or the shrinking of the bilayer. The result is an ordered bilayer which is independent of temperature changes. This result agrees with previous studies done on cholesterol interactions with ESM (Chachaty et al., 2005; Quinn & Wolf, 2009). As the molar proportion of cholesterol increased, the periodicity of sphingomyelin bilayers became more resistant to temperature induced change (Chachaty, et al., 2005).

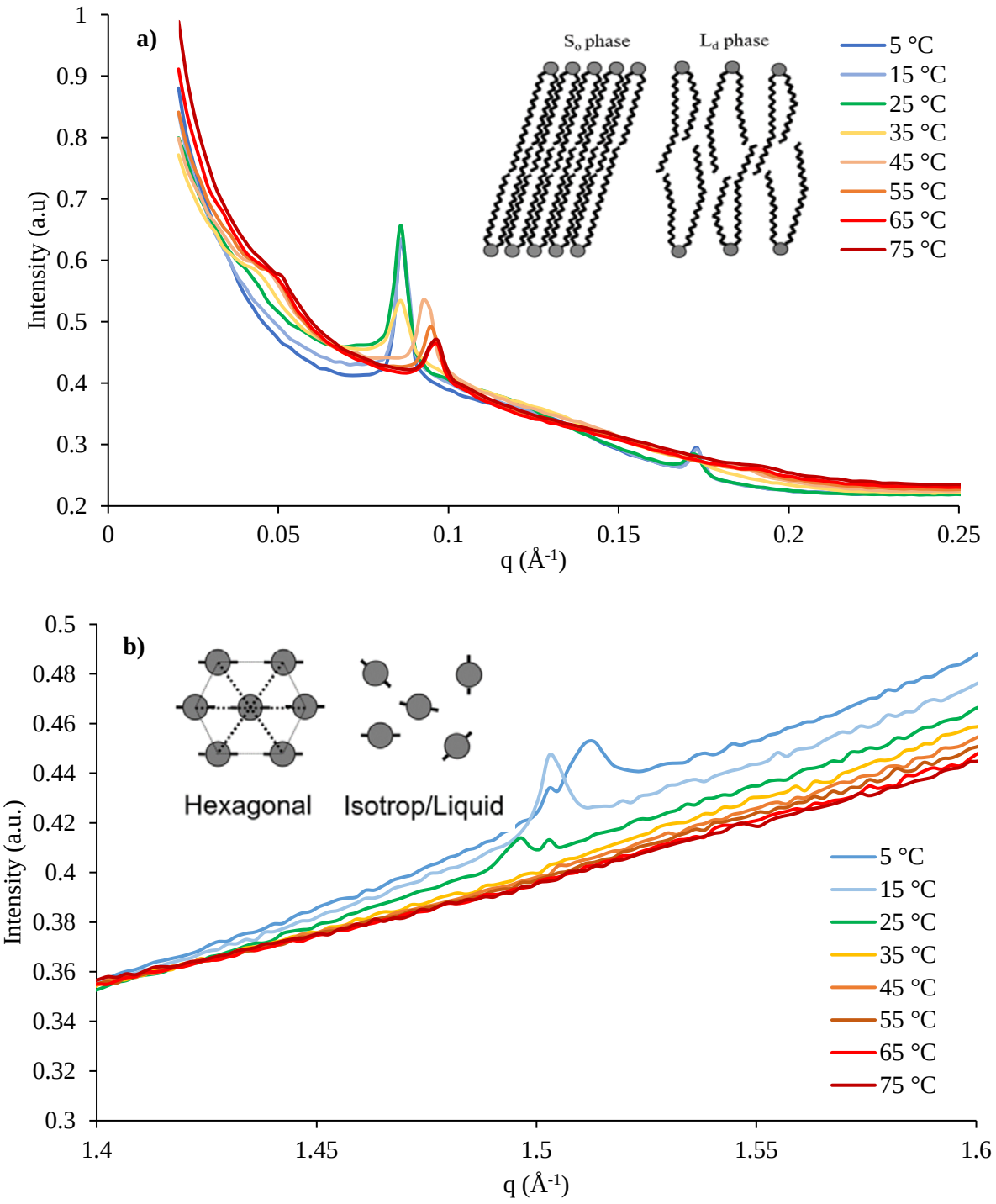

Figure 3.8. SAXS of milk sphingomyelin vesicles without cholesterol as a function of temperature. a) small-angle scattering profile; b) wide-angle scattering profile. Schematics of chain conformation and lateral chain packing were reproduced from (Schmitt & Neubert, 2018).

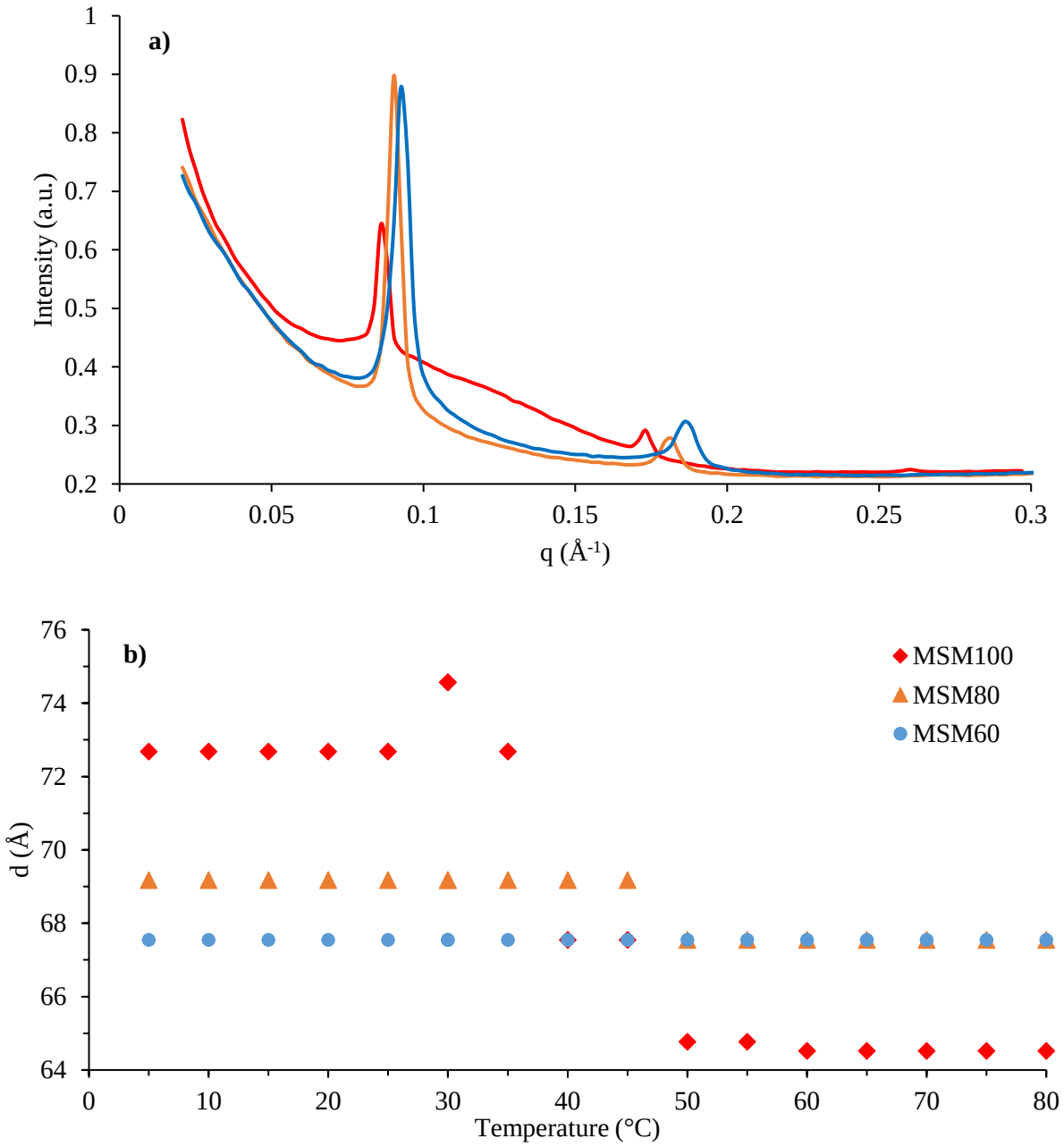

Figure 3.9. SAXS scattering of milk sphingomyelin (MSM) multilamellar vesicles (MLVs) with varying concentrations of cholesterol; red = MSM MLVs with 0% mol cholesterol; orange = 4:1 mol/mol MSM:cholesterol MLVs; blue = 3:2 mol/mol MSM:cholesterol MLVs. a) small angle scattering profiles 20 °C; b) D-spacing as a function of temperature.

SR-WAXS demonstrated that the addition of cholesterol dissipates the hexagonal packing Bragg peak at d = 4.13 Å (1.51 $Å^{-1}$), representative of the proliferation of the L_o phase (Fig. 3.9). A second peak at d = 4.16 Å (1.50 $Å^{-1}$) persisted until 30 °C regardless of the cholesterol content. Although small, this peak is not due to instrument noise, as it was also present in Fig. 3.8 b, samples created with a different batch of MSM at an earlier time.

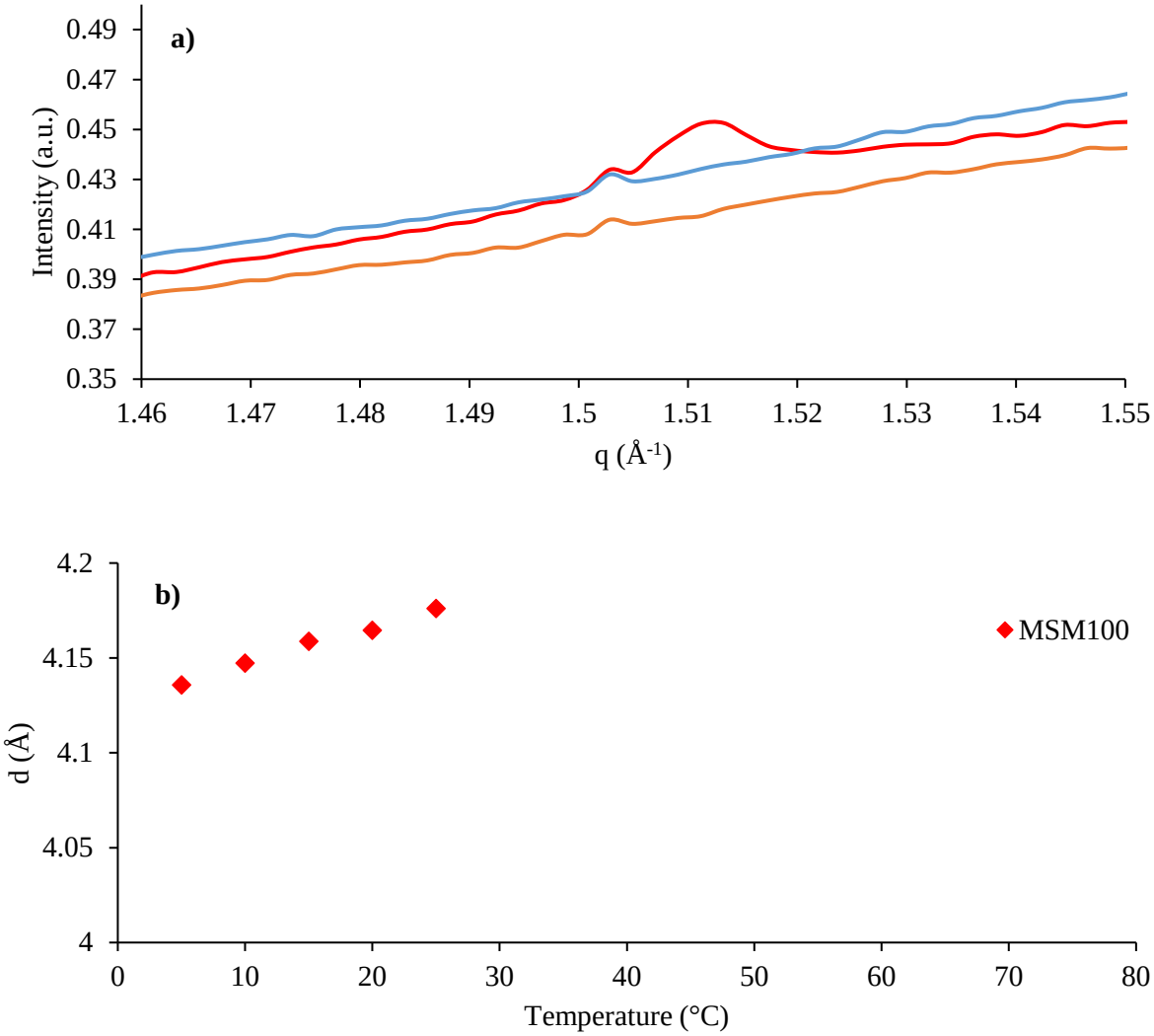

Figure 3.10. WAXS d-spacing of milk sphingomyelin (MSM) multilamellar vesicles (MLVs) with varying concentrations of cholesterol during heating. MSM100 = 0% mol cholesterol; MSM80 = 4:1 mol/mol MSM:cholesterol MLVs; MSM60 = 3:2 mol/ml MSM:cholesterol MLVs. a) WAXS scattering profiles at 20 °C; b) D-spacing as a function of temperature.

The instrument was stopped at 30 °C and restarted after an undisclosed amount of time. To account for the stop, two measurements were taken at 30 °C before and after the stop. The structural feature at d = 4.16 Å does not appear in the XRD curves after the stop. It is possible that samples resting for an extended period at 30 °C, which is close to the T_m of MSM, could have melted this feature. Conversely, the SAXS scattering profiles for MSM100 at 30 °C lack the shift in lamellar repeat d-spacing one would expect to occur from a phase transition, so the matter needs to be further investigated.

In summary, SR-SAXS and WAXS are capable of delivering high resolution data concerning the structure of phospholipid bilayers at concentrations within the same magnitude as those found in natural milk products. Preliminary structural investigations into MSM interactions with cholesterol

were confirmatory in nature – the addition of cholesterol led to a constant bilayer periodicity that was resistant to temperature-induced phase transition.

3.3.3 Intra- and inter-molecular behaviour of milk sphingomyelin bilayers

Considerable effort was taken to optimize a Raman protocol for taking the spectra of the sphingomyelin MLVs. Two additional methods considered were the use of an oil immersion lens and supporting the MLVs on parafilm. Due to high interference to the CH region from the hydrophobic components of the oil and parafilm, both these methods were deemed unsuitable. Two concentrations of MLVs (2 mM and 326 μM) were assayed to determine the concentration to be used in subsequent experiments. The 326 μM showed much better than expected signal (Fig. 3.11).

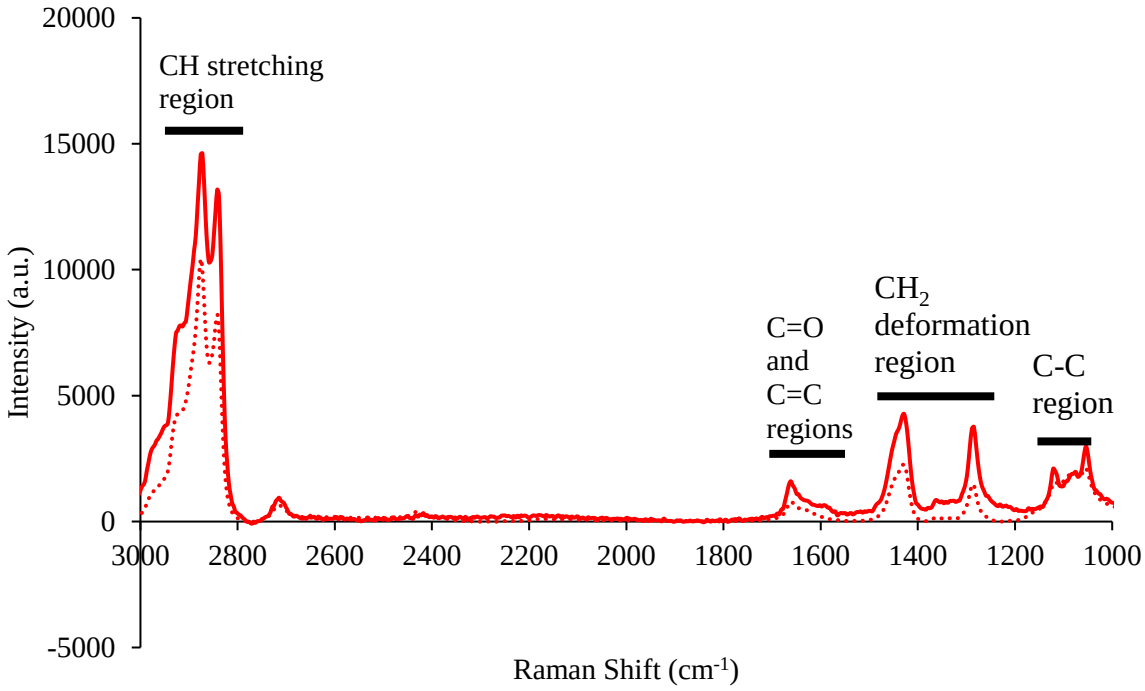

Figure 3.11. Raman spectra of milk sphingomyelin vesicles without cholesterol labelled with the regions of interest and their assignments. a) Red dotted line = 326 μM milk sphingomyelin; red line = 2 mM milk sphingomyelin

Table 3.1 details the reference vibrational modes that approximately correspond to each peak, as well as the corresponding Raman shifts on the above graph. The 2850 and 2880 cm^{-1} peaks describe the symmetric and asymmetric CH_2 stretching modes, respectively. The 2880 cm^{-1} peak is a product of Fermi resonance, the convolution of two or more vibration modes some of which may be overtones, between the symmetric 2850 cm^{-1} peak, as well as overtones from CH_2 bending modes. With a broad and complex character, the 2930 cm^{-1} shoulder is also a product of Fermi resonance. One component of the 2930 cm^{-1} peak is the 2850 cm^{-1} peak (CH_2 symmetric stretch). A second component has been suggested to be an overtone of the 1465 cm^{-1} shoulder (CH_2 bending) (Abbate, Zerbi, & Wunder, 1982) or a CH_3 symmetric stretching mode (Snyder, Strauss, & Elliger 1982). Further debate has arisen whether the 2930 cm^{-1} is in fact a binary product, whether all three previously mentioned

modes (CH_2 symmetric stretch, CH_2 deformation, and CH_3 symmetric stretch) make up the band (Lee & Bain, 2005) or whether there are contributions from overtones of modes at even lower frequencies (Snyder, Strauss, & Elliger 1982).

Table 3.1 Raman active modes for milk sphingomyelin. Reproduced from Table 2.5 for convenience.

SM Vibrational Mode	Reference Raman Shift (cm^{-1})	Actual Raman Shift (cm^{-1})	Reference
Asymmetric Stretch CH_3	2960	2955	(Czamara et al., 2015)
Fermi Resonance Symmetric Stretch CH_3	2930	2930	(Czamara et al., 2015)
Fermi Resonance Asymmetric Stretch CH_2	2880	2875	(Czamara et al., 2015)
Symmetric Stretch CH_2	2850	2840	(Czamara et al., 2015)
C=C Stretch	1670	1660	(Shirota et al., 2016)
C=O Stretch + Amide	1630	1640	(Czamara et al., 2015; Shirota et al., 2016)
Scissoring CH_2/CH_3	1425	1430	(Czamara et al., 2015)
Twisting CH_2	1280	1280	(Czamara et al., 2015)
Stretch C-C	1110, 1085, 1050	1115, 1080, 1050	(Czamara et al., 2015)

The features present in the 1600 to 1800 cm^{-1} region are unique to sphingomyelin. The C=O stretching band in glycerophospholipids is around 1730 cm^{-1} (Czamara et al., 2015). Such a band is not visible in sphingolipids even though C=O is present in sphingomyelin molecules. Krafft et al., (2005), suggest that the 1670 cm^{-1} peak coupled with the 1630 cm^{-1} shoulder takes the place of the 1730 cm^{-1} band. This suggestion disregards the 1660 cm^{-1} peaks in glycerophospholipids corresponding to Z-C=C which is also present in the sphingosine backbone. Shirota et al. (2016) therefore conclude the 1670 cm^{-1} peak is not amide-related but simply the Z-C=C peak, whereas the 1630 cm^{-1} shoulder is a combination of the C=O and N-H which, of the two, the C=O dominates (Miyazawa, Shimanouchi, & Mizushima, 1958).

The 1000 to 1500 cm^{-1} region mostly confirms the presence of the acyl chains on the phospholipid. The 1430 cm^{-1} and 1280 cm^{-1} peak are methylene deformation modes whose overtones may contribute to the CH region (2800 – 3000 cm^{-1}). The 1110, 1085, and 1050 cm^{-1} peaks denote C-C stretching with the wavenumbers used to determine the types of fatty acids present (Czamara et al., 2015), and the intensity ratios can determine the length of the hydrocarbon chains (Okotrub et al., 2020). The choline headgroup is at a lower Raman shift that was beyond the ability of the instrument to detect.

Chapter 4 will quantify the structural and orientational information that can be gleaned from Raman spectroscopy of MSM/cholesterol MLVs. The following will serve as a qualitive introduction and primer on the changes in the regions of interest. The predominately nonpolar cholesterol and the highly saturated MSM interact favourably to form L_o domains. The exact character of these interactions, the fundamental driving mechanism that creates L_o domains is still unknown; what is measured is the effect of the cholesterol on the phospholipid bilayer. The CH and C-C have the largest degree of change when cholesterol was incorporated into the MSM vesicles. In the CH region (2800 – 3000 cm^{-1}), the 2850, 2880, and 2930 cm^{-1} peak intensity ratios can be used to quantify the fluidity of the membrane, interactions between the CH_2 groups, and the packing order of the bilayer (Gallier et al., 2011). As cholesterol concentration in the MLV increases, so does the 2930 cm^{-1} peak; whereas, the 2880 cm^{-1} peak decreases (Fig. 3.12 a), representing an increase in bilayer fluidity from either an increase of *gauche* isomers or a loosening of hydrocarbon chains (Li-Chan, 2007).

As previously mentioned in this section, the 1600 – 1800 cm^{-1} region in sphingomyelin is capable of elucidating the amide/cholesterol interactions using the C=O mode at 1630 cm^{-1}. In ESM, as the concentration of cholesterol increases, the 1630 cm^{-1} peak becomes a shoulder and then dissipates at 5:1 mol/mol SM/cholesterol while the relative intensity of the 1670 cm^{-1} peak increases (Shirota et al., 2016). In Figure 3.12 b, the 1630 cm^{-1} peak (shown here at 1640 cm^{-1}) is a shoulder regardless of cholesterol content. Furthermore, it is MSM80 with a 4:1 mol/mol SM/cholesterol ratio where the C=O shoulder is at its zenith, calling into question either the contribution of NH towards the C=O stretching mode or whether a direct hydrogen bond exists between sphingomyelin amide and the cholesterol polar hydroxyl group.

When cholesterol is added to MSM vesicles, the outer peaks for the C-C stretch, triplet peaks decrease relative to the centre peak (Fig. 3.12 c). As the C-C peaks are related to the length of the hydrocarbon chains, the intensity of the peaks can be used to determine the presence of *gauche* isomers. This parameter complements the complex 2930 cm^{-1} and 2880 cm^{-1} peaks which determine hydrocarbon chain interaction with contributions from the C-C. By careful consideration of the CH and C-C regions, it is possible to isolate the *gauche/trans* contributions from the lateral hydrocarbon interactions to discern which effect dominates.

It is important to remember the direction of the orientational and structural changes of MSM vesicles (bilayer expansion or shrinkage) are dependent on the original phase state and therefore the temperature. As seen in the preliminary XRD experiments in Section 3.3.2, cholesterol is capable of affecting bilayer structures in both the S_o and L_d phases.

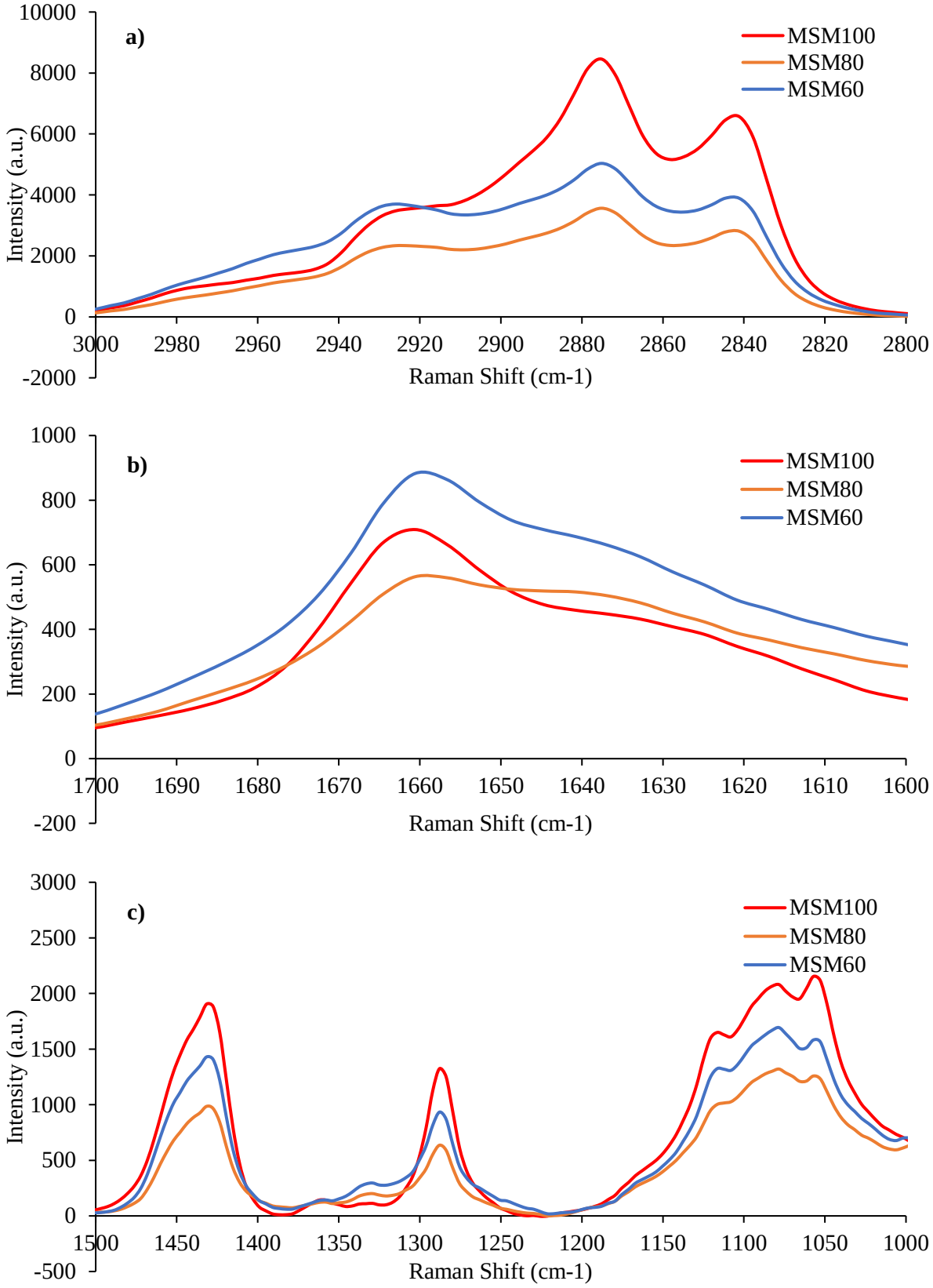

Figure 3.12. Raman spectra of milk sphingomyelin (MSM) multilamellar vesicles (MLVs) with varying concentrations of cholesterol. MSM100 = 0% mol cholesterol; MSM80 = 4:1 mol/mol MSM/cholesterol; MSM60 = 3:2 mol/mol MSM/cholesterol; a) CH region; b) C=O and C=C region; c) C-C region.

3.4 Conclusions

Milk sphingomyelin MLVs with varying concentrations of cholesterol were created. The structural changes of these MLVs due to the addition of cholesterol were evaluated by DLS, TEM, DSC, SR-XRD, and Raman spectroscopy. All instruments other than the DLS observed a distinguishable signal at relatively physiological concentrations of phospholipids and cholesterol.

Interactions between sphingomyelin and cholesterol that influenced bilayer structure were confirmed. Such an interaction was unable to be visually confirmed by TEM. Conversely, DSC techniques, Raman, and XRD clearly demonstrated cholesterol alters the structural properties of the MSM bilayers. The SAXS and WAXS went one step further, demonstrating that with the addition of cholesterol, MSM MLVs were highly resistant to temperature-induced phase transition. This is potentially physiologically relevant as the melting point of MSM is so close to 37 °C, the internal temperature for humans.

In short, there is evidence that in the presence of cholesterol, MSM may act differently under digestive condition than it would without the sterol. Extrapolating from that statement, the co-presence of MSM and cholesterol within the MFGM implies these components may be digested in a particular way. This hypothesis, the confirmation of the general trend expounded upon in the literature, and success of the techniques employed lead to the key question explored in the next chapter – what makes MSM a unique component of the MFGM?

Acknowledgements

Small-angle and wide-angle x-ray scattering data was collected with the help of Dr. Ben Boyd, Dr. Andrew Clulow, and Xiaohan Sun from Monash University. Dr. Andrew Clulow is currently employed by ANSTO.

References

Abbate, S., Zerbi, G., & Wunder, S. L. (1982). Fermi resonances and vibrational spectra of crystalline and amorphous polyethylene chains. *The Journal of Physical Chemistry*, *86*(16), 3140–3149.

Arriaga, L. R., López-Montero, I., Monroy, F., Orts-Gil, G., Farago, B., & Hellweg, T. (2009). Stiffening effect of cholesterol on disordered lipid phases: A combined neutron spin echo + dynamic light scattering analysis of the bending elasticity of large unilamellar vesicles. *Biophysical Journal*, *96*(9), 3629–3637.

Bangham, A. D., Standish, M. M., & Watkins, J. C. (1965). Diffusion of univalent ions across the lamellae of swollen phospholipids. *Journal of Molecular Biology*, *13*(1), 238-IN27.

Baxa, U. (2018). Imaging of Liposomes by Transmission Electron Microscopy. In S. E. McNeil (Ed.), *Characterization of Nanoparticles Intended for Drug Delivery* (Vol. 1682, pp. 73–88). New York, USA: Springer.

Bhattacharjee, S. (2016). DLS and zeta potential – What they are and what they are not? *Journal of Controlled Release*, *235*, 337–351.

Bitman, J., & Wood, D. L. (1990). Changes in milk fat phospholipids during lactation. *Journal of Dairy Science*, *73*(5), 1208–1216.

Böckmann, R. A., Hac, A., Heimburg, T., & Grubmüller, H. (2003). Effect of sodium chloride on a lipid bilayer. *Biophysical Journal*, *85*(3), 1647–1655.

Chachaty, C., Rainteau, D., Tessier, C., Quinn, P. J., & Wolf, C. (2005). Building up of the liquid-ordered phase formed by sphingomyelin and cholesterol. *Biophysical Journal*, *88*(6), 4032–4044.

Cheng, K., Ropers, M.-H., & Lopez, C. (2017). The miscibility of milk sphingomyelin and cholesterol is affected by temperature and surface pressure in mixed Langmuir monolayers. *Food Chemistry*, *224*, 114–123.

Chemin, C., Bourgaux, C., Péan, J.-M., Pabst, G., Wüthrich, P., Couvreur, P., & Ollivon, M. (2008). Consequences of ions and pH on the supramolecular organization of sphingomyelin and sphingomyelin/cholesterol bilayers. *Chemistry and Physics of Lipids*, *153*(2), 119–129.

Chiang, Y.-W., Shimoyama, Y., Feigenson, G. W., & Freed, J. H. (2004). Dynamic molecular structure of DPPC-DLPC-cholesterol ternary lipid system by Spin-Label Electron spin resonance. *Biophysical Journal*, *87*(4), 2483–2496.

Czamara, K., Majzner, K., Pacia, M. Z., Kochan, K., Kaczor, A., & Baranska, M. (2015). Raman spectroscopy of lipids: A review: Raman spectroscopy of lipids. *Journal of Raman Spectroscopy*, *46*(1), 4–20.

Dewettinck, K., Rombaut, R., Thienpont, N., Le, T. T., Messens, K., & Van Camp, J. (2008). Nutritional and technological aspects of milk fat globule membrane material. *International Dairy Journal*, *18*(5), 436–457.

Dua, J. S., Rana, A. C., & Bhandari, D. A. K. (2012). Liposome: Methods of preparation and applications. *International Journal of Pharmaceutical Studies and Research*, *3* (2), 14 – 20.

Evers, J. M., Haverkamp, R. G., Holroyd, S. E., Jameson, G. B., Mackenzie, D. D. S., & McCarthy, O. J. (2008). Heterogeneity of milk fat globule membrane structure and composition as observed using fluorescence microscopy techniques. *International Dairy Journal*, *18*(12), 1081–1089.

Gallier, S., Gragson, D., Jiménez-Flores, R., & Everett, D. (2010 a). Using confocal laser scanning microscopy to probe the milk fat globule membrane and associated proteins. *Journal of Agricultural and Food Chemistry*, *58*(7), 4250–4257.

Gallier, S., Gragson, D., Jiménez-Flores, R., & Everett, D. W. (2010 b). Surface characterization of bovine milk phospholipid monolayers by Langmuir isotherms and microscopic techniques. *Journal of Agricultural and Food Chemistry*, *58*(23), 12275–12285.

Gallier, S., Vocking, K., Post, J. A., Van De Heijning, B., Acton, D., Van Der Beek, E. M., & Van Baalen, T. (2015). A novel infant milk formula concept: Mimicking the human milk fat globule structure. *Colloids and Surfaces B: Biointerfaces*, *136*, 329–339.

Guyomarc'h, F., Zou, S., Chen, M., Milhiet, P.-E., Godefroy, C., Vié, V., & Lopez, C. (2014). Milk sphingomyelin domains in biomimetic membranes and the role of cholesterol: Morphology and nanomechanical properties investigated using AFM and force spectroscopy. *Langmuir*, *30*(22), 6516–6524.

Hsueh, Y.-W., Zuckermann, M., & Thewalt, J. (2005). Phase diagram determination for phospholipid/sterol membranes using deuterium NMR. *Concepts in Magnetic Resonance Part A*, *26A*(1), 35–46.

Jobin, M.-L., & Alves, I. D. (2019). The Contribution of Differential Scanning Calorimetry for the Study of Peptide/Lipid Interactions. In E. Ennifar (Ed.), *Microcalorimetry of Biological Molecules* (Vol. 1964, pp. 3–15). Springer New York.

Koynova, R., & Caffrey, M. (1995). Phases and phase transitions of the sphingolipids. *Biochimica et Biophysica Acta (BBA) - Lipids and Lipid Metabolism*, *1255*(3), 213–236.

Krafft, C., Neudert, L., Simat, T., & Salzer, R. (2005). Near infrared Raman spectra of human brain lipids. *Spectrochimica Acta Part A: Molecular and Biomolecular Spectroscopy*, *61*(7), 1529–1535.

Lee, C., & Bain, C. D. (2005). Raman spectra of planar supported lipid bilayers. *Biochimica et Biophysica Acta (BBA) - Biomembranes*, *1711*(1), 59–71.

Li-Chan, E. C. Y. (2007). Vibrational spectroscopy applied to the study of milk proteins. *Le Lait*, *87*(4–5), 443–458.

Levin, I. W., Keihn, E., & Harris, W. C. (1985). A Raman spectroscopic study on the effect of cholesterol on lipid packing in diether phosphatidylcholine bilayer dispersions. *Biochimica et Biophysica Acta (BBA) - Biomembranes*, *820*(1), 40–47.

Lopez, C., Madec, M.-N., & Jimenez-Flores, R. (2010). Lipid rafts in the bovine milk fat globule membrane revealed by the lateral segregation of phospholipids and heterogeneous distribution of glycoproteins. *Food Chemistry*, *120*(1), 22–33.

Lopez, C., Cheng, K., & Perez, J. (2018). Thermotropic phase behaviour of milk sphingomyelin and role of cholesterol in the formation of the liquid ordered phase examined using SR-XRD and DSC. *Chemistry and Physics of Lipids*, *215*, 46–55.

Lopez, C. (2020). Intracellular origin of milk fat globules, composition and structure of the milk fat globule membrane highlighting the specific role of sphingomyelin. In P. L. H. McSweeney, P. F. Fox, & J. A. O'Mahony (Eds.), *Advanced Dairy Chemistry, Volume 2* (pp. 107–131). Switzerland: Springer Nature.

Ma, Y., Ghosh, S. K., DiLena, D. A., Bera, S., Lurio, L. B., Parikh, A. N., & Sinha, S. K. (2016). Cholesterol partition and condensing effect in phase-separated ternary mixture lipid multilayers. *Biophysical Journal*, *110*(6), 1355–1366.

Magarkar, A., Dhawan, V., Kallinteri, P., Viitala, T., Elmowafy, M., Róg, T., & Bunker, A. (2015). Cholesterol level affects surface charge of lipid membranes in saline solution. *Scientific Reports*, *4*(5005), 1 – 5.

McMullen, T. P. W., Lewis, R. N. A. H., & McElhaney, R. N. (1993). Differential scanning calorimetric study of the effect of cholesterol on the thermotropic phase behaviour of a homologous series of linear saturated phosphatidylcholines. *Biochemistry*, *32*(2), 516–522.

Melcrová, A., Pokorna, S., Pullanchery, S., Kohagen, M., Jurkiewicz, P., Hof, M., Jungwirth, P., Cremer, P. S., & Cwiklik, L. (2016). The complex nature of calcium cation interactions with phospholipid bilayers. *Scientific Reports*, *6*(1), 38035.

Miyazawa, T., Shimanouchi, T., & Mizushima, S. (1958). Normal vibrations of *N* -methylacetamide. *The Journal of Chemical Physics*, *29*(3), 611–616.

Murthy, A. V. R., Guyomarc'h, F., Paboeuf, G., Vié, V., & Lopez, C. (2015). Cholesterol strongly affects the organization of lipid monolayers studied as models of the milk fat globule membrane: Condensing effect and change in the lipid domain morphology. *Biochimica et Biophysica Acta (BBA) - Biomembranes*, *1848*(10), 2308–2316.

Murthy, A. V. R., Guyomarc'h, F., & Lopez, C. (2016). The temperature-dependent physical state of polar lipids and their miscibility impact the topography and mechanical properties of bilayer models of the milk fat globule membrane. *Biochimica et Biophysica Acta (BBA) - Biomembranes*, *1858*(9), 2181–2190.

Isalomboto Nkanga, C., Murhimalika Bapolisi, A., Ikemefuna Okafor, N., & Werner Maçedo Krause, R. (2019). General Perception of liposomes: Formation, manufacturing and applications. In A. Catala (Ed.), *Liposomes—Advances and Perspectives*. IntechOpen.

Nyholm, T. K. M., Nylund, M., & Peter Slotte, J. (2003). A calorimetric study of binary mixtures of dihydrosphingomyelin and sterols, sphingomyelin, or phosphatidylcholine. *Biophysical Journal*, *84*(5), 3138–3146.

Obeid, S., Guyomarc'h, F., David-Briand, E., Gaucheron, F., Riaublanc, A., & Lopez, C. (2019). The phase and charge of milk polar lipid membrane bilayers govern their selective interactions with proteins as demonstrated with casein micelles. *Journal of Colloid and Interface Science*, *534*, 279–290.

Okotrub, K. A., Zykova, V. A., Adichtchev, S. V., & Surovtsev, N. V. (2020). Deciphering the orientation of lipid molecules by principal component analysis of Raman mapping data. *The Analyst*, *145*(4), 1466–1472.

Pabst, G., Rappolt, M., Amenitsch, H., & Laggner, P. (2000). Structural information from multilamellar liposomes at full hydration: Full *q* -range fitting with high quality x-ray data. *Physical Review E*, *62*(3), 4000–4009.

Quinn, P. J., & Wolf, C. (2009). The liquid-ordered phase in membranes. *Biochimica et Biophysica Acta (BBA) - Biomembranes*, *1788*(1), 33–46.

Schmitt, T., & Neubert, R. H. H. (2018). State of the art in Stratum Corneum research: The biophysical properties of ceramides. *Chemistry and Physics of Lipids*, *216*, 91–103.

Shaw, K. P., Brooks, N. J., Clarke, J. A., Ces, O., Seddon, J. M., & Law, R. V. (2012). Pressure–temperature phase behaviour of natural sphingomyelin extracts. *Soft Matter*, *8*(4), 1070–1078.

Shirota, K., Yagi, K., Inaba, T., Li, P.-C., Murata, M., Sugita, Y., & Kobayashi, T. (2016). Detection of sphingomyelin clusters by Raman spectroscopy. *Biophysical Journal*, *111*(5), 999–1007.

Sinn, C. G., Antonietti, M., & Dimova, R. (2006). Binding of calcium to phosphatidylcholine–phosphatidylserine membranes. *Colloids and Surfaces A: Physicochemical and Engineering Aspects*, *282–283*, 410–419.

Snyder, R. G., Strauss, H. L., & Elliger, C. A. (1982). Carbon-hydrogen stretching modes and the structure of n-alkyl chains. 1. Long, disordered chains. *The Journal of Physical Chemistry*, *86*(26), 5145–5150.

Stępniewski, M., Bunker, A., Pasenkiewicz-Gierula, M., Karttunen, M., & Róg, T. (2010). Effects of the lipid bilayer phase state on the water membrane interface. *The Journal of Physical Chemistry B*, *114*(36), 11784–11792.

Svetlovics, J. A., Wheaten, S. A., & Almeida, P. F. (2012). Phase separation and fluctuations in mixtures of a saturated and an unsaturated phospholipid. *Biophysical Journal*, *102*(11), 2526–2535.

Sułkowski, W. W., Pentak, D., Nowak, K., & Sułkowska, A. (2005). The influence of temperature, cholesterol content and pH on liposome stability. *Journal of Molecular Structure*, *744–747*, 737–747.

Ward, R. E., Watzke, H. J., Jimenez-Flores, R., German, B., (2004). Bioguided Processing: A Paradigm Change in Food Production. *Food Technology*, *58*(5), 44 – 48.

Chapter 4 – Cholesterol-phospholipid interactions resist the detergent effect of bovine bile

4.1 Introduction

Numerous health benefits newly ascribed to dietary phospholipids have increased interest in commercial applications. A complex assembly of protein and phospholipids, the milk fat globule membrane (MFGM) has received growing attention as clinical studies show the consumption of both intact MFGM and isolated milk phospholipids lowers serum lipids, total cholesterol, blood triglycerides, low-density lipoprotein cholesterol, and the alipoprotein B:alipoprotein A-I ratio (Conway et al., 2013; Rosqvist et al., 2015; Vors et al., 2019). In particular, the sphingomyelin (SM) fraction, which makes up ~20 – 25 % of the total phospholipid in the MFGM, is known to modulate cholesterol uptake in both *in vitro* and *in vivo* animal studies (Eckhardt et al., 2002; Noh & Koo., 2004; Norris et al., 2016).

Phospholipids and cholesterol solubilization and uptake occur in the small intestine (Wilde & Chu, 2011). Bile salts incorporate phospholipids into mixed micelles, then an assortment of pancreatic enzymes, including, but not limited to, alkaline sphingomyelinase (NPP-7), intestinal neutral ceramidase and pancreatic phospholipase A2 hydrolyze phospholipids before the hydrolysis products (sphingosine, ceramide, lyso-PC, etc) are absorbed across the intestinal epithelium (Nilsson & Duan, 2006). As the mixed micelles cross the unstirred water layer, (i.e. the diffusion zone of chyme immediately adjacent to the intestinal mucosal layer), monomeric cholesterol desorbs from micelles and crosses the brush-border via either passive diffusion or facilitated transport mechanisms (Yao et al., 2002; Korjamo et al., 2009).

With the fundamentals of intestinal digestion in mind, three possible mechanisms behind how dietary phospholipids inhibiting cholesterol uptake have been considered (Cohn et al., 2010). The absorption of micellar cholesterol depends upon phospholipase A2 (pPLA2) hydrolyzing phospholipids into the lyso form. The addition of phosphatidylcholine (PC) micelles has been shown to reduce the uptake of cholesterol in model intestinal Caco-2 cells, implying that a diet sufficiently high in phospholipid could cause self-inhibition in pPLA2 (Homan & Hamelehle, 1998). However, it was later discovered, that SM is not hydrolyzed by pancreatic enzymes but a brush boarder enzyme, NPP-7, commonly known as alkaline sphingomyelinase (alk-SMase), which is also dependent on bile salt concentration (Duan et al., 2003). Therefore, it is likely SM and PC modulate cholesterol absorption via different mechanisms of actions. A suggested second mechanism is that a surplus of dietary phospholipids, such as SM, can impede the conversion of cholesterol-containing vesicles into micelles (Hernell et al., 1990). Micelles are the ideal physical form for maximal cellular uptake of cholesterol whereas the vesicular (lamellar) form is poorly absorbed by the brush border cholesterol binding protein that mediates cholesterol absorption via a collision-induced transfer mechanism (Thurnhofer & Hauser,

A version of this chapter was published in Colloids and Surfaces B: Biointerfaces

1990). Saturating a vesicle that contains cholesterol with SM results in the formation of detergent-resistant liquid-ordered domains (L_o), assemblies of SM and cholesterol which hinder the bile-induced transition of vesicle → micelle. The final hypothesis is predicated on the activity of membrane proteins being dependent upon the local environment. An abundance of phospholipid may modify the folding of intestinal trans-membrane proteins through electrostatic or hydrophobic interactions, reducing cholesterol absorption (Dowhan & Bogdanov, 2009). Considering that within the MFGM, milk sphingomyelin (MSM) and cholesterol form microscopic liquid-ordered (L_o) domains (Gallier et al., 2010), analogous to the detergent-resistant lipid rafts found in cells, the interaction between MSM and cholesterol may allow cholesterol to persist in a poorly absorbed vesicular (lamellar) form in the presence of bile (Eckhardt et al., 2002). The second hypothesis and the implications of how cholesterol alters micellar structure during intestinal digestion begs further investigation.

Liquid-ordered domains possess intermediate properties of liquid-disordered (L_d) and solid-ordered (S_o) phases. For instance, electron spin resonance experiments show the motion and orientation of spin-labelled probes embedded within an L_o domain have the reorientational motion of a probe within the S_o phase whereas the lateral motion is similar to a probe found in the L_d phase (Chachaty et al., 2005; Quinn & Wolf, 2009). A primary feature of L_o domains is insolubility in the presence of detergents, designating them as detergent-resistant membranes (DRM) which are, by definition, insoluble in cold 1% Triton X-100 (Pike, 2006). This detergent resistance also applies to physiological systems. The introduction of L_o domains into 1-palmitoyl-2-oleoyl-*sn*-glycero-3-phosphocholine (POPC) membranes increases resistance against micellization by a bile salt mixture (Coreta-Gomes et al., 2015). Hydrogenated soy phosphatidylcholine/cholesterol vesicles wholly in the L_o phase produce mixed vesicles when bile salt extract — similar in composition to human bile — is added whereas soy phosphatidylcholine (SPC) vesicles in the L_d phase produce mixed micelles, bile salt-rich bile salt/lipid micelles, when bile extract is added (Hermida, Sabés-Xamaní, & Barnadas-Rodríguez, 2014). In light of these results, L_o domains present within the MFGM may resist micellization in the small intestine, leaving the cholesterol in a poorly absorbed vesicular (lamellar) structure rather than aforementioned easily absorbed micellar phase (Hernell et al., 1990; Eckhardt et al., 2002).

Complementary techniques are necessary to study the structure of phospholipid vesicles, the presence of the L_o phase, and detergent-induced micellization. Transmission electron microscopy (TEM) provides direct observation of detergent-induced vesicle dissociation. Turbidity measured as optical density, tracks the kinetics of vesicle → micelle phase transitions, and has been used to compare rates of micellization for vesicles consisting of egg phosphatidylcholine, egg sphingomyelin (ESM), and cholesterol (Moschetta et al., 2002). Vibrational spectroscopic techniques, such as attenuated total reflection – Fourier transform infrared (ATR-FTIR) and Raman spectroscopy are capable of providing

A version of this chapter was published in Colloids and Surfaces B: Biointerfaces

information about the structure and dynamics of phospholipids and are used to great effect in studying possible H-bonding between the 3-hydroxyl group on cholesterol and amide group of sphingomyelin (Arsov & Quaroni, 2008; Czamara et al., 2015; Shirota et al., 2016).

The objective of this work was to examine how phospholipids from a variety of natural sources (soy, porcine brain, and milk) interact with cholesterol and affect the ensuing mixed micellization process during *in vitro* digestion. The hypothesis is that MSM/cholesterol complexation induces structural changes in the vesicle that persist in the presence of bovine bile.

4.2. Materials and methods

4.2.1. Sample preparation

4.2.1.1 Vesicle preparation

Phospholipid vesicles were prepared in pH 6.7 buffer: PIPES 10 mM (1,4-piperazinediethane sulfonic acid; purity ≥ 99%; Sigma-Aldrich, Auckland, New Zealand), 50 mM NaCl (Analytical Reagent Grade; Thermo Fisher Scientific NZ, North Shore City, New Zealand) and 5 mM $CaCl_2$ (Millipore, Burlington, MA, USA), according to the procedure of Lopez, Cheng, & Perez, (2018). Phospholipid vesicles were composed of milk sphingomyelin (Avanti Polar Lipids, Alabaster, AL, USA), porcine brain phosphatidylcholine (Avanti Polar Lipids), and or soy phosphatidylcholine (Sigma-Aldrich), or binary mixtures of one of these three phospholipid preparations with ovine cholesterol (Sigma-Aldrich). Binary mixtures consisted of 1:0, 4:1, 7:3, 3:2 mol/mol of phospholipid/cholesterol, mol/mol. Total lipid concentration of vesicles was kept at 326 µM to more closely mimic dietary conditions (Bitman & Wood, 1990). Milk sphingomyelin and cholesterol vesicles had been confirmed to be multilamellar using SAXS in Chapter 3. There was no indication that other preparations were multilamellar.

4.2.1.2 Particle size

Particle size of phospholipid vesicles was measured using dynamic light scattering (Malvern Zetasizer Pro, Worcestershire, UK) with data analyzed using the program bundled with the machine, ZX XPLORER 1.4.0.105. The dispersant refractive index was set to 1.330 in the software. The back-scattering angle was 173 °. Before each run the machine was equilibrated to 37 °C for 60 s. Each measurement consisted of the average of 30 runs of 1.68 s each.

4.2.1.3. Bile addition

Bovine bile (dried, unfractionated, Sigma-Aldrich) was reconstituted in Milli-Q water at 37 °C for 30 min before being added to the vesicles for a final concentration of 10 mM bile and 8:1 vesicle/bile, v/v in accordance with INFOGEST recommendations (Brodkorb et al., 2019). The bovine bile dispersion consisted of 70% bile salt, 22% phospholipid, 4% cholesterol, 3% protein, and 0.3%

A version of this chapter was published in Colloids and Surfaces B: Biointerfaces

bilirubin (Hu et al., 2018). The mixture of vesicle and bile was then incubated in a shaking incubator for 2 h at 37 °C and 80 rpm. Samples were refrigerated at 4 °C for up to 2 days before analysis.

4.2.2 Interactions between vesicles and bovine bile

4.2.2.1 Negative stain transmission electron microscopy

Negative stain TEM was carried out on an FEI Tecnai G2 Spirit BioTWIN (FEI Company, Hillsboro, OR, USA) microscope. Vesicles with and without bile were applied onto 3.05 mm, 200 mesh copper grids (Agar Scientific, Essex, UK) pre-coated with Formvar. After allowing the sample to adhere to the carbon resin for 5 min, the remaining wet sample was wicked off using filter paper. Uranyl acetate (2%) was then used to stain the grid for 5 min before being wicked off, ensuring the grid was no longer wet before the sample was loaded into the microscope.

4.2.2.2 Optical density

The optical density (OD) experiments followed the method of Moschetta et al. (2002); however, due to the presence of bilirubin in the bovine bile, vesicle mixtures were measured at 630 nm to minimize bilirubin colour absorbance. OD at 630 nm (OD630) experiments were carried out at 37 °C in a BioTek Synergy 2 thermostated microplate reader (BioTek, Winooski, VT, USA). OD630 measurements were taken for the phospholipid vesicles immediately before samples were placed into the instrument (designated as time T0). Bovine bile (10 mM final concentration, 8:1 v/v vesicle/bile) or taurocholic acid (5 mM final concentration, 8:1 v/v vesicle/bile salt) was added to all samples to measure phospholipid vesicle → micelle transition kinetics. OD630 measurements were then continuously taken every minute for two hours. A control consisting of PIPES buffer and bovine bile or taurocholic acid was also measured, and any absorbance due to the bilirubin was subtracted from each sample.

4.2.2.3 Raman spectroscopy

Raman spectroscopic data were acquired using a confocal microscope adapted from a commercially available inverted fluorescence microscope (Olympus, IX70, Tokyo, Japan) and pumped by a 532-nm fiber-coupled diode laser. Mirrors were used to orient the beam into a 40× microscope objective (numerical aperture = 0.65). Raman scattered light was collected in a 180 ° back-scattering geometry through the 40× microscope objective. The scattered light was directed into a FERGIE detector (Olympus, Princeton Instruments, Trenton, NJ, USA). Samples were sandwiched between two glass microscope cover-slips and frames (250 in total) each lasting 500 ms were taken for each measurement (Shirota et al., 2016; Rankine et al., 2018). The typical power at the sample measured 100 mW.

A version of this chapter was published in Colloids and Surfaces B: Biointerfaces

4.2.3. Statistical analysis

Vesicles were prepared as five independent replicates for each phospholipid/cholesterol ratio. Each instrument collected at least two measurements from each replicate and the mean of five replicates reported. Significant differences between means were determined by mixed-effects ANOVA, with the day that each replicate was analyzed as a random effect. Post-hoc Tukey's HSD analysis ($\alpha < 0.05$) to compare means was carried out using Minitab (State College, PA, USA).

4.3. Results and discussion

4.3.1. Physical characterization of multilamellar vesicles (MLVs)

From dynamic light scattering (DLS) measurements, the average particle size for all phospholipid vesicles ranged from approximately 100 nm to 1 μm, with some larger aggregates present (Appendix 4.1). Negative stain TEM micrographs corroborated particle size data from DLS. Micrographs of the phospholipid vesicles showed a polydisperse distribution of spherical vesicles between 50 nm and 1 μm in diameter as well as the presence of larger aggregates and multilamellar vesicles (Fig. 4.1 a, b).

The majority of biliary phospholipids consist of PC in the form of micelles, unilamellar vesicles, and multilamellar vesicles (Fig. 4.1 c). In human bile, PC aggregates to form onion shell-like multilamellar structures (Konikoff et al., 2000; Gilat & Sömjen et al., 1996). Similar structures were found in the rehydrated bovine bile; albeit the aggregates were cylindrical tendrils consisting of irregularly shaped, fused planar bilayers (Fig. 4.1 d).

When 10 mM of bovine bile was added to the MLVs and the mixture was incubated for 2 h at 37 °C, the bovine bile structures subsumed the vesicles, creating superstructures of several micrometres in size (Fig. 4.1 e). Small aggregates or vesicles budded off from around the edges of these superstructures (Fig. 4.1 e, f; Fig 4.1. f is an expanded view of Fig. 4.1. e).

A version of this chapter was published in Colloids and Surfaces B: Biointerfaces

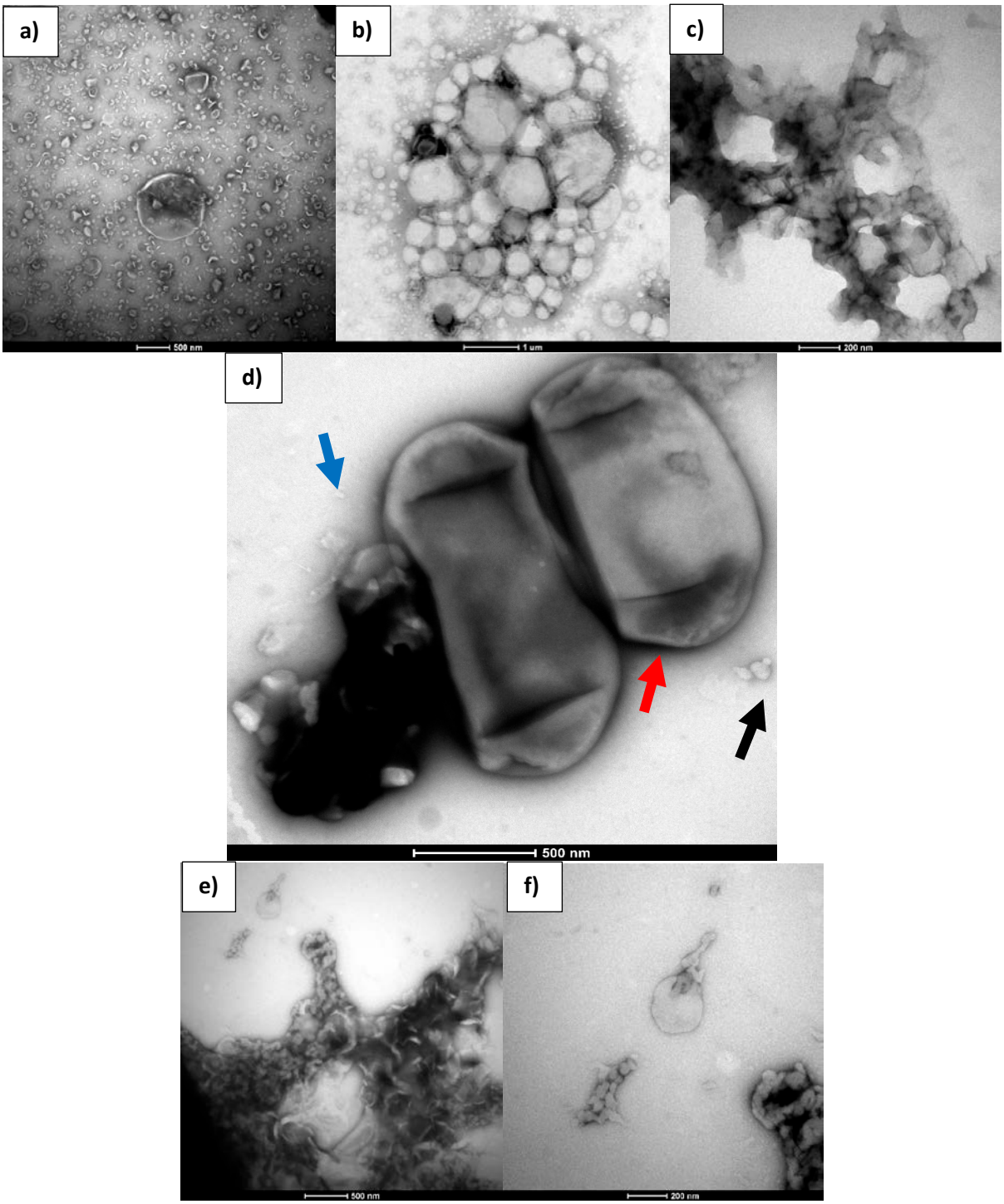

Figure 4.1. Negative stain transmission electron micrographs of milk sphingomyelin (MSM) vesicles

a) No cholesterol, 20,500×.
b) MSM vesicles and aggregates, 16,500×. 3:2 mol/mol MSM:cholesterol.
c) Rehydrated bovine bile, 60,000×. Interlocking plates and vesicles.
d) Rehydrated bovine bile, 43,000×. Red arrow: likely a multivesicular vesicle; black arrow: likely a unilamellar vesicle based on size; blue arrow: mixed micelle based on size.
e) 3:2 mol/mol MSM:cholesterol incubated with bovine bile, 26,500×.
f) Close up for Fig 4.1 e. 60,000×.

A version of this chapter was published in Colloids and Surfaces B: Biointerfaces

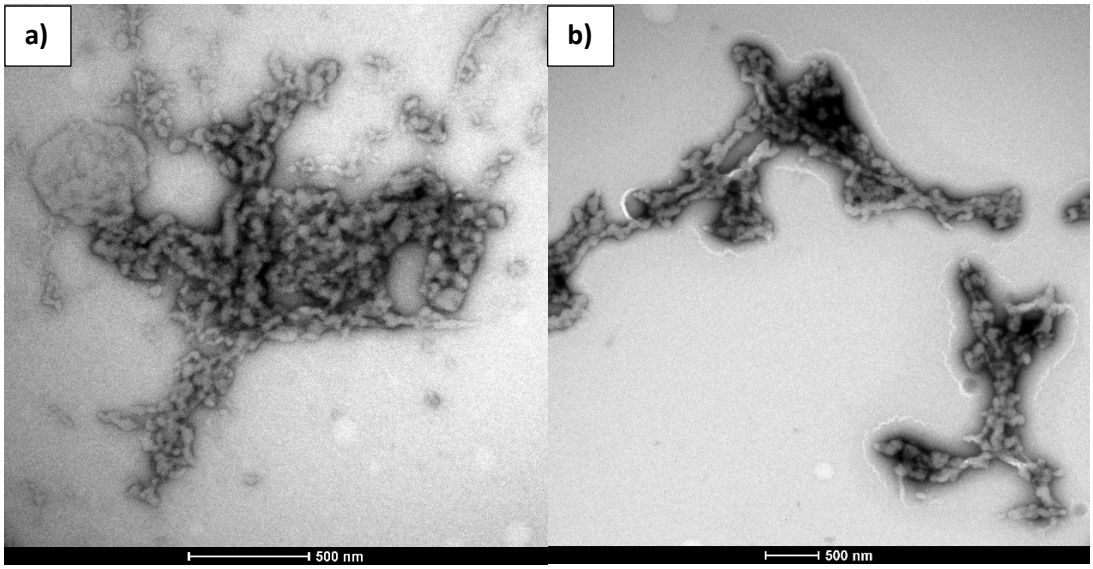

Figure 4.2. Negative stain transmission electron micrographs, brain phosphatidylcholine (BPC)

a) 3:2 mol/mol BPC:cholesterol incubated with bovine bile, 43,000×.
b) 4:1 mol/mol BPC:cholesterol incubated with bovine bile, 20,500×.

In the small intestine, the interaction between bile salts and multilamellar lipolytic products results in the budding of small unilamellar vesicles which serve as metastable cholesterol carriers (Gantz et al., 1999). These unilamellar vesicles are solubilized in the presence of bile salts to form mixed micelles (Hernell et al., 1990).

Aggregates of rod-shaped bile salt-rich vesicle/micelle intermediates were also present (Fig. 4.1 g, h). These tubular structures were not as fibrous as the worm-like micelles seen using cryo-TEM (Dao et al., 2017), but considering the high bile salt environment and the cylindrical micelles evolving from the edges of vesicle superstructures, it is likely these are an intermediate phase between mixed micelles and unilamellar vesicles (Walter et al., 1991).

Regardless of phospholipid origin and cholesterol content, the presence of all three stages of vesicle-to-micelle transformation noted above — the incorporation of phospholipid vesicles into the bile, the budding of structures suspected to be unilamellar vesicles, and the solubilization of those structures into cylindrical vesicle/micelle intermediates — was visually confirmed (Fig. 4.1 e, f; Appendix 4.2). The observed features, the subsuming of vesicles by bile, the micellization of vesicles into micelles, and the presence of rod-shaped micellization intermediates are all well observed in intestinal fluid collected from the duodenum of humans 20 min after consuming a liquid meal (Riethorst et al., 2016). This suggests the colloidal assemblies that are formed with *in vitro* experiments are (at least visually) relevant to the physiological process. However, information concerning the kinetics of detergent-induced solubilization of phospholipid preparations cannot be obtained from negative stain TEM.

A version of this chapter was published in Colloids and Surfaces B: Biointerfaces

4.3.2. The solubilization and micellization of natural phospholipid and phospholipid/cholesterol vesicles by bovine bile

4.3.2.1 Optical density of binary phospholipid/cholesterol vesicles

The optical density experiments were prepared in independent quadruplicates (n = 5). Figure 4.2. shows the optical density at 630 nm (OD630) of MSM with 0 – 40% mol cholesterol incubated with 5 mM taurocholic acid at 37 °C measured as a function of incubation time (up to 2 h). The concentration of taurocholic acid was chosen based on the concentration present in bovine bile (Hu et al., 2018). A control consisting of PIPES buffer and taurocholic acid was used to subtract any background absorbance.

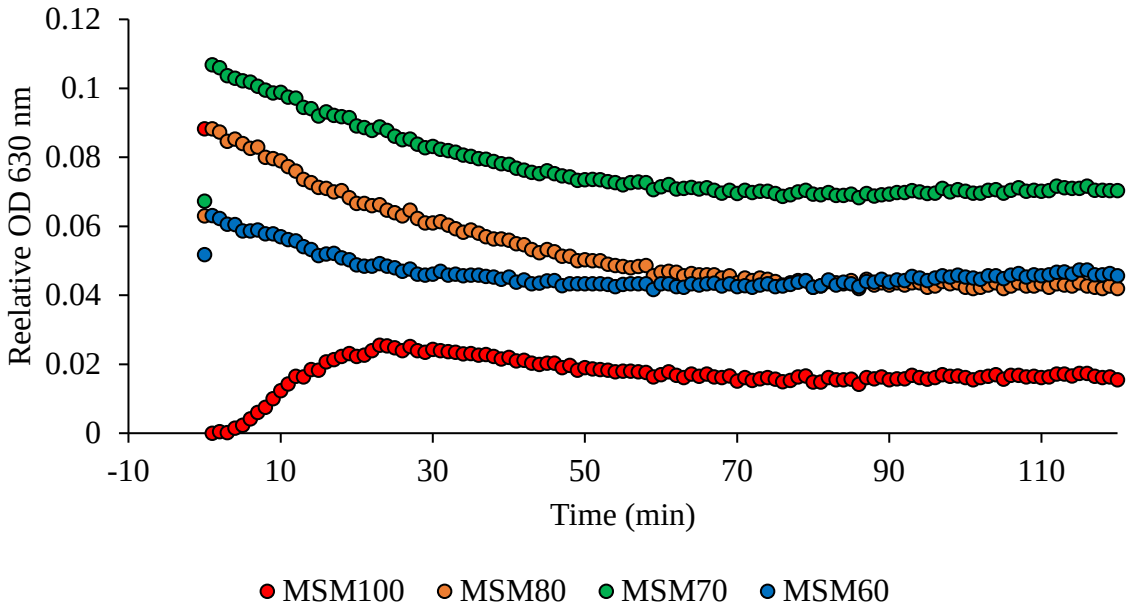

Figure 4.3. Optical density 630 nm of milk sphingomyelin (MSM) multilamellar vesicles incubated with taurocholic acid (5 mM) for 2 h at 37 °C with control (PIPES buffer with bovine bile) subtracted. T0 for each vesicle system and cholesterol ratio are displayed directly on the Y axis. Note the rapid change from T0 to T1 in each case. MSM100 = without cholesterol, MSM80 = 4:1 MSM/cholesterol, MSM70 = 7:3 mol/mol MSM/cholesterol, MSM60 = 3:2 mol/mol MSM/cholesterol.

The initial time, T0, designates the optical density of the MSM multilamellar (MLVs) immediately before taurocholic acid. The first measurement was taken a minute after the bovine bile was added and was designated as T1. For MSM100, where 100 refers to the % mol as a molar ratio of sphingomyelin/cholesterol, i.e. no cholesterol in this case, the difference between T0 and T1 showed a significant reduction in OD630, likely due to detergent-induced micellization.

This trend is reversed after the addition of cholesterol. The increase in OD630 after the addition of taurocholic acid is indicative of either the size growth of vesicle due to the insertion of bile salts, the vesicle changing shape, and/or aggregation (Andrieux et al., 2009). The increase in particle size occurs during the first stage of micellization when low concentrations of bile salts are inserted into the

A version of this chapter was published in Colloids and Surfaces B: Biointerfaces

bilayer. Conversely, the rapid decrease in OD630 and particle size of MSM100 occurs during and after the bilayer reaches a critical point R_e^{sat}, when the bile salts saturate the vesicle surface and surface tension is greatly reduced (Lichtenberg, 1985). As the expansion of vesicle was not reflected in the OD630 for MSM100, it is likely, without cholesterol, that MSM vesicles immediately reach R_e^{sat}. The marked slowing of the micellization process when cholesterol is present could be due to the formation of the more ordered L_o domains that require higher concentrations of bile salts to solubilize (Hermida, Sabés-Xamaní, & Barnadas-Rodríguez, 2014).

The use of bile salts to evaluate bioavailability of orally delivered drugs encapsulated in liposomes is relatively common in the literature (He et al., 2019). However, bile salts alone are not representative of physiological bile which also contains biliary PC, known to act synergistically with the bile salts to displace proteins, protect the intestinal epithelial layer against the cytotoxicity of bile salt monomers, and increase cholesterol solubilization (Macierzanka et al., 2009; Morita & Terada, 2014). The latter function may seem a contradiction as dietary phospholipids are known to reduce cholesterol uptake. An additional source of phospholipid decreases the bile salt:phospholipid ratio in mixed micelles, moving the equilibrium towards intermediates with a higher vesicular character. As understanding the contributions of biliary PC is of great interest, the OD630 experiments were repeated with bovine bile. The BPC and SPC vesicles with 0 – 40% mol cholesterol were included alongside the MSM vesicles (Fig. 4.4). Negative values were present due to the absorbance of the bilirubin in bile at 630 nm. A control blank, consisting of buffer and bovine bile, was used to subtract the absorbance of bilirubin (OD630 measurements, without the buffer and bile subtracted, and can be found in Appendix 4.3 and 4.4).

Once again, the initial time, T0, designates the point immediately before bovine bile was added to phospholipid vesicles. The first measurement was taken a minute after the bovine bile was added and was designated as T1. For all phospholipid vesicles without cholesterol (MSM100, BPC100, SPC100, where 100 refers to the % mol as a mole ratio of phospholipid/cholesterol, i.e. no cholesterol in these three cases), the difference between T0 and T1 showed a significant reduction in OD630. After a progressive decrease in OD630 from 1 min to 30 min, OD values did not experience further statistically significant change.

A version of this chapter was published in Colloids and Surfaces B: Biointerfaces

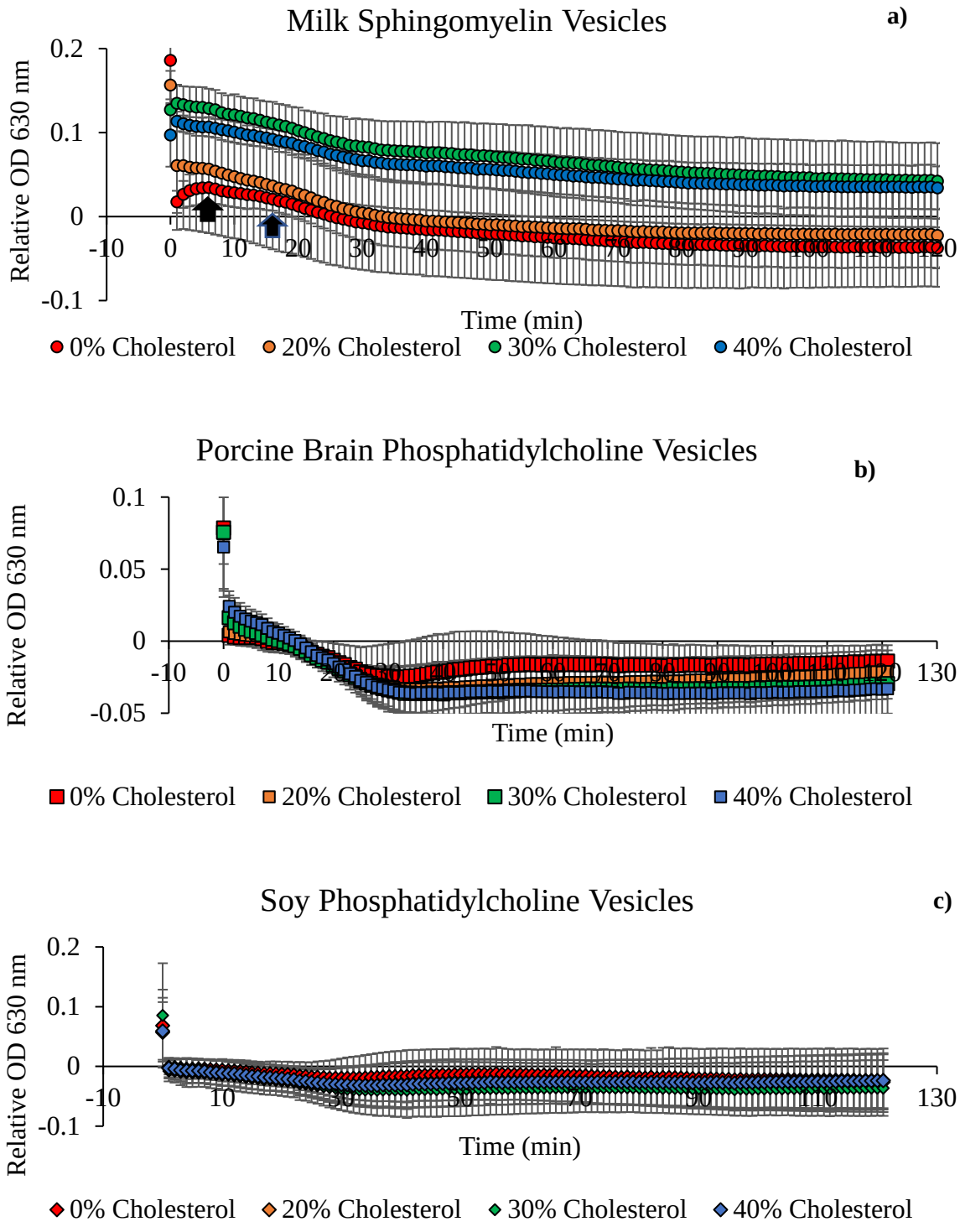

Figure 4.4. Optical density at 630 nm of phospholipid vesicles incubated with bovine bile (10 mM) for 2 h at 37 °C with control (PIPES buffer with bovine bile) subtracted. Black arrows indicate peaks believed to be due to the formation of transient vesicle/micelle intermediates.

a) Bile added to milk sphingomyelin MLVs, 0 – 40 mol % cholesterol.
b) Bile added to porcine brain phosphatidylcholine, phospholipid vesicles 0 – 40 mol % cholesterol. The T0 value for BPC80 overlaps BPC70.
c) Bile added to soy phosphatidylcholine phospholipid vesicles 0 – 40 mol % cholesterol. The T0 value for 20% cholesterol overlaps 40% cholesterol. The 20% cholesterol curve also overlaps the BPC60 curve.

A version of this chapter was published in Colloids and Surfaces B: Biointerfaces

The kinetics of vesicle-to-mixed micelles transition are well in agreement with previous data, even when the source of phospholipid and composition of bile salts differed (Moschetta et al., 2002; Belsito et al., 2000; Simões et al., 2004). The detergent solubilization of lipids is commonly described by a three-stage process with two critical lipid:detergent ratios (Helenius & Simons, 1975), R_{sat}, as previously mentioned, the lipid:detergent ratio where the detergent saturates the bilayer and solubilization of the bilayer is initiated, and R_{sol}, the complete solubilization of the bilayer. Stage one occurs before the R_{sat} is reached and involves the interactions between free detergent monomers and the bilayer. The second stage occurs after R_{sat} is reached. At first, the detergent-induced solubilization and vesicle → micelle transition produces unilamellar vesicles and then cylindrical micelles (also known as wormlike or rod-like micelles). The third stage occurs after R_{sol} and detergent-phospholipid micelles dominate (Lichtenberg, Ahyayauch, & Goñi, 2013). The concentration of bovine bile was high enough that the first stage was not visible in the OD630 profile of MSM100 and MSM80. A large immediate decrease in OD630 implies by the time of the first reading R_{sat} had already been reached and the second stage begun. On the other hand, the OD630 of MSM60 and MSM70 did not instantly decrease with the addition of bovine bile, implying higher amount of bile salt would be necessary to achieve the same degree of solubilization. It should be noted that while the three-stage model is useful for expressing the basic behaviour of lipid/detergent mixtures it is unable to account for the array of intermediate structures and structural changes that occur during micellization (Elsayed & Cevc, 2011).

The large decreases in OD630 from T0 to T1 were likely due to the second stage, rapid micellization of the phospholipid vesicles reduced particle size. For large vesicles (>5000 lipid molecules) which make much most of the phospholipid vesicles, multiple pores are formed, first solubilizing the vesicle into a network of worm-like micelles, and then mixed micelles (Haustein et al., 2015). As evident from the reductions in OD630 across all phospholipid vesicles, the bile salts rapidly intercalate and then rupture the phospholipid vesicles, producing mixed micelles and intermediates, rapidly reducing overall particle size (Belsito et al., 2000). The progressive decrease in OD630 after the rapid T0 to T1 reduction was likely due to the vesicle/micelle mixtures reaching steady state after approximately 40 min. Even at this steady-state, a lipid:bile ratio designated as R_e^{sol}, the mixture is not wholly in the micellar phase but rather as a co-existence of multilamellar vesicles, unilamellar vesicles, and mixed micelles (López et al., 1999; Garidel et al., 2007).

The reduction of OD630 from T0 to T1 for MSM100 was from 0.19 ± 0.05 to 0.017 ± 0.013, 75% of the total OD630 reduction (T0 to T120) (Fig. 4.4 a). Immediately after the T0 to T1 reduction, a peak and an inflection point were observed at 7 and 15 min, respectively (shown by arrows). Similar transient peaks found soon after the addition of detergent have been ascribed to the presence of open vesicles, the intermediate product of trans-bilayer solubilization (Moschetta et al., 2002). After bile salts saturate the bilayer and pores begin to form, a leaky membrane allows bile salts access to the

A version of this chapter was published in Colloids and Surfaces B: Biointerfaces

interior leaflet (Stuart & Boekema, 2007; Lichtenberg, Ahyayauch, & Goñi., 2013). Trans-bilayer solubilization has been linked to detergent trans-bilayer motion and a rapid rate of solubilization (85% reduction of turbidity in 1 min in egg-PC large unilamellar vesicles) (Kragh-Hansen, le Maire, & Møller, 1998; Lete et al., 2019). These reactions are typical of "fast" detergents, such as taurocholic acid which makes up 41% of bovine bile (Lete et al., 2019). As the multilamellar open vesicle intermediates were solubilized, the OD630 reached an inflection point at 30 min, after which decreases in OD630 were not statistically significant.

The T0 and T1 OD630 values for MSM MLVs with 30 and 40% cholesterol (designated as MSM70 and MSM60, respectively) were not significantly different, indicating that the rapid saturation and solubilization observed in the MSM100 (0% cholesterol) did not occur (Fig. 4.4 a). The incorporation of cholesterol into phospholipid bilayers is known to reduce vesicle sensitivity to detergents (Moschetta et al., 2002). The interaction between sphingomyelin and cholesterol is foundational to forming L_o domains, creating detergent-resistant membranes which resist micellization at high bile salt concentrations (up to 56 mM commercial bile salt extract) (Hermida, Sabés-Xamaní, & Barnadas-Rodríguez, 2014). At low concentrations of bile salt (< 2 mM), Hermida, Sabés-Xamaní, & Barnadas-Rodríguez (2014) reported that bile salts monomers are inserted into the vesicle bilayer, inducing membrane shrinkage and leakage. However, when R_e^{sat} is reached, the vesicle is once again stabilized, no longer prone to leakage. The lack of a significant initial immediate reduction from cholesterol containing MSM vesicles incubated with bovine bile agrees well with the hypothesis that the addition of cholesterol to MSM vesicles reduces detergent sensitivity. In light of previous work in *Section 3.3.2* on the properties of L_o domains, it is likely the cause for the detergent resistance is due to the appearance of such domains.

The T0 to T1 reduction for BPC100 was 80% of the total reduction, from 0.079 ± 0.024 to 0.006 ± 0.013 (Fig. 4.4 b). With the addition of cholesterol, T0 to T1 reductions were 71, 56, and 42% of the total reductions for BPC80, 70, and 60, respectively. The addition of cholesterol did not have a significant effect on the detergent sensitivity of BPC (Fig. 4.4 b) or SPC (Fig. 4.4 c) vesicles. The T0 to T1 reductions were 76, 72, 77, and 74% of total OD630 reduction for SPC100, 80, 70, and 60, respectively (Fig. 4.4 c). Although those reductions were statistically significant, the T0 and T1 for all treatments were not statistically significantly different. Therefore, based on the OD630 results, cholesterol has an negligible effect on the detergent resistance of BPC or SPC vesicles.

4.3.2.2 Optical density of ternary phospholipid vesicles

A nascent inquiry into the detergent resistance of ternary phospholipid vesicles consisting of SPC, MSM, and cholesterol confirmed the conclusions drawn from the binary MSM and cholesterol MLV experiments, but also demonstrated the limit of optical density measurements to elucidate vesicle structure during detergent induced micellization. Ternary combinations of MSM, SPC, and

A version of this chapter was published in Colloids and Surfaces B: Biointerfaces

cholesterol were used to better model the MFGM which is rich in both SM and PC and better understand the coexistence between L_o and L_d phases. As these experiments were done earlier than the previous OD630 nm experiments, OD405 nm was used. Figures without the bovine bile subtraction can been found in Appendix 4.4 – 4.6. Each vesicle system was prepared in independent duplicates (n = 2), measurements, technical replicates, were taken three times.

A binary mixture of MSM and SPC with a varying ratio illustrates the dominance of the SPC character during detergent-induced micellization (Fig. 4.5 a). Although the PC present in milk is higher in C18:1 and lower in C18:2 than in soy, ternary vesicles can be useful models for understanding the contributions of each phospholipid species in a complex system. Hints of transient peaks representative of open vesicles due to trans-bilayer micellization that are characteristic of SM detergent vesicle → micelle transition only appear at ≥ 4:1 % mol MSM to SPC. As the SM:PC within MFGM is roughly 2:3 mol/mol, the kinetics of the detergent-induced micellization was expected to follow PC.

Surprisingly, the kinetics of the detergent-induced micellization at 2:3 mol/mol MSM:SPC (Fig. 4.5 b) was constant regardless of cholesterol content. T0 and T1 decreases were not statistically significantly different between 2:3:0 and 2:3:2 % mol/mol/mol MSM:SPC:Chol. At such SM/Chol ratios, L_o domains should be present, and as Figure. 4.4 a shows, a MSM vesicle should be somewhat initially resistant to detergent. In this case, the absence of detergent resistance must be due to the solubilization and dispersion of the unsaturated PC into micellar structures. As the vesicle is majority PC, if enough of the phospholipid is solubilized a decrease in particle size and therefore optical density will occur. Whether the SM/cholesterol, L_o domains persist after being detached from the bulk PC requires further investigation.

A version of this chapter was published in Colloids and Surfaces B: Biointerfaces

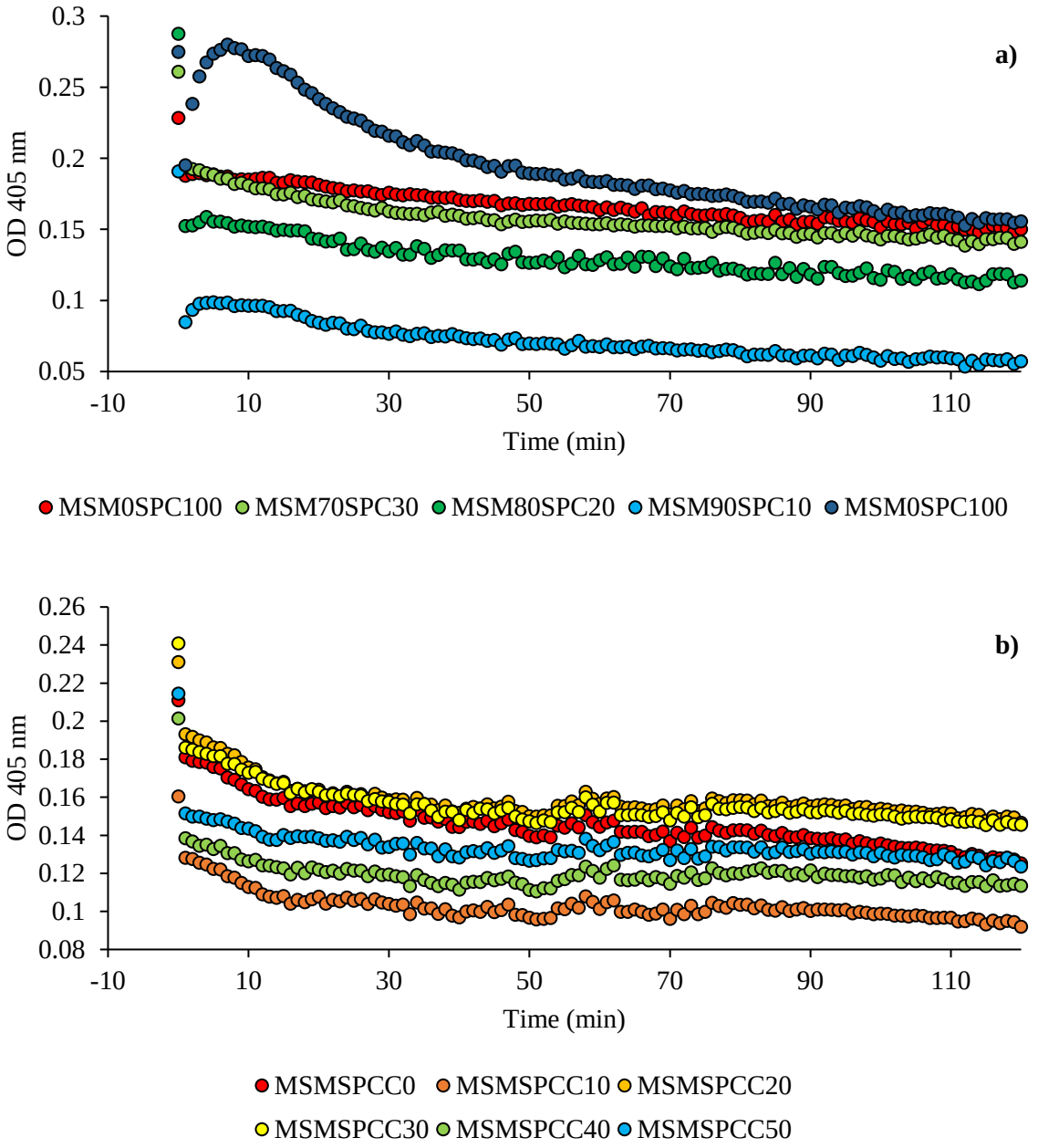

Figure. 4.5. Optical density measurements at 405 nm of the detergent-induced micellization of phospholipid vesicles for 2 h and at 37 °C.

a) Binary phospholipid vesicles consisting of milk sphingomyelin (MSM, variable % mol) and soy phosphatidylcholine (SPC, variable % mol)
b) Ternary phospholipid vesicles consisting of milk sphingomyelin, soy phosphatidylcholine (1:1.6 mol mol MSM:SPC, respectively), and cholesterol (C, variable % mol according to MSM:Cholesterol, i.e. MSMSPCC40 = 100:160:66 μM)

When the cholesterol content was held constant at 27% mol (73% mol total phospholipid), the molar proportion found in the MFGM (Lopez et al., 2018), progressive detergent resistance was observed at ≥ 1:1 MSM:SPC (Fig. 4.6). However, even in the presence of cholesterol, the concentration of MSM must be much greater than the concentration of SPC to render the vesicles wholly resistant to detergent even when the vesicles consist of a high MSM/cholesterol ratio. This is visible from Figure

A version of this chapter was published in Colloids and Surfaces B: Biointerfaces

4.5 b which demonstrates even when the MSM/cholesterol ratio is at 50/50, micellization will occur due to the high SPC content. Further investigation into the ratios necessary to render a vesicle detergent resistant in ternary model membrane systems is necessary. The detergent-induced micellization of MLVs with high SPC:MSM and MSM:cholesterol progress although the MSM/cholesterol complexation is occurring, that is, not enough of the vesicle is in a detergent resistant state to resist micellization. Such a result demonstrates the limitation of optical density techniques which cannot deliver high-resolution information about specific L_o domains or the biliary micelle → mixed micelle, only the state of the MLVs in relation to the initial intact vesicle.

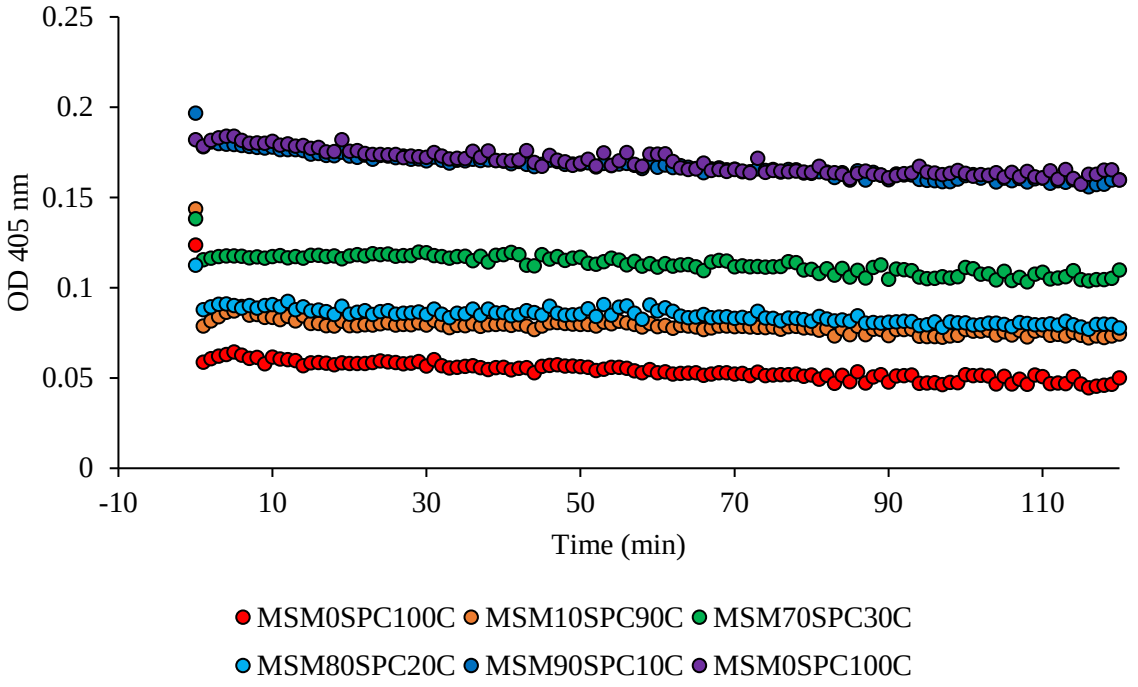

Figure 4.6. Optical density measurements of the detergent induced micellization of milk sphingomyelin (MSM, % mol variable), soy phosphatidylcholine (SPC, % mol variable), and cholesterol MLVs for 2 h and at 37 °C where cholesterol is constant (27% mol).

Besides confirming the detergent resistance of MSM/cholesterol MLVs, optical density was used to distinguish the unique properties of MSM vesicles compared to other naturally sourced phospholipids with choline headgroups. Even in the absence of cholesterol, MSM MLVs are more resistant to biliary detergents than BPC and SPC. However, the detergent resistance of MSM is attenuated in ternary vesicles containing majority SPC. As naturally occurring dietary products like eggs and milk phospholipids are never predominately SM, OD experiments are likely relegated to investigating model systems or complementing other techniques.

4.3.2.2 Raman spectroscopy

The Raman spectra of phospholipid vesicles (Raman shift 1000 – 3000 cm^{-1}) before and after incubation at 37 °C for 2 h with bile were taken (Appendix 4.7 – 4.12). The Raman spectra of samples

A version of this chapter was published in Colloids and Surfaces B: Biointerfaces

were taken at room temperature (~20 °C) as a temperature-controlled stage was unavailable. MSM vesicles without cholesterol were in the solid-ordered phase (S_o) for the duration of the experiment (MSM T_m (34 °C) > 20 °C) (Lopez et al., 2018), whereas BPC and SPC were in the liquid-disordered phase (L_d) due to a low T_m (Appendix 4.13) (O'Neill & Leopold, 1982). Table 4.1 displays literature values for vibrational modes which were used to identify peaks in the Raman spectra. Of interest were the methylene C-H stretching modes (2800 – 3000 cm^{-1}), the C-C skeletal stretching modes (1000 – 1200 cm^{1}), and the amide region (1600 – 1700 cm^{-1}).

Table 4.1. Reference Raman band assignments for phospholipid vesicles.

Reference Mode (cm^{-1})	Assignment	Reference
960	CN asymmetric stretching	(Czamara et al., 2015; Shirota et al., 2016)
1060	C-C stretching (*trans*)	(Czamara et al., 2015; Shirota et al., 2016)
1090	C-C stretching (*gauche*)	(Czamara et al., 2015; Shirota et al., 2016)
1120	C-C stretching (*trans*)	(Czamara et al., 2015; Shirota et al., 2016)
1300	CH_2 twist	(Czamara et al., 2015; Shirota et al., 2016)
1445	CH_2 deformation	(Czamara et al., 2015; Shirota et al., 2016)
1645	Amide I	(Czamara et al., 2015; Yagi et al., 2015; Shirota et al., 2016)
1676	C=C stretching	(Shirota et al., 2016)
2850	*sp3* CH_2 symmetric stretching	(Synder et al., 1982; Levin et al., 1985; Batenjany et al., 1994; Lee & Bain, 2005)
2880	*sp3* CH_2 asymmetric stretching	(Synder et al., 1982; Levin et al., 1985; Batenjany et al., 1994; Lee & Bain, 2005)
2930	Fermi resonance *sp3* CH_3 symmetric stretching	(Synder et al., 1982; Levin et al., 1985; Batenjany et al., 1994; Lee & Bain, 2005)

4.3.2.2.1 The effect of cholesterol on phospholipid acyl chain interchain interactions and gauche/trans conformational isomerism

Figure 4.7 displays two MSM MLV Raman spectra (spectra for all the phospholipid vesicle systems can be found in Appendices 4.7 and 4.8). Three peaks were of interest in the methylene region, the symmetric C-H stretching mode (2850 cm^{-1}), the asymmetric C-H stretching mode (2880 cm^{-1}), and the Fermi resonant symmetric terminal acyl stretching mode coupled with overtones from other modes (2930 cm^{-1}) (Snyder et al., 1982). The two peaks of interest in the C-C skeletal stretching region were the modes used to establish the *gauche* (1085 cm^{-1}) and *trans* isomers (1130 cm^{-1}) (Fig. 4.7 c). Frequency shifts in phospholipids are well-documented; however, the reasons for those shifts have not been thoroughly investigated. One possible reason for frequency shifts in the CH region is an increase in chain order (Lee & Bain, 2005).

Figure 4.7 – 4.9 reports the I_{2850}/I_{2880}, I_{2930}/I_{2880}, and I_{1085}/I_{1130} ratios for phospholipid vesicles before and after incubation with bovine bile (Appendix 4.14 for tabulated values). The peak intensity ratio I_{2850}/I_{2880} furnishes an index of acyl chain disorder/order arising from lateral chain-chain interactions,

A version of this chapter was published in Colloids and Surfaces B: Biointerfaces

I_{2930}/I_{2880} offers the same interchain information while also including the degree of conformational isomerism (*gauche/trans*), and I_{1085}/I_{1130} is solely the degree of intrachain interactions which includes conformational isomerism (Bunow & Levin, 1977; Yellin & Levin, 1977; Levin et al., 1985; Batenjany et al., 1994; Orendorff, Ducey, & Pemberton, 2002; Bryce et al., 2018).

Both the I_{2850}/I_{2880} (Fig. 4.7 b, c) and I_{2930}/I_{2880} (Fig. 4.8 b, c) ratios for BPC and SPC phospholipid vesicles show no significant differences in interchain disorder/order or overall bilayer order with the addition of cholesterol (no bile). The I_{1085}/I_{1130} reflects the results from the I_{2930}/I_{2880} ratio but diverges for the BPC100 (0% cholesterol, $I_{1085}/I_{1130} = 2.07 \pm 0.20$) where the addition of cholesterol (BPC 20% cholesterol, $I_{1085}/I_{1130} = 1.73 \pm 0.13$) increased the proportion of *trans* isomers in the BPC vesicles (Fig. 4.9 b). A similar trend has been previously observed in 1-octadecanoyl-2--(9Z-octadecenoyl)-*sn*-glycero-3-phosphocholine (SOPC, 18:0; 18:1)/cholesterol bilayers (Genova et al., 2018). The addition of ≥ 30% mol cholesterol induced phase separation of the cholesterol and SOPC, leading to no interchain interactions between the lipids; however, the intrachain ordering was conserved. Therefore, a weak interaction between cholesterol and a moderately saturated PC such as BPC exists through the conformational isomerization of *gauche* to *trans* acyl chain.

A version of this chapter was published in Colloids and Surfaces B: Biointerfaces

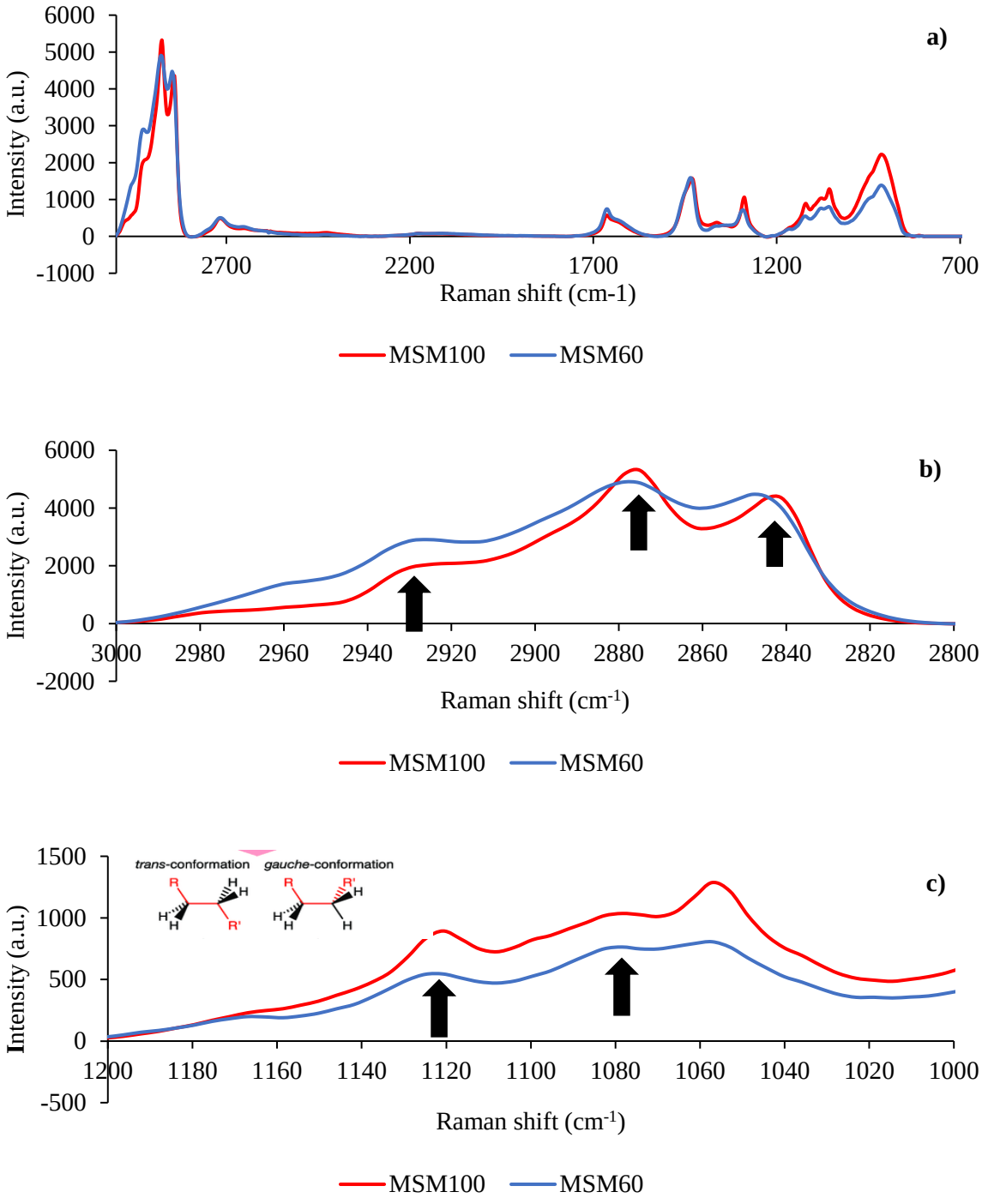

Figure 4.7. Raman spectra of milk sphingomyelin (MSM) multilamellar vesicles with no cholesterol (MSM100) and 3:2 mol:mol MSM:cholesterol (MSM60).

a) The entire spectrum taken, 700 – 3000 cm^{-1}.
b) Methylene region (2800 – 3000 cm^{-1}); from left to right, arrows indicate peaks that correspond to 2930, 2880, 2850 cm^{-1} modes.
c) C-C skeletal region (1000 – 1200 cm^{-1}); from left to right, arrows indicate peaks that correspond to 1130 and 1085 cm^{-1} modes. Includes a Natta projection of gauche and trans rotamers reproduced from Uematsu & Shimizu, (2021)

A version of this chapter was published in Colloids and Surfaces B: Biointerfaces

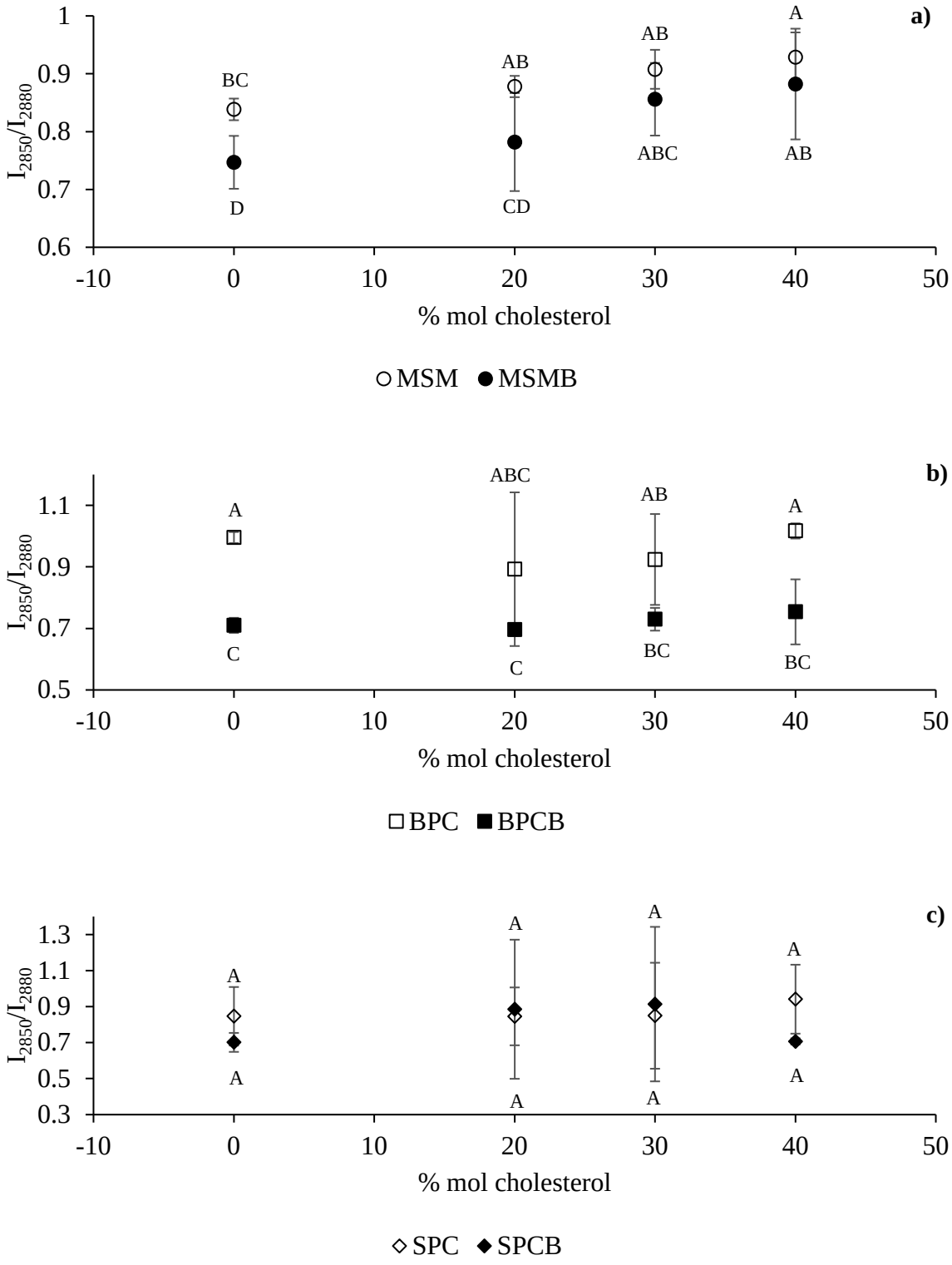

Figure 4.8. Lateral interchain packing (I_{2850}/I_{2880}) of phospholipid/cholesterol vesicles. Different letters indicate significant differences ($p \geq 0.05$) in each phospholipid type.

a) MSM = milk sphingomyelin; MSMB = milk sphingomyelin + bovine bile.
b) BPC = porcine brain phosphatidylcholine; BPCB = porcine brain phosphatidylcholine + bovine bile.
c) SPC = soy phosphatidylcholine; SPCB = soy phosphatidylcholine + bovine bile.

A version of this chapter was published in Colloids and Surfaces B: Biointerfaces

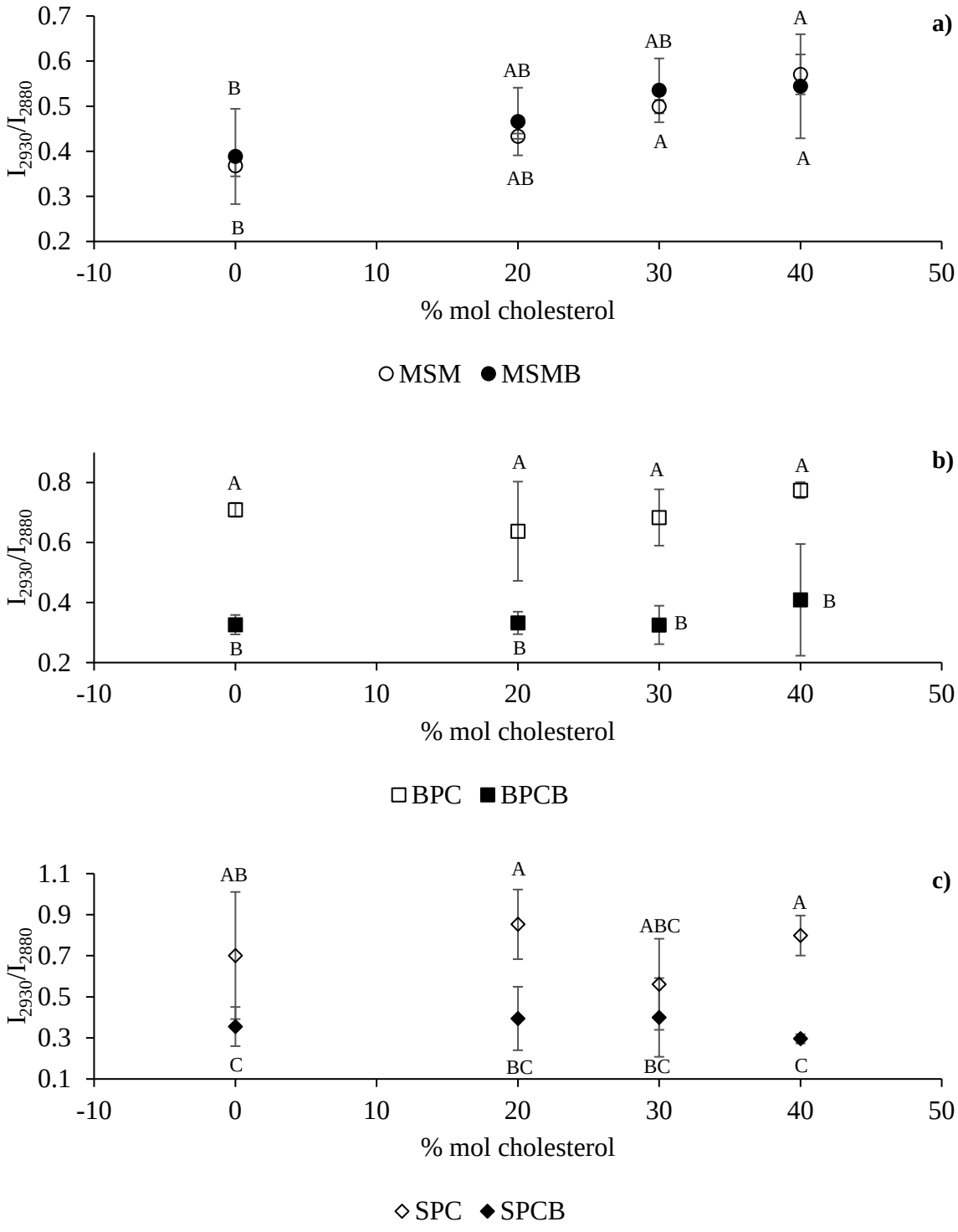

Figure 4.9. Lateral interchain plus the degree of intrachain packing (I_{2930}/I_{2880}) of phospholipid/cholesterol vesicles. Different letters indicate significant differences ($p \geq 0.05$) in each phospholipid species.

a) MSM = milk sphingomyelin; MSMB = milk sphingomyelin + bovine bile.
b) BPC = porcine brain phosphatidylcholine; BPCB = porcine brain phosphatidylcholine + bovine bile.
c) SPC = soy phosphatidylcholine; SPCB = soy phosphatidylcholine + bovine bile.

A version of this chapter was published in Colloids and Surfaces B: Biointerfaces

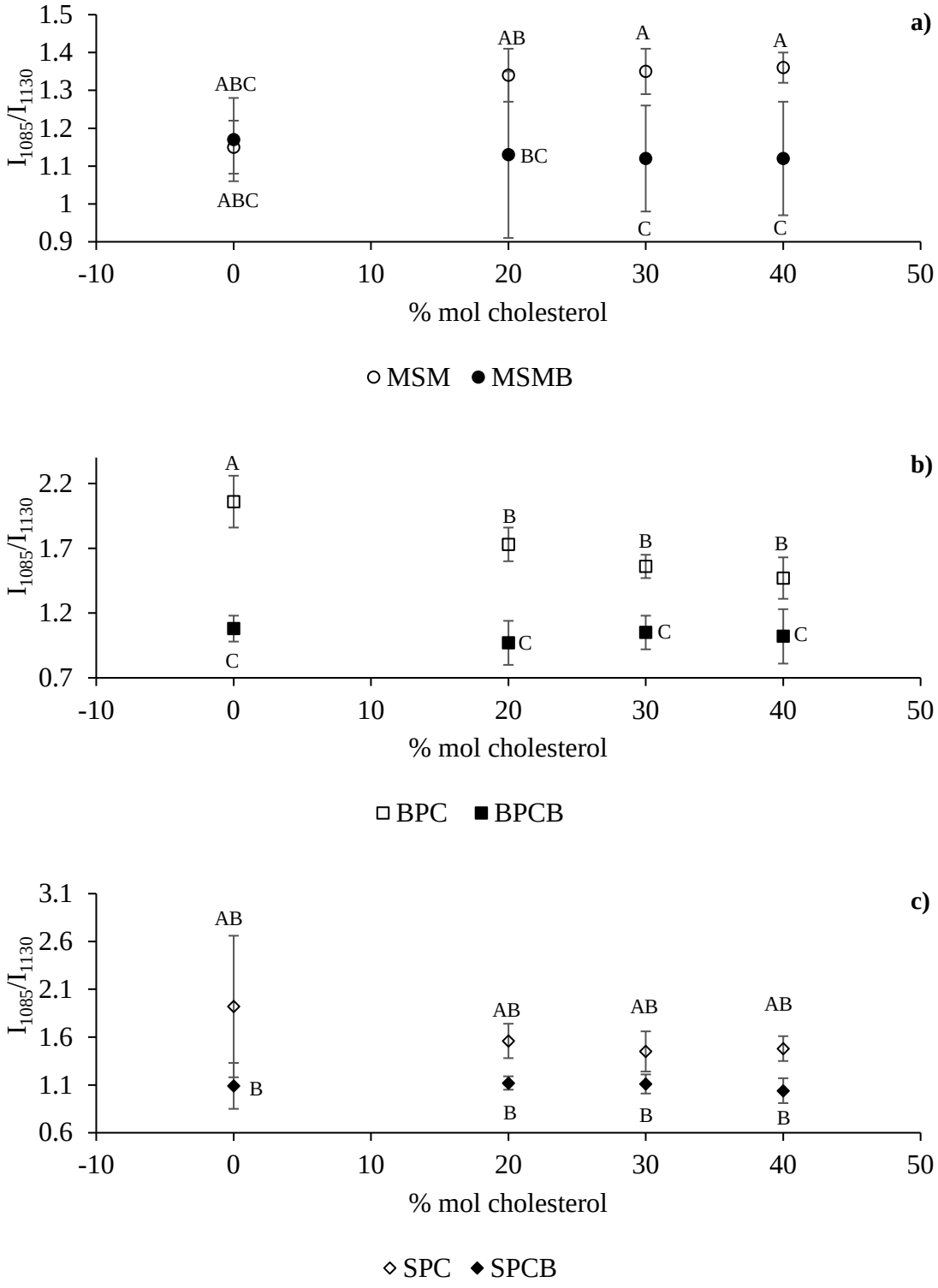

Figure 4.10. Intrachain rotational conformation (I_{1085}/I_{1130}) of phospholipid/cholesterol vesicles. Different letters indicate significant differences ($p \geq 0.05$) in each phospholipid species.

a) MSM = milk sphingomyelin; MSMB = milk sphingomyelin + bovine bile.
b) BPC = porcine brain phosphatidylcholine; BPCB = porcine brain phosphatidylcholine + bovine bile.
c) SPC = soy phosphatidylcholine; SPCB = soy phosphatidylcholine + bovine bile.

A version of this chapter was published in Colloids and Surfaces B: Biointerfaces

Conversely, the addition of cholesterol to MSM had no effect on intrachain rotational isomerization (I_{1085}/I_{1130}) (Fig 4.10. a) but significantly increased the lateral interchain packing disorder (I_{2850}/I_{2880}) from 0.838 ± 0.018 (MSM100) to 0.93 ± 0.04 (MSM60) (Fig. 4.8 a), and for I_{2930}/I_{2880}, 0.368 ± 0.023 (MSM100) to 0.57 ± 0.04 (MSM60) (Fig. 4.9 a). This elevated hydrocarbon chain disorder indicates that MSM increasingly transitioned from the S_o phase into a L_o phase as cholesterol was added. Intrachain conformation was not statistically significantly different when cholesterol was present (Fig. 4.10 a). In contrast, a phase transition from S_o to L_d shows considerable *trans*-to-*gauche* rotational isomerization (Levin et al., 1985; Batenjany et al., 1994). Consequently, the decreased bilayer periodicity observed in SAXS measurements (Lopez, Perez, & Cheng, 2018) of MSM vesicles in the S_o phase when cholesterol is added could be attributed to this increase in interchain disorder rather than increases in *gauche* isomers.

Increases in the proportion of *trans* isomers observed in the I_{1085}/I_{1130} for BPC vesicles (Fig. 4.10 b) when cholesterol was added were not reflected in the corresponding I_{2930}/I_{2880} ratio (Fig 4.9 b). This is peculiar as the change in lateral interchain packing (I_{2850}/I_{2880}) present when cholesterol was added to MSM was reflected by the corresponding I_{2930}/I_{2880} (Fig. 4.9 a). Cholesterol is known to have a greater affinity for the saturated MSM than PC (Noh & Koo, 2004). Even when hydrocarbon chain lengths are equal, SM has a higher affinity for PC (Lönnfors et al., 2011). Molecular dynamic studies show that, whereas PC can be an acceptor of hydrogen bonding from other molecules, SM is capable of forming both inter- and intralipid hydrogen bonds in bilayers (Niemelä et al., 2004). The presence of cholesterol in SM bilayers enhances interlipid hydrogen bonding to form hydrogen bonding networks (Slotte, 2016). This increased degree of hydrogen bonds pushes cholesterol molecules towards the inner leaflet, minimizing entropic penalties, and maximizing the umbrella effect where the hydrophilic headgroups of the phospholipids reduce interactions between the apolar regions of the bilayer and the bulk aqueous medium (Yasuda et al., 2014).

4.3.2.2.2 Effect of bile and cholesterol additions on phospholipid acyl chain interchain interactions and gauche/trans conformational isomerism

The addition of bile significantly decreased the disorder/order ratio of all phospholipid preparations without cholesterol (MSM100, BPC100, SPC100), increasing the degree of order in both inter or intrachain packing (Fig. 4.8, 4.9, 4.10). From the TEM micrographs (Fig 4.1), detergents solubilize vesicles into micelles, a more thermodynamically favourable state. Incorporating bile salt monomers into the phospholipid bilayer increases curvature strain leading to an excess of endothermic enthalpy (Heerklotz et al., 2008). As the bilayer reaches saturation, the excess enthalpy reaches its maximum and the vesicle transition into cylindrical micelles (Heerklotz et al., 2008). Furthermore, micelles are known to be more rigid than vesicles, due to tighter molecular packing, hence a higher degree of order (Alshehab et al., 2019).

A version of this chapter was published in Colloids and Surfaces B: Biointerfaces

For SPC and BPC vesicles, this decrease in disorder/order from detergent-induced micellization persisted regardless of cholesterol content. Egg yolk PC is known to distribute preferentially into mixed micelles and small unilamellar vesicles in the presence of taurocholate (Eckhardt et al., 1999; Yasuda et al., 2014). The OD630 for SPC and BPC showed no significant difference in the optical density at any points throughout the two-hour incubation with bovine bile, suggestive of "complete" micellization or at least a lipid:bile salt ratio greater than R_{sol} (Fig. 4.4 b, c). Although the overall decrease in disorder/order could be ascribed to micellization, the nature and degree of this ordering differs, depending upon the source of the PC and therefore its hydrocarbon chain length and saturation.

Both lateral interchain packing (I_{2850}/I_{2880}) and intrachain rotational conformation (I_{1085}/I_{1130}) of SPC vesicles containing cholesterol incubated with bovine bile were not significantly different to vesicles without bovine bile (Fig. 4.8 c, 4.10 c); however, SPC with 0%, 20%, and 40% cholesterol with added bile had a reduced I_{2930}/I_{2880} compared to vesicles without bile, implying an increase in either interchain or intrachain order (Fig. 4.9 b). Although this result may seem contradictory at first, the presence of a large standard deviation for the I_{2850}/I_{2880} and I_{1085}/I_{1130} for SPC100 (0% cholesterol) (Fig. 4.8 a, c) without bile in the mixed effects ANOVA model yields non-significant differences.

The addition of bile to SPC bilayers and subsequent micellization had no effect on the interchain packing but did increase intrachain order in the SPC acyl chains regardless of cholesterol content, likely increasing the proportion of *trans* isomers in the SPC bilayer. Although the exact orientation of acyl chains in phospholipid/bile salt micelles has yet to be elucidated, detergent micelles are known to consist of either all *trans* or partially *gauche* acyl chains (Kalyansundaram & Thomas, 1976; Lichtenberg et al., 1983). Bile-induced *gauche* to *trans* isomerization was also present for BPC, regardless of the cholesterol content (Fig. 4.9 b).

The MSM MLV interactions with bile and cholesterol were the most complex to parse. There was no significant difference in I_{2930}/I_{2880} for vesicles with or without bile (Fig. 4.8 b). However, the I_{2850}/I_{2880} of MSM100 and MSM80 decreased from 0.838 ± 0.018 to 0.75 ± 0.05, and 0.878 ± 0.018 to 0.78 ± 0.09, before and after bile addition respectively, indicating an increase of order in the interchain packing (Fig. 4.8 a). The I_{1085}/I_{1130} for the MSM was the opposite, with an increase of *trans* isomers for MSM70 and MSM60 from 1.35 ± 0.06 to 1.12 ± 0.14, and 1.36 ± 0.04 to 1.12 ± 0.15 before and after bile addition, respectively (Fig. 4.8 c). That is to say, the ordering effect of bovine bile on the MSM vesicle system depended upon the concentration of cholesterol present. In the absence of cholesterol, MSM MLVs were in the S_o phase. The S_o phase will be directly converted into the micellar form and is known to require a lower concentrations of bile salt and less time to solubilize than PC (Moschetta et al., 2002) at temperatures below the T_m of the lipid. However, cholesterol-rich membranes do not disintegrate when detergent is added; these form larger resistant

A version of this chapter was published in Colloids and Surfaces B: Biointerfaces

particles that coexist with detergent micelles (Apel-Paz et al., 2005). With the cholesterol already acting as a "cement" for the bilayer, it is unlikely that the addition of bile adds an observable amount of additional lateral order to the bilayer. The order that bovine bile supplies is seemingly intrachain order. At cholesterol concentrations ≥ 30%, the addition of bile increased intrachain order. Such I_{1085}/I_{1130} values for vesicles with ≥ 30% cholesterol and incubated with bile were similar to values for the MSM MLVs in the S_o phase (MSM100), implying less of an inverse effect, but conservation of the original hydrocarbon chain order (Appendix 4.14).

Based on the Raman peak intensity ratios above, MSM/cholesterol vesicle systems are resistant to solubilization by physiological concentrations of bile. Therefore, it stands to reason that MSM and cholesterol complexes may slow down the micellization of dietary and possibly even biliary cholesterol, as well as other lipids, during intestinal digestion.

4.3.2.2.3. Bovine bile interactions with the PC ester and MSM amide regions

When embedded in a bilayer, cholesterol is known to align so that the polar hydroxyl group is pointed towards the hydrophilic choline headgroup of PC or SM (Smondyrey & Berkowitz, 1999). This orientation not only minimizes hydrophobic size mismatch between sterol molecules and long hydrocarbon chains, but also has been speculated to promote hydrogen bonding networks throughout the bilayer (Pandit, Bostick, & Berkowitz, 2004; Jaikishan & Slotte, 2011). Molecular dynamics models have postulated that the cholesterol embedded in PC bilayers forms hydrogen bonds with the CH groups on the choline headgroup. Although CH to O hydrogen bonds alone (i.e. in CH_4) only have 7% of the bond strength of a typical hydrogen bonds, the electron withdrawing properties of the PC choline head group $-N(CH_3)_3$ substantially increases the strength of the CH to O hydrogen bond (Pandit, Bostick, & Berkowtiz, 2004).

In SM bilayers, the cholesterol polar hydroxyl group has been suggested to form hydrogen bonds with the SM amide group (Arsov & Quaroni, 2008). Methylation of either the hydroxyl group of cholesterol or the amide group minimizes interaction of sphingomyelin with cholesterol (Lönnfors et al., 2011). The interactions involved with this amide group can be tracked in the 1600 – 1700 cm^{-1} region, in particular, the 1670 cm^{-1} and 1654 cm^{-1} reference modes which are the C=O stretching vibrations and the N-H bending vibrations (Czamara et al., 2015). Shirota et al., (2016) assigns 1670 cm^{-1} as the C=C stretching and 1654 cm^{-1} as the C=O stretch with contributions from N-H.

A version of this chapter was published in Colloids and Surfaces B: Biointerfaces

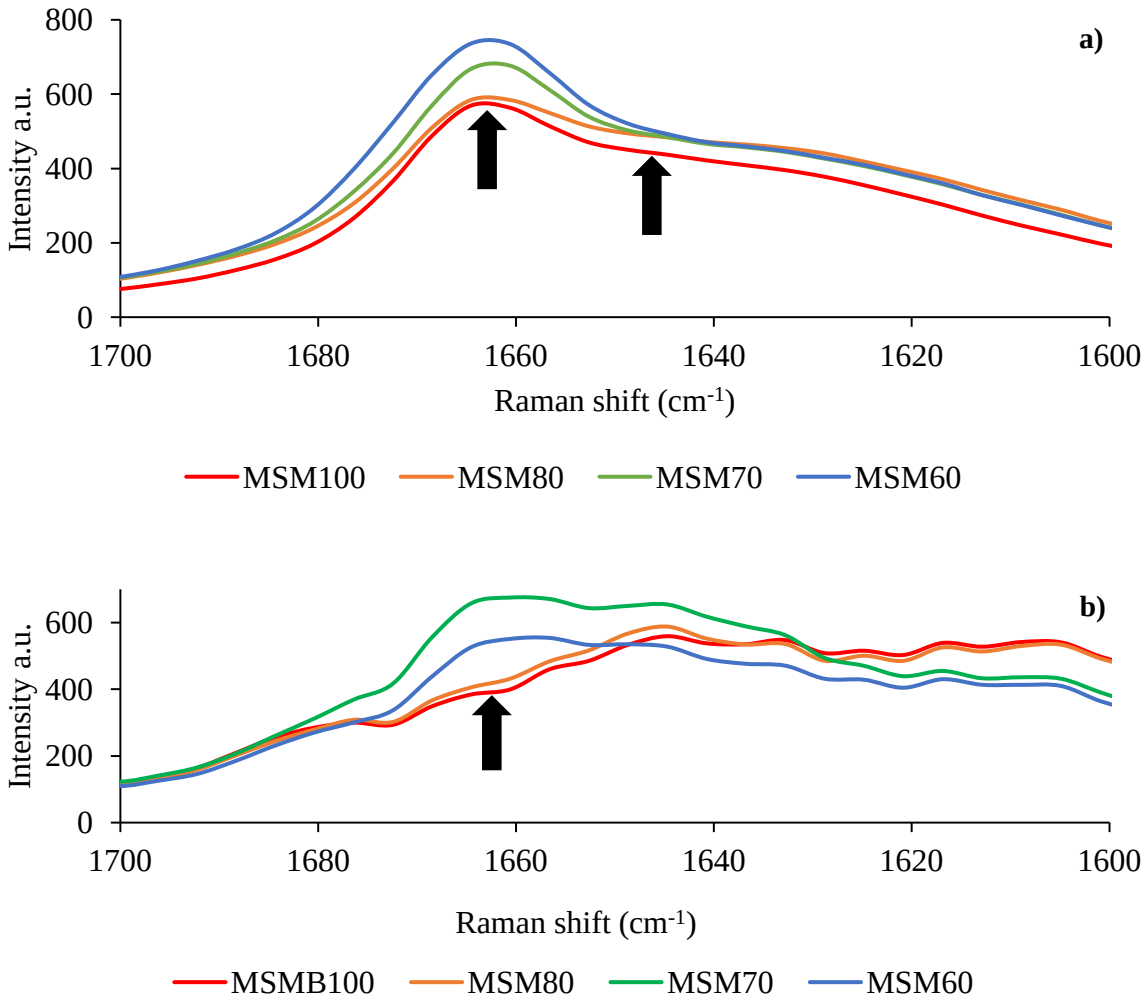

Figure 4.11. Raman spectra of the MSM vesicle amide region (1600 – 1700 cm^{-1}).

a) MSM vesicles with 0 – 40% cholesterol added. From left to right, arrows indicate the corresponding 1670 and 1654 cm^{-1} reference modes.

b) MSM vesicles with 0 – 40% cholesterol added, incubated with bile. Arrow indicates the 1670 cm^{-1} mode. The peak has almost completely disappeared at ≤ 20% cholesterol.

Egg sphingomyelin vesicles without cholesterol show a peak at 1654 cm^{-1} (Shirota et al., 2016). This feature dissipates as higher concentrations of cholesterol are added to the vesicle, disappearing when the cholesterol concentration is ≥ 40%. The disappearance of the peak has been attributed to cholesterol inhibiting hydrogen bonding between SM molecules (Levin et al., 1985; Arsov & Quaroni, 2008; Yagi et al., 2015; Shirota et al., 2016). Yet, as Figure 4.11 demonstrates, although the faint outline of an amide feature was present, the addition of cholesterol had no visible effect on its intensity. If a direct hydrogen bond between the polar hydroxyl group of cholesterol and the amide group on SM does not exist it is possible the hydrogen bonding network encloses the cholesterol, reducing the probability of desorption from the bilayer and therefore increasing total order without the need for a direct stabilizing hydrogen bond between cholesterol and SM (Lala et al., 1981; Yasuda et al., 2014).

A version of this chapter was published in Colloids and Surfaces B: Biointerfaces

The 1670 and 1654 cm^{-1} modes for MSM disappeared when bovine bile was added to MSM vesicles with ≤ 20% cholesterol. However, the carboxyl ester peak (1664 cm^{-1}) was clearly visible at ≥ 30% cholesterol (Fig. 4.11 b). Furthermore, MSM vesicles with ≤ 20% cholesterol were shown to have significantly higher T0 to T1 reductions in the OD630 and had increased order in interchain packing when incubated with bovine bile (Fig. 4.4, Appendix 4.14). The disappearance of the carboxyl mode at these lower cholesterol concentrations suggests that MSM was transitioning from vesicle to micellar forms. For MSM vesicles with concentrations of cholesterol that were ≥ 30%, the persistence of the carboxyl ester mode suggests a retention of vesicle structure.

4.4. Conclusions

In conclusion, the addition of cholesterol and bovine bile modifies phospholipid bilayer hydrocarbon chains within vesicles. Cholesterol delays the micellization of MSM MLVs, as measured by optical density. This did not occur for SPC and BPC vesicles. From Raman spectroscopy, the addition of cholesterol to BPC and SPC vesicles in the L_d phase increased the proportion of *trans* isomers present without changing the vesicle interchain lateral packing. Conversely, in MSM bilayers, cholesterol only affected interchain lateral packing and had no effect on the intrachain rotational isomerization. Therefore, the detergent resistance of SM/cholesterol complexes seemingly originates from the ability of cholesterol to change lateral packing when embedded in an MSM bilayer.

Interactions between cholesterol and phospholipid acyl chains were an observable factor in providing SM and cholesterol complexes with detergent resistance. These interactions have been hypothesized to be intermolecular hydrogen bonds, hydrophobic interactions, and Van der Waals forces (Shirota et al., 2016). No direct evidence of hydrogen bonds between hydroxyl groups of cholesterol and amide groups in SM could be found when cholesterol was added to MSM bilayers with the techniques used, as shown in Figure 4.10. Additional research into bile salt and amide interactions may shed new light on how cholesterol modification of SM bilayers renders the bilayer detergent-resistant, and without cholesterol SM undergoes a high degree of trans bilayer micellization.

Furthermore, the presence of ≥ 30% cholesterol in SM MLV systems that contained concentrations of SM similar to that of liquid milk nullified the detergent effect of bovine bile as evident from the bilayer order ratios obtained from Raman spectroscopy. The detergent-resistant SM and cholesterol complexation persists in a physiologically relevant bile preparations. This is not the case for either soy or porcine brain PC. This result once again highlights the uniqueness of SM in combination with cholesterol in modulating digestive processes.

The verification of the bile resistance in SM/cholesterol complexes in bovine bile contributes to a better understanding of how phospholipids behave during digestion, as well as the structural changes induced from the addition of complex, physiological detergents such as bile. Further questions are raised on the effect of lipase on the structure of dietary phospholipid assemblies, the evolutionary

A version of this chapter was published in Colloids and Surfaces B: Biointerfaces

purpose of detergent resistance domains in food products, such as milk, and the impact on those who suffer from hypercholesterolemia.

Acknowledgements

The Python program used to baseline, average, and process the Raman data was coded by Dr. Mark Waterland of Massey University.

References

Alshehab, M., Budamagunta, M. S., Voss, J. C., & Nitin, N. (2019). Real-time measurements of milk fat globule membrane modulation during simulated intestinal digestion using electron paramagnetic resonance spectroscopy. *Colloids and Surfaces B: Biointerfaces*, *184* (110511), 1 – 9.

Andrieux, K., Forte, L., Lesieur, S., Paternostre, M., Ollivon, M., & Grabielle-Madelmont, C. (2009). Solubilisation of dipalmitoylphosphatidylcholine bilayers by sodium taurocholate: A model to study the stability of liposomes in the gastrointestinal tract and their mechanism of interaction with a model bile salt. *European Journal of Pharmaceutics and Biopharmaceutics*, *71*(2), 346–355.

Apel-Paz, M., Doncel, G. F., & Vanderlick, T. K. (2005). Impact of membrane cholesterol content on the resistance of vesicles to surfactant attack †. *Langmuir*, *21*(22), 9843–9849.

Arsov, Z., & Quaroni, L. (2008). Detection of lipid phase coexistence and lipid interactions in sphingomyelin/cholesterol membranes by ATR-FTIR spectroscopy. *Biochimica et Biophysica Acta (BBA) - Biomembranes*, *1778*(4), 880–889.

Batenjany, M. M., Wang, Z., Huang, C., & Levin, I. W. (1994). Bilayer packing characteristics of mixed chain phospholipid derivatives: Raman spectroscopic and differential scanning calorimetric studies of 1-stearoyl-2-capryl-sn-glycero-3-phosphocholine (C(18): C(10)PC) and 1-stearoyl-2-capryl-sn-glycero-3-phospho-N-trimethylpropanolamine (C(18): C(10)TMPC). *Biochimica et Biophysica Acta (BBA) - Biomembranes*, *1192*(2), 205–214.

Belsito, S., Bartucci, R., Montesano, G., Marsh, D., & Sportelli, L. (2000). Molecular and mesoscopic properties of hydrophilic polymer-grafted phospholipids mixed with phosphatidylcholine in aqueous dispersion: Interaction of dipalmitoyl n-poly(ethylene glycol) phosphatidylethanolamine with dipalmitoylphosphatidylcholine studied by spectrophotometry and spin-label electron spin resonance. *Biophysical Journal*, *78*(3), 1420–1430.

Brodkorb, A., Egger, L., Alminger, M., Alvito, P., Assunção, R., Ballance, S., Bohn, T., Bourlieu-Lacanal, C., Boutrou, R., Carrière, F., Clemente, A., Corredig, M., Dupont, D., Dufour, C., Edwards, C., Golding, M., Karakaya, S., Kirkhus, B., Le Feunteun, S., … Recio, I. (2019). INFOGEST static in vitro simulation of gastrointestinal food digestion. *Nature Protocols*, *14*(4), 991–1014.

Bitman, J., & Wood, D. L. (1990). Changes in milk fat phospholipids during lactation. *Journal of Dairy Science*, *73*(5), 1208–1216.

Bryce, D. A., Kitt, J. P., & Harris, J. M. (2018). Confocal-Raman Microscopy Characterization of Supported Phospholipid Bilayers Deposited on the Interior Surfaces of Chromatographic Silica. *Journal of the American Chemical Society*, *140*(11), 4071–4078.

Bunow, M. R., & Levin, I. W. (1977). Comment on the carbon-hydrogen stretching region of vibrational raman spectra of phospholipids. *Biochimica et Biophysica Acta (BBA) - Lipids and Lipid Metabolism*, *487*(2), 388–394.

Chachaty, C., Rainteau, D., Tessier, C., Quinn, P. J., & Wolf, C. (2005). Building up of the liquid-ordered phase formed by sphingomyelin and cholesterol. *Biophysical Journal*, *88*(6), 4032–4044.

Cohn, J., Kamili, A., Wat, E., Chung, R. W., & Tandy, S. (2010). Dietary phospholipids and intestinal cholesterol absorption. *Nutrients*, *2*(2), 116–127.

Coreta-Gomes, F. M., Martins, P. A. T., Velazquez-Campoy, A., Vaz, W. L. C., Geraldes, C. F. G., & Moreno, M. J. (2015). Interaction of bile salts with model membranes mimicking the gastrointestinal epithelium: A study by isothermal titration calorimetry. *Langmuir*, *31*(33), 9097–9104.

A version of this chapter was published in Colloids and Surfaces B: Biointerfaces

Conway, V., Couture, P., Richard, C., Gauthier, S. F., Pouliot, Y., & Lamarche, B. (2013). Impact of buttermilk consumption on plasma lipids and surrogate markers of cholesterol homeostasis in men and women. *Nutrition, Metabolism and Cardiovascular Diseases*, *23*(12), 1255–1262.

Czamara, K., Majzner, K., Pacia, M. Z., Kochan, K., Kaczor, A., & Baranska, M. (2015). Raman spectroscopy of lipids: A review: Raman spectroscopy of lipids. *Journal of Raman Spectroscopy*, *46*(1), 4–20.

Dao, T. P. T., Brûlet, A., Fernandes, F., Er-Rafik, M., Ferji, K., Schweins, R., Chapel, J.-P., Fedorov, A., Schmutz, M., Prieto, M., Sandre, O., & Le Meins, J.-F. (2017). Mixing block copolymers with phospholipids at the nanoscale: From hybrid polymer/lipid wormlike micelles to vesicles presenting lipid nanodomains. *Langmuir*, *33*(7), 1705–1715.

Dowhan, W., & Bogdanov, M. (2009). Lipid-dependent membrane protein topogenesis. *Annual Review of Biochemistry*, *78*(1), 515–540.

Duan, R.-D., Bergman, T., Xu, N., Wu, J., Cheng, Y., Duan, J., Nelander, S., Palmberg, C., & Nilsson, Å. (2003). Identification of human intestinal alkaline sphingomyelinase as a novel ecto-enzyme related to the nucleotide phosphodiesterase family. *Journal of Biological Chemistry*, *278*(40), 38528–38536.

Eckhardt, E. R. M., Moschetta, A., Renooij, W., Goerdayal, S. S., van Berge-Henegouwen, G. P., & van Erpecum, K. J. (1999). Asymmetric distribution of phosphatidylcholine and sphingomyelin between micellar and vesicular phases: Potential implications for canalicular bile formation. 12.

Elsayed, M. M. A., & Cevc, G. (2011). The vesicle-to-micelle transformation of phospholipid–cholate mixed aggregates: A state of the art analysis including membrane curvature effects. *Biochimica et Biophysica Acta (BBA) - Biomembranes*, *1808*(1), 140–153.

Gantz, D. L., Wang, D. Q.-H., Carey, M. C., & Small, D. M. (1999). Cryoelectron microscopy of a nucleating model bile in vitreous ice: Formation of primordial vesicles. *Biophysical Journal*, *76*(3), 1436–1451.

Genova, J., Petrov, M., Bivas, I., Rafailov, P., Naradikian, H., & Katranchev, B. (2018). Fourier-transform infrared and Raman characterization of bilayer membranes of the phospholipid SOPC and its mixtures with cholesterol. *Colloids and Surfaces A: Physicochemical and Engineering Aspects*, *557*, 85–93.

Haustein, M., Wahab, M., Mögel, H.-J., & Schiller, P. (2015). Vesicle solubilization by bile salts: Comparison of macroscopic theory and simulation. *Langmuir*, *31*(14), 4078–4086.

He, H., Lu, Y., Qi, J., Zhu, Q., Chen, Z., & Wu, W. (2019). Adapting liposomes for oral drug delivery. *Acta Pharmaceutica Sinica B*, *9*(1), 36–48.

Heerklotz, H. (2008). Interactions of surfactants with lipid membranes. *Quarterly Reviews of Biophysics*, *41*(3–4), 205–264.

Helenius, A., & Simons, K. (1975). Solubilization of membranes by detergents. *Biochimica et Biophysica Acta (BBA) - Reviews on Biomembranes*, *415*(1), 29–79.

Hernell, O., Staggers, J. E., & Carey, M. C. (1990). Physical-chemical behaviour of dietary and biliary lipids during intestinal digestion and absorption. 2. Phase analysis and aggregation states of luminal lipids during duodenal fat digestion in healthy adult human beings. *Biochemistry*, *29*(8), 2041–2056.

Hermida, L. G., Sabés-Xamaní, M., & Barnadas-Rodríguez, R. (2014). Characteristics and behaviour of liposomes when incubated with natural bile salt extract: Implications for their use as oral drug delivery systems. *Soft Matter*, *10*(35), 6677–6685.

Homan, R., & Hamelehle, K. L. (1998). Phospholipase A2 relieves phosphatidylcholine inhibition of micellar cholesterol absorption and transport by human intestinal cell line Caco-2. *Journal of Lipid Research*, *39*, 1197 – 1209.

Hu, P.-L., Yuan, Y.-H., Yue, T.-L., & Guo, C.-F. (2018). Bile acid patterns in commercially available oxgall powders used for the evaluation of the bile tolerance ability of potential probiotics. *PLOS ONE*, *13*(3), 1 – 11.

Jaikishan, S., & Slotte, J. P. (2011). Effect of hydrophobic mismatch and interdigitation on sterol/sphingomyelin interaction in ternary bilayer membranes. *Biochimica et Biophysica Acta (BBA) - Biomembranes*, *1808*(7), 1940–1945.

Gallier, S., Gragson, D., Jiménez-Flores, R., & Everett, D. (2010). Using confocal laser scanning microscopy to probe the milk fat globule membrane and associated proteins. *Journal of Agricultural and Food Chemistry*, *58*(7), 4250–4257.

Garidel, P., Hildebrand, A., Knauf, K., & Blume, A. (2007). Membranolytic activity of bile salts: Influence of biological membrane properties and composition. *Molecules*, *12*(10), 2292–2326.

Kalyanasundaram, K., & Thomas, J. K. (1976). The conformational state of surfactants in the solid state and in micellar form. A laser-excited Raman scattering study. *The Journal of Physical Chemistry*, *80*(13), 1462–1473.

Korjamo, T., Heikkinen, A. T., & Mönkkönen, J. (2009). Analysis of unstirred water layer in *in vitro* permeability experiments. *Journal of Pharmaceutical Sciences*, *98*(12), 4469–4479.

Kragh-Hansen, U., le Maire, M., & Møller, J. V. (1998). The mechanism of detergent solubilization of liposomes and protein-containing membranes. *Biophysical Journal*, *75*(6), 2932–2946.

Lala, A. K. (1981). Cholesterol and phospholipids in membranes: The hydrogen bonding problem. *International Journal of Quantum Chemistry*, *20*(1), 93–97.

Lee, C., & Bain, C. D. (2005). Raman spectra of planar supported lipid bilayers. *Biochimica et Biophysica Acta (BBA) - Biomembranes*, *1711*(1), 59–71.

Levin, I. W., Thompson, T. E., Barenholz, Y., & Huang, C. (1985). Two types of hydrocarbon chain interdigitation in sphingomyelin bilayers. *Biochemistry*, *24*(22), 6282–6286.

Lete, M. G., Monasterio, B. G., Collado, M. I., Medina, M., Sot, J., Alonso, A., & Goñi, F. M. (2019). Fast and slow biomembrane solubilizing detergents: Insights into their mechanism of action. *Colloids and Surfaces B: Biointerfaces*, *183*, 110430.

Lichtenberg, D., Robson, R. J., & Dennis, E. A. (1983). Solubilization of phospholipids by detergents structural and kinetic aspects. *Biochimica et Biophysica Acta (BBA) - Reviews on Biomembranes*, *737*(2), 285–304.

Lichtenberg, D. (1985). Characterization of the solubilization of lipid bilayers by surfactants. *Biochimica et Biophysica Acta (BBA) - Biomembranes*, *821*(3), 470–478.

Lichtenberg, D., Ahyayauch, H., & Goñi, F. M. (2013). The mechanism of detergent solubilization of lipid bilayers. *Biophysical Journal*, *105*(2), 289–299.

Lönnfors, M., Doux, J. P. F., Killian, J. A., Nyholm, T. K. M., & Slotte, J. P. (2011). Sterols have higher affinity for sphingomyelin than for phosphatidylcholine bilayers even at equal acyl-chain order. *Biophysical Journal*, *100*(11), 2633–2641.

López, O., Cócera, M., Wehrli, E., Parra, J. L., & de la Maza, A. (1999). Solubilization of liposomes by sodium dodecyl sulfate: New mechanism based on the direct formation of mixed micelles. *Archives of Biochemistry and Biophysics*, *367*(2), 153–160.

Lopez, C., Cheng, K., & Perez, J. (2018). Thermotropic phase behaviour of milk sphingomyelin and role of cholesterol in the formation of the liquid ordered phase examined using SR-XRD and DSC. *Chemistry and Physics of Lipids*, *215*, 46–55.

Lopez, C., Cauty, C., & Guyomarc'h, F. (2018). Unravelling the complexity of milk fat globules to tailor bioinspired emulsions providing health benefits: The key role played by the biological membrane. *European Journal of Lipid Science and Technology*, *121*, 1800201.

Macierzanka, A., Sancho, A. I., Mills, E. C., Rigby, N. M., & Mackie, A. R. (2009). Emulsification alters simulated gastrointestinal proteolysis of β-casein and β-lactoglobulin. *Soft Matter*, *5*(3), 538–550.

Meister, A., Blume, A., 2017. (Cryo) transmission electron microscopy of phospholipid model membranes interacting with amphiphilic and polyphilic molecules. *Polymers* 9, 521, 1-17.

Morita, S., & Terada, T. (2014). Molecular mechanisms for biliary phospholipid and drug efflux mediated by ABCB4 and bile salts. *BioMed Research International*, *2014*, 1–11.

Moschetta, A., Frederik, P. M., Portincasa, P., vanBerge-Henegouwen, G. P., & van Erpecum, K. J. (2002). Incorporation of cholesterol in sphingomyelin- phosphatidylcholine vesicles has profound effects on detergent-induced phase transitions. *Journal of Lipid Research*, *43*(7), 1046–1053.

Nilsson, Å., & Duan, R.-D. (2006). Absorption and lipoprotein transport of sphingomyelin. *Journal of Lipid Research*, *47*(1), 154–171.

Noh, S. K., & Koo, S. I. (2004). Milk sphingomyelin is more effective than egg sphingomyelin in inhibiting intestinal absorption of cholesterol and fat in rats. *The Journal of Nutrition*, *134*(10), 2611–2616.

Norris, G. H., Jiang, C., Ryan, J., Porter, C. M., & Blesso, C. N. (2016). Milk sphingomyelin improves lipid metabolism and alters gut microbiota in high fat diet-fed mice. *The Journal of Nutritional Biochemistry*, *30*, 93–101.

O'Neill, S. D., & Leopold, A. C. (1982). An assessment of phase transitions in soybean membranes. *Plant Physiology*, *70*(5), 1405–1409.

Orendorff, C. J., Ducey, M. W., & Pemberton, J. E. (2002). Quantitative correlation of Raman spectral indicators in determining conformational order in alkyl chains. *The Journal of Physical Chemistry A*, *106*(30), 6991–6998.

Pandit, S. A., Bostick, D., & Berkowitz, M. L. (2004). Complexation of phosphatidylcholine lipids with cholesterol. *Biophysical Journal*, *86*(3), 1345–1356.

Pike, L. J. (2006). Rafts defined: A report on the Keystone symposium on lipid rafts and cell function. *Journal of Lipid Research*, *47*(7), 1597–1598.

Quinn, P. J., & Wolf, C. (2009). The liquid-ordered phase in membranes. *Biochimica et Biophysica Acta (BBA) - Biomembranes*, *1788*(1), 33–46.

Rankine, C. D., Atkinson, S. J., Waterland, M. R., Masters, S. L., & Wann, D. A. (2018). The structure of tris(chloromethyl)amine in the gas phase using quantum chemical calculations and gas electron diffraction and as a solid and melt using Raman spectroscopy. *Structural Chemistry*, *29*(3), 803–813.

Riethorst, D., Baatsen, P., Remijn, C., Mitra, A., Tack, J., Brouwers, J., & Augustijns, P. (2016). An in-depth view into human intestinal fluid colloids: Intersubject variability in relation to composition. *Molecular Pharmaceutics*, *13*(10), 3484–3493.

Rosqvist, F., Smedman, A., Lindmark-Månsson, H., Paulsson, M., Petrus, P., Straniero, S., Rudling, M., Dahlman, I., & Risérus, U. (2015). Potential role of milk fat globule membrane in modulating plasma lipoproteins, gene expression, and cholesterol metabolism in humans: A randomized study1. *The American Journal of Clinical Nutrition*, *102*(1), 20–30.

Stuart, M. C. A., & Boekema, E. J. (2007). Two distinct mechanisms of vesicle-to-micelle and micelle-to-vesicle transition are mediated by the packing parameter of phospholipid–detergent systems. *Biochimica et Biophysica Acta (BBA) - Biomembranes*, *1768*(11), 2681–2689.

Shirota, K., Yagi, K., Inaba, T., Li, P.-C., Murata, M., Sugita, Y., & Kobayashi, T. (2016). Detection of sphingomyelin clusters by Raman spectroscopy. *Biophysical Journal*, *111*(5), 999–1007.

Simões, S. I., Marques, C. M., Cruz, M. E. M., Cevc, G., & Martins, M. B. F. (2004). The effect of cholate on solubilisation and permeability of simple and protein-loaded phosphatidylcholine/sodium cholate mixed aggregates designed to mediate transdermal delivery of macromolecules. *European Journal of Pharmaceutics and Biopharmaceutics*, *58*(3), 509–519.

Slotte, J. P. (2016). The importance of hydrogen bonding in sphingomyelin's membrane interactions with co-lipids. *Biochimica et Biophysica Acta (BBA) - Biomembranes*, *1858*(2), 304–310.

Smondyrev, A. M., & Berkowitz, M. L. (1999). Structure of dipalmitoylphosphatidylcholine/cholesterol bilayer at low and high cholesterol concentrations: Molecular dynamics simulation. *Biophysical Journal*, *77*(4), 2075–2089.

Snyder, R. G., Strauss, H. L., & Elliger, C. A. (1982). Carbon-hydrogen stretching modes and the structure of n-alkyl chains. 1. Long, disordered chains. *The Journal of Physical Chemistry*, *86*(26), 5145–5150.

Thurnhofer, H., & Hauser, H. (1990). Uptake of cholesterol by small intestinal brush border membrane is protein-mediated. *Biochemistry*, *29*(8), 2142–2148.

Uematsu, M., & Shimizu, T. (2021). Raman microscopy-based quantification of the physical properties of intracellular lipids. *Communications Biology*, *4*(1), 1176.

Vors, C., Joumard-Cubizolles, L., Lecomte, M., Combe, E., Ouchchane, L., Drai, J., Raynal, K., Joffre, F., Meiller, L., Le Barz, M., Gaborit, P., Caille, A., Sothier, M., Domingues-Faria, C., Blot, A., Wauquier, A., Blond, E., Sauvinet, V., Gésan-Guiziou, G., … Michalski, M.-C. (2019). Milk polar lipids reduce lipid cardiovascular risk factors in overweight postmenopausal women: Towards a gut sphingomyelin-cholesterol interplay. *Gut*, *2019 (0)*. 1 – 15.

Wilde, P. J., & Chu, B. S. (2011). Interfacial & colloidal aspects of lipid digestion. *Advances in Colloid and Interface Science*, *165*(1), 14–22.

Yagi, K., Li, P.-C., Shirota, K., Kobayashi, T., & Sugita, Y. (2015). A weight averaged approach for predicting amide vibrational bands of a sphingomyelin bilayer. *Physical Chemistry Chemical Physics*, *17*(43), 29113–29123.

Yao, L., Heubi, J. E., Buckley, D. D., Fierra, H., Setchell, K. D. R., Granholm, N. A., Tso, P., Hui, D. Y., & Woollett, L. A. (2002). Separation of micelles and vesicles within lumenal aspirates from healthy humans: Solubilization of cholesterol after a meal. *Journal of Lipid Research*, 7.

Yasuda, T., Kinoshita, M., Murata, M., & Matsumori, N. (2014). Detailed comparison of deuterium quadrupole profiles between sphingomyelin and phosphatidylcholine bilayers. *Biophysical Journal*, *106*(3), 631–638.

Yellin, N., & Levin, I. W. (1977). Hydrocarbon chain trans-gauche isomerization in phospholipid bilayer gel assemblies. *Biochemistry, 16*(4), 642–647.

Chapter 5 – Structural analysis of vesicles comprised of milk fat globule membrane phospholipid extracted from bovine beta-serum

5.1. Introduction

The milk fat globule membrane (MFGM) is an interface that separates the triacylglyceride core of milk fat globules from casein micelles and the bulk serum phase of milk. This complex phospholipid tri-layer plays a large role in the digestion of milk lipids (Gallier et al. 2012); yet, the molecular interactions underlying MFGM digestion are not well understood.

The majority of MFGM research before the 2010s has focused on characterizing and determining the functionality of the unique proteins embedded within the membrane, such as xanthine oxidase, mucins, and butyrophilin (Reinhardt & Lippolis, 2006; Mather, 2011). Less prominent at the time were a myriad of animal and clinical studies which consistently showed that buttermilk (a byproduct of butter production) or beta-serum (the aqueous phase of butter) acted as an anticholesteremic agent (Howards & Marks, 1979; Cohn et al., 2010; Baumgartner et al., 2013; Conway et al., 2013). The anticholesteremic effect of buttermilk has been hypothesized to be a consequence of the abundant amount of MFGM polar lipids concentrated in buttermilk during butter production. The rise of phospholipids as a possible bioactive ingredient and the discovery of lateral liquid-ordered (L_o) domains of sphingomyelin (SM) and cholesterol in the MFGM, analogous to biological lipid rafts, using confocal laser scanning microscopy (Gallier et al., 2010 a; Lopez, Madec, & Jimenez-Flores, 2010) sparked interest in the possible health benefits of dairy polar lipid fractions and the use of milk polar lipids to better mimic biological emulsions such as breast milk (Gallier et al., 2015; Lopez, Cauty, & Guyomarc'h, 2018 a).

The polar lipid composition of the bovine MFGM is dependent upon the animal source of the fraction and extraction method, but generally consists of glycerophospholipids (PC = phosphatidylcholine; PE = phosphatidylethanolamine; PI = phosphatidylinositol, PS = phosphatidylserine) and sphingolipids (SM = sphingomyelin) with a diverse variety of saturated and unsaturated acyl moieties (Sánchez-Juanes et al., 2009). The inner monolayer that originates from the endoplasmic reticulum of lactocytes within the mammary gland is rich in PI, PS whereas MSM, PC, and cholesterol are concentrated within the outer bilayer that originates from the apical plasma membrane of the lactocyte (Deeth, 1997; Mather & Keenan, 1998; Jeong et al., 2013). The location of PE within the MFGM has been a point of contention. Deeth (1997) reported that PE existed within the inner monolayer; however, Zheng (2014) asserted that, due to the PE critical packing parameter (which determines the preferred association structure of molecular shapes and is dependent upon the effective volume of FA, length of

A version of this chapter was published in Colloids and Surfaces B: Biointerfaces

FA, and head group area) being >1, the phospholipid has the packing of an inverted truncated cone and therefore suited towards the inner leaflet of the bilayer (Israelachvili, 2010).

The cholesterol associated with the MFGM is typically distributed in the outer bilayer where it may complex with SM to form detergent resistant L_o domains. These unique structural assemblies possess intermediate properties of solid-ordered (S_o) gel phases and liquid-disordered (L_d) phases (Chachaty et al., 2005; Quinn & Wolf, 2009). Moreover, due to the wide array of hydrocarbon chain lengths and degrees of saturation of polar lipids found in milk, multiple phases will coexist depending upon temperature, pressure, and cholesterol concentration (Murthy, Guyomarc'h, & Lopez, 2016 a). The temperatures at which these phase transitions occur can be determined by differential scanning calorimetry (DSC) (Murthy et al., 2015). Additionally, wide-angle synchrotron x-ray diffraction (Lopez, Cheng, & Perez, 2018 b) and *in silico* models (Sodt et al., 2015) have shown that the addition of cholesterol perturbs the hexagonal packing of S_o-packed phospholipids. With mounting evidence showing the importance of cholesterol as a structural component of the MFGM, further investigation is necessary to determine how cholesterol and L_o domains dictate the digestion of milk lipids.

The previous chapter only focused on one specific component of the MFGM, milk sphingomyelin (MSM) and its interactions with cholesterol. To investigate the role of cholesterol in MFGM digestion, polar lipids were extracted from beta-serum and hydrated to create phospholipid vesicles. The composition of these vesicles was characterized and the physical properties investigated with varying cholesterol/SM ratios (100/0, 80/20, 70/30, 60/40 mol/mol). The phospholipid vesicles were then incubated with bovine bile at 37 °C for 2 h to examine the role of cholesterol in detergent-induced vesicle → micelle phase transitions to determine structural changes in the presence of a digestive factor. The micellization behaviour of MFGM phospholipid vesicles was attempted to be understood by comparing the results of Chapter 4.

5.2. Materials and methods

5.2.1. MFGM phospholipid extraction

MFGM lipids from beta-serum powder (BSP2; Tatua Dairy Company, Tatuanui, New Zealand) obtained from spray drying fresh beta-serum was extracted using the Folch method with 2:3:1 v/v of methanol:chloroform:8.76% NaCl (Folch, Lees, & Sloane 1957; Eggers and Schwudke, 2016). The solid to total extract solvent ratio was 1:24 w/v. Samples were thoroughly mixed then centrifuged at 1,000 × g for 10 min at 20 °C. The top methanol layer and precipitate were siphoned and discarded. The bottom chloroform layer was concentrated with a Rota-Vap and solubilized with hexane to produce a crude extraction with approximately 100 mg lipid/mL.

Phospholipids were separated from the crude hexane extract by solid phase extraction according to Bitman and Wood (1990) as modified by Gallier et al., (2010 b). Silica cartridges (12 mL) with a bed weight of 2 g (Discovery DSC-Si, Sigma Aldrich, Auckland, New Zealand) were conditioned with

two volumes of methanol and the crude extract (200 mg lipid) loaded. The neutral lipids were eluted out with 40 mL hexane:ethyl ether (1:1). The phospholipids were first eluted with methanol (20 mL), followed by chloroform:methanol:water (20 mL; 3:5:2 v/v/v). Both phospholipid fractions were collected, concentrated by rotary evaporation, and solubilized in 2:1 v/v chloroform:methanol to approximately 10 mg SM/mL before being stored in the dark at –20 °C until used.

5.2.2 MFGM phospholipid characterization

Thin layer chromatography (TLC) was carried out on the MFGM phospholipid extract to test for purity (Gallier et al., 2010 b). Milk phospholipid extract (20 µL) was spotted onto a 2.5 × 20 cm silica plate (MilliporeSigma, Burlington, MA, USA) and placed inside a sealed chamber with chloroform:methanol:water (65:25:4) to separate the phospholipids. After being dried, the plate was developed within the chamber using iodine.

Quantitative analysis of the phospholipids was determined using HPLC-ELSD (evaporative light scattering detector) (Shimadzu, Kyoto, Japan) equipped with two LC-10 ADvp pumps, a SCL-10 ADvp gradient system, a DGU-14 ADvp module degaser, and SIL-10ADvp autosampler (Su et al., 2019). The analytical column was a YMC – pack PVA-SIL-NP column (250 × 4.6 mm, 5 µm) and the mobile phase followed a linear, binary gradient according to the following scheme: t_0 = 0% B, t_{30} = 40% B and then isocratic (40% B) for 30 min at a constant flow rate of 1.0 mL/min. Eluent A consisted of chloroform:isopropanol:triethylamine:acetic acid (75:25:0.08:1.0, v/v/v/v) and eluent B was methanol:water:triethylamine:acetic acid (95:5:0.08:1.0, v/v/v/v). An ELSD-LT II Shimadzu model ELSD was used for detection; the pressure of nebulizer gas (nitrogen) was maintained at 350 kPa and the drift tube temperature was set to 80 °C. Identification of glycerophospholipids and sphingomyelin was carried out by comparing against the retention time of pure standards. Calibration curves for each compound were calculated from maximum peak heights obtained by injecting different volumes containing soy-PE (Cayman Chemical Company, Ann Arbor, MI, USA), soy-PI, soy-PS, milk-SM (Avanti Polar Lipids, Alabaster, AL, USA), and soy-PC (Sigma-Aldrich, MI, USA) standards dissolved in chloroform (Appendix 5.1).

5.2.3 Vesicle preparation and characterization

The MFGM phospholipid extract was used to prepare vesicles suspended in pH 6.7 PIPES buffer: PIPES 10 mM (1,4-piperazinediethane sulfonic acid; purity ≥ 99%; Sigma-Aldrich, Auckland, New Zealand), 50 mM NaCl (Analytical Reagent Grade; Thermo Fisher Scientific NZ, North Shore City, New Zealand) and 5 mM $CaCl_2$ (Millipore, Burlington, MA, USA), according to the procedure of Lopez, Cheng, & Perez (2018 b). Phospholipid vesicles were binary mixtures that consisted of MFGM phospholipid extract and cholesterol. Cholesterol concentration was measured as SM:cholesterol (1:0, 4:1, 7:3, 3:2 of SM/cholesterol, mol/mol). Total SM and cholesterol

concentration was 326 µM. Table 5.1 displays the calculated concentrations of all phospholipids in each vesicle preparation.

Table 5.1. Polar lipid concentration of vesicles created from recombined MFGM phospholipid extract.

Given name	SM (µM)	Chol (µM)	PC (µM)	PE (µM)	PI (µM)	PS (µM)	Sum (µM)
MFGM100	326	0	419	550	97	332	1723
MFGM80	261	65	335	440	77	266	1444
MFGM70	228	98	293	385	68	232	1303
MFGM60	196	130	252	331	58	200	1166

MFGM100 = milk fat globule membrane phospholipid vesicles without cholesterol; MFGM80 = milk fat globule membrane phospholipid vesicles with 4:1 mol/mol sphingomyelin:cholesterol; MFGM70 = milk fat globule membrane phospholipid vesicles with 7:3 mol/mol sphingomyelin:cholesterol; MFGM60 = milk fat globule membrane phospholipid vesicles with 3:2 mol/mol sphingomyelin:cholesterol. SM = sphingomyelin; Chol = cholesterol; PC = phosphatidylcholine; PE = phosphatidylethanolamine; PI = phosphatidylinositol; PS = phosphatidylserine.

Particle size of phospholipid vesicles was measured using a dynamic light scattering (DLS) system (Malvern Zetasizer Pro, Worcestershire, UK) with a backscattering angle of 173°. Data were analyzed using the program supplied with the machine, ZX XPLORER version 1.4.0.105. Before each run, the machine was equilibrated to 37 °C for 60 s. Each measurement consisted of the average of 30 runs, each run 1.68 s. Zeta potential was measured using the same instrument and program with PIPES buffer as the dispersant.

Thermograms were taken using a Nano DSC (TA instruments, New Castle, DE, USA). MFGM phospholipid vesicles (300 µL) were injected and compared to the PIPES buffer as a reference. Samples and the corresponding reference were injected into the instrument, cooled to 5 °C, pressurized to 300 kPa, further cooled to 1 °C and allowed to equilibrate for 5 min. Heating scans were from 1 °C to 60 °C at 1 °C/min. The startup hook (1 – 5 °C), the endothermic shift that appears as the sample approaches steady-state, was discarded. Data were analyzed with the NanoAnalyze software (TA Instruments).

5.2.4. Bovine bile addition to MFGM phospholipid vesicles

Bovine bile (dried, unfractionated, Sigma-Aldrich) was rehydrated in Milli-Q water at 37 °C for 30 min before being added to the vesicles to achieve a final concentration of 10 mM bile and 8:1 vesicle/bile, v/v in accordance with INFOGEST recommendations (Brodkorb et al., 2019). The mixture of vesicles and bile was then incubated in a shaking incubator for 2 h at 37 °C and 80 rpm. Samples were refrigerated at 4 °C for up to 2 days before analysis.

5.2.4.1 Transmission electron microscopy

Negative stain transmission electron microscopy (TEM) was carried out at the Manawatu Microscopy and Imaging Centre (Palmerston North, New Zealand) on samples using an FEI Tecnai G2 Spirit BioTWIN (FEI Company, Hillsboro, OR, USA). Vesicles before and after incubation with bovine bile were applied onto 3.05 mm, 200 mesh copper grids (Agar Scientific, Essex, UK) pre-coated with Formvar. After allowing the sample to adhere to the carbon resin for 5 min, the remaining wet sample was wicked off using filter paper. Uranyl acetate (2%) was then used to stain the grid for 5 min before being blotted off, ensuring the grid was no longer wet before the sample was loaded into the microscope.

5.2.4.2 Optical density

The optical density at 630 nm (OD630) experiments followed Tai et al. (2021) and were carried out at 37 °C in a BioTek Synergy 2 thermostated microplate reader (BioTek, Winooski, VT, USA). OD630 measurements were taken for the MFGM phospholipid vesicles immediately before samples were placed into the instrument (designated as time zero, T0). Bovine bile (10 mM final concentration, 8:1 v/v, vesicle/bile) was incubated with samples to measure vesicle → micelle transition kinetics. OD630 measurements were then continuously taken every minute for 2 h. A control consisting of PIPES buffer and bovine bile was also measured, and any absorbance due to the bilirubin in bile was subtracted from each sample.

5.2.4.3 Raman spectroscopy

Raman spectroscopic data were acquired using a confocal microscope adapted from a commercially available inverted fluorescence microscope (Olympus IX70) (Olympus New Zealand Limited, Auckland, NZ) and pumped by a 532-nm fiber-coupled diode laser. Mirrors were used to orient the beam into a 40× microscope objective lens (numerical aperture = 0.65). Raman scattered light was collected in a 180° back-scattering geometry through the 40× microscope objective. The scattered light was directed into a FERGIE detector (Princeton Instruments, Trenton, NJ, USA). Samples were sandwiched between two glass microscope cover-slips and frames (250 in total) each lasting 500 ms were taken for each measurement (Shirota et al., 2016; Rankine et al., 2018). The typical power at the sample measured 100 mW.

5.2.4.4 X-ray diffraction

Small angle X-ray diffraction data was obtained from the BioSAXS beamline at the European Molecular Biology Laboratory (EMBL) in the German Electron Synchrotron DESY (Hamburg, Germany). MFGM phospholipid vesicles were made in New Zealand and mailed to Hamburg. Shipping took approximately 1 week – samples were kept in a Styrofoam box with cooler packs but were not refrigerated. The mailed samples were diluted by the beamline staff and submitted to X-rays operating at 10 KeV (λ= 1.23983) and 20 °C. The sample-detector distance was set to 3 m to record

X-ray diffraction patterns from 0.02 – 8 $Å^{-1}$. Diffraction patterns were displayed as a series of concentric rings as a function of the radial scattering vector $q = 4\pi\sin\theta/\lambda$, where 2θ was the scattering angle and λ the wavelength of the incident beam.

5.2.5. Statistical analysis

Phospholipid vesicles were prepared as five independent replicates for each MFGM phospholipid/cholesterol ratio. Each instrument collected at least two measurements from each independent replicate and the mean of five replicates was reported. Significant differences between means were determined with mixed-effects ANOVA with the day the samples analyzed as a random effect. Post-hoc analysis in the form of Tukey's HSD ($\alpha \leq 0.05$) was used to compare means on MiniTab (State College, PA, USA).

5.3. Results and discussion

5.3.1. Polar lipid composition of beta-serum extract

Polar lipid composition and typical chromatograms are reported in Table 5.2 and Fig 5.1, respectively. The beta-serum phospholipid extract contained 16.16 ± 2.4 mg polar lipid/mL extract (~0.5 mg polar lipid/g milk) which is significantly higher than the amount of PL extracted from whole bovine milk (0.23 mg polar lipid/mL milk, 0.14 mg polar lipid/g milk) (Lopez, Briard-Bion, & Ménard, 2014; Yao et al., 2016 a). This roughly comes down to a recovery of 75% of the total phospholipids present in the beta-serum.

The relative proportion of polar lipids in the BSP2 extract were PE > PC > SM = PS > PI based on the HPLC results. This sequence slightly differed from the composition on the product specification sheet (PE > PC > SM > PS > PI) (Appendix 5.2). The extraction resulted in small relative losses to PE, PC, and SM while PS and PI were concentrated when compared to the supplier's product specification sheet. These results differed considerably to those of Gallier et al., (2010 b) who saw large losses to PE and PI when employing the Folch/Bitman extraction on commercial buttermilk powders. After Folch extraction and without a SPE purification step, Brink et al. (2020) reported the relative proportion of phospholipids in BSP2 to be PC > SM > PE > PS > PI, from greatest to least using UPLC-MS.

Table 5.2. Relative proportion of polar lipids found in beta-serum powder.

Polar Lipids	% wt	% mol	Typical Composition % wt[1]
PI	5.61 ± 0.38	5.00 ± 0.34	8.5
PE	31.91 ± 0.26	33.70 ± 0.26	30.8
PS	19.26 ± 1.04	18.53 ± 1.01	12.1
PC	24.29 ± 0.31	24.18 ± 0.31	26.6
SM	18.92 ± 0.45	18.59 ± 0.45	20.8

Polar Lipid	mg/g beta-serum powder	Typical Composition (mg)
PI	2.72 ± 0.17	4.93
PE	15.54 ± 2.00	17.86
PS	9.42 ± 1.67	7.02
PC	11.82 ± 1.40	17.86
SM	9.20 ± 1.04	12.06
Total	48.71 ± 6.25	59.74

PE = phosphatidylethanolamine; PI = phosphatidylinositol; PS = phosphatidylserine; PC = phosphatidylcholine; SM = sphingomyelin. Values are means ± standard deviation (n = 5). [1]Typical composition refers to composition supplied in the BSP2 product specification sheet (Appendix 5.2).

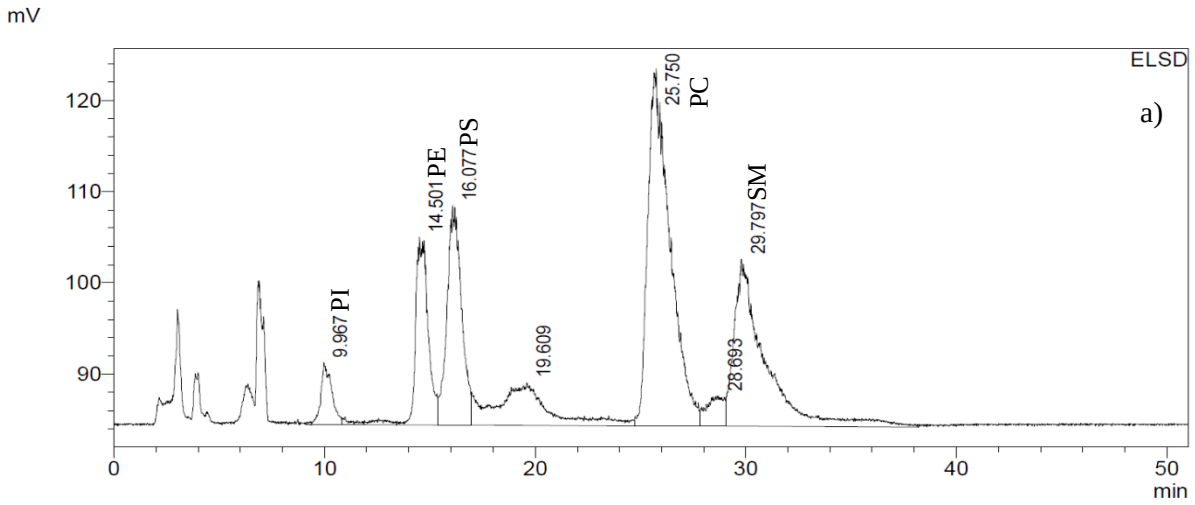

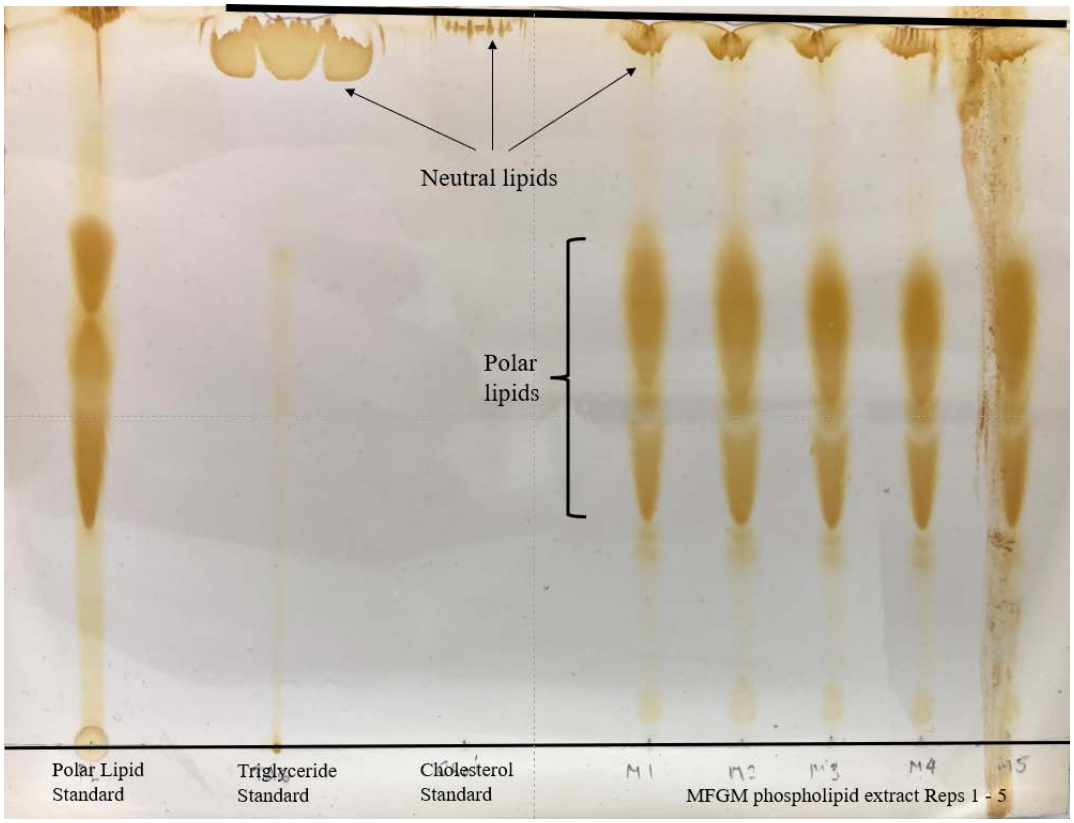

Figure 5.1. Chromatograms of MFGM phospholipid extracts. a) HPLC-ELSD example chromatogram. PE = phosphatidylethanolamine; PI = phosphatidylinositol; PS = phosphatidylserine; PC = phosphatidylcholine; SM = sphingomyelin. b) TLC plates showing separated phospholipids extracted from beta-serum powder. Polar lipid standard is the same standard used for HPLC experiments. Triglyceride standard is soy bean oil dissolved in 4:1 v/v methanol:chloroform. Cholesterol standard was 3 mg/mL of cholesterol dissolved in 4:1 v/v methanol:choloroform. The dark line at the top of the TLC plate is the solvent front. An artifact was present in the TLC plate for the MFGM Rep 5 column.

Based on the TLC results (Fig. 5.1 b), it is likely that the unidentified peaks in the HPLC-ESLD chromatogram (Fig 5.1 a) are neutral lipids. Furthermore, Gallier et al., (2010 b) has also reported the possible presence of residual neutral lipids after Bitman SPE purification. Peaks corresponding to possible polar lipid degradation products (i.e. lyso-phospholipids) were found between the PS and PC peaks at 19.07 min. These degradation products may be due to oxidation from the beta-serum spray-drying process.

5.3.2. Physical and thermotropic properties of MFGM phospholipid vesicles

Particle size and DSC thermograms of MFGM phospholipid vesicles with varying concentrations of cholesterol are shown in Figure 5.2. Individual vesicles had a diameter of ~100 – 200 nm; however, these vesicles aggregate to form irregularly shaped structures that can be larger than 1 μm as shown by the DLS size measurements (Fig. 5.2 a). Cholesterol content had no significant effect on particle size or the visible morphology of the MFGM vesicles as expected based on the results for milk sphingomyelin (MSM) and porcine brain phosphatidylcholine (BPC) in *Section 4.3.1*.

The ζ–potentials for the MFGM vesicles were –9.08 ± 0.40, –9.46 ± 0.55, –9.68 ± 0.24, –10.96 ± 1.45 mV for MFGM100, 80, 70, and 60, respectively. The ζ–potential of MFGM60 was statistically significantly more negative than MFGM100; however, the large standard deviation, as well as the small magnitude of the decrease indicates that cholesterol has a negligible effect on the ζ–potential. The consistent negative ζ–potential of MFGM phospholipids regardless of cholesterol concentration is due to the negative headgroups on PI and PS. Obied et al., (2019) observed a ζ–potential of –4.6 ± 1.2 mV for MFGM phospholipid extracts that contained 3.6% PI and 2.5% PS, whereas the PI and PS content of the BSP2 extract was significantly higher (Table 5.2), resulting in a more negative ζ–potential. For reference, the ζ–potential of milk fat globules is roughly –10 mV (Singh, 2019).

The heating curve of the MFGM phospholipid vesicle DSC thermogram consists of a broad peak that persists until approximately 37 °C, the temperature of human digestion (Fig. 5.2 b). The characteristic broad isotherm that extends from 5 to 37 °C is due to the progressive melting of complex mixtures of phospholipids with varying hydrocarbon chain length and saturation. The MFGM100 (no cholesterol) had a melting temperature peak (T_m) at 25 °C and a shoulder at 30 °C. In comparison, a T_m of 36 °C (Murthy et al., 2015) when heated and a T_m of 30.3 °C with a shoulder present at 5 °C when cooled (Murthy, Guyomarc'h, & Lopez, 2016 a) for MFGM phospholipid vesicles has been reported. The polar lipid composition for the MFGM phospholipid extract used in Murthy, Guyomarc'h, & Lopez (2016 a) was 38.7% SM, 31.6% PC, 3.5% PE, 3.4% PI, 2.8% PS. With more than double the relative amount of SM, the most saturated of the milk polar lipids, and almost ten times less PE, the most unsaturated of the milk polar lipids (Gallier et al., 2010 b; Yao et al., 2016 a), it is not surprising that there is such a large difference in T_m.

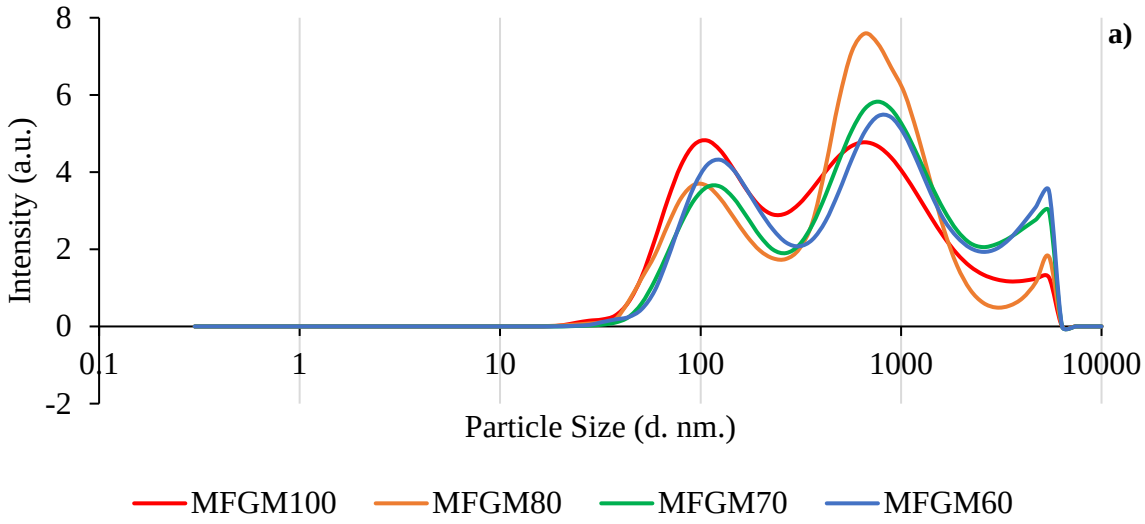

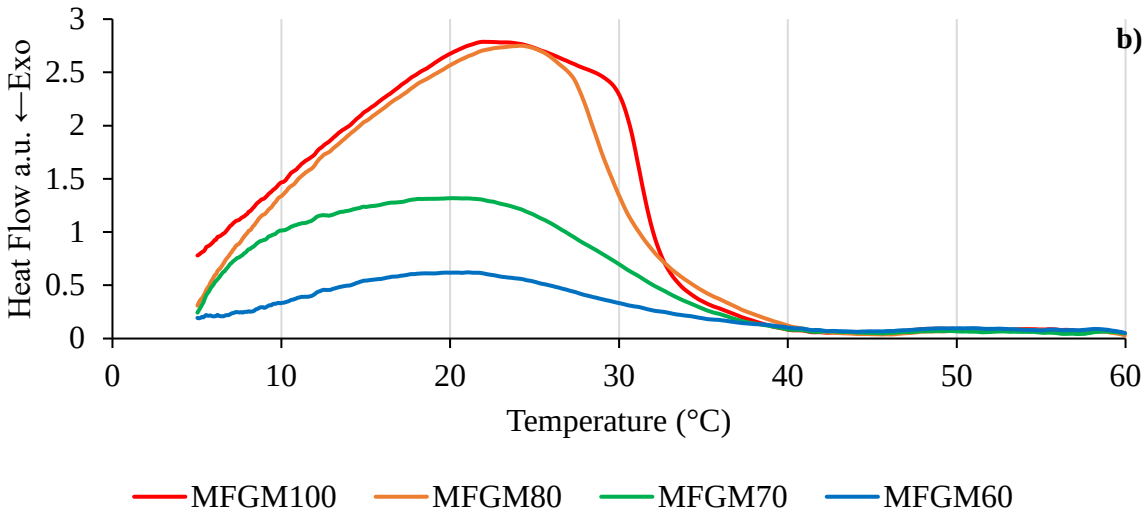

Figure 5.2. Size and thermotropic behaviour properties of vesicles created from milk fat globule membrane phospholipids derived from beta-serum (MFGM). MFGM100 = without cholesterol; MFGM80 = 4:1 mol/mol sphingomyelin:cholesterol; MFGM70 = 7:3 mol/mol sphingomyelin:cholesterol; MFGM60 = 3:2 mol/mol sphingomyelin:cholesterol. a) Particle size distribution from dynamic light scattering; b) Thermotropic properties of milk fat globule membranes phospholipid vesicles.

Increasing the amount of cholesterol incorporated into the MFGM phospholipid vesicles reduced the magnitude of the endothermic peak area, the enthalpy of transition, indicative of a progressive decrease in the S_o phase as L_o domains form (Gao et al., 2008). Furthermore, as cholesterol content increased, the T_m of the MFGM phospholipid vesicles decreased from 25 °C (MFGM100) to 20 °C (MFGM70 and 60). These features are consistent with the thermotropic behaviour of L_o domains being established in binary MSM/cholesterol bilayers (Chemin et al., 2008; Lopez, Cheng, & Perez, 2018 b). Unlike MSM60 in Fig. 3.5, MFGM60 still possess a prominent endothermic event centered around 20 °C, indicative of residual $S_o \rightarrow L_d$ phase transition.

Murthy, Guyomarc'h, & Lopez (2016 b) reported that a 73:27 MFGM phospholipid:cholesterol (50:50 mol/mol MSM:cholesterol) ratio was necessary for MFGM vesicles to be entirely in the L_o phase. The MFGM60 preparation is 8:1 MFGM phospholipid:cholesterol (60:40 mol/mol MSM:cholesterol) with a high ratio of phospholipid to cholesterol due to the low relative SM content present (18.5 % mol of total phospholipid). What is apparent from the DSC result is that even with the higher relative proportion of unsaturated PE, the addition of cholesterol still readily reduces the T_m and the enthalpy of transition. Figure 5.3 exhibits some of the aforementioned characteristics of the MFGM phospholipid vesicles.

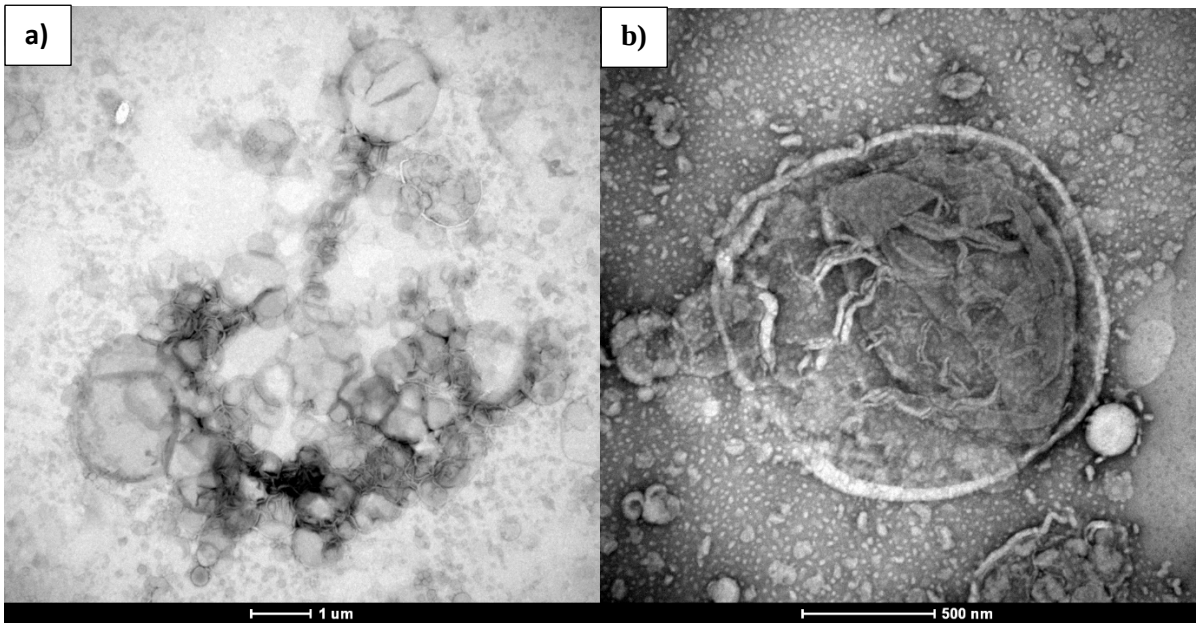

Figure 5.3. Transmission electron micrographs of vesicles made from milk fat globule membrane (MFGM) phospholipids extracted from beta-serum powder.
a) MFGM phospholipid vesicles with 4:1 mol/mol MSM/cholesterol, 9,900×
b) MFGM phospholipid vesicles without cholesterol, 43,000×

To summarize, vesicles were created from MFGM phospholipids extracted from beta-serum. The DSC thermograms showed that with the incorporation of cholesterol, the ablation of the $S_o \rightarrow L_d$ phase that is characteristic of the appearance of a L_o phase, was still present. The atypical composition (PE > PC > SM) is one novelty compared to the PC > SM> PE model membrane systems that are more commonly studied. The MFGM samples submitted to SAXS that will be detailed later in this chapter did not show Bragg peaks representative of a multilamellar structure; thus, these vesicles cannot be confirmed to be multilamellar.

5.3.3. Detergent-induced micellization of MFGM phospholipid vesicles

Sphingomyelin and cholesterol associate to forms L_o domains in the MFGM (Singh and Gallier, 2017). These microdomains are analogous in phospholipid structure to lateral lipid rafts in cellular systems which are dynamic protein sorting platforms that rest on L_o domains (Pike, 2006). One well-documented property of lipid rafts is detergent resistance, which extends to MSM and cholesterol model membrane systems as shown in Chapter 4 (Tai et al. 2021). The detergent-induced micellization of MFGM phospholipids and MFG core triacylglycerides is a vital component of intestinal lipid digestion (Gallier, Ye, & Singh, 2012). As MSM is one of the most abundant phospholipids in the MFGM, and confocal microscopy has shown L_o microdomains are present on the MFGM surface, the SM:cholesterol ratio may be related to MFGM phospholipid vesicle resistance to physiological surfactants.

Transmission electron micrographs taken of MFGM phospholipid vesicles that had been incubated with 10 mM of bovine bile were consistent with previous images of MSM MLVs incubated with

bovine bile (Tai et al. 2021) (Fig. 5.4). The rehydrated bovine bile appeared as irregular plates that subsumed the vesicles with particles that resembled mixed micelles budding from aggregates (Fig. 5.4 a – c). Most interestingly, MFGM60 (3:2 mol/mol MSM:cholesterol) retained a degree of vesicular structure in the presence of bovine bile, supplying visual evidence that MFGM phospholipid vesicles were resistant to detergent-induced micellization.

To confirm the detergent resistance of MFGM phospholipid/cholesterol vesicles, optical density at 630 nm (OD630) was employed to elucidate the kinetics of MFGM phospholipid detergent-induced vesicle → micelle transition (Fig. 5.5). The bilirubin in bovine bile has a wide-ranging absorbance spectrum; therefore, a blank consisting of PIPES buffer and bovine bile was subtracted from each measurement resulting in some negative values; however, it is the shape of the curve rather than the absolute values which are important (Appendix 5.3).

The addition of detergent and subsequent solubilization of liposome and vesicle systems result in disruption to the bilayer, reducing particle size. This particle size reduction can be measured as a reduction in turbidity or optical density. The detergent-induced micellization time-course can be divided into three stages: the rapid initial micellization, the aggregation of micellar intermediates, and then micellization reaching an endpoint equilibrium, $R_{sol,}$ when the entire system is in the micellar phase (Moschetta et al., 2002). An initial, almost instantaneous micellization can be seen where the optical density at T0 (time zero in minutes, an initial optical density measurement of the MFGM vesicles) is significantly higher than the optical density at T1 (time 1 min, the first OD630 measurement after bile had been added).

The MFGM phospholipid vesicles that contained cholesterol (MFGM80 – MFGM60) followed the detergent-induced micellization kinetics of PC as expected (*Section 4.3.2*). The OD630 of the MFGM phospholipid vesicles without cholesterol (MFGM100) progressively increased after bovine bile addition, reaching a maximum at 10 min, before progressively decreasing. This has been previously observed in MSM without cholesterol and was attributed to the presence of open vesicles, which are partially solubilized vesicular structures. These intermediate products of trans-bilayer solubilization have pores resulting in a leaky membrane (Haustein et al., 2015).

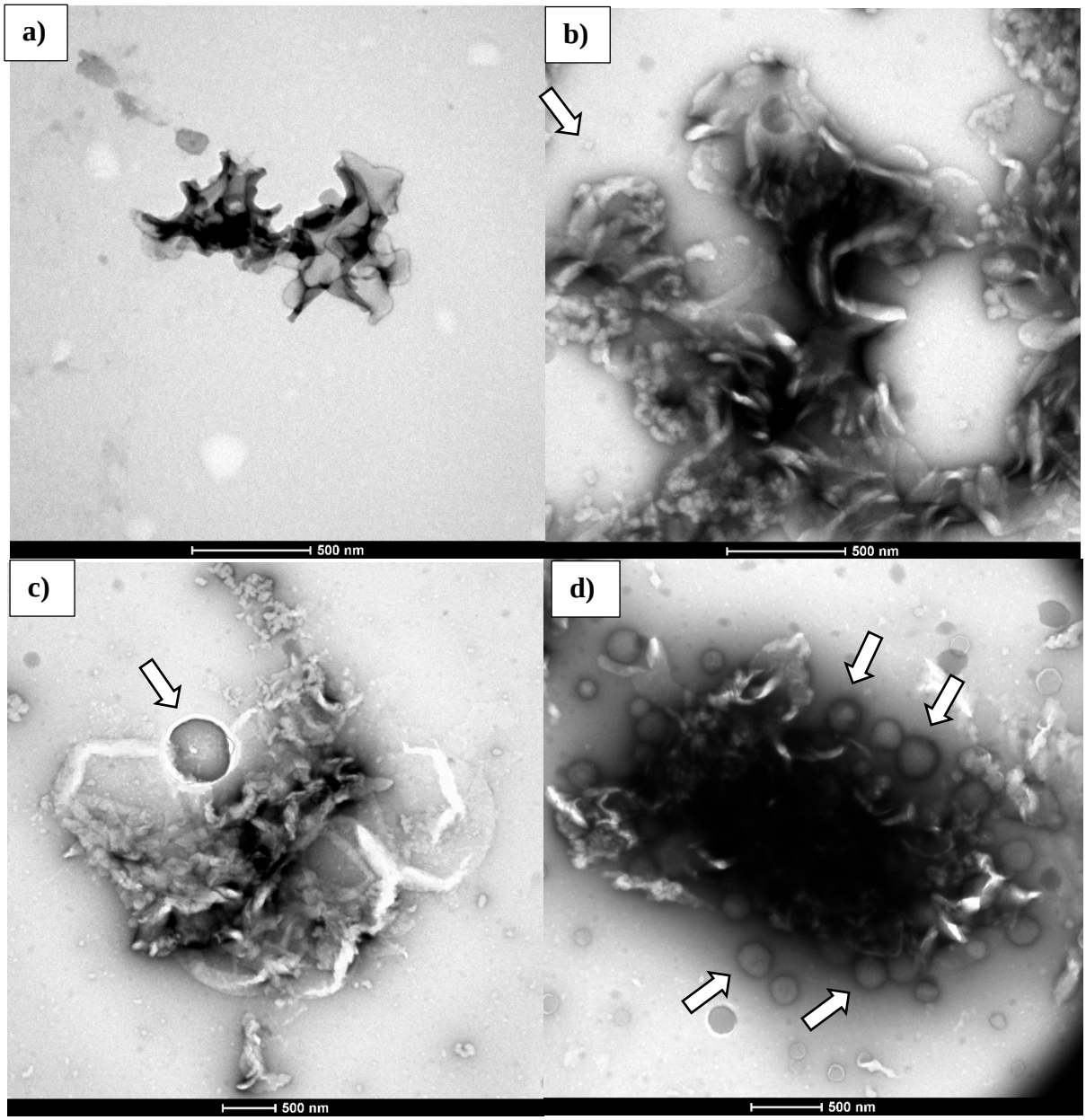

Figure 5.4. Transmission electron microscopy of milk fat globule membrane (MFGM) phospholipid vesicles after incubation with bovine bile

a) PIPES Buffer and bovine bile; 43,000× magnification.
b) MFGM phospholipid vesicles without cholesterol after incubation with bovine bile; 43,000× magnification. Arrow indicates a micellular product budding off from the bile/phospholipid vesicle aggregate.
c) MFGM phospholipid vesicles 4:1 mol/mol sphingomyelin/cholesterol after incubation with bovine bile; 20,500× magnification. Arrow indicates an artifact in the Fomvar grid.
d) MFGM phospholipid vesciles 3:2 mol/mol sphingomyelin/cholesterol; 16,500× magnification. Arrows indicate intact MFGM phospholipid vesicles.

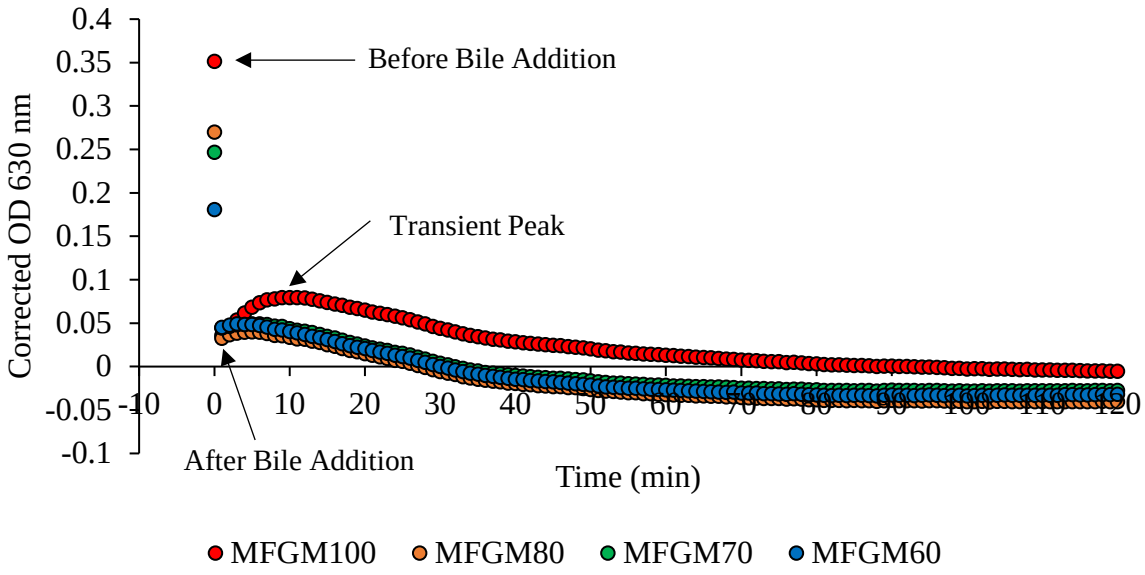

Figure 5.5. The kinetics of detergent-induced micellization of milk fat globule membrane (MFGM) phospholipid vesicles by optical density. MFGM100 = without cholesterol, MFGM80 = 4:1 sphingomyelin/cholesterol, MFGM70 = 7:3 sphingomyelin/cholesterol, MFGM60 = 3:2 sphingomyelin/cholesterol. SM makes up 18.6% mol of the MFGM phospholipid extract.

The micellization of porcine brain (BPC) and soy phosphatidylcholine (SPC) did not produce the same transient maximum in OD630 in the experiments performed in Chapter 4 (Fig. 4.3. b, c); hence, the suggestion that even without cholesterol, PC vesicles lack a degree of detergent resistance that pure SM MLVs possess at 37 °C. This inherent resistance, likely related to the phase state of the phospholipid vesicles, results in the formation and aggregation of open vesicles. Furthermore, the transient maximum did not appear in binary MSM:SPC phospholipid vesicles unless the ratio was at least 4:1 mol/mol (Fig. 4.4 a). The SM:PC in the MFGM phospholipid vesicles is 13:10 mol/mol. High T_m PC derived from milk which are more saturated than the PC present in soy (Yao et al., 2016 a) may contribute to the formation of open vesicles. Nevertheless, it is peculiar that with such high levels of PC and PE, the MFGM phospholipid vesicles possessed a MSM characteristic (open vesicle micellar intermediates).

Overall, the MFGM phospholipid/cholesterol vesicles did not possess the same level of detergent resistance as MSM/cholesterol vesicles. Although the magnitude of the T0 to T1 reduction significantly decreased with the addition of cholesterol (Fig. 5.5), detergent-induced micellization still occurs, as a statistically significant decrease in T0 to T1 for each vesicle system is apparent. The PE- and PC-rich MFGM phospholipid vesicles are likely solubilized, and the detergent resistant SM/cholesterol complexes are dispersed amongst a sea of micellar intermediates. As an illustration, in Fig. 5.4 c, there is a large aggregate of bile and vesicle fragments. It is possible that portions of these aggregates are made up of SM/cholesterol complexes; however, due to the large quantity of L_d phase, the size of SM/cholesterol complexes are indistinguishable from other micellar intermediates. As

optical density has no specificity towards L_o domains, there is no indication of the presence of SM/cholesterol complexation even if the L_o structure is maintained.

Furthermore, unlike the binary MSM/cholesterol MLVs, the MFGM60 OD630 endpoint at 120 minutes was not significantly different from MFGM100, implying that the addition of 10 mM bovine bile to MFGM phospholipid vesicles with or without cholesterol reached roughly the same equilibrium state or degree of micellization. The question now becomes whether the resulting micellar products of MFGM phospholipids vesicles, with or without cholesterol at the endpoint (120 min), are structurally similar or if it is possible that the presence of L_o domains induces the formation of detergent resistant micellar structures?

5.3.4. The effect of detergent-induced micellization on the inter- and intra hydrocarbon chain order of MFGM phospholipid vesicles

Raman spectroscopy was used to investigate the structural arrangement and bilayer order of the hydrocarbon chains within MFGM phospholipid vesicles before and after bile addition. Table 5.3 reiterates the literature reference values for Raman active vibrational modes and includes the Raman active bands for the MFGM phospholipid vesicles. Figure 5.6 shows the mean Raman spectra of MFGM100 and 60 before bile addition, and Figure 5.7 shows the spectra for MFGM100 and 60 after incubation with bovine bile for 2 h at 37 °C (Appendices 5.4 and 5.5 display individual average spectra for all MFGM phospholipid vesicles). Similar to Chapter 4, the Raman spectra of the samples were taken at room temperature (~20 °C) rather than 37 °C due to the absence of a temperature control unit. Based on the DSC thermogram of MFGM100 (Fig. 5.1 b), the MFGM phospholipid vesicles without cholesterol were a mix of S_o and L_d (MFGM100 T_m > 20 °C) and the MFGM phospholipid vesicles with cholesterol were a mix of S_o, L_d, and a varying amount of L_o depending upon the cholesterol content.

Figures 5.6 b and 5.7 b exhibit the methylene C–H stretching modes (2800 – 3000 cm^{-1}) of which four peaks are visible at approximately 2855 cm^{-1} (CH_2 symmetric stretching), 2885 cm^{-1} (CH_2 asymmetric stretching), 2935 cm^{-1} (Fermi resonance of the symmetric CH_3 stretching), and 2963 cm^{-1} (asymmetric CH_3 stretching). The first three are used to obtain intensity ratios that are of interest. The I_{2850}/I_{2880} ratio is inverse to the lateral interchain order of the bilayer. The I_{2930}/I_{2880} ratio is inverse to the combined interchain and intra-chain order of the bilayer. Figures 5.6 c and 5.7 c focus on hydrocarbon chain *trans/gauche* rotational isomerization (1000 – 1200 cm^{-1}). Three peaks are visible at 1070 cm^{-1} (*trans* C–C stretching), 1085 cm^{-1} (*gauche* C-C stretching), 1130 cm^{-1} (*trans* C-C stretching) (Shirota et al., 2016); the I_{1085}/I_{1130} ratio is directly proportional to the number of *gauche* isomers that make up the bilayer.

Table 5.3 Raman assignments, reference modes and Raman active bands for MFGM phospholipid vesicles before and after bovine bile addition.

Reference Mode (cm^{-1})	Without Bile Raman Shift (cm^{-1})	With Bile Raman Shift (cm^{-1})	Assignment/Structural Information	Reference
2960	2963	2960	Asymmetric CH_3 stretching	Batenjany et al. 1994
2930	2935	2935	Fermi resonance of CH_3 symmetric stretching	Batenjany et al. 1994
2880	2885	2881	CH_2 asymmetric stretching	Batenjany et al. 1994
2850	2855	2847	CH_2 symmetric stretching	Batenjany et al. 1994
1737	1740	N/A	C=O ester stretching	Czamara et al. 2015
1657	1660	1644	Z–C=C stretching	Czamara et al. 2015
1442	1443	1439	CH_2 scissoring mode	Czamara et al. 2015
1300	1304	1296	CH_2 twisting mode	Czamara et al. 2015
1267	1267	1267	=C–H in-plane deformation	Czamara et al. 2015
1135	1130	1129	C-C stretching *(trans)*	Shirota et al. 2016
1097	1086	1091	C-C stretching *(gauche)*	Shirota et al. 2016
1067	1070	1061	C-C stretching *(trans)*	Shirota et al. 2016

The intensity ratios of the I_{2930}/I_{2880} for MFGM vesicles without bile (MFGM100 = 0.66 ± 0.04, MFGM80 = 0.67 ± 0.03, MFGM70 = 0.69 ± 0.03, MFGM = 0.677 ± 0.018) (Appendix 5.6) were not significantly different; cholesterol had no effect on overall MFGM vesicles hydrocarbon chain order. To answer why the overall acyl chain order remained the same requires scrutinizing the hydrocarbon inter- and intra-chain parameters.

The I_{2850}/I_{2880} of MFGM60 (3:2 mol/mol MSM/cholesterol) is significantly higher than MFGM100 (no cholesterol) (0.85 ± 0.03 vs 0.91 ± 0.01, respectively); the decrease in interchain order is consistent with an $S_o \rightarrow L_o$ phase transition (Tai et al., 2021). The introduction of cholesterol into the MFGM phospholipid vesicles also led to a significant decrease in the I_{1085}/I_{1130} (MFGM100 = 1.65 ± 0.04 vs MFGM60 = 1.48 ± 0.03), that is a higher proportion of rigid *trans* isomers. At first glance, the increase in intrachain order, as the phospholipid vesicles transitions from a predominately $S_o \rightarrow L_o$, seems contradictory as the fluidization of hydrocarbon chains would result in greater acyl chain mobility. However, MFGM is a complex mixture of polar lipids with acyl chains of varying size and saturation of which SM is only a fraction. *Section 4.3.2.2.1* demonstrated that incorporating cholesterol into vesicles made from BPC rich in (1,2-dipalmitoyl-*sn*-glycero-3-PC) (DPPC) and (1,2-dioleoyl-*sn*-glycero-3-phosphocholine) (DOPC) significantly reduces I_{1085}/I_{1130}, increasing intrachain order (Fig. 4.10 b). Furthermore, (1-palmitoyl-2-oleoyl-*sn*-glycero-3-PE (POPE) bilayer order also increases when cholesterol is added (Paré & Lafleur, 1998). Therefore, due to the higher proportion of PE and PC, there is in fact a higher amount of *trans* isomers when cholesterol is added which is quantified by the I_{1085}/I_{1130} ratio. The same trend is expected to occur at 37 °C, albeit the MFGM100 I_{1085}/I_{1130} would be higher as the MFGM phospholipid vesicles would almost entirely be in the L_d

phase. In summary, the addition of cholesterol to MFGM phospholipid vesicles at 20 °C decreases lateral order but increases the intrachain order. These two effects cancel each other out, preserving the native order of MFGM phospholipid vesicles. This property showcases the synergistic nature of the MFGM phospholipids and is perhaps an important structural consideration during the insertion and adhesion of protein to the proximal leaflet of the native MFGM.

In dairy food science, Raman spectroscopy, in particular confocal Raman spectroscopy, is often applied to determine differences in the composition of fat globules (Gallier et al., 2011; Yao et al., 2016 b) and also to investigate the interactions that occur between the fat globules and molecules of different hydrophobicity (Zheng et al., 2013). It is therefore difficult to compare spectra of whole milk fat globules to that of the MFGM phospholipid vesicles due to the lack of triacylglycerides in the model membrane system. One other study of the Raman spectra of MFGM was found (Forrest, 1978) which was in agreement with Fig. 5.6 and 5.7. It is likely the Forrest (1978) preparation had a higher proportion of MSM, as at 20 °C the I_{2850}/I_{2880} was lower than the MFGM phospholipids vesicles. Milk sphingomyelin, having the highest proportion of long (> C20) and saturated hydrocarbon chains results in more of the bilayer being in the S_o phase, hence, reduced lateral disorder.

Of slight concern is the presence of an amide I peak at 1643 cm^{-1}, which Forrest (1978) attributed to protein remnants from separation of the membrane material from the triglyceride. The 1643 cm^{-1} band is quite pronounced in the sphingomyelin MLV spectra (Fig. 4.11) due to the amide present on the sphingosine moiety (Shirota et al. 2016); however, the amide I band is not present in bovine, human, or caprine milk fat globule spectra (Yao et al., 2016 b), nor is it prominent enough in Figure 5.6 a to be distinct. Without the composition of phospholipids in hand, it is difficult to offer anything beyond speculation on the existence of the amide I band in Forrest's spectra.

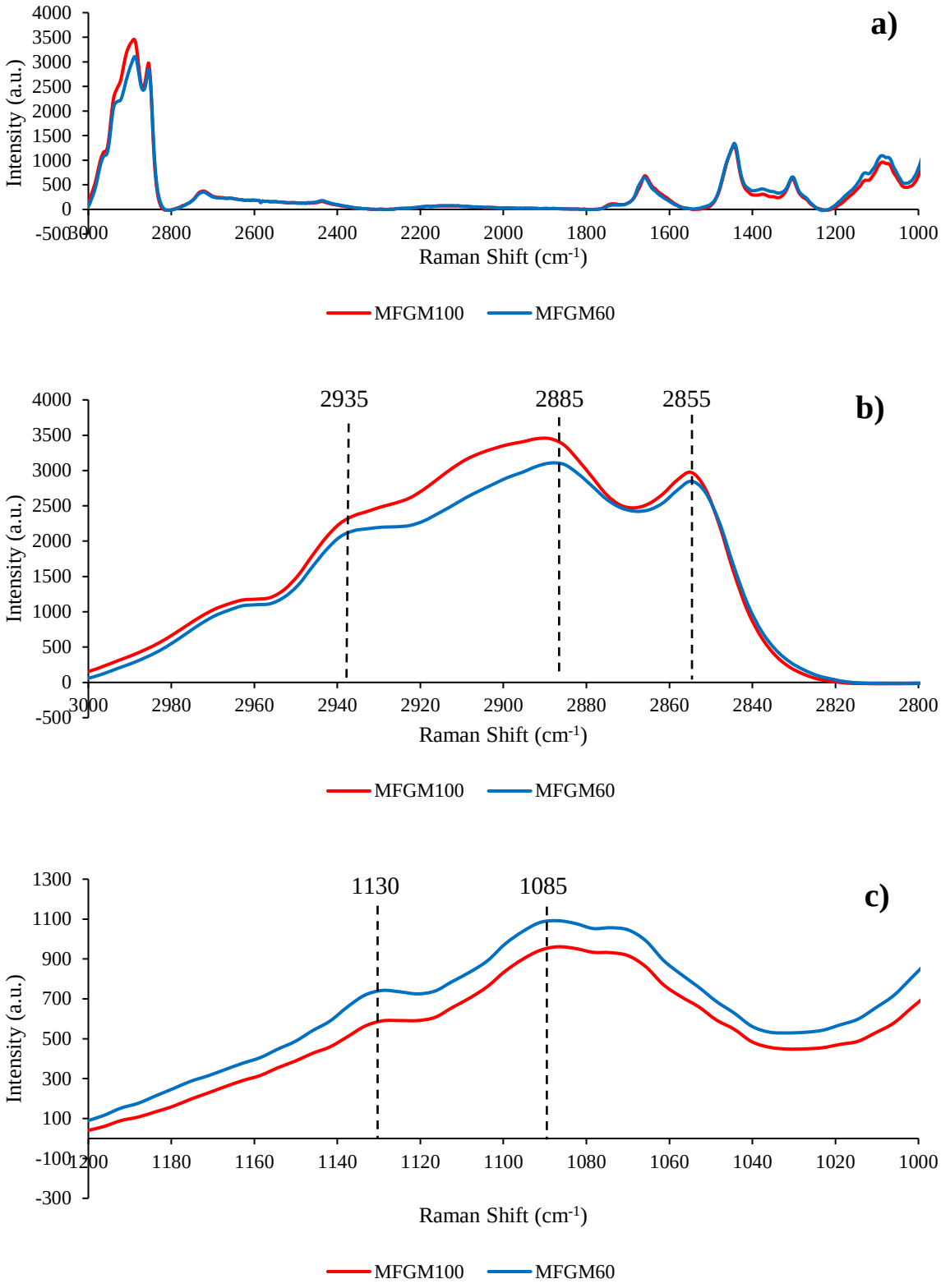

Figure 5.6. Raman spectra of MFGM100 and MFGM60 phospholipid vesicles. MFGM100 = milk fat globule membrane phospholipid vesicles without cholesterol; MFGM60 = milk fat globule membrane phospholipid vesicles with 3:2 MSM:cholesterol.

a) Raman spectra of MFGM100 and MFGM60 (1000 – 3000 cm^{-1}).
b) Methylene region (2800 – 3000 cm^{-1}); the dotted lines indicate the Raman active bands.
c) C-C skeletal region (1000 – 1200 cm^{-1}); the dotted lines indicate the Raman active bands.

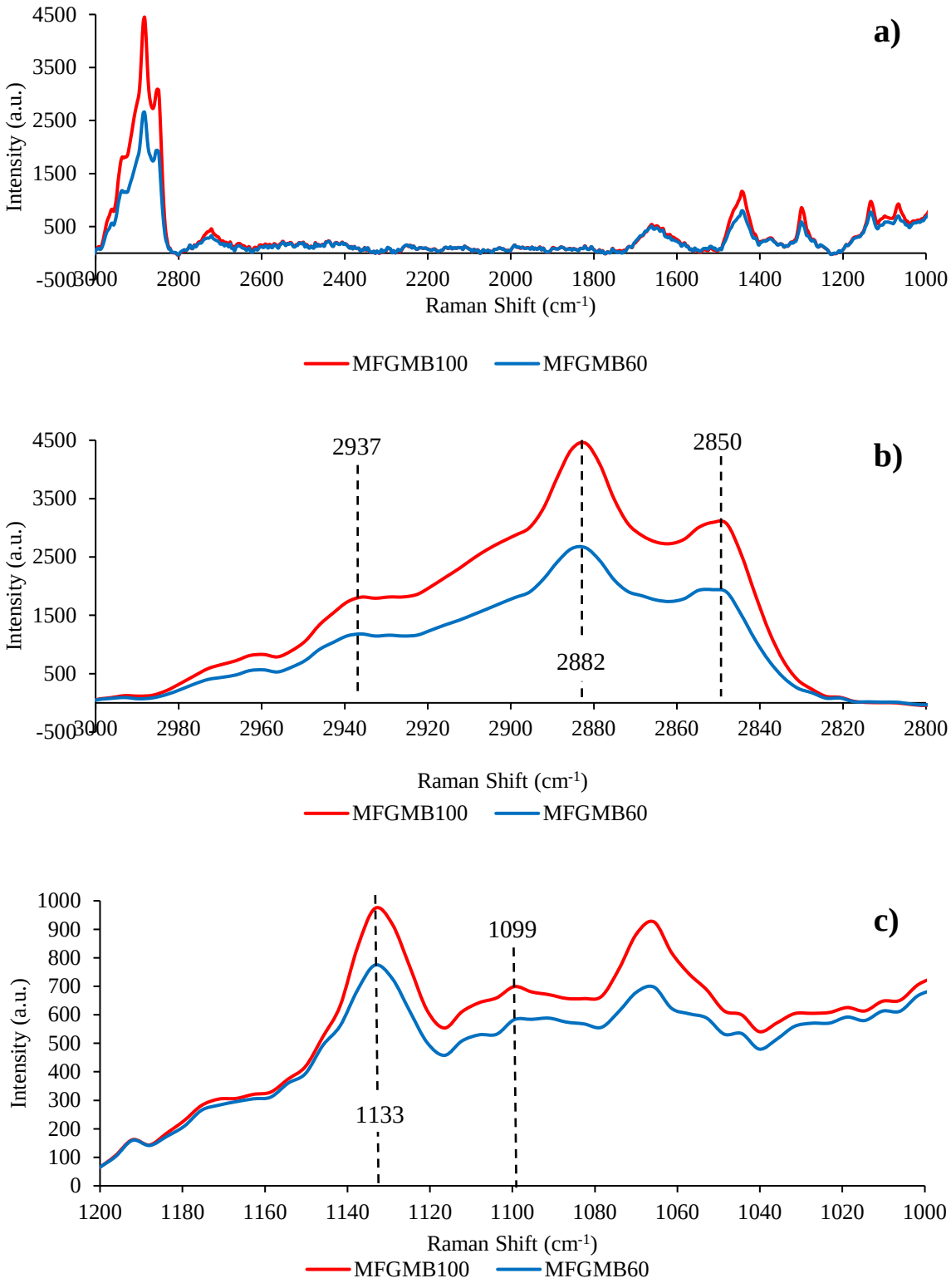

Figure 5.7. Raman spectrum of MFGM100 and MFGM60 phospholipid vesicles after bile addition. MFGMB100 = milk fat globule membrane phospholipid vesicles without cholesterol after bovine bile addition; MFGMB60 = milk fat globule membrane phospholipid vesicles with 3:2 MSM:cholesterol after bovine bile addition.

a) Raman spectra of MFGMB100 and MFGMB60 (1000 – 3000 cm^{-1}).
b) Methylene region (2800 – 3000 cm^{-1}); the dotted lines indicate the Raman active bands.
c) C-C skeletal region (1000 – 1200 cm^{-1}); the dotted lines indicate the Raman active bands.

Consistent with previous instances of detergent-induced vesicle → micelle transitions, MFGM vesicles that were incubated with bovine bile for 2 h at 37 °C decreased in both interchain order (I_{2850}/I_{2880}) and intrachain order (I_{1085}/I_{1130}), regardless of the cholesterol concentration. The considerable increase in hydrocarbon chain order from the introduction of bovine bile is due to the increasing curvature as vesicles transition to micelles with smaller radii (Almgren, 2000) imposing order, or rigidity, to the acyl chains (Alshehab et al., 2019). As the MFGM phospholipid vesicles are saturated with bile salts, the heightened curvature strain results in an excess of endothermic enthalpy. As curvature strain reaches a maximum, the release of cylindrical micelles from the bilayer relaxes the excess enthalpy (Heerklotz, 2008). The enthalpy of the cylindrical micelles is once again reduced after a rod → sphere (mixed micelle) transition. Mixed micelles are comprised of components with a lower packing parameter (< ⅓) compared to those that make up bilayer assemblies (½ to 1) (Stuart & Boekema, 2007). The molecular parameter is a common unitless measurement defined as the ratio between the volume of the apolar tail (V_o) and the product of the tail length (l_o) and the surface area of the headgroup (a_o) (Nagarajan, 2002). Whereas a packing parameter ~ 1 is indicative of a cylinder packing, a low packing parameter implies the headgroup surface area multiplied by the tail length is greater than the volume of the tail, producing cone shaped packing resulting in spherical micelles. The increased curvature constricts the lateral and rotational freedom of the hydrocarbon chains resulting in higher chain order (Kundu, Banik, & Sarkar, 2018). Yet even after detergent-induced micellization, the I_{1085}/I_{1130} of the MFGM phospholipid vesicles is rather high. The intensity of the C-C stretching bands favour true *trans/gauche* conformations rather than rotational *gauche/trans* isomerization (Orendorff et al., 2002). The PE which makes up a plurality of the phospholipid vesicle preparation is highly unsaturated (Yao et al., 2016 a), thus, the I_{1085}/I_{1130} ratio of the MFGM phospholipid vesicles before and after bovine bile is added is quite similar to the SPC and BPC in *Section 4.3.2.2.1*.

Interestingly, the high degree of lateral and rotational order that emerges after the MFGM phospholipids vesicles that have been incubated with bovine bile resembles milk fat globules that have been frozen at –90 °C (Forrest, 1978). Not only do the sharpness and overall shape of the peaks match Fig. 5.7 a, but the hydrocarbon interchain intensity ratio (0.59) of milk fat globules at – 90 °C agrees quite well with MFGM phospholipids vesicles after being incubated with bovine bile (~0.70). On the other hand, the intrachain order of the milk fat globules at –90 °C is several orders of magnitude higher than the bilayer order found in the MFGM phospholipid vesicles, likely due to the dense packing of solid triglycerides present within fat globules. Nevertheless, the high I_{1085}/I_{1130} of the vesicular and micellar intermediates after detergent-induced solubilization implies an abundance of *trans* rotamers.

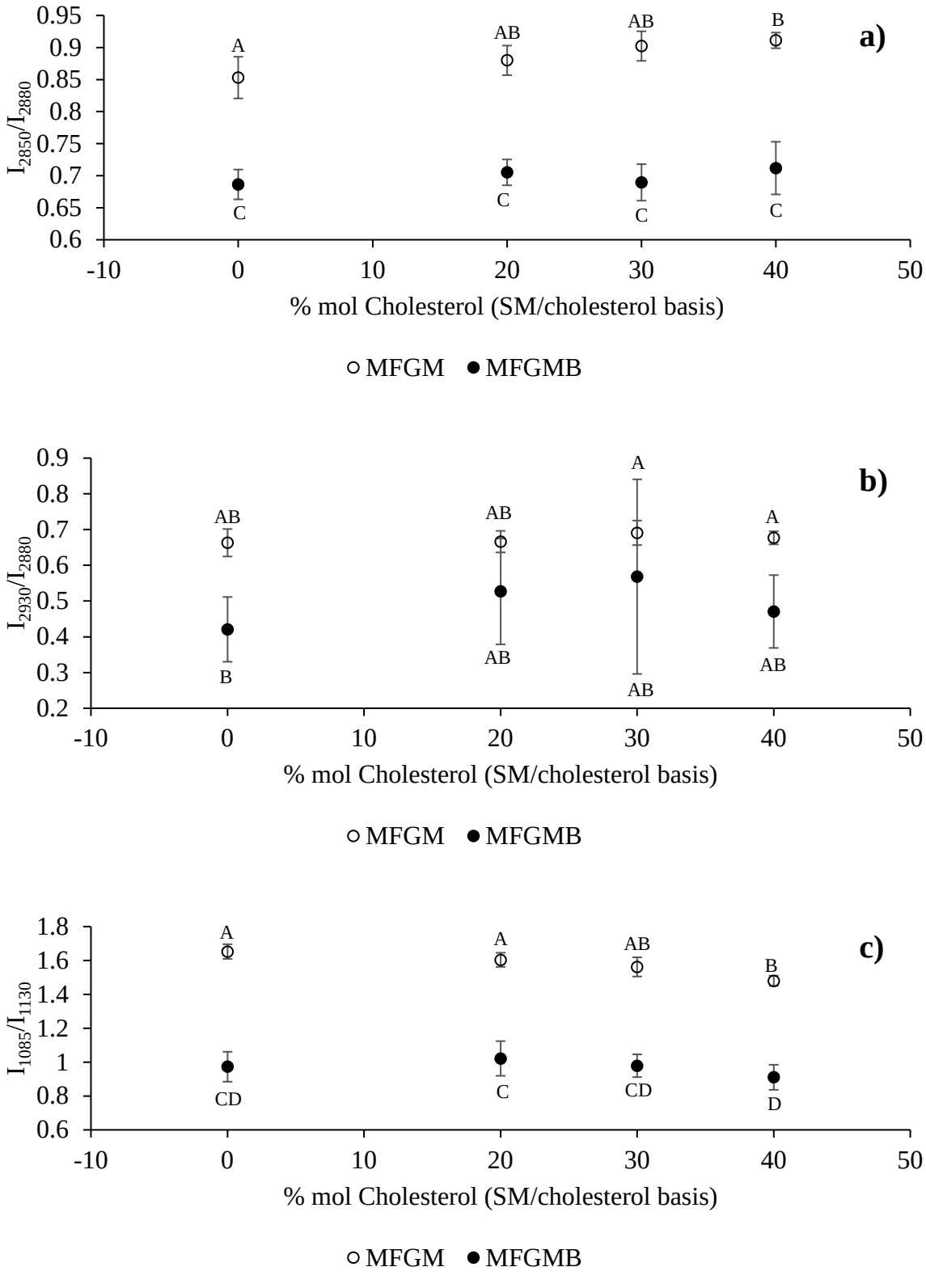

Figure 5.8. Raman peak intensity ratios for hydrocarbon inter and intrachain order of milk fat globule phospholipid vesicles with varying concentrations of cholesterol before (MFGM) and after (MFGMB) bovine bile addition. The tabulated form can be found in Appendix 5.6.

a) Hydrocarbon interchain order (I_{2850}/I_{2880})
b) Combined hydrocarbon inter- and intra-chain order (I_{2930}/I_{2880})
c) Hydrocarbon intrachain order (I_{1085}/I_{1130})

The structural status of the lateral hydrocarbon packing of the mixed micelles is less obvious. As previously mentioned, the structure of a mixed micelle depends upon the molar ratio of lipid and surface-active molecules (R_{sat} and R_{sol}) (Hjelm et al., 1988). Evidently the formation of micellar intermediates also persists even when there is an excess of bile salt (Fig. 5.4). The microstructure of a bile salt/phospholipid mixed micelle generally consists of the phospholipids forming a bilayer, with the bulky hydrophobic portion of the bile salt intercalated between the phospholipids, adding a higher curvature so the micelle resembles a disc or an ellipsoid, depending upon the phospholipid packing and the bile salt in question (Lichtenberg, Robson, & Dennis, 1983). It is also possible for the hydrophilic portion of the bile salt to be in association with itself so that the sterol ring is positioned parallel to the phospholipid hydrocarbon chains (Mazer, Benedek, & Carey, 1980) to form what is known as a mixed disc bilayer at high bile salt concentrations (Maldonado-Valderrama et al., 2011). In either model, the bile salts do not afford the vesicle a high degree of molecular mobility, therefore, the low degree of bilayer disorder shown by Figure 5.8. The digestive implication of such rigidity in mixed micelles comprised of milk polar lipids may be profound, but not yet well understood.

Incorporating cholesterol into the MFGM phospholipid vesicles did not increase detergent resistance of vesicles as the I_{2850}/I_{2880} and I_{1085}/I_{1130} ratios displayed no significant differences when bovine bile was added, no matter the cholesterol content (Fig. 5.8 a, c). This result is in agreement with the optical density measurements which show that, after a 2 h incubation at 37 °C, the detergent-induced micellization of the MFGM phospholipid vesicles reach a similar endpoint regardless of cholesterol content (Fig. 5.5). Even though evidence from DSC and from the statistically significant increase in interchain order when cholesterol is added imply a $S_o \rightarrow L_o$ phase transition is occurring, the MFGM phospholipid vesicles lack of detergent resistance. The spectra gathered from MFGM phospholipid vesicle system after bile has been added is an aggregate of micelles and intermediates. The MFGM extract is a complex blend of phospholipids that has been recombined into liposomes/vesicles. Less of the vesicle surface area may be present as L_o regions compared to a binary phospholipid vesicle. To account for this, MFGM phospholipid vesicles were manufactured with 326 uM of SM+cholesterol, so the amount of L_o domains should be the same as reported in *Section 4.3.2.2.1*, although the total quantity of phospholipids will be higher. MFGM phospholipid vesicles not becoming detergent resistant in the presence of cholesterol is not an unexpected result. After all, if MFGM phospholipids were wholly detergent resistant in the presence of cholesterol, the membrane would be nigh impossible to digest.

5.3.5. Small angle X-ray scattering

Preliminary results from X-ray scattering experiments of MFGM phospholipid vesicles showed weak scattering underneath hints of diffraction peaks at d = 89 Å (q = 0.07 $Å^{-1}$) and 41 Å (q = 0.15 $Å^{-1}$) (Fig. 5.9 a), where the diffraction peaks were present in MSM MLVs (Fig. 3.6). The incorporation of cholesterol so that the SM/cholesterol ratio was 3:2 saw the disappearance of the two hints (Fig. 5.9

b). As the addition of cholesterol either decreased or increased the d-spacing of lamellar features depending upon the phase state of the bilayer, it is mostly likely that either an insufficient concentration or low lamellarity was the cause of the absent peaks (Appendix 5.7).

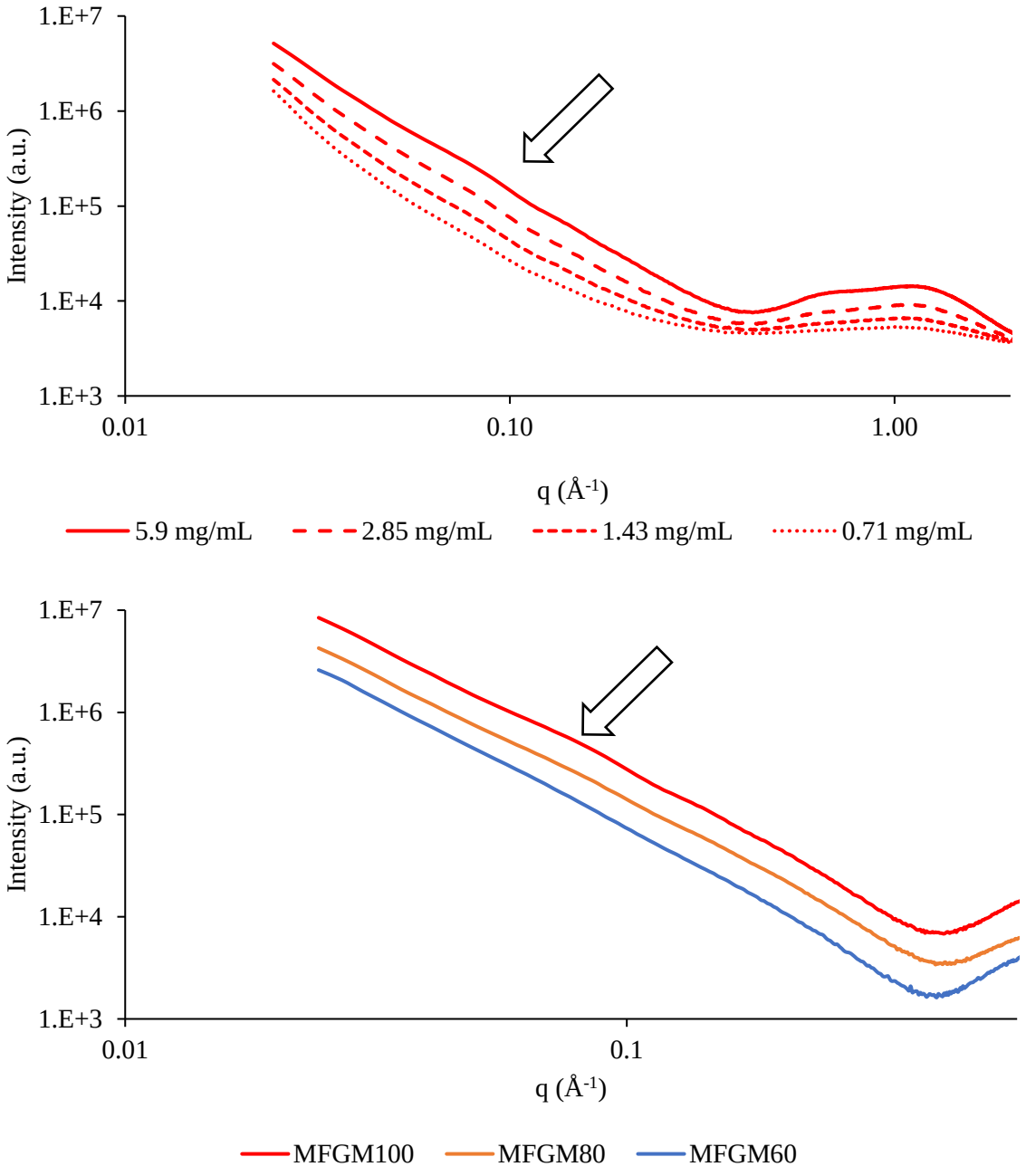

Figure 5.9. Small angle X-ray scattering profiles of milk fat globule membrane (MFGM) phospholipid vesicles.

a) Concentration gradient of MFGM100 = without cholesterol. Intensity has been normalized to account for concentration. Arrow indicates a small degree of possible diffraction. Units are mg total polar lipid/mL.
b) MFGM phospholipids with varying concentrations of cholesterol with PIPES buffer subtracted. MFGM100, 5.9 mg total polar lipid/mL; MFGM80 = 4:1 MSM/cholesterol, 4.8 mg total polar lipid/mL; MFGM60 = 3:2 MSM/cholesterol, 3.6 mg total polar lipid/mL. Offset has been added for clarity. Arrow indicates possible diffraction peak.

Diluting MFGM100 with PIPES buffer may have changed the structure of the vesicles. After accounting for differences in concentration, the shoulder at d = 9.3 Å (q = 0.66 $Å^{-1}$) as well as the d = 5.3 Å (q = 1.18 $Å^{-1}$) which are present in the 5.9 mg/mL preparation progressively disappear as the concentration of total polar lipid decreases (Fig. 5.9 a). These changes to the scattering profiles could be due in part to reduced interparticle repulsion between the negative MFGM phospholipid vesicles. The anionic surface of the native MFGM repulses casein micelles and other fat globules (Obeid et al., 2019). Diluting the MFGM phospholipid preparation increases the distance between the fat globules, reducing the tendency for electrostatic interactions and aggregation to occur, as well as any structural changes due to electrostatic interactions. As the preliminary WAXS study of MFGM phospholipid vesicles has been unfruitful, it will be more useful to focus on the SAXS focus on the q = 0 – 0.2 Å region where the greater amount of scattering is present.

5.4. Conclusions

In Chapter 4, the structural properties and detergent resistance of model membrane systems with binary combinations of naturally sourced phospholipids and cholesterol were examined. The techniques and methods used to do so were expanded upon in this chapter and applied to a more complex system, a model membrane system created from recombined MFGM phospholipids that were extracted from beta-serum. The phospholipids were extracted from beta-serum, a byproduct of anhydrous milk fat (AMF) production. There are generally two ways to produce AMF, the creation and then melting of butter and phase inversion of high fat cream (Bylund, 1995). Centrifugation is used to concentrate cream to achieve such high fat contents and the supernatant is disposed of as buttermilk. The beta-serum used in this study comes from the final centrifugation after the phase inversion.

MFGM phospholipids were recovered at a reasonably high purity, although impurities, likely to be residual neutral lipids, were detected. Phospholipid oxidation products possibly formed during the spraying drying of liquid beta-serum were also possibly present. The Folch/Bitman extraction did not selectively concentrate any one of the phospholipid species measured when compared to the typical composition of phospholipids found in the beta-serum used. The high PE content originated from the MFGM inner monolayer which may be attached to triacylglyceride core during AMF production.

Due to the high unsaturated PE content, the MFGM phospholipid vesicles had a T_m (25 °C), lower than a previously reported T_m of 36 °C (Murthy et al., 2015). The presence of a high proportion of unsaturated phospholipids leads to the absence of liquid ordering when cholesterol is added (Martinez-Seara et al., 2008). However, evidence of the onset of L_o domains was present in the MFGM phospholipid vesicles as the enthalpy of the $S_o \rightarrow L_d$ transition decreased as cholesterol content increased, implying a cholesterol-induced dissipation of the phase transition. Secondly, the

lateral hydrocarbon chain packing (I_{2850}/I_{2880}) disorder of MFGM phospholipid in the S_o phase increased when cholesterol was added, also indicative of the onset of an L_o phase.

In light of the evidence indicating that an L_o phase existed within the MFGM phospholipid vesicles, the detergent resistance of the vesicles was investigated, providing mixed results concerning the fate of the L_o domains when incubated with bovine bile. Milk fat globule membrane phospholipid vesicles with higher concentrations of cholesterol seemed to initially be more resistant to immediate detergent-induced solubilization due to lower T0 to T1 reductions in OD630 when bovine bile was added. After being incubated in bovine bile for 2 h, the OD630 of the MFGM phospholipid vesicle system at the endpoint of digestion were not statistically significantly different, indicating the MFGM phospholipid vesicle systems had reached a similar equilibrium. This was in agreement with the results from Raman spectroscopy – at the endpoint of the reaction, bilayer order between phospholipid vesicles that contained cholesterol and those that did not were not significantly different. As such, further investigation into the digestion of MFGM systems should focus on the polymorphism of micellar structures formed at the onset of the reaction and detection of L_o domains at the endpoints. X-ray diffraction may be one tool that is capable of aiding in this. The current concentration of MFGM phospholipid vesicles was too low for the lamellar features to be visible in small angle x-ray diffraction. Despite these difficulties, vesicles created from phospholipids extracted from beta-serum have proven to be model system worth investigating – the interplay of phospholipid components and cholesterol has led to interesting structural modifications and a degree of detergent resistance. The implications are potentially far reaching in the nutritional field considering that the phospholipid composition of milk fat globules is size dependent and therefore differently sized milk fat globules may produce micellar intermediates of varying structure and function during digestion.

Acknowledgements

The beta serum powder (BSP2) was kindly donated by TATUA Co-operative Dairy Company. The Python program used to baseline, average, and process the Raman data was developed and coded by Dr. Waterland of Massey University. The small-angle x-ray scattering data was collected and normalized by Dr. Andrew Clulow of ANSTO during a remote seminar course at the European Molecular Biology Laboratory (EMBL) Hamburg, Germany.

References

Almgren, M. (2000). Mixed micelles and other structures in the solubilization of bilayer lipid membranes by surfactants. *Biochimica et Biophysica Acta (BBA) - Biomembranes*, *1508*(1–2), 146–163.

Alshehab, M., Budamagunta, M. S., Voss, J. C., & Nitin, N. (2019). Real-time measurements of milk fat globule membrane modulation during simulated intestinal digestion using electron paramagnetic resonance spectroscopy. *Colloids and Surfaces B: Biointerfaces*, *184*(2019), 110511.

Batenjany, M. M., Wang, Z., Huang, C., & Levin, I. W. (1994). Bilayer packing characteristics of mixed chain phospholipid derivatives: Raman spectroscopic and differential scanning calorimetric studies of 1-stearoyl-2-capryl-sn-glycero-3-phosphocholine (C(18): C(10)PC) and 1-stearoyl-2-capryl-sn-glycero-3-phospho-N-trimethylpropanolamine (C(18): C(10)TMPC). *Biochimica et Biophysica Acta (BBA) - Biomembranes*, *1192*(2), 205–214.

Baumgartner, S., Kelly, E. R., van der Made, S., Berendschot, T. TJM., Husche, C., Lütjohann, D., & Plat, J. (2013). The influence of consuming an egg or an egg-yolk buttermilk drink for 12 wk on serum lipids, inflammation, and liver function markers in human volunteers. *Nutrition*, *29*(10), 1237–1244.

Bitman, J., & Wood, D. L. (1990). Changes in milk fat phospholipids during lactation. *Journal of Dairy Science*, *73*(5), 1208–1216.

Brink, L. R., Herren, A. W., McMillen, S., Fraser, K., Agnew, M., Roy, N., & Lönnerdal, B. (2020). Omics analysis reveals variations among commercial sources of bovine milk fat globule membrane. *Journal of Dairy Science*, *103*(4), 3002–3016.

Brodkorb, A., Egger, L., Alminger, M., Alvito, P., Assunção, R., Ballance, S., Bohn, T., Bourlieu-Lacanal, C., Boutrou, R., Carrière, F., Clemente, A., Corredig, M., Dupont, D., Dufour, C., Edwards, C., Golding, M., Karakaya, S., Kirkhus, B., Le Feunteun, S., … Recio, I. (2019). INFOGEST static in vitro simulation of gastrointestinal food digestion. *Nature Protocols*, *14*(4), 991–1014.

Chachaty, C., Rainteau, D., Tessier, C., Quinn, P. J., & Wolf, C. (2005). Building up of the liquid-ordered phase formed by sphingomyelin and cholesterol. *Biophysical Journal*, *88*(6), 4032–4044.

Chemin, C., Bourgaux, C., Péan, J.-M., Pabst, G., Wüthrich, P., Couvreur, P., & Ollivon, M. (2008). Consequences of ions and pH on the supramolecular organization of sphingomyelin and sphingomyelin/cholesterol bilayers. *Chemistry and Physics of Lipids*, *153*(2), 119–129.

Cohn, J., Kamili, A., Wat, E., Chung, R. W., & Tandy, S. (2010). Dietary phospholipids and intestinal cholesterol absorption. *Nutrients*, *2*(2), 116–127.

Conway, V., Couture, P., Richard, C., Gauthier, S. F., Pouliot, Y., & Lamarche, B. (2013). Impact of buttermilk consumption on plasma lipids and surrogate markers of cholesterol homeostasis in men and women. *Nutrition, Metabolism and Cardiovascular Diseases*, *23*(12), 1255–1262.

Czamara, K., Majzner, K., Pacia, M. Z., Kochan, K., Kaczor, A., & Baranska, M. (2015). Raman spectroscopy of lipids: A review: Raman spectroscopy of lipids. *Journal of Raman Spectroscopy*, *46*(1), 4–20.

Deeth, H. (1997). The role of phospholipids in the stability of milk fat globules. *The Australian Journal of Dairy Technology*, 52, 44 – 46.

Eggers, L. F., & Schwudke, D. (2016). Liquid Extraction: Folch. In M. R. Wenk (Ed.), *Encyclopedia of Lipidomics* (pp. 1–6). Netherlands: Springer.

Folch, J., Lees, M., & Sloane Stanley, G. (1957). A simple method for the isolation and purification of total lipides from animal tissues. *J Biol Chem*, *226*(1), 497–509.

Gallier, S., Gragson, D., Jiménez-Flores, R., & Everett, D. (2010 a). Using confocal laser scanning microscopy to probe the milk fat globule membrane and associated proteins. *Journal of Agricultural and Food Chemistry*, *58*(7), 4250–4257.

Gallier, S., Gragson, D., Cabral, C., Jiménez-Flores, R., & Everett, D. W. (2010 b). Composition and fatty acid distribution of bovine milk phospholipids from processed milk products. *Journal of Agricultural and Food Chemistry*, *58*(19), 10503–10511.

Gallier, S., Gordon, K. C., Jiménez-Flores, R., & Everett, D. W. (2011). Composition of bovine milk fat globules by confocal Raman microscopy. *International Dairy Journal*, *21*(6), 402–412.

Gallier, S., Ye, A., & Singh, H. (2012). Structural changes of bovine milk fat globules during in vitro digestion. *Journal of Dairy Science*, *95*(7), 3579–3592.

Gallier, S., Vocking, K., Post, J. A., Van De Heijning, B., Acton, D., Van Der Beek, E. M., & Van Baalen, T. (2015). A novel infant milk formula concept: Mimicking the human milk fat globule structure. *Colloids and Surfaces B: Biointerfaces*, *136*, 329–339.

Gao, W.-Y., Quinn, P. J., & Yu, Z.-W. (2008). The role of sterol rings and side chain on the structure and phase behaviour of sphingomyelin bilayers. *Molecular Membrane Biology*, *25*(6–7), 485–497.

Haustein, M., Wahab, M., Mögel, H.-J., & Schiller, P. (2015). Vesicle solubilization by bile salts: Comparison of macroscopic theory and simulation. *Langmuir*, *31*(14), 4078–4086.

Heerklotz, H. (2008). Interactions of surfactants with lipid membranes. *Quarterly Reviews of Biophysics*, *41*(3–4), 205–264.

Hjelm, R. P., Thiyagarajan, P., & Alkan, H. (1988). A small-angle neutron scattering study of the effects of dilution on particle morphology in mixtures of glycocholate and lecithin. *Journal of Applied Crystallography*, *21*(6), 858–863.

Howards, A., & Marks, J. (1979). Effect of milk products on serum-cholesterol. *The Lancet*. *314*(8149), 957.

Israelachvili, J. N. (2010). Soft and biological structures. In *Intermolecular and Surface Forces* (pp. 535 – 576). Burlington: Elsevier Science.

Jeong, J., Lisinski, I., Kadegowda, A. K. G., Shin, H., Wooding, F. B. P., Daniels, B. R., Schaack, J., & Mather, I. H. (2013). A Test of current models for the mechanism of milk-lipid droplet secretion: Mechanism of milk-lipid secretion. *Traffic*, *14*(9), 974–986.

Keenan, T.W., Patton, S. (1995). The milk lipid globule membrane. In R. G. Jensen (Ed.), *Handbook of Milk Composition* (pp. 5–62). San Diego: Academic Press.

Kundu, N., Banik, D., & Sarkar, N. (2018). Self-Assembly of amphiphiles into vesicles and fibrils: Investigation of structure and dynamics using spectroscopy and microscopy techniques. *Langmuir*, *34*(39), 11637–11654.

Lichtenberg, D., Robson, R. J., & Dennis, E. A. (1983). Solubilization of phospholipids by detergents structural and kinetic aspects. *Biochimica et Biophysica Acta (BBA) - Reviews on Biomembranes*, *737*(2), 285–304.

Lopez, C., Madec, M.-N., & Jimenez-Flores, R. (2010). Lipid rafts in the bovine milk fat globule membrane revealed by the lateral segregation of phospholipids and heterogeneous distribution of glycoproteins. *Food Chemistry*, *120*(1), 22–33.

Lopez, C., Briard-Bion, V., & Ménard, O. (2014). Polar lipids, sphingomyelin and long-chain unsaturated fatty acids from the milk fat globule membrane are increased in milks produced by cows fed fresh pasture based diet during spring. *Food Research International*, *58*, 59–68.

Lopez, C., Cauty, C., & Guyomarc'h, F. (2018 a). Unravelling the complexity of milk fat globules to tailor bioinspired emulsions providing health benefits: The key role played by the biological membrane. *European Journal of Lipid Science and Technology*, 1800201.

Lopez, C., Cheng, K., & Perez, J. (2018 b). Thermotropic phase behaviour of milk sphingomyelin and role of cholesterol in the formation of the liquid ordered phase examined using SR-XRD and DSC. *Chemistry and Physics of Lipids*, *215*, 46–55.

Maldonado-Valderrama, J., Wilde, P., Macierzanka, A., & Mackie, A. (2011). The role of bile salts in digestion. *Advances in Colloid and Interface Science*, *165*(1), 36–46.

Martinez-Seara, H., Róg, T., Pasenkiewicz-Gierula, M., Vattulainen, I., Karttunen, M., & Reigada, R. (2008). Interplay of unsaturated phospholipids and cholesterol in membranes: effect of the double-bond position. *Biophysical Journal*, *95*(7), 3295–3305.

Mather, I. H. (2011). Milk lipids | Milk fat globule membrane. In J. W. Fuquay, P. F. Fox, P. L. H. McSweeney (Eds.), *Encyclopedia of Dairy Sciences* (pp. 680–690). San Diego: Academic Press.

Mather, I. H., & Keenan, T. W. (1998). Origin and Secretion of Milk Lipids. *Journal of Mammary Gland Biology and Neoplasia. 3*(3), 259 – 273.

Mazer, N. A., Benedek, G. B., & Carey, M. C. (1980). Quasielastic light-scattering studies of aqueous biliary lipid systems. Mixed micelle formation in bile salt-lecithin solutions. *Biochemistry*, *19*(4), 601–615.

Morin, P., Jiménez-Flores, R., & Pouliot, Y. (2007). Effect of processing on the composition and microstructure of buttermilk and its milk fat globule membranes. *International Dairy Journal*, *17*(10), 1179–1187.

Moschetta, A., Frederik, P. M., Portincasa, P., vanBerge-Henegouwen, G. P., & van Erpecum, K. J. (2002). Incorporation of cholesterol in sphingomyelin- phosphatidylcholine vesicles has profound effects on detergent-induced phase transitions. *Journal of Lipid Research*, *43*(7), 1046–1053.

Murthy, A. V. R., Guyomarc'h, F., Paboeuf, G., Vié, V., & Lopez, C. (2015). Cholesterol strongly affects the organization of lipid monolayers studied as models of the milk fat globule membrane: Condensing effect and change in the lipid domain morphology. *Biochimica et Biophysica Acta (BBA) - Biomembranes*, *1848*(10), 2308–2316.

Murthy, A. V. R., Guyomarc'h, F., & Lopez, C. (2016 a). The temperature-dependent physical state of polar lipids and their miscibility impact the topography and mechanical properties of bilayer models of the milk fat globule membrane. *Biochimica et Biophysica Acta (BBA) - Biomembranes*, *1858*(9), 2181–2190.

Murthy, A. V. R., Guyomarc'h, F., & Lopez, C. (2016 b). Cholesterol decreases the size and the mechanical resistance to rupture of sphingomyelin rich domains, in lipid bilayers studied as a model of the milk fat globule membrane. *Langmuir*, *32*(26), 6757–6765.

Nagarajan, R. (2002). Molecular packing parameter and surfactant self-assembly: The neglected role of the surfactant tail. *Langmuir*, *18*(1), 31–38.

Obeid, S., Guyomarc'h, F., Francius, G., Guillemin, H., Wu, X., Pezennec, S., Famelart, M.-H., Cauty, C., Gaucheron, F., & Lopez, C. (2019). The surface properties of milk fat globules govern their interactions with the caseins: Role of homogenization and pH probed by AFM force spectroscopy. *Colloids and Surfaces B: Biointerfaces*, *182*, 110363.

Orendorff, C. J., Ducey, M. W., & Pemberton, J. E. (2002). Quantitative correlation of raman spectral indicators in determining conformational order in alkyl chains. *The Journal of Physical Chemistry A*, *106*(30), 6991–6998.

Paré, C., & Lafleur, M. (1998). Polymorphism of POPE/Cholesterol system: A 2H nuclear magnetic resonance and infrared spectroscopic investigation. *Biophysical Journal*, *74*(2), 899–909.

Pike, L. J. (2006). Rafts defined: A report on the Keystone symposium on lipid rafts and cell function. *Journal of Lipid Research*, *47*(7), 1597–1598.

Quinn, P. J., & Wolf, C. (2009). The liquid-ordered phase in membranes. *Biochimica et Biophysica Acta (BBA) - Biomembranes*, *1788*(1), 33–46.

Rankine, C. D., Atkinson, S. J., Waterland, M. R., Masters, S. L., & Wann, D. A. (2018). The structure of tris(chloromethyl)amine in the gas phase using quantum chemical calculations and gas electron diffraction and as a solid and melt using Raman spectroscopy. *Structural Chemistry*, *29*(3), 803–813.

Reinhardt, T. A., & Lippolis, J. D. (2006). Bovine milk fat globule membrane proteome. *Journal of Dairy Research*, *73*(04), 406.

Sánchez-Juanes, F., Alonso, J. M., Zancada, L., & Hueso, P. (2009). Distribution and fatty acid content of phospholipids from bovine milk and bovine milk fat globule membranes. *International Dairy Journal*, *19*(5), 273–278.

Shirota, K., Yagi, K., Inaba, T., Li, P.-C., Murata, M., Sugita, Y., & Kobayashi, T. (2016). Detection of sphingomyelin clusters by Raman spectroscopy. *Biophysical Journal*, *111*(5), 999–1007.

Singh, H. (2019). Symposium review: Fat globules in milk and their structural modifications during gastrointestinal digestion. *Journal of Dairy Science*, *102*(3), 2749–2759.

Singh, H., & Gallier, S. (2017). Nature's complex emulsion: The fat globules of milk. *Food Hydrocolloids*, *68*, 81–89.

Sodt, A. J., Pastor, R. W., & Lyman, E. (2015). Hexagonal substructure and hydrogen bonding in liquid-ordered phases containing palmitoyl sphingomyelin. *Biophysical Journal*, *109*(5), 948–955.

Stuart, M. C. A., & Boekema, E. J. (2007). Two distinct mechanisms of vesicle-to-micelle and micelle-to-vesicle transition are mediated by the packing parameter of phospholipid–detergent systems. *Biochimica et Biophysica Acta (BBA) - Biomembranes*, *1768*(11), 2681–2689.

Su, M., Subbaraj, A. K., Fraser, K., Qi, X., Jia, H., Chen, W., Gomes Reis, M., Agnew, M., Day, L., Roy, N. C., & Young, W. (2019). Lipidomics of brain tissues in rats fed human milk from chinese mothers or commercial infant formula. *Metabolites*, *9*(253), 1–19.

Tai, P., Golding, M., Singh, H., Waterland, M., & Everett, D. W. (2021). Cholesterol-phospholipid interactions resist the detergent effect of bovine bile. *Colloids and Surfaces B: Biointerfaces*, *205*(111842), 1 – 11.

TATUA (2017). BSP2, Ver. 2. The TATUA Co-operative Dairy Company Limited.

van Meer, G., Voelker, D. R., & Feigenson, G. W. (2008). Membrane lipids: Where they are and how they behave. *Nature Reviews Molecular Cell Biology*, *9*(2), 112–124.

Yao, Y., Zhao, G., Xiang, J., Zou, X., Jin, Q., & Wang, X. (2016 a). Lipid composition and structural characteristics of bovine, caprine and human milk fat globules. *International Dairy Journal*, *56*, 64–73.

Yao, Y., Zhao, G., Yan, Y., Mu, H., Jin, Q., Zou, X., & Wang, X. (2016 b). Milk fat globules by confocal Raman microscopy: Differences in human, bovine and caprine milk. *Food Research International*, *80*, 61–69.

Zheng, H., Gordon, K. C., & Everett, D. W. (2013). Innovative application of confocal Raman microscopy to investigate the interaction between trans-2-hexenal and bovine milk fat globules. *International Dairy Journal*, *32*(2), 68–70.

Zheng, H., Jiménez-Flores, R., Gragson, D., & Everett, D. W. (2014). Phospholipid architecture of the bovine milk fat globule membrane using giant unilamellar vesicles as a Model. *Journal of Agricultural and Food Chemistry*, *62*(14), 3236–3243.

Chapter 6 – The structural fate of liquid-ordered domains during *in vitro* digestion of phospholipid/cholesterol vesicles

6.1. Introduction

The milk fat globule membrane (MFGM) interface of the milk fat globule (MFG) undergoes digestive processes to not only provide nutrients to the human body, but to also provide putative functional effects. Both *in vitro* and *in vivo* gastrointestinal digestion models have been utilized to study the macro and microstructural changes that occur during digestion; however, previous studies have not delved into the molecular mechanisms and interactions that occur between phospholipids and cholesterol under gastrointestinal conditions. These two components make up the foundation of the MFGM, and act as a cement for the interface, respectively. Analysis of the structural fate of these dairy components may shed light or even bridge gaps of understanding between the role of lipidic structures and bioactive functionality, in particular, the anticholesteremic effect that arises from the consumption of MFGM-derived products.

Phospholipids and proteins account for over 95% of the dry weight of the MFGM (Walstra, Wouters & Geurts, 2006). The inner monolayer and proteins located within the interlamellar space originate from the ectoplasmic reticulum of the lactocytes whereas the outer bilayer is from the secretory regions of the apical membrane of the plasma lactocytes (Thum et al., 2021). Sphingomyelin and cholesterol are capable of associating to form L_o domains, structural analogues to the phospholipid/sterol foundation underlying lipid rafts in biological systems. These domains possess high lateral mobility and display a lower rupture force than the MFGM bulk L_d phase (Murthy, Guyomarc'h, & Lopez, 2016), while at the same time, displaying higher intermolecular attraction than pure phases of either sphingomyelin or cholesterol (Cheng, Ropers, & Lopez, 2017), highlighting the fluidizing and condensing effect that cholesterol has on sphingomyelin. The structural and mechanical features of L_o domains may impact how milk phospholipids, cholesterol, and perhaps even milk triglycerides are digested.

The nuances in the digestion of MFGM are often overlooked or under-emphasized due to the milk fat globule membrane only making up 2 – 6% of the MFG mass (Heid & Keenan, 2005) and the complexity of the interface, comprising of phospholipid, protein, and glycoprotein. On the other hand, the unique variety of proteins and phospholipids are responsible for an increasing interest in the health benefits of MFGM consumption. Furthermore, as the MFGM is the interface between the MFG triacylglyceride core and the bulk aqueous phase, it is involved in all digestive processes. Understanding the structural transformations of these phospholipids during gastrointestinal digestion will promote the valorisation of MFGM-rich products, such as beta-serum (byproduct of anhydrous milk fat production) and buttermilk (byproduct of butter production).

The current model proposed model of MFG and MFGM digestion is mainly concerned with the hydrolysis of proteins and lipolysis of triacylglycerides (Gallier, Ye, & Singh, 2012). In addition to the well-reported protein aggregation and hydrolysis due to the acidic pH and pepsin, respectively (Ye, Cui, & Singh, 2011), the gastric digestion of milk results in a vast degree of structural changes to the MFG. Dynamic *in vitro* systems that do not include gastric lipase have demonstrated the shearing force from the formation of protein clots is enough disrupt the membrane, resulting in coalescence of MFGs (Roy et al., 2019). Fat globules in dairy products with relatively low protein content, such as cream, also become trapped within small protein aggregates, i.e., clots (Gallier, Ye, & Singh, 2012) but retain their globular structure. Static *in vitro* digestion models show that the native membrane allows the MFGs to resist coalescence and to retain the lateral distribution of phospholipids.

Gastric lipase has not been commonly used in the *in vitro* digestion of MFG due to its former commercial unavailability. The enzyme is an important addition, responsible for hydrolysing 10 – 30% of the lipids and, although it is inhibited by the neutral pH and bile salts in the intestine, is necessary for the complete digestion of milk triacylglycerides (Bernbäck, Bläckberg, Hernell, 1990). *In vivo* studies inherently incorporate gastric lipases, or in the case of rats, an acid-stable lingual lipase that acts similarly to human gastric lipase (Hamosh and Scow, 1973). The acid-stable lingual lipase is capable of producing needle-shaped crystals on the surface of the MFG (Gallier et al., 2013) which transform into small protrusions as the gastric digestion progresses. These protrusions are hypothesized to be plugs composed of fatty acids and gastric lipase, responsible for preventing the enzyme from reaching further into the triacylglyceride core (Pafumi et al., 2003). These clusters of mostly free fatty acids that accumulate on the surface of the globule, promote the binding of the pancreatic lipase-colipase complex (Singh & Gallier, 2014). This model of gastric lipase activity has two weaknesses: considering that gastric lipase is responsible for a high degree of hydrolysis, such small protrusions, only 200 nm in size, are solely responsible for limiting gastric lipase activity. Furthermore, the model of gastric digestion proposed by Gallier, Ye, & Singh (2012) only applies to dairy products with lower casein content and intact fat globules (i.e., cream). In a semi-dynamic gastric *in vitro* digestion system, the addition of rabbit gastric lipase to standardized bovine milk showed increased aggregation in the raw milk and the pasteurized milk but limited the aggregation of homogenized milk (Bourlieu et al., 2015). The authors argue that MFGM and interfaces after processing are recognized differently by gastric lipase.

Intestinal digestion of MFGs can be split into three categories, the displacement of phospholipids and proteins by bile salts, the further hydrolysis of lipids by pancreatic lipases, and absorption of lipolytic products across the intestinal epithelial. Bile salts cover the MFG interface forming liquid-crystalline lamellae composed of phospholipids, bile salts, and lipolytic products such as long chain fatty acids. These fatty acids are highly hydrophobic, accumulating at the polar-apolar interface (Carey, Small, & Bliss, 1983). The bile salts partially displace MFGM components (Gallier, Ye, & Singh 2012)

promoting pancreatic colipase and lipase adsorption onto bile salt-rich interfacial regions. In the first 5 min of intestinal digestion, roughly 25% of the free fatty acids are already released (Gallier, Ye, & Singh, 2012). Without a gastric digestive phase (i.e., with gastric lipase) a lag phase to intestinal lipolysis is present (Berton et al., 2009). Thus, the presence of fatty acids as a result of the gastric phase promotes the binding of pancreatic co-lipase and lipase to the surface of the MFG. Caseins and whey proteins adhering to the MFGM due to homogenization and interfacial adsorption have also been shown to hinder the kinetics of intestinal lipolysis (Berton et al., 2012). These authors suggest that, although the presence of the proteins create larger available area for the pancreatic lipase to adhere to, the quality of the interface decreases, implying that the phospholipid composition of the interface surface enhances milk lipid digestion. Quality, in this case, refers to the electrostatic properties of the interface. The active site of pancreatic lipase is negative (Colin et al., 2008) much like the surface of casein micelles and whey protein. The lipase complex is far more attracted to the zwitterionic phospholipids, PC and SM, which make up the majority of phospholipids of the native surface of the MFGM. The lipolytic products, phospholipids, and bile salts self-assemble to form micellar intermediates and mixed micelles. The amphiphilic nature of the micelles is required for transport across the unstirred water layer to come into contact with the mucosal layer and epithelial transporters.

Studies reviewed above have noted the possibility of rigid sphingomyelin-rich domains being involved in digestive mechanisms (Gallier, Ye, & Singh, 2012; Et-Thakafy, Guyomarc'h, & Lopez, 2017) but the topic has not been further investigated. Laterally organized on the surface of the distal leaflet, L_o domains would come into contact with all the digestive processes mentioned above. Furthermore, sphingomyelin is not hydrolysed by pancreatic phospholipase (PLA2) but by mucosal and biliary (only in humans) alkaline sphingomyelinase (alk-SMase), the activity of which is bile salt-dependent. The role of PLA2 in overall phospholipid digestion, especially PC digestion, should not be underestimated in the digestion of MFGM as the majority of membrane phospholipid is PC. Studying the interactions between L_o domains and digestive components may increase our understanding of why dairy products are structured the way they are for optimal digestion.

Investigation into the structural role of cholesterol in model membrane systems that are comprised of naturally sourced phospholipids has shown that L_o domains are resistant to the physiological detergent, rehydrated bovine bile extract (Tai et al., 2021). Conversely, in Chapter 5, recombined MFGM phospholipid vesicles were shown to be quite susceptible to detergent-induced solubilization. Hence, the objective of the current study was to determine whether L_o domains are not only detergent-resistant, but also resistant to *in vitro* gastrointestinal digestive conditions. The hypothesis is that bile salts are primarily the agent by which phospholipids are displaced from the MFGM interface – the detergent resistance offered by cholesterol nullifies the vesicle → micelle transition. As gastric lipase is substrate-specific to triacylglycerides, and pancreatic the lipase/co-lipase complex requires

partial displacement of the MFGM to optimally function, MSM/cholesterol multilamellar vesicles (MLVs) that possess L_o domains should be more resistant to both enzymes. Whether the L_o domains are resistant to alk-SMase remains to be seen. The strategy for determining if the detergent resistant L_o domains persist during gastrointestinal digestion consisted of incorporating varying proportions of cholesterol into milk sphingomyelin (MSM), brain phosphatidylcholine (BPC), soy phosphatidylcholine (SPC), and MFGM phospholipid vesicles which were then subjected to *in vitro* gastrointestinal digestion. The microstructure, thermotropic behaviour, and the bilayer order of the vesicles pre-digestion, post-gastric, and post-intestinal were analysed and compared.

6.2. Materials and methods

6.2.1 Milk fat globule membrane phospholipid extraction

The MFGM phospholipid extract used in this study was derived from beta-serum powder (BSP2, Tatua Dairy Company, Tatuanui, New Zealand) obtained from spray-drying fresh beta-serum. Lipids were extracted using the Folch method with 2:3:1 v/v of methanol:chloroform:8.76% NaCl (Folch, Lees, Sloane Stanley, 1957; Eggers and Schwudke, 2016). The solid to total extract solvent ratio was 1:24 w/v. Samples were thoroughly mixed then centrifuged at 1,000 × g for 10 min at 20 °C. The top methanol layer was siphoned off, the aqueous layer as well as any precipitate was discarded, and the chloroform layer containing phospholipids was decanted. The phospholipid-rich chloroform layer was concentrated by rotary evaporation and solubilized with hexane to produce a crude extract that was approximately 100 mg lipid/mL based on previous calculations.

Phospholipids were separated from the crude hexane extract by solid phase extraction according to Bitman and Wood (1990) as modified by Gallier et al. (2010). Silica cartridges (12 mL) with a bed weight of 2 g (Discovery DSC-Si, Sigma-Aldrich, Auckland, New Zealand) were conditioned with 2 volumes of methanol before the crude extract (~200 mg lipid) was loaded. The neutral lipids were eluted out with 40 mL hexane:ethyl ether (1:1). The phospholipids were first eluted with methanol (20 mL), followed by chloroform:methanol:water (20 mL; 3:5:2 v/v/v). Both phospholipid fractions were collected, concentrated by rotary evaporation and solubilized in 2:1 v/v chloroform:methanol to approximately 10 mg SM/mL before being stored in the dark at –20 °C until used.

The BSP2 used in this experiment and the BSP2 used in Chapter 5 originated from different batches. The phospholipid composition of the batch used in this chapter was found to be 4.0 ± 0.1% mol PI, 47.7 ± 0.7 % mol PE, 7.1 ± 0.2 % mol PS, 25.0 ± 0.4% mol PC, 16.2 ± 0.3% mol SM and the total phospholipid content was 15.7 ± 0.4 mg total polar lipids/mL extract. The HPLC protocol, the standard curves, and an example chromatogram can be found in Appendices 6.1 – 6.3.

6.2.2 Phospholipid vesicle preparation

Phospholipid vesicles were prepared in pH 6.7 buffer: PIPES 10 mM (1,4-piperazinediethane sulfonic acid; purity ≥ 99%; Sigma-Aldrich), 50 mM NaCl (Analytical Reagent Grade; Thermo Fisher Scientific NZ, North Shore City, New Zealand) and 5 mM $CaCl_2$ (Millipore, Burlington, MA, USA), according to the procedure of Lopez, Cheng, & Perez (2018) using the same method as Chapter 3 and 4.

Vesicles were composed of milk sphingomyelin (Avanti Polar Lipids, Alabaster, AL, USA), porcine brain phosphatidylcholine (Avanti Polar Lipids), soy phosphatidylcholine (Sigma-Aldrich), and MFGM phospholipids or binary mixtures of one of these four phospholipid preparations with ovine cholesterol (Sigma-Aldrich). Binary mixtures consisted of 100/0, 4/1, 7/3, 3/2 of phospholipid/cholesterol, mol/mol. In the case of the MFGM phospholipid vesicles, the same ratios were used but to an SM/cholesterol, mol/mol ratio. Total lipid concentration of the MSM, SPC, and BPC vesicles was 2.6 mM so that the post-intestinal digestate would contain 326 µM total phospholipid plus cholesterol. This is the same concentration of lipid used in previous experiments and is two times the concentration of SM found in milk (Bitman & Wood, 1990), ensuring the experiments are somewhat physiologically relevant. The MFGM phospholipids vesicles were constructed so that the total of SM/cholesterol was 2.6 mM. Table 6.1 details the concentrations used to create MFGM phospholipid vesicles.

Table 6.1. Phospholipid and cholesterol concentrations used for MFGM phospholipid vesicles.

Given name	PI (mM)	PE (mM)	PS (mM)	PC (mM)	SM (mM)	Chol (mM)	Total PL (mM)
MFGM100	0.72	7.33	1.13	4.00	2.6	0	16
MFGM80	0.58	5.86	0.9	3.20	2.08	0.52	13.1
MFGM70	0.5	5.13	0.79	2.80	1.82	0.78	11.8
MFGM60	0.43	4.40	0.68	2.40	1.56	1.04	10.5

PE = phosphatidylethanolamine; PI = phosphatidylinositol; PS = phosphatidylserine; PC = phosphatidylcholine; SM = sphingomyelin; Chol = cholesterol. MFGM100 = milk fat globule membrane phospholipid without cholesterol; MFGM80 = milk fat globule membrane phospholipid with 4:1 SM/cholesterol; MFGM70 = milk fat globule membrane phospholipid with 7:3 SM/cholesterol; MFGM60 = milk fat globule membrane phospholipid with 3:2 cholesterol.

6.2.3 Gastrointestinal static in vitro digestion

Static *in vitro* digestion followed the INFOGEST protocol set forth by Brodkorb et al., (2019) with slight modifications. Simulated salivary, gastric, and intestinal fluid (SSF, SGF, SIF, respectively) were prepared to 1.25× strength of the final reagent used in the experiment (Brodkorb et al., 2019). As the phospholipids did not contain starch and protein digestion was not the focus of the experiment, amylase and pepsin were not included. The simulated digestion fluids were diluted to 1× strength before use and $CaCl_2$ (aq.) was added immediately before the digestion experiment to achieve final concentrations of 1.5 mM, 0.15 mM, and 0.6 mM for the SSF, SGF, and SIF, respectively.

The oral phase consisted of incubating 1 mL of phospholipid vesicle with an equivalent volume of SSF (pH 7) at 37 °C for 2 min. The gastric phase consisted of incubating the resulting 2 mL from the oral phase with an equivalent volume of SGF that contained rabbit gastric extract (RGE, 60 lipase U/mL total digesta, Lipolytech, Marseille, France) at 37 °C for 2 h. The pH was adjusted to 3.0 ± 0.1 with 2 M HCl and each sample was vortexed intermittently during the gastric digestion. After the gastric phase was complete, 2 mL of each sample was aliquoted for further analysis. The pH of each aliquot was raised to 7.0 ± 0.1 with 4M NaOH to inhibit residual gastric lipase activity.

For the MSM samples alone, the remaining post-gastric 2 mL and additional NaOH was incubated with an equivalent volume of SIF at 37 °C for a further 2 h. Other than salts (KCl, KH_2PO_4, $NaHCO_3$, NaCl, etc), the SIF contained 10 mM of rehydrated bovine bile (final concentration, Sigma-Aldrich) and pancreatin (8× USP, 100 U trypsin activity/mL Sigma-Aldrich). Intestinal digestion was performed both with alk-SMase (0.35 nmol/min/mL) and without. The pH was adjusted to 7.0 ± 0.1 with 4M NaOH and samples were vortexed intermittently during digestion. After the intestinal phase was complete, the pH was lowered to 5.0 ± 0.1 with 2 M HCl and a heat treatment applied (60 °C for 20 min) to inhibit the pancreatin enzyme cocktail. The low pH and heat treatment caused some of the intestinal fraction precipitate so the pH was readjusted to 7.0 ± 0.1 with 4M NaOH to redissolve the precipitate. This precipitate was likely due to the protein fraction of the pancreatin as it only formed after the addition of the pancreatin and was exacerbated with heat treatment and pH changes. The bovine bile and gastric lipase did not show this behavior when heated or had the pH changed.

For the BPC, SPC, and MFGM samples, the remaining 2 mL was incubated with an equivalent volume of SIF at 37 °C for a further 2 h. Other than the aforementioned salts, the SIF contained 10 mM (final concentration) of rehydrated bovine bile (Sigma-Aldrich), and pancreatin (8× USP, 100 U trypsin activity/mL Sigma-Aldrich). The digestate was aliquoted into two, 2 mL portions. Alk-SMase (0.35 nmol/min/mL) was added to one aliquot. The pH was adjusted to 7.0 ± 0.1 with 4M NaOH and samples were vortexed intermittently during the digestion. After the intestinal phase was complete, the pH was lowered to 5.0 ± 0.1 with 2M HCl and a heat treatment applied (60 °C for 20 min) to inhibit the enzyme cocktail. The low pH and heat treatment cause some enzyme to precipitate so the pH was readjusted to 7.0 ± 0.1 with 4M NaOH to redissolve the precipitated enzyme.

The concentrations of chemicals used, as well as assays performed to determine enzyme activity, were in accordance with the INFOGEST protocol and recommendations (Minekus et al., 2014; Brodkorb et al., 2019) and can be found in Appendix 6.4. The one exception was the enzyme activity assay for alk-SMase for which a colorimetric assay kit was used (abcam241039, Abcam, Melbourne, Australia) (Appendix 6.5). A diagram of the static *in vitro* digestion process and the differences in MSM compared to the other preparations can be found as Fig. 6.1.

6.2.4 Negative stain transmission electron microscopy

Negative stain TEM was carried out on an FEI Tecnai G2 Spirit BioTWIN (FEI Company, Hillsboro, OR, USA) microscope. Phospholipid vesicles pre-digestion, post-gastric, and post-intestinal were applied onto 3.05 mm, 200 mesh copper grids (Agar Scientific, Essex, UK) pre-coated with Formvar. After allowing the sample to adhere to the carbon resin for 5 min, the remaining wet sample was wicked off using filter paper. Uranyl acetate (2%) was then used to stain the grid for 5 min before being blotted off, ensuring the grid was no longer wet before the sample was loaded into the microscope.

6.2.5 Raman spectroscopy

Raman spectroscopic data were acquired using a confocal microscope adapted from a commercially available inverted fluorescence microscope (Olympus, IX70, Tokyo, Japan) and pumped by a 532-nm fiber-coupled diode laser. Mirrors were used to orient the beam into a 40× microscope objective (numerical aperture = 0.65). Raman scattered light was collected in a 180° back-scattering geometry through the 40× microscope objective. The scattered light was directed into a FERGIE detector (Princeton Instruments, Trenton, NJ, USA). Samples were sandwiched between two glass microscope coverslips and frames (250 in total) each lasting 500 ms were taken for each measurement (Shirota et al., 2016; Rankine et al., 2018). The typical power at the sample measured 100 mW.

6.2.6 Differential scanning calorimetry

Differential scanning calorimetry (DSC) measurements were taken using a Nano DSC (TA Instruments, DE, USA). Samples (300 µL) were injected into a capillary cell and compared to 300 µL of PIPES buffer. Samples and corresponding controls were cooled to 1 °C, pressurized to 303 kPa, and allowed to equilibrate for 5 min. Heating scans were from 1 °C to 60 °C at 2 °C/min. The startup hook from 1 – 5 °C was removed. Data was analyzed with the NanoAnalyze software (TA Instruments).

6.2.7 Statistical analysis

A power analysis was conducted using preliminary MSM MLV Raman results. Diagnostics testing for outliers, non-normality of residuals, and homoscedasticity of the I_{2850}/I_{2880} and I_{2930}/I_{2880} data returned negative results (Appendix 6.6, 6.7). A balanced one-way ANOVA was used to test the H_0: the mean peak intensity ratio was the same for all cholesterol concentrations. Effect size was determined using:

$$f = \sqrt{\frac{\sigma^2_{means}}{\sigma^2}} \tag{6.1}$$

with f as the effect size, σ^2_{means} as the variance of k means, and σ^2 as the common variance of k groups. For a $1\text{-}\beta = 0.8$, $k = 4$. Five independent replicates were chosen for the Raman and DSC. The figures provided are constructed from the mean of five spectra and thermograms. The means and standard deviations of the Raman intensity ratios have been reported. The model for the ANOVA of

BPC, SPC, and MFGM was constructed using R (R Foundation of Statistical Computing, Vienna, Austria) and was:

$$response = \beta_0 + \beta_1(conc) + \beta_2(stage_{gs}) + \beta_3(stage_{ns}) + \beta_4(stage_s) + \beta_5(conc \times stage_{gs}) + \beta_6(conc \times stage_{ns}) + \beta_7(conc \times stage_s) + \in \quad (6.2)$$

where β_0 is the baseline group (3:2 phospholipid/cholesterol or 3:2 SM/cholesterol), the cholesterol concentration (conc) is one factor, and the pre-digestion, gastric stage (gs), and intestinal (with alk-SMase (s) and without alk-SMase (ns)) are four factors. To examine the difference between the peak intensity ratios for alk-SMase and without alk-SMase, data were treated as paired, as each pair of observations came from a single gastric stage sample (Fig 6.1 b). The difference was then tested with a t-test and the following liner regression model:

$$difference = \beta_0 + \beta_1(conc) + \in \quad (6.3)$$

where β_0 is the intercept, and β_1 is the expected change in difference as cholesterol concentration decreased.

The model for the MSM Raman peak ratios differed, as ten replicates were present for all stages of digestion with five independent replicates for the alk-SMase groups and the "without alk-SMase" group, allowing alk-SMase/no alk-SMase to be an additional factor that could be crossed with cholesterol concentration as well as digestion stage. The model is as follows:

$$response = \beta_0 + \beta_1(conc) + \beta_2(stage_{gs}) + \beta_3(stage_{ma}) + \beta_4(smase_y) + \beta_5(conc \times stage_{gs}) + \beta_6(conc \times stage_{ma}) + \beta_7(conc \times smase_y) + \beta_8(stage_{gs} \times smase_y) + \beta_9(stage_{ma} \times smase_y) + \beta_{10}(conc \times stage_{gs} \times smase_y) + \beta_{11}(conc \times stage_{ms} \times smase_y) + \in \quad (6.4)$$

The abbreviations are the same as the previous model with the exception of $stage_{ma}$ which is the intestinal phase and $smase_y$ is the presence of alk-SMase. The baseline group is the pre-digestion peak intensities for 3:2 MSM/cholesterol MLVs without alk-SMase added.

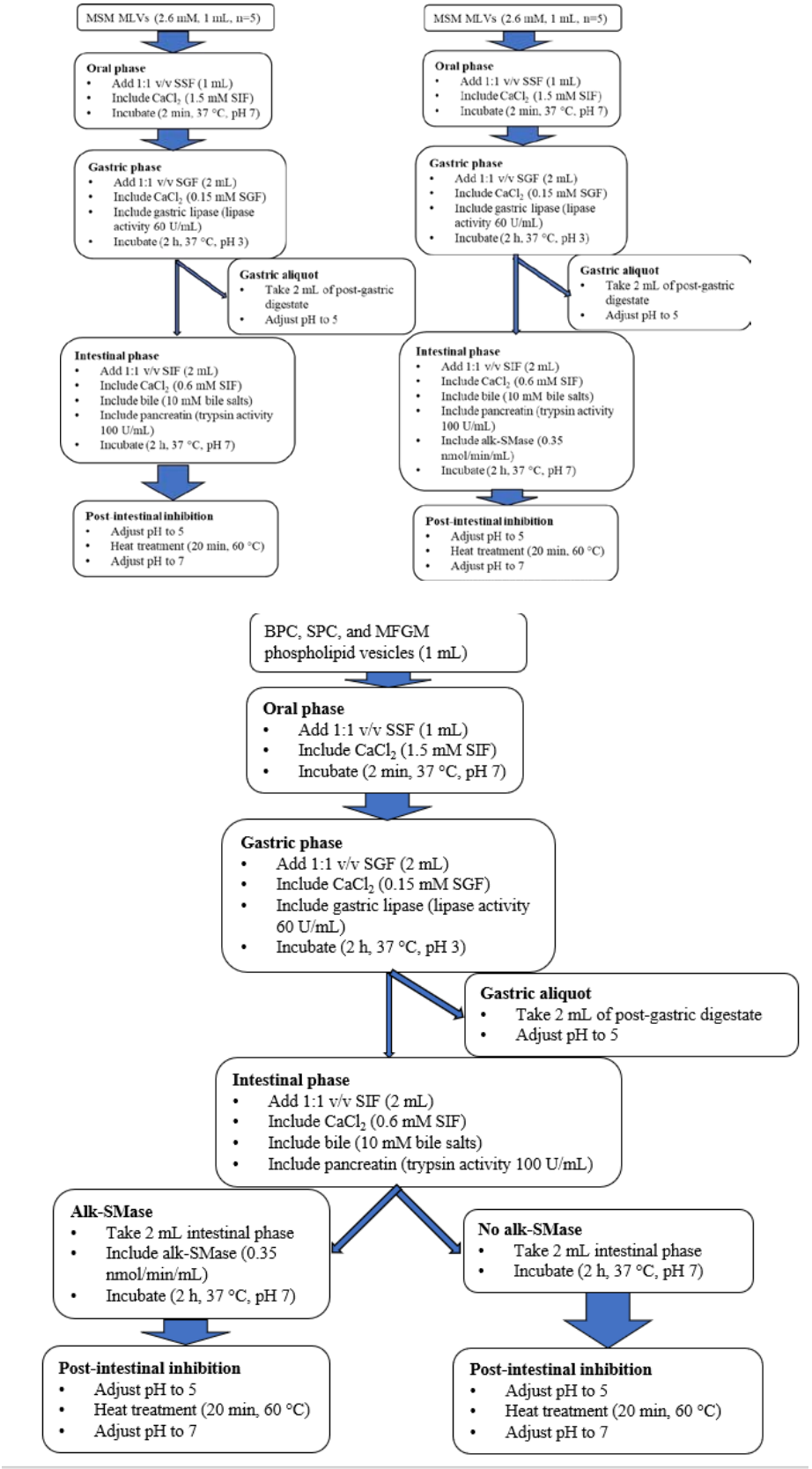

Figure 6.1. Experimental design for static *in vitro* digestion of phospholipid multilamellar vesicles. SSF = simulated salivary fluid; SGF = simulated gastric fluid; SIF = simulated intestinal fluid; alk-SMase = alkaline sphingomyelinase; MLVs = multilamellar vesicles. a) Experimental design of MSM MLVs. b) Experimental design for BPC, SPC, and MFGM phospholipid vesicles.

6.3.1 Results and discussion

6.3.1. Microstructure of phospholipid/cholesterol vesicles under in vitro digestion conditions

The microstructure of phospholipid vesicles visible by TEM and the non-effect of cholesterol on the morphology have been detailed in Chapter 4 and 5. The morphology of rehydrated rabbit gastric extract (RGE) was similar to the ox gallbladder extract used in Chapter 4 (Fig. 6.2 a, 4.1. c). Both extracts aggregate to form networks of threads (Fig 6.2 a), but unlike the bovine bile which contains PC, vesicular structures are absent from the gastric extract. When the gastric extract came into contact with phospholipid vesicles, it adhered to the surface but seemed incapable of penetrating the outer bilayer (Fig. 6.2 b, c). Since the RGE used contained 8.1 % w/w and 7.5% w/w of rabbit gastric lipase and pepsin, respectively (Sams et al., 2018), one cannot be certain it was the gastric lipase alone that adhered onto the surface of the vesicle. However, at the concentration of gastric lipase used vesicle morphology was clearly maintained. It is well observed that gastric lipase does not hydrolyze phospholipids (Bénarouche et al., 2017); however, the gastric lipase is capable of penetrating the milk fat globule membrane. The release of fatty acids from the limited hydrolysis of the triacylglyceride core is essential for further hydrolysis by the pancreatic lipase and colipase complex (Bénarouche et al., 2017). From the micrographs, this adhesion may be capable of changing the bilayer, either by compression (Fig. 6.2 c) or aiding in creation of aggregates (Fig. 6.2 d).

The inclusion of intestinal digestion components such as bovine bile and pancreatin into the system added additional vesicular structures to the digestive milieu (Fig 6.3 a). From the shape and size of these irregular vesicles, they are comprised of the same PC vesicles that were present in the bovine bile (Fig. 4.1 c). The addition of pancreatin introduced sharp crystals greater than > 3 µm in length (Fig 6.3 b). Negative stain TEM was unable distinguish between the gastric extract and the pancreatin; however, in both the gastric and intestinal phases the extracts clearly adhere to the vesicle surface (Fig 6.3 c, d).

The presence of vesicles with open pores confirmed that detergent-induced trans-bilayer solubilization of phospholipid vesicles was occurring (Fig 6.3 e). As previously mentioned in Chapter 4, trans-bilayer solubilization is the ability of some detergents to flip from the distal leaflet into the proximal leaflet. The saturation of the proximal leaflet by bile salt results in the rapid solubilization of both layers (85% reduction of turbidity in 1 min in egg-PC large unilamellar vesicles) (Kragh-Hansen, le Marie, & Møller, 1998; Lichtenberg, Ahyayauch, & Goñi, 2013; Lete et al., 2019). These reactions are typical of “fast” detergents, such as taurocholic acid which makes up 41% of bovine bile (Lete et al., 2019). The remaining lamealle in the perforated vesicle then take up multiple flake-like structures (Almgren, 2000).

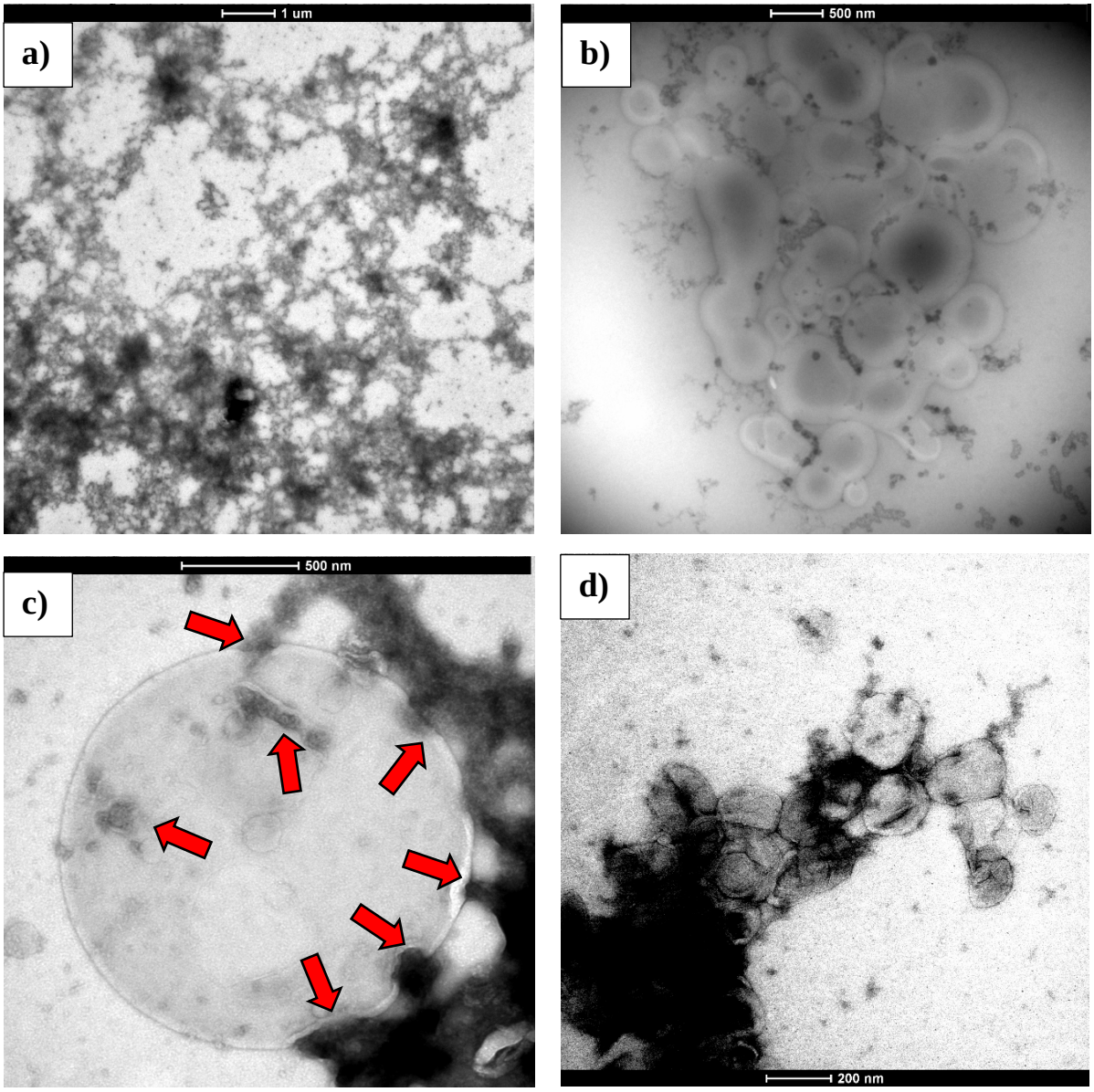

Figure 6.2. The addition of rabbit gastric extract to phospholipid/cholesterol vesicles. pH = 7.0 ± 0.1.

a) PIPES buffer and gastric lipase, 9,900 ×.
b) Milk sphingomyelin and cholesterol vesicles post-gastric digestion, 0.66 mM total lipid, 4:1 phospholipid/cholesterol, 20,500 ×, the black dots are rabbit gastric extract interspersed among the vesicles.
c) Milk sphingomyelin and cholesterol vesicles after gastric digestion, 0.66 mM total lipid, 7:3 phospholipid/cholesterol, 60,000 ×, the red arrows indicate where the rabbit gastric extract is compressing the bilayer.
d) Milk fat globule membrane phospholipid and cholesterol vesicles after gastric digestion, 1.33 mM total lipid, 3:2 SM/cholesterol, 60,000 ×.

The disruption of the vesicle lamellae led to the formation of tubular micellar intermediates (Fig. 6.4 a). These structures are morphologically similar to worm-like micelles elongated: flexible, and dynamic aggregates that are formed by the self-assembly of amphiphilic molecules with packing parameters of $1/3 < P < 1/2$ (Dreiss, 2017). The formation of worm-like micelles occurs in bile salt/phospholipid systems when the spontaneous curvature of the system i.e., the molecular

asymmetry between the packing areas of the polar and apolar portions of the molecular favour a cylindrical structure. The combination of bile salts, sodium deoxycholate, and 1,2-dimyristoyl-*sn*-glycero-3-phosphocholine (DMPC), can create worm-like micelles (Forooqi Motlaq et al., 2021). These have been reported to be present as a product of detergent-induced solubilization of other phospholipid and bile salt combinations (Moschetta et al., 2002). The tubular micelles shown in Figure 6.4. a have a larger diameter than worm-like micelles (Fig. 6.4.c) which are usually 4 – 6 nm thick (Dreiss, 2017). It is more likely that these filaments are analogous to the lace-like structures that appear from the solubilization of the "flakes" of perforated bilayers (Almgren, 2000). As bile salt is incorporated into these lace-like net, surface tension is decreased and surface curvature increases, and the nets are micellized into worm-like micelles.

In summary, the addition of gastric lipase adheres to and compresses the phospholipid vesicles. The addition of the intestinal enzyme and components resulted in visible detergent-induced solubilization. Both trans-bilayer solubilization and multilamellar vesicle → unilamellar vesicle → micellar intermediates transitions were visible. Tubular micelles similar to worm-like micelles were present. These structures were likely lace-like micellar intermediates that originated from the solubilization of perforated bilayer flakes. The observations of Patton and Carey (1979) that apply to fat digestion, the formation of a birefringent liquid crystalline product and extrusion of a "viscous isotropic" phase were not seen in this experiment. This is likely due to the minimal triacylglyceride present. However, the micrographs above do show that even without triacyglyceride, bile salts are capable of dispersing phospholipid to produce the mixed micellar phase (Patton and Carey, 1979). There were no visible differences between phospholipid vesicles that were incubated with alk-SMase and those without.

6.3.2. Bilayer order of phospholipid vesicles after being subjected to in vitro digestion

Similar to the results reported in Chapters 4 and 5, the hydrocarbon chain order of the phospholipids that make up the phospholipid vesicles (i.e. order of the bilayer or bilayer order) pre-digestion, post-gastric, and post-intestinal was determined with Raman spectroscopy. The methylene C-H stretching modes (2800 – 3000 cm^{-1}) and the C-C skeletal stretching modes (1000 – 1200 cm^{1}) were the regions of focus. The literature reference values for Raman activate vibrational modes can be found in Tables 4.1 and 5.3. The peak intensity ratios of interest were once again: I_{2850}/I_{2880} which furnishes an index of acyl chain disorder/order arising from lateral chain-chain interactions, I_{2930}/I_{2880} offers the same interchain information while also including the degree of conformational isomerism (*gauche*/*trans*), and I_{1085}/I_{1130} is the degree of conformational isomerism and intrachain order. As a general rule, an increase in either one of the three ratios expresses an increase in disorder. Once again, the spectra of the phospholipids were taken at room temperature (~20 °C) as a temperature-controlled stage was unavailable. Frequency shifts of the vibrational modes of interest occurred when the vesicles underwent gastric and intestinal digestion.

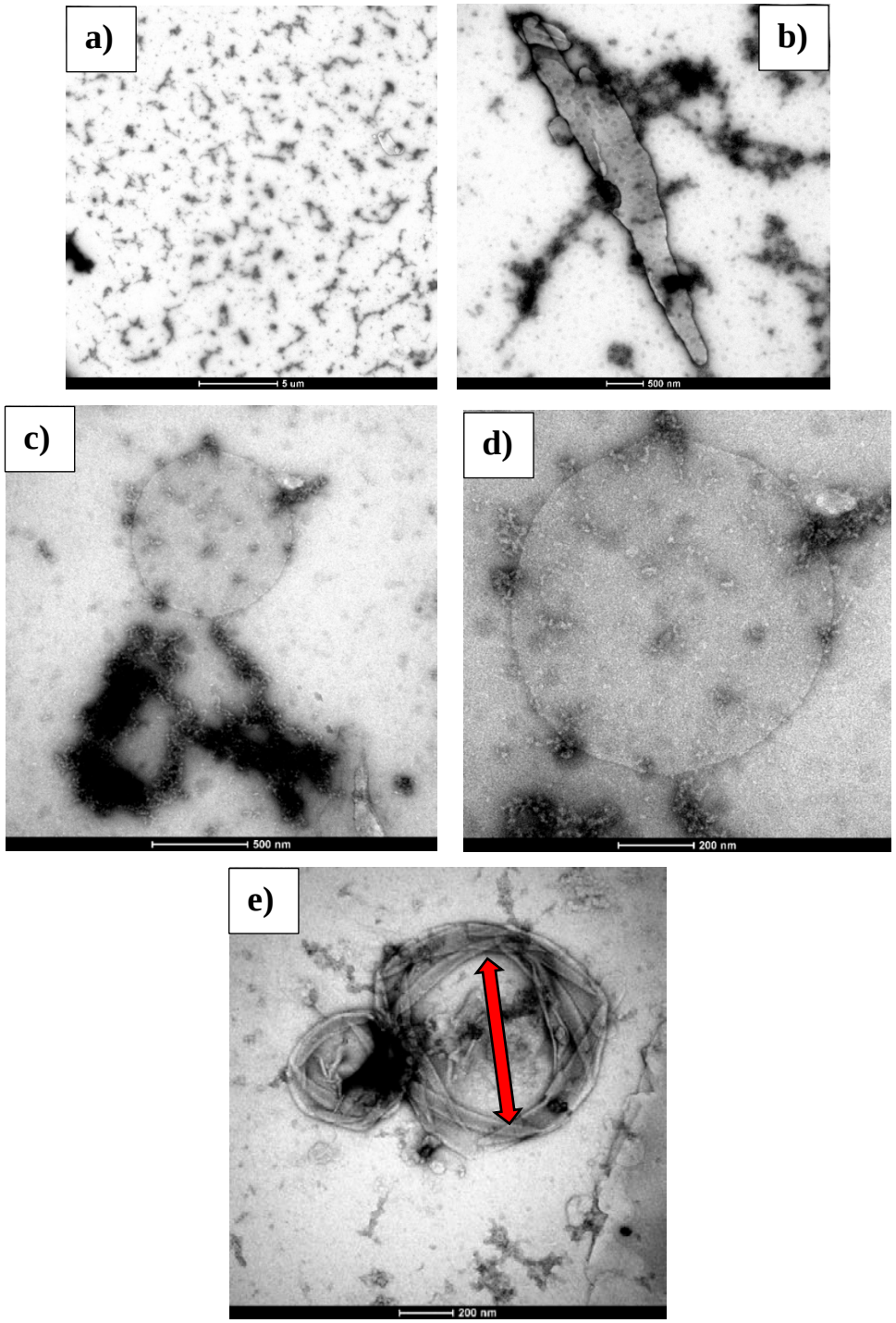

Figure 6.3. Phospholipid vesicles post-gastric and intestinal *in vitro* digestion. The biochemical digestive components present in all micrographs are gastric lipase, bovine bile, and pancreatin. pH = 5.0 ± 0.1.

a) PIPES buffer, 4,200 ×.
b) PIPES buffer, 20,500 ×.
c) Milk sphingomyelin/cholesterol 7:3 mol/mol multilamellar vesicle digested with alk-SMase, 43,000 ×.
d) Close up of 6.3 c, 87,000 ×.

e) Milk sphingomyelin multilamellar vesicle without cholesterol, digested without alk-SMase, 60,000 ×. The red arrow indicates the diameter of the empty space in the middle of the vesicle.

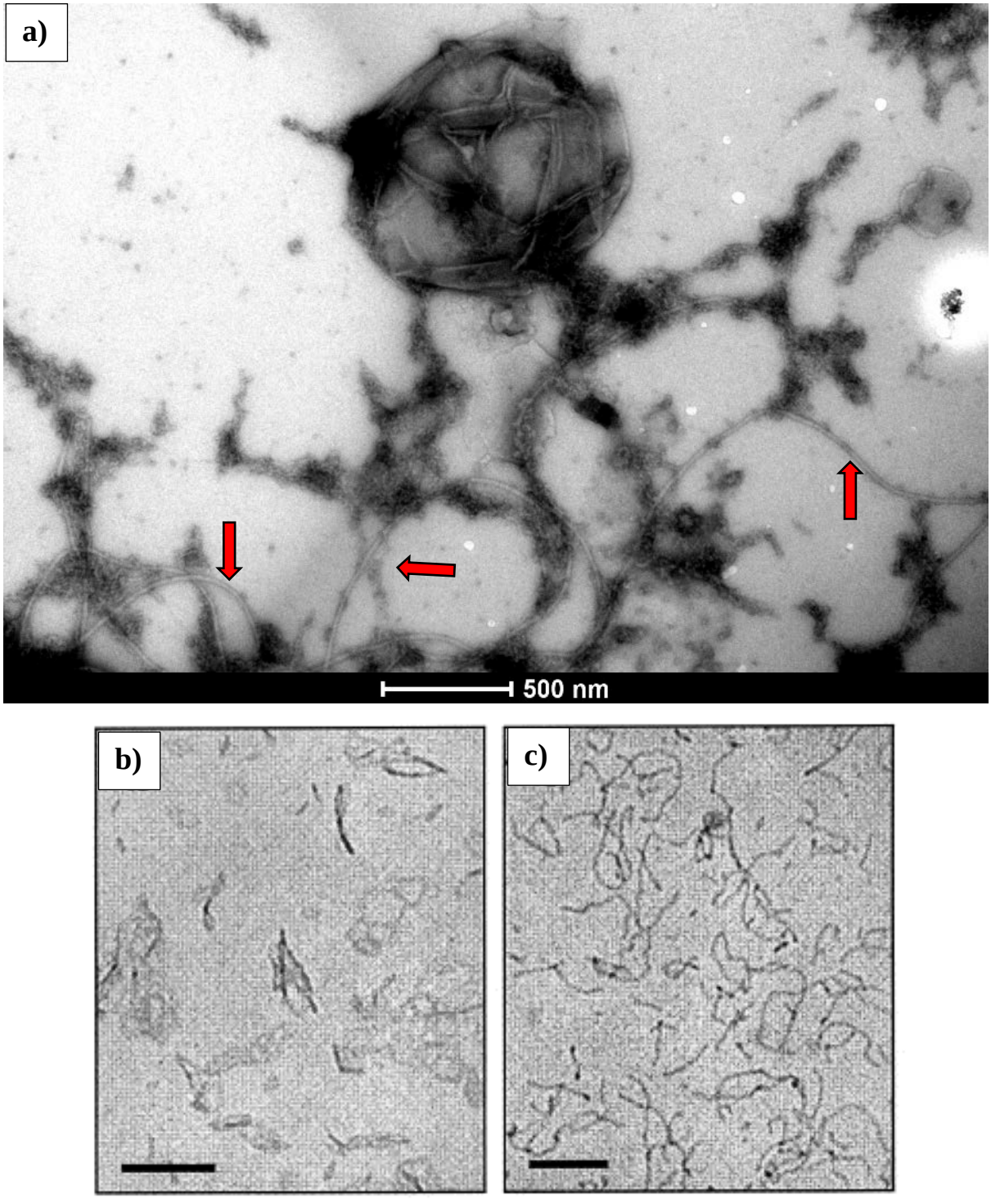

Figure 6.4 The morphology of micellar intermediates from perforated vesicles and open bilayers; b) and c) are reproduced from Almgren (2000).

a) Tubular micelles extending out from a milk sphingomyelin vesicle post-intestinal digestion, 26,500 ×. Arrows indicate the most obvious threads.
b) Cryo-TEM image of lace-like nets created from incubating 80% hexadecyltrimethylammonium chloride with egg phosphatidylcholine SUVs for 24 h. Scale bar is 100 nm.

c) Cryo-TEM image of worm-like micelles created from incubating 80% hexadecyltrimethylammonium chloride with egg phosphatidylcholine SUVs for 24 h. Scale bar is 100 nm.

The experimental and statistical design of the bilayer order experiments may seem confusing at first. The *in vitro* digestion of the MSM MLVs served as the preliminary experiment for the power analysis, so the following experimental design was informed by the analysis. The main difference in the digestion of the MSM MLVs was the inclusion of alk-SMase as an individual factor that could be crossed with cholesterol concentration and stage of digestion. Practically, the design gave rise to two independent experiments – one where the MSM MLVs were submitted to digestion without alk-SMase and one where alk-SMase was included during the intestinal phase.

In the BPC, SPC, and MFGM experiments, the alk-SMase and no alk-SMase treatments were paired as they came from same post-gastric sample (Fig 6.1 b). That is, after the gastric digestion the digesta was separated into two aliquots. One aliquot had alk-SMase added to it and the second did not during intestinal digestion. Although this design means that the presence of alk-SMase was not a separate factor and unable to be crossed with cholesterol concentration, the pairing allowed for the exclusion of the individual gastric replicates as a random effect allowing for a higher degree of power when testing for differences in the intestinal stage, with and without alk-SMase.

As the analysis was only performed within phospholipid type and no conclusions were drawn by attempting to compare across phospholipid types i.e. Gastric BPC to Intestinal MSM, the difference in experimental designs should have little impact on the overall trends derived from the results. Due to the interference from the biochemical digestive components in the 1000 – 1200 cm^{-1} region, the I_{1085}/I_{1130} ratio was unable to be taken from all phospholipid vesicles post intestinal digesta. Example spectra of the control, PIPES buffer, post gastric and post intestinal are included in Appendix 6.9 – 6.13.

6.3.2.1. Bilayer order of milk sphingomyelin and cholesterol multilamellar vesicles under in vitro digestive conditions

The I_{2850}/I_{2880}, I_{2930}/I_{2880}, and I_{1085}/I_{1130} peak intensity ratios for the MSM MLVs pre-digestion (Appendix 6.8) were similar to the corresponding peak intensity values reported in Chapter 4 (Appendix 4.10) for the MSM MLVs that were not yet incubated with bile, indicating the bilayer order of MSM MLVs is quite reproducible. From the statistical analysis employed, the cholesterol concentration and the stage of digestion had the largest impact on the hydrocarbon chain order. Increasing cholesterol concentration in MSM MLVs decreased lateral interchain hydrocarbon chain order (I_{2850}/I_{2880}) and increased intrachain hydrocarbon chain disorder (I_{1085}/I_{1130}) (Fig. 6.5 a, c). The former increase in lateral hydrocarbon chain disorder was expected of a $S_o \rightarrow L_o$ transition (Tai et al., 2021). The latter conformational change and increase in rotational mobility did not match the results from Chapter 4 where the addition of cholesterol had no statistically significant effect on the

intrachain bilayer order, even though the mean I_{1085}/I_{1130} values of both experiments (Appendix 4.10, Appendix 6.9) were comparable. As the current experiment consisted of twice the replicates used in the experiment performed in Chapter 4 (n = 10, MSM pre-digestion vs. n = 5, MSM without bile), it is likely that there is indeed statistically significant increase in the amount of *gauche* isomers when MSM100 (without cholesterol) is compared to MSM60 (4:1 mol/mol MSM/cholesterol). Conversely, molecular dynamic simulations have shown the addition of up to 50% mol cholesterol to stearoylsphingomyelin (SSM, C18:0) at temperatures > T_m significantly decreases the fatty acid angle tilt and the number of *gauche* isomers (Róg & Pasenkiewicz-Gierula, 2006) implying the $S_o \rightarrow L_o$ phase transition should provide intrachain (I_{1085}/I_{1130}) order, the opposite of what is shown in Figure 6.5 a. Small angle synchrotron X-ray diffraction performed on MSM MLVs < T_m show that incorporating cholesterol into the MLV decreases overall d-spacing (Lopez, Cheng, & Perez, 2018), that is, the bilayer length shrinks. If the number of *gauche* isomers and tilt decrease with increasing cholesterol content, the bilayer thickness should extend, increasing the d-spacing (the sum of bilayer thickness and interlamellar space). X-ray diffraction studies on phospholipid/cholesterol vesicle systems will be elaborated upon in Chapter 7. The difference in results between Róg & Pasenkiewicz-Gierula's (2006) study and the current one is possibly due to different composition of the bilayers. A stearoylsphingomyelin (SSM) bilayer consists of a single type of SM whereas a MSM bilayer consists of complex array of hydrocarbon chain lengths. The lower T_m SM molecules of the MSM bilayer act as "defects," disrupting the lateral packing of the S_o bilayer (Et-Thakafy et al., 2018) which exacerbates the disorder within the bilayer as cholesterol is added to the system. A bilayer system that consists of only one type of SM would lack these "defects."

The second factor that engendered the greatest structural change to the MSM MLVs was the stage of digestion. As pictured in Section 6.3.1 and extensively reviewed (Bénarouche et al., 2017), gastric lipase tends to adsorb onto phospholipid interfaces due to the enzyme's high tensioactivity and penetration capacity (Bénarouche et al., 2013) even though the enzyme has no inherent phospholipase activity. The adhesion of the gastric lipase in the form of rabbit gastric extract to the MSM MLVs had no statistically significant impact on the lateral bilayer order (I_{2850}/I_{2880}) (Fig. 6.5 a). This lack of a change in lateral hydrocarbon chain order was expected as the enzyme is known to only penetrate 5 nm into monolayers and therefore will interact with the head groups of the phospholipids (Bourlieu et al., 2016). This does not contradict the author's claims that overall lateral organization is rearranged as the I_{2850}/I_{2880} peak intensity ratio only informs the lateral hydrocarbon chain packing. In DOPC/DPPC/DOPS monolayers with coexisting S_o/L_d phases, canine gastric lipase is known to adhere onto the L_d phase and S_o/L_d phase boundaries (Bourlieu et al., 2016). Unlike AFM, Raman spectroscopy is unable to detect the locations to which the rabbit gastric lipase adheres. The non-significant impact of the enzyme on the overall bilayer order of MSM80, MSM70, and MSM60

implied that although the gastric lipase is possibly adhering to the vesicles (Fig 6.2 d), hydrocarbon chain order is not affected.

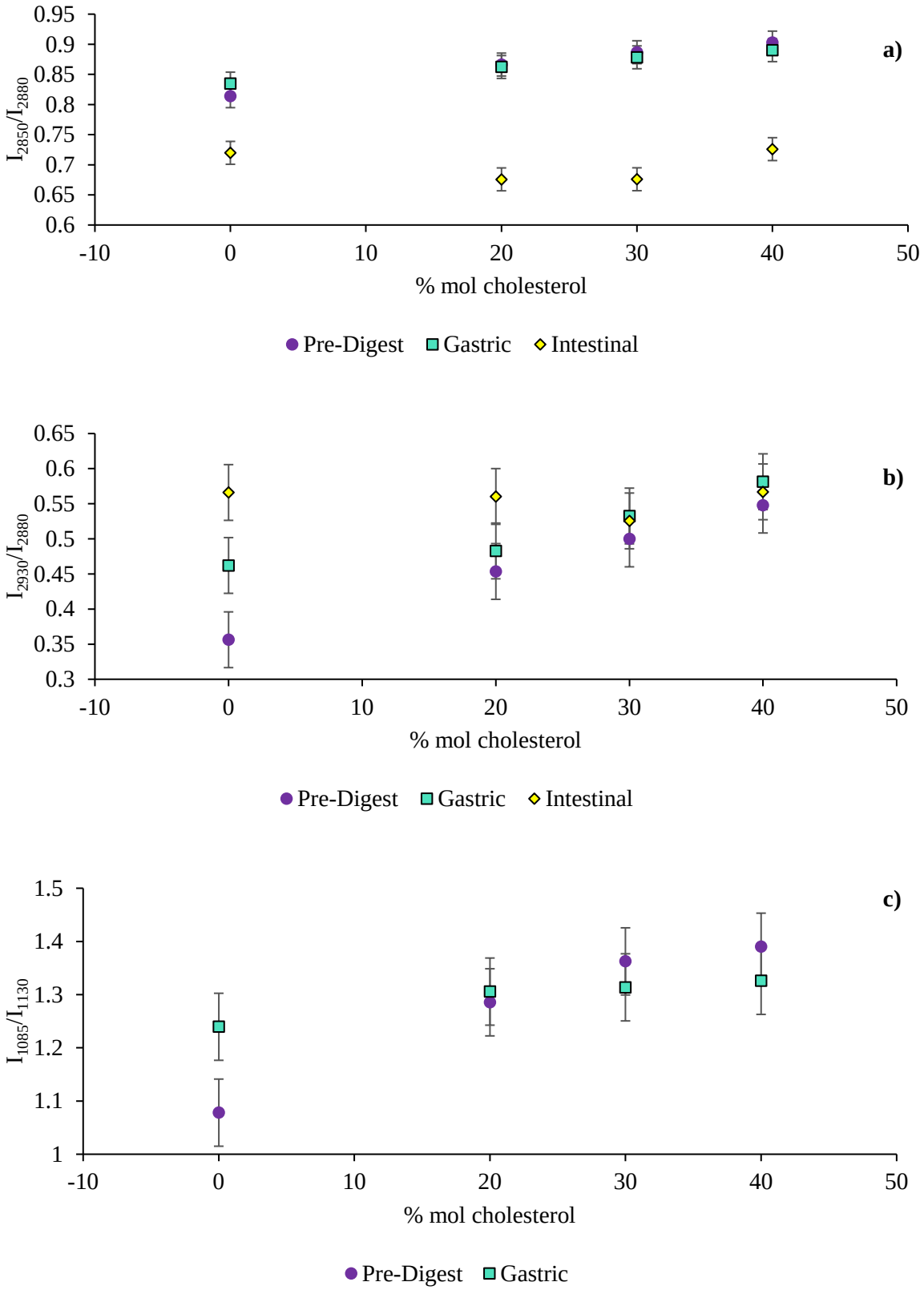

Figure. 6.5. Marginal means of the overall peak intensity ratios of milk sphingomyelin multilamellar vesicles (i.e., no alk-SMase and with alk-SMase results have been pooled together). The error bars the standard deviation.

a) interchain bilayer order; (I_{2850}/I_{2880}).
b) interchain and intrachain bilayer order; (I_{2930}/I_{2880}).
c) intrachain bilayer order; (I_{1085}/I_{1130}).

Rabbit gastric extract adsorption onto the interface alters the intrachain order of MSM MLVs that do not contain cholesterol. Pre-digestion MSM MLVs without cholesterol (MSM100) showed a greater degree of intrachain order (I_{1085}/I_{1130}) compared to GMSM100 (post gastric MSM without cholesterol). One peculiarity of the experiment was that the gastric lipase is added to the MSM100 MLVs at 37 °C and incubated for 2 h but the samples were analyzed at 20 °C. As DSC has shown, the T_m of pure MSM is ~34 °C (Lopez, Cheng, & Perez, 2018), thus, when the gastric lipase was added, the system was mostly in the L_d phase (> T_m) whereas the analysis took place when the MLV was predominately in the S_o phase (< T_m). The degree of intrachain order induced by the gastric lipase may have changed during the L_d (gastric digestion) → S_o (Raman analysis) transition. A second possibly confounding factor is that the gastric portion of the *in vitro* digestion was performed at pH 3 whereas Raman analysis was performed after enzyme inhibition at pH 7.0 ± 0.1. For example, the interfacial binding of dog gastric lipase to an Intralipid emulsion (soybean oil stabilized with egg lecithin) is ~ 70% at pH 3 but decreases to 40% at pH 7 (Chahinian et al., 2006). The interfacial binding of RGL may too be dependent on pH, thus the degree of conformational order may be over or underestimated. Nevertheless, there is a clear increase in the intrachain disorder (Fig. 6.5 c), implying that once the gastric lipase has penetrated the L_d bilayer, even a phase transition towards a tightly ordered S_o phase will not nullify the effect of the enzyme nor expel the enzyme. The resulting increase in intrachain disorder is analogous to the adsorption of pancreatic lipase onto the MFGM (Alshehab et al., 2019). The resulting compression upon the membrane results in increased surface pressure upon the distal leaflet, leading to a lateral expansion of the proximal leaflet. This expansion frees the apolar tails of amphiphilic interface, allowing for greater rotational freedom.

The intestinal phase paints two seemingly disparate pictures of MSM/cholesterol MLV digestion. With the addition of bile salt and pancreatic lipase, the lateral hydrocarbon chain order (I_{2850}/I_{2880}) of MSM MLVs plummets, regardless of the cholesterol concentration (Fig 6.5 a). This decrease in chain-chain order is due to the solubilization and formation of micellar structures, a key part of intestinal digestion. However, the MSM MLVs containing cholesterol are known to contain L_o domains which are resistant to bile salts (Moschetta et al., 2002; Tai et al., 2021). Even the L_o domain-rich MSM60 was converted into micelles in the presence of pancreatin after the MLVs had been pretreated with gastric lipase. Conversely, the total bilayer order (I_{2930}/I_{2880}) of IMSM60 and 70 (3:2 MSM/cholesterol and MSM 7:3 MSM/cholesterol, post-intestinal digestion) were not significantly different to the corresponding gastric and pre-digestion versions whereas the total bilayer order of IMSM100 and IMSM80 (MSM without cholesterol and 4:1 MSM/cholesterol, post-intestinal digestion) significantly increased (Fig. 6.5 b). The addition of cholesterol and the formation of L_o domains was unable to resist micellization during the intestinal phase but did retain overall hydrocarbon chain order whereas the MSM MLVs without cholesterol (MSM100) did not. This is

slight evidence that the micellar intermediates of MSM60 MLVs retained some degree of hydrocarbon chain order.

The increase of overall bilayer disorder (I_{2930}/I_{2880}) to IMSM100 and IMSM80 compared to the pre-digestion and gastric counterparts is not due to the presence of bovine bile (Fig. 6.5). In Chapter 4, the addition of bovine bile to MSM100 and 80 had no significant effect on the total (I_{2930}/I_{2880}) and intrachain (I_{1085}/I_{1130}) bilayer order (Fig. 4.7. a, 4.9. a). The increased disorder is most likely due to the adhesion of the pancreatin onto micellar intermediates such as open vesicles. Although it would be fascinating to further delve into the kinetics of the interactions between pancreatin enzymes, bile salts, and the MLVs, the design of the experiment only allowed for the analysis of the intestinal digestion endpoint. Unexpectantly, the presence of SMase in the intestinal phase of *in vitro* digestion had no significant effect on bilayer order (Fig. 6.6). That may be partially due to the high degree of variance of MSM MLV subjected to intestinal digestion. The post-intestinal digestate for the MSM MLVs that contained alk-SMase also consisted of the MLVs, rabbit gastric, bovine bile, pancreatin.

The addition of cholesterol induced structural changes to the MSM MLVs were consistent with previous experiments (Fig. 4.8 a – 4.10 a). Gastric lipase adheres to MSM MLVs, increasing hydrocarbon rotational freedom when the system does not contain cholesterol. An unknown synergistic effect between bile salts and either pancreatic phospholipase or lipase results in the solubilization of the detergent resistant MSM60 (3:2 mol/mol MSM/cholesterol) to produce micelles. The overall bilayer order (I_{2930}/I_{2880}) of MSM60 was retained. Further work investigating the interaction and reaction kinetics of each digestive component is warranted. The data obtained provide some evidence that when MSM and cholesterol MLVs are micellized a degree of order is retained.

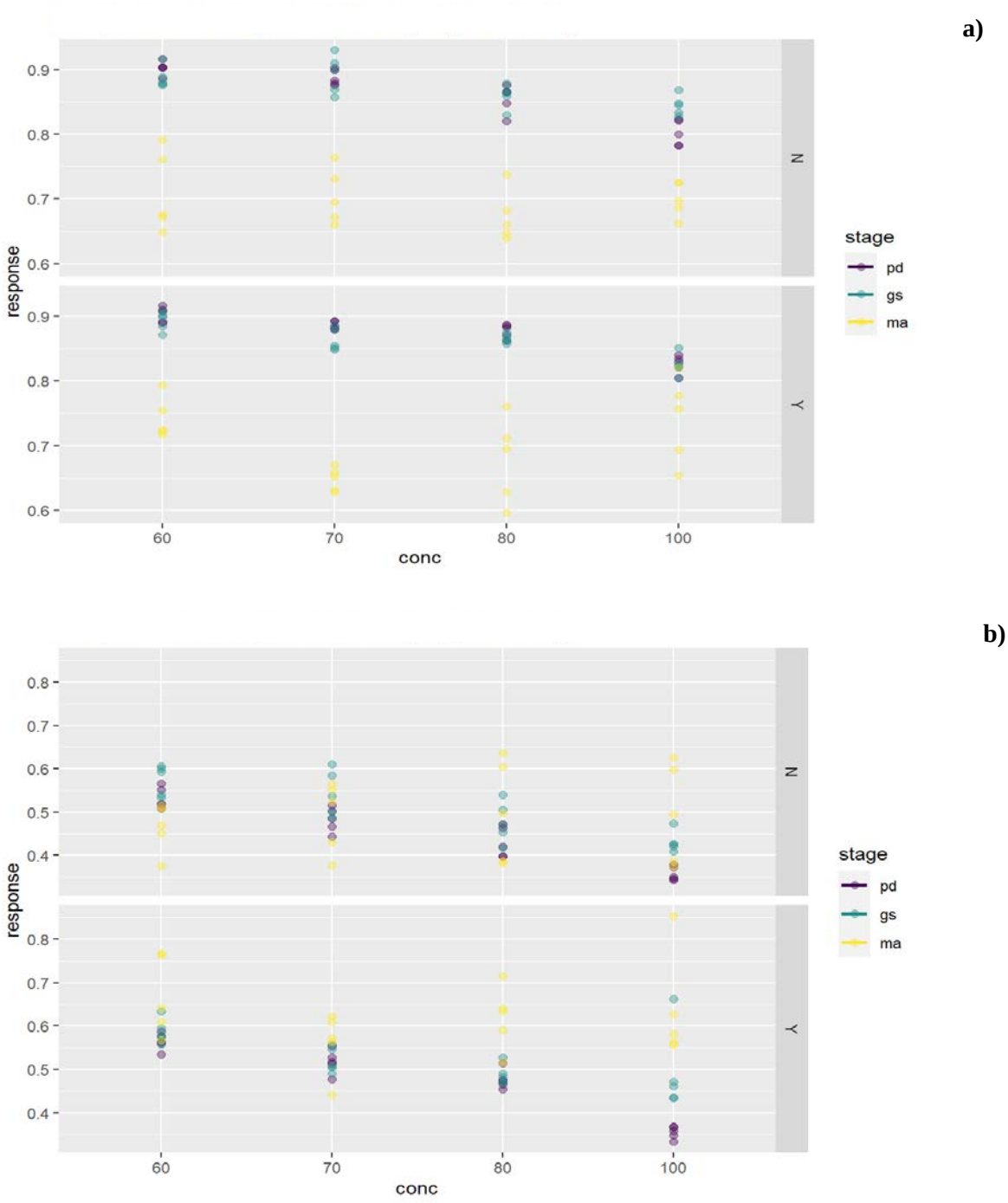

Figure 6.6. Milk sphingomyelin and cholesterol multilamellar vesicles have been divided into two independent experiments. Pre-digestion, gastric, and intestinal digestion with alk-SMase and without. pd = pre-digestion, gs = gastric phase, ma = intestinal phase, n = no alk-SMase, y= alk-SMase. Each point represents one replicate.

a) Interchain bilayer order, (I_{2850}/I_{2880}).
b) Overall bilayer order, (I_{2930}/I_{2880}).

6.3.2.2. Bilayer order of phosphatidylcholine and cholesterol vesicles under in vitro digestive conditions

The digestive behaviour of SPC and BPC vesicles are quite straightforward, highlighting the complexity of MSM interactions with the digestive milieu by comparison. Consistent with the results from Chapter 4, the addition of cholesterol had no significant effect on the lateral hydrocarbon chain packing (I_{2850}/I_{2880}) (Fig. 6.7 a, Fig. 6.8 a), nor did it shift the overall bilayer order (I_{2930}/I_{2880}) (Fig. 6.7 b, Fig 6.8. b). Both BPC and SPC vesicles saw a decrease to the intrachain bilayer disorder (I_{1085}/I_{1130}) (Fig. 6.7. c, Fig. 6.8 c), confirming that the previously determined intercalation between BPC and cholesterol was present. Previous results determined there to be no significant difference in SPC intrachain bilayer order (I_{1085}/I_{1130}) when cholesterol was added (Fig. 4.10 c); in the current experiment that was not the case. The most likely explanation for the difference in results is the higher concentration of SPC used in the pre-digestion samples for the current experiment compared to the previous one (2.6 mM vs. 326 uM), allowing for the recovery of higher quality spectra. Soy PC is known to consist of 15% DPPC (16:0) and 3% DSPC (18:0) which interact with cholesterol to form L_o domains (Zhao et al., 2007; Wang et al., 2016). As to the particular intrachain order that is occurring in the SPC hydrocarbon chains, DMPC/cholesterol (dimyristoylphosphatidylcholine-cholesterol) molecular dynamic simulations show reductions in the average amount of *gauche* isomers when the phospholipid is in proximity to the cholesterol molecules (Róg & Pasenkiewicz-Gierula, 2001). However, the authors conclude that the decrease in *gauche* isomers only moderately accounts for the bilayer ordering, proposing it is the un-tilting of the hydrocarbon chains and headgroups that result in a more ordered bilayer. Although the Raman data were capable of confirming an increase in intrachain order (I_{1085}/I_{1130}) when cholesterol was added to SPC vesicles, the data are of little use when deciding whether that increase is due either a higher amount of *trans* isomers, the un-tilting of the phospholipids, or a combination of both. The I_{1085}/I_{1130} is a ratio derived from hydrocarbon length and the ratio alone cannot be used discriminate between contributions by conformational order and those by phospholipid orientation (Okotrub et al., 2020).

In both BPC and SPC vesicles, the concentration effect of adding cholesterol, shown by an increase in intrachain ($I_{1085}I_{1130}$) bilayer order, persisted in the presence of gastric lipase (Fig. 6.7 c, Fig. 6.8 c). Phospholipids are not a valid substrate for gastric lipase, yet the post-gastric state of MSM MLVs showed that physical interaction between the RGE and vesicles could change the vesicle surface structure (Fig. 6.5 c). The addition of RGE increased SPC vesicle intrachain (I_{1085}/I_{1130}) bilayer order (Fig 6.8 c) but had little effect on BPC vesicle (Fig. 6.7 c). Gastric lipase preferentially adheres to the L_d phase (Bourlieu et al., 2016). Considering a majority of the BPC vesicle should have been in the L_d phase at both 20 and 37 °C, it was expected that any gastric lipase adsorbed to the interface compressed the surface, expanding the proximal leaflet, leading to a greater degree of intrachain

disorder. It is possible that due to the already high degree of intrachain disorder (BPC100, 2.391 ± 0.039), the gastric lipase would not contribute much additional rotational freedom.

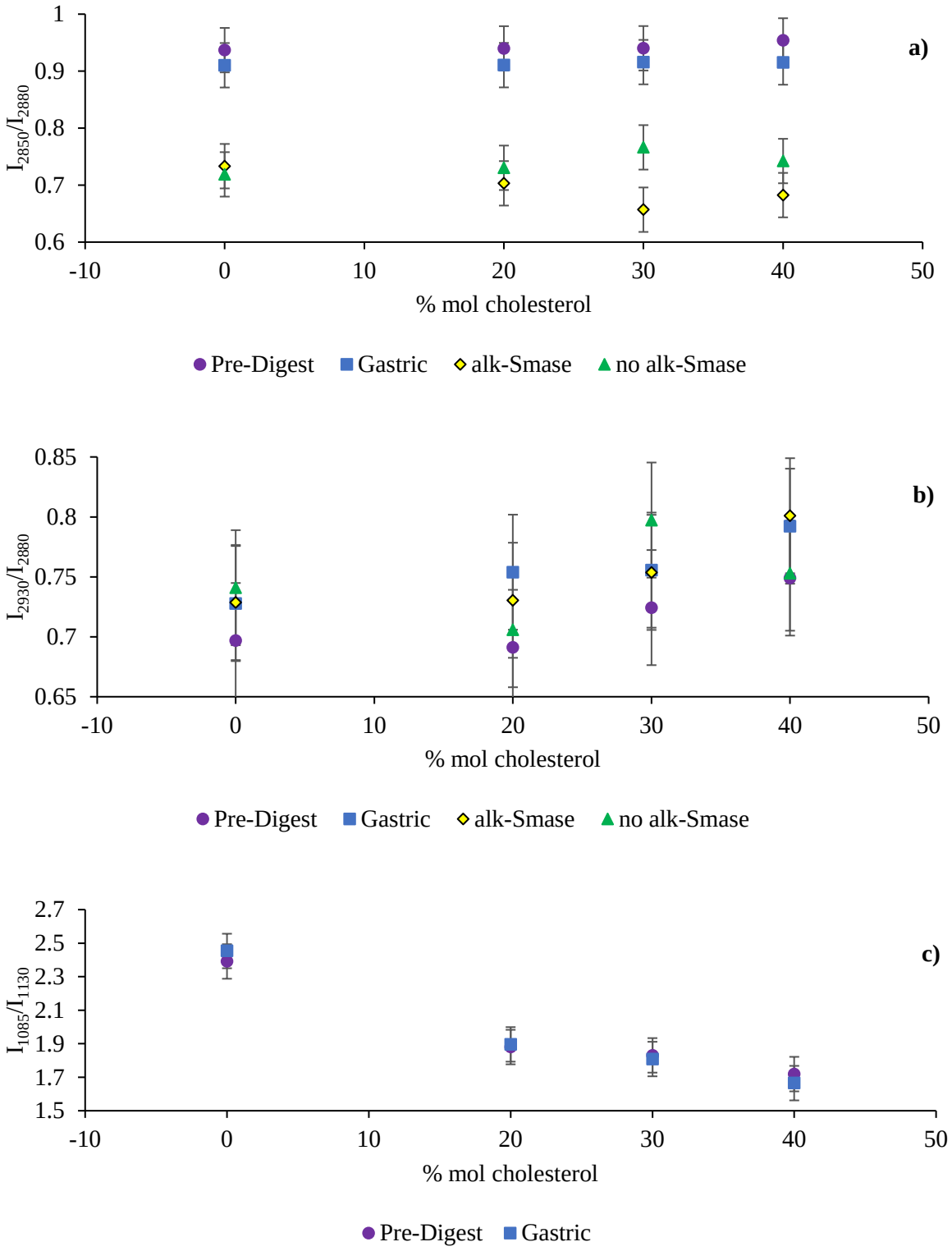

Figure 6.7. Marginal means of the overall peak intensity ratios of brain phosphatidylcholine vesicles.
a) Interchain bilayer order (I_{2850}/I_{2880}).
b) Interchain and intrachain bilayer order (I_{2930}/I_{2880}).
c) Intrachain bilayer order (I_{1085}/I_{1130}).

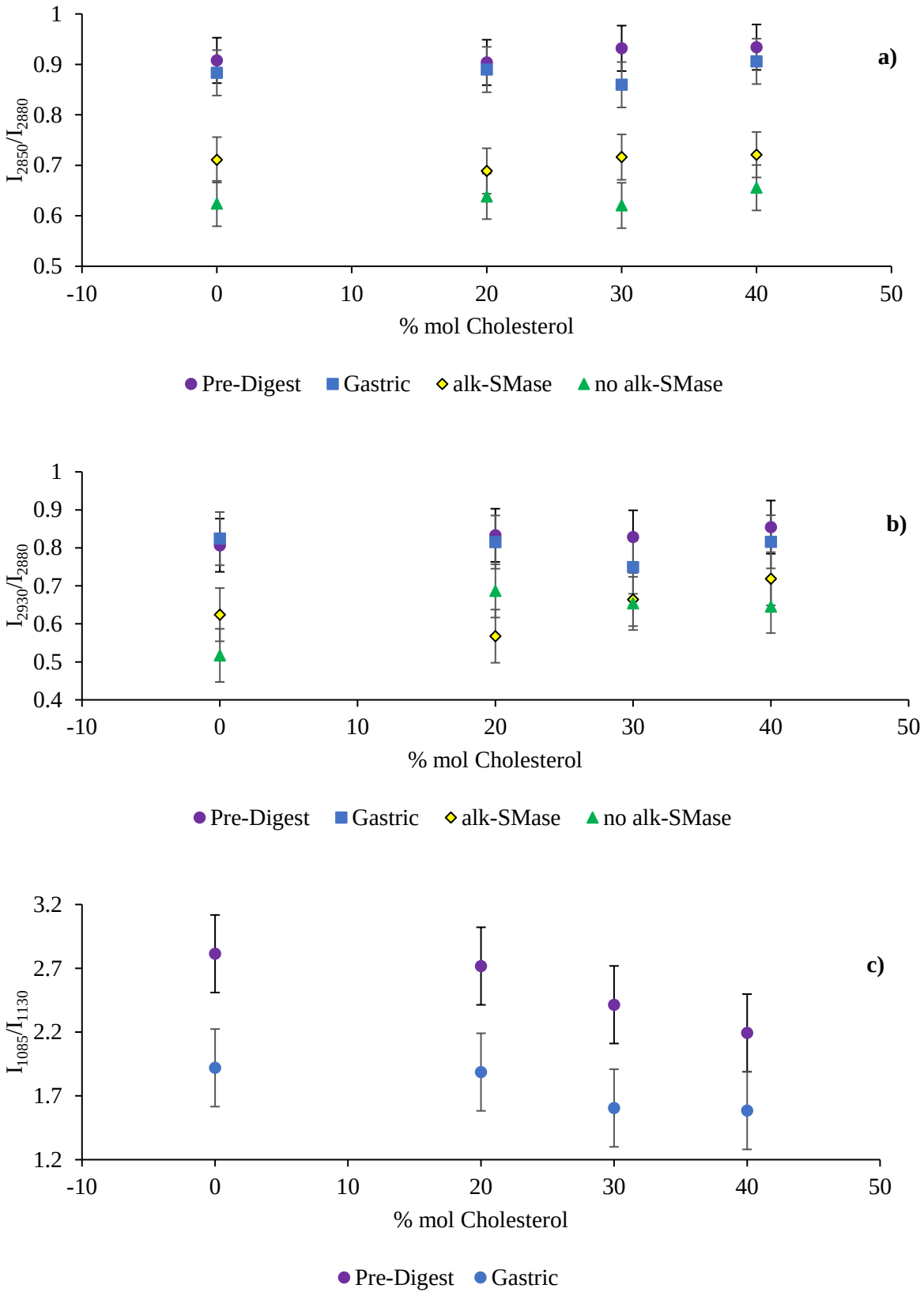

Figure 6.8. Marginal means of the overall peak intensity ratios of soy phosphatidylcholine vesicles.
a) Interchain bilayer order, (I_{2850}/I_{2880}).
b) Interchain and intrachain bilayer order, (I_{2930}/I_{2880}).
c) Intrachain bilayer order, (I_{1085}/I_{1130}).

The interpretation that a membrane with a high degree of fluidity is less affected by surface pressure does not align with the results for the SPC vesicles. When the RGE was added to the SPC vesicles, the intrachain (I_{1085}/I_{1130}) bilayer order increased regardless of cholesterol concentration (Fig. 6.8 c). The hydrocarbon chains that make up the SPC vesicles are more unsaturated than the BPC hydrocarbon chains and therefore the system is less interactive with cholesterol, i.e., fewer L_o domains. Hence, more of the SPC vesicle surfaces are in the L_d phase compared to BPC vesicles, which should indicate greater rotational freedom for the long and kinked hydrocarbon chains.

Based on the I_{1085}/I_{1130} ratios for the binary phospholipid/cholesterol, the intrachain structural modifications that occur when RGE adheres to the vesicle is influenced by the phase state. For the rigid MSM100 that is predominately in the S_o phase, the increased surface pressure results in a lateral expansion in the proximal leaflet, whereas the fluid SPC vesicles which are predominately in the L_d phase do not suffer the same lateral expansion and are instead compressed. When comparing dog gastric lipase adhesion and lateral restructuring of the monolayer of human milk and bovine milk polar lipid extract, Bourlieu et al., (2020) discovered that gastric lipase favoured the human milk monolayer and the high PUFA content in human milk resulted in lower molecular packing. The lateral expansion of visible S_o microdomains were only on average 4 nm compared to the 20 nm of S_o domains on the bovine milk monolayer. Although the complexity of a human and bovine milk system is much greater than for the phospholipid vesicle systems examined, both results indicate that the effect of gastric lipase is more strongly felt by systems with tighter molecular packing, possibly explaining why gastric lipase had little effect on the I_{1085}/I_{1130} of BPC. However, this reasoning does not explain why the intrachain order of SPC increases when gastric lipase is added. One possible rationale is that the phase state of BPC vesicles at 20 °C serves as an intermediate where the surface pressure from the gastric lipase is cancelled out by the bilayer expansion which occurs on the proximal leaflet.

The addition of simulated intestinal fluid with bovine bile and pancreatin to the SPC and BPC vesicles saw severe decreases in interchain hydrocarbon order (I_{2850}/I_{2880}) (Fig. 6.7 a, Fig. 6.8 a). As with the MSM MLVs, these decreases are likely from vesicle solubilization and conversion to mixed micelles. The addition of cholesterol had no effect on the interchain packing of the two vesicle systems in question. The overall bilayer order (I_{2930}/I_{2880}) of the SPC vesicles post-intestinal stage was significantly lower than it was in the pre-digestion and post-gastric stage (Fig. 6.8 b). The same could not be said about the post-intestinal BPC vesicles (IaBPC100 – 60 and InBPC100 – 60), for which the overall bilayer order (I_{2930}/I_{2880}) was not significantly different to that of the pre-digestion (BPC100 – 60) and post-gastric (GBPC100 – 60) counterparts (Fig. 6.7 b). Considering that in Chapter 4 the addition of bovine bile alone greatly decreased the overall bilayer order of the BPC vesicles, the pancreatin must be at least partially responsible.

Alkaline sphingomyelinase had no effect on the bilayer order of BPC vesicles, as expected; however, there was significantly higher lateral hydrocarbon chain (I_{2850}/I_{2880}) order for SPC vesicles that were incubated with the SMase compared to those without (Fig. 6.8 a). The slight difference indicated by the test for difference in response (Fig. 6.9) is most likely due to physical interactions between the enzyme and the SPC vesicles rather than enzymatic activity, as although the alk-SMase active site is capable of binding to phosphatidylcholine (Gorelick et al., 2017), it does not hydrolyze PC.

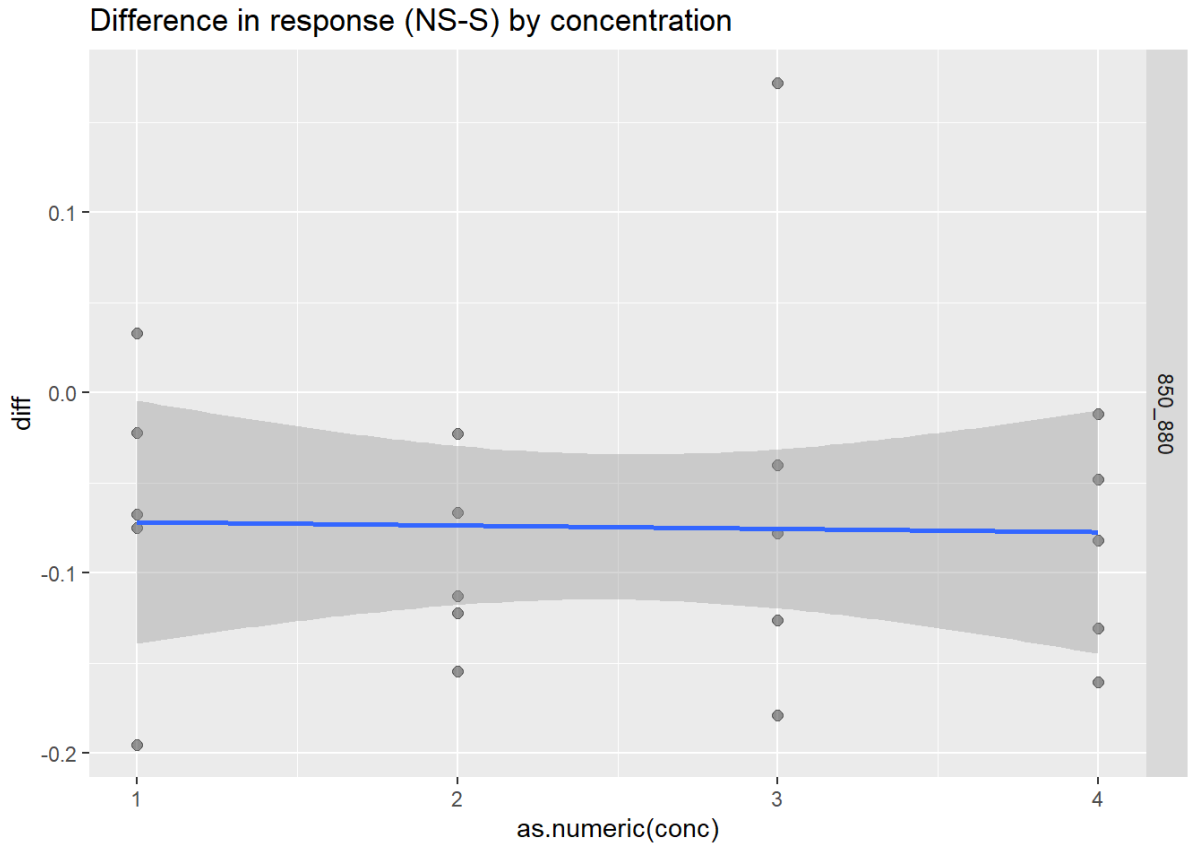

Figure 6.9. Difference in I_{2850}/I_{2880} (No SMase - SMase) for intestinal SPC vesicles. 850_880 = label for I_{2850}/I_{2880}. X axis: 1 = 3:2 mol/mol SPC/cholesterol; 2 = 7:3 mol/mol SPC/cholesterol; 3 = 4:1 mol/mol SPC/cholesterol; 4 = SPC vesicles without cholesterol. Each point represents the difference between one set of paired replicates.

In summary, the addition of cholesterol introduces a condensation effect which increases BPC and SPC intrachain order (I_{1085}/I_{1130}). This condensation results in rotational isomerization or the reversing of chain tilt. Cholesterol in SPC and BPC vesicles has no effect on the lateral bilayer order. The addition of gastric lipase has no effect on the bilayer order of BPC vesicles and the cholesterol effect on the intrachain bilayer order is still present. For SPC vesicles, the cholesterol effect on the intrachain bilayer order persisted in the presence of gastric lipase. Unlike BPC vesicles, SPC vesicles showed a systematic increase in intrachain (I_{2930}/I_{2880}) bilayer order, suggesting the pressure induced by the compression of the distal leaflet was greater than any expansion of the proximal leaflet. The introduction of bile and pancreatin leads to vesicle → micellar transitions as indicated by the decrease

in lateral hydrocarbon chain packing (I_{2850}/I_{2880}), and for SPC vesicles, the overall bilayer order (I_{2930}/I_{2880}). The overall bilayer order of BPC pre-digestion, post-gastric, and post-intestinal were not significantly different, implying either a degree of resistance against digestion, high statistical random error, or some other reason that requires further investigation.

6.3.2.3. Bilayer order of milk fat globule membrane phospholipid extract and cholesterol vesicles under in vitro *digestive conditions*

The digestion of the MSM, BPC, and SPC model membrane systems serve as points of comparison for the MFGM phospholipid vesicles. It is difficult to parse out the exact contributions of each phospholipid type in the MFGM vesicles, so having three points of references (highly saturated, moderately saturated, highly unsaturated) was determined to be key to understand the digestion of MFGM phospholipid vesicles.

In Chapter 5, the addition of cholesterol (3:2 mol/mol SM:cholesterol) was reported to significantly decrease MFGM phospholipid vesicles interchain bilayer order (I_{2850}/I_{2880}) while increasing intrachain bilayer order (I_{1085}/I_{1130}) resulting in no net change to the overall bilayer order (I_{2930}/I_{2880}). This was not the case in another set of MFGM phospholipid vesicles which saw no change in either interchain or intrachain bilayer order (Fig. 6.10). The difference between the sets of results is likely due to the differing phospholipid compositions of the beta-serum extract used. The new MFGM phospholipid vesicles have a higher content of PE (47.7 ± 0.7 % mol vs. 33.7 ± 0.3 % mol), lower PS (7.1 ± 0.2 % mol vs. 18.5 % mol) and SM (16.2 ± 0.3 % mol vs. 18.6 ± 0.5 % mol). Since SM is the premier phospholipid that forms L_o domains with cholesterol, the loss of even a small amount can render any change in intrachain bilayer order statistically non-significant. To illustrate this point, the absolute difference between means of the MFGM100 and MFGM60 intrachain bilayer order (I_{1085}/I_{1130}) reported in Chapter 5 (Fig. 5.8 a) was only 0.06 ($p < 0.05$) – the difference in the current experiment is 0.03.

In the previous chapter, the intrachain peak intensity ratio of MFGM100 was significantly higher than that of MFGM60 (Fig. 5.8 c). One thing to note is that the I_{1085}/I_{1130} values in Figure 6.10 c are lower than those in Figure 5.8 c. This increased intrachain order may be due to the higher proportion of PE making up the MFGM extract (47.7 % mol vs. 33.7 % mol). It bears mentioning the NH_3^+ of the PE headgroup can form hydrogen bonds with the PO_2^- of other PE (Pink et al., 1998), thus PE bilayers have stronger interlipid interactions than PC bilayers (Murzyn et al., 2005). Furthermore, as previously mentioned, PE is localized towards the proximal leaflet due to its low packing parameter >1 (Israelachvili, 2010). Due to the hydrogen bonding capacity of PE and its preferential localization in the inner leaflet of bilayer systems, bilayers which have an asymmetrical phospholipid distribution that contains PE have been shown to be more ordered than bilayers with a symmetrical phospholipid

distribution (Son & London, 2013). How the PE hydrogen bonds affect the intrachain order is unknown.

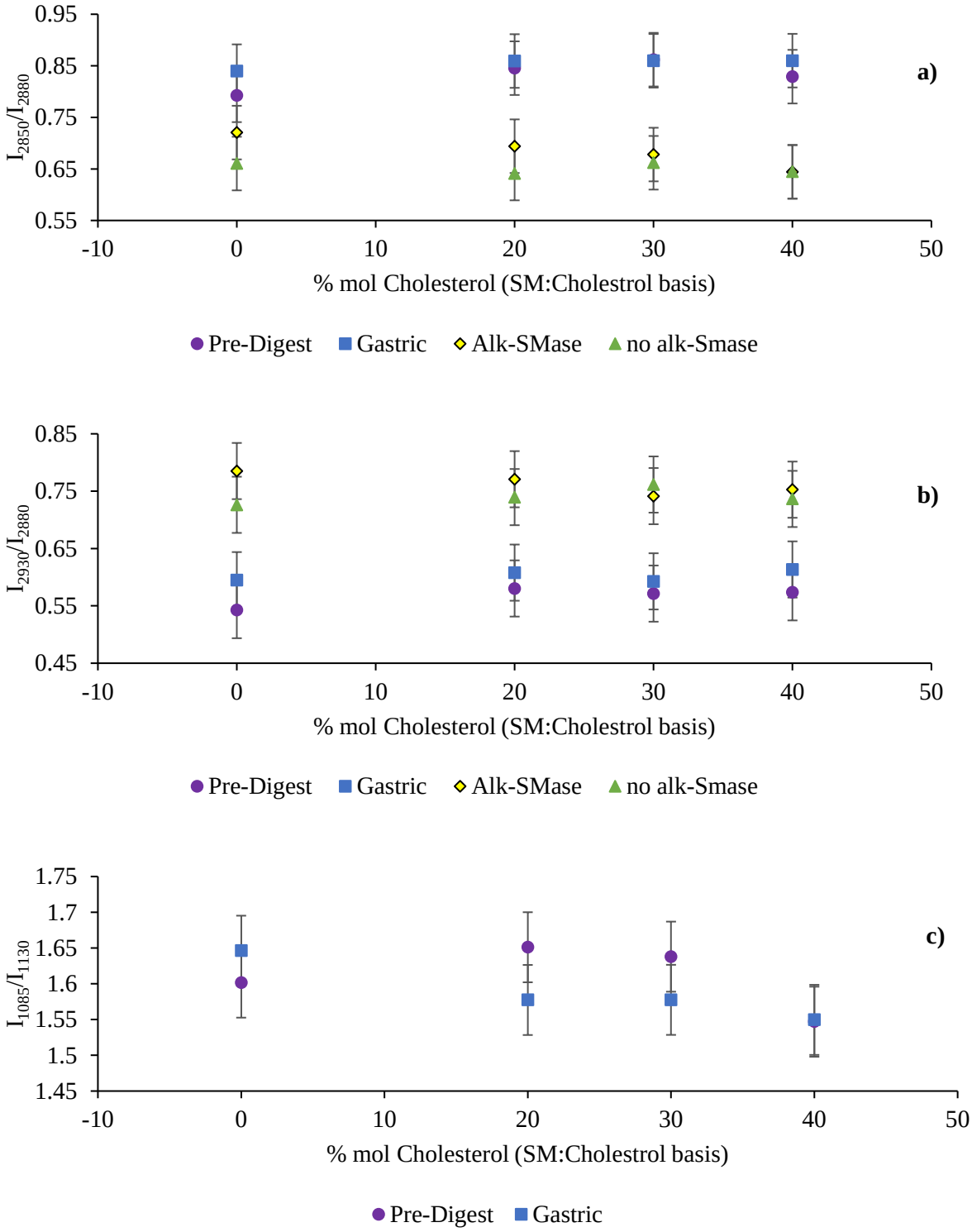

Figure 6.10. Marginal means of the overall peak intensity ratios of milk fat globule membrane phospholipid vesicles.

a) Interchain bilayer order, (I_{2850}/I_{2880}).
b) Interchain and intrachain bilayer order, (I_{2930}/I_{2880}).
c) Intrachain bilayer order, (I_{1085}/I_{1130}).

The addition of gastric lipase had no observable effect on the bilayer order of the MFGM phospholipid vesicles. Rather than the RGE being unable to affect the hydrocarbon order of the membrane, it is more likely Raman spectroscopy was unable to parse any changes that were occurring as gastric lipase is known to greatly affect the lateral portioning of the S_o and L_d phases of milk fat globules (Bourlieu et al., 2016).

With the addition of the intestinal digestive components, the lateral hydrocarbon packing order (I_{2850}/I_{2880}) of the MFGM phospholipid vesicles increased, indicative of disruption of the vesicle and subsequent micellization. The I_{2850}/I_{2880} ratios of the no alk-SMase treatment (Fig. 6.10 a) were very consistent with the values obtained in Chapter 5 for MFGM after bile addition (Fig. 5.8 a), implying that pancreatin had little effect on the lateral hydrocarbon order of the resulting micelles. The overall bilayer order (I_{2930}/I_{2880}) of the MFGM vesicles post-intestinal digestion (Fig. 6.10 b) breaks a trend. As reported in Chapter 4, the addition of bovine bile without pancreatin to phospholipid/cholesterol systems increased the overall bilayer order, in-line with an increase in lateral hydrocarbon chain (I_{2850}/I_{2880}) order which represents the solubilization and micellization of the phospholipids was observed. With the addition of both bovine bile and pancreatin, the lateral hydrocarbon chain order (I_{2850}/I_{2880}) of all the phospholipid vesicles increased once again, indicative of micellization, but the overall bilayer order of each phospholipid type did not consistently increase. The SPC vesicles post-intestinal overall bilayer order (I_{2930}/I_{2880}) was the only ratio that was greater than its pre-digestion and post-gastric counterparts (Fig. 6.8 b). The BPC vesicles post-intestinal overall bilayer order was not significantly different to its counterparts (Fig. 6.7 b). The MSM MLV post-intestinal overall bilayer order was either not different from its counterparts (40 – 20% mol cholesterol) or significantly more disordered (Fig. 6.5 b). Regardless of the cholesterol incorporated into the MFGM phospholipid vesicles, the addition the simulated intestinal fluid along with intestinal enzymes increased the overall bilayer disorder. That is the opposite effect to what befell the SPC vesicles. Considering that in Chapter 4 and 5, the addition of bovine bile alone increased the overall bilayer order (I_{2930}/I_{2880}) for all types of phospholipids, the bilayer order modulating or disordering effect must be due to either the phospholipase activity in pancreatin or the physical interaction between the pancreatin and the surface of the vesicles.

Unfortunately, the Raman data is unable to distinguish these two hypotheses, and to add to the complexity, pancreatin consists of several types of enzymes which may alter the surface structure of the MFGM vesicles. Pancreatic lipase is known to adhere to the surface of milk fat globules, expanding the proximal leaflet (Alshehab et al., 2019) whereas PC is hydrolyzed from PL-rich bile salt/PL micelles (disk-like bilayers; Maldonado-Valderrama et al., 2011) via secretory pancreatic phospholipase A2 IB (sPLA2 IB) and mucosal phospholipase B (PLB) (Nilsson & Duan, 2019). The sPLA2 IB enzyme activity is known to be dependent on the interfacial properties and bile salt concentration whereas the latter has broad substrate specificity. Although it is difficult to pinpoint the

contributions of the intestinal phase and the exact mechanisms, the Raman data were able to provide a frame of reference for further research with instruments specialize in determining interfacial binding.

As an aside, there is weak statistical evidence that the inclusion of alk-SMase into the intestinal digestion of MFGM phospholipid vesicles without cholesterol results in higher lateral hydrocarbon chain disorder (Appendix 6.14). The one sample t-test for an overall difference between the no alk-SMase and alk-SMase returned a significant value i.e., a difference between the treatments existed. On the other hand, the model summary stated there were no significant differences between each of the treatments (SM/cholesterol ratios). Furthermore, a cholesterol effect was not reflected in the overall bilayer order (I_{2930}/I_{2880}) for the alk-SMase MFGM vesicles (Fig. 6.10 b). If this ethereal trend is nonexistent, it would imply that alk-SMase at the concentration of its inclusion had a negligible effect on the bilayer order of MFGM vesicles during *in vitro* digestion. The reason for this is most likely due to inhibition by phospholipids other than sphingomyelin. At pH 7.4, the total activity of 0.1 μg of intestinal alk-SMase is partially inhibited by 16 μM of PC (~50 % of the activity of the enzyme activity inhibited), PI (~90 %), PE (~25 %), PS (~90 %) (Liu et al., 2000). Although the enzyme's affinity for SM is higher than that for PC, competition among the two for the enzyme's binding site (a pocket and groove that fits the choline head group) and apolar tails, respectively, still exists (Gorelik et al., 2017). The non-effect of alk-SMase is therefore a symptom of the phospholipid composition of the MFGM and the bovine bile. Phospholipid inhibition of alk-SMase is less of an issue in the native small intestine where hydrolysis of SM predominately takes place in the jejunum. At that time, a large portion of the PC has already been absorbed (Nyberg et al., 1997). Therein lies the limitation of static *in vitro* digestion. In the body, not only are the phases of digestion (oral, gastric, intestinal, colonic) sequential but the organ dimensions allow for separate biochemical reactions to be favoured at different times. It is therefore of great interest to first attempt to understand the possible structural changes to MSM and MFGM that hydrolysis by alk-SMase may engender before moving to more complex systems.

6.3.3. Phase transitions and thermotropic behaviour of milk phospholipids

Similar to the Raman spectroscopy, the thermotropic behaviour of MSM and MFGM phospholipid vesicles was analyzed by DSC under pre-digestive, gastric, and intestinal digestive conditions. Measurements for BPC vesicles for all three phases were taken; however, as the T_m of BPC was under the minimum temperature the instrument could analyze (5 °C) and thus the results were inconclusive. The pre-digestion SPC vesicles were also analyzed. Much like the BPC vesicles, the T_m was too low for the instrument to analyze any possible phase transitions.

6.3.3.1. Thermotropic behaviour of milk sphingomyelin multilamellar vesicles before and after in vitro digestion

The T_m and phase transition enthalpies of pre-digestion MSM MLVs were consistent with previous thermograms presented in Chapter 3 (Fig. 3.5). For MSM100 (no cholesterol), the $S_o \rightarrow L_d$ phase transition was a broad, asymmetric endothermic feature centered around 33 °C, a typical value for MSM (Lopez, Cheng, & Perez, 2018). Once again, the presence of a post-T_m transition was detected as a shoulder at 36 °C, possibly due to the influence of high T_m SM components. The endothermic events broadened and flattened when cholesterol was incorporated into the MLV system, lowering the enthalpy of the phase transition. The enthalpy of transition is proportional to the amount of $S_o \rightarrow L_d$ phase transition present which decreases as MSM and cholesterol complexation establishes an L_o state (Nyholm, Nylund, & Slotte, 2003). The overall T_m decreases with the addition of cholesterol due to a hydrophobic mismatch between the MSM and cholesterol. Hydrophobic mismatch in phospholipid/cholesterol bilayers occur when the hydrophobic length of the sterol does not match the hydrophobic length of the apolar phospholipid tail, causing lateral inhomogeneities in the bilayer (Mouritsen & Bloom, 1984). The addition of cholesterol is known to decrease the T_m of PC that are comprised of < 17 carbon atoms and increases the T_m of PC comprised of > 18 carbon atoms, implying that the best fit for cholesterol is a hydrophobic length of about 17.5 Å (McMullen, Lewis, & McElhaney, 1993). Saturated sphingomyelin with 16 carbon chains was determined to have the most favourable binding to cholesterol when comparing C14:0 – C24:0 sphingomyelin species (Jaikishan & Slotte, 2011). Using MSM80 as an example to explain the influence of cholesterol on SM bilayers, T_m was reduced from 33 °C (MSM100) to 29 °C due to the hydrophobic mismatch of the longer chain hydrocarbons after the cholesterol had complexed with C16:0 (~16% of MSM fatty acid) sphingomyelin. As minimal interaction with the longer hydrocarbon chains occurred, the post-T_m shoulder remains at the same location.

Such a hypothesis explains how the addition of cholesterol modifies bilayer lateral structure but may seem counterintuitive in respect to *in vivo* studies that demonstrate consumption of MSM has a greater anticholesteremic effect in rats compared to egg sphingomyelin (ESM) (Noh & Koo, 2004). Milk sphingomyelin is composed of 16% C16:0 whereas ESM has 86%, therefore, if matching hydrophobic length was the driving force behind SM and cholesterol complexation, ESM should complex more favourably with cholesterol than MSM (Engberg et al., 2020). However, the biological fate of MSM and ESM (Noh & Koo, 2004) seem to indicate that factors other than hydrophobic mismatch is responsible for the anticholesteremic effect of SM.

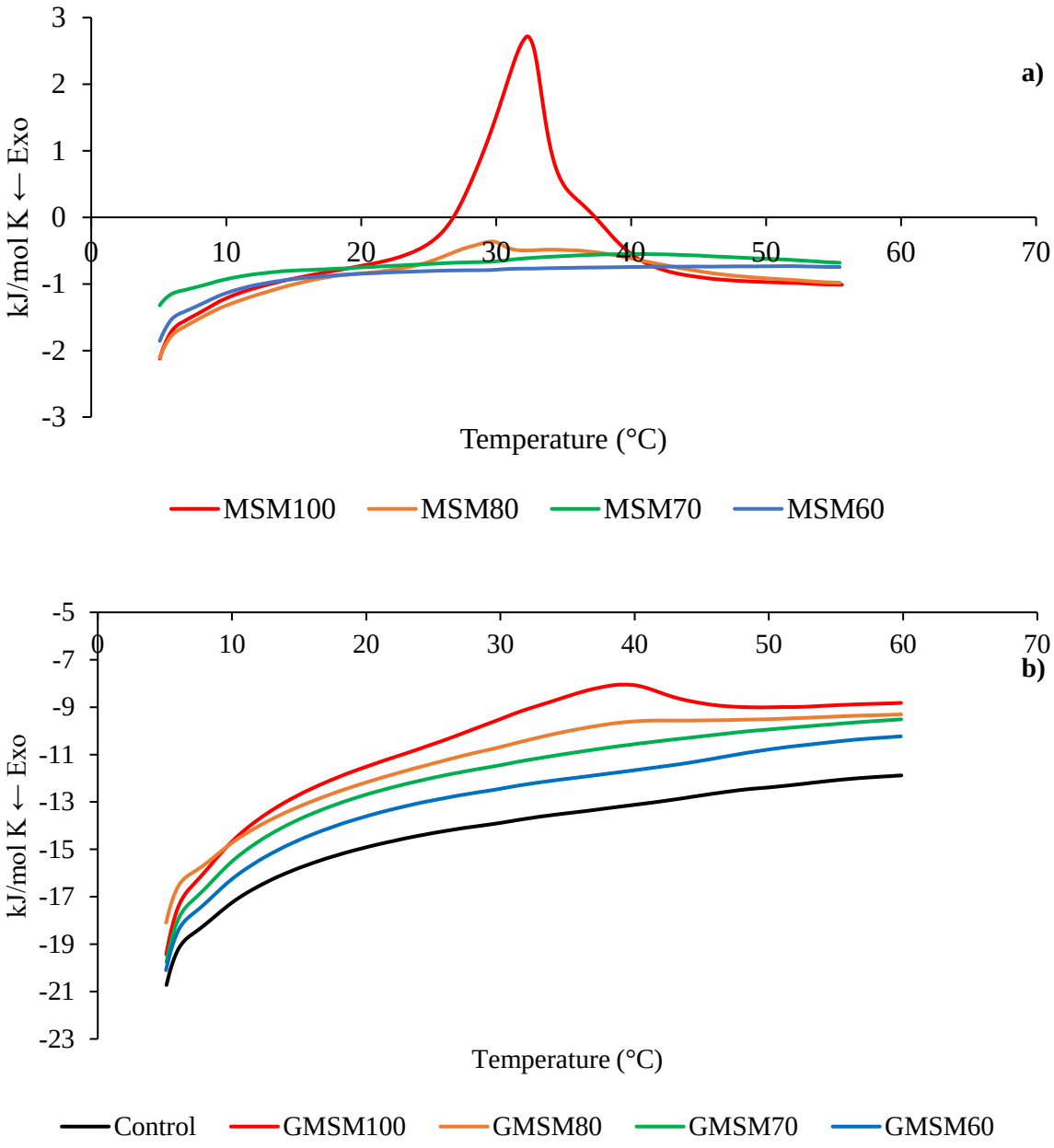

Figure 6.12. Thermotropic behaviour of milk sphingomyelin (MSM) multilamellar vesicles during *in vitro* digestion. The start-up hook from 1 – 5 °C has been discarded. Offsets have been added to the thermographs so they can be better distinguished.

a) Pre-digestion. MSM100 = without cholesterol, MSM80 = 4:1 mol/mol MSM/cholesterol, MSM70 = 7:3 mol/mol MSM/cholesterol, MSM60 = 3:2 MSM/cholesterol.
b) Post-gastric digestion. GMSM100 = without cholesterol, GMSM80 = 4:1 mol/mol MSM/cholesterol, GMSM70 = 7:3 mol/mol MSM/cholesterol, GMSM60 = 3:2 MSM/cholesterol.

The thermotropic behaviour of the MSM MLVs changed after the addition of gastric lipase (Fig. 6.12 b). The control, consisting of gastric lipase and PIPES buffer alone, confirmed that the enzyme did not unfold at the temperature range assayed, thus all endothermic events in the post-gastric MSM thermograms are due to the physical interactions between the RGE and the bilayer. The most obvious change was the higher T_m of GMSM100 compared to the pre-digestion counterpart (39 °C vs. 34 °C).

Furthermore, the $S_o \rightarrow L_d$ endothermic event developed a negative skew; that is, there is a greater degree of melting that occurs pre-T_m than post. Finally, the post-transition shoulder at 36 °C is no more and was likely subsumed into the main T_m peak.

The addition of RGE caused no change to lateral hydrocarbon (I_{2880}/I_{2930}) chain order of MSM MLVs without cholesterol (Fig 6.5 a) but did impact the intrachain (I_{1085}/I_{1130}, Fig 6.5 c) bilayer order and therefore for the overall bilayer order (I_{2930}/I_{2880}, Fig. 6.5 b). The shift in the T_m and transition enthalpy is due to intrachain interactions which are occurring i.e., an increase in *gauche* isomers or the un-tilting of the phospholipids. This is a novel interpretation which to the author's knowledge has not been previously proposed. A few inferences can be made regarding how the expansion of the proximal leaflet impacts the $S_o \rightarrow L_d$. Destabilization of the S_o phase in SM bilayer can occur due to the asymmetry of the sphingosine chain and the acyl chain (Fig. 6.13) resulting in a mixed interdigitated phase (Fig. 3.7) where the shorter sphingosine chains pack end to end with the longer acyl chain on the opposing leaflet (Jaikishan & Slotte, 2011). This form of packing forces the terminal end of the sphingosine to be *gauche* to fill space under the terminal methyl group for the acyl chain (Mason & Huang, 1981). It is possible that the expansion of the proximal leaflet by the gastric lipase exacerbates this rotameric disorder as there is more space to fill, thus a higher amount of *gauche* isomers are necessary to fill that space. A higher amount of *gauche* isomers among the high T_m phospholipids would result in a lower transition enthalpy, but does not explain why the T_m increased by 5 °C.

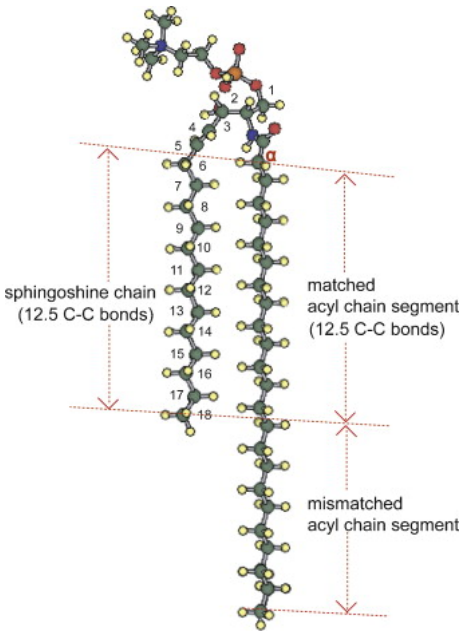

Figure 6.13. Structural model of D-*erythro*-sphingomyelin molecule. The effective length of the sphingosine chain is 12.5 C–C bonds estimated by the equation: (18 − 1) + (5.5 − 1), and the effective length of the acyl chain is 22 (= 24 − 1 − 1) C–C bonds, so that the mismatched C–C bonds (ΔC) are 9.5 (= 22 − 12.5). Reproduced from Kodama and Kawasaki, (2010).

Although the addition of alk-SMase had no observable effect on the bilayer order of the MSM MLVs, there were distinct differences in the thermograms of MSM MLVs post-intestinal with and without alk-SMase (Fig. 6.14.). The control for with alk-SMase post-intestinal samples consisted of pancreatin, bovine bile, and alk-SMase whereas the control for the without alk-SMase post-intestinal did not contain the alk-SMase. A phase transition can be seen for both controls at ~ 26 °C which is too low to be attributed to bile salts (128 °C) (Trivedi, et al., 2015) and pancreatic enzymes. When analyzing the structural aspects of sodium taurodeoxycholate and disteraoyl phosphatidylcholine (DSPC) mixed micelles (4:1 mol/mol), two peaks were present, one at 50 °C which was determined to be from the phospholipid and a second at 14 °C which the authors (Müller, 1984) determined was from the complexation of the bile salts and the phospholipid. With the addition of 8% mol cholesterol, this peak at 14 °C disappears. Although the T_m are different, the transition occurring for both controls are most likely also an interaction between the biliary PC and bile salts.

When the digestive components of the intestinal phase are applied to MSM MLVs, the T_m of this bile salt/phospholipid interaction increases. The degree to which the T_m increases depends on the presence of alk-SMase. For the IaMSM (MSM MLVs after intestinal digestion with alk-SMase) samples, the T_m is ~ 30 °C and specifically for IaMSM100 (MSM MLVs without cholesterol after intestinal digestion with alk-SMase), there is a second peak at 39 °C (Fig. 6.14. a). Although the temperatures may vary, the order of the peaks resembles MSM100 (Fig. 6.12.), a main transition and then a post-transition. With the addition of cholesterol, the post-transition peak broadens and disappears at 20% mol cholesterol. The primary phase transition at ~ 30 °C remains. Without the inclusion of alk-SMase to the intestinal digestive cocktail, the T_m of the primary transition occurs at ~ 30 °C and there is no post-transition peak for InMSM100 (MSM MLVs without cholesterol which have undergone the intestinal phase without alk-SMase) (Fig. 6.14 b).

Without any helpful complementary information from the Raman spectra regarding the MSM phospholipid MLVs post-intestinal digestion, it is difficult to identify the phase transitions that are occurring in the intestinal stage and their impact on the system writ large. From the DSC data available, it is possible to consider the post-transition peak as an $S_o \rightarrow L_d$ phase transition of free sphingomyelin hydrolysis products produced from the enzymatic activity of alk-SMase. One product of SM hydrolysis, ceramide (Gorelik et al., 2017) can be solubilized and incorporated into L_o domains (Castro et al., 2009). It should be noted that an excess of ceramide is known to displace cholesterol in model membranes (Chiantia et al., 2006). In such a case, it is expected that the InMSM MLVs (MSM MLVs after intestinal digestion without alk-SMase) which cannot hydrolyze MSM would not show a post-transition peak.

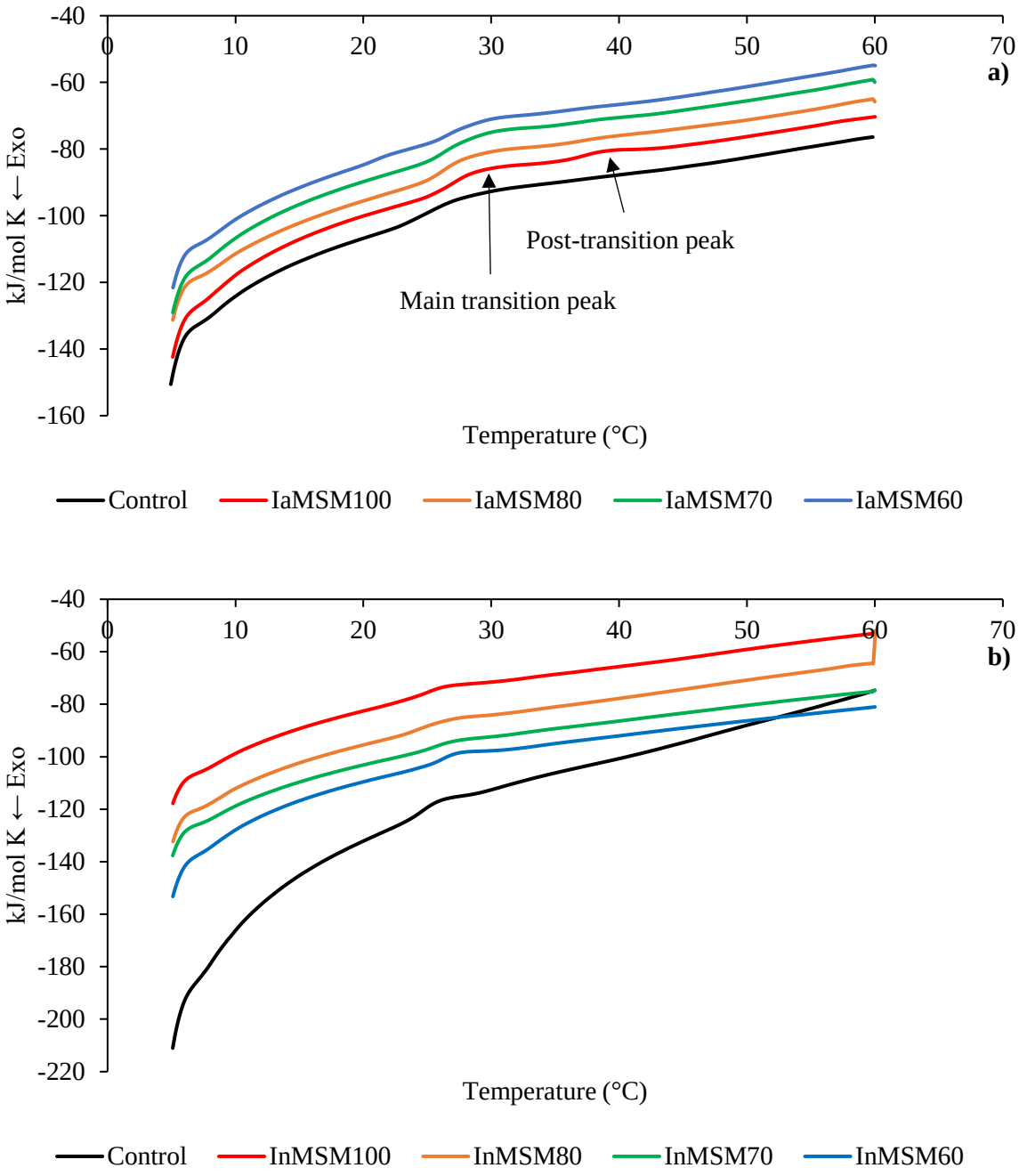

Figure. 6.14. Thermotropic behaviour of milk sphingomyelin (MSM) multilamellar vesicles (MLVs) during *in vitro* intestinal digestion. Offsets have been added to the thermographs so they can be better distinguished.

a) control consists of bovine bile, pancreatin, and alk-SMase suspended in PIPES buffer. IaMSM100 = Intestinal alk-SMase MSM MLVs without cholesterol; IaMSM80 = Intestinal alk-SMase MSM MLVs with 4:1 mol/mol SM/cholesterol; IaMSM70 = Intestinal alk-SMase MSM MLVs with 7:3 mol/mol SM/cholesterol; IaMSM60 = Intestinal alk-SMase MSM MLVs with 3:2 mol/mol SM/cholesterol.

b) control consists of bovine bile and pancreatin suspended in PIPES buffer. InMSM100 = Intestinal, no alk-SMase, MSM MLVs without cholesterol; InMSM80 = Intestinal, no alk-SMase, MSM MLVs with 4:1 mol/mol SM/cholesterol; InMSM70 = Intestinal, no alk-SMase, MSM MLVs with 7:3 mol/mol SM/cholesterol; InMSM60 = Intestinal, no alk-SMase, MSM MLVs with 3:2 mol/mol SM/cholesterol.

6.3.3.2. Thermotropic behaviour of milk fat globule membrane phospholipid vesicles before and after in vitro *digestion*

Figures 6.15 and 6.16 show the thermograms for MFGM phospholipid vesicles pre-digestion, post-gastric, and post-intestinal digestion. The MFGM phospholipid vesicles were created on an SM/cholesterol basis, meaning the total lipid concentration of each treatment varies. The thermograms have been normalized to account for concentration effects.

Pre-digestion, a broad endothermic event was visible from 5 to 40 °C, representing the melting of the phospholipids. This breadth is due to the assortment of milk phospholipid types and the varying hydrocarbon chain lengths that make up the MFGM phospholipid vesicles. The temperature range of the melting is similar to the profile reported in Chapter 5 (Fig. 5.2). One of the two contrasts between the data previously obtained and the current data is for the MFGM100, the shoulder at 30 °C (Fig. 5.2) is no longer present. The second is that the addition of cholesterol had no effect on the $S_o \rightarrow L_d$ phase transition. The latter was foreshadowed in the Raman data (Fig. 6.10 a) where increasing cholesterol composition did not significantly impact the lateral hydrocarbon packing. The key difference between the MFGM phospholipid vesicles discussed in Chapter 5 and the current ones is phospholipid composition. The current MFGM phospholipid vesicles have a higher PE content (+ 13%) and lower amounts of SM (- 3%). Since the phospholipid vesicles were created based on SM/cholesterol ratios, the current total phospholipid/cholesterol ratio is higher than previously discussed (Chapter 5), meaning even if there is the same amount of SM and cholesterol association, less of the vesicle is in the L_o state. One insight this assessment provides is that as the size of an MFG impacts its phospholipid composition (Lopez et al., 2011; Mesilati-Stahy, Mida, & Argov-Argaman, 2011), it may also impact the presence of L_o domains and therefore any L_o domain-driven bioactivity.

With the addition of the gastric lipase, the baseline trends towards an upward slope (Fig. 6.15 a). This slope represents the increasing heat capacity of the enzyme and MFGM phospholipid vesicles as the system is being heated (Höhne, Hemminger, &Flammersheim 1996). The presence of the enzyme had no effect on the phase transitions regardless of cholesterol content, similar to what was seen in the Raman spectra.

The broad phase transition from 5 – 40 °C disappears in the intestinal phase regardless of alk-SMase, suggesting as the Raman spectra indicates, solubilization and micellization by intestinal digestive components. Some features are present in the thermograms. For IaMFGM80, there is a peak at 39 °C (Fig. 6.16 a) around the same location as the post-T_m peak in IaMSM100 (Fig. 6.14 a). With the current lack of information, it is difficult to correlate the peaks with any potential interaction between bile salts and phospholipids.

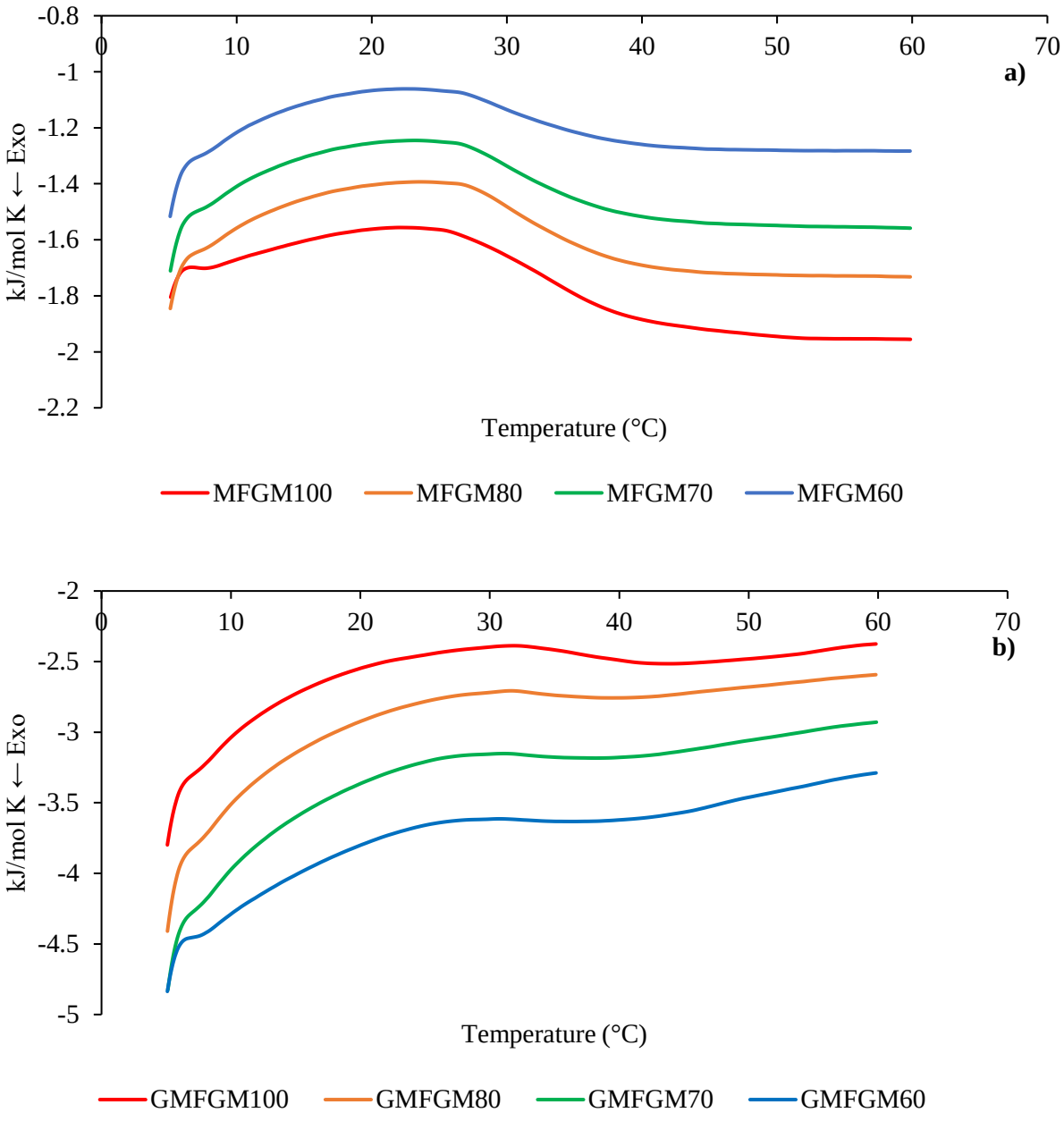

Figure. 6.15. Thermotropic behaviour of milk fat globule membrane (MFGM) phospholipid vesicles during *in vitro* digestion. Offsets have been added to the thermographs so they can be better distinguished.

a) Pre-digestion. MFGM100 = MFGM phospholipid vesicles without cholesterol; MFGM80 = MFGM phospholipid vesicles with 4:1 SM/cholesterol; MFGM70 = MFGM phospholipid vesicles with 7:3 SM/cholesterol; MFGM60 = MFGM phospholipid vesicles with 3:2 SM/cholesterol.

b) Post-gastric. GMFGM100 = MFGM phospholipid vesicles without cholesterol; GMFGM80 = MFGM phospholipid vesicles with 4:1 SM/cholesterol; GMFGM70 = MFGM phospholipid vesicles with 7:3 SM/cholesterol; GMFGM60 = MFGM phospholipid vesicles with 3:2 SM/cholesterol.

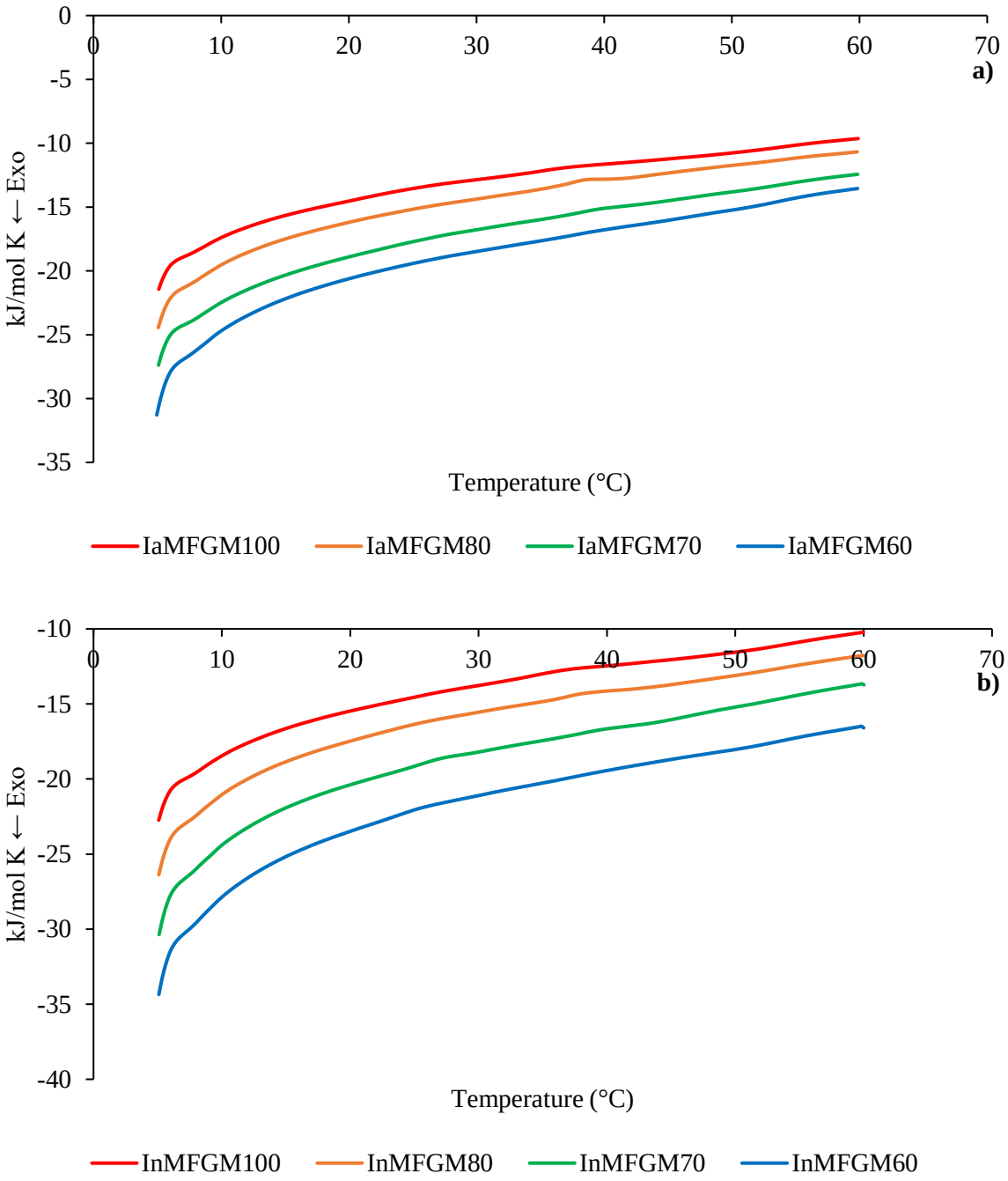

Figure. 6.16. Thermotropic behaviour of milk fat globule membrane (MFGM) phospholipid vesicles post-intestinal *in vitro* digestion. Offsets have been added to the thermographs so they can be better distinguished.

a) Post-intestinal with alk-SMase. IaMFGM100 = MFGM phospholipid vesicles without cholesterol; IaMFGM80 = MFGM phospholipid vesicles with 4:1 SM/cholesterol; IaMFGM70 = MFGM phospholipid vesicles with 7:3 SM/cholesterol; IaMFGM60 = MFGM phospholipid vesicles with 3:2 SM/cholesterol.

b) Post-intestinal without alk-SMase. InMFGM100 = MFGM phospholipid vesicles without cholesterol; InMFGM80 = MFGM phospholipid vesicles with 4:1 SM/cholesterol; InMFGM70 = MFGM phospholipid vesicles with 7:3 SM/cholesterol; InMFGM60 = MFGM phospholipid vesicles with 3:2 SM/cholesterol.

6.4 Conclusions

Phospholipids that originated from different natural sources were used to make vesicles and were submitted to static *in vitro* digestion. It was revealed phospholipid vesicle systems that contained L_o domains exhibited unique gastric behavior, rabbit gastric extract had no effect on the intrachain bilayer order of vesicle system that contained L_o domains. On the other hand, L_o domains had no effect on intestinal digestive behavior.

After the gastric digestion stage, the adhesion of RGE to the phospholipid vesicles was observed. This physical interaction did not change the lateral modifications that the presence of cholesterol makes in MSM MLVs (i.e., $S_o \rightarrow L_o$ phase transition). The presence of gastric lipase enzyme increased intrachain bilayer disorder (as measured by I_{1085}/I_{1130}) for MSM MLVs that did not contain cholesterol (MSM100) whereas it had no effect on MSM MLVs with cholesterol, demonstrating that the L_o phase is resistant to surface modification by gastric lipase. The changes in intrachain order due to the physical interaction between MSM100 and gastric lipase resulted in an increase in T_m and a lowering of the $S_o \rightarrow L_d$ enthalpy of transition. The gastric digestion of BPC and SPC suggested that the ordering and disordering which accompanies the adhesion of the gastric lipase to the vesicle surface may be dependent on the phase state of the phospholipid vesicles and therefore the phospholipid composition.

The data obtained for the post-intestinal digestion was not as conclusive. All phospholipid vesicles were solubilized and micellized regardless of cholesterol content. Transmission electron micrographs captured various vesicular and micellar intermediates that were formed during intestinal digestion. Of note was the presence of open vesicles, the product of trans-bilayer micellization, and the presence of what could only described as “lace-like” micelles, a precursor to worm-like micelles.

The statistical non-significance of interchain peak intensity ratios (I_{2850}/I_{2880}) of post-intestinal digestion of the phospholipid vesicles indicated that no matter what the prior phase state was (S_o, L_o, or L_d), the digestive components were capable of solubilizing the vesicles to form the structures observed by TEM. Milk sphingomyelin MLVs containing cholesterol showed some possible resistance to the intestinal stage of *in vitro* digestion. Milk sphingomyelin MLVs post-intestinal without cholesterol (IMSM100) showed an increase in overall bilayer disorder, whereas with 40% mol cholesterol (IMSM60), there was no change in overall bilayer disorder implying that although the IMSM60 had been micellized, some degree of unquantified type of order that was similar to what was in the original bilayer remained. The intestinal *in vitro* digestion components also had no effect on the overall bilayer order of the BPC vesicles.

The presence or absence of alk-SMase had no effect on the bilayer order for any of the phospholipid vesicles and is likely not a useful addition to static *in vitro* digestion models that contain an excess of phospholipids other than sphingomyelin. Due to the presence of phospholipids inhibiting alk-SMase,

the enzyme may be more of use in structural studies where only alk-SMase and phospholipid vesicles are present, or a dynamic system that better resembles the small intestine.

The results from the model membrane systems were used to better understand of the digestion of phospholipid vesicles comprised of MFGM phospholipids extracted from beta-serum. These vesicles showed a broad melting isotherm, and the thermotropic behaviour did not change with the addition of cholesterol, i.e., no indication of the formation of L_o domains were detected as suggested from Raman data, but not measured directly using confocal microscopy. When submitted to *in vitro* digestion, the change in bilayer order of the MFGM phospholipid vesicles was more similar to the BPC and SPC vesicles than the MSM. This may be due to the high unsaturated PE content of the beta-serum used to construct the MFGM phospholipid vesicles. As Figure. 4.5 a demonstrated, no matter the SM/cholesterol ratio, as long as the majority of the vesicle consists of unsaturated phospholipids, the detergent-induced solubilization kinetics will favour micellization.

Static *in vitro* digestion of naturally occurring phospholipids revealed that SM and cholesterol complexation is able retain some degree of bilayer order under intestinal digestive conditions. Further work is required to understand whether the micellar intermediates created during the digestion of SM/cholesterol assemblies are capable impacting lipid absorption. Secondly, the phospholipid composition of MFGM greatly alters its capacity to form L_o domains, which in turn alters its thermotropic behaviour, and perhaps even if its digestive behaviour. That is, phospholipid composition informs structure which informs digestive behaviour. Understanding the nuances behind the digestion of MFGM in this manner opens up new avenues of research on the role of the microstructure in determining nutritional outcomes.

Acknowledgements

The beta serum powder (BSP2) was kindly donated by TATUA Co-operative Dairy Company. The Python program used to baseline, average, and process the Raman data was developed and coded by Dr. Waterland of Massey University. Statistical analysis (Power, model creation and outputs) for the Raman spectroscopy portion of the work was performed by Dr. Rina Hannaford of AgResearch NZ.

Note

A condensed version of this chapter is currently being prepared as a manuscript to be considered for publication.

References

Almgren, M. (2000). Mixed micelles and other structures in the solubilization of bilayer lipid membranes by surfactants. Biochimica et Biophysica Acta (BBA) - Biomembranes, 1508(1–2), 146–163.

Alshehab, M., Budamagunta, M. S., Voss, J. C., & Nitin, N. (2019). Real-time measurements of milk fat globule membrane modulation during simulated intestinal digestion using electron paramagnetic resonance spectroscopy. Colloids and Surfaces B: Biointerfaces, 184, 110511. https://doi.org/10.1016/j.colsurfb.2019.110511

Bénarouche, A., Sams, L., Bourlieu, C., Vié, V., Point, V., Cavalier, J. F., & Carrière, F. (2017). Studying gastric lipase adsorption onto phospholipid monolayers by surface tensiometry, ellipsometry, and atomic force microscopy. A.M. Pyle, D.W. Christianson (Eds.) Methods in Enzymology (Vol. 583, pp. 255–278). Cambridge: Elsevier.

Bénarouche, A., Point, V., Parsiegla, G., Carrière, F., & Cavalier, J.-F. (2013). New insights into the pH-dependent interfacial adsorption of dog gastric lipase using the monolayer technique. Colloids and Surfaces B: Biointerfaces, 111, 306–312.

Bernbäck, S., Bläckberg, L., & Hernell, O. (1990). The complete digestion of human milk triacylglycerol in vitro requires gastric lipase, pancreatic colipase-dependent lipase, and bile salt-stimulated lipase. Journal of Clinical Investigation, 85(4), 1221–1226.

Berton, A., Sebban-Kreuzer, C., Rouvellac, S., Lopez, C., & Crenon, I. (2009). Individual and combined action of pancreatic lipase and pancreatic lipase-related proteins 1 and 2 on native versus homogenized milk fat globules. Molecular Nutrition & Food Research, 53(12), 1592–1602.

Berton, A., Rouvellac, S., Robert, B., Rousseau, F., Lopez, C., & Crenon, I. (2012). Effect of the size and interface composition of milk fat globules on their in vitro digestion by the human pancreatic lipase: Native versus homogenized milk fat globules. Food Hydrocolloids, 29(1), 123–134.

Bitman, J., & Wood, D. L. (1990). Changes in Milk Fat Phospholipids During Lactation. Journal of Dairy Science, 73(5), 1208–1216.

Bourlieu, C., Ménard, O., De La Chevasnerie, A., Sams, L., Rousseau, F., Madec, M.-N., Robert, B., Deglaire, A., Pezennec, S., Bouhallab, S., Carrière, F., Dupont, D., 2015. The structure of infant formulas impacts their lipolysis, proteolysis and disintegration during in vitro gastric digestion. Food Chemistry 182, 224–235.

Bourlieu, C., Paboeuf, G., Chever, S., Pezennec, S., Cavalier, J.-F., Guyomarc'h, F., Deglaire, A., Bouhallab, S., Dupont, D., Carrière, F., & Vié, V. (2016). Adsorption of gastric lipase onto multicomponent model lipid monolayers with phase separation. Colloids and Surfaces B: Biointerfaces, 143, 97–106.

Bourlieu, C., Mahdoueni, W., Paboeuf, G., Gicquel, E., Ménard, O., Pezennec, S., Bouhallab, S., Deglaire, A., Dupont, D., Carrière, F., & Vié, V. (2020). Physico-chemical behaviours of human and bovine milk membrane extracts and their influence on gastric lipase adsorption. Biochimie, 169, 95–105.

Brodkorb, A., Egger, L., Alminger, M., Alvito, P., Assunção, R., Ballance, S., Bohn, T., Bourlieu-Lacanal, C., Boutrou, R., Carrière, F., Clemente, A., Corredig, M., Dupont, D., Dufour, C., Edwards, C., Golding, M., Karakaya, S., Kirkhus, B., Le Feunteun, S., … Recio, I. (2019). INFOGEST static in vitro simulation of gastrointestinal food digestion. Nature Protocols, 14(4), 991–1014.

Castro, B. M., Silva, L. C., Fedorov, A., de Almeida, R. F. M., & Prieto, M. (2009). Cholesterol-rich fluid membranes solubilize ceramide domains. Journal of Biological Chemistry, 284(34), 22978–22987.

Carey, M. C., Small, D. M., & Bliss, C. M. (1983). Lipid Digestion and Absorption. Ann. Rev. Physiol. 45, 651-677.

Chahinian, H., T. Snabe, C. Attias, P. Fojan, S.B. Petersen, and F. Carrière. 2006. How gastric lipase, an interfacial enzyme with a Ser-His-Asp catalytic triad, acts optimally at acidic pH. Biochemistry 45:993–1001. doi:10.1021/bi0518803.

Cheng, K., Ropers, M.-H., & Lopez, C. (2017). The miscibility of milk sphingomyelin and cholesterol is affected by temperature and surface pressure in mixed Langmuir monolayers. Food Chemistry, 224, 114–123.

Chiantia, S., Kahya, N., Ries, J., & Schwille, P. (2006). Effects of ceramide on liquid-ordered domains investigated by simultaneous AFM and FCS. Biophysical Journal, 90(12), 4500–4508.

Colin, D. Y., Deprez-Beauclair, P., Allouche, M., Brasseur, R., & Kerfelec, B. (2008). Exploring the active site cavity of human pancreatic lipase. Biochemical and Biophysical Research Communications, 370(3), 394–398.

Dreiss, C.A., (2018). Wormlike micelles: An introduction. C.A. Dreiss, Y. Feng (Ed.) Wormlike micelles: Advances in systems, characterisation and applications, 2017, pp. 1-8

Eggers, L. F., & Schwudke, D. (2016). Liquid Extraction: Folch. In M. R. Wenk (Ed.), Encyclopedia of Lipidomics (pp. 1–6). Netherlands: Springer.

Engberg, O., Lin, K.-L., Hautala, V., Slotte, J. P., & Nyholm, T. K. M. (2020). Sphingomyelin acyl chains influence the formation of sphingomyelin- and cholesterol-enriched domains. Biophysical Journal, 119(5), 913–923.

Et-Thakafy, O., Guyomarc'h, F., & Lopez, C. (2017). Lipid domains in the milk fat globule membrane: Dynamics investigated in situ in milk in relation to temperature and time. Food Chemistry, 220, 352–361.

Et-Thakafy, O., Delorme, N., Guyomarc'h, F., & Lopez, C. (2018). Mechanical properties of milk sphingomyelin bilayer membranes in the gel phase: Effects of naturally complex heterogeneity, saturation and acyl chain length investigated on liposomes using AFM. Chemistry and Physics of Lipids, 210, 47–59.

Folch, J., Lees, M., & Sloane Stanley, G. (1957). A simple method for the isolation and purification of total lipides from animal tissues. J Biol Chem, 226(1), 497–509.

Forooqi Motlaq, V., Ortega-Holmberg, M., Edwards, K., Gedda, L., Lyngsø, J., Pedersen, J. S., & Bergström, L. M. (2021). Investigation of the enhanced ability of bile salt surfactants to solubilize phospholipid bilayers and form mixed micelles. Soft Matter, 17(33), 7769–7780.

Gallier, S., Gragson, D., Cabral, C., Jiménez-Flores, R., & Everett, D. W. (2010). Composition and Fatty Acid Distribution of Bovine Milk Phospholipids from Processed Milk Products. Journal of Agricultural and Food Chemistry, 58(19), 10503–10511.

Gallier, S., Ye, A., & Singh, H. (2012). Structural changes of bovine milk fat globules during in vitro digestion. Journal of Dairy Science, 95(7), 3579–3592.

Gallier, S., Cui, J., Olson, T. D., Rutherfurd, S. M., Ye, A., Moughan, P. J., & Singh, H. (2013). In vivo digestion of bovine milk fat globules: Effect of processing and interfacial structural changes. I. Gastric digestion. Food Chemistry, 141(3), 3273–3281.

Gorelik, A., Liu, F., Illes, K., & Nagar, B. (2017). Crystal structure of the human alkaline sphingomyelinase provides insights into substrate recognition. Journal of Biological Chemistry, 292(17), 7087–7094.

Hamosh, M., & Scow, R. O. (1973). Lingual lipase and its role in the digestion of dietary lipid. Journal of Clinical Investigation, 52(1), 88–95.

Heid, H. W., & Keenan, T. W. (2005). Intracellular origin and secretion of milk fat globules. European Journal of Cell Biology, 84(2–3), 245–258.

Höhne, G. W. H., Hemminger, W., & Flammersheim, H.-J. (1996). The DSC Curve. In G. W. H. Höhne, W. Hemminger, & H.-J. Flammersheim (Eds.), Differential Scanning Calorimetry: An Introduction for Practitioners (pp. 81–104). Heidelberg Berlin: Springer.

Israelachvili, J. N. (2010). Soft and biological structures. In Intermolecular and surface forces (3rd edn. pp. 535–576). Massachusetts, USA: Elsevier Science

Jaikishan, S., & Slotte, J. P. (2011). Effect of hydrophobic mismatch and interdigitation on sterol/sphingomyelin interaction in ternary bilayer membranes. Biochimica et Biophysica Acta (BBA) - Biomembranes, 1808(7), 1940–1945.

Kodama, M., & Kawasaki, Y. (2010). Structural role of mismatched C–C bonds in a series of d-erythro-sphingomyelins as studied by DSC and electron microscopy. Chemistry and Physics of Lipids, 163(6), 514–523.

Kragh-Hansen, U., le Maire, M., & Møller, J. V. (1998). The mechanism of detergent solubilization of liposomes and protein-containing membranes. Biophysical Journal, 75(6), 2932–2946.

Lete, M. G., Monasterio, B. G., Collado, M. I., Medina, M., Sot, J., Alonso, A., & Goñi, F. M. (2019). Fast and slow biomembrane solubilizing detergents: Insights into their mechanism of action. Colloids and Surfaces B: Biointerfaces, 183, 110430.

Lichtenberg, D., Ahyayauch, H., & Goñi, F. M. (2013). The mechanism of detergent solubilization of lipid bilayers. Biophysical Journal, 105(2), 289–299.

Liu, J.-J., Nilsson, Å., & Duan, R.-D. (2000). Effects of phospholipids on sphingomyelin hydrolysis induced by intestinal alkaline sphingomyelinase: An in vitro study. The Journal of Nutritional Biochemistry, 11(4), 192–197.

Lopez, C., Briard-Bion, V., Ménard, O., Beaucher, E., Rousseau, F., Fauquant, J., Leconte, N., & Robert, B. (2011). Fat globules selected from whole milk according to their size: Different compositions and structure of the biomembrane, revealing sphingomyelin-rich domains. Food Chemistry, 125(2), 355–368.

Lopez, C., Cheng, K., & Perez, J. (2018). Thermotropic phase behaviour of milk sphingomyelin and role of cholesterol in the formation of the liquid ordered phase examined using SR-XRD and DSC. Chemistry and Physics of Lipids, 215, 46–55.

Mason, J. T., & Huang, C.-H. (1981). Chain length dependent thermodynamics of saturated symmetric-chain phosphatidylcholine bilayers. Lipids, 16(8), 604–608.

Maldonado-Valderrama, J., Wilde, P., Macierzanka, A., & Mackie, A. (2011). The role of bile salts in digestion. Advances in Colloid and Interface Science, 165(1), 36–46.

McMullen, T. P. W., Lewis, R. N. A. H., & McElhaney, R. N. (1993). Differential scanning calorimetric study of the effect of cholesterol on the thermotropic phase behaviour of a homologous series of linear saturated phosphatidylcholines. Biochemistry, 32(2), 516–522.

Mesilati-Stahy, R., Mida, K., & Argov-Argaman, N. (2011). Size-dependent lipid content of bovine milk fat globule and membrane phospholipids. Journal of Agricultural and Food Chemistry, 59(13), 7427–7435.

Minekus, M., Alminger, M., Alvito, P., Ballance, S., Bohn, T., Bourlieu, C., Carrière, F., Boutrou, R., Corredig, M., Dupont, D., Dufour, C., Egger, L., Golding, M., Karakaya, S., Kirkhus, B., Le Feunteun, S., Lesmes, U., Macierzanka, A., Mackie, A., … Brodkorb, A. (2014). A standardised static in vitro digestion method suitable for food – an international consensus. Food Funct., 5(6), 1113–1124.

Moschetta, A., Frederik, P. M., Portincasa, P., vanBerge-Henegouwen, G. P., & van Erpecum, K. J. (2002). Incorporation of cholesterol in sphingomyelin- phosphatidylcholine vesicles has profound effects on detergent-induced phase transitions. Journal of Lipid Research, 43(7), 1046–1053.

Mouritsen, O. G., & Bloom, M. (1984). Mattress model of lipid-protein interactions in membranes. Biophysical Journal, 46(2), 141–153.

Müller, K. (1984). Structural aspects of bile salt-lecithin mixed micelles. Hepatology, 4(S2), 134S-137S.

Murthy, A. V. R., Guyomarc'h, F., & Lopez, C. (2016). Cholesterol decreases the size and the mechanical resistance to rupture of sphingomyelin rich domains, in lipid bilayers studied as a model of the milk fat globule membrane. Langmuir, 32(26), 6757–6765.

Murzyn, K., Róg, T., & Pasenkiewicz-Gierula, M. (2005). Phosphatidylethanolamine-phosphatidylglycerol bilayer as a model of the inner bacterial membrane. Biophysical Journal, 88(2), 1091–1103.

Nilsson, Å., & Duan, R.-D. (2019). Pancreatic and mucosal enzymes in choline phospholipid digestion. American Journal of Physiology-Gastrointestinal and Liver Physiology, 316(4), G425–G445.

Noh, S. K., & Koo, S. I. (2004). Milk Sphingomyelin Is More Effective than Egg Sphingomyelin in Inhibiting Intestinal Absorption of Cholesterol and Fat in Rats. The Journal of Nutrition, 134(10), 2611–2616.

Nyberg, L., Nilsson, Å., Lundgren, P., & Duan, R.-D. (1997). Localization and capacity of sphingomyelin digestion in the rat intestinal tract. The Journal of Nutritional Biochemistry, 8(3), 112–118.

Nyholm, T. K. M., Nylund, M., & Peter Slotte, J. (2003). A calorimetric study of binary mixtures of dihydrosphingomyelin and sterols, sphingomyelin, or phosphatidylcholine. Biophysical Journal, 84(5), 3138–3146.

Okotrub, K. A., Zykova, V. A., Adichtchev, S. V., & Surovtsev, N. V. (2020). Deciphering the orientation of lipid molecules by principal component analysis of Raman mapping data. The Analyst, 145(4), 1466–1472.

Pafumi, Y., Lairon, D., de la Porte, P. L., Juhel, C., Storch, J., Hamosh, M., & Armand, M. (2002). Mechanisms of inhibition of triacylglycerol hydrolysis by human gastric lipase. Journal of Biological Chemistry, 277(31), 28070–28079.

Pink, D. A., McNeil, S., Quinn, B., & Zuckermann, M. J. (1998). A model of hydrogen bond formation in phosphatidylethanolamine bilayers. Biochimica et Biophysica Acta (BBA) – Biomembranes, 1368(2), 289 – 305.

Rankine, C. D., Atkinson, S. J., Waterland, M. R., Masters, S. L., & Wann, D. A. (2018). The structure of tris(chloromethyl)amine in the gas phase using quantum chemical calculations and gas electron diffraction and as a solid and melt using Raman spectroscopy. Structural Chemistry, 29(3), 803–813.

Róg, T., & Pasenkiewicz-Gierula, M. (2001). Cholesterol effects on the phosphatidylcholine bilayer nonpolar region: A molecular simulation study. Biophysical Journal, 81(4), 2190–2202.

Róg, T., & Pasenkiewicz-Gierula, M. (2006). Cholesterol-sphingomyelin interactions: A molecular dynamics simulation study. Biophysical Journal, 91(10), 3756–3767.

Roy, D., Ye, A., Moughan, P. J., & Singh, H. (2021). Structural changes in cow, goat, and sheep skim milk during dynamic in vitro gastric digestion. Journal of Dairy Science, 104(2), 1394–1411.

Shirota, K., Yagi, K., Inaba, T., Li, P.-C., Murata, M., Sugita, Y., & Kobayashi, T. (2016). Detection of sphingomyelin clusters by Raman spectroscopy. Biophysical Journal, 111(5), 999–1007.

Singh, H., & Gallier, S. (2014). Processing of food structures in the gastrointestinal tract and physiological responses. M. Boland, M. Golding, H. Singh (Eds.) Food structures, digestion and health (1st edn, pp. 51-81). London, UK: Elsevier.

Son, M., & London, E. (2013). The dependence of lipid asymmetry upon polar headgroup structure. Journal of Lipid Research, 54(12), 3385–3393.

Tai, P., Golding, M., Singh, H., Waterland, M., & Everett, D. W. (2021). Cholesterol-phospholipid interactions resist the detergent effect of bovine bile. Colloids and Surfaces B: Biointerfaces, 205, 111842.

Thum, C., Roy, N. C., Everett, D. W., & McNabb, W. C. (2021). Variation in milk fat globule size and composition: A source of bioactives for human health. Critical Reviews in Food Science and Nutrition, 1–27.

Trivedi, M. K. (2015). Thermal and physical properties of biofield treated bile salt and proteose peptone. Journal of Analytical & Bioanalytical Techniques, 6(4). 1–6.

Walstra, P., Wouters, J., Geurts, T. (2006). Dairy science and technology (2nd edn., Chapt. 3).

Florida, USA: Taylor & Francis Group, LLC.

Wang, Y., Gkeka, P., Fuchs, J. E., Liedl, K. R., & Cournia, Z. (2016). DPPC-cholesterol phase diagram using coarse-grained Molecular Dynamics simulations. Biochimica et Biophysica Acta (BBA) - Biomembranes, 1858(11), 2846–2857.

Ye, A., Cui, J., & Singh, H. (2011). Proteolysis of milk fat globule membrane proteins during in vitro gastric digestion of milk. Journal of Dairy Science, 94(6), 2762–2770.

Zhao, J., Wu, J., Heberle, F. A., Mills, T. T., Klawitter, P., Huang, G., Costanza, G., & Feigenson, G. W. (2007). Phase studies of model biomembranes: Complex behaviour of DSPC/DOPC/Cholesterol. Biochimica et Biophysica Acta (BBA) - Biomembranes, 1768(11), 2764–2776.

Chapter 7 – Structural alterations of biliary micelles in the presence of phospholipid/cholesterol vesicles during detergent-induced solubilization by bile salts

7.1 Introduction

The structure and biological functions of plasma membranes have received much attention in the past two decades (Levental, Levental, & Heberle, 2020). Advancements in membrane sciences have resulted in a burgeoning interest about the role and dietary function of phospholipids that comprise the milk fat globule membrane (MFGM). These functional properties include, but are not limited to, emulsion stabilization (He & Ye, 2019), serum cholesterol modulation (Vors et al., 2019), and encapsulation of bioactive compounds (Jash et al., 2020). Attempts have been made to mimic the natural structure of the MFGM to better tailor food products, such as infant formula (Gallier et al., 2015; Lopez, Cauty, & Guyomarc'h, 2019). Research efforts in these areas are directly or indirectly spurred on by the potential health benefits from consuming MFGM material (Dewettinck et al., 2008). However, there is little available knowledge regarding the structural changes that occur when the MFGM is digested and the role of those structures in delivering nutritional benefits.

The model of MFG digestion proposed from *in vitro* (Gallier, Ye, & Singh, 2012) and *in vivo* studies (Gallier et al., 2013 a; Gallier et al., 2013 b) serves as an appreciable survey of MFGM digestion. Key insights include gastric lipase adhering to the MFGM surface to hydrolyse the MFG triacylglyceride core, forming free fatty acid protrusions on the surface of the fat globule which limits gastric lipolysis to a small degree (Gallier et al., 2013 a). Bile salts adsorb and then solubilize the surface of the membrane allowing for the adhesion of pancreatic lipase and its co-lipase (Gallier, Ye, & Singh, 2012). The fat globule becomes crenated as lipolytic products form a liquid-crystalline lamellar phase rich in calcium and fatty acids (Patton & Carey, 1979). At a critical stage, the lamellar phase cracks and unhydrolyzed oil leaves the globule. The lamellar phase is solubilized to form bile salt/fatty acid/phospholipid/cholesterol mixed micelles which are absorbed through the intestinal epithelium (Gallier, Ye, & Singh, 2012). The studies by Gallier makes note of the presence of lateral liquid ordered (L_o) domains on the MFGM surface; however, did not propose how the domains were affected by gastrointestinal digestion.

These L_o domains are detergent resistant sphingomyelin (SM) and cholesterol assemblies which have intermediate properties of a solid ordered (S_o) and liquid disordered (L_d) phase (Quinn & Wolf, 2009; Tai et al., 2021). Previous work in Chapters 4 and 6 tracking the changes in lateral inter-hydrocarbon chain and intrachain (a combination of *gauche/trans* rotational isomerization and chain tilt) order with Raman spectroscopy showed that vesicles comprising of milk sphingomyelin (MSM) and cholesterol were capable of partially resisting the slew of conditions and biochemical factors that make up *in vitro* digestion. Post-intestinal digestion, the lateral chain-to-chain order of MSM and cholesterol (3:2

mol/mol respectively) MLVs increased which was indicative of micellization – however, the overall bilayer order of the MLVs did not change during any of the *in vitro* digestion processes. In contrast, the overall bilayer order of MSM MLVs that did not contain cholesterol decreased with the addition of gastric lipase and decreased once again with the introduction of intestinal digestive factors. It is possible that even though MSM/cholesterol ML tVs were solubilized, the L_o domains were incorporated into micellar intermediates. This result illustrates the limitations of the Raman analysis; differences in bilayer order are capable of being determined but the lyotropic structures, as well as alterations to those structures, are unable to be identified and must be inferred.

Lyotropic structures, also known as liquid crystalline mesophases, are ordered structures that are dependent on the critical packing parameter of the amphiphilic components that make them up (Pham, Clulow, & Boyd, 2021). As obvious as it may seem, liposomes and multilamellar vesicles possess lamellar bilayer structure. During intestinal digestion in the small intestine, these bilayers come into contact with bile, a physiological assortment of various bile salts and biliary phosphatidylcholine (PC) vesicles (Macierzanka et al., 2019). Intestinal fluids that simulate the fasted state only contain bile salt/PC mixed micelles, those that simulate the postprandial state additionally contain lipid aggregates and vesicles (Riethorst et al., 2016). The detergent-induced micellization of phospholipid membranes by bile salts alters native bilayer structures to form mixed micelles and various intermediates e.g. worm-like micelles. Conversely, the detergent resistant L_o domains should be more resistant to structural alterations caused by bile.

Small angle x-ray diffraction has shown to be proficient in identifying the mesophases (Hyde, 2001) of triacylglycerides that have been enzymatically treated with pancreatic lipase and incubated with bile salts (Salentinig et al., 2011). Furthermore, x-ray diffraction techniques have also been paramount in determining the conditions under which L_o domains are formed (Chachaty et al., 2005), as well as the thermotropic behaviour (Quinn & Wolf, 2009) of these SM/cholesterol assemblies. Within the small angle region ($q = 0.1 – 0.4$ Å^{-1}), SM and cholesterol MLVs are known to demonstrate at least two Bragg peaks, the first and second order diffraction peaks (Lopez, Cheng, & Perez, 2018). A second peak at $q = 0.099$ Å^{-1} ($d = 62.9$ Å) close to the first lamellar repeat has been reported to be the interdigitated S_o phase (Chachaty et al., 2015). When cholesterol is added to MSM MLVs, the d-spacing of the MLV decreases if the vesicle is in the S_o phase which occurs at temperatures lower than the melting point (i.e. $< T_m$) and increases if the vesicle is in the L_d phase ($> T_m$) (Fig. 3.9), reaching an intermediate bilayer periodicity that is resistant to temperature-induced phase transitions.

Consequently, synchrotron small angle x-ray diffraction has proven to be a powerful tool for determining the structural fate of L_o domains under intestinal digestive conditions. This study aims to first compare the thermotropic properties of various phospholipid vesicles composed of naturally occurring phospholipids: milk sphingomyelin (MSM), egg sphingomyelin (ESM), soy

phosphatidylcholine (SPC), and milk fat globule membrane phospholipids extracted from beta-serum (MFGM). The second objective was to determine how the lamellar structure of the phospholipid vesicles is altered in the presence of bovine bile and then investigate the structural changes of the biliary micelles during the detergent-induced micellization by bile salts. Studying the structural changes that occur in these model membrane systems will shed light not only on the unique biophysical properties of phospholipids with different T_m, but provide the opportunity to compare the properties of the complex phospholipid composition of MFGM in a digestive context. The hypothesis that will be tested is similar to the one in Chapter 4 – the detergent resistance inherent to L_o domains is predominately due to increase lateral hydrocarbon ordering from chain-to-chain interactions. In this experiment, a retention of lamellar structure during detergent-induced micellization is expected of phospholipid vesicles that contain a high number of L_o domains, i.e., vesicles that contain a high concentration of cholesterol and are composed of high T_m phospholipids.

7.2 Materials and methods

7.2.1 Milk fat globule membrane phospholipid extraction

The MFGM phospholipid extract used in this study was derived from beta-serum powder (BSP2, Tatua Dairy Company, Tatuanui, New Zealand) obtained from spray drying fresh beta-serum. Lipids were extracted using the Folch method with 2:3:1 v/v of methanol:chloroform:NaCl (aq. 8.76%) (Folch, Lees, & Sloane Stanley, 1957; Eggers and Schwudke, 2016). The solid-to-total extract solvent ratio was 1:24 w/v. Samples were thoroughly mixed then centrifuged at 1,000 × g for 10 min at 20 °C. The top methanol layer and the aqueous layer that included the precipitate were siphoned and discarded. The phospholipid-rich chloroform layer was concentrated by rotary evaporation and solubilized with hexane to produce a crude extract with an estimated 100 mg lipid/mL based on prior calculations using the manufacturer specifications.

Phospholipids were separated from the crude hexane extract by solid phase extraction according to Bitman and Wood (1990) as modified by Gallier et al. (2010). Silica cartridges (12 mL) with a bed weight of 2 g (Discovery DSC-Si, Sigma-Aldrich, Auckland, New Zealand) were conditioned with 2 volumes of methanol before the crude extract (200 mg lipid) was loaded. The neutral lipids were eluted out with 40 mL hexane:ethyl ether (1:1). The phospholipids were first eluted with methanol (20 mL), followed by chloroform:methanol:water (20 mL; 3:5:2 v/v/v). Both phospholipid fractions were collected, concentrated by rotary evaporation, and solubilized in 2:1 v/v chloroform:methanol to approximately 10 mg SM/mL before being stored in the dark at –20 °C until used.

The BSP2 used in this experiment and the BSP2 used in Chapter 5 originated from different batches. The phospholipid composition for the sample used in this chapter was found to be 4.0 ± 0.1% mol PI, 47.7 ± 0.7 % mol PE, 7.1 ± 0.2 % mol PS, 25.0 ± 0.4% mol PC, 16.2 ± 0.3% mol SM and the total

phospholipid contents was 15.7 ± 0.4 mg total polar lipids/mL extract. The HPLC protocol, the standard curves, and an example chromatogram can be found in Appendices 6.1 – 6.3.

7.2.2 Phospholipid vesicle preparation for temperature-controlled SR-XRD and detergent-induced vesicle → micelle transition by bovine bile

Phospholipid vesicles were prepared in pH 6.7 buffer: PIPES 10 mM (1,4-piperazinediethane sulfonic acid; purity ≥ 99%; Sigma-Aldrich), 50 mM NaCl (Analytical Reagent Grade; Thermo Fisher Scientific NZ, North Shore City, New Zealand) and 5 mM $CaCl_2$ (Millipore, Burlington, MA, USA), according to the procedure of Lopez, Cheng, & Perez (2018). Phospholipid vesicles were composed of milk sphingomyelin (Avanti Polar Lipids, Alabaster, AL, USA), egg sphingomyelin (Avanti Polar Lipids), soy phosphatidylcholine (Sigma-Aldrich), MFGM phospholipids or binary mixtures of one of these four phospholipid preparations with ovine cholesterol (Sigma-Aldrich). Binary mixtures consisted of 100/0, 4/1, 7/3, 3/2 of phospholipid/cholesterol, mol/mol. In the case of the MFGM phospholipid vesicles, the same ratios were used, but with an SM/cholesterol, mol/mol ratio. Total lipid concentration of the MSM, SPC, and ESM vesicles were 0.66 mM, ~ 4 × the SM content in liquid milk (Bitman & Wood, 1990), based on preliminary results assessing how close to the SM content in milk was detectable with synchrotron radiation small angle x-ray scattering (SR-SAXS) (Fig. 3.6 a). Table 7.1 details the concentrations used to create MFGM phospholipid vesicles.

Table 7.1. Phospholipid and cholesterol concentrations used for MFGM phospholipid vesicles.

Given name	PI (µM)	PE (µM)	PS (µM)	PC (µM)	SM (µM)	Chol (µM)	Total PL (µM)
MFGM100	0.18	1.83	0.28	1.00	0.66	0.00	4.0
MFGM80	0.15	1.47	0.23	0.80	0.52	0.13	3.3
MFGM70	0.13	1.28	0.20	0.70	0.46	0.20	2.7
MFGM60	0.11	1.10	0.17	0.60	0.40	0.26	2.6

PE = phosphatidylethanolamine; PI = phosphatidylinositol; PS = phosphatidylserine; PC = phosphatidylcholine; SM = sphingomyelin; Chol = cholesterol. MFGM100 = milk fat globule membrane phospholipid without cholesterol; MFGM80 = milk fat globule membrane phospholipid with 4:1 SM/cholesterol; MFGM70 = milk fat globule membrane phospholipid with 7:3 SM/cholesterol; MFGM60 = milk fat globule membrane phospholipid with 3:2 cholesterol.

7.2.3 Temperature-controlled SR-SAXS experiments

Synchrotron x-ray diffraction experiments were performed at the Australian Synchrotron (ANSTO, Melbourne, Australia) on the small-angle and wide-angle x-ray scattering beamline. Phospholipid vesicles sedimented during transit and were vortexed before being loaded into glass capillaries (100 – 200 µL of sample). The capillaries were oriented horizontally onto a capillary rack perpendicular to the beam direction. Mylar sheets (6 µm thick, Sietronics Laboratory Services, Mitchell, ACT, Australia) were taped onto the measurement window for thermal insulation (Appendix 7.1). An automated scan sequence calibrated the position of the capillaries. The independent scanning points were obtained by moving the capillaries laterally through the beam, scanning the length of the capillary.

The samples were submitted to controlled heating from 6.6 °C – 65.0 °C ± 0.2 °C. 6.6 °C was the lowest temperature possible with the configuration used. The samples were equilibrated at this temperature for 30 min and then heated to 10 °C. Measurements took 5 min to complete and each sample was equilibrated at the scanning temperature for at least 5 min. After the first measurement, samples were heated with a minimum of 5 min equilibration time at each set point. Measurements were taken every 10 °C. The final measurement at 65 °C was equilibrated for at least 10 min. At the beginning of the experiment, the vesicles had sedimented once more and the data recorded was from the sediment at the bottom of the capillary.

The sample-detector distance was set to 840 mm and q ranges were calibrated against silver behenate. The diffraction patterns consisted of concentric circles as a function of the scattering vector $q = \frac{4\pi}{\lambda}\sin(\theta)$ where 2θ is the scattering angle and λ the wavelength of the incident beam (λ = 0.816 Å; 15.2 keV). These parameters covered q = 0.022 – 2.284 $Å^{-1}$. The mean of three XRD patterns was taken and reported as the integrated signal from the concentric circle versus q.

7.2.4 Detergent-induced vesicle → micelle transition by bile salt SR-SAXS experiments

This series of experiments consisted of a custom in-house setup where bovine bile (10 mM final concentration, Sigma-Aldrich) reconstituted in simulated intestinal fluid (SIF) (Brodkorb et al., 2019) was added to a thermostatted glass vessel held at 37 °C containing phospholipid vesicles. The simulated intestinal fluid consisted of 5.4 mM KCl, 0.6 mM KH_2PO_4, 68.0 mM $NaHCO_3$, 30.7 mM NaCl, 0.2 mM $MgCl_2(H_2O)_6$, and 0.5 mM $CaCl_2$ (Bordkorb et al., 2019). To facilitate this set-up, a capillary was clamped to hang above a glass vessel atop a stirrer plate equipped with a thermostat. A peristaltic pump was mounted on a stand above the vessel to allow the phospholipid vesicles and bile dispersion to flow through the capillary back into the vessel (Appendix 7.2).

The sample-detector distance was set to 2339 mm and calibrated against silver behenate. The diffraction patterns consisted of concentric circles as a function of the scattering vector (refer to *Section 7.2.2* for the scattering equation). The wavelength used was 1.033 Å; 12.0 keV. These parameters covered q = 0.007 – 0.669 $Å^{-1}$. The SAXS pattern was integrated and the intensity from the concentric circle versus q was reported.

Phospholipid vesicle dispersions (4.8 mL) were vortexed until homogenous and loaded into the digestion vessel. Approximately 10 scattering profiles of the vesicle dispersion were acquired before bovine bile was injected into the vessel that contained the vesicle dispersion. The bovine bile dispersion was loaded into a 3 mL syringe attached to a 0.58 mm ID tube for injection. A Nemesys syringe driver (CETONI, Korbußen, Germany) was used to deliver the bovine bile into the digestion vessel. Exposures took 5 s and there was a 15 s delay between exposure, i.e., one measurement every 20 s. These experiments were performed for at least 25 min before the vessel was cleaned and the next sample loaded.

7.2.5 SR-SAXS data analysis

An in-house developed software package, ScatterBrain, was used to convert the 2D SAXS pattern recorded using a Pilatus 1 M detector to plot I (q) versus q by radial integration of the scattered x-ray intensity about the calibrated beam centre position.

For the temperature-controlled experiments, all spectra were plotted on a log-log scale. During the experiment, bubbles in the capillaries began to swell at temperatures >40 °C. Each scattering profile taken at or above 40 °C was checked for artefacts due to air bubbles (low intensity, distorted scattering patterns). Nothing resembling air bubbles were apparent. Scattering profiles of two independent replicates, each consisting of three measurements at different locations in the capillary were taken and averaged. The background scattering from the PIPES buffer was then subtracted from the average scattering profile. Peak location was identified with the peak finding tool in Origin Academic (2018, 95E, Northampton, MA, USA).

Peak location for the vesicle → micelle transition scattering profiles were obtained using the same program. Due to limited beam time, scattering profiles were only taken from one replicate. The bilayer periodicity (d-spacing) was determined from the q values of the first Bragg peak using:

$$q = \frac{2\pi}{d} \tag{7.1}$$

A power-law was subtracted from the low q region of the vesicle → micelle transition scattering profiles before Guinier approximations were attempted due to aggregation of the vesicles and other large particles. An example of how this power law subtraction was performed is detailed Appendix 7.3.

After the power-law was subtracted from each scattering profile, the BioXTAS RAW software package (Hopkins, Gililan, & Skou, 2017) was used for the Guinier approximation to obtain an approximate radius of gyration (R_g) by fitting a straight line to a plot of ln (I) and q^2. This approximation is only valid for $qR_g < 1.3$ and for spherical particles. The approximation states that at low q, the scattering profile can be approximated using:

$$\lim_{q \to 0} I = I_0 \exp\left(-\frac{1}{3} q^2 R_g^2\right) \tag{7.2}$$

where R_g is the radius of gyration of the particle and I_0 is the calculated intensity of the scattering profile at q = 0. Using the value for R_g, the radius of a sphere can be obtained using:

$$R_s = \sqrt{5/3} \times R_g \tag{7.3}$$

where R_s is the radius of a sphere. The R_g obtained underestimates the radius of the particle, assuming it is a sphere.

7.3 Results and discussion

7.3.1 Diffuse scattering of milk fat globule membrane and soy phosphatidylcholine vesicles

For both the temperature controlled and detergent-induced vesicle → micelle experiments, SPC and MFGM scattering profiles showed weak scattering (Fig. 7.1) rather than sharp Bragg peaks. Diffuse scattering of the MFGM phospholipid vesicles had been seen in Figure 5.9 and the concentration of vesicles was doubled in the current experiment. Considering no diffraction was visible, it is likely the MFGM and SPC vesicles measured were LUVs rather than MLVs.

A diffuse scattering pattern is a feature of unilamellar lipid vesicles (Brzustowicz & Brunger, 2005). The diffuse maxima present in both scattering profiles are due to the contrast between the electron densities of the solvent (i.e., PIPES buffer + simulated intestinal fluid (SIF)) and the vesicle membrane (Rappolt, 2006). The maxima for the SPC scattering profile are at q = ~0.095 with a repeat diffraction at 0.186 $Å^{-1}$. The maxima were broader for the MFGM phospholipids, covering a higher q range (Fig. 7.2 b).

7.3.2. Sphingomyelin and cholesterol multilamellar vesicles retain lamellar structure when heated

Scattering profiles of milk (MSM) and egg sphingomyelin (ESM), highlighting the structural transformations that occur when temperature was raised, can be observed in Figure 7.2 and 7.3. Both a heating and cooling step was attempted; however, diffraction peaks did not return when vesicles were cooled, suggesting sedimentation of the vesicles during the heating step. Sedimentation of the vesicles had been present when the samples arrived at the Synchrotron facility.

First order Bragg peaks at q = 0.06 – 0.09 $Å^{-1}$, were present for both MSM and ESM MLVs. The wide-angle q region 1.4 – 1.7 $Å^{-1}$ was devoid of scattering (Appendix 7.4). The amount of diffraction from the phospholipid vesicles of the concentration used cannot be observed over the water background plus capillary. A single peak was present in all scattering profiles at q = 1.16 $Å^{-1}$ due to the diffraction from the Mylar used to insulate the capillary rack (Appendix 7.5).

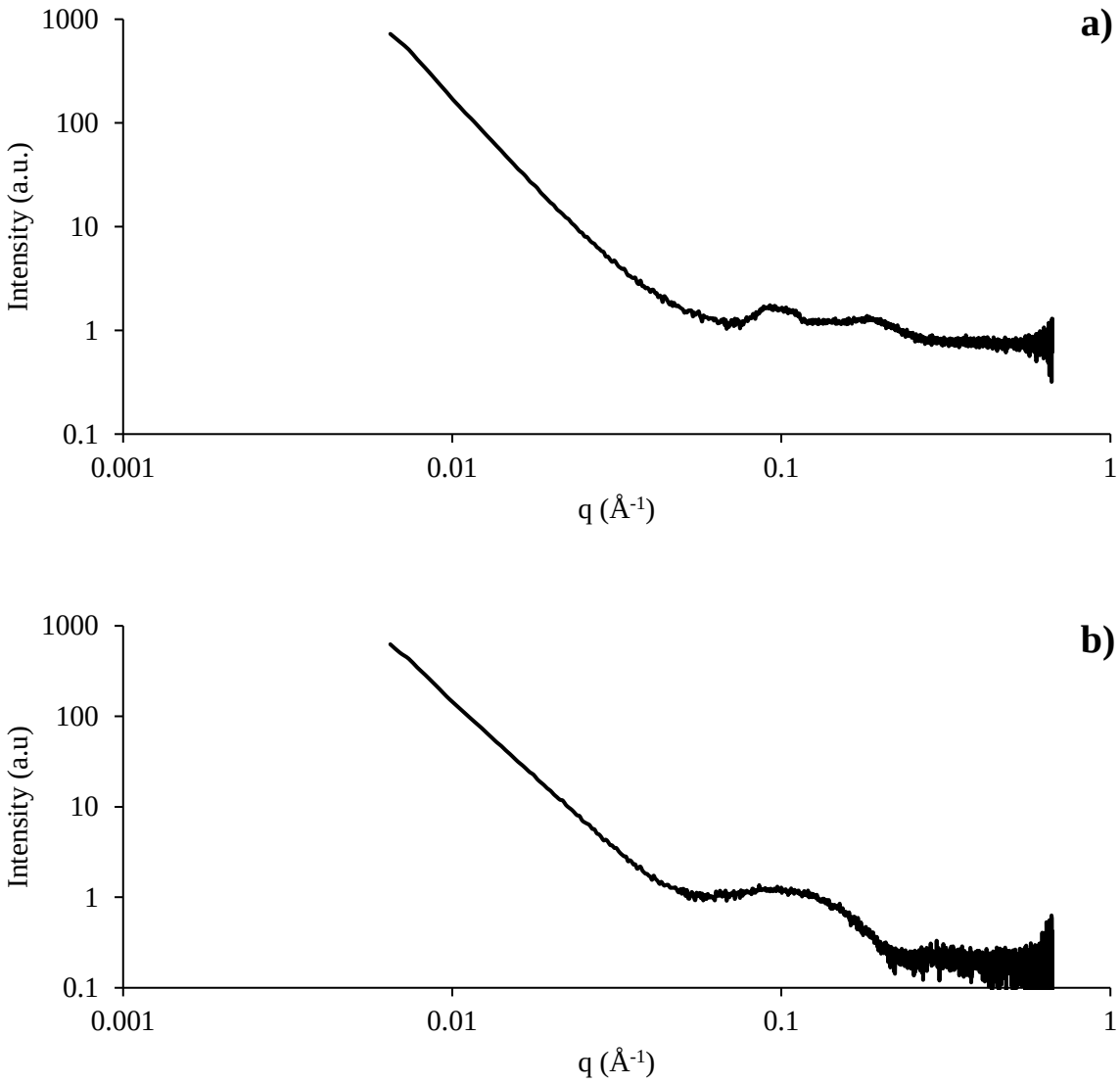

Figure 7.1. Diffuse scattering of a) soy phosphatidylcholine vesicles and b) milk fat globule membrane phospholipid vesicle

Two orders of Bragg peaks are visible at $q < 0.2$ Å^{-1} for MSM and ESM MLVs (Fig. 7.2 a, Fig. 7.3 a). These peaks represent the lamellar repeat spacing, the sum of the bilayer width of the membrane and interlamellar space (Costigan et al., 2000; Scott et al., 2019). For the MSM100 which is entirely in the S_o phase at 6.6 °C, the d-spacing of the first order Bragg refraction was 74.5 Å, which is in agreement with both preliminary data (72.6 Å, Fig. 3.9.) and literature values (75.5 Å) (Lopez, Cheng, & Perez, 2018). As temperature approaches T_m (34 °C), the hydrocarbon chains un-tilt, temporarily increasing the bilayer periodicity. The SM molecules with acyl chains longer than the C18:0 sphingosine form the fully interdigitated S_o phase where the methyl end of the sphingosine tail is directly across from the acyl chain tail (Levin et al., 1985). This polymorphism increased the lamellar repeat, the bilayer periodicity, to 77.4 Å. Further increases in temperature that complete the S_o transitions to L_d, decrease the bilayer periodicity. Moreover, at temperatures > 55 °C, the lamellar repeat of MSM100 has broadened so far that a d-spacing cannot be obtained.

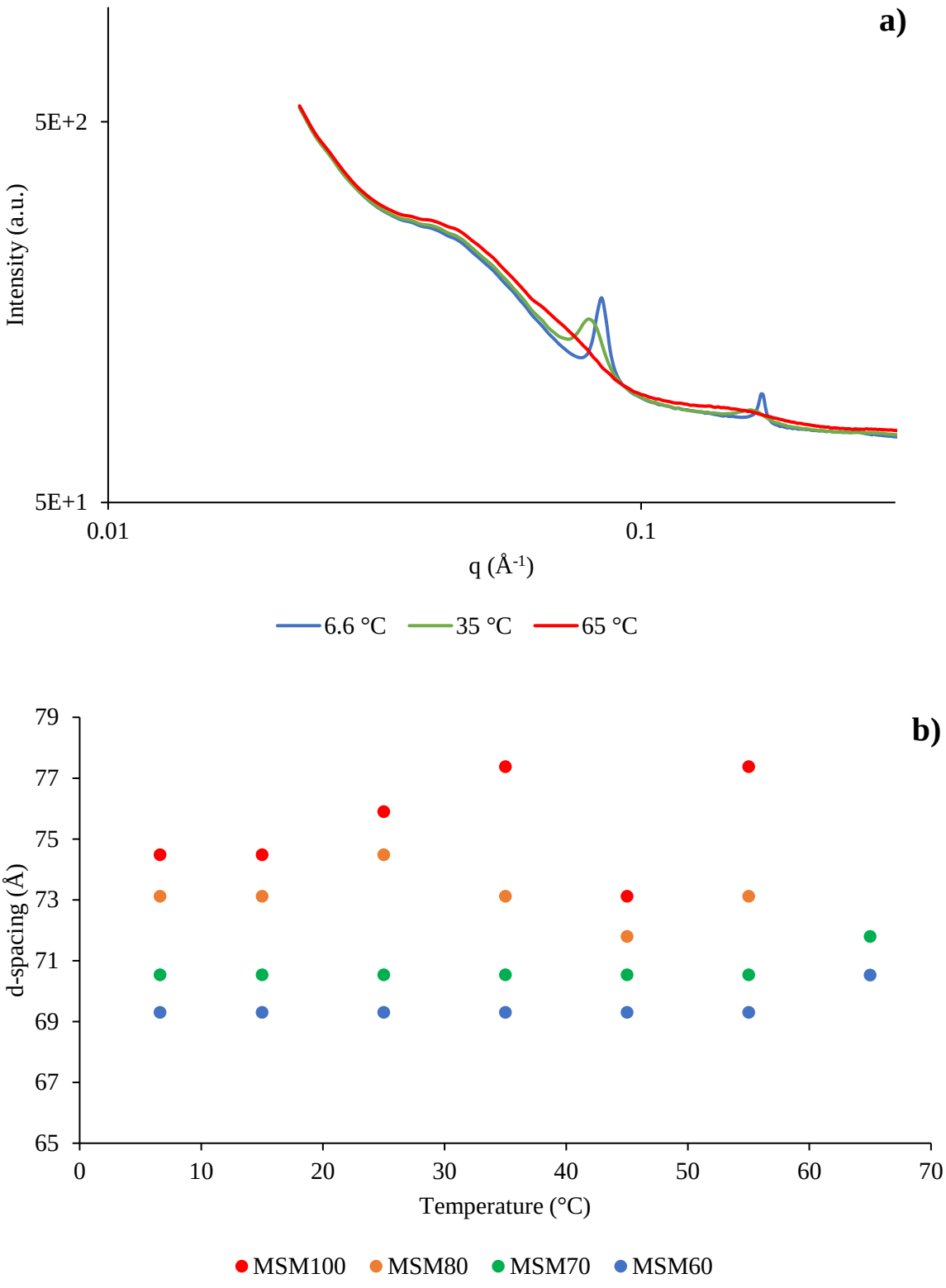

Figure 7.2. Small angle x-ray scattering of milk sphingomyelin and cholesterol multilamellar vesicles.

a) Milk sphingomyelin multilamellar vesicles without cholesterol < T_m, ~ T_m, > T_m
b) The bilayer repeat spacing of MSM100 = milk sphingomyelin without cholesterol; MSM80 4:1 mol/mol, milk sphingomyelin/cholesterol; MSM70 = 7:3 mol/mol, milk sphingomyelin/cholesterol; MSM60 = 3:2 mol/mol, milk sphingomyelin/cholesterol.

The scattering profiles of ESM MLVs without cholesterol (ESM100) were inconsistent. Below T_m, Bragg peaks were not detected (Fig. 7.3. a). It was only until 45 °C that two orders of Bragg refractions become visible at q = 0.094 and 0.189 $Å^{-1}$ (d = 66.97 and 33.25 Å, respectively) (Fig. 7.3 a). The absence of Bragg peaks at < T_m may be due to sedimentation of the vesicles and the formation of structures with different thermotropic properties to vesicles.

With the addition of cholesterol, the d-spacing of MSM MLVs < T_m decreased as an increasing proportion of the bilayer shifted from $S_o \rightarrow L_o$ (Fig. 7.2 b). As elucidated in Chapter 4, $S_o \rightarrow L_o$ transitions increase the lateral chain-chain disorder as well as intrachain disorder. An increase in disorder laterally shrinks the bilayer in a cholesterol concentration dependent manner. At the same time, the cholesterol nullifies the un-tilting of the hydrocarbon chains that occurs close to T_m (Fig. 7.3. b).

One peculiarity in the data is the increase in d-spacing when temperatures are > T_m for MSM MLVs with 0% and 20% mol cholesterol (MSM100, MSM80). As previously mentioned, the $S_o \rightarrow L_d$ phase transition is known to fluidize the membrane and increase the proportion of *gauche* isomers – it stands to reason and has been shown – the phase transition causes the bilayer width to shrink (Fig 3.9). The expansion of the interlamellar water layer offsets the reduction in d-spacing to a degree (Quinn & Wolf, 2009), but in almost all cases, the d-spacing of the L_d phase is lower than the d-spacing of the mixed interdigitated S_o phase (Maulik & Shipley, 1995; Quinn, 2013; Lopez, Cheng, & Perez, 2018). The opposite occurred in the MSM100 where the d-spacing of the MSM100 and 80 (0 and 20% mol cholesterol) increased at temperatures > T_m (Fig. 7.2 b). This phenomenon has previously been reported in ESM MLVs without cholesterol (Arsov et al., 2018); however, no explanation was provided. Furthermore, the d-spacing of an L_o phase should be lower than that of the S_o phase and higher than that of the L_d phase (Fig. 3.9.). Once again, this was not the case in Figure 7.2 and 7.3. In both phospholipid vesicle systems, the d-spacing of the vesicles with 40% mol cholesterol is consistently lower than counterparts with high phospholipid:cholesterol ratios. This peculiarity has also been previously reported in the literature (Chachaty et al., 2005), but not yet been expounded upon. For the vesicles in the current experiment, it is likely a phenomenon associated with the sedimentation of the vesicles; however, uncovering the possible structural differences between the sedimented and dispersed vesicles will required additional research efforts.

In summary, the addition of cholesterol to MSM and ESM MLV systems removes the $S_o \rightarrow L_d$, transitions and the polymorphic transformations which accompany that phase transition. The lamellar structure of high cholesterol MSM and ESM bilayers remains prominent no matter the temperature. This is apparent from the lower decrease in I (q) for the Bragg refractions of MLVs with cholesterol versus those without.

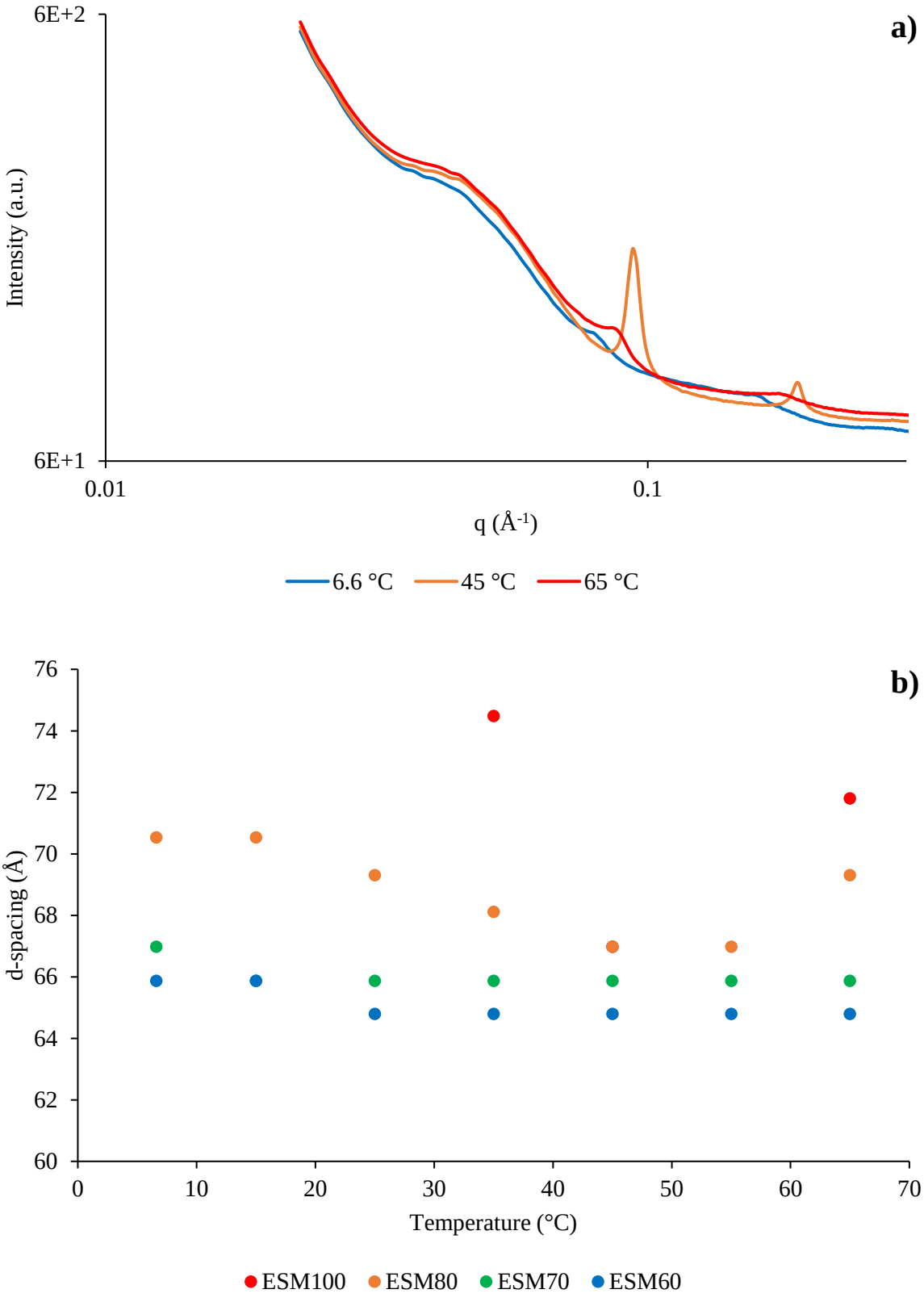

Figure 7.3. Small angle x-ray scattering of egg sphingomyelin and cholesterol multilamellar vesicles.
a) Egg sphingomyelin multilamellar vesicles without cholesterol < T_m, > T_m
b) The first order lamellar repeat spacing of ESM100 = egg sphingomyelin without cholesterol; ESM80 = 4:1 mol/mol, egg sphingomyelin/cholesterol; ESM70 = 7:3 mol/mol, egg sphingomyelin/cholesterol; ESM60 = 3:2 mol/mol, egg sphingomyelin/cholesterol.

7.3.3. Sphingomyelin and cholesterol multilamellar vesicles retain lamellarity during detergent-induced micellization by bile salts

The complexation of sphingomyelin and cholesterol in MLV systems has shown to produce detergent resistant membranes (Moschetta et al., 2002). This bile resistance preserves the bilayer order of SM and cholesterol MLVs (Tai et al., 2021). Although optical density and Raman techniques can evaluate the integrity of a vesicle, neither provides information on the lamellarity of the vesicle. Bilayer order alone gives no indication of the potential intermediate structures that emerge from the interactions between phospholipid/cholesterol vesicles, biliary micelles, and biliary PC vesicles.

When bovine bile is added to the PIPES, a peak at q = 0.133 $Å^{-1}$ (d = 48.3 Å) is present. This feature is present in all scattering profiles, indicating the feature is not the result of bile and phospholipid interactions (Fig. 7.4). This peak developed two additional orders of scattering at q = 0.26 and 0.39 $Å^{-1}$, corresponding to lamellar geometry (Miller index n = 1, 2, 3 ...) (Pullmannová et al., 2019). Lamellar peaks at the same q have been observed during the digestion of milk triglycerides (Clulow et al., 2018) and shown to be calcium soaps, precipitation formed from the binding of calcium ions and free fatty acids. The buffer used to rehydrate the bovine bile contained calcium chloride and the bovine bile was unfractionated ox gall powder, not pure bile salts (Hu et al., 2018). It is possible that trace fatty acids complexed with the calcium to form calcium soaps. At the same time, the ox gall powder is composed of 22% phospholipids (Sigma-Aldrich). The dilution of high lipid:bile salt micelles has shown to induce micelle → vesicle transition (Hjelm et al., 1988; Clulow et al., 2017).

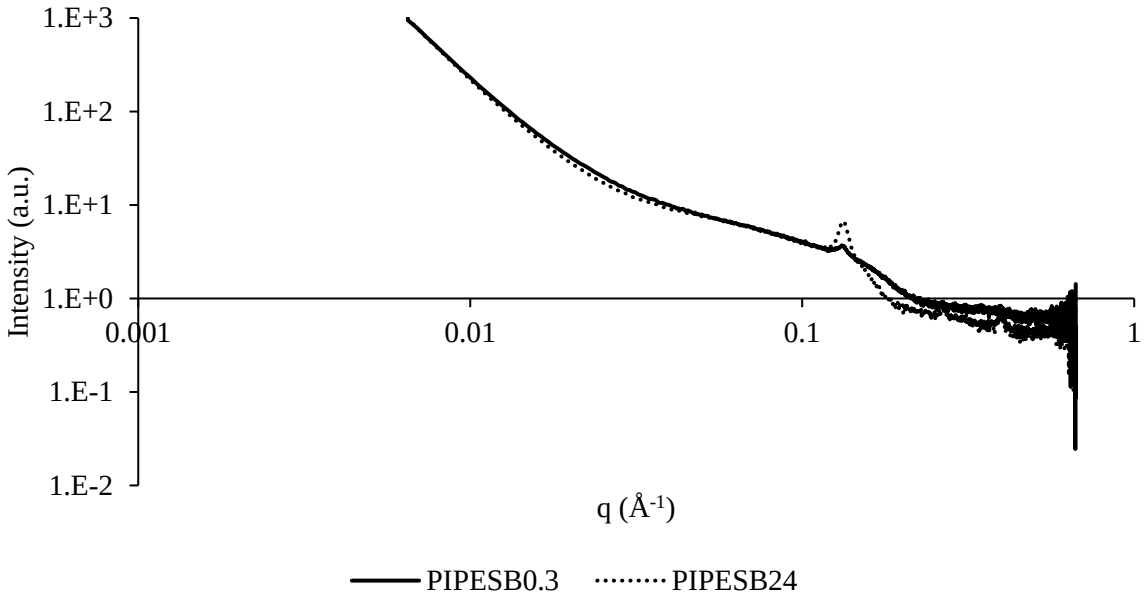

Figure. 7.4. Small angle x-ray scattering of PIPES buffer after bile addition on a log-log scale. PIPESB0.3 = 20 s after bovine bile addition; B24 = 24 min after bovine bile addition.

The change, or the lack of change, that occurs in the intensity and the position of a Bragg peak provides direct information on the status of the lamellar state of the MLV (Lopez, Cheng, & Perez, 2018). Figure 7.5 d confirms that the lamellar structure of 3:2 mol/mol MSM/cholesterol MLVs are resistant to detergent-induced micellization by bovine bile. For the two Bragg peak at q = 0.09 and 0.18 $Å^{-1}$, the diffraction pattern of the MSM60 sample remains unchanged when bile was added to the glass vessel (MSM60B0.3, MSM60 20 s after bile addition) and persist after 24 min of incubation at 37 °C (MSM60B24). The Bragg peaks associated with the lamellar phase were slightly shifted towards a higher q (lower d-spacing). This shrinkage is likely due to the incorporation of the bile salt into the L_o. Although it may at first seem counter-intuitive, the insertion of bile salts into an MLVs shrinks the bilayer – this pattern of behaviour has been demonstrated in hydrogenated SPC/cholesterol systems (Hermida et al., 2014). The insertion of a concentration of bile below the R_{sol} (the lipid:bile salt ratio to completely solubilize the membrane) lowers mechanical bilayer stability facilitating fluctuations in bilayer width (Elsayed & Cevc, 2011). This has been called a "quaking" state, where the removal of phospholipid material from the surface of the bilayer by surfactant requires phospholipids in the proximal leaflet to "flip-flop" to plug the gap in the bilayer (Nomura et al., 2001). During this "quaking" state, interlamellar water molecules are discharged, shrinking the bilayer. In the case of vesicles without cholesterol, repeated "quaking" results in the perforation of the bilayer resulting in a leaky membrane. It would seem that when the majority of the MLV is in the L_o phase, the bilayer integrity is minimally impacted.

The two broad diffraction peaks at q = 0.08 and 0.16 $Å^{-1}$ are visible for the MSM100 atop some diffuse scattering (Fig. 7.5 a). With the addition of cholesterol, these peaks become sharper. Nominally, this indicates a higher number of layers or an increased order in the bilayer – a more consistent interplanar spacing. The degree of lamellarity (vesicular nature) of a particle and its ability to retain that lamellar quality during intestinal digestion has been suggested to responsible for the anticholesteremic property of MFGM (Eckhardt et al., 2002). If SM/cholesterol vesicles are unable to be converted to micellar form, the cholesterol that comprises these vesicles is unable to be absorbed through the intestinal epithelial. The physiological temperature of digestion, 37 °C, is > T_m for MSM. From previous DSC experiments (Fig. 3.5) the MSM MLVs without cholesterol (MSM100) are predominately in the L_d phase with some S_o phase character present. The addition of cholesterol disorders the MSM lateral and intrachain bilayer order as the model membrane undergoes an $S_o \rightarrow L_o$ transition (Fig. 4.8). The reverse is occurring at 37 °C, where the fluid L_d phase is transitioning to the L_o phase, so it is not unexpected that MSM60 has sharper peaks, a more consistent lamellar character, than MSM100 (Fig. 7.5 a, d).

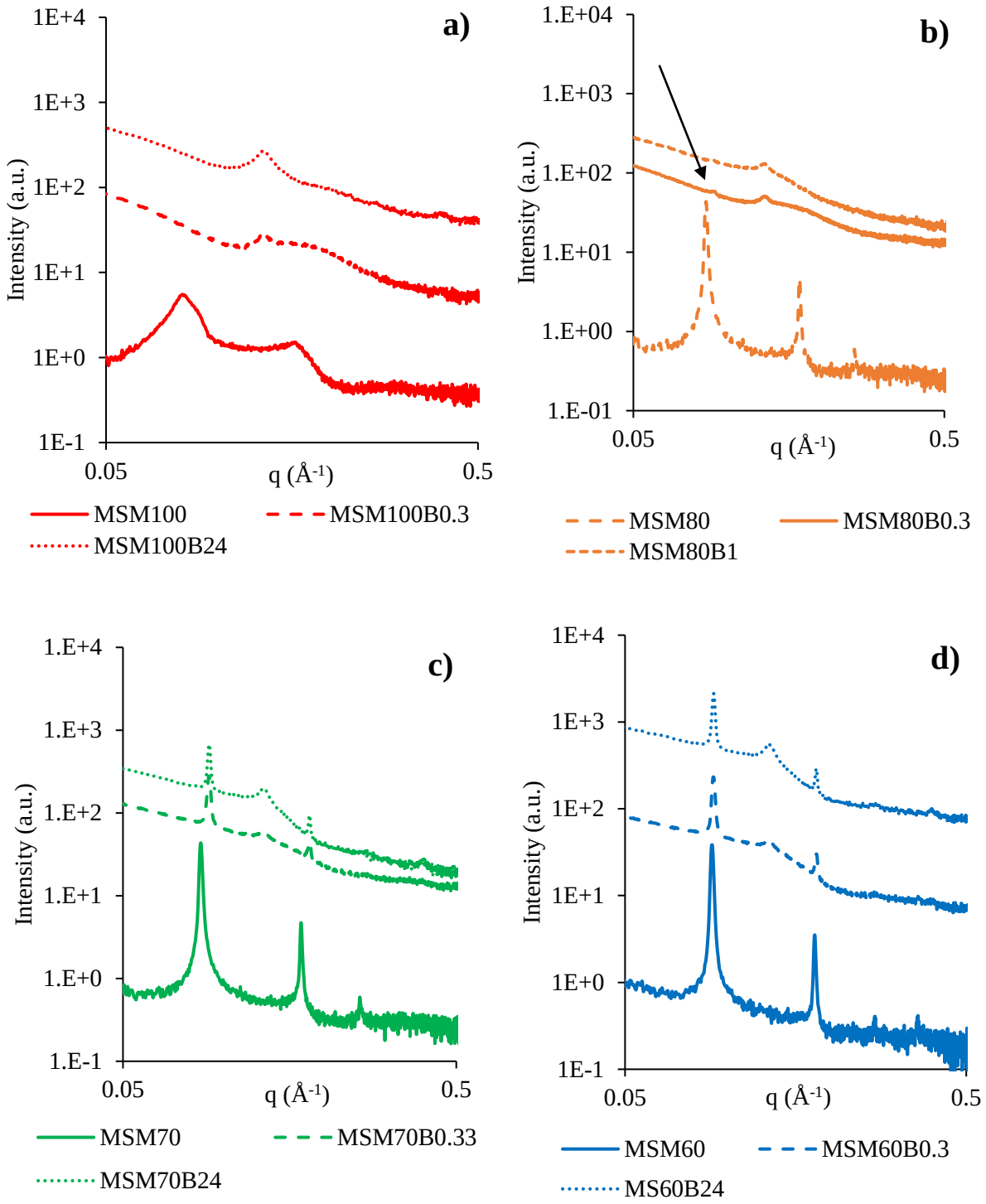

Figure. 7.5. Small angle x-ray scattering of milk sphingomyelin multilamellar vesicles on a log-log scale. Offsets in intensity values have been added for clarity.

a) MSM100 = no cholesterol; B0.3 = 20 s after bovine bile addition; B24 = 24 min after bovine bile addition.
b) MSM80 = before bovine bile addition; B0.3 = 20 s after bovine bile addition; B1 = 1 min after bovine bile addition. Arrow indicates the remnant of the lamellar repeat at q = 0.085 $Å^{-1}$.
c) MSM70 = 7:3 mol/mol milk sphingomyelin/cholesterol; B0.3 = 20 s after bovine bile addition; B24 = 24 min after bovine bile addition.
d) MSM60 = 3:2 mol/mol milk sphingomyelin/cholesterol; B0.3 = 20 s after bovine bile addition; B24 = 24 min after bovine bile addition.

The disappearance of the vesicle lamellar peaks after the addition of the bovine bile (Fig. 7.5 a) suggests that without cholesterol, sphingomyelin is equally susceptible to detergent-induced solubilization as SPC vesicles at 37 °C. The presence of cholesterol is not enough to confer a high degree of resistance to bile as seen with MSM80 (Fig 7.5 b); there is a concentration dependence at work which confirms the optical density work in Chapter 4 (*Section 4.3.2*).

The lamellar structure of MSM60 persisting at 37 °C in the presence of bovine bile may have implications in the digestive process. When MSM is consumed as is, it would be in the L_d phase, but MSM is commonly consumed as a component of the MFGM where it is complexed with cholesterol (Murthy et al., 2016). Although, it has been previously demonstrated in Chapter 5 that MFGM phospholipids are not resistant to detergent-induced solubilization and micellization, the persistence of the lamellar structure in Figure 7.5 c and d suggests it may be possible that the MSM continues to complex with cholesterol in the intestinal tract. It is important to note that in a food system, MSM and cholesterol would exist in fat globule. The lyotropic structure of triglycerides in fat globules morph in the presence of pancreatic lipase and colipase (Pham et al., 2021); therefore, it is almost the case the phase behavior of mixed micelles with phospholipid as well as triglyceride also change.

The diffraction peaks of MSM and ESM without cholesterol completely disappear with the addition of bile (Fig 7.5 b, Appendix 7.6) indicating the absence of MLVs or a concentration below the background. The first time point after bovine bile was added to MSM100 shows no Bragg peaks at q = 0.08 and 0.16 $Å^{-1}$ (MSM100B0.3). There may be residual vesicles with high phospholipid:bile salt ratios present which are unable to be detected due to their aggregation in the bile. As cholesterol content increased, the ESM and MSM MLVs became more resistant to bile salt. Inclusion of 20% mol cholesterol into MSM vesicles (MSM80) led to a slight retention of the first lamellar repeat but was shifted to higher q (lower d-spacing). This feature was short-lived, disappearing within a minute (Fig. 7.5 b) which confirms that L_o phases are resistant to bile salts at 4:1 mol/mol MSM/cholesterol. However, at such a molar ratio, the L_o domains make up a minority of the vesicle surface area. Such a small amount of detergent resistant L_o phase was unable to protect the vesicle from disruption. Based on that line of reasoning, it is clear why the bilayer order (lateral, intrachain, and total) of MSM80B was not significantly different to MSM100B (Fig. 4.7 a). At 30% mol cholesterol (MSM70), the lamellar repeats are completely visible after bovine bile addition and persisted for the duration of incubation (~30 min). The critical MSM/cholesterol ratio that dictates whether the bovine bile was capable of solubilizing and disintegrating the lamellar structure of the vesicle lies between 4:1 and 7:3. It should also be noted that even if the lamellar phase persisted throughout the incubation for MSM70 and MSM60 (Fig 7.5 c, d), the bile addition slightly reduced the vesicle d-spacing (< 1 Å).

The ESM followed a similar trend to the MSM. The only difference was that the lamellar repeat in ESM80 (20% mol) persisted throughout the incubation (Fig. 7.6). The critical ESM/cholesterol ratio

would between 1:0 and 4:1. Interestingly, this implies ESM MLVs require less cholesterol than MSM MLVs to retain lamellar structure in the presence of bile, i.e., ESM/cholesterol complexation leads to a higher degree of detergent resistance. This is not unexpected as C16:0 SM was determined to have the most favourable binding to cholesterol when compared to C14:0 – C24:0 sphingomyelin (Jaikishan & Slotte, 2011). The C16:0 fatty acid makes up ~86 % of ESM hydrocarbon chains whereas it only makes up ~16 % of the MSM fatty acids. Even though cholesterol is known to complex more favourably with more hydrophobic and saturated fatty acids, in a bilayer, the packing frustrations from the hydrophobic mismatch of the sterol and phospholipid apolar tail is also a key factor when considering detergent-resistance.

In short, the presence of the MLV Bragg peaks when bovine bile was present corresponds nicely to the resistance to bilayer order change seen using Raman spectroscopy. The lateral hydrocarbon order of MSM60 and 70 was maintained after bile addition (Fig. 4.8 a) and so was the lamellar integrity of the vesicle (Fig. 7.5 b, c). Furthermore, small-angle x-ray scattering has proven to be a useful tool when determining the kinetics of detergent-induced solubilization, capable of distinguishing between the disintegration of the lamellar structure or its persistence.

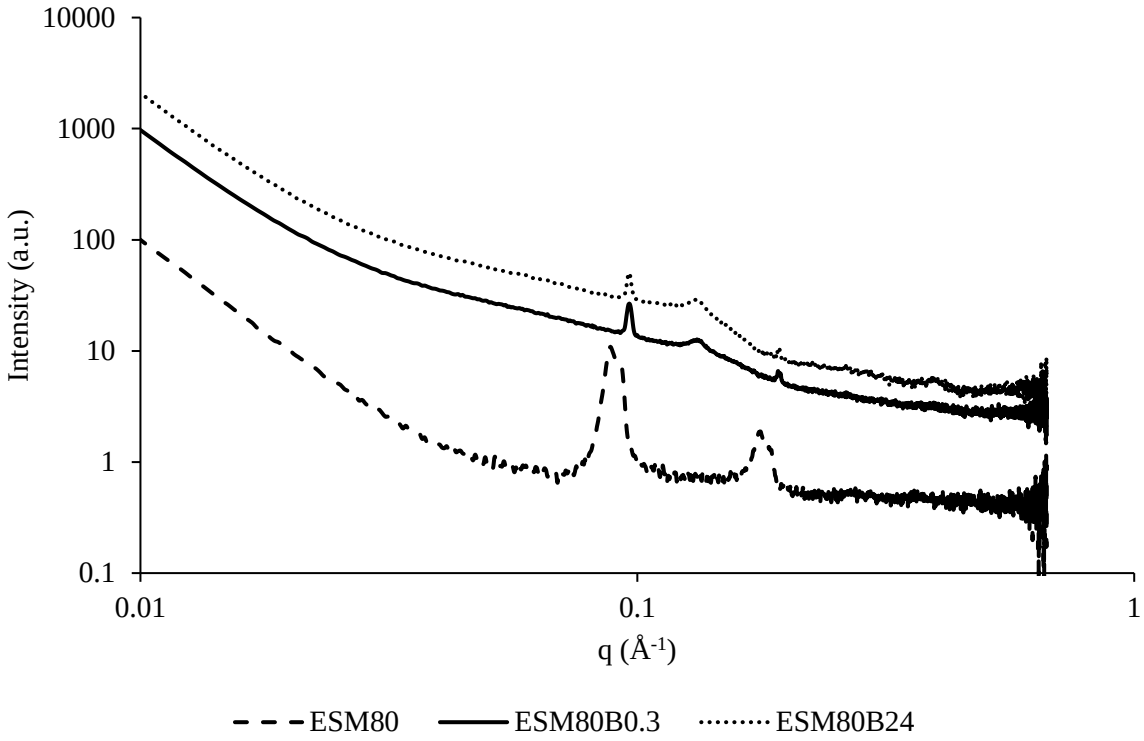

Figure 7.6. Small angle x-ray scattering of 4:1 egg sphingomyelin/cholesterol. ESM80 = before bovine bile addition; B0.3 = 20 s after bovine bile addition; B24 = 24 min after bovine bile addition.

7.3.4. Increasing cholesterol concentration reduces micellar swelling during detergent-induced solubilization by bile salt

A power-law was evident in the low-q region which indicates the presence of large aggregate particles (Jacques & Trewhella, 2010) in all of the scattering profiles. This was expected based on the TEM

images taken of the vesicles before and after bile addition (Fig 4.1). This power-law at low q was subtracted to obtain Guinier fittings (Sorensen & Wang, 1999) – a sample subtraction is present in Appendix 7.3. After the power-law was subtracted, a sufficiently wide region of the scattering profile of the control (bovine bile + PIPES buffer) and the other phospholipid vesicle dispersions still had an acceptable Guinier fitting region out to a qR_g of ~1.3. The low q region where over subtraction (negative or outlying values) occurred was neglected during the fitting. All radii of gyration (R_g) obtained from those fittings that are reported should be considered approximations (Fig. 7.7). Appendix 7.7 – 7.11 contains the Guinier fits for the first five minutes of incubation with bovine bile, for all the phospholipid vesicle systems and the control (PIPES buffer). The residual scattering was consistent with spherical or slightly ellipsoidal micelles.

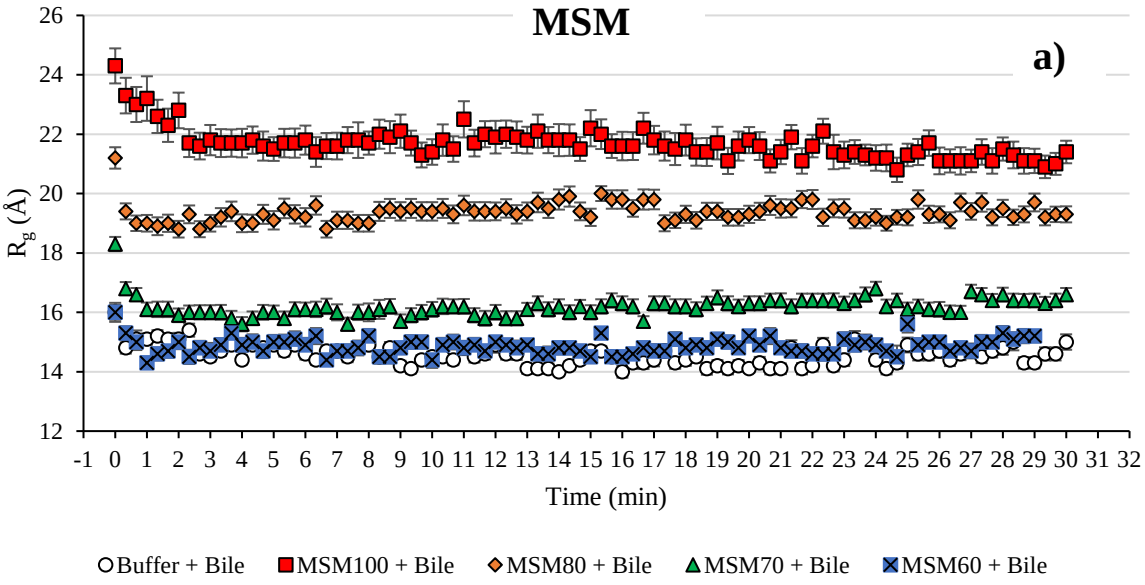
MSM
a)
R_g (Å)
Time (min)
Buffer + Bile
MSM100 + Bile
MSM80 + Bile
MSM70 + Bile
MSM60 + Bile

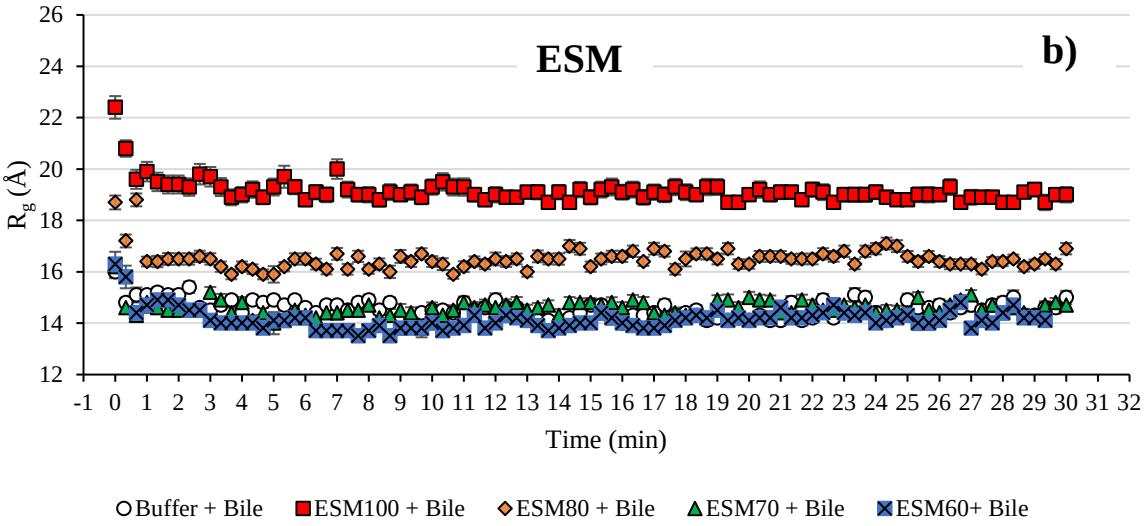
ESM
b)
R_g (Å)
Time (min)
Buffer + Bile
ESM100 + Bile
ESM80 + Bile
ESM70 + Bile
ESM60+ Bile

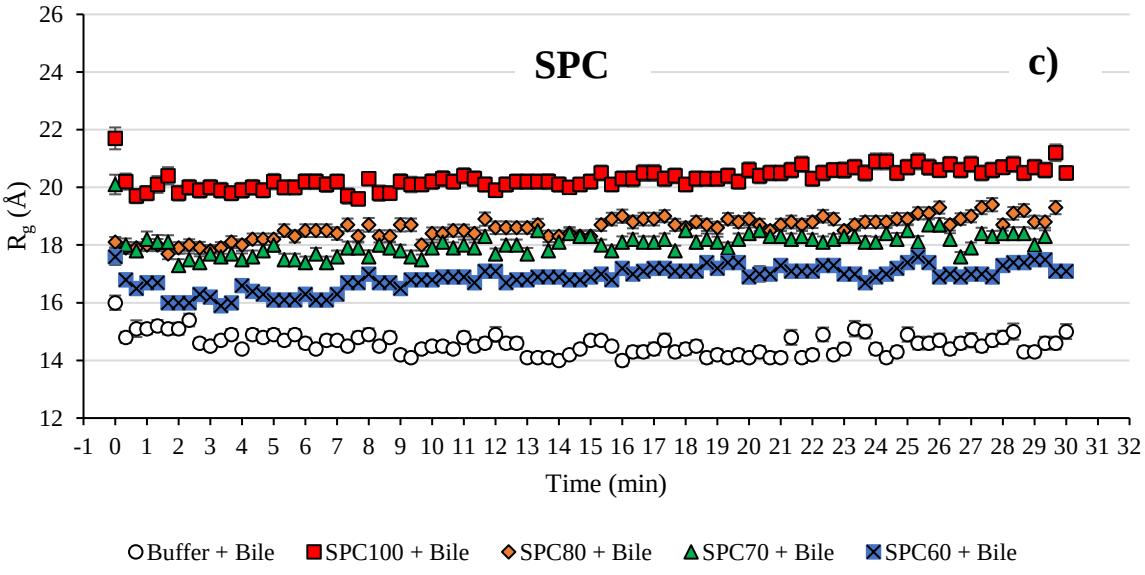
SPC
c)
R_g (Å)
Time (min)
Buffer + Bile
SPC100 + Bile
SPC80 + Bile
SPC70 + Bile
SPC60 + Bile

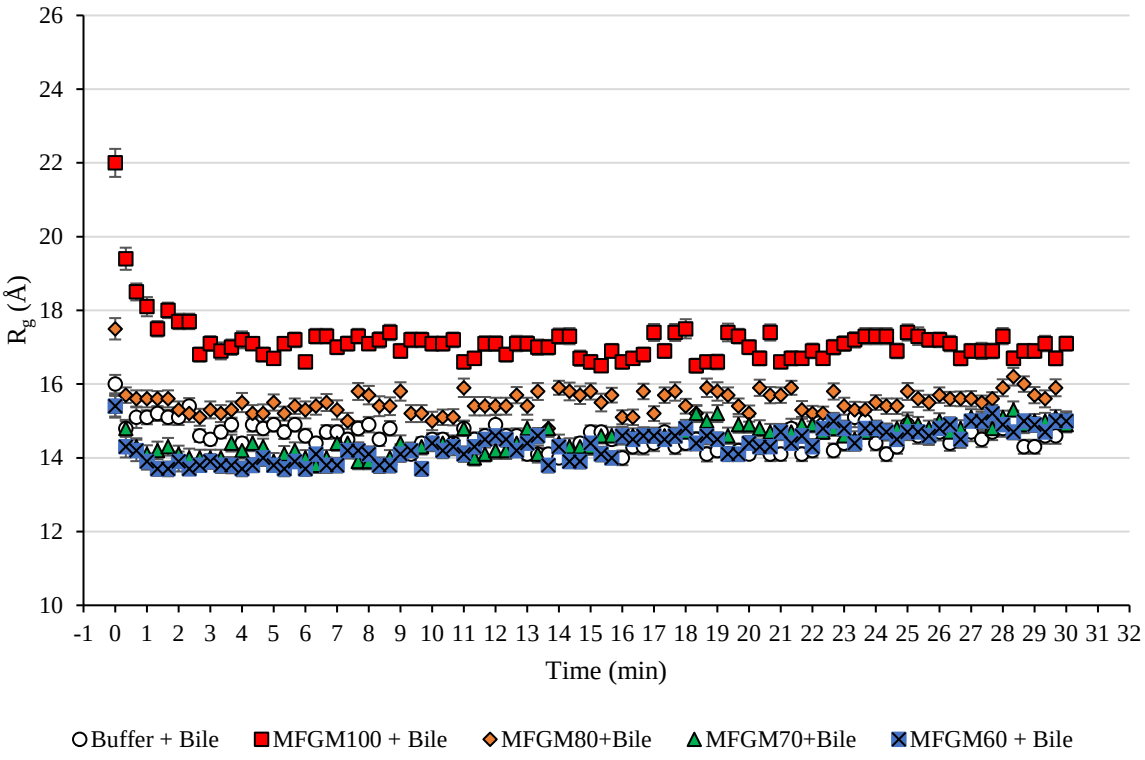

Figure 7.7. The radius of gyration (R_g) of phospholipid vesicles during incubation with bovine bile. Buffer + Bile, consists of bovine bile added to PIPES buffer and therefore did not contain any phospholipid vesicles before bile addition. Bovine bile was injected at 0 min. Each individual point is 20 s apart. The R_g of scattering profiles before bile addition were unable to be obtained due to the high amount of aggregation from the vesicles.

a) Milk sphingomyelin (MSM). MSM100 = no cholesterol; MSM80 = 4:1 mol/mol MSM/cholesterol; MSM70 = 7:3 MSM/cholesterol; MSM60 = 3:2 MSM/cholesterol.
b) Egg sphingomyelin (ESM). ESM100 = no cholesterol; ESM80 = 4:1 mol/mol ESM/cholesterol; MSM70 = 7:3 ESM/cholesterol; ESM60 = 3:2 MSM/cholesterol.
c) Soy phosphatidylcholine (SPC). SPC100 = no cholesterol; SPC80 = 4:1 mol/mol SPC/cholesterol; SPC70 = 7:3 SPC/cholesterol; MSM60 = 3:2 SPC/cholesterol.
d) Milk fat globule membrane phospholipid (MFGM). Molar ratios are based on a sphingomyelin (SM)/cholesterol basis. MFGM100 = no cholesterol; MFGM80 = 4:1 mol/mol SM/cholesterol; MFGM70 = 7:3 SM/cholesterol; MSM60 = 3:2 SM/cholesterol.

The Guinier approximations of biliary micelles were within the expected R_g range (Clulow et al., 2017). The change in the R_g of the biliary micelles as incubation progressed was used to examine the kinetics of detergent-induced solubilization by bile salts. In Chapter 4, optical density at 630 nm (OD630) was utilized to track the solubilization of phospholipid vesicles (Fig. 4.4). Changes in optical density were caused by changes in vesicle particle size and structure which could be used to extrapolate how the micelles must have been acting. The Guinier fittings measure the R_g of bile micelles as the incubation with vesicle progresses.

The detergent-induced solubilization kinetics of the phospholipid vesicles closely followed the commonly used three-stage model (Lichtenberg, Ahyayauch, & Goñi, 2013) that was explained in *Section 4.3.2.1*. Briefly, there are two critical lipid:detergent ratios, R_{sat}, the ratio when detergent

saturates the bilayer and solubilization of the bilayer is initiated, and R_{sol}, the complete solubilization of the bilayer. It was previously observed that the required lipid:bile salt ratios required to initiate and solubilize (R_{sat} and R_{sol}, respectively) phospholipid vesicles without cholesterol, such as MSM100, is lower than the ratio present when bovine bile (10 mM) is added to the phospholipid vesicle system (Fig. 4.4). Therefore, solubilization was effectively immediate.

This is reflected by the increase in bile micelle R_g values (Fig. 7.7 a – d) immediately after the addition of bile to the phospholipid vesicles without cholesterol (within 5 s). The phospholipids that make up the phospholipid vesicles are incorporated into the micelles, increasing the lipid:bile salt ratio of bile micelles which then become mixed micelles. Due to the higher lipid content, these mixed micelles were larger than the biliary micelles (~ + 4 Å). The plateau at low q after the power law has been subtracted (Appendix. 7.3) implies that even after the vesicles are solubilized, the micelles remained spherical, perhaps with a degree of elongation which is in agreement with the discoidal structure of mixed micelles (Lasic, 1988: Clulow et al., 2017).

After the initial size increase, the mixed micelles for ESM100 progressively decrease in size within the first minute (Fig. 7.7 b). The MFGM100 takes approximately three minutes to reach a steady R_g (Fig. 7.7 d). Without lipase, lipolysis of the mixed micelles should be absent. More likely, the phospholipids that make up an outer bilayer (Maldonado-Valderrama et al., 2011) of the swollen mixed micelles are redistributed until an equilibrium is reached. Although often pictured as static systems, micellar assemblies are dynamic. Biliary micelles exchange monomers with the bulk phase and the micelles themselves form and reform. These two processes are known as micellar relaxation (Patist et al., 1999). For MSM100, the mixed micelles reached an equilibrium within the first five minutes of incubation. Conversely, the phospholipid vesicles do not reach a size equilibrium until > 20 min of incubation (Fig. 4.4) and the presence of open vesicles was determined after 5 min of incubation. The question naturally becomes, if the mixed micelles reach a size equilibrium at 5 min why don't the phospholipid vesicles do likewise?

Kinetic traps such as the presence of an S_o phase and multiple lamellae can hamper the micellization of high T_m MLVs (Lichtenberg, Ahyayauch, & Goñi, 2013). Although the T_m of MSM is nominally ~34 °C, the complex array of fatty acids renders the endothermic event broad enough that only part of the transition occurs at 34 °C. The T_m of ESM is 40 °C. Equilibration between lipids in the S_o phase and detergents has shown to stall, reaching a kinetically trapped steady state where solubilization takes of the order of days to reach equilibrium (Schnitzer, Lichtenberg, & Kozlov, 2003). The steady state may include aggregates and micellar intermediates that are not present if the lipid was solubilized > T_m (Schnitzer, Lichtenberg, & Kozlov, 2003). Secondly, the solubilization of an MLV occurs layer by layer – similar to peeling an onion. Even if the bile:lipid ratio exceeds the $R_{sol,}$ each bilayer, or at the very least bilayer portions, are sequentially solubilized (Alonso et al., 1987). Though

the outer layer has been incorporated into mixed micelles and a steady state established, features that occur before R_{sat} such as detergent-induced vesicle fusion and size growth may be present (Lichtenberg, Ahyayauch, & Goñi, 2013) as inner layers are solubilized. Due to these kinetic traps, MSM solubilization is expected to lag behind the redistribution of phospholipids among mixed micelles and micellar size growth.

The SPC vesicles without cholesterol (SPC100) showed negligible size reduction (Fig. 7.7 c) during incubation with bovine bile compared to the other phospholipid model membranes. Furthermore, the SPC100 vesicles did not show an increase in OD630 that was present in both the MSM and MFGM vesicles (Fig. 4.4). It is possible that due to the phase state of SPC100 at physiological temperatures (L_d) and the high amount of unilamellar vesicles present (Fig. 7.1. a), the vesicles were rapidly solubilized, that is, there were fewer kinetic traps in the micellization process in the SPC system. The complete disintegration of vesicular structure and incorporation in the biliary micelles would explain why there was no vesicle fusion or aggregation present in the OD630 of SPC100 vesicles.

When cholesterol was incorporated into the phospholipid vesicles, the behaviour of the biliary micelles was utterly divergent to when cholesterol was absent for MSM, ESM, and MFGM (Fig. 7.7 a, b, d). No matter the type of phospholipid, when 40% mol of the vesicles consisted of cholesterol (in the case of the MFGM, 3:2 SM/cholesterol), the bile micelles did not grow to the same size as the vesicle counterpart without cholesterol (Fig. 7.7 a, b, d). Combined with the fact that the diffraction peaks did not change, the absence of a difference in R_g may indicate there was minimal phospholipid exchange between the 3:2 mol/mol phospholipid/cholesterol vesicles and the biliary micelles. The composition of biliary micelles at the end of incubation period must be different if R_g was dependent on cholesterol concentration. Considering that the lateral hydrocarbon chain order of MSM60 after bile addition is not significantly different from MSM60 (Fig. 4.8 a), it is likely that the phospholipid exchange between the biliary micelles and the MSM60 vesicle which is rich in cholesterol is low enough that lamellar integrity is not greatly disturbed (Fig. 7.5 d).

The bile micelles added to SPC60 increased in size more so than when added to the other phospholipids (Fig. 7.7 c). However, the R_g did not reach the same size as when added to SPC100, which has no cholesterol (Fig. 7.7 c). As the fatty acid composition of SPC is predominately linolenic acid, L_o domains are unlikely to dominate the vesicle. Absent a coherent structural hypothesis, the decreased size of the mixed micelles in SPC60 compared to SPC100 could be due to the lower concentration of PC present in the system. Similar to SPC100, as the incubation progressed there seems to be a positive slope (Fig. 7.7 c) indicating that phospholipid exchange between SPC vesicles and the mixed micelles continued over the 30 min incubation period.

Most surprisingly, bile micelles added to MFGM60, which was shown not to be detergent resistant (Fig. 5.5, 5.8), were similar to the control that did not contain any phospholipid vesicles before bile

was added, Buffer + Bile (Fig. 7.7 d). The hypothesis posited above to explain why the mixed micelles did not grow in size when added to MSM60 and ESM60 used a structural argument: the presence of L_o domains which are known to be resistant to bile salts prevents solubilization and therefore minimizes biliary micelles → mixed micelle transition and a subsequent increase in the mixed micellar lipid:bile salt ratio. This structural hypothesis alone is insufficient in explaining why the R_g of bile micelles added to MFGM60 did not increase in size. Bovine bile has been shown to alter the lateral bilayer order of MFGM60 systems, implying detergent-induced solubilization was occurring (Fig. 5.8.). Large unilamellar vesicles composed of 1-palmitoyl-2-oleoyl-*sn*-glycero-3-phosphocholine (POPC), a low T_m phospholipid, and > 30% mol cholesterol are known to form large, leak-resistant vesicles which coexist with the detergent micelles in the presence of detergents such as SDS and N-9 (Apel-Paz, Doncel, & Vanderlick, 2005); however, as the diffuse scattering of MFGM60 vesicles disappeared, the formation of large detergent-resistant vesicles is unlikely to be occurring. Thus, even though the lateral structures of MFGM60 vesicles were altered, the R_g of the bile micelles was similar to the bovine bile suspended in buffer (Fig. 7.7 d).

In the presence of bile, the behaviour of MFGM phospholipid vesicles is as complex as its phospholipid composition. Without cholesterol, the solubilization kinetics of MFGM phospholipid vesicles are similar to a high T_m phospholipid, like MSM (Fig. 5.5). With cholesterol, the kinetics resemble SPC which has a minimal potential to form L_o domains (Fig. 5.5). Not matter the cholesterol content, the lateral bilayer order will increase in the presence of detergent, indicative of micellization (Fig. 5.8 a). This micellization can be confirmed for the MFGM100 as the biliary micelle R_g increases when added to the MFGM100 vesicles (Fig. 7.7 d). This is not the case for bile micelles added to MFGM60 which better resembles the behaviour of biliary micelles added to MSM60 and ESM60 vesicles.

7.4. Conclusions

Using synchrotron radiation small angle x-ray scattering, the thermotropic properties of phospholipid/cholesterol vesicles and the transformation of these vesicles during detergent-induced solubilization by physiologically relevant concentrations of bovine bile was investigated.

The addition of cholesterol alters the structural and thermotropic properties of phospholipid vesicles that favourably interaction with the sterol. The structural stability and lamellar character of ESM and MSM MLVs were increased. The condensation effect of the cholesterol decreases molecular area taken by cholesterol/phospholipid complexes so that d-spacing of the vesicles in the L_o phase was lower than for vesicles in the S_o phase. The opposite was expected at temperatures > T_m. The d-spacing of the L_o phase should be higher than that of the L_d phase – this did not occur and bears further investigation.

The structural stability and higher lamellar quality aided the SM/cholesterol bilayers against detergent-induced solubilization. The lamellar repeats of these MLVs resisted detergent-induced micellization by bovine bile, albeit with the d-spacing slightly decreasing. When bile micelles were added to these cholesterol rich MLV systems, negligible micellar size growth was observed, evidence for the absence or at least a minimal amount of phospholipid incorporation into mixed micelles. When bile was added to ESM MLV systems without cholesterol, micellar R_g immediately increased after bile addition. A re-equilibration occurred and the R_g of the mixed micelles progressively decreased reaching a steady state within 1 min. For MFGM vesicle systems without cholesterol, roughly 3 min was necessary to reach a steady state. The detergent-induced solubilization of MFGM phospholipid vesicles comprised of 3:2 SM/cholesterol by bovine bile was shown to be more similar to MSM and ESM with the same cholesterol content.

The complex behaviour of MFGM phospholipid vesicles during detergent-induced solubilization by bile salts highlights the compositional and structural complexity of milk fat globule membrane phospholipids. Vesicles composed of milk phospholipids and enriched with cholesterol are both susceptible to detergent-induced solubilization but at the same, the solubilization of the phospholipid vesicles seems to negligibly affects the R_g of the bile salt micelles. During solubilization, one would expect the phospholipid from the vesicle to be incorporated into the bile salt micelles, increasing the R_g as seen with the SPC vesicles. However, this was not the case – the R_g of the MFGM60 was similar to the R_g of the Buffer + Bile, the control. One possible conclusion that can be drawn from this disparity is that although MFGM60 vesicles are solubilized, the phospholipids are not incorporated – perhaps the intermediates from the solubilization are partially resistant to bile salts. That is, as the biliary or mixed micelles saw minimal increases to R_g, no matter what structural alterations occur to the MFGM phospholipid vesicles, the micellar phase is minimally affected. This finding is unprecedented and may be key to understanding the mechanism behind the anticholesteremic effect of consuming MFGM fractions. This phenomenon is ripe for further investigation, especially in digestion-relevant settings. In the physiological digestive system, bile does not act alone, but in concert with proteases, lipase, and phospholipases. Further SAXS studies on this topic should not only include how the enzymes interact with milk phospholipids when alone and with bile, but whether a synergistic interaction between the milk phospholipids and triacylglycerides exist during digestion to better understand both the nutritional qualities and possible technological applications of dairy products.

Acknowledgements

Phospholipid vesicles samples were created in Te Ohu Rangahau Kai, Massey University and shipped to the Australian Synchrotron where Dr. Andrew Clulow from ANSTO conducted the thermotropic and detergent-induced solubilization small-angle x-ray scattering experiments. The raw data was

converted into scattering profiles with his aid before being sent to me. His assistance and feedback was also instrumental in determining the experimental design and the approach towards data interpretation.

Funding

This research was part of Australian Synchrotron Beamtime Application #16276: Liquid-ordered phases in milk fat globule membrane and its role in digestion. Funding for the sample shipping costs were provided by the New Zealand Synchrotron Group Ltd.

Notes

This chapter is currently being prepared as a manuscript for publication.

References

Alonso, A., Urbaneja, M.-A., Goñi, F. M., Carmona, F. G., Cánovas, F. G., & Gómez-Fernández, J. C. (1987). Kinetic studies on the interaction of phosphatidylcholine liposomes with Triton X-100. *Biochimica et Biophysica Acta (BBA) - Biomembranes*, *902*(2), 237–246.

Apel-Paz, M., Doncel, G. F., & Vanderlick, T. K. (2005). Impact of membrane cholesterol content on the resistance of vesicles to surfactant attack †. *Langmuir*, *21*(22), 9843–9849.

Arsov, Z., González-Ramírez, E. J., Goñi, F. M., Tristram-Nagle, S., & Nagle, J. F. (2018). Phase behaviour of palmitoyl and egg sphingomyelin. *Chemistry and Physics of Lipids*, *213*, 102–110.

Brodkorb, A., Egger, L., Alminger, M., Alvito, P., Assunção, R., Ballance, S., Bohn, T., Bourlieu-Lacanal, C., Boutrou, R., Carrière, F., Clemente, A., Corredig, M., Dupont, D., Dufour, C., Edwards, C., Golding, M., Karakaya, S., Kirkhus, B., Le Feunteun, S., … Recio, I. (2019). INFOGEST static in vitro simulation of gastrointestinal food digestion. *Nature Protocols*, *14*(4), 991–1014.

Brzustowicz, M. R., & Brunger, A. T. (2005). X-ray scattering from unilamellar lipid vesicles. *Journal of Applied Crystallography*, *38*(1), 126–131.

Chachaty, C., Rainteau, D., Tessier, C., Quinn, P. J., & Wolf, C. (2005). Building up of the liquid-ordered phase formed by sphingomyelin and cholesterol. *Biophysical Journal*, *88*(6), 4032–4044.

Clulow, A. J., Parrow, A., Hawley, A., Khan, J., Pham, A. C., Larsson, P., Bergström, C. A. S., & Boyd, B. J. (2017). Characterization of solubilizing nanoaggregates present in different versions of simulated intestinal fluid. *The Journal of Physical Chemistry B*, *121*(48), 10869–10881.

Clulow, A. J., Salim, M., Hawley, A., & Boyd, B. J. (2018). A closer look at the behaviour of milk lipids during digestion. *Chemistry and Physics of Lipids*, *211*, 107–116.

Costigan, S. C., Booth, P. J., & Templer, R. H. (2000). Estimations of lipid bilayer geometry in fluid lamellar phases. *Biochimica et Biophysica Acta*, 1468. 41 – 54.

Dewettinck, K., Rombaut, R., Thienpont, N., Le, T. T., Messens, K., & Van Camp, J. (2008). Nutritional and technological aspects of milk fat globule membrane material. *International Dairy Journal*, *18*(5), 436–457.

Eckhardt, E. R. M., Wang, D. Q. –H., Donovan, J. M., & Carey, M. C. (2002). Dietary sphingomyelin suppresses intestinal cholesterol absorption by decreasing thermodynamic activity of cholesterol monomers. *Gastroenterology*, *122*(4), 948–956.

Eggers, L. F., & Schwudke, D. (2016). Liquid Extraction: Folch. In M. R. Wenk (Ed.), Encyclopedia of Lipidomics (pp. 1–6). Netherlands: Springer.

Elsayed, M. M. A., & Cevc, G. (2011). The vesicle-to-micelle transformation of phospholipid–cholate mixed aggregates: A state of the art analysis including membrane curvature effects. *Biochimica et Biophysica Acta (BBA) - Biomembranes*, *1808*(1), 140–153.

Folch, J., Lees, M., & Sloane Stanley, G. (1957). A simple method for the isolation and purification of total lipides from animal tissues. *J Biol Chem*, *226*(1), 497–509.

Gallier, S., Gragson, D., Cabral, C., Jiménez-Flores, R., & Everett, D. W. (2010). Composition and fatty acid distribution of bovine milk phospholipids from processed milk products. *Journal of Agricultural and Food Chemistry*, *58*(19), 10503–10511.

Gallier, S., Ye, A., & Singh, H. (2012). Structural changes of bovine milk fat globules during in vitro digestion. *Journal of Dairy Science*, *95*(7), 3579–3592.

Gallier, S., Cui, J., Olson, T. D., Rutherfurd, S. M., Ye, A., Moughan, P. J., & Singh, H. (2013 a). In vivo digestion of bovine milk fat globules: Effect of processing and interfacial structural changes. I. Gastric digestion. *Food Chemistry*, *141*(3), 3273–3281.

Gallier, S., Zhu, X. Q., Rutherfurd, S. M., Ye, A., Moughan, P. J., & Singh, H. (2013 b). In vivo digestion of bovine milk fat globules: Effect of processing and interfacial structural changes. II. Upper digestive tract digestion. *Food Chemistry*, *141*(3), 3215–3223.

Gallier, S., Vocking, K., Post, J. A., Van De Heijning, B., Acton, D., Van Der Beek, E. M., & Van Baalen, T. (2015). A novel infant milk formula concept: Mimicking the human milk fat globule structure. *Colloids and Surfaces B: Biointerfaces*, *136*, 329–339.

He, S., & Ye, A. (2019). Formation and gastrointestinal digestion of β-carotene emulsion stabilized by milk fat globule membrane. *Journal of Food Process Engineering*, *42*(8), e13301.

Hu, P.-L., Yuan, Y.-H., Yue, T.-L., & Guo, C.-F. (2018). Bile acid patterns in commercially available oxgall powders used for the evaluation of the bile tolerance ability of potential probiotics. *PLOS ONE*, *13*(3), e0192964.

Hermida, L. G., Sabés-Xamaní, M., & Barnadas-Rodríguez, R. (2014). Characteristics and behaviour of liposomes when incubated with natural bile salt extract: Implications for their use as oral drug delivery systems. *Soft Matter*, *10*(35), 6677–6685.

Hjelm, R. P., Thiyagarajan, P., & Alkan, H. (1988). A small-angle neutron scattering study of the effects of dilution on particle morphology in mixtures of glycocholate and lecithin. *Journal of Applied Crystallography*, *21*(6), 858–863.

Hopkins, J. B., Gillilan, R. E., & Skou, S. (2017). *BioXTAS RAW*: Improvements to a free open-source program for small-angle X-ray scattering data reduction and analysis. *Journal of Applied Crystallography*, *50*(5), 1545–1553.

Hyde, S. (2001). Identification of Lyotropic Liquid Crystalline Mesophases. In *Handbook of Applied Surface and Colloid Chemistry* (pp. 299–332). John Wiley & Sons Inc.

Jacques, D. A., & Trewhella, J. (2010). Small-angle scattering for structural biology—Expanding the frontier while avoiding the pitfalls. *Protein Science*, *19*(4), 642–657.

Jaikishan, S., & Slotte, J. P. (2011). Effect of hydrophobic mismatch and interdigitation on sterol/sphingomyelin interaction in ternary bilayer membranes. *Biochimica et Biophysica Acta (BBA) - Biomembranes*, *1808*(7), 1940–1945.

Jash, A., Ubeyitogullari, A., & Rizvi, S. S. H. (2020). Synthesis of multivitamin-loaded heat stable liposomes from milk fat globule membrane phospholipids by using a supercritical-CO_2 based system. *Green Chemistry*, *22*(16), 5345–5356.

Lasic, D. D. (1988). The mechanism of vesicle formation. *Biochem. J*, *256*, 1 – 11.

Levental, I., Levental, K. R., & Heberle, F. A. (2020). Lipid rafts: Controversies resolved, mysteries remain. *Trends in Cell Biology*, *30*(5), 341–353.

Levin, I. W., Thompson, T. E., Barenholz, Y., & Huang, C. (1985). Two types of hydrocarbon chain interdigitation in sphingomyelin bilayers. *Biochemistry*, *24*(22), 6282–6286.

Lichtenberg, D., Ahyayauch, H., & Goñi, F. M. (2013). The mechanism of detergent solubilization of lipid bilayers. *Biophysical Journal*, *105*(2), 289–299.

Lopez, C., Cheng, K., & Perez, J. (2018). Thermotropic phase behaviour of milk sphingomyelin and role of cholesterol in the formation of the liquid ordered phase examined using SR-XRD and DSC. *Chemistry and Physics of Lipids*, *215*, 46–55.

Lopez, C., Cauty, C., & Guyomarc'h, F. (2019). Unraveling the Complexity of Milk Fat Globules to Tailor Bioinspired Emulsions Providing Health Benefits: The Key Role Played by the Biological Membrane. *European Journal of Lipid Science and Technology*, *121*(1), 1800201.

Macierzanka, A., Torcello-Gómez, A., Jungnickel, C., & Maldonado-Valderrama, J. (2019). Bile salts in digestion and transport of lipids. *Advances in Colloid and Interface Science*, *274*, 102045.

Maldonado-Valderrama, J., Wilde, P., Macierzanka, A., & Mackie, A. (2011). The role of bile salts in digestion. *Advances in Colloid and Interface Science*, *165*(1), 36–46.

Maulik, P. R., & Shipley, G. G. (1995). X-ray diffraction and calorimetric study of N-lignoceryl sphingomyelin membranes. *Biophysical Journal*, *69*(5), 1909–1916.

Moschetta, A., Frederik, P. M., Portincasa, P., vanBerge-Henegouwen, G. P., & van Erpecum, K. J. (2002). Incorporation of cholesterol in sphingomyelin- phosphatidylcholine vesicles has profound effects on detergent-induced phase transitions. *Journal of Lipid Research*, *43*(7), 1046–1053.

Murthy, A. V. R., Guyomarc'h, F., & Lopez, C. (2016). Cholesterol decreases the size and the mechanical resistance to rupture of sphingomyelin rich domains, in lipid bilayers studied as a model of the milk fat globule membrane. *Langmuir*, *32*(26), 6757–6765.

Nomura, F., Nagata, M., Inaba, T., Hiramatsu, H., Hotani, H., & Takiguchi, K. (2001). Capabilities of liposomes for topological transformation. *Proceedings of the National Academy of Sciences*, *98*(5), 2340–2345.

Patist, A., Jha, B. K., Oh, S.-G., & Shah, D. O. (1999). Importance of micellar relaxation time on detergent properties. *Journal of Surfactants and Detergents*, *2*(3), 317–324.

Patton, J. S., & Carey, M. C. (1979). Watching fat digestion: The formation of visible product phases by pancreatic lipase is described. *Science*, *204*(4389), 145–148.

Pham, A. C., Clulow, A. J., & Boyd, B. J. (2021). Formation of self-assembled mesophases during lipid digestion. *Frontiers in Cell and Developmental Biology*, *9*, 657886.

Pullmannová, P., Ermakova, E., Kováčik, A., Opálka, L., Maixner, J., Zbytovská, J., Kučerka, N., & Vávrová, K. (2019). Long and very long lamellar phases in model stratum corneum lipid membranes. *Journal of Lipid Research*, *60*(5), 963–971.

Quinn, P. J. (2013). Structure of sphingomyelin bilayers and complexes with cholesterol forming membrane rafts. *Langmuir*, *29*(30), 9447–9456.

Quinn, P. J., & Wolf, C. (2009). Thermotropic and structural evaluation of the interaction of natural sphingomyelins with cholesterol. *Biochimica et Biophysica Acta (BBA) - Biomembranes*, *1788*(9), 1877–1889.

Rappolt, M. (2006). The Biologically Relevant Lipid Mesophases as "Seen" by X-Rays. In *Advances in Planar Lipid Bilayers and Liposomes* (Vol. 5, pp. 253–283). Elsevier.

Riethorst, D., Baatsen, P., Remijn, C., Mitra, A., Tack, J., Brouwers, J., & Augustijns, P. (2016). An in-depth view into human intestinal fluid colloids: Intersubject variability in relation to composition. *Molecular Pharmaceutics*, *13*(10), 3484–3493.

Salentinig, S., Sagalowicz, L., Leser, M. E., Tedeschi, C., & Glatter, O. (2011). Transitions in the internal structure of lipid droplets during fat digestion. *Soft Matter*, *7*(2), 650–661.

Schnitzer, E., Lichtenberg, D., & Kozlov, M. M. (2003). Temperature-dependence of the solubilization of dipalmitoylphosphatidylcholine (DPPC) by the non-ionic surfactant Triton X-100, kinetic and structural aspects. *Chemistry and Physics of Lipids*, *126*(1), 55–76.

Scott, H. L., Skinkle, A., Kelley, E. G., Waxham, M. N., Levental, I., & Heberle, F. A. (2019). On the mechanism of bilayer separation by extrusion, or why your LUVs are not really unilamellar. *Biophysical Journal*, *117*(8), 1381–1386.

Sorensen, C. M., & Wang, G. M. (1999). Size distribution effect on the power law regime of the structure factor of fractal aggregates. *Physical Review E*, *60*(6), 7143–7148.

Tai, P., Golding, M., Singh, H., Waterland, M., & Everett, D. W. (2021). Cholesterol-phospholipid interactions resist the detergent effect of bovine bile. *Colloids and Surfaces B: Biointerfaces*, *205*, 111842.

Vors, C., Joumard-Cubizolles, L., Lecomte, M., Combe, E., Ouchchane, L., Drai, J., Raynal, K., Joffre, F., Meiller, L., Le Barz, M., Gaborit, P., Caille, A., Sothier, M., Domingues-Faria, C., Blot, A., Wauquier, A., Blond, E., Sauvinet, V., Gésan-Guiziou, G., … Michalski, M.-C. (2019). Milk polar

lipids reduce lipid cardiovascular risk factors in overweight postmenopausal women: Towards a gut sphingomyelin-cholesterol interplay. *Gut*, gutjnl-2018-318155.

Chapter 8 – Key findings, limitations, and future research directions

8.1. Key findings

The research undertaken has aimed to undercover the possible mechanisms underlying the anticholesteremic effect observed in human and animal studies when consuming milk fat globule membrane (MFGM) material. The primary hypothesis tested was that the putative effect was due to structural modifications of the MFGM phospholipids during digestion, decreasing both biliary and dietary cholesterol absorption in the small intestine. Particular emphasis was placed on the fate of liquid-ordered (L_o) domains which are found on the MFGM surface and comprised of sphingomyelin and cholesterol. Through *in vitro* digestion of model membrane systems, the impact of digestive factors on bilayer structure, order, and in particular L_o domains were investigated.

8.1.1. Cholesterol induces structural changes in sphingomyelin multilamellar vesicles at near-physiological concentrations

The research conducted builds upon the work: "Understanding the Structure of Bovine Milk Fat Globule and its Membrane by Means of Microscopic Techniques and Model Systems," by Sophie Gallier. At the end of the thesis, she carries out a preliminary study to set up the basis of future phospholipid bilayer model system experiments, nominally, this work. The multilamellar vesicles (MLVs) created and reported in her thesis were noted to be a few microns in size, too small to observe the surface using confocal laser scanning microscopy (CLSM). This technique was and still is the only method that can determine L_o domains on the surface of milk fat globules via direct observation.

The challenge in understanding how L_o domains behave in a digestive setting is identification and then quantification. Using a high concentration of phospholipids compensates for the difficulty in observing these model membrane systems; however, concentration dependent effects that occur during *in vitro* digestion are an additional confounding factor. The phospholipid content in liquid milk is small, only 1% of the milk lipid (Jensen, Ferris, & Lammi-Keefe, 1991); therefore, determining techniques and optimizing them to reliably detect structural changes at micromolar concentrations of sphingomyelin/cholesterol MLV systems was the primary objective of the preliminary studies conducted at the start of this work.

Differential scanning calorimetry (DSC), transmission electron microscopy (TEM), Raman spectroscopy, and synchrotron radiation small-angle x-ray scattering (SR-SAXS) are techniques capable of gathering intelligible data from milk sphingomyelin (MSM)/cholesterol MLV systems. With DSC, the T_m (melting transition temperature) of binary MSM/cholesterol vesicles was determined. The incorporation of cholesterol into the system led to a reduction of both the T_m and the enthalpy of the $S_o \rightarrow L_d$ transition. A post-transition shoulder was detected for the MSM MLVs without cholesterol (MSM100). That shoulder is likely due to high T_m SM components rather than

poor homogeneity (Lopez, Cheng, & Perez, 2018). Complete Raman spectra of MSM from 1000 to 3000 cm^{-1} were obtained and relevant peaks identified. Changes in peak intensity ratios in the CH region (2800 – 3000 cm^{-1}) that were indicative of modifications to hydrocarbon chain order were noted. Preliminary experiments in SR-SAXS showed the d-spacing (i.e., bilayer width + interlamellar space) of 3:2 mol/mol MSM/cholesterol (MSM60) was in between the S_o and L_d phases for MSM100.

The DSC and SR-SAXS results largely mirror those gathered by Lopez, Cheng, & Perez, (2018). The difference was this thesis used a phospholipid concentration much closer to physiological reality, 326 μM vs. 250 mM to obtain comparable results. Furthermore, interactions between SM and cholesterol have been investigated using Raman spectroscopy, but only to show there is a direct hydrogen bond between the cholesterol hydroxyl group and the sphingosine amide on SM (Shirota et al., 2016). Cholesterol induces significant changes to the thermotropic behaviour, structure, and molecular order of MSM vesicles. These changes are detectable in near-physiological concentrations of phospholipids, ~ 2 – 4 × what is found in whole milk (11 mg/dL) (Bitman & Wood, 1990).

The fundamental limitation of using vesicles as a model bilayer system is the water-water interface compared to the oil-water interface of the MFGM trilayer. The micellization of the MFGM outer bilayer results in the release of triacylglycerides and fatty acids which form lipolytic products when hydrolyzed by enzymes. The structural fate of lipolytic products will affect the structure of phospholipid vesicles and mixed micelles. However, as trilayers are notoriously difficult to construct *in vitro* (Gallier et al., 2015) bilayer are useful for isolating the fundamental chemistry behind phospholipid/cholesterol interactions.

As mentioned in Chapter 4, the bilirubin in the bile hindered the optical density and the Raman spectroscopy. This limitation was taken into consideration and preliminary studies had been performed with bile salts alone to confirm a trend before progressing with bovine bile. It may be possible to use simulated bile created from phospholipid vesicles and bile salts.

8.1.2. Sphingomyelin and cholesterol multilamellar vesicles resist detergent-induced solubilization by bovine bile

The biological lipid raft was erroneously first reported as a detergent-resistant membrane (Simons & Vaz, 2004) due to precipitation in cold Triton X-100 at 4 °C (Pike, 2006). As an aside, the consensus in the biological sciences is that lipid rafts are detergent resistant, but not all detergent resistant membranes are lipid rafts. In the context of the MFGM, L_o domains, which are the phospholipid foundation of lipid raft systems, have been visualized on the surface of milk fat globules (MFGs) (Gallier et al., 2010; Lopez, Madec, & Jimenez-Flores, 2010). Chapter 3 of this thesis has shown MSM/cholesterol model membrane systems possess properties associated with L_o domains: the condensation and fluidization effect of cholesterol and the absence of an $S_o \rightarrow L_d$ transition. In all

likelihood, the features that Gallier and Lopez visualized with RD-DOPE fluorescence dyes and CLSM are not entirely due to drastic rearrangement of the MFGM creating patches of electron dense material (Wooding & Mather, 2016), but assemblies of SM and cholesterol. The detergent insolubility of lipid raft systems is currently underemphasized in membrane sciences as detergent resistant membranes extracted from cells using cold detergents are not necessarily lipid rafts. In the sphere of digestion, detergent in the form of bile salts is essential to digestive function (Macierzanka et al., 2019), therefore, the question must be asked, are L_o domains insoluble in bile, and does this mean L_o domains are capable of resisting micellization?

The results from optical density and Raman spectroscopy indicated that at 3:2 mol/mol MSM/cholesterol (MSM60), the lateral and total bilayer order of the vesicle was conserved when incubated with a physiological concentration of bovine bile (10 mM) for 2 h. Optical density at 630 nm (OD630) that tracked the turbidity of the MSM/cholesterol MLV system after bile addition retained a higher optical density, i.e., turbidity, compared to MSM100. Without cholesterol, MSM100 underwent rapid micellization starting with the formation of intermediates, most likely open vesicles, around 7 min into the incubation. These open vesicles or leaky bilayers were the result of trans-bilayer solubilization (Stuart & Boekema, 2007) where the vesicle grows pores during detergent-induced solubilization by bovine bile (Fig 8.1 b). This leaky membrane allows the bile salts access to the interior leaflet or in the case of MLVs, subsequent bilayers. The same phenomena did not occur in the soy (SPC) and brain phosphatidylcholine (BPC) vesicles.

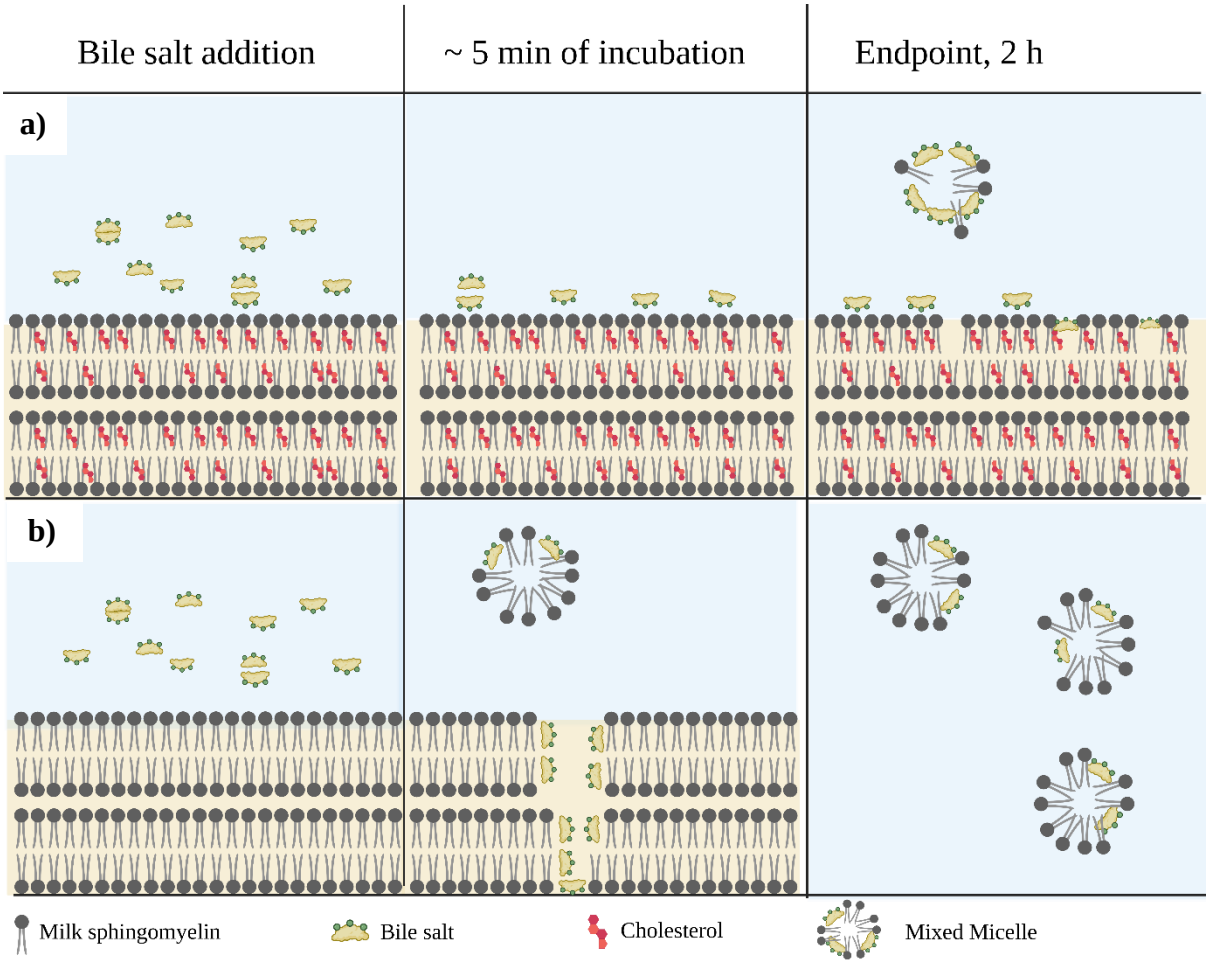

Figure 8.1. Schematic of the proposed solubilization behaviour of MSM multilamellar vesicles (MLV) at 37 °C. a) 3:2 mol/mol MSM/cholesterol bilayer. At the 2 h endpoint, bilayer order is conserved in the presence of bile salts however mixed micelles that originated from the bilayer are detected with TEM. The radius of gyration (R_g) of these micelles is similar to biliary and mixed micelles from bovine bile and PIPES buffer; therefore, minimal phospholipid is being exchanged from bilayer to micelle. Whether these mixed micelles are bile salt/cholesterol/phospholipid or only bile salt/phospholipid is unknown. b) MSM bilayer. 5 – 10 min after bile addition the MSM bilayer undergoes trans-bilayer solubilization. Not to scale. Created on Biorender.com.

Although the T_m of the MSM is ~34 °C and the optical density experiments were performed at 37 °C, there is still an appreciable amount of S_o phase that has yet to melt. The S_o phase is known to reduce the speed of micellization and encourage partial re-vesiculation as the open MLVs fuse (Schnitzer et al., 2003). These kinetically trapped intermediates can persist on the order of days for systems far below the T_m of the phospholipid. As the majority of the MSM100 vesicle is in the L_d phase, the OD630 quickly decreased, reaching an equilibrium at ~30 min. The SPC and BPC vesicles with cholesterol were immediately solubilized, the presence of cholesterol having no significant effect on the kinetics of solubilization. These results can be explained quite well with the three-stage model of micellization (Helenius & Simons, 1975). They key parameter is the detergent:lipid ratio that initiates ($R_{sat,}$ ratio of saturation) or completes (R_{sol}, ratio of solubilization) micellization. When cholesterol is incorporated into the MSM MLVs, a higher R_{sat} and R_{sol} than what is sufficient to solubilize

MSM100 is required. At 3:2 mol/mol MSM/cholesterol the necessary R_{sat} is higher than bovine bile:lipid concentration in the system (Fig 8.1 a).

Changes to the bilayer order of the three phospholipid vesicle systems were assessed using Raman spectroscopy which was also used to assess detergent-induced solubilization. An increase in the bilayer order intuitively indicates an increasingly S_o character. In the presence of bile, the result may be confounding as a high increase in lateral bilayer order is also indicative of micellization. Due to the high curvature, a mixed micelle is a smaller particle than a vesicle. This is reflected in the particle by a loss of fluidity and increased rigidity as the phospholipids and surfactant are tightly packed together, therefore a higher degree of order. The same phenomenon has been recorded using electron spin resonance techniques on milk fat globules digested with bile salts (Alshehab et al., 2019). In this case, the lack of a significant difference in the lateral bilayer order of the vesicle before and after bile addition suggests the vesicle is detergent insoluble. When there is a significant decrease in lateral chain order, micellization can be assumed to be occurring.

MSM MLVs with ≤ 20% cholesterol were susceptible to micellization but resistant to alterations in the intrachain order (un-tilting of hydrocarbon chains, *gauche/trans* rotational isomerization). Conversely MSM MLVs with ≥ 30% cholesterol were resistant to micellization but saw increases in the intrachain order. The latter is interesting, as the peak intensity ratio of the intrachain order of MSM60 and 70 after bile had been added was similar to MSM100 before bile had been added. It would seem the intrachain hydrocarbon chain order of MSM MLVs with high cholesterol content is conserved in the presence of bile salt.

Where cholesterol greatly impacts the lateral bilayer order of MSM, the sterol greatly increases the intrachain disorder of BPC and SPC vesicles at 20 °C. Intrachain disorder has traditionally been attributed to the ratio of *gauche/trans* rotational isomers (Batenjany et al., 1994); however, the I_{1085}/I_{1130} measures the hydrocarbon length (Okotrub et al., 2020) of which the proportion of *gauche/trans* rotamers is only one component. The tilt of the hydrocarbon chain is another possible factor when considering changes to intrachain order (Róg & Pasenkiewicz-Gierula, 2001).

Due to scheduling conflicts with the Raman spectrometer, the phospholipid vesicles needed to be refrigerated (4 °C) overnight before being analyzed. They were then returned to room temperature before analysis. An extended period of time at temperatures has shown to change the L_o domain behavior of MFGs (Et-Thakafy et al., 2017).

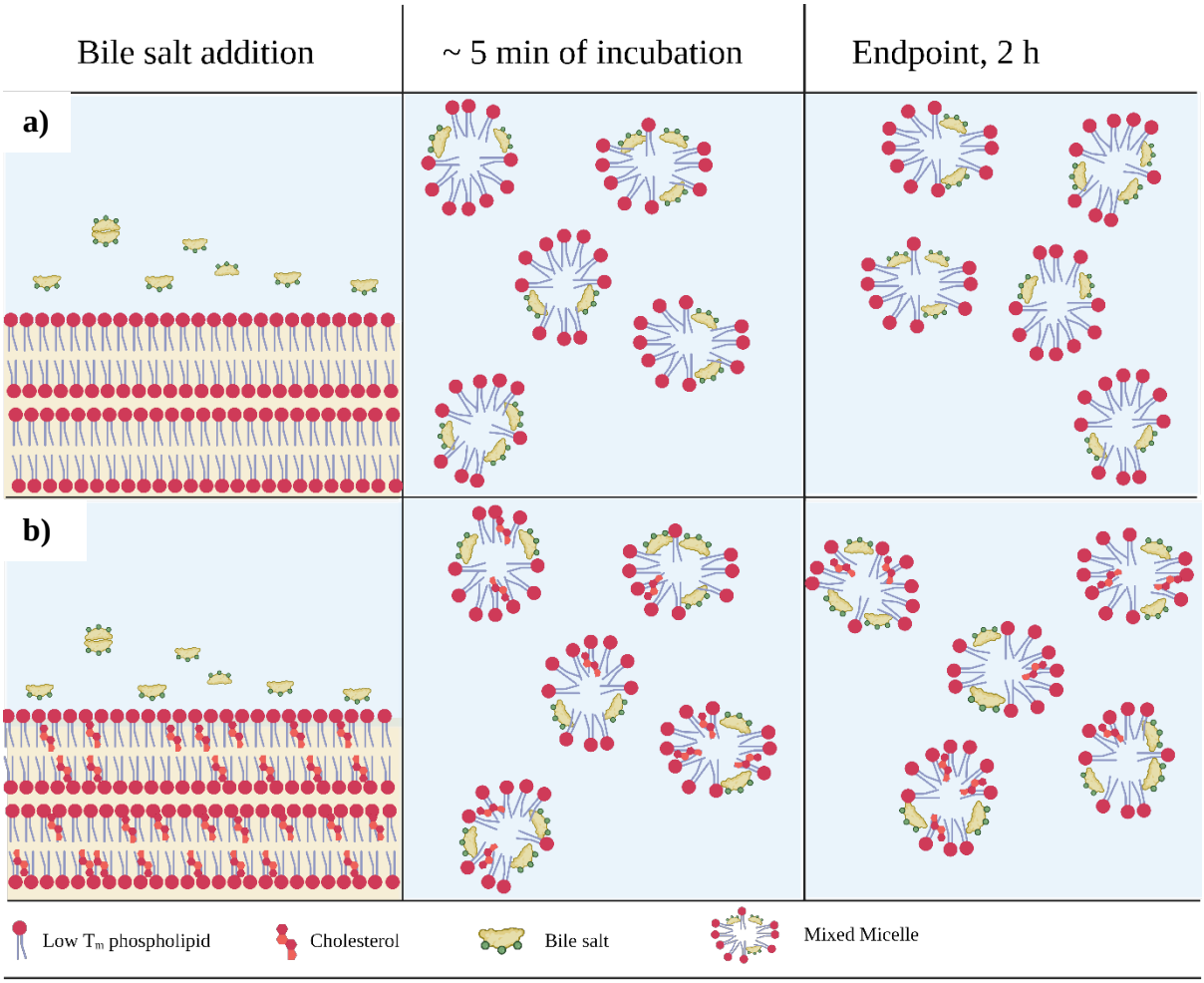

Figure 8.2. Schematic of the proposed solubilization behaviour of BPC and SPC vesicles at 37 °C. Within 5 min, the vesicles are completely micellized. a) BPC or SPC vesicle without cholesterol. b) 3:2 mol/mol BPC or SPC/cholesterol vesicles. There was no observed difference to the solubilization behaviour with and without cholesterol. Not to scale. Created on Biorender.com

The detergent-induced solubilization kinetics and the resulting bilayer order of MSM MLVs are exceedingly different to BPC and SPC (Fig. 8.2). The molecular differences between the SM and PC culminates in MSM complexation with cholesterol which allows the vesicle to resist micellization by a physiological concentration of bovine bile. Although at first glance, this result may seem simply confirmatory of literature pertaining to lipid rafts, it is an important step in elucidating the possible dietary function of Lo domains during digestion, a topic that has not yet been studied. Now that it is known Lo domains composed of a dietary phospholipid, MSM, are resistant to bile, the structural fate of the SM/cholesterol assemblies and the MFGM in the small intestine are further called in question.

8.1.3. Milk fat globule membrane phospholipid vesicles are susceptible to detergent-induced solubilization by bovine bile

Milk fat globule membrane phospholipids were extracted from beta-serum and recombined into a model vesicle system. The thermotropic behaviour of the MFGM vesicles was determined and a

small-angle x-ray scattering profile was obtained. Further experiments investigated the bile-induced solubilization kinetics of MFGM as well the bilayer order.

The steps involved in processing cream to produce beta-serum result in a particular phospholipid profile that serves as a limitation to using beta-serum extract to study the surface of the milk fat globule membrane. Two byproduct streams, buttermilk and beta-serum originate from the production of anhydrous milk fat. Buttermilk is also a direct product of butter manufacturing. In the anhydrous milk fat process stream, the buttermilk comes from the initial centrifugation of cream whereas the beta-serum comes from a final centrifugation after the phase inversion of the concentrated cream. Other than batch-to-batch differences in phospholipids, the extraction method may have led to a variable composition of the phospholipids obtained. Coupling Folch extraction with SPE is well reported to ensure the highest recovery of phospholipid from dairy foods (Pimentel et al., 2016). The variability of phospholipid extraction in food systems is quite high as seen in Table 5.1. Furthermore, the chromatograms clearly show other compounds that are not polar lipids. It would have been advantageous to identify and quantify these compounds to access the purity of the MFGM phospholipid extract.

DSC showed that the endothermic event of MFGM phospholipid vesicles that occurs during the $S_o \rightarrow L_d$ phase transition was broad, extending from 5 to 35 °C. This broadness is from the complex composition of phospholipid types and fatty acids lengths. Similar to MSM, with the addition of cholesterol, the enthalpy of transition decreases as the $S_o \rightarrow L_d$ transition dissipates, giving rise to the L_o phase. The Raman data confirmed this, as the lateral bilayer disorder increased when cholesterol was added to the MFGM phospholipid vesicles. The SAXS scattering profile of the MFGM vesicles showed weak, diffuse scattering. Bragg peaks indicating multi-lamellarity were unable to be confirmed.

With the addition of bovine bile, the detergent-induced solubilization kinetics of MFGM100 were similar to that of MSM100. There was a sharp initial decrease in OD630 followed by the formation of a transient peak at 10 min. On the other hand, with the addition of cholesterol, the kinetics of MFGM phospholipid vesicles resembled SPC and BPC – a sharp initial decrease of OD630 and further decreases until an equilibrium was reached at 30 min. The lateral and intrachain bilayer order of the MFGM phospholipid vesicles after bile addition were also similar to SPC and BPC: no detergent resistance could be observed.

Based on the DSC and Raman spectroscopy, the addition of cholesterol to MFGM phospholipid vesicles results in bilayer modifications which are consistent with the formation of L_o domains. The complexation that occurs between SM and cholesterol does not protect the MFGM phospholipid vesicle against detergent-induced solubilization by bile salt. This may seem contrary to the hypothesis being tested, that L_o domains promote detergent resistance. Yet, intuitively it makes sense when

thinking about the milk fat globule as an agent for lipid delivery. The membrane is meant to be solubilized so that the triacylglyceride and phospholipid payload can be absorbed. Furthermore, the detergent-induced solubilization kinetics of ternary MSM/SPC/cholesterol vesicles in Chapter 3 has shown that even if the MSM/cholesterol is 3:2 mol/mol, if the MSM/SPC ratio is > 0.5, the vesicles are vulnerable to detergent-induced solubilization. The SM content of the MFGM phospholipid vesicles was ~19 % mol and therefore make up a minority of the vesicle. Even if 20% of the MFGM phospholipid vesicle was in the L_o phase, as the solubilization of MSM80 showed, the vesicle would still be disrupted.

One limitation of this study is that although food components are being used, the system itself has little relevance to actual dietary conditions. The value of this experiment is in offering an avenue for future experiments that may be more physiologically relevant. For instance, the knowledge that the vesicular structure of MFGM phospholipids are broken down provides a comparison point against the MFGM which also contains transmembrane and surface protein.

8.1.4. Bile and pancreatin solubilize the detergent-resistant L_o phase

After having determined the detergent resistance of MSM/cholesterol MLVs, the next step was to submit the phospholipid vesicle systems to the INFOGEST static *in vitro* digestion protocol (Brodkorb et al., 2019). Alkaline sphingomyelinase (alk-SMase), the primary enzyme that hydrolyzes SM in the gastrointestinal tract, was added to the intestinal stage. The concentration of vesicle used in this experiment ensured that, during the intestinal stage, the vesicles had been diluted to a concentration of 326 μM. This overestimates the physiological concentration of SM that would enter the small intestine. The concentration of SM in milk is approximately 11.9 mg/dL or ~152 μM which would be further diluted by gastric and intestinal fluids. Even with vesicles at 326 μM in the intestinal phase, the bilirubin in the bovine bile caused absorbance, making discerning between the signal and noise of the Raman spectra from 1000 – 2000 cm^{-1} nigh impossible.

The gastric stage performed in this experiment was more akin to the gastric digestion of cream or other low casein, high fat dairy product than it was for whole milk. In the case of whole milk, the low pH and pepsin activity cause the casein to coagulate, forming a clot. The dynamics of the stomach create enough shear that the fat globules embedded within the protein clot will partially or wholly coalesce (Roy et al., 2021). An *in vivo* study on the gastric digestion of cream has shown that although fat globules increased in size, the presence of L_o domains in the chyme suggested the presence of intact fat globules and MFGM trilayers (Gallier et al., 2013 a). Gastric lipase has no lipolytic activity against phospholipids but will adhere onto phospholipid interfaces (Bénarouche et al., 2013). The enzyme partially penetrates the MFG trilayer and can incompletely hydrolyze the triacylglyceride core. Based on the changes in bilayer order from the Raman experiments conducted, rabbit gastric extract (RGE) which contains gastric lipase compresses the bilayer. The surface pressure on the distal

leaflet increases which results in the expansion of the proximal leaflet, allowing proximal hydrocarbon chains greater motional freedom (Fig. 8.2). Higher motional freedom corresponds to a higher proportion of intrachain disorder. Similar events occur when pancreatic lipase is added to milk fat globules (Alshehab et al., 2019). The increased motional freedom of the hydrocarbon chains also alters the thermotropic behaviour of MSM MLVs without cholesterol – the T_m increases and the enthalpy of the $S_o \rightarrow L_d$ transition decreases.

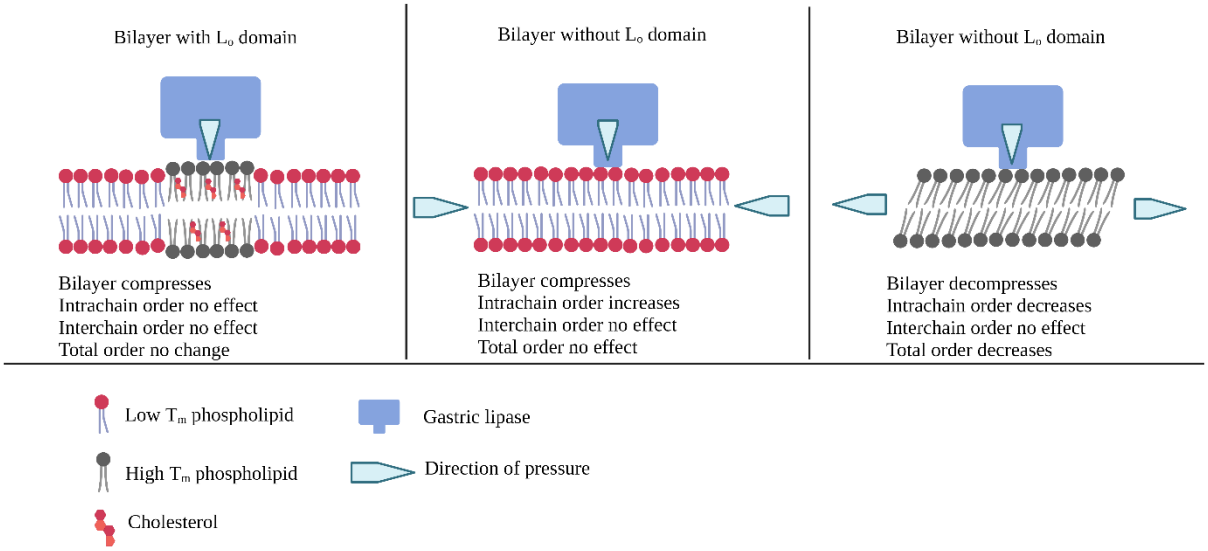

Figure 8.3. Schematic of hypothesized gastric lipase interactions with bilayers and the resulting effect on bilayer order. The high T_m phospholipids are tilted in the schematic since the Raman spectra was taken at 20 °C; however, when MSM100 underwent the gastric phase the hydrocarbon chains would have been un-tilted. For a more in-depth explanation see *Section 6.3.2.1*. The liquid-ordered domain pictured is symmetrical, asymmetrical liquid-ordered domains also exist. Not to scale. Created with Biorender.com.

The intrachain modifications of phospholipid vesicles due to RGE may be dependent on phase state. Soy phosphatidylcholine vesicles display an increased amount of order when gastric lipase is adhered to the vesicle surface. Since the lateral order of MSM MLVs is quite high, the expansion of the proximal leaflet dominates. For SPC vesicles, the lateral order is quite low, therefore increases to vesicle surface pressure dominates. Although changes to the vesicles during the gastric stage were minimal, the physics of gastric lipase adhesion are quite interesting and further study could prove essential for biotailoring emulsions or encapsulated food systems with triacylglyceride cores.

The detergent-resistance exhibited by MSM/cholesterol MLVs was no longer present when pancreatin was included in the intestinal stage. Regardless of cholesterol content, the lateral bilayer order increased, i.e., micellization of MSM MLVs occurred during the intestinal phase. On the other hand, the total bilayer order of MSM/cholesterol MLVs were not significantly different from the pre-digestion and gastric counterparts. This is some evidence that although micellization was occurring, some degree of bilayer order was conserved in MSM/cholesterol MLVs.

The BPC vesicles followed a similar trend, an increase in lateral bilayer order after the intestinal phase indicated micellization took place, and no significant difference in the total bilayer order of pre-digestion, post-gastric, and post-intestinal phases was determined. The statistical variation of the peak intensity ratios for the total bilayer order of BPC vesicles was quite high, so it is possible there was an effect that was missed. The SPC vesicles showed clear micellization and the total bilayer order of the SPC vesicles after the intestinal stage was significantly higher ($p < 0.05$) than the pre-digestion and gastric stage.

The inclusion of alkaline sphingomyelinase (alk-SMase), the enzyme found in the small intestine, and human bile that hydrolyzes dietary and biliary sphingomyelin (Nilsson et al., 2021) in the intestinal phase had no effect on the bilayer order of the phospholipid vesicles at the post-intestinal phase. Choosing a physiological concentration of alk-SMase to include was a challenge. There is abundant literature on the purification and the activity of human intestinal and bile alk-SMase; however, those enzyme activities are reported on a protein/enzyme basis (Duan et al., 1996; Nyberg et al., 1996; Duan & Nilsson, 1997; Duan et al., 2003). It proved difficult to convert enzyme activity into a protein concentration that a food product might expect to encounter during intestinal digestion. If the concentration used (0.35 nmol/min/mL digesta) was physiologically relevant, the second hurdle was that the enzyme is severely inhibited by other phospholipids, such as phosphatidylcholine (PC) (Liu et al., 2000). In an anatomically correct digestive system, this is not an issue as PC absorption occurs before SM hydrolysis in the jejunum (Nyberg et al., 1997). In a static system, the biliary PC vesicles compete for the alk-SMase active site.

This study was the first *in vitro* digestion performed that focused on the structural aspects of milk-derived phospholipids, and the first time alk-SMase was included in an *in vitro* digestion protocol in the context of examining molecular lipid structures. The digestion was effective, the synergy between bile salts and pancreatin was capable of solubilizing detergent-resistant L_o domains. Gastric lipase may not hydrolyze phospholipids, but it did alter the interchain order of the bilayer and the thermotropic properties of MSM MLVs. If L_o domains are capable of persisting during the intestinal phase, the assemblies will do so as micellar intermediates that are beyond the ability of Raman spectroscopy to detect.

8.1.5. Milk sphingomyelin and cholesterol multilamellar vesicles retain lamellar structure in the presence of bovine bile

Raman spectroscopy offers insight into the bilayer order of the phospholipid vesicles. Observing changes in bilayer order indirectly signifies structural changes. Small angle x-ray diffraction is capable of directly resolving the structure of the vesicle – furthermore, specialized equipment allows the kinetics of detergent-induced micellization to be elucidated.

Based on small-angle x-ray scattering, two orders of lamellar repeats at q = 0.08 and 0.16 $Å^{-1}$ were detected for MSM100 at 6.6 °C which gives the MLVs an S_o d-spacing of 74.5 Å. The thermotropic behaviour of the MSM MLVs were atypical. The d-spacing of the MSM MLVs without cholesterol increased up until T_m before decreasing from 40 – 50 °C then increasing once more before the peak was too broad to obtain a d-spacing (> 55 °C). Typically, the d-spacing would progressively decrease above T_m as the MLV is becoming increasingly fluid. There is no indication from the scattering profiles why the d-spacing is so high at temperatures > T_m. Furthermore, the addition of cholesterol to the MSM and egg sphingomyelin (ESM) MLVs decreased the d-spacing. This is expected at temperatures < T_m as the L_o phase is a more disordered phase compared to the S_o phase. This should not be the case for temperatures > T_m where the MLV is predominately in the L_d. For these temperature-controlled experiments, the measurements were taken from vesicles that had sedimented to the bottom of the capillary. The sedimentation indicates aggregation and perhaps even structural changes that may affected the thermotropic behaviour of the MLVs. Further investigation into the structural properties of the SM and cholesterol polymorphs may prove fruitful in determining a novel phase state or structures.

The detergent-induced solubilization of MSM is in agreement with the Raman results. Without cholesterol, MSM100 MLVs are immediately disrupted. MSM/cholesterol (4:1 mol/mol), is mostly disrupted, with a small Bragg peak present for a minute before finally disappearing. At MSM/cholesterol ratios > than 7:3, the diffraction pattern is wholly conserved. Egg sphingomyelin (ESM) proved to be more detergent resistant than MSM – only 4:1 mol/mol ESM/cholesterol was necessary to conserve the diffraction pattern throughout the 30 min incubation period. Based on the hydrophobic mismatch of sterol and hydrocarbon chains, ESM should complex more favourably with cholesterol than MSM (Jaikishan & Slotte, 2011); however, it has been shown that MSM has a greater anticholesteremic effect than ESM (Noh & Koo, 2004). The reason for this is currently unknown but is likely due to the biochemical factors in digestion rather than the thermodynamic considerations. As seen in the previous section, synergies between bile salts and enzyme can result in the solubilization of otherwise detergent resistant vesicles. Thus, detergent-resistance cannot be the primary predictor of putative nutritional effect.

By subtracting the power-law at low q that was symptomatic of vesicle aggregation, Guinier fittings of the biliary and mixed micelles were obtained after disregarding the over-subtracted region at low q. The radius of gyration (R_g) of bovine bile micelles added to PIPES buffer was roughly 16 Å, an R_g within the expected size range (Clulow et al., 2017). When bile was added to phospholipid vesicle systems without cholesterol, the R_g of the micelles increased. As the vesicles → micelle transition occurs, phospholipid is incorporated into the biliary micelles, creating mixed micelles (Lichtenberg, Ahyayauch, Goñi, 2013). Immediately after the bile was added (within 20 s), these mixed micelles begin to reduce in R_g as the phospholipids underwent re-equilibration during micellar relaxation

(Patist et al., 1999). That is, phospholipid exchange between the vesicle and micelle, as well as micelle to micelle, was occurring as the micelles relax and re-equilibrate to reach an equilibrium.

When ESM, MSM, and MFGM vesicles contained cholesterol, the R_g of the biliary micelles increased to a lesser degree. Furthermore, no re-equilibration occurred for the duration of incubation. As the diffraction peaks of 3:2 mol/mol SM/cholesterol did not change when bile was added, and the R_g of the bile micelles did not grow to the same size as the phospholipid vesicle counterpart without cholesterol, it is possible there was minimal phospholipid exchange between the biliary micelles and the vesicle. In previous sections, it has been shown that MFGM phospholipid vesicles will solubilize in the presence of detergent with the fate of the L_o domains being unknown. Considering the R_g of the bile micelles remained constant when added to the MFGM phospholipid vesicles with cholesterol throughout the incubation, one may hazard a guess that, although solubilization of the MFGM phospholipids was taking place, minimal micellization was occurring (Fig. 8.4). The intermediates produced must have mainly consisted of non-micelles or the number of micelles so few

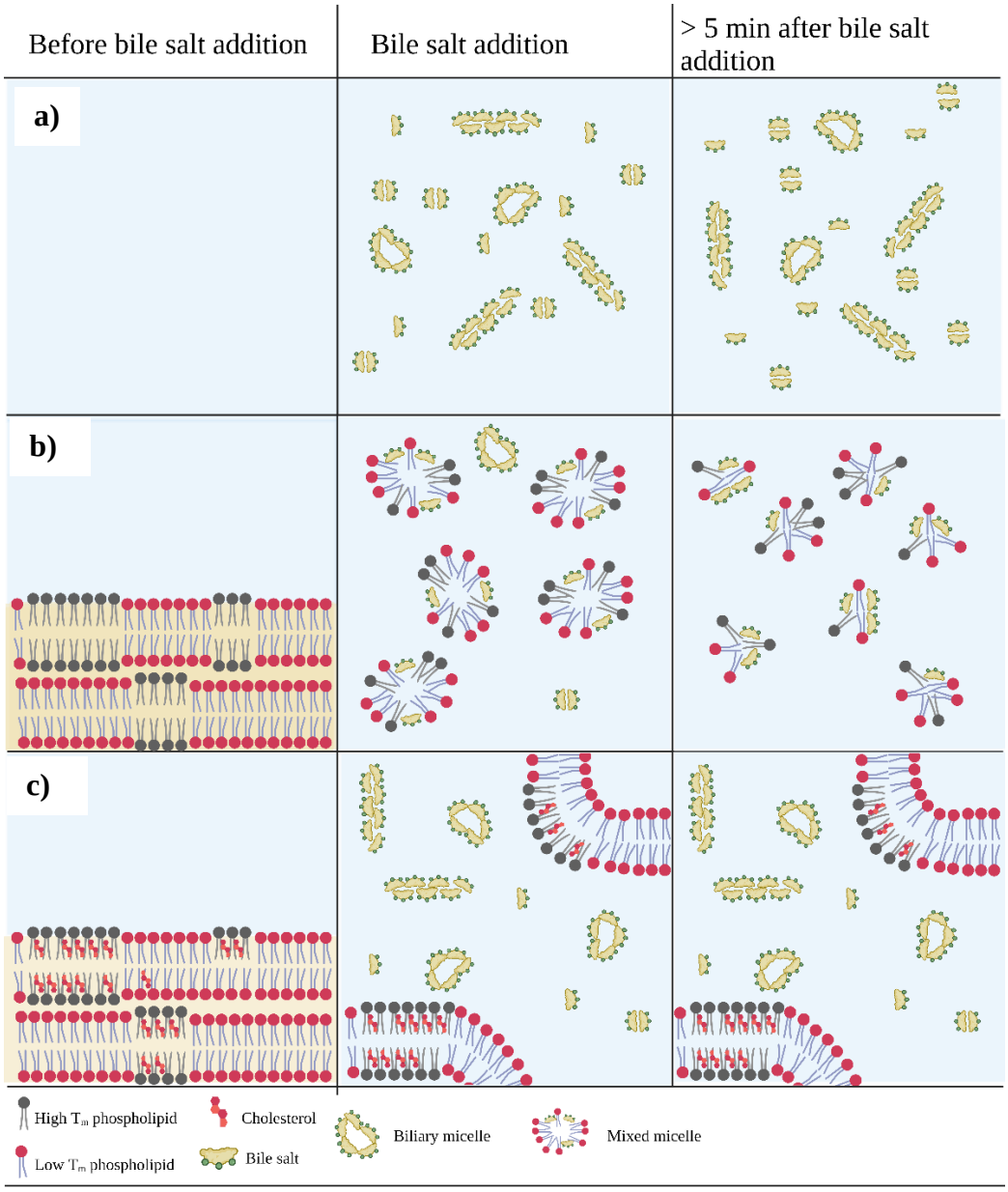

Figure 8.4. Schematic for the solubilization of milk fat globule membrane (MFGM) phospholipid vesicles by bile salts. This schematic only pertains to the activity of bile salts. Bovine bile also contains biliary phosphatidylcholine which form mixed micelles with the bile salts. Biliary phosphatidylcholine has not been included in the figure. a) control, bile salts added to buffer. b) MFGM bilayer with no cholesterol added. 5 min after bile addition the radius of gyration (R_g) of the mixed micelles decreases but is still higher than that of the control. c) 3:2 mol/mol SM/cholesterol MFGM bilayer. Both immediately and 5 min after bile salt addition, micellar R_g remains similar to R_g of control. The exact structures of the vesicle → micelle intermediates are currently unknown, but they are likely to be unilamellar vesicles.

8.1.6 Reflection of objectives and novelty of the research conducted

The research conducted has taken various well-trodden paths, the detergent-resistance of lipid rafts, the anticholesteremic effect of consuming milk phospholipids, detergent solubilization kinetics of phospholipid vesicles and combined them to synthesize a new path in investigating the lipid digestion of dairy products.

The value of the MFGM and milk phospholipids in the human diet is well documented (Dewettick et al., 2008); however, the fundamental "why" behind the bioactivity of MFGM constituents has yet to be rigorously studied. One step beyond why a component may be chemically bioactive (antioxidant, antimicrobial, etc) are the transforms and reactions that occur during digestion. Understanding not only the changes that occur during digestion, but also why those changes occur, provides a new perspective on food products.

The key novelty in this research project is the exploration of L_o domains in the context of digestion. While the physical and chemical properties of L_o domains have been quite well studied, these domains have never been explored in a digestive milieu. Exploring the digestion of L_o domains has led to a deeper understanding of how different phospholipid fractions in complex phospholipid mixtures contribute to form unique functionality. The unexplored physical chemistry between digestive components have been partially elucidated. Key novel findings include:

- The ordering and disordering effect of cholesterol and bovine bile on the bilayer order of vesicles composed of phospholipids derived from natural sources.
- The solubilization kinetics of MFGM phospholipids in the presence of bovine bile.
- Characterizing the physical interactions that occur between gastric lipase and phospholipid vesicles.
- The use of alk-SMase in an *in vitro* digestion protocol.
- The changes and absence of changes to the R_g of biliary and mixed micelles during detergent solubilization with bovine bile.

Finally, due to the physiological nature of this research topic, although all experiments have been performed *in vitro*, data has been collected on micromolar concentrations of phospholipids, similar to what one might find in milk. The results which have been obtained are comparable to experiments that have required the use of much higher concentrations of material.

8.2. Further research

As the research was conducted, a number of gaps and possible divergence points were noted. Possible future avenues of research can be categorized into two broad sections: the dietary function of L_o domains, and changes to lipid structure during digestion.

8.2.1 The function of liquid ordered domains on the milk fat globule membrane

The evidence for lipid raft systems was a breakthrough in the biological sciences and shifted the paradigm of how membranes organization was considered (Levental et al., 2020). The discovery of L_o domains on the milk fat globule membrane has not been met with as much fanfare, but merely seen as an interesting footnote. Milk is one of the only naturally produced biological secretions that is meant to be consumed by neonates. It is not too much of a leap to consider that evolution has designed the

MFGM to include L_o domains. If nature has designed the MFGM to include L_o domains and the MFGM is a product that is designed to be consumed, these assemblies have two possible roles: a purely structural function, insuring delivery of the other MFG components, a nutritional function, providing a putative nutritional benefit, or both – a synergy that exists between the structural function and the nutritional function.

This work takes the latter position, that the L_o domains where membrane cholesterol is localized reduces micellization and therefore impacts the absorption of dietary and biliary cholesterol. The other major hypothesis for the function of L_o domains is to serve as a decoy for strains of pathogenic bacteria (Sprong, Hulstein, & van der Meer, 2002). In biological systems, host lipid rafts serve as the entry point for viruses and other pathogens (Mañes et al., 2003; Ripa et al., 2021). In the small intestine, the pathogens that adhere to the MFGM components would be excreted, protecting the neonate from infection (Sprong, Hulstein, & van der Meer, 2002).

Lipid rafts in biological systems are considered elusive (Munro, 2003). Investigating dietary L_o domains during digestion is similar to attempting to find a needle in a haystack. Of the techniques used, TEM was to the only method where it was possible to visually confirm the subject of study; however, TEM lacks the ability to distinguish different phase states. Furthermore, the style of TEM used, negative stain, was incapable of clarifying the lamellarity of a vesicle. Cryo-TEM whenever possible is recommend to confirm the lamellarity of phospholipid vesicles.

The other techniques applied were also unable to definitively indicate an L_o domain, so an assessment of the phase state was made by comparing phospholipid vesicles with varying cholesterol concentrations and measuring the impact of the cholesterol on the system. Nuclear magnetic resonance and optical traps are two techniques not employed in this study, but which could further advance the field. Deuterium labelling of the sphingomyelin incorporated into model membranes and conducting 2 (H)-NMR has been used to determine bilayer order and mobility (Keyvanloo et al., 2018). This method has also been used in investigating whether the elusive hydrogen bond between the amide group of SM and the hydroxyl group of cholesterol exists (Guo et al., 2002). Nuclear magnetic resonance is rarely applied to dairy phospholipids beyond identification (Maher & Rochfort, 2014), but has proved to be a useful tool to study *in vitro* lipolysis (Nieva-Echevarría et al., 2016). After optimizing the experimental parameters, it may be possible to obtain a higher degree of information using NMR techniques on the phospholipid orientation and phase state after the gastric and intestinal stages. During the time when this work was conducted, Friddin et al., (2019) developed an optical trapping technique that allowed for the direct manipulation of L_o domains in giant unilamellar vesicles. The heat from the laser can induce phase transitions in individual vesicles (Friddin et al., 2019). Coupled with microfluidics technology and Raman spectroscopy, it may be possible to investigate exactly how the bilayer order of a single vesicle changes during *in vitro*

digestion. This optical tweezer technique is one method to overcome a severe limitation of the current Raman regimen; the current Raman data cannot observe a single L_o domain, only the average spectra of one or an aggregate of phospholipid vesicles are being taken. While this is useful for determining micellization of the vesicle, it is much less sensitive than observing the changes in order for a single domain.

This work has attempted to produce multilamellar vesicles as the model membrane system. Although more difficult to make, GUV are another possibility. Due to their unilamellar nature, Bragg peaks could not be measured using SAXS; however coupled with optical trapping and Raman spectroscopy it may be possible to directly obtain spectra of L_o domains, rather than an aggregate of multiple vesicles.

One limitation that needs to be addressed in studies that use vesicle systems, is storage time and temperature. Whenever possible, data should be collected immediately after incubation or digestion. Due to the length of time necessary for digestion protocols, this is not always possible. Refrigeration, storage at 4 °C after inihibition of enzyme is the common way to preserve the vesicle. Studies on the morphologies of L_o domains in MFG after cooling show phase separation that between the S_o phase that arises from saturated phospholipids that are not in association with cholesterol and the L_d phase (Et-Thakafy et al., 2017). Prolonged storage at this state is speculated to result in mechanical heterogeneities in the bilayer which could have functional consequences.

Throughout this work, L_o domains have been correlated with phospholipid assemblies, but that is not the case in the native MFGM. Both phospholipids and proteins play an important role in the structure of the MFGM. The primary function of the lipid rafts in cellular systems is to serve as a mobile protein recruiting platform (Simons & Ikonen, 1997). Protein localization is visible on the surface of the MFGM. For instance, glycoproteins which are part of the MFGM glycocalyx are not associated with L_o domains (Lopez, Madec, & Jimenez-Flores., 2010). In the native MFGM, L_o domains are laterally interspersed throughout the membrane (Gallier et al., 2010; Et-Thakafy et al., 2017) whereas the liquid-ordered phase in model membrane systems is a large phase-separated platform (Zheng et al., 2014). Although it is unlikely that trans-membrane proteins should exist within L_o domains, raft associated proteins such as GPI-anchored proteins exist in biological systems (Lucero & Robbins, 2004). Additional work on the localization of proteins on the surface and within the MFGM in relation to the phase state of the globule would be a novel research path.

There is a clear trend of following the progress of the biological sciences when evaluating the future research direction of MFGM L_o domains. The current focus should be on developing more robust methods for L_o domain detection during *in vitro* digestion of model systems. The long-term goals would be to apply the same techniques to track the structural alterations of these microdomains in actual food systems, such as cheese, after dynamic *in vitro* or even *in vivo* digestion.

8.2.2 Additional considerations for investigating the in vitro digestion of milk fat globule membrane phospholipids

To the author's knowledge, this was the first *in vitro* digestion experiment performed on milk phospholipid vesicles. In the process of conducting this set of experiments, various opportunities for further research were observed. These include the further investigation into the kinetics of lipolysis by pancreatic lipase, the impact of fat globule size, the effect of processing, and the effect of sphingomyelin and hydrolysis products on the microbiome.

The first limitation of a bilayer system is that the native milk fat globule membrane is a trilayer system. With this in mind, a bilayer system can only accurately model what occurs in the outer bilayer of a milk fat globule. Recombining MFGM phospholipids and producing vesicles of that extract combines monolayer and bilayer phospholipids, thus, the bilayers produces are not wholly representative of the MFGM phospholipid bilayer structure either. Until trilayer systems become widely available, these bilayer systems are the closest proxy we have to a MFGM.

One large limitation of investigating structural assemblies in digestive systems are impurities. Not only are impurities present due to extraction, but unless pure bile salt and enzyme are used in the *in vitro* digestion, side reactions occur and interference is present. This was most obvious in Chapter 4 where the presence of bilirubin in the rehydrated bovine bile resulted in unwanted absorbance. At the same time, if the goal is to eventually understand phospholipid systems *in vivo*, it is necessary to use *in vitro* models as close as physiologically possible – the body does not utilize pure bile salt or pure enzyme, they exist in complex solutions.

Two major experiments were the detergent-induced solubilization by bile salt and the *in vitro* digestion of phospholipid vesicles. A gap between these two experiments is the investigation the digestive enzymes without bile on the vesicle systems. There is an argument to be made that such a study is extraneous as the activity of alk-SMase is dependent on bile salt. Incubating the vesicles with pancreatic lipase alone may provide a deeper understanding of enzyme-phospholipid interactions. Investigating these phospholipid-enzyme interactions through SAXS would prove complementary to the studies focused on the lyotropic phases that occur during the lipolysis of bovine milk triacylglycerides (Clulow et al., 2018). These studies demonstrate a large limitation in the present studies – milk phospholipids are rarely digested alone. In the case of milk fat globules, the phospholipids are digested with triacylglycerides and in the case of butter milk or beta-serum, proteins such as casein or whey proteins. As our understanding of what structural changes occur to phospholipids during lipolysis, we must also be able to reconcile how these compounds will be interact or fail to interact with lipolytic or proteolytic components.

Outside of the scope of this thesis, but deeply connected is the question of whether structural changes to the intestinal micellar phase have an observable effect on cholesterol absorption. This question has

been partially investigated by Eckhardt et al., (2002) who showed a difference in cholesterol absorption by Caco-2 cells when provided a milk sphingomyelin or egg yolk phosphatidylcholine suspension. Future pre-clinical studies including typical cell models should focus on simulating the physiological absorption process as closely as possible with either ternary vesicle systems or even phospholipid extracts.

The nutritional consequence of fat globule size has risen as a topic of interest in the dairy food sciences. Fat globule size has shown to be dependent upon, or the result of differences in membrane phospholipid and protein content (Lopez et al., 2011; Mesilati-Stahy et al., 2011). As the phospholipid architecture of large and small milk fat globules are different due to alternative directions through the biosynthetic pathway, it may be possible that the digestion (kinetics, alterations in structure, intermediates form) may differ between differently sized milk fat globules. In the same vein, the MFGM phospholipids used in this work were extracted from beta-serum which has a higher PE, but lower SM content compared to liquid whole milk (Yao et al., 2016). It would be worthwhile to study the digestion of phospholipid vesicles constructed with MFGM phospholipids extracted from buttermilk powder against those of beta-serum and from raw milk. Buttermilk powder and beta-serum are currently seen as low value byproducts to be used as emulsifiers or thickeners. An in-depth look at the digestive behaviour of these byproducts may unlock value beyond physical functionality.

For research on dairy phospholipids, the material is either obtained from beta-serum, buttermilk powder or raw milk. The latter is not commonly consumed due to the greater potential for microbial contamination. Both pasteurization and homogenization are known to alter the MFGM surface. Serum proteins, α-lactalbumin and β-lactoglobulin, bind to the surface of the fat globule when heated above 65 °C (Corredig & Dalgleish, 1996) and various membrane proteins associated with lipid synthesis and boosting immunity are heat-labile (Ma et al., 2019). Homogenization disrupts the membrane – the decrease in fat globule size and increased relative surface area means there is not enough membrane material to encapsulate the fat globules (Lee & Sherbon, 2002). Casein adsorbs onto the surface of the membrane to plug the gaps while changing the electrostatic and hydrophobic properties of the fat globule (Obeid et al., 2019), thus altering lipase binding (Reis et al., 2008). Tracking the fate of polar lipids during the digestion of these systems is a promising, novel, and applicable area of research.

Recently, there has been much interest in understanding the link between the milk fat globule membrane and a healthy microbiota (Thum et al., 2020; Chichlowski et al., 2021; Wu et al., 2021; Ye et al., 2021). With a greater emphasis on personal health, an increased awareness of colonic health, and more accessible computing power, investigating the fermentation of dairy products by gut microbial communities may even become a mandatory practice in holistic digestion studies.

8.3 Closing remarks

In conferences and symposiums, I have often been asked: what is the novelty of this research?

I've been told the individual components, the complexation of sphingomyelin and cholesterol, the kinetics of detergent-induced solubilization, and the digestion of milk fat globules are published in the literature. The results obtained from each experiment that compose my work are for the most part in agreement with current literature and therefore the conclusions are seemingly confirmatory in nature.

Although this work has not answered how sphingomyelin affects cholesterol absorption, the novelty of lies within applying the aforenoted fundamental interpretations and optimizing the techniques used to investigate a more complex system (MFGM phospholipids). The complexation of sphingomyelin and cholesterol has been noted; the kinetic model of detergent-induced micellization is widely spread; and there is a model of milk fat globule digestion in circulation. These have all been guides and tools for my research. If the sum that is produced is greater than the parts, then the sum much also be more complex than the individual parts. If the conclusions drawn have sounded confirmatory, then it is because after stringing together all this seemingly disparate fundamental science through rigorous experimentation, the conclusions still hold true. These fundamental principles are applicable to answering the simple sounding question of, "what happens to L_o domains during digestion?" and, "will L_o domains impact how cholesterol is absorbed?" These are two questions have been pondered (the latter more so than the former) but never attempted to be answered. This has been the first attempt – I hope there will be more.

References

Alshehab, M., Budamagunta, M. S., Voss, J. C., & Nitin, N. (2019). Real-time measurements of milk fat globule membrane modulation during simulated intestinal digestion using electron paramagnetic resonance spectroscopy. *Colloids and Surfaces B: Biointerfaces*, 110511.

Batenjany, M. M., Wang, Z., Huang, C., & Levin, I. W. (1994). Bilayer packing characteristics of mixed chain phospholipid derivatives: Raman spectroscopic and differential scanning calorimetric studies of 1-stearoyl-2-capryl-sn-glycero-3-phosphocholine (C(18): C(10)PC) and 1-stearoyl-2-capryl-sn-glycero-3-phospho-N-trimethylpropanolamine (C(18): C(10)TMPC). *Biochimica et Biophysica Acta (BBA) - Biomembranes*, *1192*(2), 205–214.

Bénarouche, A., Sams, L., Bourlieu, C., Vié, V., Point, V., Cavalier, J. F., & Carrière, F. (2017). Studying gastric lipase adsorption onto phospholipid monolayers by surface tensiometry, ellipsometry, and atomic force microscopy. In *Methods in Enzymology* (Vol. 583, pp. 255–278). Cambridge: Elsevier.

Bitman, J., & Wood, D. L. (1990). Changes in milk fat phospholipids during lactation. *Journal of Dairy Science*, *73*(5), 1208–1216.

Brodkorb, A., Egger, L., Alminger, M., Alvito, P., Assunção, R., Ballance, S., Bohn, T., Bourlieu-Lacanal, C., Boutrou, R., Carrière, F., Clemente, A., Corredig, M., Dupont, D., Dufour, C., Edwards, C., Golding, M., Karakaya, S., Kirkhus, B., Le Feunteun, S., … Recio, I. (2019). INFOGEST static in vitro simulation of gastrointestinal food digestion. *Nature Protocols*, *14*(4), 991–1014.

Chichlowski, M., Bokulich, N., Harris, C. L., Wampler, J. L., Li, F., Berseth, C. L., Rudolph, C., & Wu, S. S. (2021). Effect of bovine milk fat globule membrane and lactoferrin in infant formula on gut microbiome and metabolome at 4 months of age. *Current Developments in Nutrition*, *5*(5), nzab027.

Clulow, A. J., Parrow, A., Hawley, A., Khan, J., Pham, A. C., Larsson, P., Bergström, C. A. S., & Boyd, B. J. (2017). Characterization of solubilizing nanoaggregates present in different versions of simulated intestinal fluid. *The Journal of Physical Chemistry B*, *121*(48), 10869–10881.

Clulow, A. J., Salim, M., Hawley, A., & Boyd, B. J. (2018). A closer look at the behaviour of milk lipids during digestion. *Chemistry and Physics of Lipids*, *211*, 107–116.

Corredig, M., & Dalgleish, D. G. (1996). Effect of different heat treatments on the strong binding interactions between whey proteins and milk fat globules in whole milk. *Journal of Dairy Research*, *63*(3), 441–449.

Duan, R.-D., Hertervig, E., Nyberg, L., Hauge, T., Sternby, B., Lillienau, J., Farooqi, A., & Nilsson, Å. (1996). Distribution of alkaline sphingomyelinase activity in human beings and animals: Tissue and species differences. *Digestive Diseases and Sciences*, *41*(9), 1801–1806.

Duan, R., & Nilsson, A. (1997). Purification of a newly identified alkaline sphingomyelinase in human bile and effects of bile salts and phosphatidylcholine on enzyme activity. *Hepatology*, *26*(4), 823–830.

Duan, R.-D., Cheng, Y., Hansen, G., Hertervig, E., Liu, J.-J., Syk, I., Sjöström, H., & Nilsson, Å. (2003). Purification, localization, and expression of human intestinal alkaline sphingomyelinase. *Journal of Lipid Research*, *44*(6), 1241–1250.

Et-Thakafy, O., Guyomarc'h, F., & Lopez, C. (2017). Lipid domains in the milk fat globule membrane: Dynamics investigated in situ in milk in relation to temperature and time. *Food Chemistry*, *220*, 352–361.

Fenske, D. B., Jarrell, H. C., Guo, Y., & Hui, S. W. (1990). Effect of unsaturated phosphatidylethanolamine on the chain order profile of bilayers at the onset of the hexagonal phase transition. A deuterium NMR study. *Biochemistry*, *29*(51), 11222–11229.

Friddin, M. S., Bolognesi, G., Salehi-Reyhani, A., Ces, O., & Elani, Y. (2019). Direct manipulation of liquid ordered lipid membrane domains using optical traps. *Communications Chemistry*, *2*(1), 1–6.

Gallier, S., Gragson, D., Jiménez-Flores, R., & Everett, D. (2010). Using confocal laser scanning microscopy to probe the milk fat globule membrane and associated proteins. *Journal of Agricultural and Food Chemistry*, *58*(7), 4250–4257.

Gallier, S., Cui, J., Olson, T. D., Rutherfurd, S. M., Ye, A., Moughan, P. J., & Singh, H. (2013 a). In vivo digestion of bovine milk fat globules: Effect of processing and interfacial structural changes. I. Gastric digestion. *Food Chemistry*, *141*(3), 3273–3281

Guo, W., Kurze, V., Huber, T., Afdhal, N. H., Beyer, K., & Hamilton, J. A. (2002). A solid-state NMR study of phospholipid-cholesterol interactions: Sphingomyelin-cholesterol binary systems. *Biophysical Journal*, *83*(3), 1465–1478.

Helenius, A., & Simons, K. (1975). Solubilization of membranes by detergents. *Biochimica et Biophysica Acta (BBA) - Reviews on Biomembranes*, *415*(1), 29–79.

Jaikishan, S., & Slotte, J. P. (2011). Effect of hydrophobic mismatch and interdigitation on sterol/sphingomyelin interaction in ternary bilayer membranes. *Biochimica et Biophysica Acta (BBA) - Biomembranes*, *1808*(7), 1940–1945.

Jensen, R. G., Ferris, A. M., & Lammi-Keefe, C. J. (1991). The Composition of Milk Fat. *Journal of Dairy Science*, *74*(9), 3228–3243.

Keenan, T.W., & Patton, S. (1995). The milk lipid globule membrane. In R. G. Jensen (ed.), *Handbook of milk composition* (pp. 5–62), San Diego; Academic Press.

Keyvanloo, A., Shaghaghi, M., Zuckermann, M. J., & Thewalt, J. L. (2018). The phase behaviour and organization of sphingomyelin/cholesterol membranes: A deuterium NMR Study. *Biophysical Journal*, *114*(6), 1344–1356.

Lee, S. J., & Sherbon, J. W. (2002). Chemical changes in bovine milk fat globule membrane caused by heat treatment and homogenization of whole milk. *Journal of Dairy Research*, *69*(4), 555–567.

Levental, I., Levental, K. R., & Heberle, F. A. (2020). Lipid rafts: Controversies resolved, mysteries remain. *Trends in Cell Biology*, *30*(5), 341–353.

Lichtenberg, D., Ahyayauch, H., & Goñi, F. M. (2013). The mechanism of detergent solubilization of lipid bilayers. *Biophysical Journal*, *105*(2), 289–299.

Lopez, C., Madec, M.-N., & Jimenez-Flores, R. (2010). Lipid rafts in the bovine milk fat globule membrane revealed by the lateral segregation of phospholipids and heterogeneous distribution of glycoproteins. *Food Chemistry*, *120*(1), 22–33.

Lopez, C., Briard-Bion, V., Ménard, O., Beaucher, E., Rousseau, F., Fauquant, J., Leconte, N., & Robert, B. (2011). Fat globules selected from whole milk according to their size: Different compositions and structure of the biomembrane, revealing sphingomyelin-rich domains. *Food Chemistry*, *125*(2), 355–368.

Lopez, C., Cheng, K., & Perez, J. (2018). Thermotropic phase behaviour of milk sphingomyelin and role of cholesterol in the formation of the liquid ordered phase examined using SR-XRD and DSC. *Chemistry and Physics of Lipids*, *215*, 46–55.

Lucero, H. A., & Robbins, P. W. (2004). Lipid rafts–protein association and the regulation of protein activity. *Archives of Biochemistry and Biophysics*, *426*(2), 208–224.

Ma, Y., Zhang, L., Wu, Y., & Zhou, P. (2019). Changes in milk fat globule membrane proteome after pasteurization in human, bovine and caprine species. *Food Chemistry*, *279*, 209–215.

Macierzanka, A., Torcello-Gómez, A., Jungnickel, C., & Maldonado-Valderrama, J. (2019). Bile salts in digestion and transport of lipids. *Advances in Colloid and Interface Science*, *274*, 102045.

Maher, A., & Rochfort, S. (2014). Applications of NMR in dairy research. *Metabolites*, *4*(1), 131–141.

Mañes, S., del Real, G., & Martínez-A, C. (2003). Pathogens: Raft hijackers. *Nature Reviews Immunology*, *3*(7), 557–568.

Mesilati-Stahy, R., Mida, K., & Argov-Argaman, N. (2011). Size-Dependent lipid content of bovine milk fat globule and membrane phospholipids. *Journal of Agricultural and Food Chemistry*, *59*(13), 7427–7435.

Morin, P., Jiménez-Flores, R., & Pouliot, Y. (2007). Effect of processing on the composition and microstructure of buttermilk and its milk fat globule membranes. *International Dairy Journal*, *17*(10), 1179–1187.

Munro, S. (2003). Lipid rafts: Elusive or illusive? *Cell*, *115*(4), 377–388.

Nieva-Echevarría, B., Goicoechea, E., Manzanos, M. J., & Guillén, M. D. (2016). A study by 1H NMR on the influence of some factors affecting lipid in vitro digestion. *Food Chemistry*, *211*, 17–26.

Nilsson, Å., Duan, R.-D., & Ohlsson, L. (2021). Digestion and absorption of milk phospholipids in newborns and adults. *Frontiers in Nutrition, 8*, 724006.

Noh, S. K., & Koo, S. I. (2004). Milk sphingomyelin is more effective than egg sphingomyelin in inhibiting intestinal absorption of cholesterol and fat in rats. *The Journal of Nutrition*, *134*(10), 2611–2616.

Nyberg, L., Duan, R.-D., Axelson, J., & Nilsson, Å. (1996). Identification of an alkaline sphingomyelinase activity in human bile. *Biochimica et Biophysica Acta (BBA) - Lipids and Lipid Metabolism*, *1300*(1), 42–48.

Nyberg, L., Nilsson, Å., Lundgren, P., & Duan, R.-D. (1997). Localization and capacity of sphingomyelin digestion in the rat intestinal tract. *The Journal of Nutritional Biochemistry*, *8*(3), 112–118.

Obeid, S., Guyomarc'h, F., Francius, G., Guillemin, H., Wu, X., Pezennec, S., Famelart, M.-H., Cauty, C., Gaucheron, F., & Lopez, C. (2019). The surface properties of milk fat globules govern their interactions with the caseins: Role of homogenization and pH probed by AFM force spectroscopy. *Colloids and Surfaces B: Biointerfaces*, *182*, 110363.

Okotrub, K. A., Zykova, V. A., Adichtchev, S. V., & Surovtsev, N. V. (2020). Deciphering the orientation of lipid molecules by principal component analysis of Raman mapping data. *The Analyst*, *145*(4), 1466–1472.

Patist, A., Jha, B. K., Oh, S.-G., & Shah, D. O. (1999). Importance of micellar relaxation time on detergent properties. *Journal of Surfactants and Detergents*, *2*(3), 317–324.

Pham, A.C., Clulow, A.J., & Boyd, B.J. (2021). Formation of self-assembled mesophases during lipid digestion. Front. Cell Dev. Biol. 9, 657886.

Pimentel, L., Gomes, A., Pintado, M., Miguel Rodriguez-Alcala, L. (2016). Isolation and analysis of phospholipids in dairy foods. *Journal of Analytical Methods in Chemistry, 2016*, 9827369

Reis, P., Miller, R., Krägel, J., Leser, M., Fainerman, V. B., Watzke, H., & Holmberg, K. (2008). Lipases at interfaces: Unique interfacial properties as globular proteins. *Langmuir*, *24*(13), 6812–6819.

Ripa, I., Andreu, S., López-Guerrero, J. A., & Bello-Morales, R. (2021). Membrane rafts: Portals for viral entry. *Frontiers in Microbiology*, *12*, 631274.

Róg, T., & Pasenkiewicz-Gierula, M. (2001). Cholesterol effects on the phosphatidylcholine bilayer nonpolar region: A molecular simulation study. *Biophysical Journal*, *81*(4), 2190–2202.

Roy, D., Ye, A., Moughan, P. J., & Singh, H. (2021). Structural changes in cow, goat, and sheep skim milk during dynamic in vitro gastric digestion. *Journal of Dairy Science*, *104*(2), 1394–1411.

Schnitzer, E., Lichtenberg, D., & Kozlov, M. M. (2003). Temperature-dependence of the solubilization of dipalmitoylphosphatidylcholine (DPPC) by the non-ionic surfactant Triton X-100, kinetic and structural aspects. *Chemistry and Physics of Lipids*, *126*(1), 55–76.

Shirota, K., Yagi, K., Inaba, T., Li, P.-C., Murata, M., Sugita, Y., & Kobayashi, T. (2016). Detection of sphingomyelin clusters by Raman spectroscopy. *Biophysical Journal*, *111*(5), 999–1007.

Simons K, Ikonen E (1997). Functional rafts in cell membranes. *Nature*. 387(6633), 569-572.

Simons, K., & Vaz, W. L. C. (2004). Model systems, lipid rafts, and cell membranes. *Annual Review of Biophysics and Biomolecular Structure*, *33*(1), 269–295.

Sprong, R. C., Hulstein, M. F. E., & van der Meer, R. (2002). Bovine milk fat components inhibit food-borne pathogens. *International Dairy Journal*, *12*(2–3), 209–215.

Stuart, M. C. A., & Boekema, E. J. (2007). Two distinct mechanisms of vesicle-to-micelle and micelle-to-vesicle transition are mediated by the packing parameter of phospholipid–detergent systems. *Biochimica et Biophysica Acta (BBA) - Biomembranes*, *1768*(11), 2681–2689.

Thum, C., Roy, N. C., Everett, D. W., & McNabb, W. C. (2021). Variation in milk fat globule size and composition: A source of bioactives for human health. *Critical Reviews in Food Science and Nutrition*, 1–27.

Virtanen, J., Ruonala, M., Vauhkonen, M., & Somerharju, P. (1995). Lateral organization of liquid-crystalline cholesterol-dimyristoylphosphatidylcholine bilayers. Evidence for domains with hexagonal and centered rectangular cholesterol superlattices. *Biochemistry*, *34*(36), 11568–11581.

Wooding, F. B. P., & Mather, I. H. (2017). Ultrastructural and immunocytochemical evidence for the reorganisation of the milk fat globule membrane after secretion. *Cell and Tissue Research*, *367*(2), 283–295.

Wu, Y., Zhang, X., Han, D., Pi, Y., Tao, S., Zhang, S., Wang, S., Zhao, J., Chen, L., & Wang, J. (2021). Early life administration of milk fat globule membrane promoted SCFA-producing bacteria colonization, intestinal barriers and growth performance of neonatal piglets. *Animal Nutrition*, *7*(2), 346–355.

Yao, Y., Zhao, G., Xiang, J., Zou, X., Jin, Q., & Wang, X. (2016). Lipid composition and structural characteristics of bovine, caprine and human milk fat globules. *International Dairy Journal*, *56*, 64–73.

Ye, L., Zhang, Q., Xin, F., Cao, B., Qian, L., & Dong, Y. (2021). Neonatal milk fat globule membrane supplementation during breastfeeding ameliorates the deleterious effects of maternal high-fat diet on metabolism and modulates gut microbiota in adult mice offspring in a sex-specific way. *Frontiers in Cellular and Infection Microbiology*, *11*, 621957.

Zheng, H., Jiménez-Flores, R., Gragson, D., & Everett, D. W. (2014). Phospholipid architecture of the bovine milk fat globule membrane using giant unilamellar vesicles as a model. *Journal of Agricultural and Food Chemistry*, *62*(14), 3236–3243.

Appendix

Appendix: Chapter 3

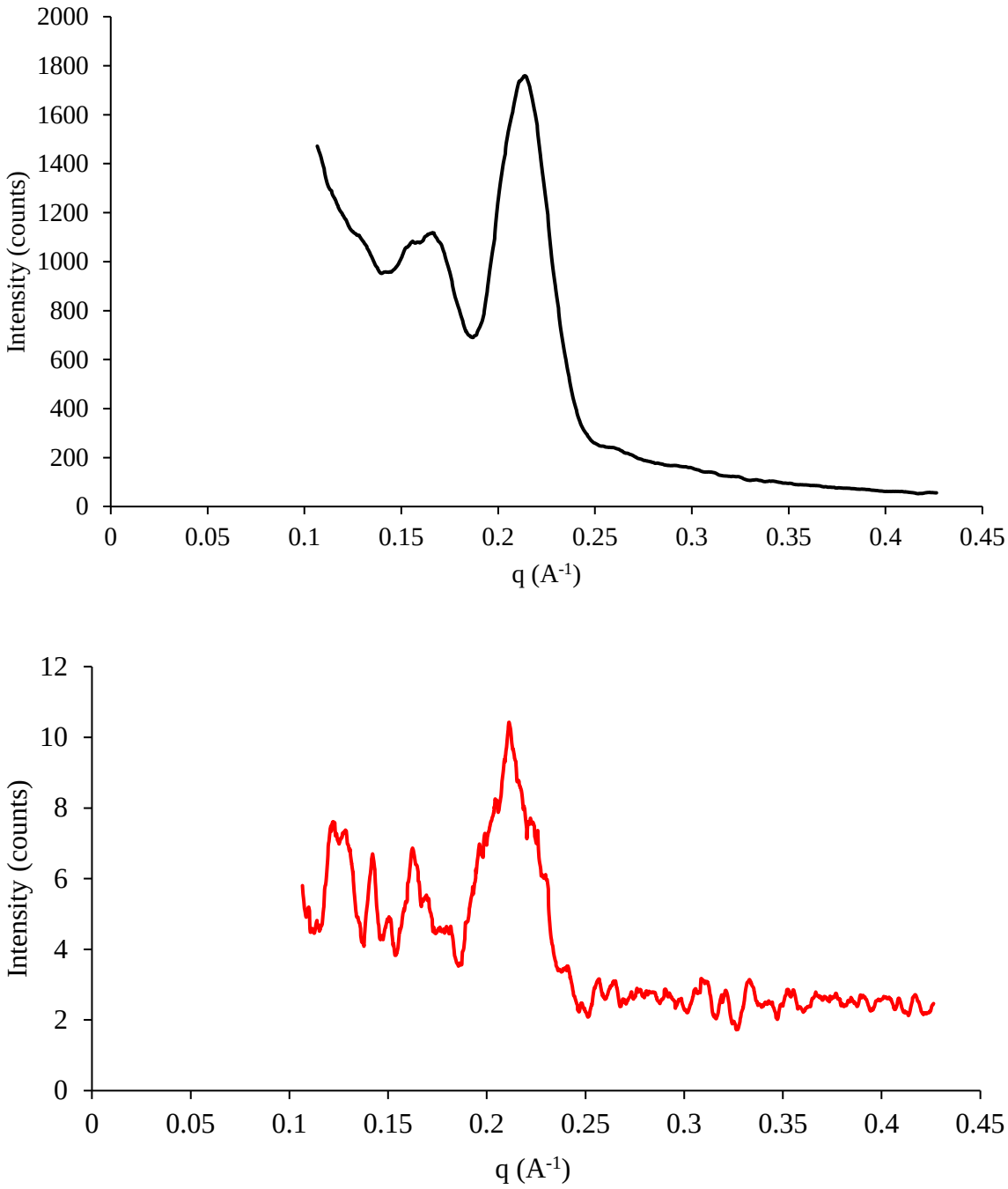

Appendix 3.1. Quasi-small angle x-ray scattering of a) PIPES buffer; b) 2 mM of phospholipid vesicles made with recombined MFGM phospholipids without cholesterol on a Rigaku Spider X-ray diffractometer. No diffraction of lamellar features was observed.

Appendix: Chapter 4

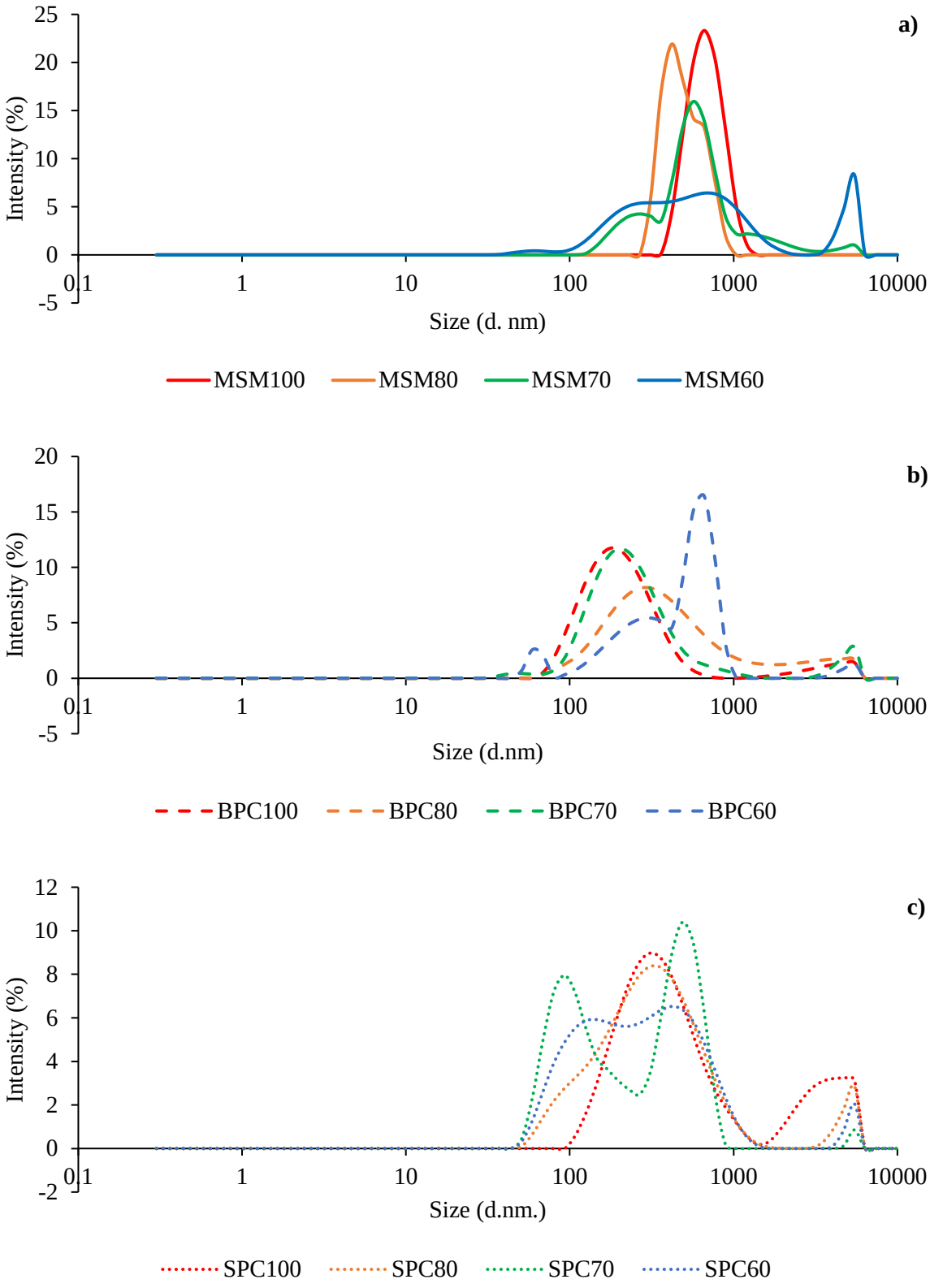

Appendix 4.1. Particle size of phospholipid vesicles. Readings larger than 1 μm are aggregates.

a) Milk sphingomyelin with 0 – 40% cholesterol
b) Brain phosphatidylcholine with 0 – 40% cholesterol
c) Soy phosphatidylcholine with 0 – 40% cholesterol

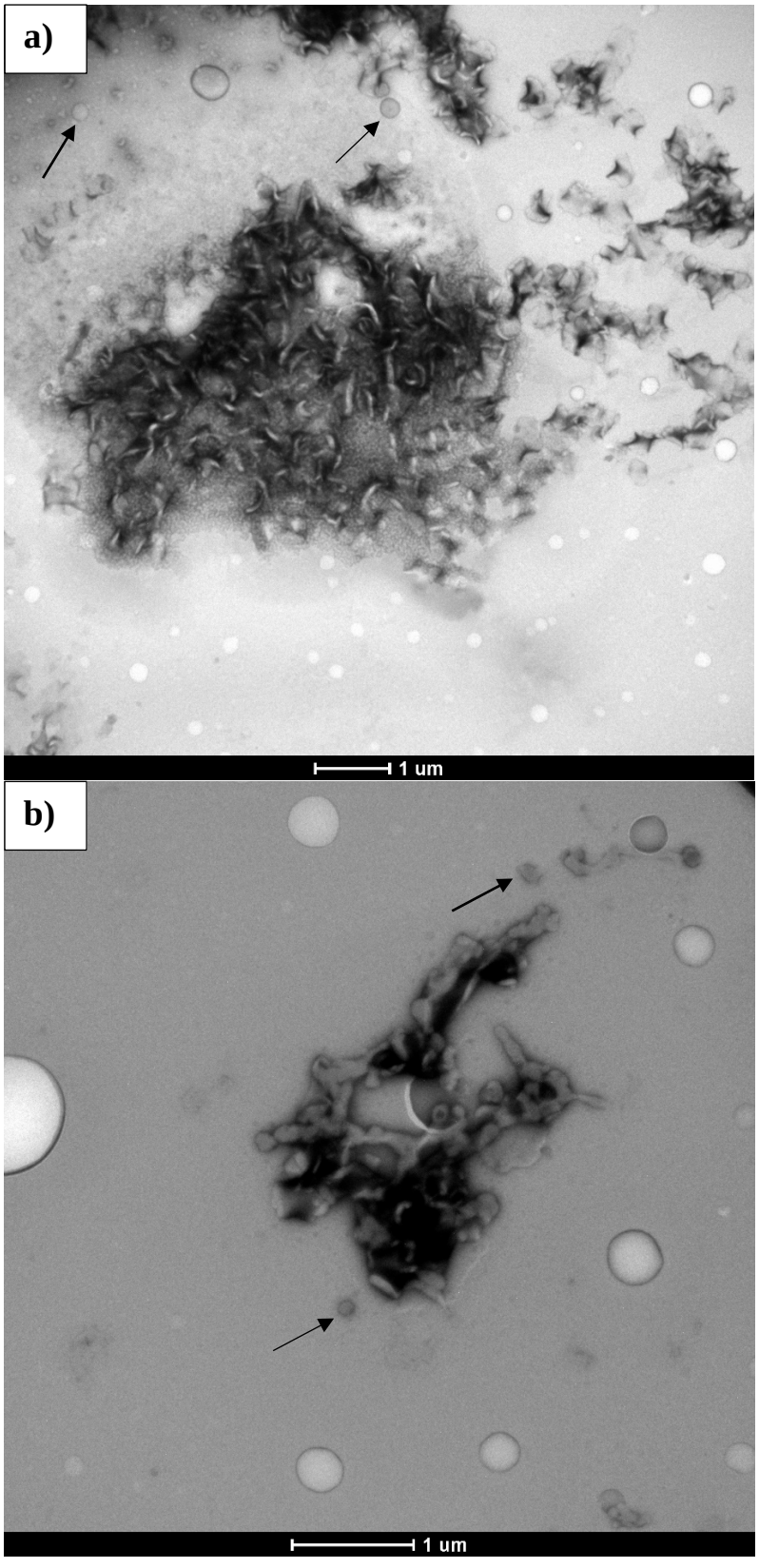

Appendix 4.2. Negative stain transmission electron micrographs

a) Soy phosphatidylcholine vesicles, 0% mol cholesterol incubated with bovine bile, 9,900 x. White circles are holes in the carbon formvar grid. Black arrow points to unilamellar vesicles.
b) Soy phosphatidylcholine vesicle, 20% mol cholesterol incubated with bovine bile, 16,500 x. White circles are holes in the carbon formvar. Black arrow points to intermediates budding off from the superstructure.

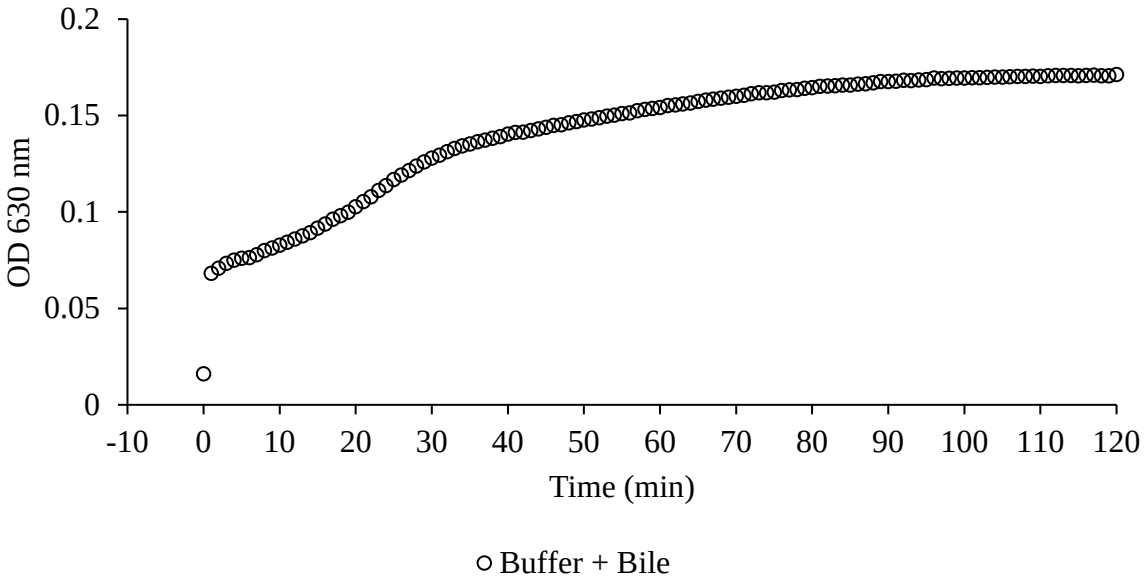

Appendix 4.3. Optical density at 630 nm of (PIPES buffer + bovine bile).

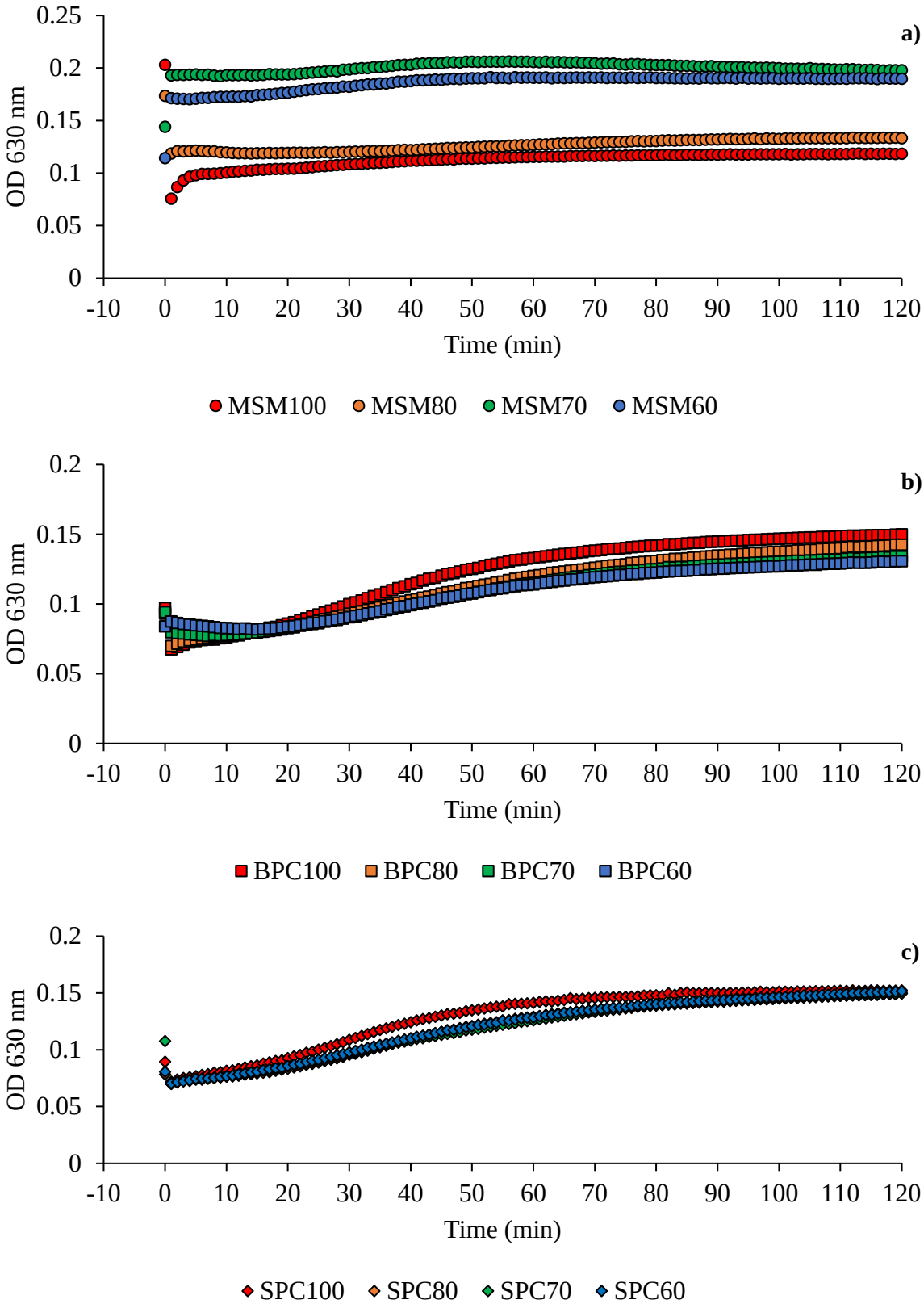

Appendix 4.4. Optical density at 630 nm of vesicle systems incubated with bovine bile (10 mM) for 2 h at 37 °C without any subtraction from the blank (PIPES buffer + bovine bile).

a) Bile added to milk sphingomyelin MLVs 0 – 40% cholesterol.

b) Bile added to brain phosphatidylcholine vesicles 0 – 40% cholesterol.

c) Bile added to soy phosphatidylcholine vesicles 0 – 40% cholesterol.

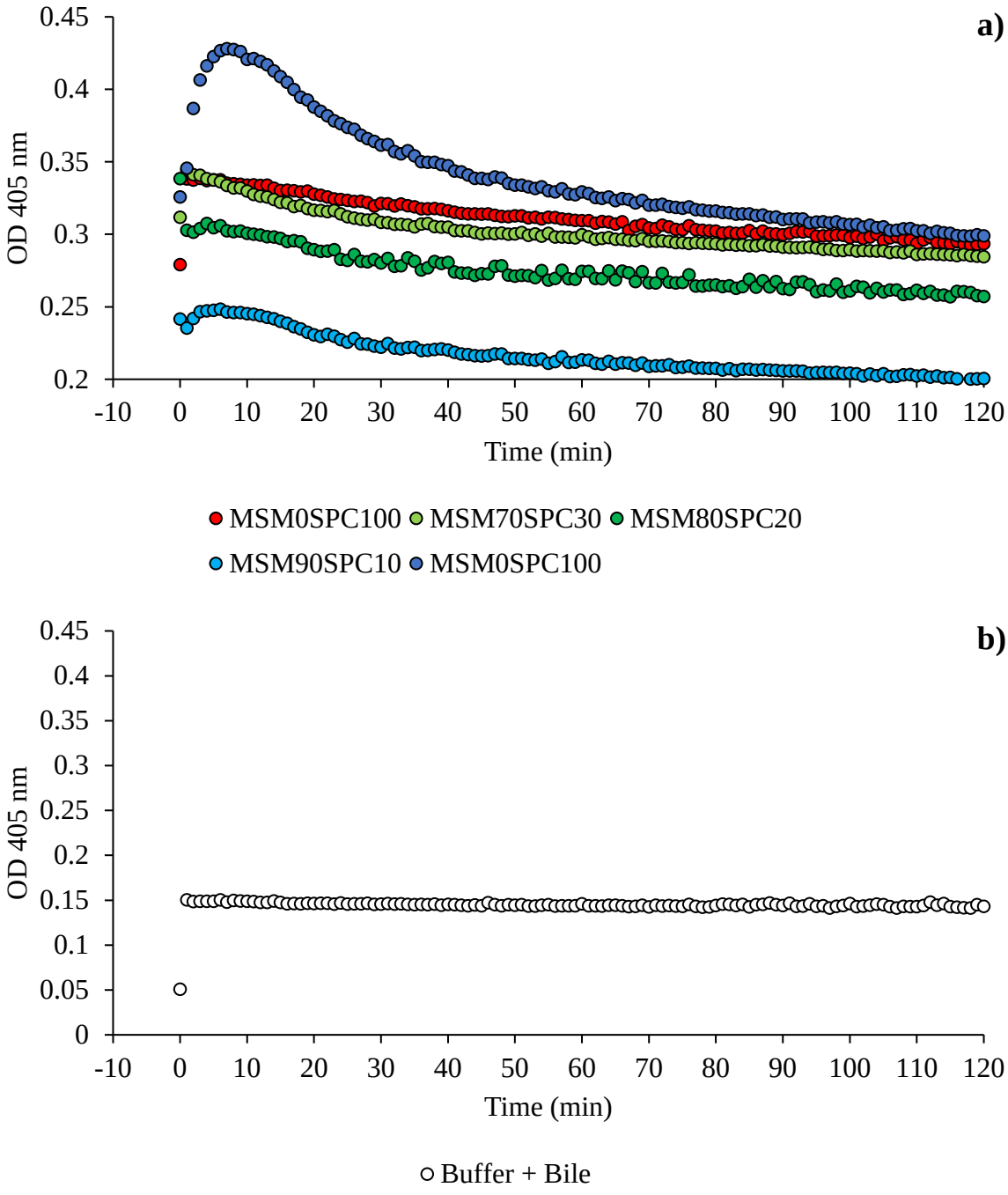

Appendix 4.4. Optical density at 405 nm of binary phospholipid vesicles consisting of milk sphingomyelin (MSM, variable % mol) and soy phosphatidylcholine (SPC, variable % mol) incubated with bovine bile; a) Figure 4.4 a, without the buffer + bile subtracted; b) PIPES buffer + bile

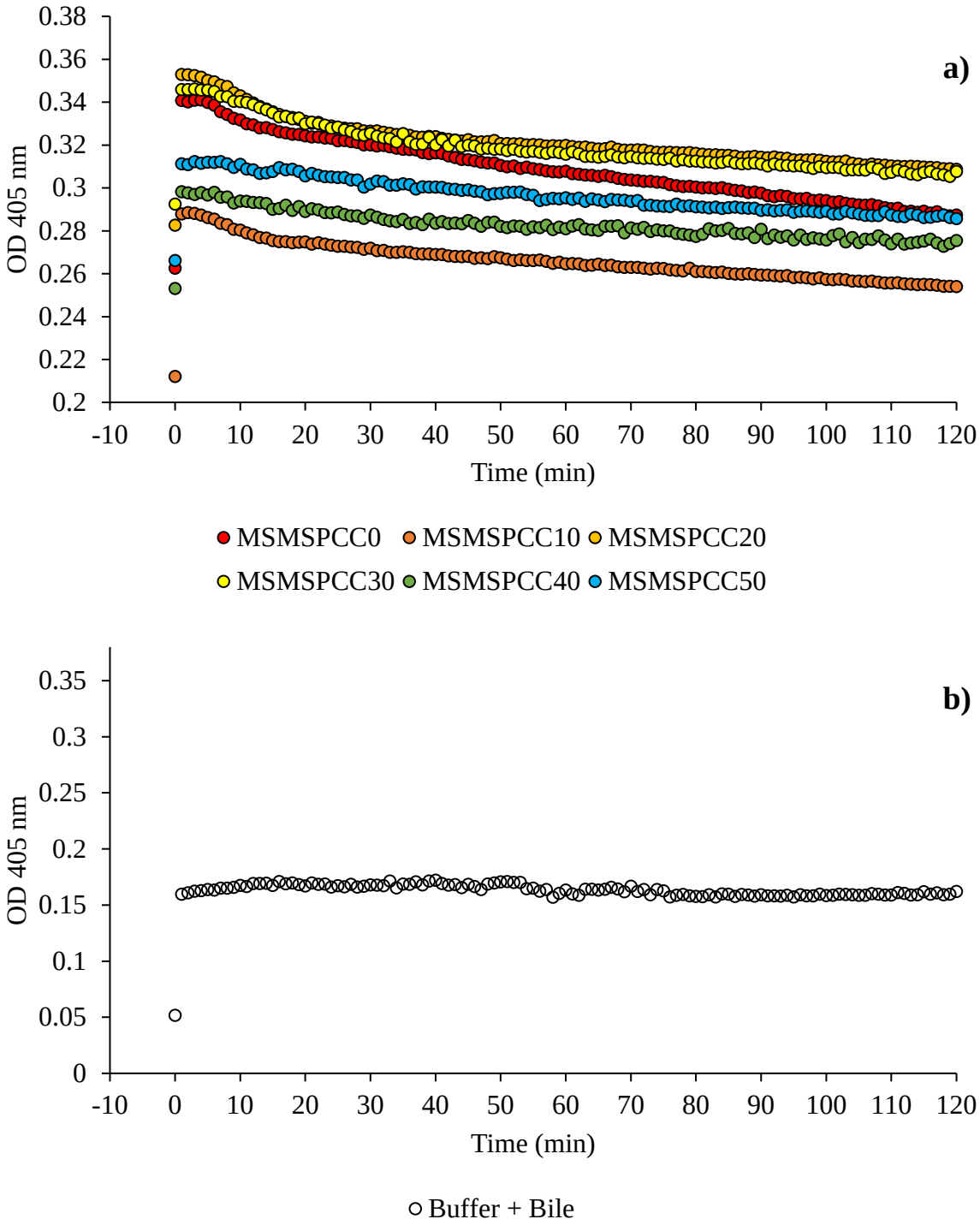

Appendix 4.5. Optical density at 405 nm of ternary phospholipid vesicles consisting of milk sphingomyelin, soy phosphatidylcholine (1:1.6 mol mol MSM:SPC, respectively), and cholesterol (C, variable % mol according to MSM:Cholesterol, i.e. MSMSPCC40 = 100:160:66 μM) incubated with bovine bile a) Figure 4.4 b, without the buffer + bile subtracted; b) PIPES buffer + bile

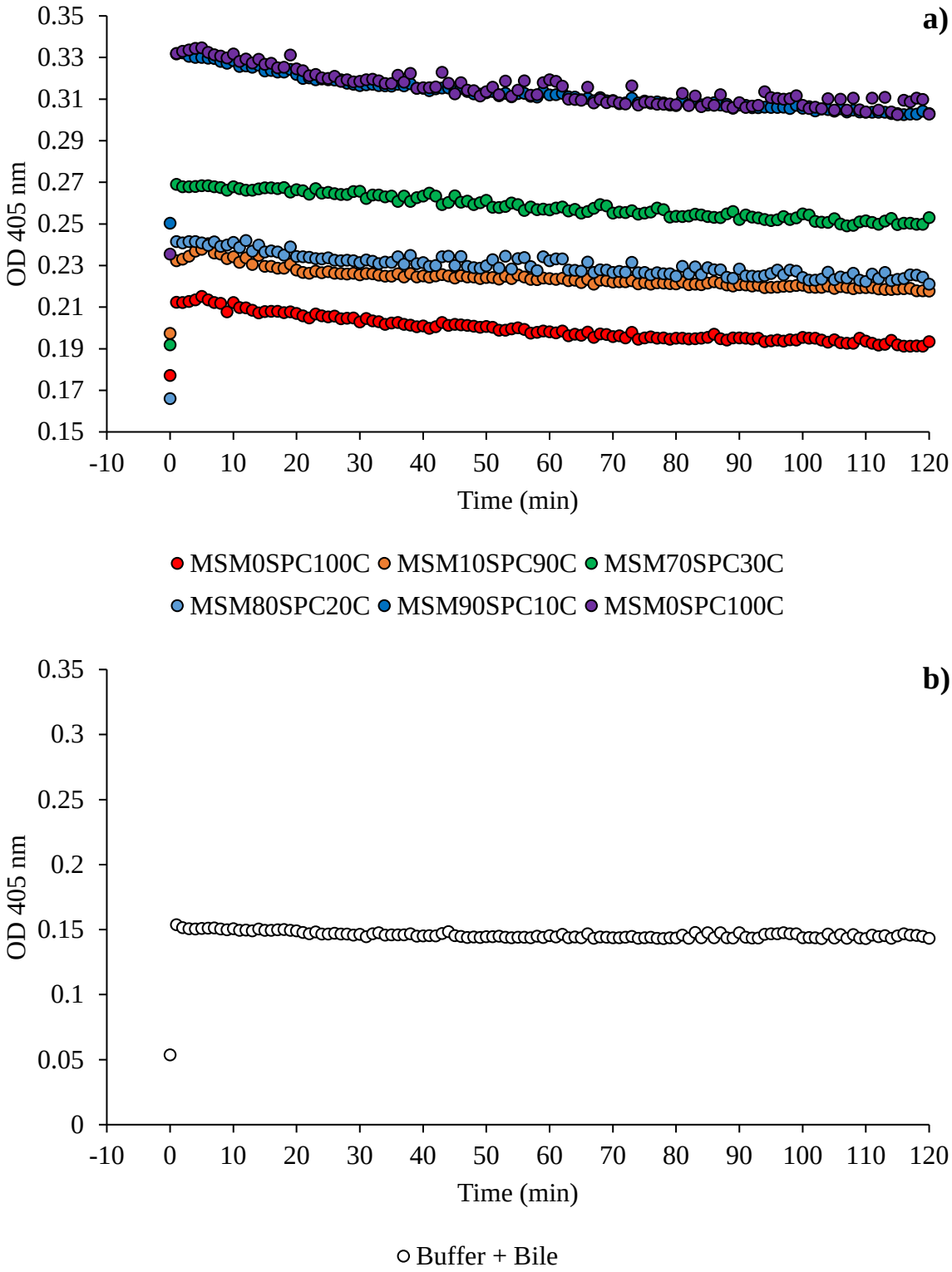

Appendix 4.6. Optical density at 405 nm of ternary phospholipid vesicles consisting of sphingomyelin (% mol variable), soy phosphatidylcholine (% mol variable), and cholesterol vesicles incubated with bovine bile; a) Fig. 4.5, without the buffer + bile subtracted; b) PIPES buffer + bile

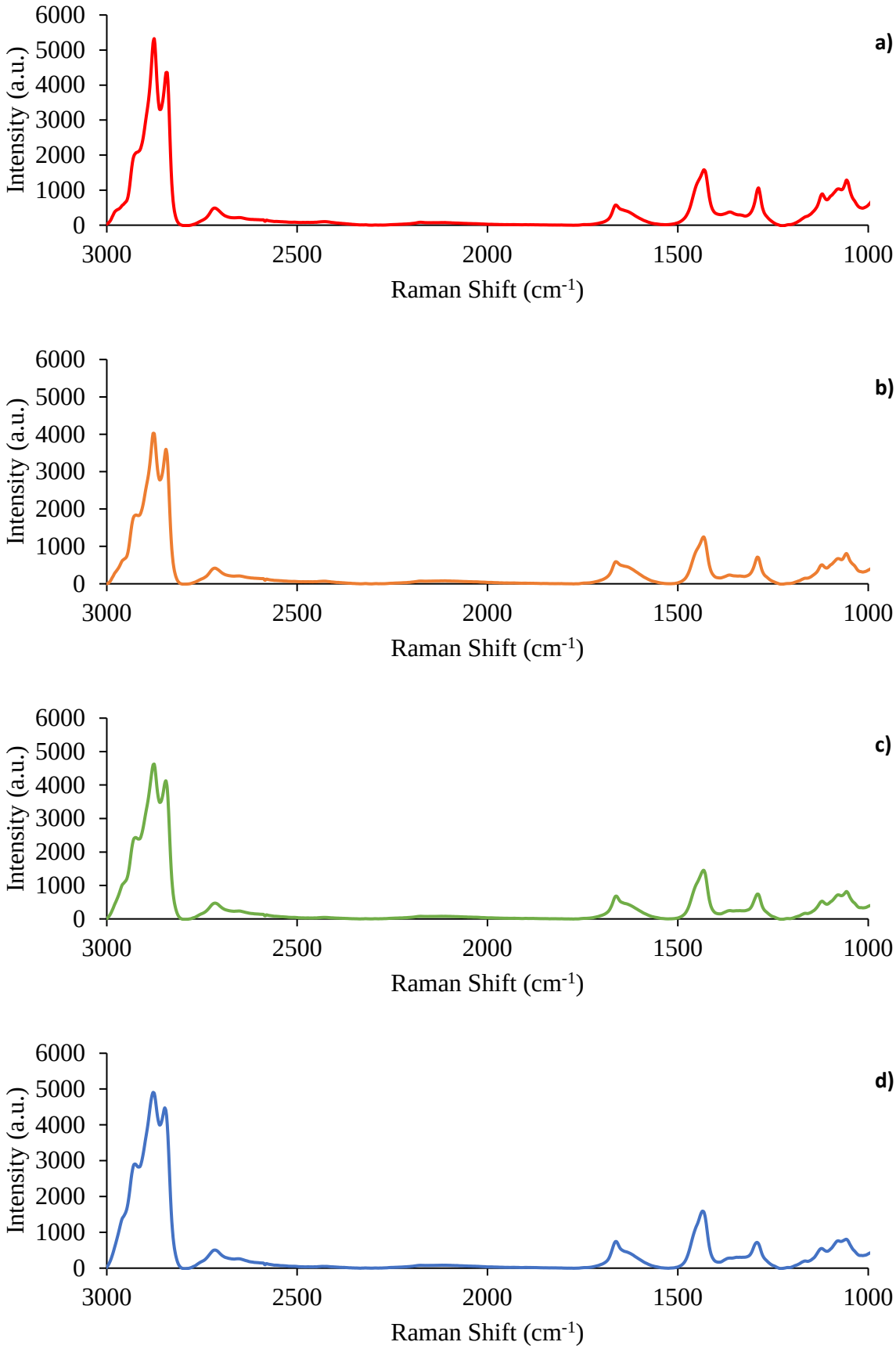

Appendix 4.7. Raman spectra of milk sphingomyelin (MSM) multilamellar vesicles (1000 – 3000 cm^{-1}). a) without cholesterol; b) 4:1 MSM/cholesterol; c) 7:3 MSM/cholesterol; d) 3:2 MSM/cholesterol

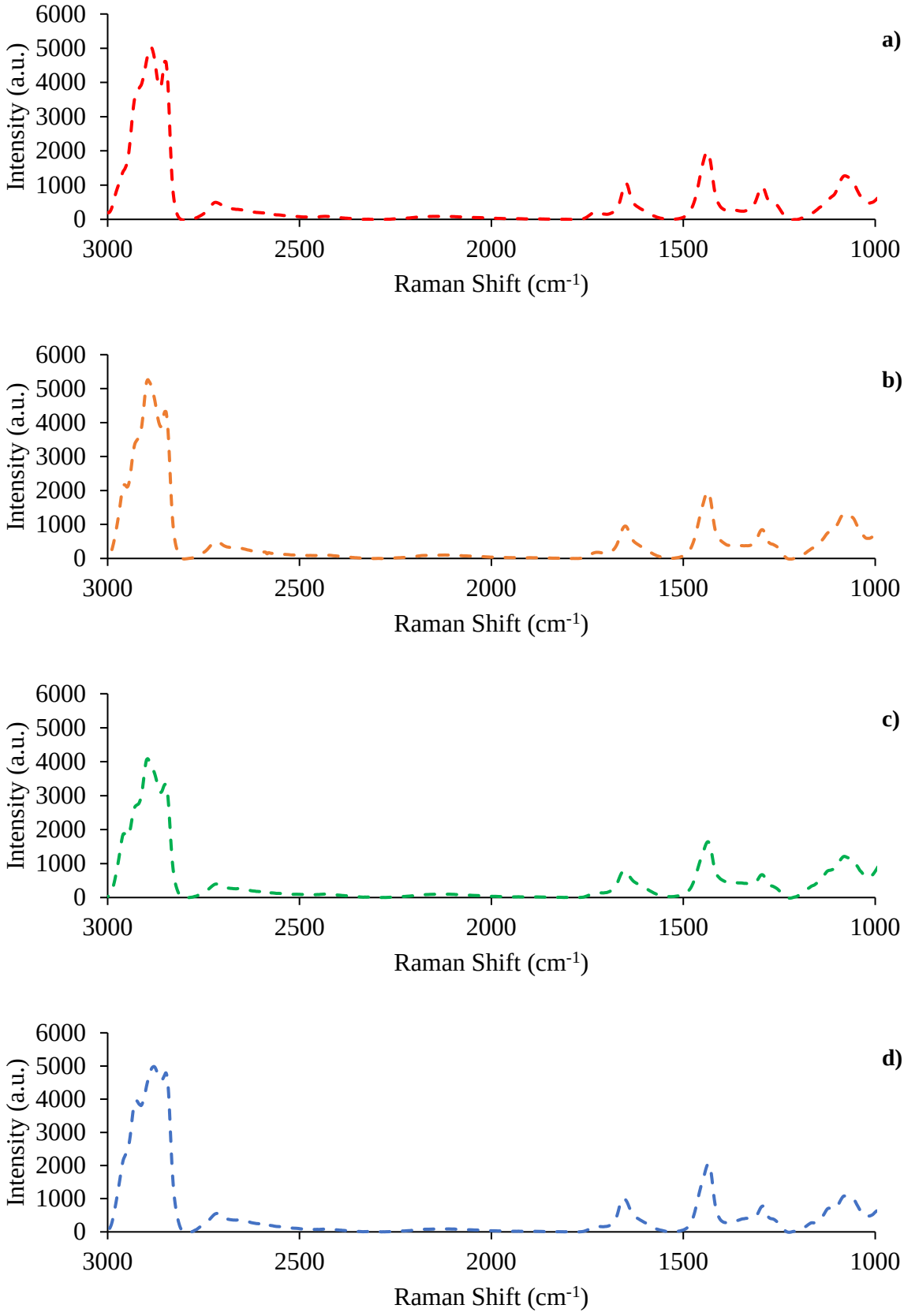

Appendix 4.8. Raman spectra of brain phosphatidylcholine (BPC) vesicles (1000 – 3000 cm^{-1}). a) without cholesterol; b) 4:1 BPC/cholesterol; c) 7:3 BPC/cholesterol; d) 3:2 BPC/cholesterol

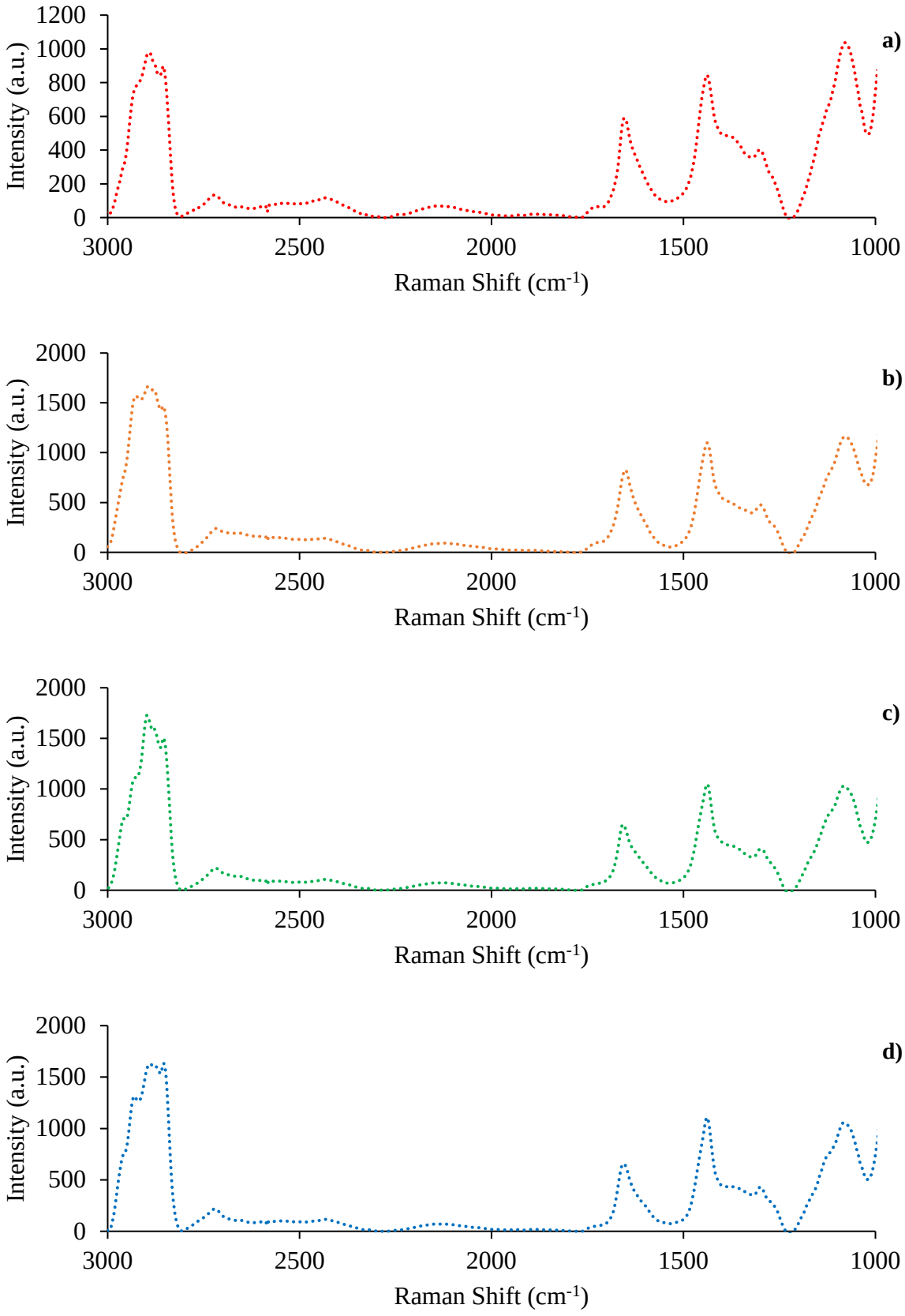

Appendix 4.9. Raman spectra of soy phosphatidylcholine (SPC) vesicles (1000 – 3000 cm^{-1}). a) without cholesterol; b) 4:1 SPC/cholesterol; c) 7:3 SPC/cholesterol; d) 3:2 SPC/cholesterol

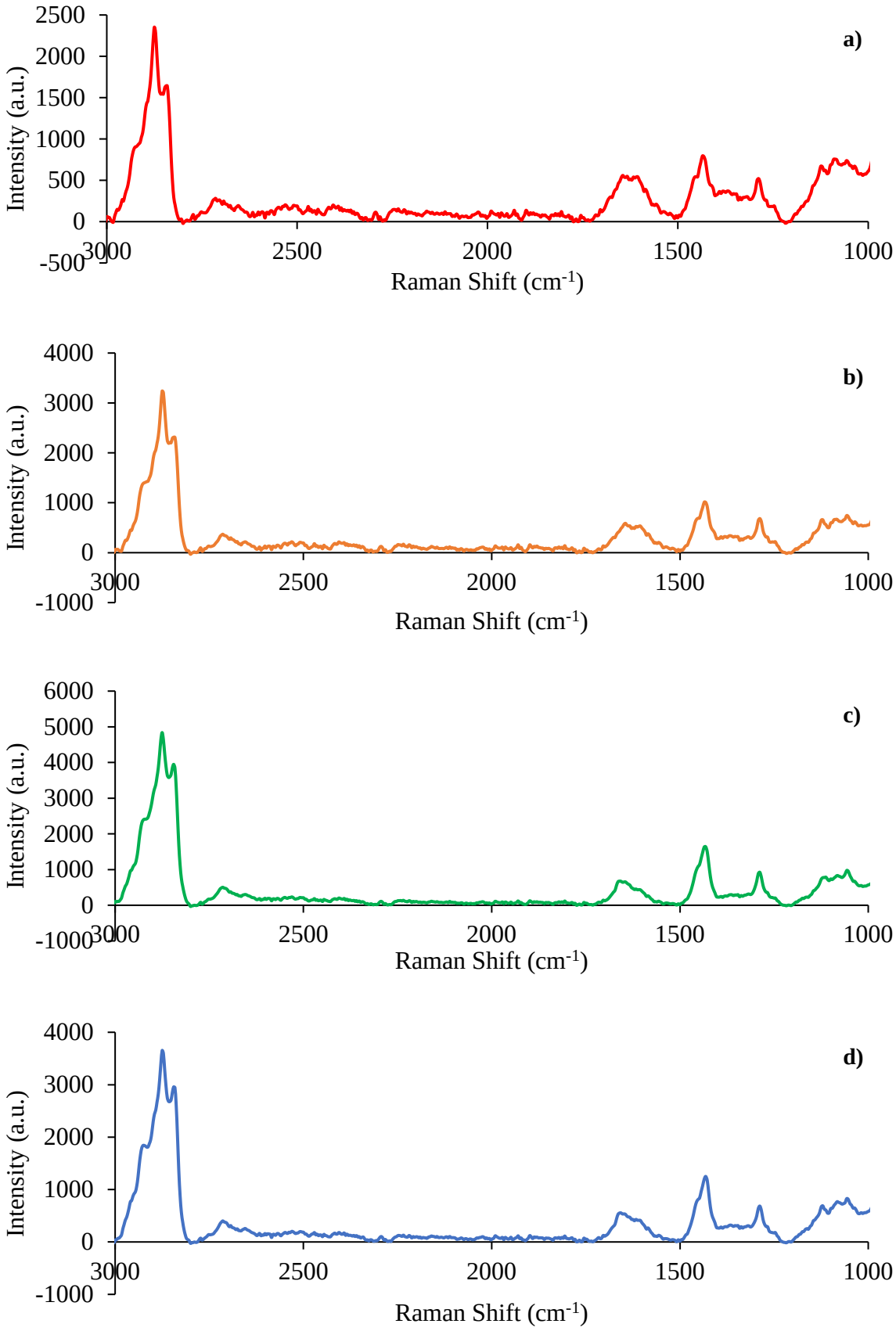

Appendix 4.10. Raman spectra of milk sphingomyelin (MSM) vesicles after incubation with bovine bile (1000 – 3000 cm^{-1}). a) without cholesterol; b) 4:1 MSM/cholesterol; c) 7:3 MSM/cholesterol; d) 3:2 MSM/cholesterol.

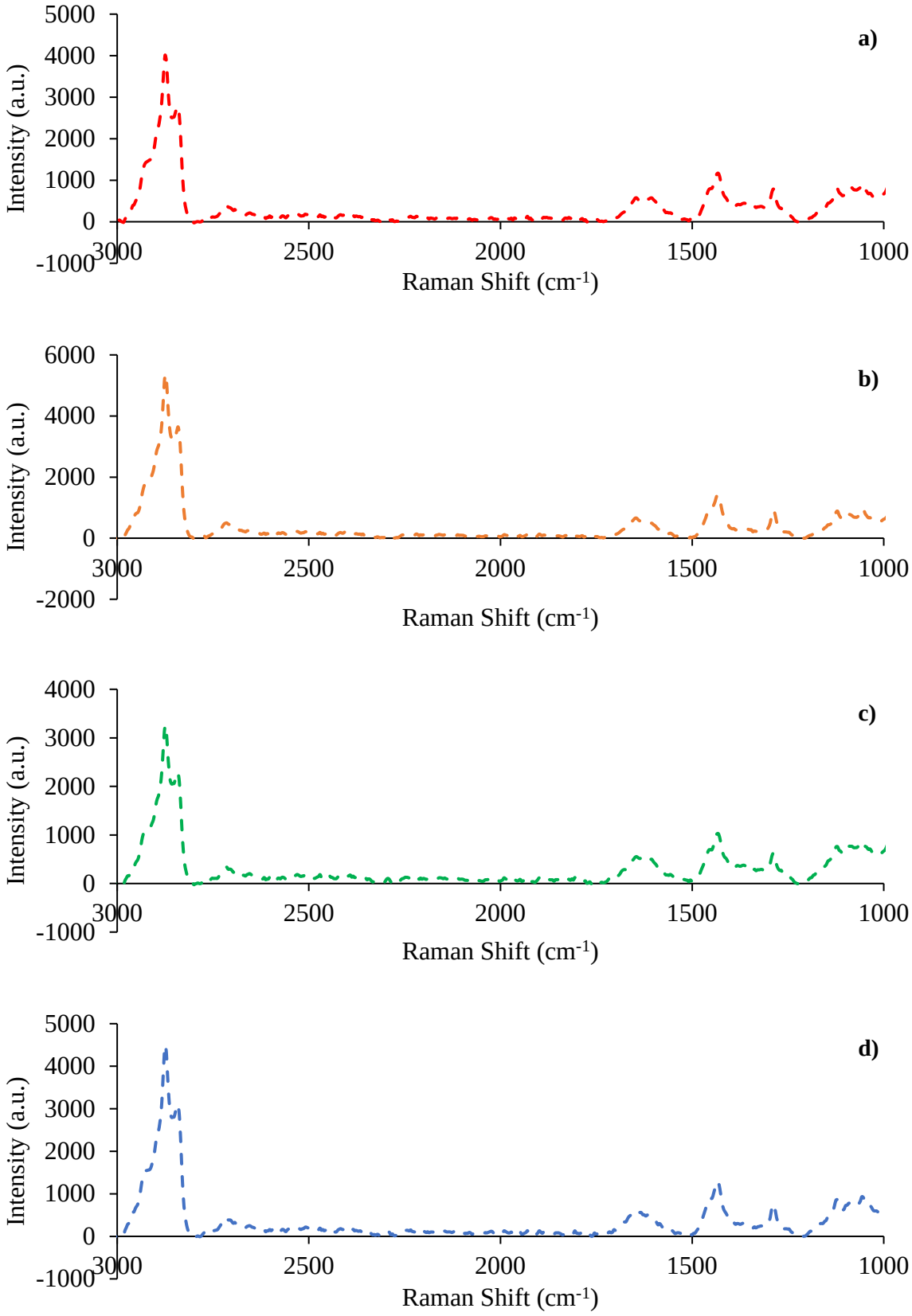

Appendix 4.11. Raman spectra of brain phosphatidylcholine (BPC) vesicles after incubation with bovine bile (1000 – 3000 cm^{-1}). a) without cholesterol; b) 4:1 BPC/cholesterol; c) 7:3 BPC/cholesterol; d) 3:2 BPC/cholesterol.

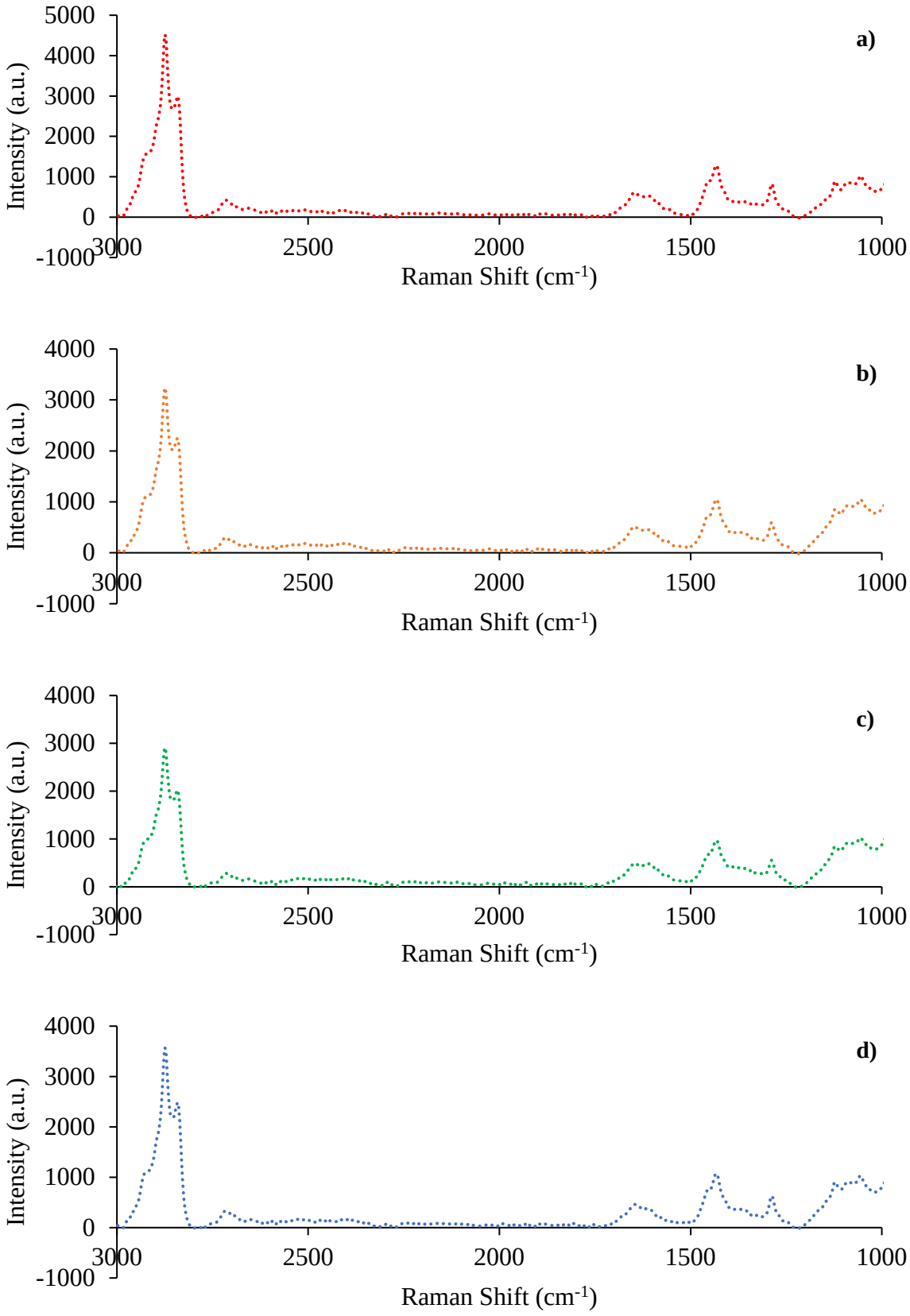

Appendix 4.12. Raman spectra of soy phosphatidylcholine (SPC) vesicles after incubation with bovine bile (1000 – 3000 cm^{-1}). a) without cholesterol; b) 4:1 SPC/cholesterol; c) 7:3 SPC/cholesterol; d) 3:2 SPC/cholesterol.

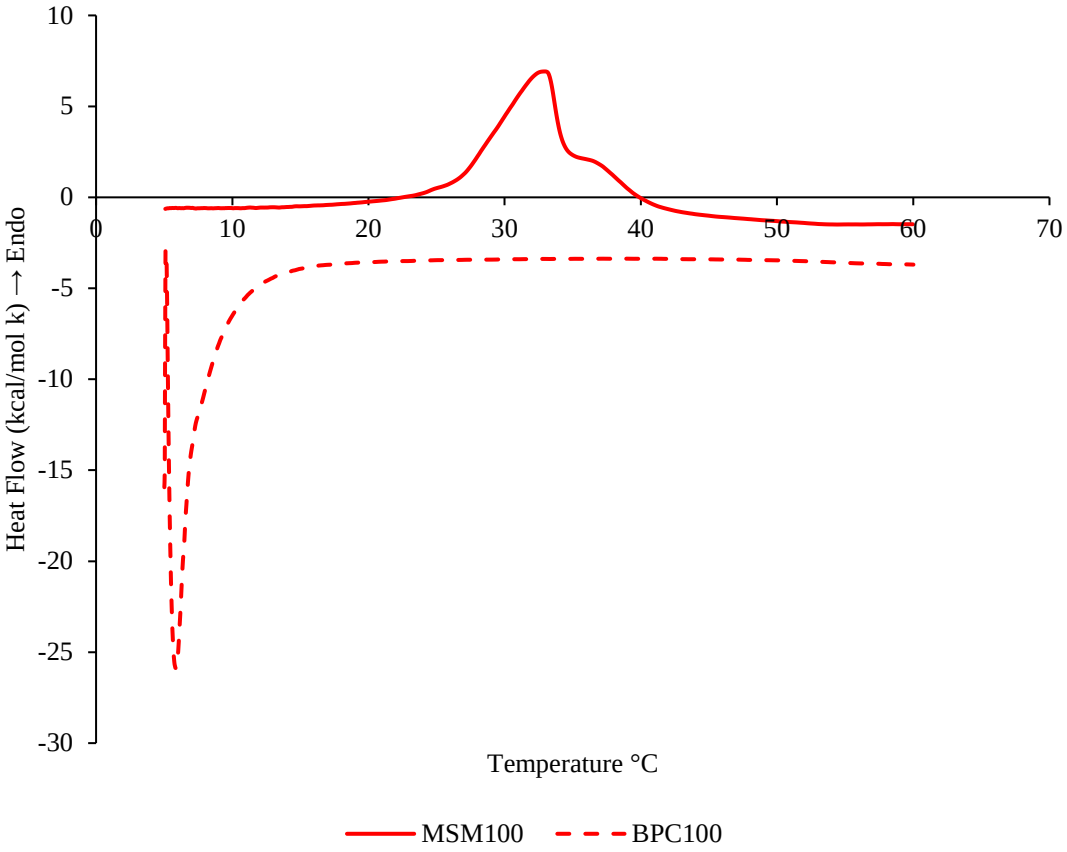

Appendix 4.13. DSC thermograms of phospholipid vesicles without cholesterol. BPC transition temperature is not visible and therefore under 20 °C. Likely, the BPC vesicles were in the L_d phase during the Raman experiments. The peak in the BPC thermogram from 8 to 10 °C is not a phase transition, but the instrument startup hook. An MSM thermograph has been supplied for comparison.

Appendix 4.14. Phospholipid vesicle system disorder/order ratios from Raman spectroscopy with and without bovine bile.

		I_{2850}/I_{2880}		I_{2930}/I_{2880}		I_{1085}/I_{1130}	
		No Bile	Bile Added	No Bile	Bile Added	No Bile	Bile Added
MSM	0% Cholesterol	0.838±0.018 BC	0.75±0.05 D	0.368±0.023 B	0.39±0.11 B	1.15±0.07 ABC	1.17±0.11 ABC
	20% Cholesterol	0.878±0.018 AB	0.78±0.09 CD	0.434±0.005 AB	0.47±0.08 AB	1.34±0.07 AB	1.13±0.22 BC
	30% Cholesterol	0.901±0.033 AB	0.86±0.06 ABC	0.499±0.015 AB	0.54±0.07 A	1.35±0.06 A	1.12±0.14 C
	40% Cholesterol	0.93±0.04 A	0.88±0.10 AB	0.57±0.04 A	0.54±0.12 A	1.36±0.04 A	1.12±0.15 C
BPC	0% Cholesterol	0.995±0.018 A	0.710±0.024 C	0.709±0.023 A	0.33±0.03 B	2.07±0.20 A	1.08±0.10 C
	20% Cholesterol	0.89±0.25 ABC	0.696±0.021 C	0.64±0.17 A	0.33±0.04 B	1.73±0.13 B	0.97±0.17 C
	30% Cholesterol	0.92±0.15 AB	0.73±0.04 BC	0.68±0.09 A	0.33±0.06 B	1.56±0.09 B	1.05±0.13 C
	40% Cholesterol	1.016±0.025 A	0.75±0.11 BC	0.77±0.04 A	0.40±0.19 B	1.47±0.16 B	1.02±0.21 C
SPC	0% Cholesterol	0.85±0.16 A	0.70±0.05 A	0.70±0.31 AB	0.36±0.10 C	1.92±0.74 A	1.09±0.24 B
	20% Cholesterol	0.85±0.16 A	0.9±0.4 A	0.85±0.17 A	0.39±0.16 BC	1.56±0.18 AB	1.12±0.09 B
	30% Cholesterol	0.85±0.29 A	0.9±0.4 A	0.56±0.22 ABC	0.40±0.19 BC	1.45±0.21 AB	1.11±0.10 B
	40% Cholesterol	0.94±0.19 A	0.706±0.017 A	0.80±0.10 A	0.296±0.022 C	1.48±0.14 AB	1.04±0.13 B

Different letters represent significant ($p < 0.05$) differences in disorder/order ratios for a specific phospholipid group and its intensity ratio; I_{2850}/I_{2880} informs the interchain interactions between neighboring acyl chains, the I_{2930}/I_{2880} informs both the interchain interactions, as well as intrachain *gauche/trans* isomerization, and I_{1085}/I_{1130} informs intrachain packing such as *gauche*/*trans* isomerization; MSM = milk sphingomyelin; BPC = brain phosphatidylcholine, SPC = soy phosphatidylcholine

Appendix: Chapter 5

a) Table of phospholipid concentrations for standard curve

Integration | Identification | Quantitative | Compound | Group | Performance | Custom | QC Check | Retention Index

ID#	Name	Type	Channel	Ret. Time	Conc.(1)	Conc.(2)	Conc.(3)	Conc.(4)	Conc.(5)
1	PI	Target	ELSD - Ch1	10.246	5	10	15	25	30
2	PE	Target	ELSD - Ch1	14.728	10	20	30	50	60
3	PS	Target	ELSD - Ch1	18.233	5	10	15	25	30
4	PC	Target	ELSD - Ch1	24.954	10	20	30	50	60
5	SM	Target	ELSD - Ch1	29.631	10	20	30	50	60

b) Phosphatidylinositol standard curve

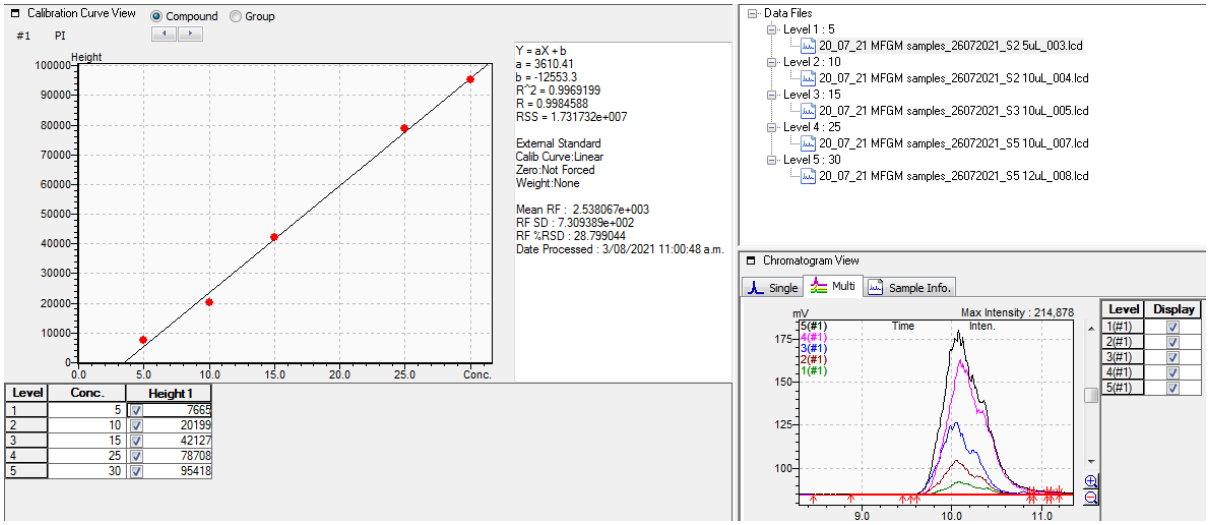

c) Phosphatidylethanolamine standard curve

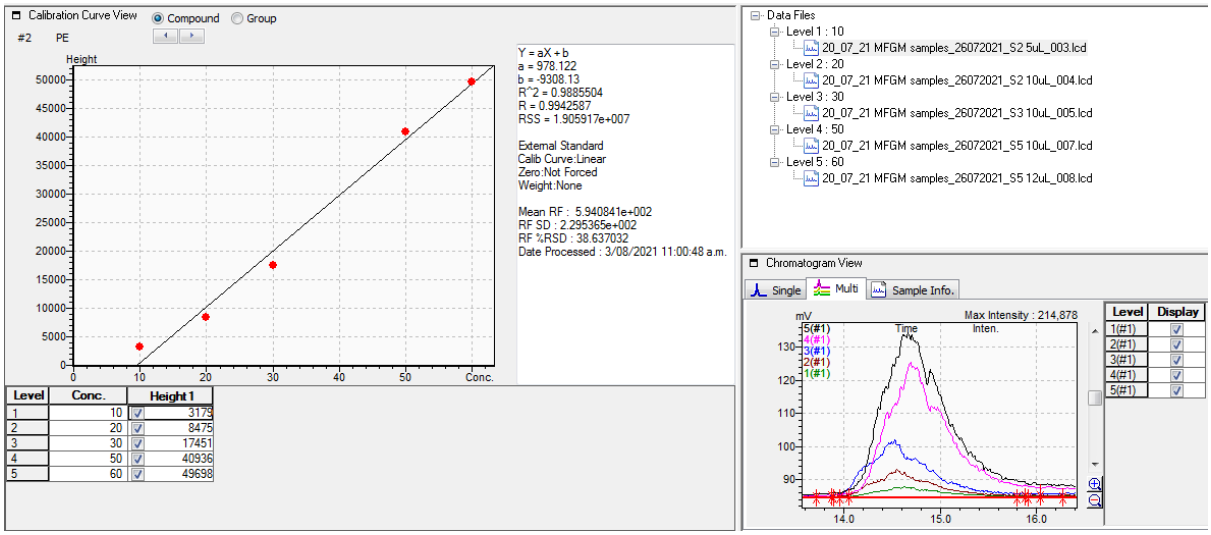

d) Phosphatidylserine standard curve

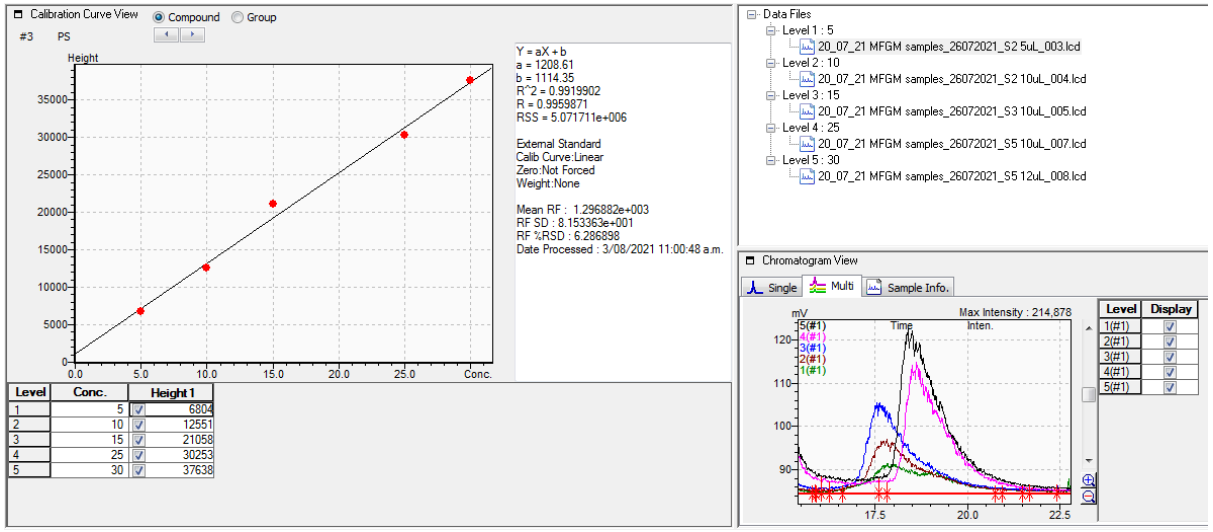

e) Phosphatidylcholine standard curve

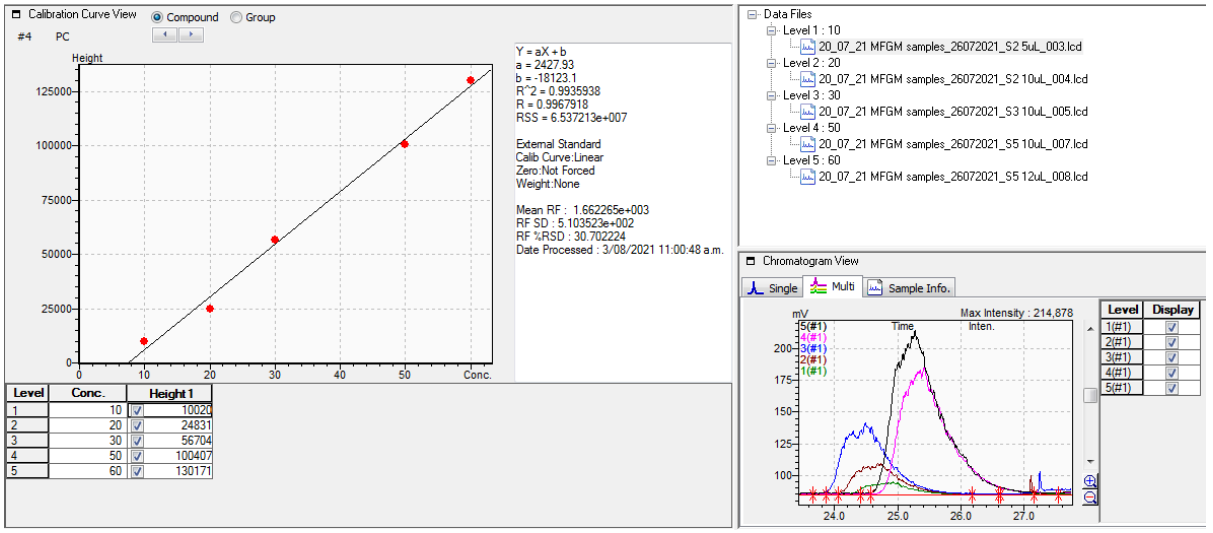

f) Sphingomyelin standard curve

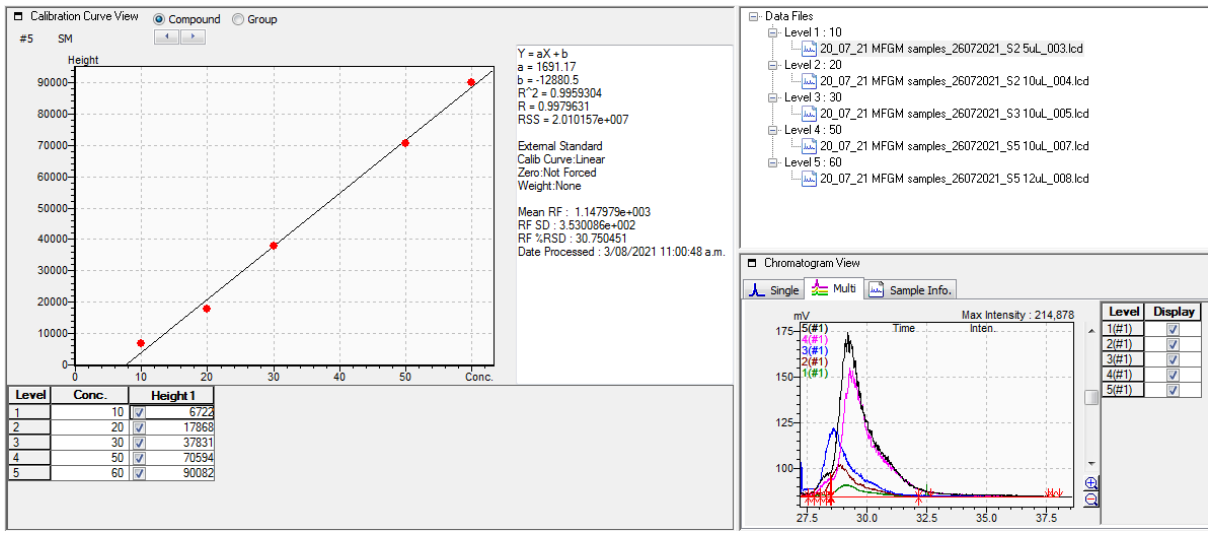

Appendix 5.1. Milk fat globule membrane phospholipid extract HPLC concentration and standard curves.

a) Mass of each phospholipid type to make standard curves. Units are in (ug).
b) Phosphatidylinositol standard curve, $y = 3610.41X-12553$, $r^2 = 0.997$
c) Phosphatidylethanolamine standard curve, $y = 978.1X – 9308.1$, $r^2 = 0.989$
d) Phosphatidylserine standard curve, $y = 1208.61X-1114.35$, $r^2 = 0.992$
e) Phosphatidylcholine standard curve, $y = 2427.93X-18123.1$, $r^2 = 0.994$
f) Sphingomyelin standard curve, $y = 1691.17X-12880.5$, $r^2 = 0.996$

Typical Composition		
Parameter	**Unit of Measure**	**Value**
Chemical		
Protein (TN x 6.38)	%	30.8
Moisture	%	3.6
Ash	%	6.5
Fat (total)	%	15.2
Phospholipid (as is)	%	5.8
pH (5% TS/20 °C)		6.8
Lactose	%	47.2
Physical		
Foreign Matter	/100 g	Absent
Scorched Particles	/100 g	Absent
Sensory		
Flavour/Odour		Typical
Microbiological		
Aerobic Plate Count	cfu/g	< 30000
Coliform	/g	Not Detected
E.coli	/g	Not Detected
Yeasts and Moulds	cfu/g	50
Coagulase +ve Staphylococci	cfu/g	Not Detected
Salmonella	/750 g	Absent
Listeria	/750 g	Absent
Phospholipids		
Phosphatidylcholine	%	26.6
Phosphatidylserine	%	12.1
Phosphatidylinositol	%	8.5
Phosphatidylethanolamine	%	30.8
Sphingomyelin	%	20.8
Glycolipid		
Ganglioside (GD3)	mg/g	2.2

Appendix 5.2. Beta serum powder (BSP2): Beta serum is the aqueous phase removed from pasteurised cream during the process of Anhydrous Milk Fat (AMF) production. Beta serum powder is obtained by spray drying fresh liquid beta serum. Reproduced from TATUA BSP2 Typical Composition, (2017)

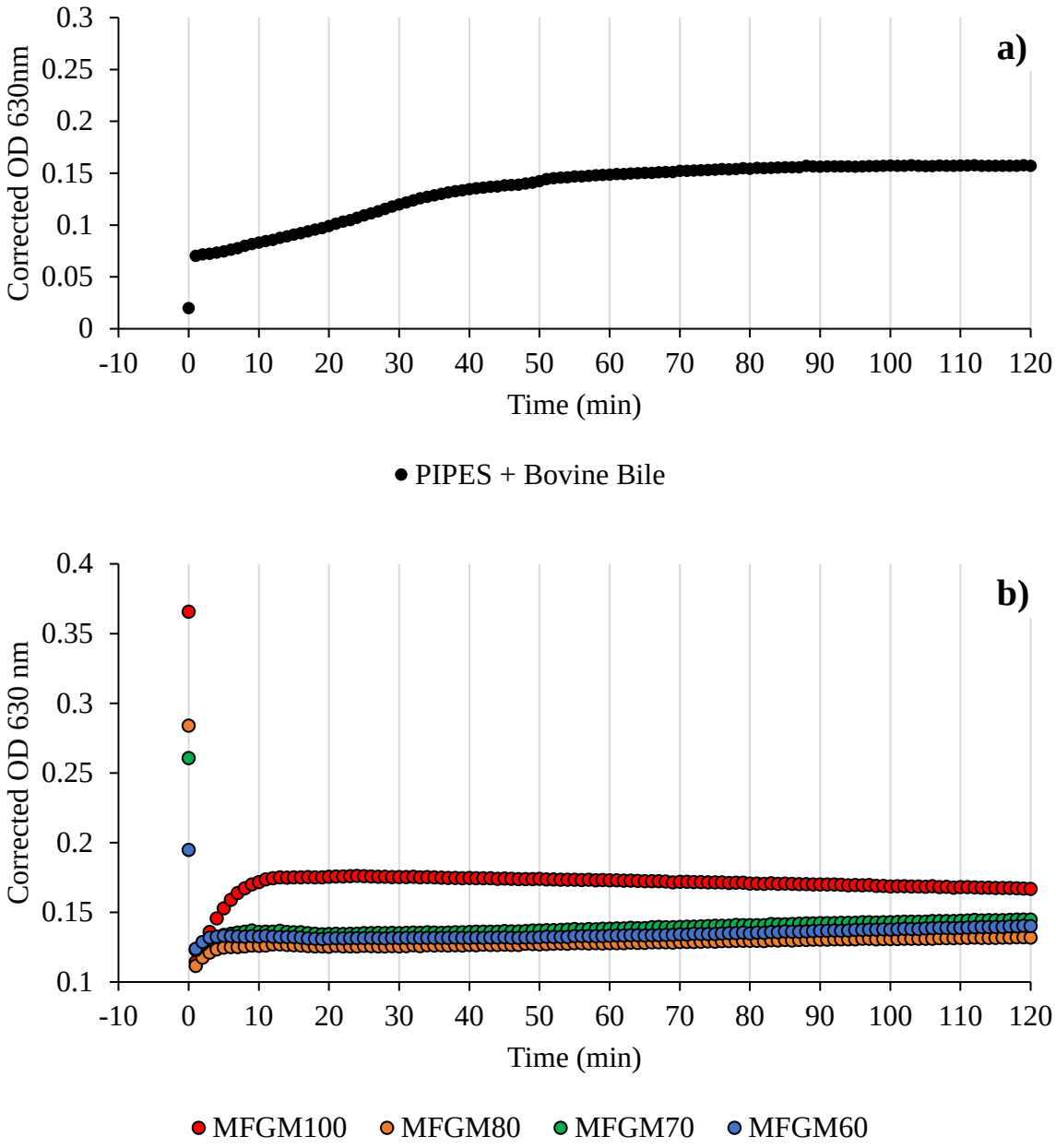

Appendix 5.3. Optical density 630 nm of milk fat globule membrane (MFGM) phospholipid vesicles incubated with bovine bile. a) The blank used to subtract the bovine bile background to produce Fig. 5.5 b. b) Detergent-induced micellization of MFGM phospholipid vesicles without bovine bile subtraction. MFGM100 = without cholesterol, MFGM80 = 4:1 sphingomyelin/cholesterol, MFGM70 = 7:3 sphingomyelin/cholesterol, MFGM60 = 3:2 sphingomyelin/cholesterol. SM makes up 18.5% mol of the MFGM phospholipid extract

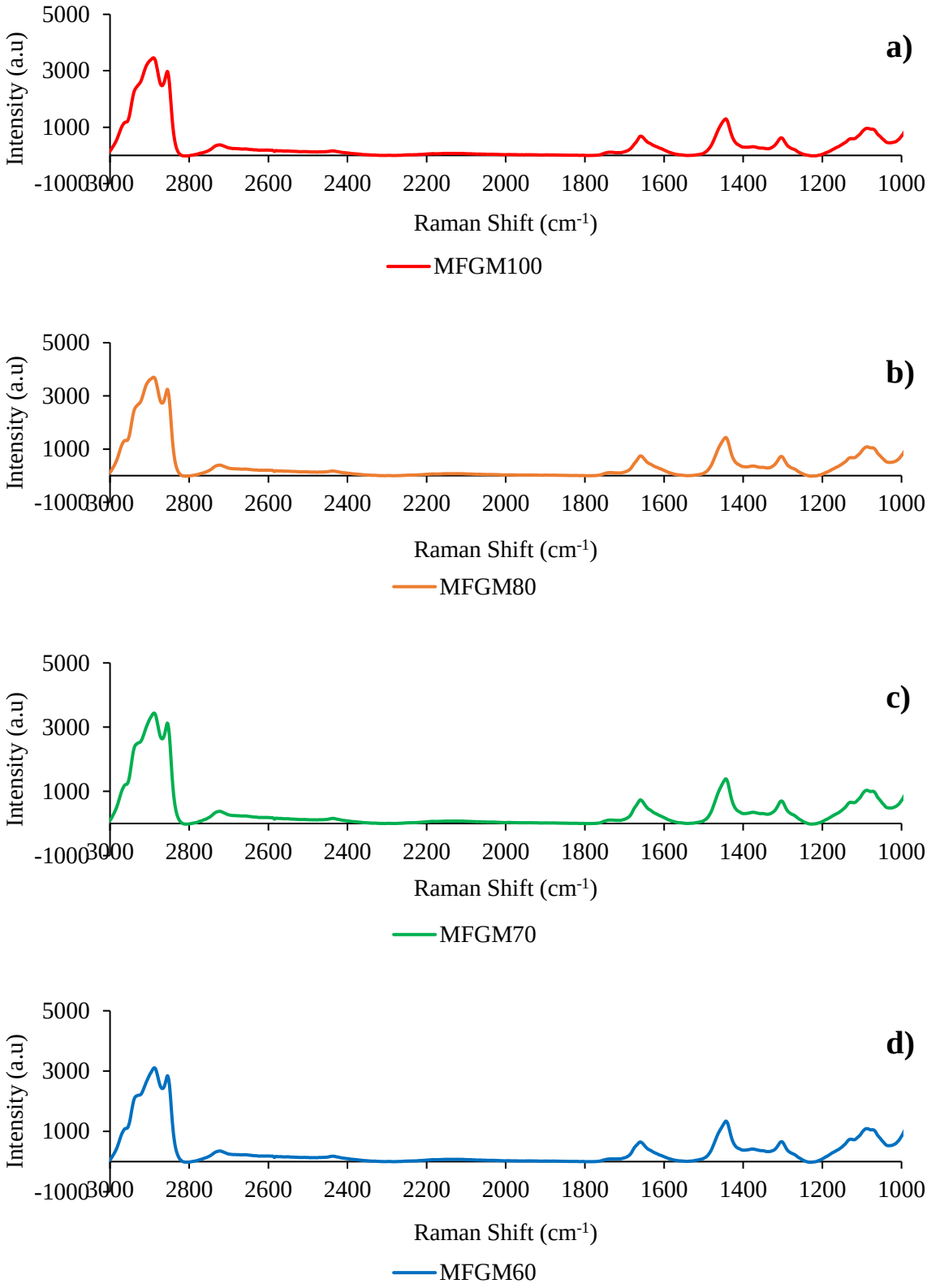

Appendix 5.4. Raman spectroscopy of milk fat globule (MFGM) phospholipid vesicles without bovine bile addition with varying concentrations of cholesterol.

a) MFGM phospholipid vesicles without cholesterol
b) MFGM phospholipid vesicles with 4:1 sphingomyelin/cholesterol
c) MFGM phospholipid vesicles with 7:3 sphingomyelin/cholesterol
d) MFGM phospholipid vesicles with 3:2 sphingomeylin/cholesterol

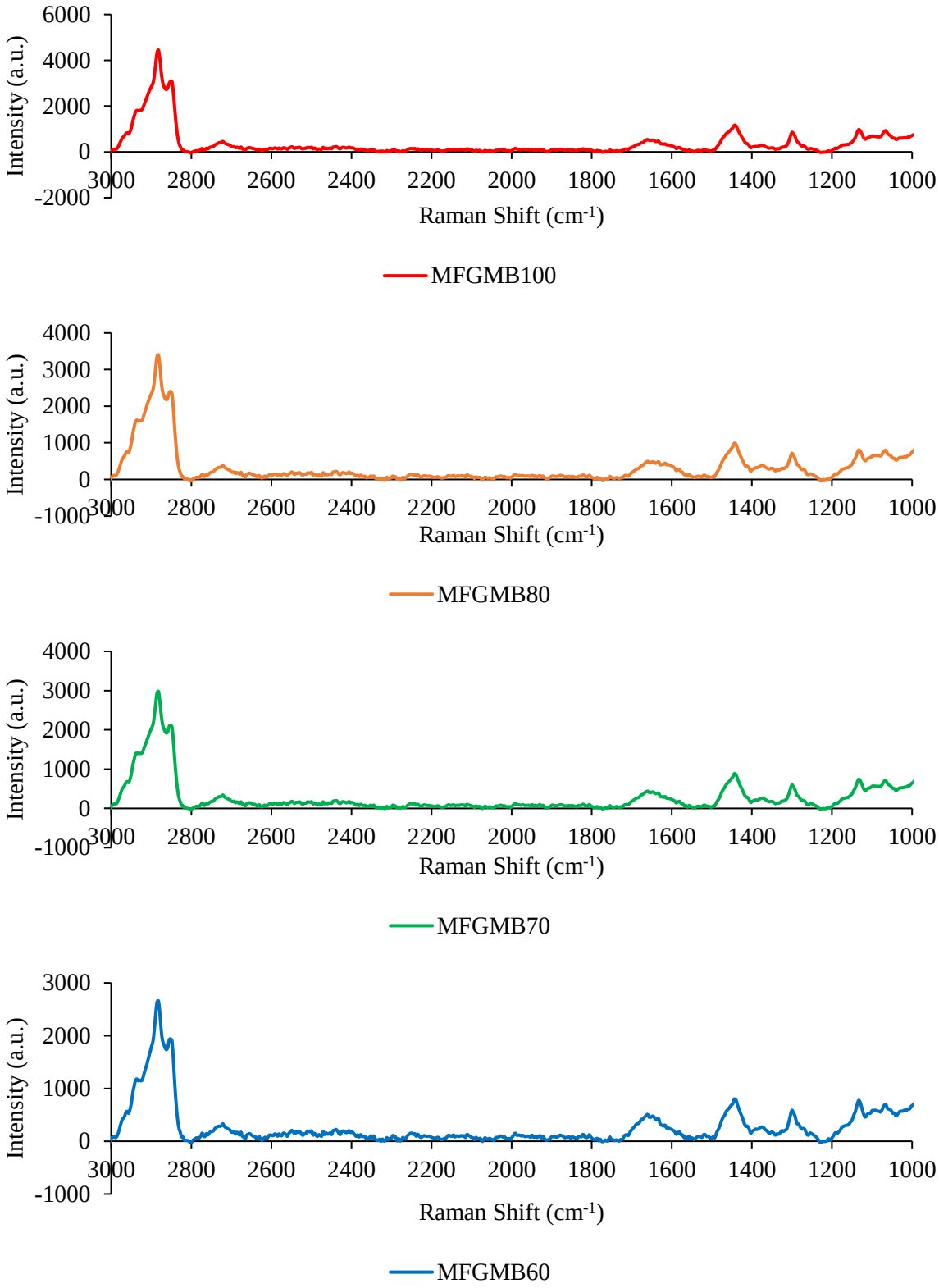

Appendix 5.5. Raman Spectroscopy of milk fat globule membrane (MFGM) phospholipid vesicles after bovine bile (10 mM, 8:1 v/v) addition with varying concentrations of cholesterol.

a) MFGM phospholipid vesicles without cholesterol
b) MFGM phospholipid vesicles with 4:1 sphingomyelin/cholesterol
c) MFGM phospholipid vesicles with 7:3 sphingomyelin/cholesterol
d) MFGM phospholipid vesicles with 3:2 sphingomyelin/cholesterol

Appendix 5.6. Milk fat globule membrane phospholipid extract vesicle hydrocarbon inter- and intra-chain Raman peak intensity ratios

		I_{2850}/I_{2880}		I_{2930}/I_{2880}		I_{1085}/I_{1130}	
		No Bile	Bile Added	No Bile	Bile Added	No Bile	Bile Added
MFGM	0% Cholesterol	0.85 ± 0.03 A	0.686 ± 0.023 C	0.66 ± 0.04 AB	0.42 ± 0.09 B	1.65 ± 0.04 A	0.97 ± 0.09 CD
	20% Cholesterol	0.880 ± 0.023 AB	0.705 ± 0.020 C	0.67 ± 0.03 AB	0.52 ± 0.14 AB	1.60 ± 0.04 A	1.02 ± 0.10 C
	30% Cholesterol	0.902 ± 0.023 AB	0.689 ± 0.028 C	0.69 ± 0.03 A	0.57 ± 0.27 AB	1.56 ± 0.05 AB	0.98 ± 0.07 CD
	40% Cholesterol	0.911 ± 0.012 B	0.71 ± 0.04 C	0.677 ± 0.018 A	0.47 ± 0.10 AB	1.48 ± 0.03 B	0.91 ± 0.07 D

Different letters within each ratio denote significant differences for both no bile and bile added

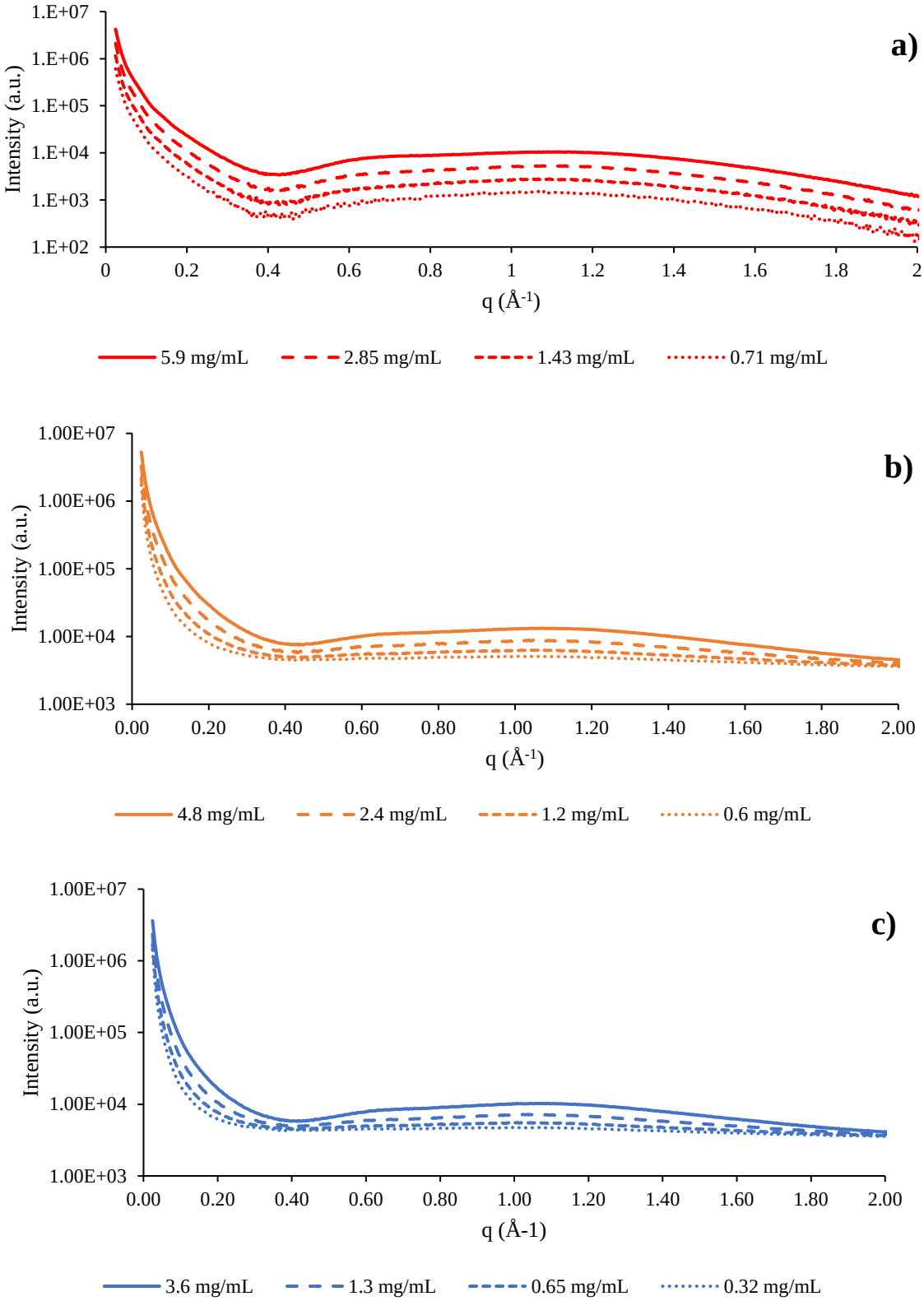

Appendix 5.7. Small angle x-ray scattering of milk fat globule membrane phospholipid vesicles normalized to account for concentration. a) MFGM100 = milk fat globule membrane without cholesterol, reproduction of Fig. 5.9. a; b) MFGM80 = milk fat globule membrane with 4:1 mol/mol MSM/cholesterol; c) MFGM60 = milk fat globule membrane with 3:2 mol/mol MSM/cholesterol

Appendix: Chapter 6

Appendix 6.1.

The protocol for phospholipid determination by HPLC-ELSD (evaporative light scattering detector) is presented in Chapter 5. For convenience, it is reproduced here. Quantitative analysis of the phospholipids was determined using HPLC-ELSD (Shimadzu, Kyoto, Japan) equipped with two LC-10 ADvp pumps, an SCL-10 ADvp gradient system, a DGU-14 ADvp module de-gaser, and SIL-10ADvp autosampler (Su et al., 2019). The analytical column was a YMC – pack PVA-SIL-NP column (250 × 4.6 mm, 5 µm) and the mobile phase followed a linear, binary gradient according to the following scheme: t0 = 0% B, t30 = 40% B and then isocratic (40% B) for 30 min at a constant flow rate of 1.0 mL/min. Eluent A consisted of chloroform:isopropanol:triethylamine:acetic acid (75:25:0.08:1.0, v/v/v/v) and eluent B was methanol:water:triethylamine:acetic acid (95:5:0.08:1.0, v/v/v/v). An ELSD-LT II Shimadzu model ELSD was used for detection; the pressure of nebulizer gas (nitrogen) was maintained at 350 kPa and the drift tube temperature was set to 80 °C. Identification of glycerophospholipids and sphingomyelin was carried out by comparing against the retention time of pure standards. Calibration curves for each compound were calculated from maximum peak heights obtained by injecting different volumes containing soy-PE (Cayman Chemical Company, Ann Arbor, MI, USA), soy-PI, soy-PS, milk-SM (Avanti Polar Lipids, Alabaster, AL, USA), and soy-PC (Sigma-Aldrich, MI, USA) standards dissolved in chloroform.

A) Phosphatidylinositol Standard Curve, r^2 = 0.998, f(x)=18041.3*x-53249.4

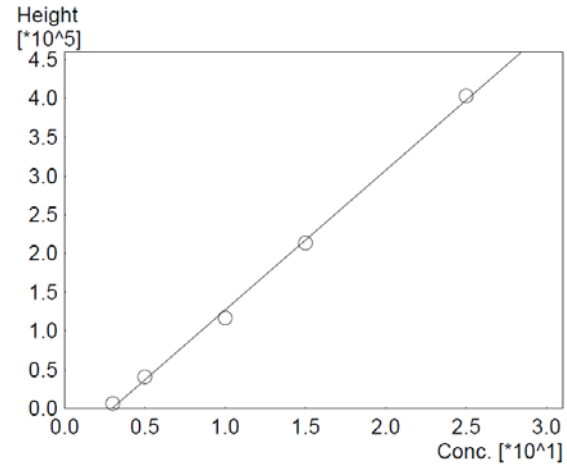

#	Conc.(Ratio)	MeanHeight	Height
1	3	6188	6188
2	5	40862	40862
3	10	116830	116830
4	15	213367	213367
5	25	402898	402898

B) Phosphatidylethanolamine Standard Curve, r^2 = 0.993, f(x)=2252.45x-15896.0

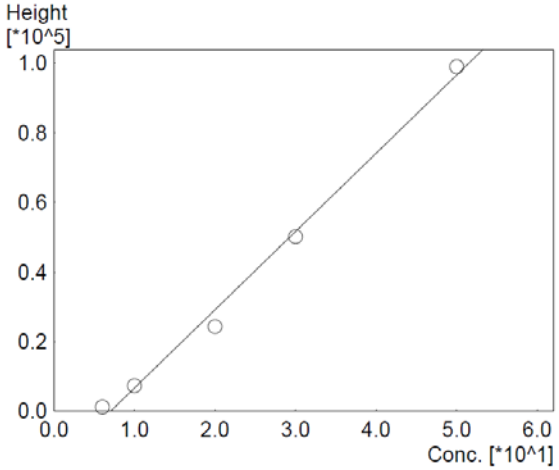

#	Conc.(Ratio)	MeanHeight	Height
1	6	1117	1117
2	10	7211	7211
3	20	24273	24273
4	30	50136	50136
5	50	99067	99067

C) Phosphatidylserine Standard Curve, r^2 = 0.993, f(x)=3474.25x-12728.9

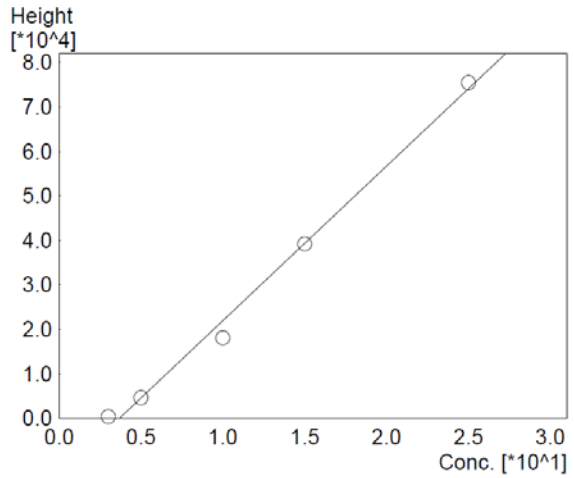

#	Conc.(Ratio)	MeanHeight	Height
1	3	404	404
2	5	4679	4679
3	10	18114	18114
4	15	39200	39200
5	25	75466	75466

D) Phosphatidylcholine Standard Curve, r^2 = 0.993, f(x)=3214.97x-20162.9

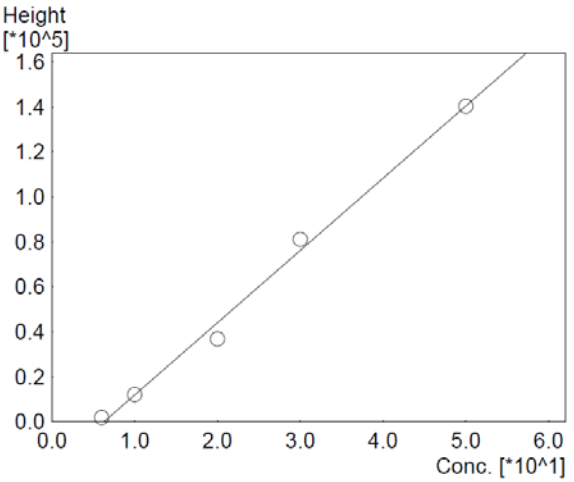

#	Conc.(Ratio)	MeanHeight	Height
1	6	1821	1821
2	10	12114	12114
3	20	36781	36781
4	30	81139	81139
5	50	140268	140268

E) Sphingomyelin Standard Curve, r^2 = 0.995, f(x)=3056.54x-21160.6

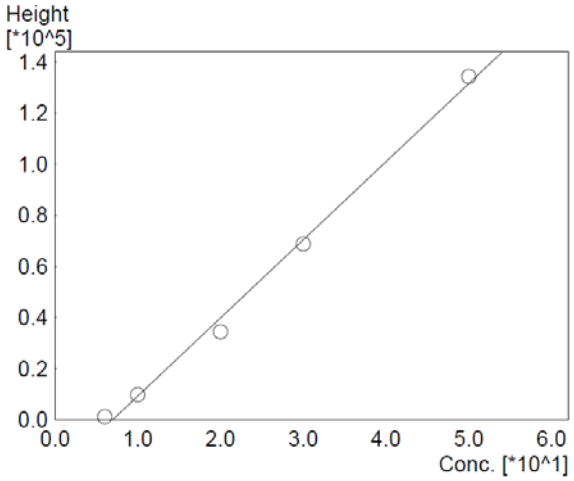

#	Conc.(Ratio)	MeanHeight	Height
1	6	1262	1262
2	10	9913	9913
3	20	34443	34443
4	30	68825	68825
5	50	134312	134312

Appendix 6.2. Phospholipid standard curves for HPLC-ELSD. Conc.(Ratio) = Label for the mass of phospholipid present (ng).

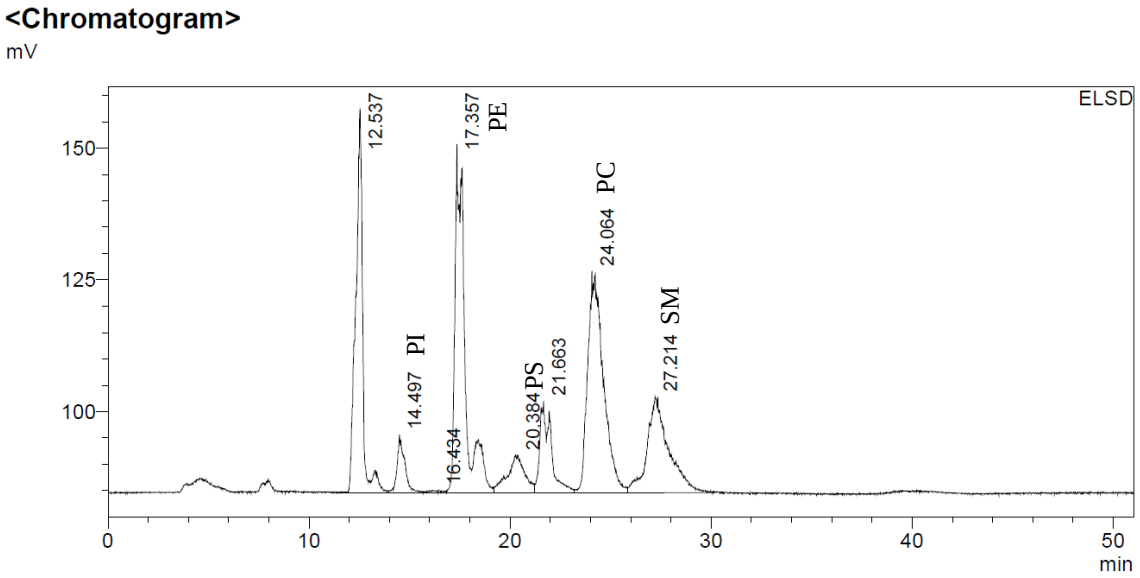

Appendix 6.3. Example chromatogram of phospholipids extracted from bovine beta-serum extract. PI = phosphatidylinositol; PE = phosphatidylethanolamine; PS = phosphatidylserine; PC = phosphatidylcholine; SM = sphingomyelin.

Units/mg powder = $\frac{R(NaOH) \times 1000}{v\,[E]}$

R(NaOH): Rate of NaOH delivery in µmol NaOH/min. Equivalent to µmol free fatty acid released per min.
V: volume [uL] of enzyme solution in the pH stat vessel
[E]: concentration of enzyme solution [mg powder/mL]

Blank = 0 units/mg powder

Rabbit gastric extract at pH 5 after 20 min at 60 °C = 0 units/mg powder

Rabbit gastric extract no modifications = 8.16 ± 2.84 units/mg powder

Appendix 6.4. Equation and results of gastric lipase enzymatic assay. Protocol used as reported in (Brodkorb et al., 2019).

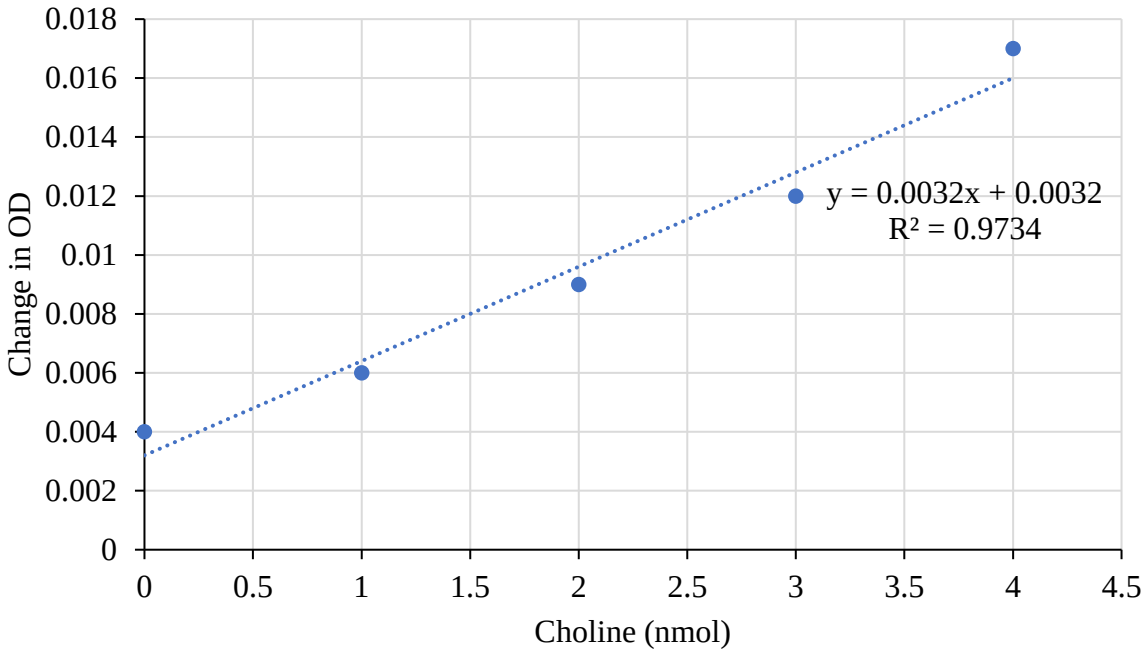

Sample alk-SMase activity = $\{\frac{B}{\Delta T \times V}\} \times D$

where B is the amount of choline in the sample calculated from the standard curve, ΔT is the change in reaction time (min), V is the sample volume added to the well(mL), and D is the sample dilution factor.

alk-SMase concentration assayed = 3.49 ± 0.00 nmol/min/mL (n = 3)

Appendix 6.5. Standard curve and equation for alk-SMase activity determination.

a)

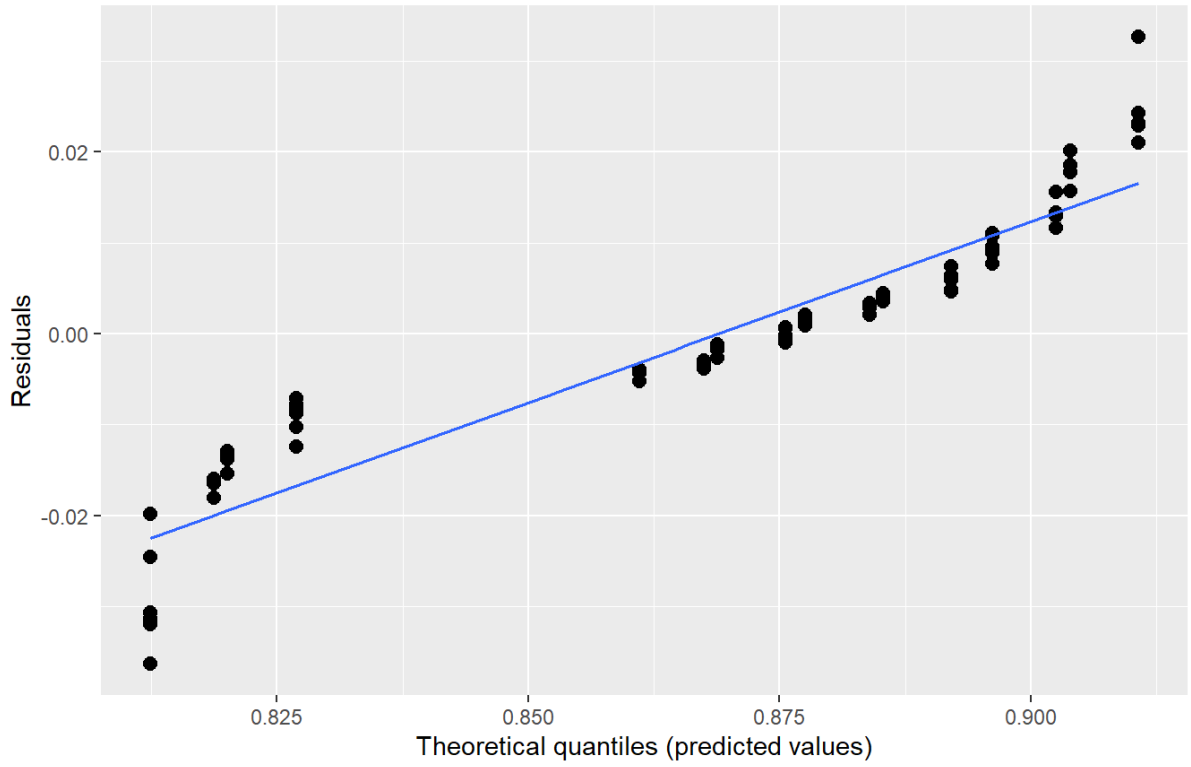
Residuals
0.02
0.00
-0.02
0.825
0.850
0.875
0.900
Theoretical quantiles (predicted values)

b)

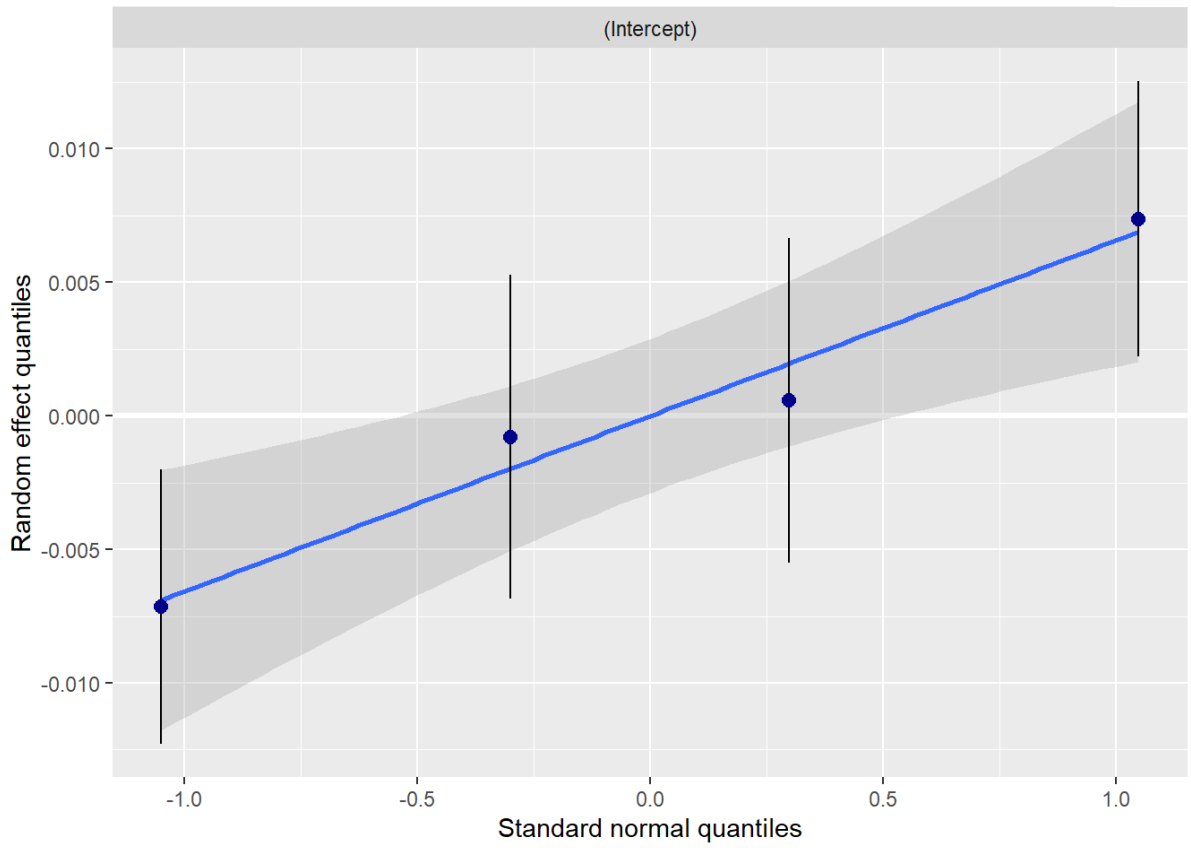
(Intercept)
Random effect quantiles
0.010
0.005
0.000
-0.005
-0.010
-1.0
-0.5
0.0
0.5
1.0
Standard normal quantiles

c)

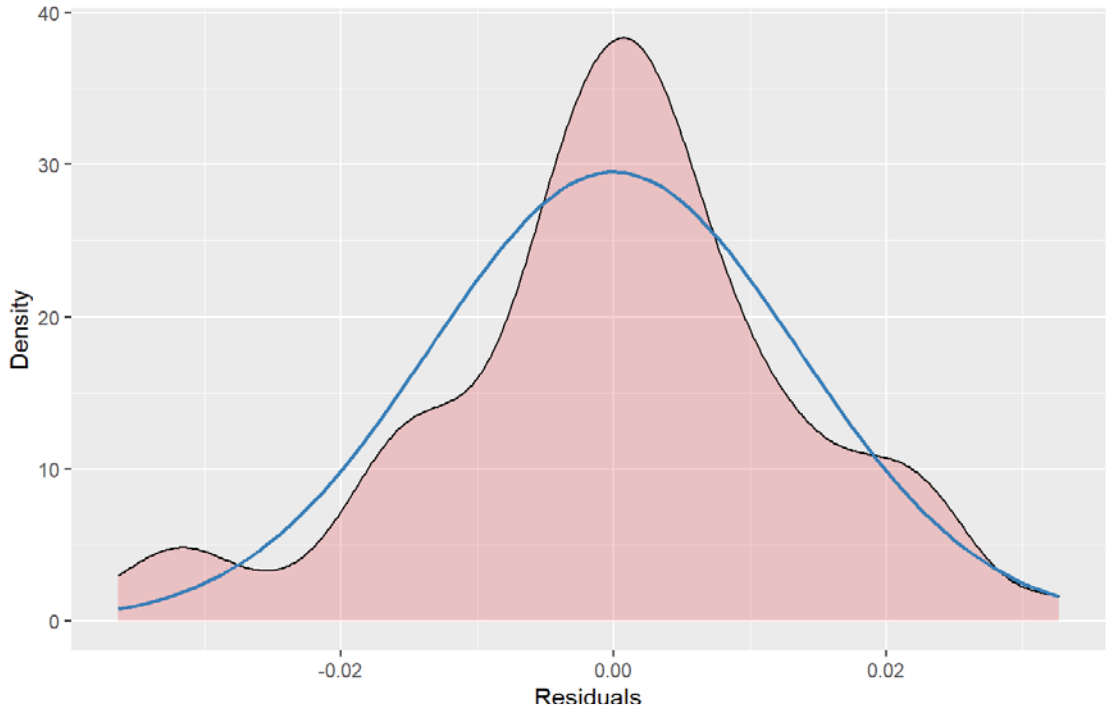

d)

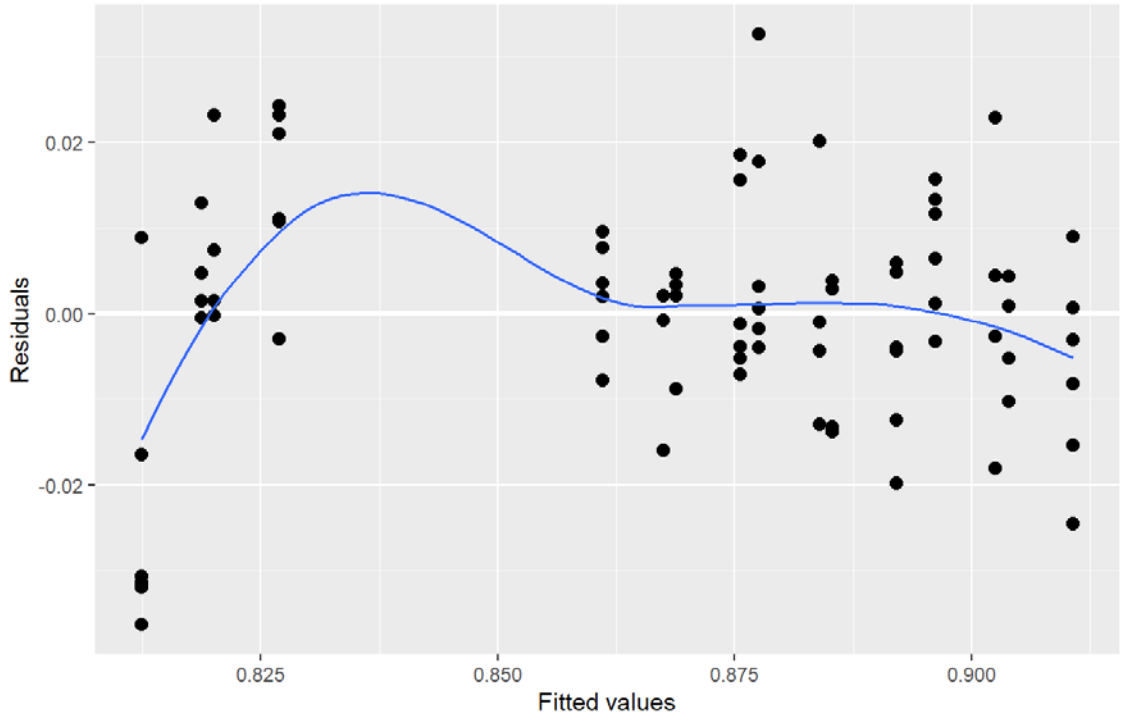

Appendix 6.6. Statistical diagnostics performed on MSM MLVs I_{2850}/I_{2880} pre-digestion.
a, b) Normality test of residuals and outliers. (Normal data = dots plotted along the line).
c) Normality test of residuals (Normal data = should resemble a normal curve).
d) Homoscedasticity, the constant variance of residuals. Amount and distance of points scattered above and below the line is equal or randomly spread.

a)

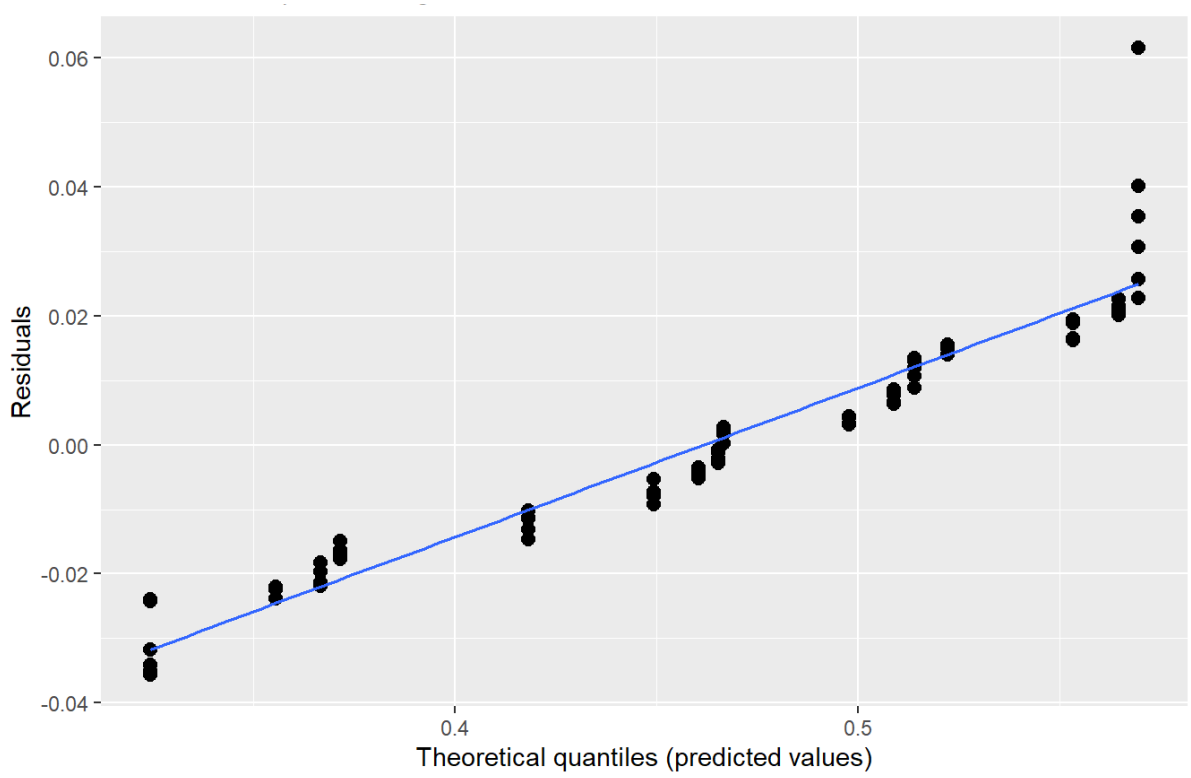
0.06
0.04
0.02
0.00
-0.02
-0.04
Residuals
0.4
0.5
Theoretical quantiles (predicted values)

b)

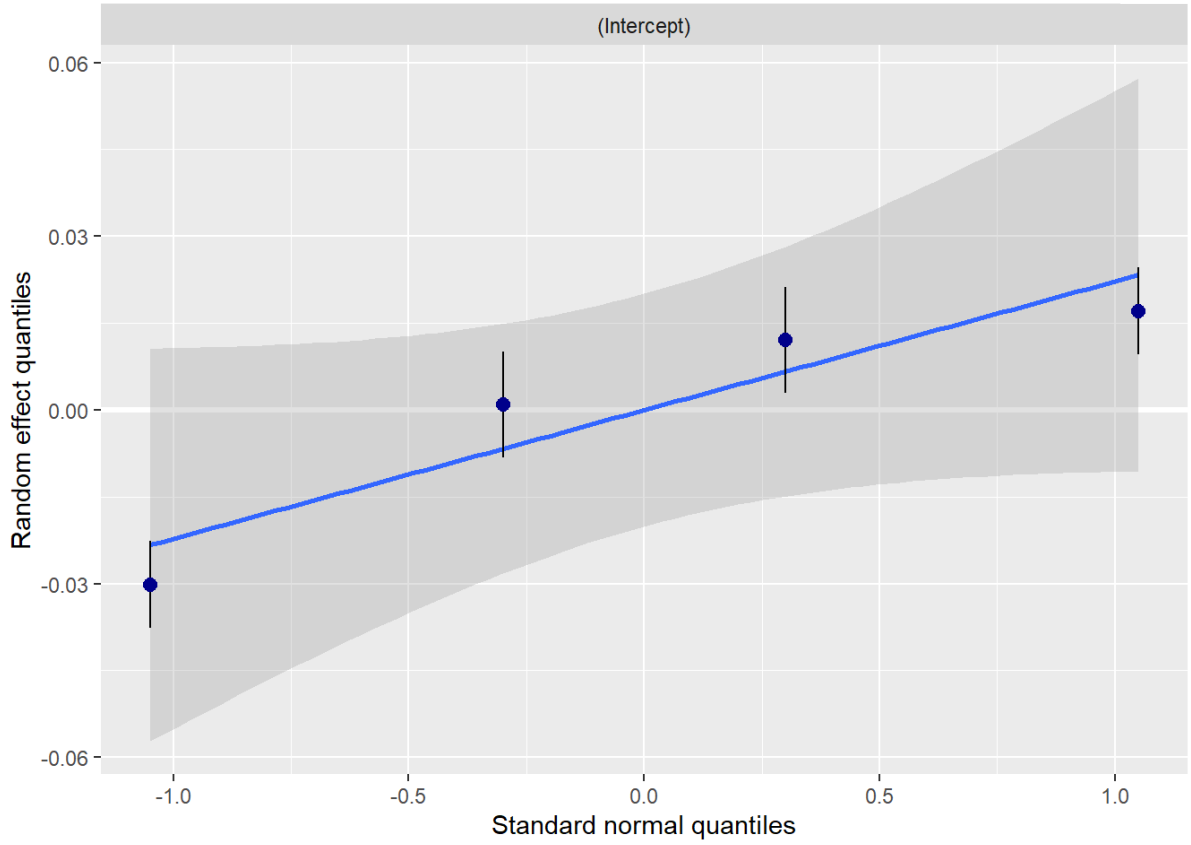
(Intercept)
0.06
0.03
0.00
-0.03
-0.06
Random effect quantiles
-1.0
-0.5
0.0
0.5
1.0
Standard normal quantiles

c)

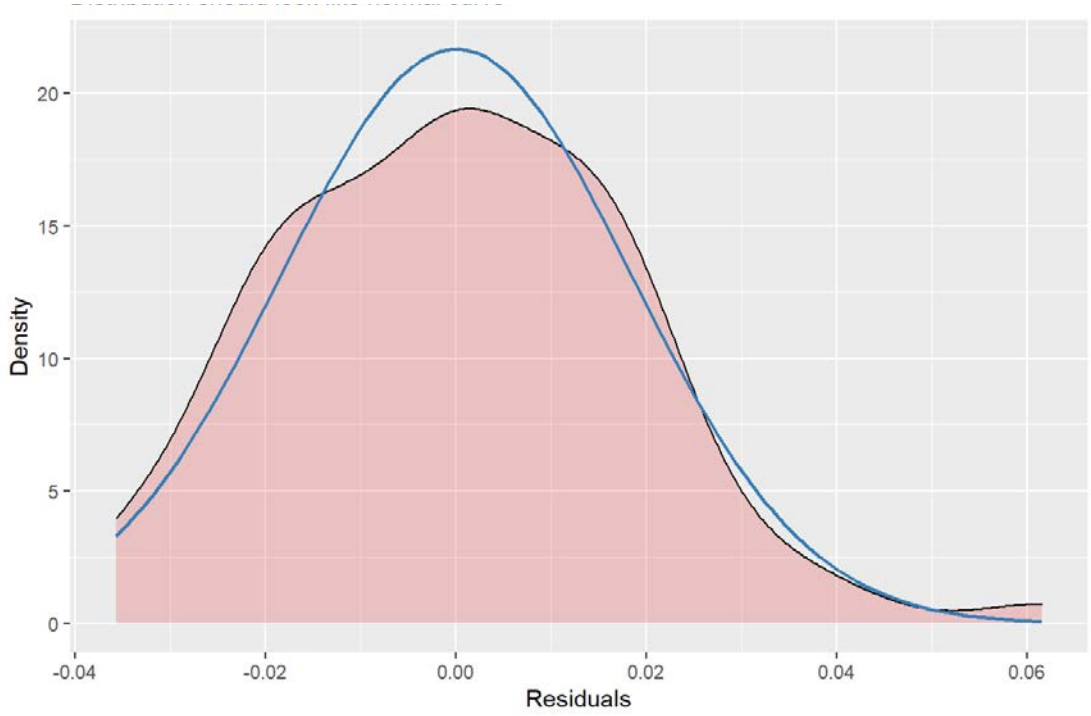

d)

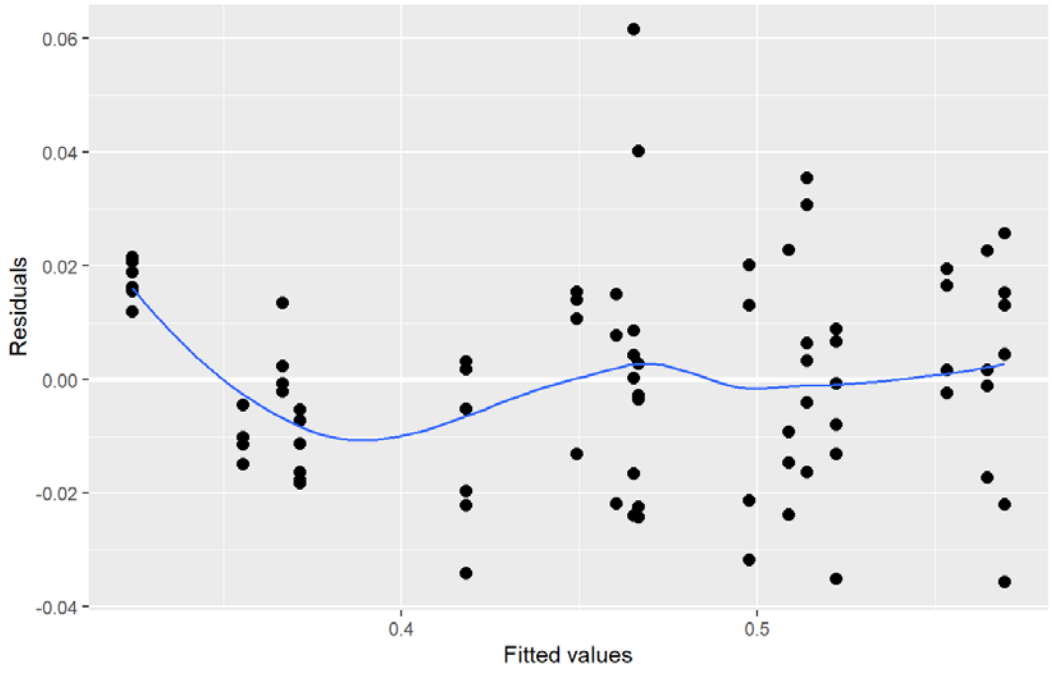

Appendix. 6.7. Statistical diagnostics performed on the I_{2930}/I_{2880} of MSM MLVs.

a, b) Normality test of residuals and outliers. (Normal data = dots plotted along the line).
c) Normality test of residuals (Normal data = distribution should resemble a normal curve).
d) Homoscedasticity, the constant variance of residuals. Amount and distance of points scattered above and below the line is equal or randomly spread.

a)

No SMase	Phospholipid/ Cholesterol (mol/mol)	Pre-Digestion	Post Gastric	Post Intestinal
		I_{2850}/I_{2880}		
MSM100	1:0	0.801 ± 0.019	0.88 ± 0.06	0.70 ± 0.03
MSM80	4:1	0.854 ± 0.021	0.86 ± 0.02	0.67 ± 0.04
MSM70	7:3	0.888 ± 0.012	0.86 ± 0.08	0.70 ± 0.04
MSM60	3:2	0.902 ± 0.010	0.88 ± 0.02	0.71 ± 0.06
		I_{2930}/I_{2880}		
MSM100	1:0	0.358 ± 0.017	0.44 ± 0.06	0.49 ± 0.12
MSM80	4:1	0.431 ± 0.036	0.47 ± 0.05	0.50 ± 0.12
MSM70	7:3	0.482 ± 0.029	0.54 ± 0.05	0.49 ± 0.08
MSM60	3:2	0.532 ± 0.025	0.57 ± 0.03	0.46 ± 0.06
		I_{1085}/I_{1130}		
MSM100	1:0	0.999 ± 0.034	1.18 ± 0.08	
MSM80	4:1	1.210 ± 0.100	1.26 ± 0.14	
MSM70	7:3	1.300 ± 0.110	1.25 ± 0.15	
MSM60	3:2	1.320 ± 0.070	1.27 ± 0.12	
SMase	Phospholipid/ Cholesterol (mol/mol)	Pre-Digestion	Post Gastric	Post Intestinal
		I_{2850}/I_{2880}		
MSM100	1:0	0.825 ± 0.014	0.824 ± 0.017	0.740 ± 0.066
MSM80	4:1	0.877 ± 0.010	0.864 ± 0.001	0.678 ± 0.065
MSM70	7:3	0.886 ± 0.006	0.863 ± 0.017	0.648 ± 0.018
MSM60	3:2	0.903 ± 0.011	0.893 ± 0.015	0.742 ± 0.032
		I_{2930}/I_{2880}		
MSM100	1:0	0.354 ± 0.015	0.493 ± 0.096	0.64 ± 0.13
MSM80	4:1	0.476 ± 0.023	0.488 ± 0.023	0.62 ± 0.07
MSM70	7:3	0.517 ± 0.028	0.521 ± 0.029	0.56 ± 0.07
MSM60	3:2	0.563 ± 0.020	0.588 ± 0.029	0.67 ± 0.09
		I_{1085}/I_{1130}		
MSM100	1:0	1.16 ± 0.04	1.29 ± 0.21	
MSM80	4:1	1.36 ± 0.05	1.35 ± 0.06	
MSM70	7:3	1.42 ± 0.05	1.38 ± 0.05	
MSM60	3:2	1.45 ± 0.06	1.38 ± 0.07	

b)

Name	Phospholipid/ Cholesterol (mol/mol)	Pre-Digestion	Post-Gastric	Post-Intestinal SMase	Post-Intestinal no SMase
			I_{2850}/I_{2880}		
BPC100	1:0	0.936 ± 0.007	0.910 ± 0.004	0.733 ± 0.058	0.719 ± 0.058
BPC80	4:1	0.939 ± 0.012	0.910 ± 0.011	0.703 ± 0.076	0.730 ± 0.059
BPC70	7:3	0.940 ± 0.009	0.916 ± 0.013	0.657 ± 0.025	0.766 ± 0.075
BPC60	3:2	0.953 ± 0.013	0.915 ± 0.012	0.682 ± 0.066	0.742 ± 0.046
			I_{2930}/I_{2880}		
BPC100	1:0	0.697 ± 0.010	0.728 ± 0.015	0.729 ± 0.066	0.740 ± 0.110
BPC80	4:1	0.691 ± 0.018	0.754 ± 0.006	0.730 ± 0.093	0.710 ± 0.070
BPC70	7:3	0.724 ± 0.006	0.756 ± 0.007	0.753 ± 0.064	0.800 ± 0.070
BPC60	3:2	0.749 ± 0.017	0.792 ± 0.017	0.800 ± 0.070	0.750 ± 0.020
			I_{1085}/I_{1130}		
BPC100	1:0	2.39 ± 0.23	2.45 ± 0.09		
BPC80	4:1	1.87 ± 0.08	1.90 ± 0.09		
BPC70	7:3	1.83 ± 0.08	1.81 ± 0.08		
BPC60	3:2	1.72 ± 0.12	1.66 ± 0.04		

c)

Name	Phospholipid/ Cholesterol (mol/mol)	Pre-Digestion	Post-Gastric	Post-Intestinal SMase	Post-Intestinal no SMase
			I_{2850}/I_{2880}		
SPC100	1:0	0.908 ± 0.022	0.883 ± 0.018	0.71 ± 0.04	0.62 ± 0.04
SPC80	4:1	0.904 ± 0.009	0.900 ± 0.023	0.69 ± 0.04	0.64 ± 0.10
SPC70	7:3	0.932 ± 0.019	0.860 ± 0.043	0.72 ± 0.06	0.62 ± 0.07
SPC60	3:2	0.934 ± 0.019	0.906 ± 0.005	0.72 ± 0.09	0.66 ± 0.07
			I_{2930}/I_{2880}		
SPC100	1:0	0.807 ± 0.008	0.824 ± 0.010	0.62 ± 0.13	0.52 ± 0.07
SPC80	4:1	0.833 ± 0.012	0.815 ± 0.048	0.57 ± 0.10	0.69 ± 0.12
SPC70	7:3	0.829 ± 0.008	0.750 ± 0.120	0.66 ± 0.08	0.65 ± 0.08
SPC60	3:2	0.855 ± 0.023	0.815 ± 0.021	0.72 ± 0.10	0.65 ± 0.09
			I_{1085}/I_{1130}		
SPC100	1:0	2.814 ± 0.022	1.900 ± 0.200		
SPC80	4:1	2.700 ± 0.500	1.900 ± 0.300		
SPC70	7:3	2.400 ± 0.5	1.600 ± 0.300		
SPC60	3:2	2.200 ± 0.4	1.600 ± 0.200		

d)

Name	Phospholipid/ Cholesterol (mol/mol)	Pre-Digestion	Post-Gastric	Post-Intestinal SMase	Post-Intestinal no SMase
			I_{2850}/I_{2880}		
MFGM100	1:0	0.79 ± 0.12	0.84 ± 0.09	0.72 ± 0.10	0.66 ± 0.03
MFGM80	4:1	0.85 ± 0.05	0.86 ± 0.03	0.69 ± 0.02	0.64 ± 0.07
MFGM70	7:3	0.86 ± 0.04	0.86 ± 0.01	0.68 ± 0.04	0.66 ± 0.07
MFGM60	3:2	0.83 ± 0.05	0.86 ± 0.04	0.64 ± 0.04	0.64 ± 0.03
			I_{2930}/I_{2880}		
MFGM100	1:0	0.54 ± 0.05	0.59 ± 0.03	0.79 ± 0.04	0.73 ± 0.09
MFGM80	4:1	0.58 ± 0.03	0.61 ± 0.01	0.77 ± 0.06	0.74 ± 0.07
MFGM70	7:3	0.57 ± 0.03	0.59 ± 0.02	0.74 ± 0.05	0.76 ± 0.07
MFGM60	3:2	0.57 ± 0.05	0.61 ± 0.02	0.75 ± 0.09	0.74 ± 0.05
			I_{1085}/I_{1130}		
MFGM100	1:0	1.60 ± 0.10	1.65 ± 0.12		
MFGM80	4:1	1.65 ± 0.09	1.58 ± 0.11		
MFGM70	7:3	1.64 ± 0.10	1.58 ± 0.10		
MFGM60	3:2	1.55 ± 0.08	1.55 ± 0.06		

Appendix 6.8. Tabulated values of peak intensity ratios of phospholipid vesicles.

a) Milk sphingomyelin (MSM) multilamellar vesicles (MLVs), MSM100 = with no cholesterol, MSM80 = 4:1 MSM/cholesterol, MSM70 = 7:3 MSM/cholesterol, MSM60 = 3:2 MSM/cholesterol.
b) Brain phosphatidylcholine (BPC) vesicles, BPC100 = no cholesterol, BPC80 = 4:1 BPC/cholesterol, BPC70 = 7:3 BPC/cholesterol, BPC60 = 3:2 BPC/cholesterol.
c) Soy phosphatidylcholine (SPC) vesicles, SPC100 = no cholesterol, SPC80 = 4:1 SPC/cholesterol, SPC70 = 7:3 SPC/cholesterol; SPC60 = 3:2 SPC/cholesterol.
d) Milk fat globule membrane (MFGM) phospholipid vesicles, MFGM100 = no cholesterol, MFGM80 = 4:1 SM/cholesterol, MFGM70 = 3:2 SM/cholesterol.

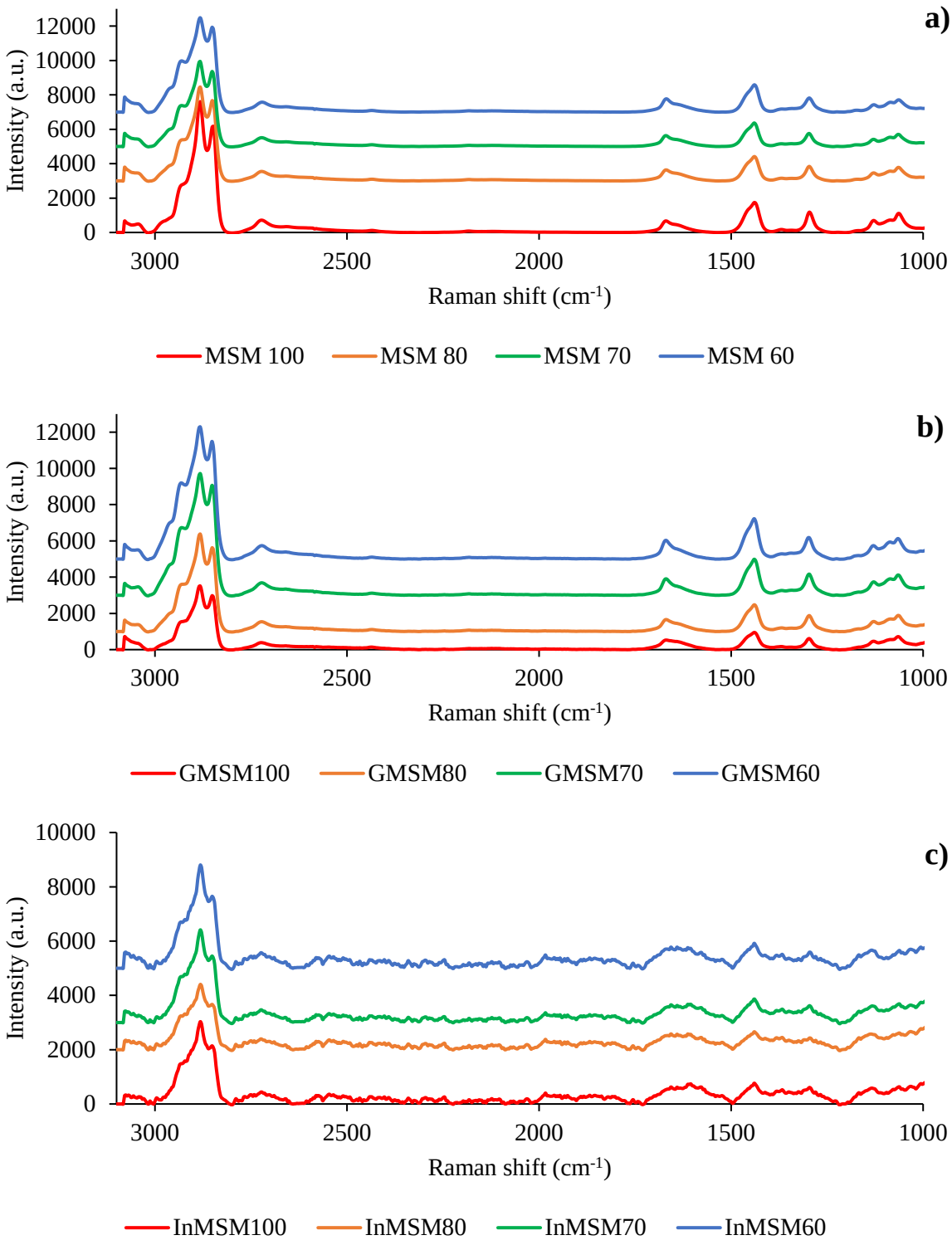

Appendix 6.9. Average Raman spectra of milk sphingomyelin (MSM) multilamellar vesicles. 100 = without cholesterol; 80 = 4:1 BPC/cholesterol; 70 = 7:3 mol/mol BPC/cholesterol; 60 = 3:2 mol/mol BPC/cholesterol. a) pre-digestion; b) post-gastric; c) post-intestinal without alk-SMase

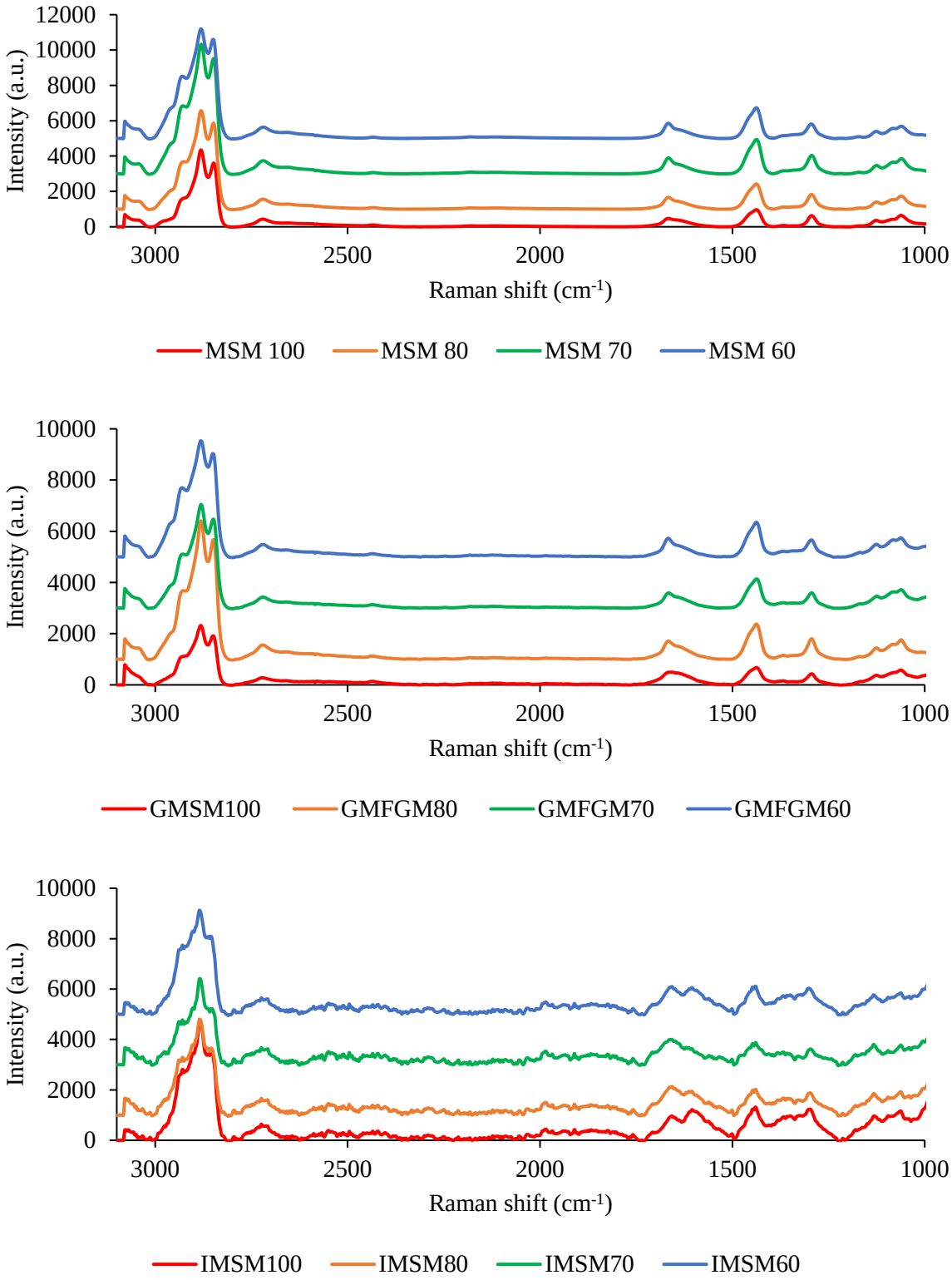

Appendix 6.10. Average Raman spectra of milk sphingomyelin (MSM) multilamellar vesicles. 100 = without cholesterol; 80 = 4:1 BPC/cholesterol; 70 = 7:3 mol/mol BPC/cholesterol; 60 = 3:2 mol/mol BPC/cholesterol. a) pre-digestion; b) post-gastric; c) post-intestinal with alk-SMase

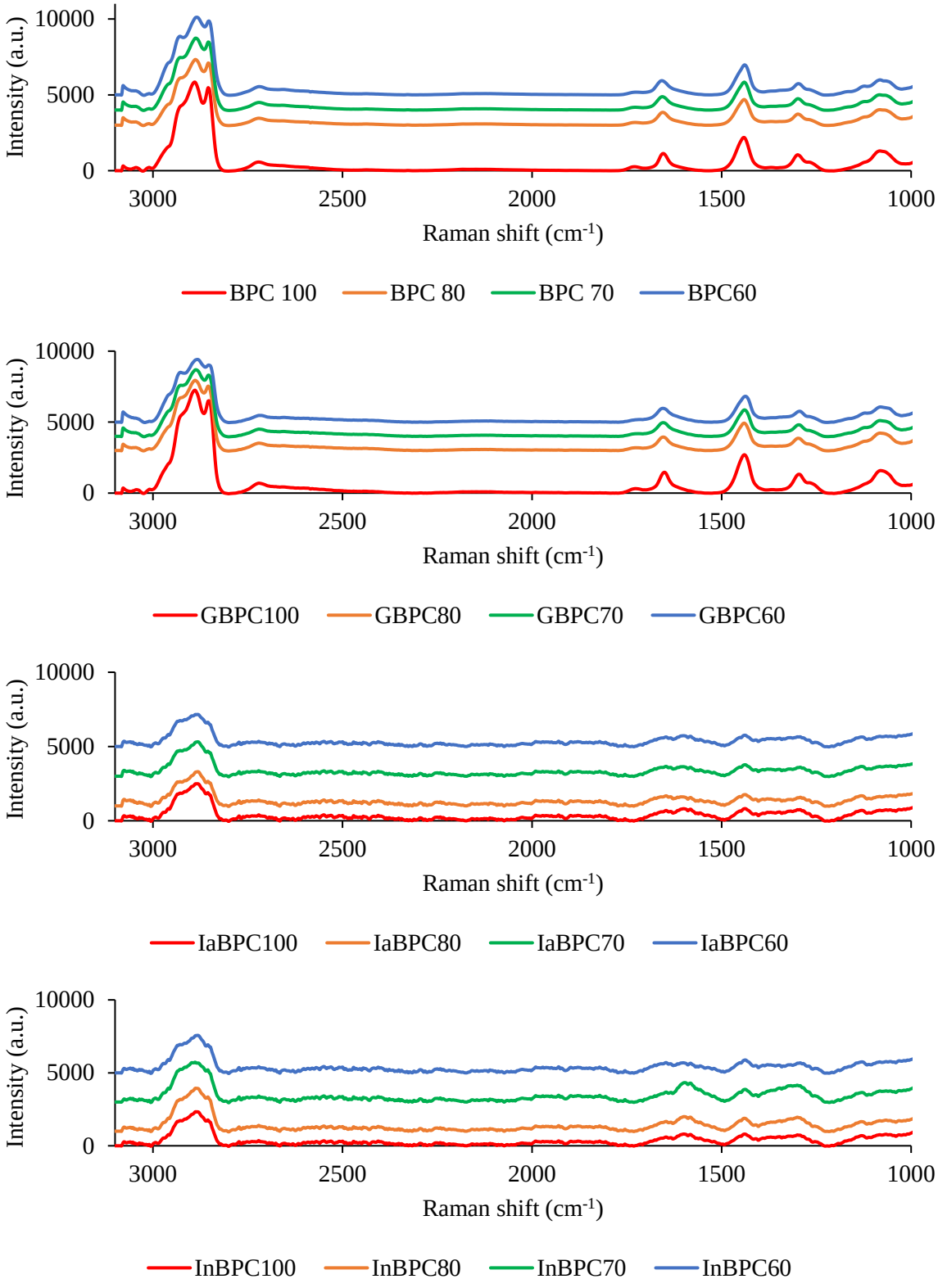

Appendix 6.11. Average Raman spectra of brain phosphatidylcholine (BPC) vesicles. 100 = without cholesterol; 80 = 4:1 BPC/cholesterol; 70 = 7:3 mol/mol BPC/cholesterol; 60 = 3:2 mol/mol BPC/cholesterol. a) pre-digestion; b) post-gastric; c) post-intestinal with alk-SMase; d) post-intestinal without alk-SMase

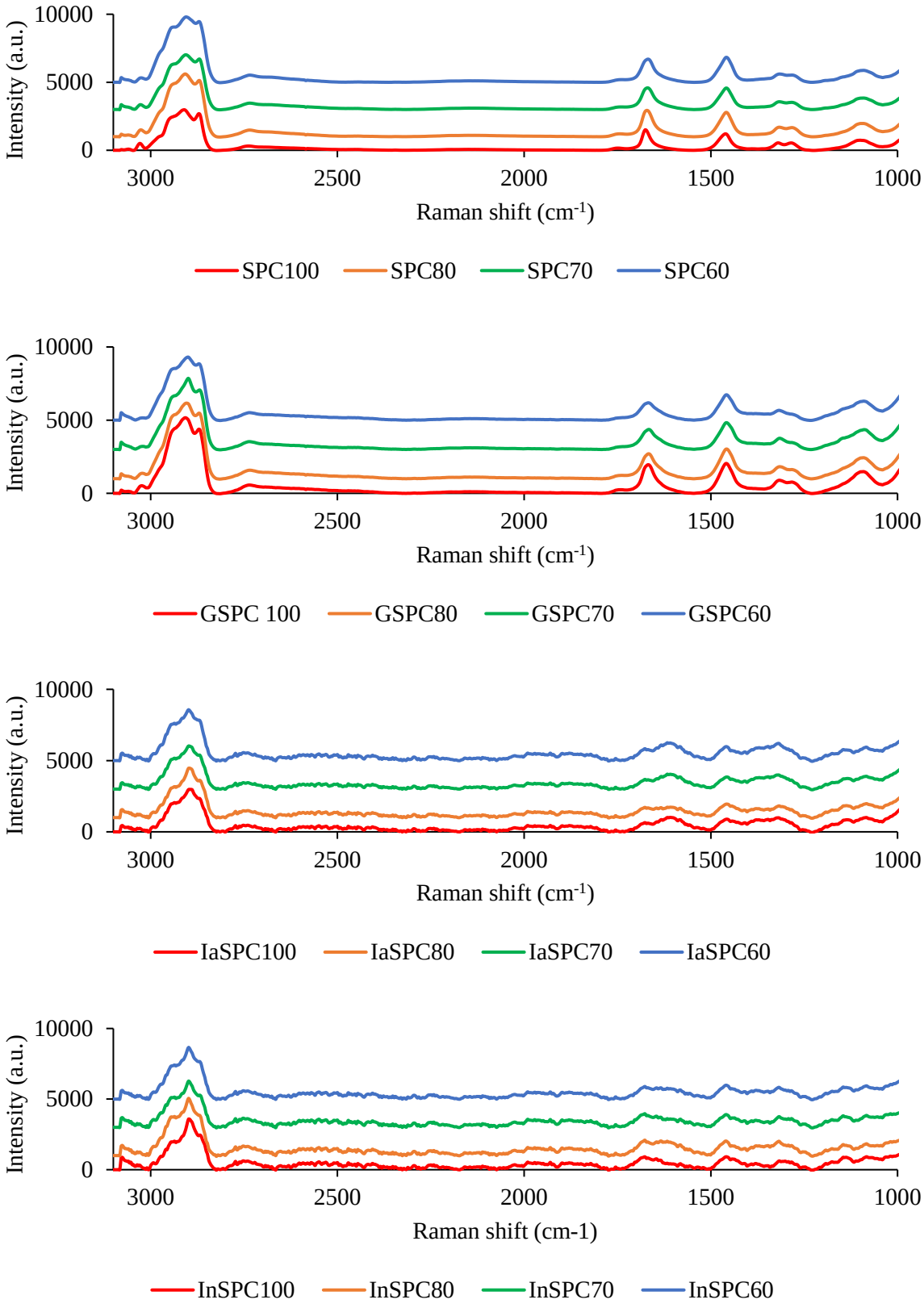

Appendix 6.12 Average Raman spectra of soy phosphatidylcholine (SPC) vesicles. 100 = without cholesterol; 80 = 4:1 SPC/cholesterol; 70 = 7:3 mol/mol SPC/cholesterol; 60 = 3:2 mol/mol SPC/cholesterol. a) pre-digestion; b) post-gastric; c) post-intestinal with alk-SMase; d) post-intestinal without alk-SMase

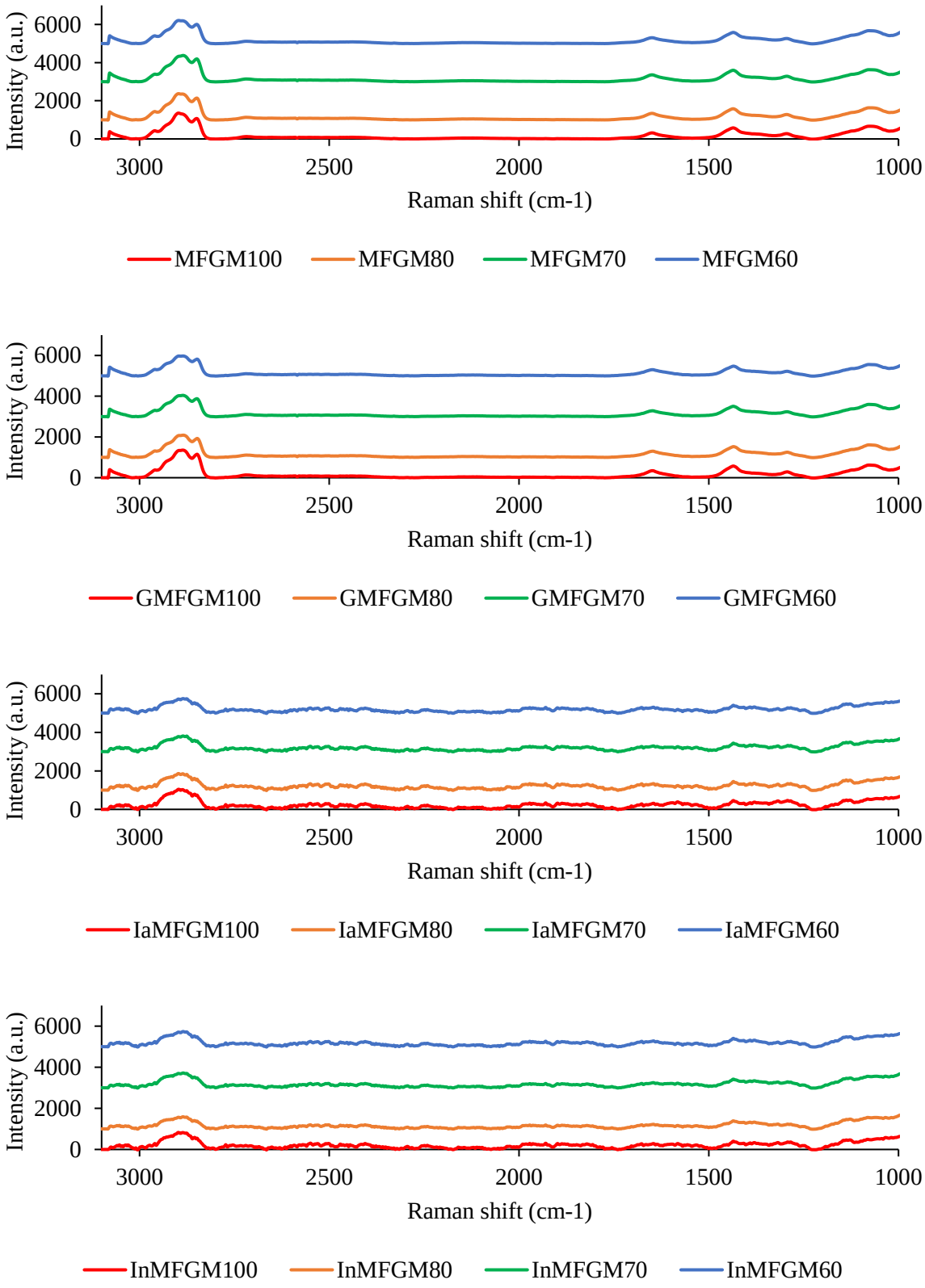

Appendix 6.13. Average Raman spectra of milk fat globule membrane (MFGM) phospholipid vesicles. 100 = without cholesterol; 80 = 4:1 MFGM/cholesterol; 70 = 7:3 mol/mol MFGM/cholesterol; 60 = 3:2 mol/mol MFGM/cholesterol. a) pre-digestion; b) post-gastric; c) post-intestinal with alk-SMase; d) post-intestinal without alk-SMase

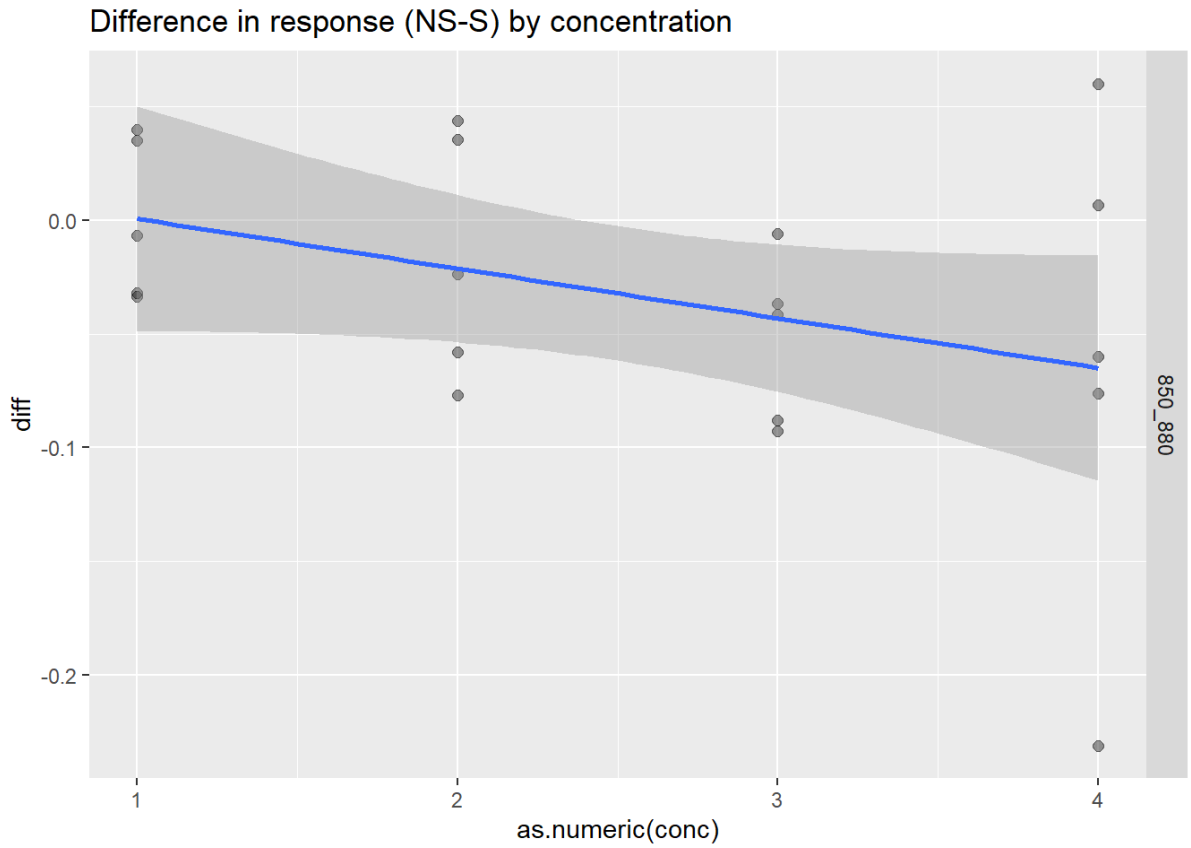

Appendix 6.14. Lateral hydrocarbon chain order difference test between MFGM phospholipid vesicle post intestinal digestion with and without alk-SMase. NS = no alk-SMase; S = with alk-SMase. 850_880 = label for I2850/I2880; as.numeric (conc) = label for SM/cholesterol ratio. 1 = IMFGM100, MFGM phospholipid vesicle without cholesterol post-intestinal, 2 = IMFGM80, MFGM phospholipid vesicle 4:1 mol/mol post-intestinal 3 = IMFGM70 = 7:3 mol/mol post-intestinal, 4 = IMFGM60 3:2 mol/mol post-intestinal.

Appendix: Chapter 7

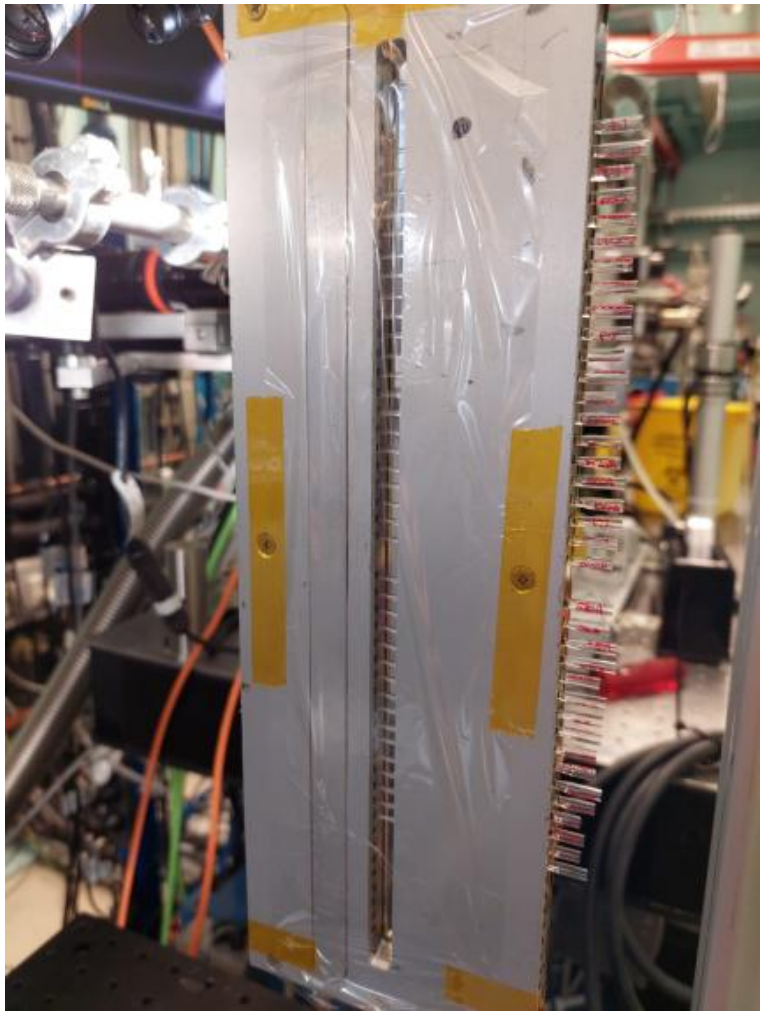

Appendix 7.1. Capillaries oriented on capillary rack. Mylar sheets (clear) taped onto measurement window.

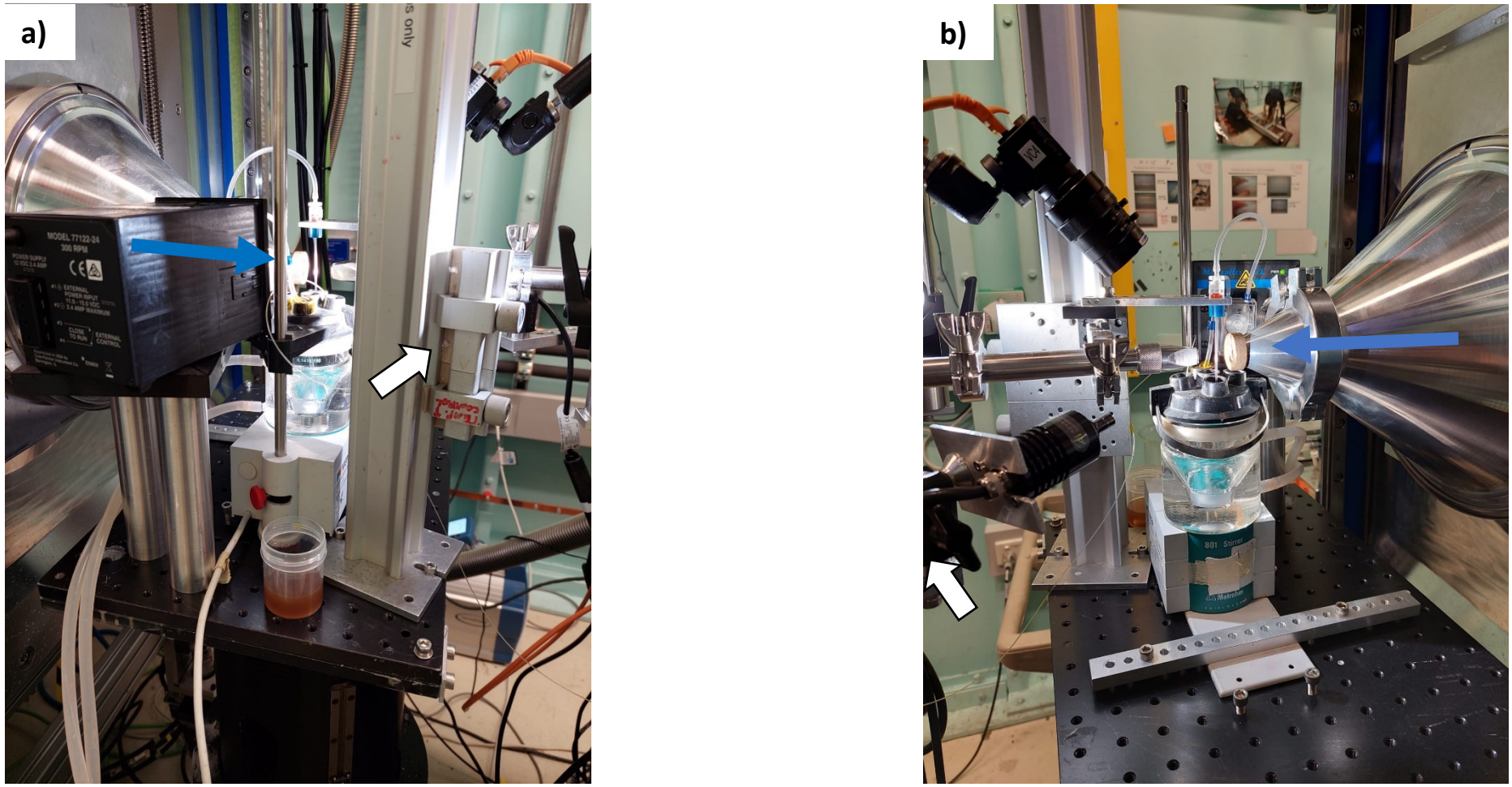

Appendix 7.2. Front (a) and back (a) of detergent-induced vesicle → micelle transition SR-SAXS experiment set-up. Thin tubing (white arrow) remotely injects bile from a syringe driver (not pictured). Blue arrow indicates the direction of the x-ray beam. Glass vessel holds and stirs the phospholipid vesicles. Solution is stirred in the vessel and aspirated through the capillary via peristaltic pump. Clamp holds the capillary and stand holds the stirrer plate and vessel in place.

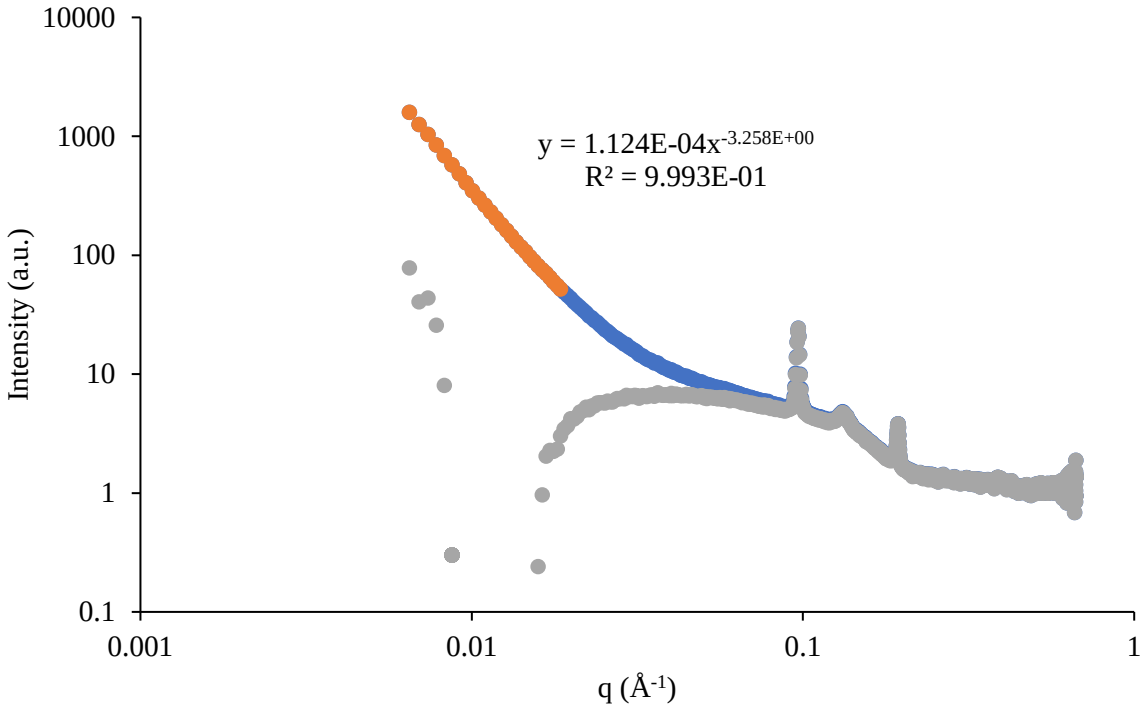

Appendix. 7.3. Original scattering profile (blue), power law portion of scattering profile (orange) with equation, and the subtracted scattering profile (grey). Power law is determined when $R^2 > 0.999$

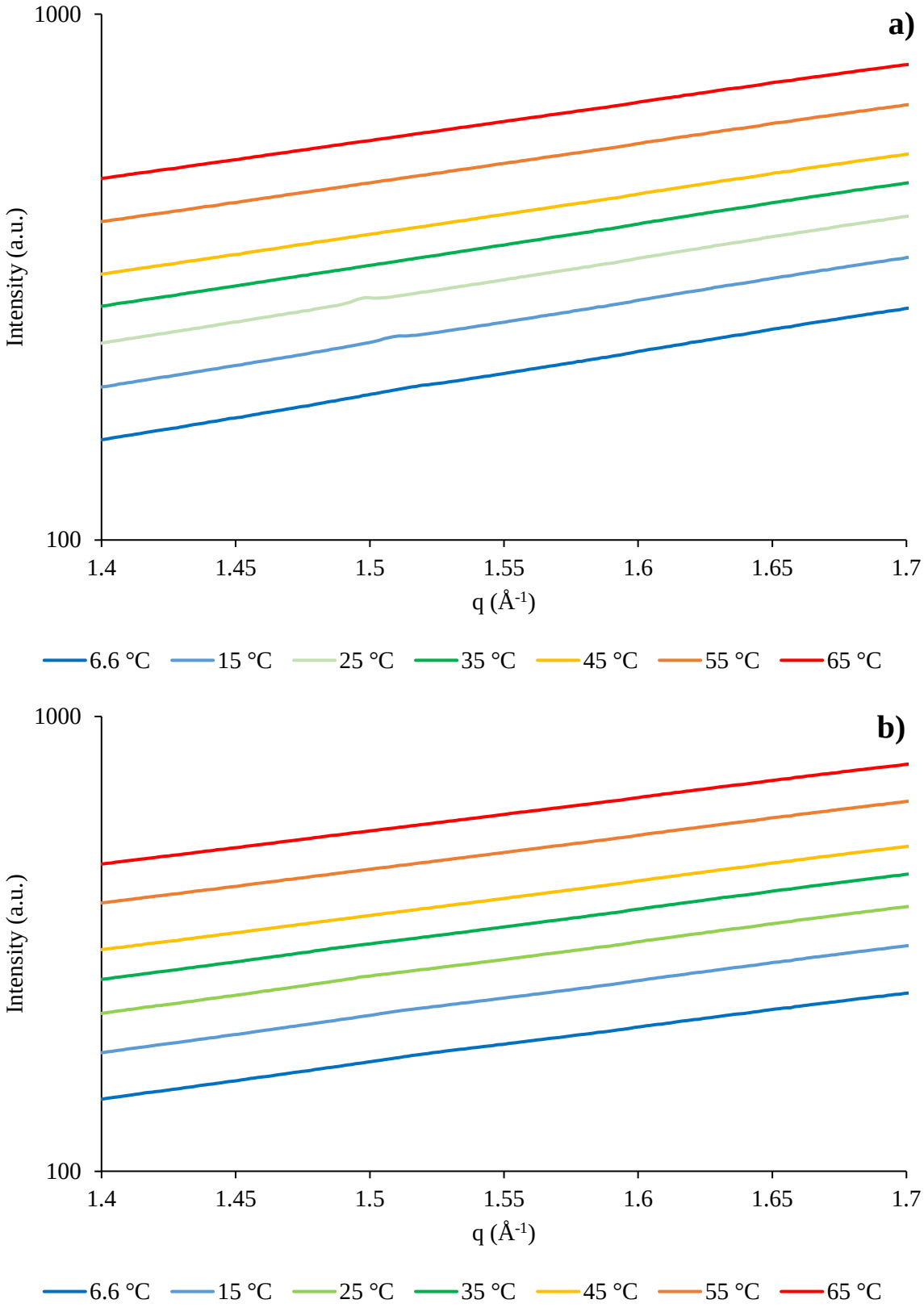

Appendix 7.4. Wide angle scattering profiles for the heating of a) milk sphingomyelin multilamellar vesicles without cholesterol; b) egg sphingomyelin multilamellar vesicles. No scattering was visible.

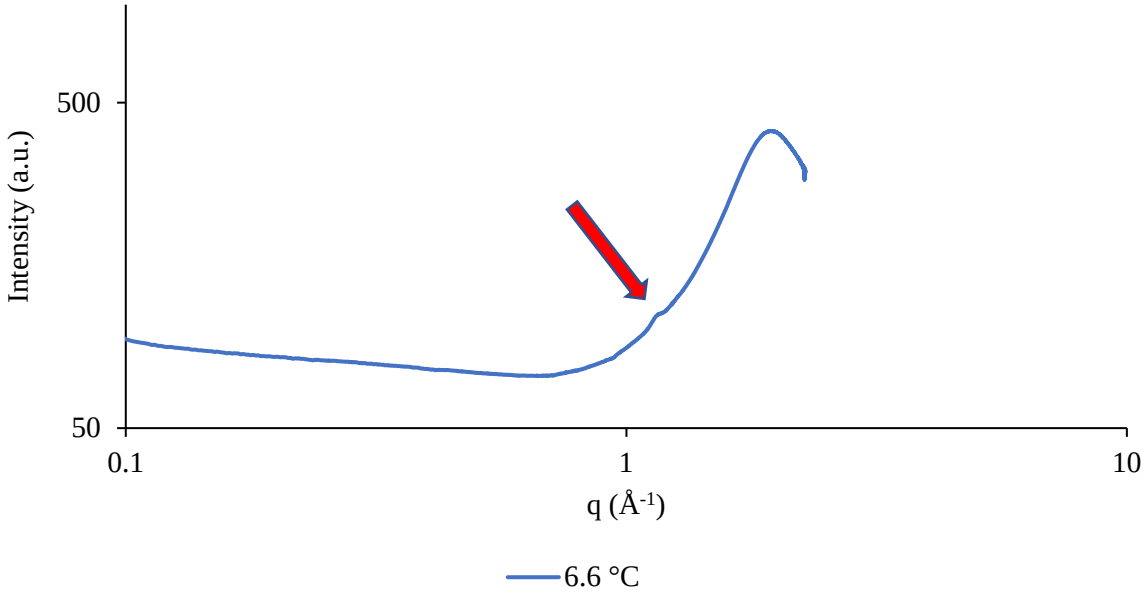

Appendix 7.5 Wide angle x-ray scattering profile of PIPES Buffer at 6.6 °C. Red arrow indicates the Mylar artefact at q = 1.16 Å. The broad peak on the right of the Bragg peak comes from a combination of scattering from the capillary and water.

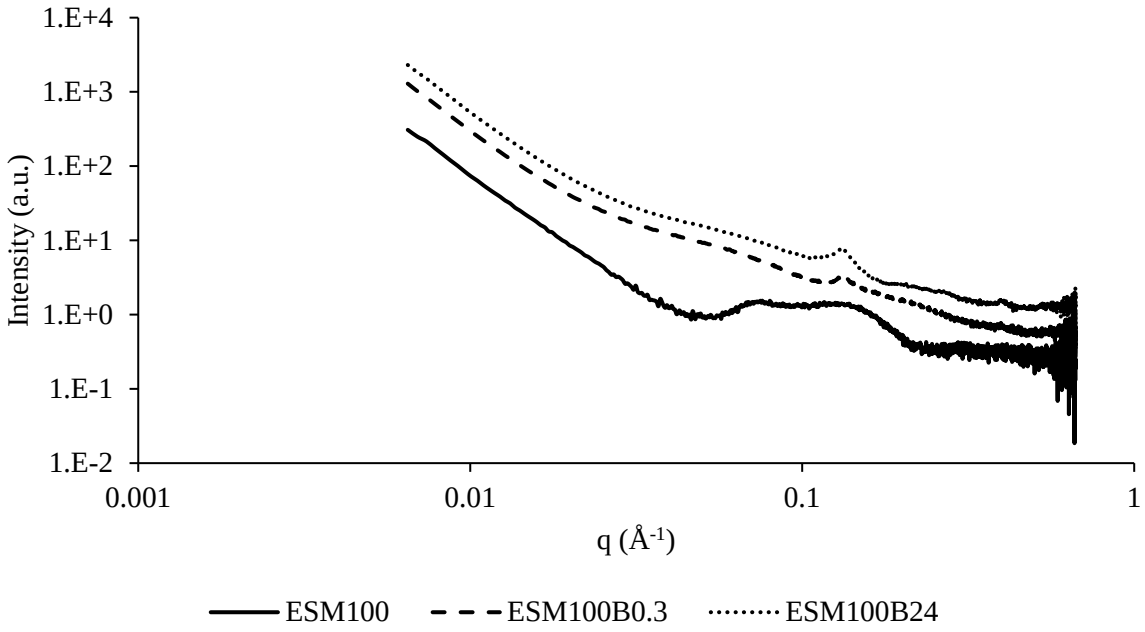

Appendix. 7.6. Small angle x-ray scattering of egg sphingomyelin multilamellar vesicles on log-log scale. Offsets have been added for clarity. ESM100 = no cholesterol; B0.3 = 20 s after bovine bile addition; B24 = 24 min after bovine bile addition.

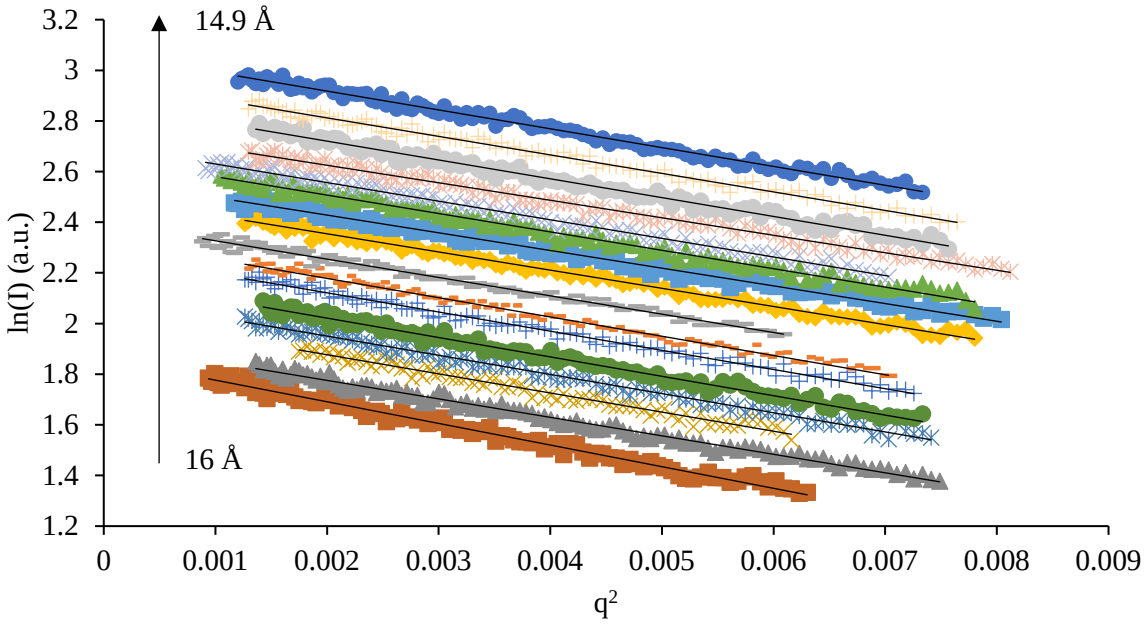

Appendix 7.7. Guinier fits of the biliary micelles after being added to the PIPES buffer after power law subtraction for the first 5 min of incubation. Brown squares = immediately after bile addition; grey triangles = 20 s; yellow crosses = 40 s; blue asterisk = 1 min; green circles = 1 min 20 s; blue crosses = 1 min and 40 s; orange dash = 2 min; grey dash = 2 min 20 s; yellow diamonds = 2 min 40s; blue squares = 3 min; green triangle = 3 min 20 s; blue crosses = 3 min 40 s; orange asterisk = 4 min, grey circles = 4 min 20 s; yellow crosses = 4 min 40 s; blue circles = 5 min.

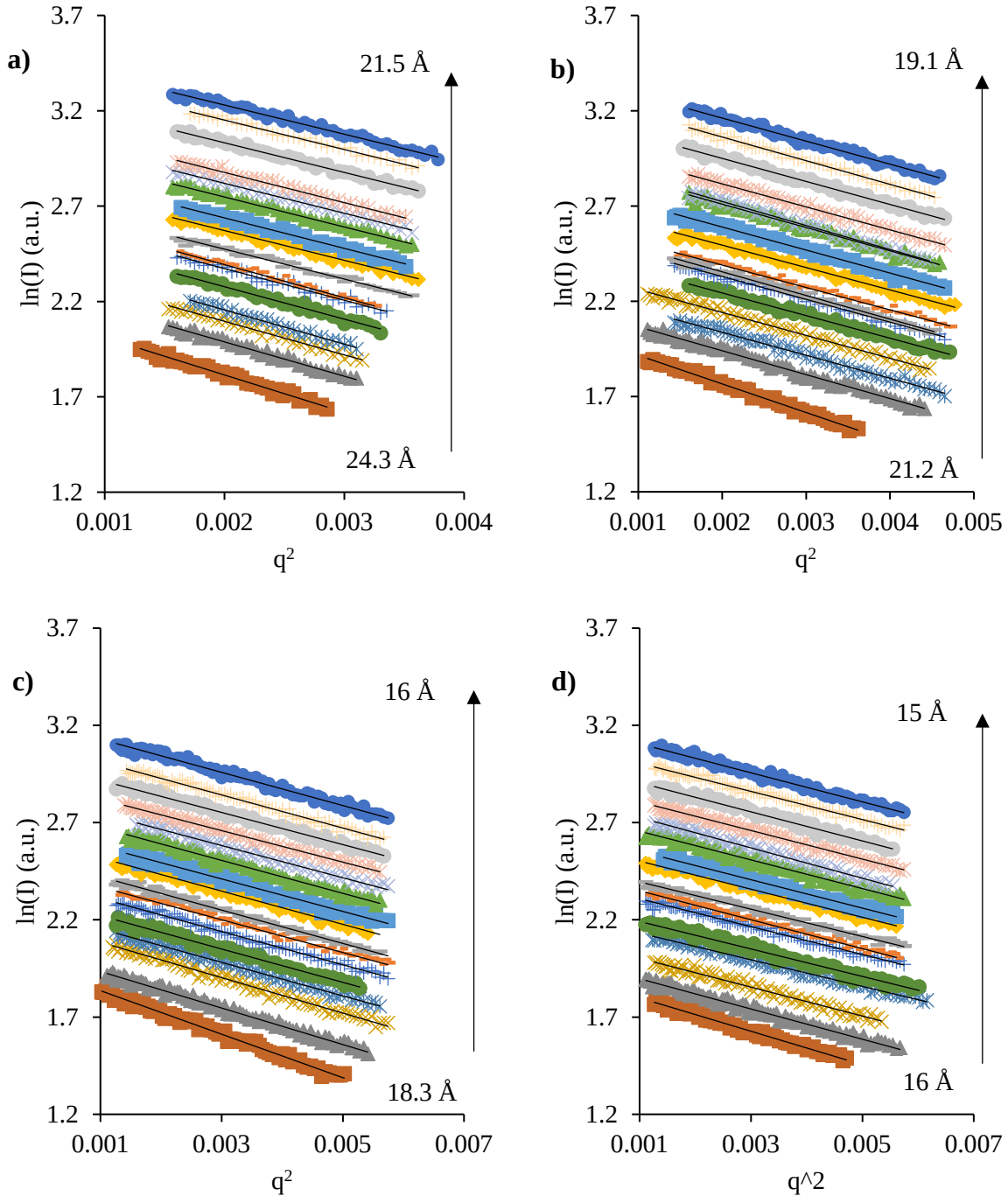

Appendix 7.8. Guinier fits of the biliary and mixed micelles after being added to the milk sphingomyelin (MSM) vesicles after power law subtraction for the first 5 min of incubation. Nonlinear q-range has been truncated. Offsets on the y- axis have been added for clarity. Brown squares = immediately after bile addition; grey triangles = 20 s; yellow crosses = 40 s; blue asterisk = 1 min; green circles = 1 min 20 s; blue crosses = 1 min and 40 s; orange dash = 2 min; grey dash = 2 min 20 s; yellow diamonds = 2 min 40s; blue squares = 3 min; green triangle = 3 min 20 s; blue crosses = 3 min 40 s; orange asterisk = 4 min, grey circles = 4 min 20 s; yellow crosses = 4 min 40 s; blue circles = 5 min. a) MSM100 = no cholesterol; b) MSM80 = 4:1 mol/mol MSM/cholesterol; c) MSM70 = 7:3 mol/mol MSM/cholesterol; d) ESM60 = 3:2 mol/mol MSM/cholesterol.

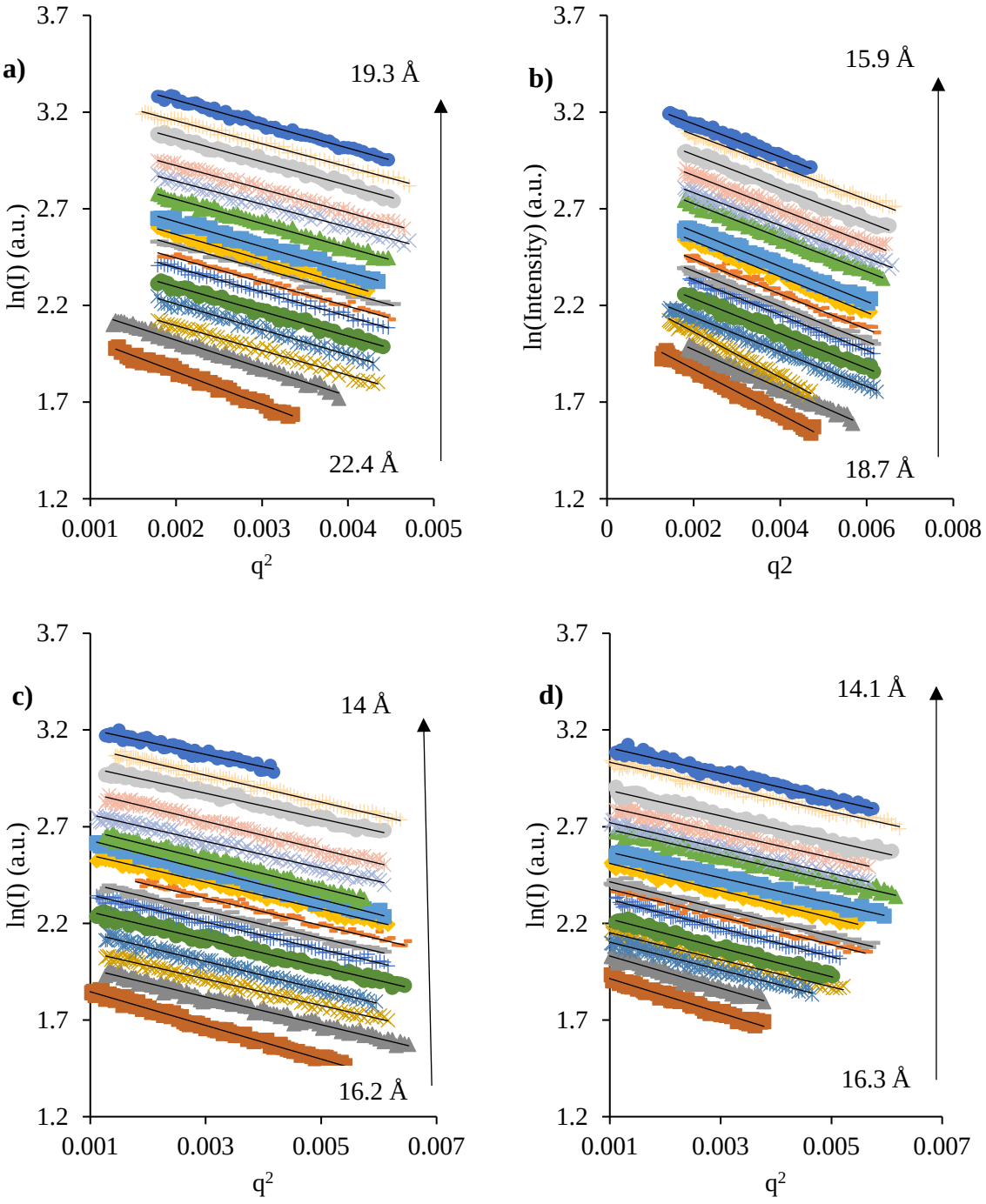

Appendix 7.9. Guinier fits of the biliary and mixed micelles after being added to the egg sphingomyelin (ESM) vesicles after power law subtraction for the first 5 min of incubation. Nonlinear q-range has been truncated. Offsets for the y-axis have been added for clarity. Brown squares = immediately after bile addition; grey triangles = 20 s; yellow crosses = 40 s; blue asterisk = 1 min; green circles = 1 min 20 s; blue crosses = 1 min and 40 s; orange dash = 2 min; grey dash = 2 min 20 s; yellow diamonds = 2 min 40s; blue squares = 3 min; green triangle = 3 min 20 s; blue crosses = 3 min 40 s; orange asterisk = 4 min, grey circles = 4 min 20 s; yellow crosses = 4 min 40 s; blue circles = 5 min. a) ESM100 = no cholesterol; b) ESM80 = 4:1 ESM/cholesterol; c) ESM70 = 7:3 ESM/cholesterol; d) ESM60 = 3:2 ESM/cholesterol.

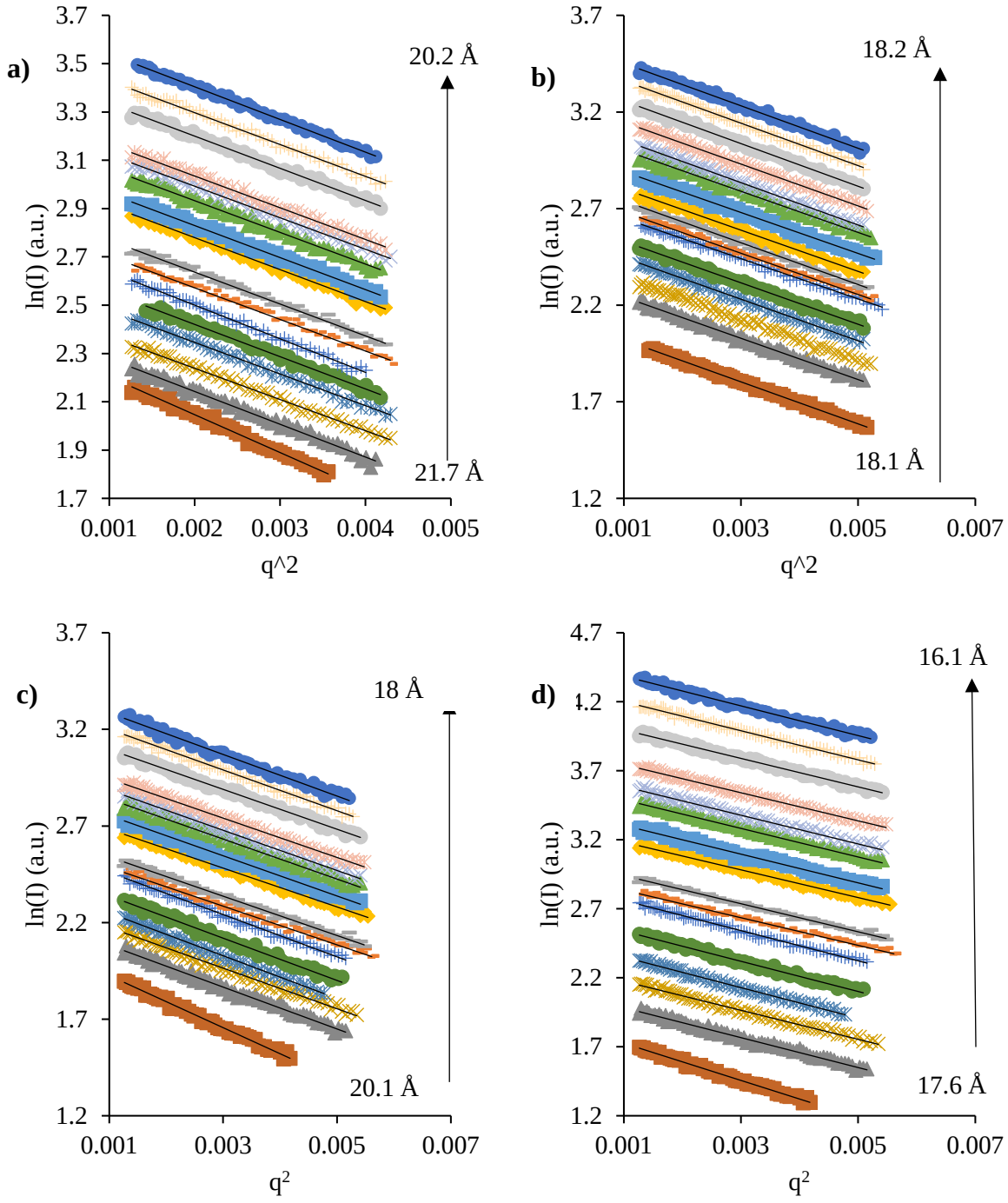

Appendix 7.10. Guinier fits of the biliary and mixed micelles after being added to the soy phosphatidylcholine (SPC) vesicles after power law subtraction for the first 5 min of incubation. Nonlinear q-range has been truncated. Offsets for the y-axis have been added for clarity. Brown squares = immediately after bile addition; grey triangles = 20 s; yellow crosses = 40 s; blue asterisk = 1 min; green circles = 1 min 20 s; blue crosses = 1 min and 40 s; orange dash = 2 min; grey dash = 2 min 20 s; yellow diamonds = 2 min 40s; blue squares = 3 min; green triangle = 3 min 20 s; blue crosses = 3 min 40 s; orange asterisk = 4 min, grey circles = 4 min 20 s; yellow crosses = 4 min 40 s; blue circles = 5 min. a) SPC100 = no cholesterol; b) SPC80 = 4:1 mol/mol SPC/cholesterol; c) SPC70 = 7:3 mol/mol SPC/cholesterol; d) SPC60 = 3:2 mol/mol ESM/cholesterol.

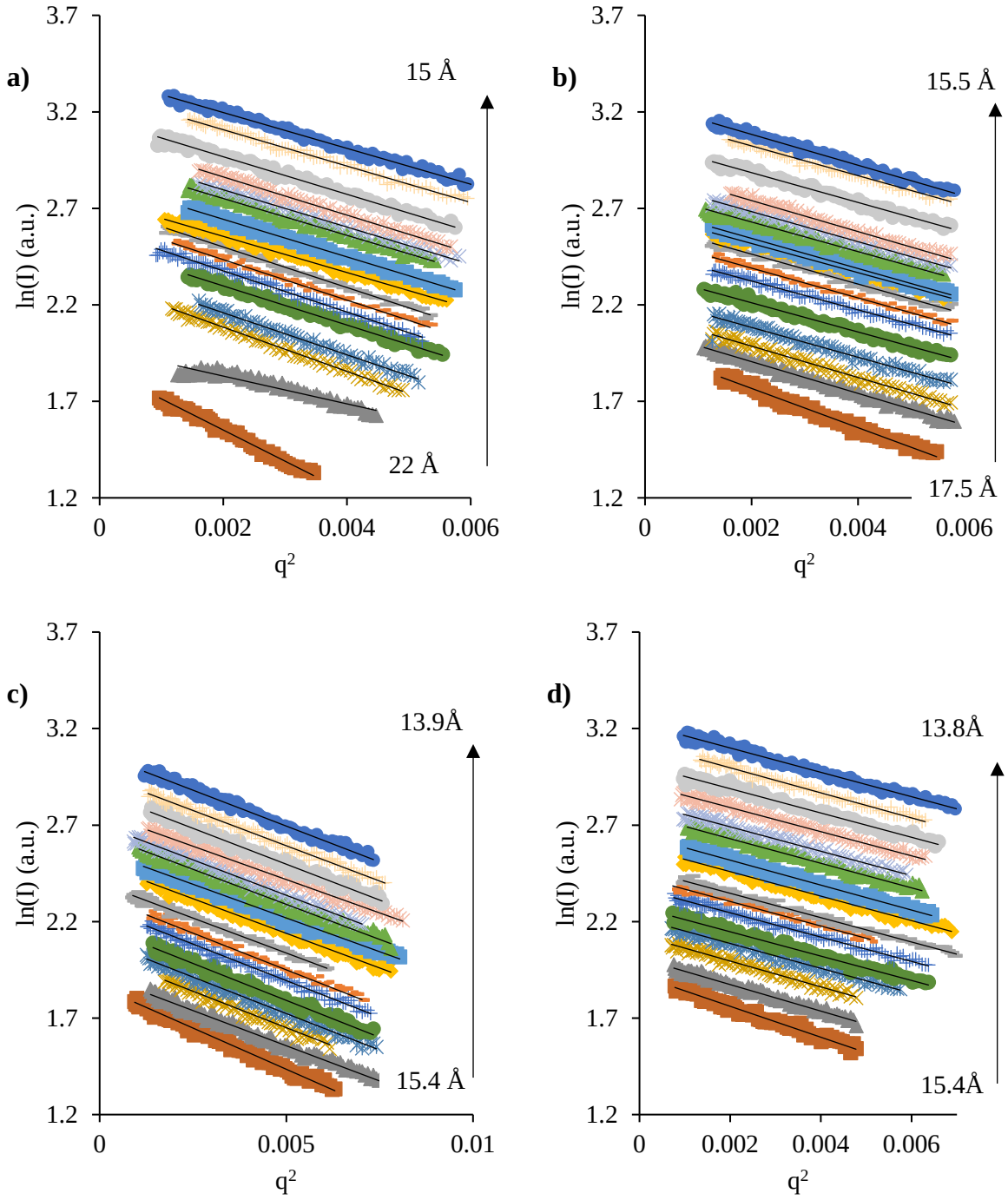

Appendix 7.11. Guinier fits of the biliary and mixed micelles after being added to the milk fat globule membrane phospholipid (MFGM) vesicles after power law subtraction for the first 5 min of incubation. Nonlinear q-range has been truncated. Offsets for the y-axis have been added for clarity. Brown squares = immediately after bile addition; grey triangles = 20 s; yellow crosses = 40 s; blue asterisk = 1 min; green circles = 1 min 20 s; blue crosses = 1 min and 40 s; orange dash = 2 min; grey dash = 2 min 20 s; yellow diamonds = 2 min 40s; blue squares = 3 min; green triangle = 3 min 20 s; blue crosses = 3 min 40 s; orange asterisk = 4 min, grey circles = 4 min 20 s; yellow crosses = 4 min 40 s; blue circles = 5 min. a) MFGM100 = no cholesterol; b) MFGM80 = 4:1 mol/mol sphingomyelin/cholesterol; c) SPC70 = 7:3 mol/mol sphingomyelin/cholesterol; d) SPC60 = 3:2 mol/mol sphingomyelin/cholesterol.

MASSEY UNIVERSITY
TE KUNENGA KI PŪREHUROA
UNIVERSITY OF NEW ZEALAND

GRADUATE RESEARCH SCHOOL

STATEMENT OF CONTRIBUTION
DOCTORATE WITH PUBLICATIONS/MANUSCRIPTS

We, the candidate and the candidate's Primary Supervisor, certify that all co-authors have consented to their work being included in the thesis and they have accepted the candidate's contribution as indicated below in the *Statement of Originality*.

Name of candidate:	Patrick Tai
Name/title of Primary Supervisor:	Harjinder Singh
In which chapter is the manuscript /published work:	2

Please select one of the following three options:

(●) The manuscript/published work is published or in press

- Please provide the full reference of the Research Output:

Tai, P., Golding, M., Singh, H., & Everett, D. (2022). The bovine milk fat globule membrane – Liquid ordered domain formation and anticholesteremic effects during digestion. Food Reviews International, 1–27.

( ) The manuscript is currently under review for publication – please indicate:

- The name of the journal:

- The percentage of the manuscript/published work that was contributed by the candidate:

- Describe the contribution that the candidate has made to the manuscript/published work:

( ) It is intended that the manuscript will be published, but it has not yet been submitted to a journal

Candidate's Signature:	Patrick Tai Digitally signed by Patrick Tai DN: cn=Patrick Tai, o=Riddet Institute, ou=Graduate Student, email=P.Tai@massey.ac.nz, c=NZ Date: 2022.07.13 09:36:11 -07'00'
Date:	14-Jul-2022
Primary Supervisor's Signature:	Harjinder Singh Digitally signed by Harjinder Singh Date: 2022.07.15 13:39:13 +12'00'
Date:	15-Jul-2022

This form should appear at the end of each thesis chapter/section/appendix submitted as a manuscript/ publication or collected as an appendix at the end of the thesis.

MASSEY UNIVERSITY
TE KUNENGA KI PŪREHUROA
UNIVERSITY OF NEW ZEALAND

GRADUATE RESEARCH SCHOOL

STATEMENT OF CONTRIBUTION
DOCTORATE WITH PUBLICATIONS/MANUSCRIPTS

We, the candidate and the candidate's Primary Supervisor, certify that all co-authors have consented to their work being included in the thesis and they have accepted the candidate's contribution as indicated below in the *Statement of Originality*.

Name of candidate:	Patrick Tai
Name/title of Primary Supervisor:	Harjinder Singh
In which chapter is the manuscript /published work:	4

Please select one of the following three options:

(●) The manuscript/published work is published or in press

- Please provide the full reference of the Research Output:

Tai, P., Golding, M., Singh, H., Waterland, M., & Everett, D. W. (2021). Cholesterol-phospholipid interactions resist the detergent effect of bovine bile. Colloids and Surfaces B: Biointerfaces, 205, 111842.

( ) The manuscript is currently under review for publication – please indicate:

- The name of the journal:

- The percentage of the manuscript/published work that was contributed by the candidate:

- Describe the contribution that the candidate has made to the manuscript/published work:

( ) It is intended that the manuscript will be published, but it has not yet been submitted to a journal

Candidate's Signature:	Patrick Tai Digitally signed by Patrick Tai DN: cn=Patrick Tai, o=Riddet Institute, ou=Graduate Student, email=P.Tai@massey.ac.nz, c=NZ Date: 2022.07.13 09:34:09 -07'00'
Date:	14-Jul-2022
Primary Supervisor's Signature:	Harjinder Singh Digitally signed by Harjinder Singh Date: 2022.07.15 13:40:30 +12'00'
Date:	15-Jul-2022

This form should appear at the end of each thesis chapter/section/appendix submitted as a manuscript/ publication or collected as an appendix at the end of the thesis.

MASSEY UNIVERSITY
TE KUNENGA KI PŪREHUROA
UNIVERSITY OF NEW ZEALAND

GRADUATE RESEARCH SCHOOL

STATEMENT OF CONTRIBUTION
DOCTORATE WITH PUBLICATIONS/MANUSCRIPTS

We, the candidate and the candidate's Primary Supervisor, certify that all co-authors have consented to their work being included in the thesis and they have accepted the candidate's contribution as indicated below in the *Statement of Originality*.

Name of candidate:	Patrick Tai
Name/title of Primary Supervisor:	Harjinder Singh
In which chapter is the manuscript /published work:	6

Please select one of the following three options:

○ The manuscript/published work is published or in press

- Please provide the full reference of the Research Output:

○ The manuscript is currently under review for publication – please indicate:

- The name of the journal:

- The percentage of the manuscript/published work that was contributed by the candidate:

- Describe the contribution that the candidate has made to the manuscript/published work:

◉ It is intended that the manuscript will be published, but it has not yet been submitted to a journal

Candidate's Signature:	Patrick Tai Digitally signed by Patrick Tai DN: cn=Patrick Tai, o=Riddet Institute, ou=Graduate Student, email=P.Tai@massey.ac.nz, c=NZ Date: 2022.07.13 09:35:05 -07'00'
Date:	14-Jul-2022
Primary Supervisor's Signature:	Harjinder Singh Digitally signed by Harjinder Singh Date: 2022.07.15 13:41:22 +12'00'
Date:	15-Jul-2022

This form should appear at the end of each thesis chapter/section/appendix submitted as a manuscript/ publication or collected as an appendix at the end of the thesis.

MASSEY UNIVERSITY
TE KUNENGA KI PŪREHUROA
UNIVERSITY OF NEW ZEALAND

GRADUATE RESEARCH SCHOOL

STATEMENT OF CONTRIBUTION
DOCTORATE WITH PUBLICATIONS/MANUSCRIPTS

We, the candidate and the candidate's Primary Supervisor, certify that all co-authors have consented to their work being included in the thesis and they have accepted the candidate's contribution as indicated below in the *Statement of Originality*.

Name of candidate:	Patrick Tai
Name/title of Primary Supervisor:	Harjinder Singh
In which chapter is the manuscript /published work:	7

Please select one of the following three options:

○ The manuscript/published work is published or in press

- Please provide the full reference of the Research Output:

○ The manuscript is currently under review for publication – please indicate:

- The name of the journal:

- The percentage of the manuscript/published work that was contributed by the candidate:

- Describe the contribution that the candidate has made to the manuscript/published work:

◉ It is intended that the manuscript will be published, but it has not yet been submitted to a journal

Candidate's Signature:	Patrick Tai Digitally signed by Patrick Tai DN: cn=Patrick Tai, o=Riddet Institute, ou=Graduate Student, email=P.Tai@massey.ac.nz, c=NZ Date: 2022.07.13 09:36:54 -07'00'
Date:	14-Jul-2022
Primary Supervisor's Signature:	Harjinder Singh Digitally signed by Harjinder Singh Date: 2022.07.15 13:37:32 +12'00'
Date:	15-Jul-2022

This form should appear at the end of each thesis chapter/section/appendix submitted as a manuscript/ publication or collected as an appendix at the end of the thesis.